

Power Electronics and Power Systems

Savu C. Savulescu *Editor*

Real-Time Stability in Power Systems

Techniques for Early Detection
of the Risk of Blackout

2nd Edition

 Springer

Power Electronics and Power Systems

Series Editors

Dr. Joe H. Chow
Rensselaer Polytechnic Institute
New York, USA

Dr. Alex M. Stankovic
Tufts University
Massachusetts, USA

Dr. David Hill
The University of Hong Kong
Pokfulam, Hong Kong

For further volumes:
<http://www.springer.com/series/6403>

The Power Electronics and Power Systems Series encompasses power electronics, electric power restructuring, and holistic coverage of power systems. The Series comprises advanced textbooks, state-of-the-art titles, research monographs, professional books, and reference works related to the areas of electric power transmission and distribution, energy markets and regulation, electronic devices, electric machines and drives, computational techniques, and power converters and inverters. The Series features leading international scholars and researchers within authored books and edited compilations. All titles are peer reviewed prior to publication to ensure the highest quality content. To inquire about contributing to the Power Electronics and Power Systems Series, please contact Dr. Joe Chow, Administrative Dean of the College of Engineering and Professor of Electrical, Computer and Systems Engineering, Rensselaer Polytechnic Institute, Jonsson Engineering Center, Office 7012, 110 8th Street, Troy, NY USA, 518-276-6374, chowj@rpi.edu.

Savu C. Savulescu
Editor

Real-Time Stability in Power Systems

Techniques for Early Detection
of the Risk of Blackout

2nd Edition

 Springer

Editor
Savu C. Savulescu
Energy Consulting International, Inc.
New York, NY
USA

ISSN 2196-3185 ISSN 2196-3193 (electronic)
ISBN 978-3-319-06679-0 ISBN 978-3-319-06680-6 (eBook)
DOI 10.1007/978-3-319-06680-6
Springer Cham Heidelberg New York Dordrecht London

Library of Congress Control Number: 2014942460

© Springer International Publishing - Switzerland 2006, 2014

This work is subject to copyright. All rights are reserved by the Publisher, whether the whole or part of the material is concerned, specifically the rights of translation, reprinting, reuse of illustrations, recitation, broadcasting, reproduction on microfilms or in any other physical way, and transmission or information storage and retrieval, electronic adaptation, computer software, or by similar or dissimilar methodology now known or hereafter developed. Exempted from this legal reservation are brief excerpts in connection with reviews or scholarly analysis or material supplied specifically for the purpose of being entered and executed on a computer system, for exclusive use by the purchaser of the work. Duplication of this publication or parts thereof is permitted only under the provisions of the Copyright Law of the Publisher's location, in its current version, and permission for use must always be obtained from Springer. Permissions for use may be obtained through RightsLink at the Copyright Clearance Center. Violations are liable to prosecution under the respective Copyright Law.

The use of general descriptive names, registered names, trademarks, service marks, etc. in this publication does not imply, even in the absence of a specific statement, that such names are exempt from the relevant protective laws and regulations and therefore free for general use.

While the advice and information in this book are believed to be true and accurate at the date of publication, neither the authors nor the editors nor the publisher can accept any legal responsibility for any errors or omissions that may be made. The publisher makes no warranty, express or implied, with respect to the material contained herein.

Printed on acid-free paper

Springer is part of Springer Science+Business Media (www.springer.com)

*Dedicated to my children
Felicia and Crivat
and to the memory of my parents
Felicia and Savu*

Preface

The revised and updated version of the original *Real-Time Stability in Power Systems* is most timely, given the myriad changes in the electric power industry and the significant technology advances in computing, control and communications fields since its initial publication. Dr. Savulescu and his hand-picked group of experts have accomplished an impressive effort to provide in a single tome a comprehensive treatment of the power system real-time stability assessment area.

While the physics of the power systems has not changed in the liberalized, competitive electricity market environment, within which they operate, the decision making process has undergone major transformations as an aftermath of the restructuring in the industry. The rapidly evolving implementation of the *smarter grid* has impacted significantly the quality and quantity of data available around the clock to system operators. Indeed, the establishment of the Advanced Metering Infrastructure (*AMI*) in many power systems and the growing presence of Phasor Measurement Units (*PMUs*) in interconnected networks are two salient features of the new power system. The massive amounts of data brought in 24×7 by these new devices—the so-called *Big Data* explosion—represents the reality of the environment in which today's operators make real-time decisions. The new book provides the basis for the construction of the analytics to deal with the multiple facets of the huge masses of data that are collected, stored and processed for arriving at decisions based on improved and more timely information.

The original version of the book was an explicit acknowledgment that the electric power industry was shifting away from the seat-of-the-pants, hand waving methods of the past to formal approaches based on a solid analytical footing that make detailed use of system and network theoretic concepts. Since that time, many of the approaches have matured and come of age and the power industry has garnered valuable experience in their deployment. Indeed, we have witnessed the broader acceptance of the metrics to quantify the distance to instability as a useful measure to reflect the risk of a reliability event. In addition, the introduction of effective visualization tools has made possible the improved comprehension of the power system state in the dynamic regime. Also, the better understanding of dynamic phenomena in voltage stability, the application of appropriate tools from control and communications domains and the advancements in computing have brought about

major progress in the formulation and implementation of effective control strategies for the power grid.

The new version of the book captures all these important developments and incorporates them in the revised edition. Together with the newly added chapters, the book offers a comprehensive treatment of the essential components of decision support systems for dynamic stability. Their effective deployment can undoubtedly result in more timely decisions, incorporating better information, in this critically important area of power system operations and control. The book is destined to become an essential reference for industry practitioners and academic researchers.

I conclude this section with my heartfelt congratulations to Dr. Savulescu and his team of experts in the production of this new and important reference tome. I also express my hope that, given the many new developments underway in microgrids, renewable resource integration and distributed decision making, to name just a few areas, the updated version of the next edition will be available with a shorter lapse in time than the present one.

April 8, 2014

George Gross

Department of Electrical and Computer Engineering
University of Illinois at Urbana-Champaign

Introduction

In the aftermath of the series of blackouts that had affected utilities in the US, UK and mainland Europe in 2003 and 2004, the August 2004 cover of the IEEE Spectrum was telling its readers that “studies of electrical networks come to the same conclusion: big blackouts are inevitable” (left side picture¹ in Fig. 1).

Less than two months later, the industry and academia experts invited to the *Real-Time Stability Challenge* panel session at the IEEE Power Systems Conference & Exposition (PSCE) on October 13, 2004 in New York (right side of Fig. 1) sent a different, yet upbeat message to the power system engineering community: stability applications capable of providing for the early detection of the risk of blackout were available and ready for being used and relied upon in power system control centers.

The proceedings of that memorable event, complemented with contributions from leading experts in the field, were assembled by Springer in 2005 in the volume *Real Time Stability in Power Systems*, the first book that was ever published on this transcendental topic.

The real-time stability theme was again focused upon: in subsequent panel sessions, held at the IEEE PES PSCE meetings in Atlanta, GA, 2006 and Seattle, WA, 2009; and in a 2009 book², which documented the experience from actually using real-time stability applications in energy control centers.

Now it’s time to step back and assess the broad picture.

Certain approaches that originally seemed promising did not, or not yet, materialize, but the overall balance is positive:

¹ © 2004 IEEE. Reprinted, with permission, from IEEE Spectrum Volume 41, Issue 8.

² Savulescu, S. C., *Real-Time Stability Assessment in Modern Power System Control Centers* (Editor), Wiley & IEEE Press, 2009, New York, NY.

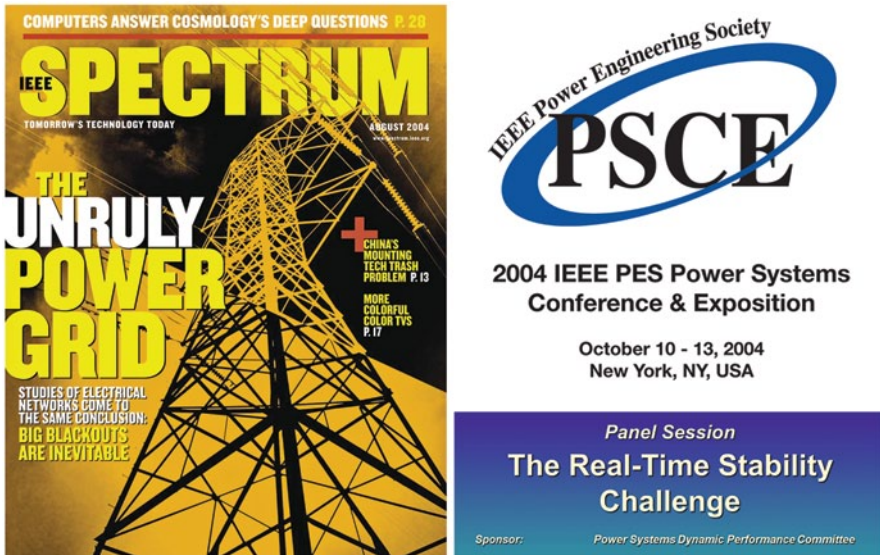


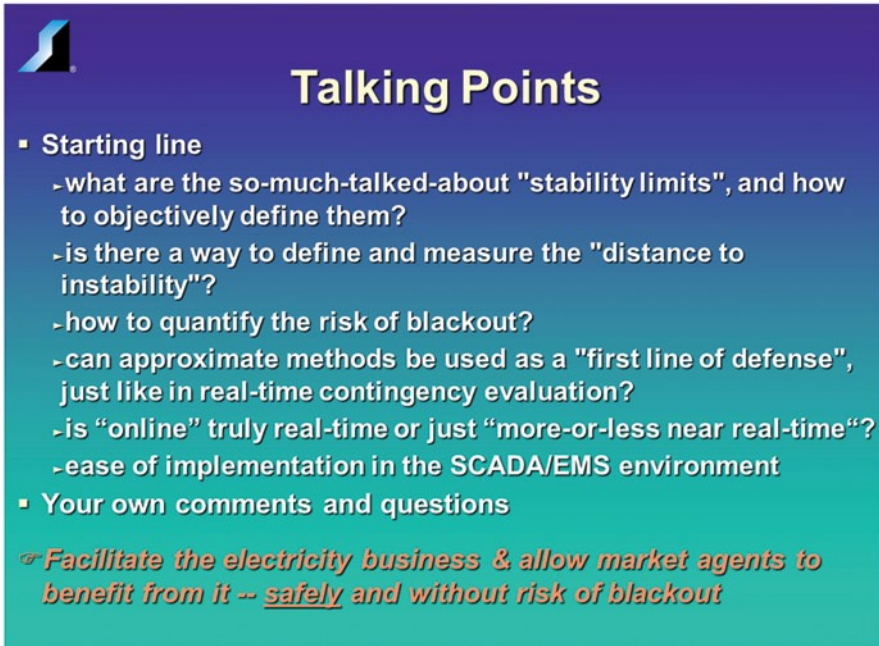
Fig. 1 Are blackouts inevitable? The community of power system engineers does not think so

- Two major system vendors have seamlessly integrated real-time stability monitoring tools in their SCADA/EMS baselines and now are offering them as *off-the-shelf* products^{3,4}
- Third-party stability software continues to be implemented on an “add-on” basis in new and existing systems
- Utilities, practitioners and academia have a clearer picture of what works, what doesn’t and why; and, last but not least
- The stability-related applications of PMUs and synchrophasor technologies have matured and are increasingly being accepted by the industry.

The second edition of *Real-Time Stability in Power Systems* addresses all these developments and much more. Before we get into more details, though, let us first summarize the key points that will be addressed in the book.

³ Eichler, R., Heyde, C. O., Stottok, B. O., Composite Approach for the Early Detection, Assessment and Visualization of the Risk of Instability in the Control of Smart Transmission Grids, in *Real-Time Stability in Power Systems*, 2nd edition, Springer, 2014, New York, NY.

⁴ Giri, J., Parashar, M., Avila-Rosales, R., and Wilson, D., The Case for Using Wide-Area Monitoring and Control to Improve the Resilience and Capacity of the Electric Power Grid, in *Real-Time Stability in Power Systems*, 2nd edition, Springer, 2014, New York, NY.



Talking Points

- **Starting line**
 - what are the so-much-talked-about "stability limits", and how to objectively define them?
 - is there a way to define and measure the "distance to instability"?
 - how to quantify the risk of blackout?
 - can approximate methods be used as a "first line of defense", just like in real-time contingency evaluation?
 - is "online" truly real-time or just "more-or-less near real-time"?
 - ease of implementation in the SCADA/EMS environment
- **Your own comments and questions**

☞ Facilitate the electricity business & allow market agents to benefit from it -- safely and without risk of blackout

Fig. 2 October 13, 2004 Real-Time Stability Challenge panel session "talking points" slide

Talking Points

The talking points set for the October 13, 2004 PSCE panel session (Fig. 2) are still valid today. Consider, for example, the need for *metrics* that define the distance to instability and quantify the risk of blackout.

In order to be truly useful in the control room, where, in addition to other duties, the operators monitor *limits*, an important requirement for the stability software is the ability to identify, quantify and visualize the *stability limit*, or *limits*, as opposed to just determining if a postulated contingency may cause instability.

However, according to Professor Kundur, many stability programs in the market would not pass this test—they "determine whether a given condition is stable or unstable, [but] have not been efficient in quickly and automatically determining the stability limits"⁵.

Let us add that, traditionally, the research community focuses on transient and voltage stability techniques, but when it comes up to quantifying system-wide

⁵ Kundur, P., Introduction to *Techniques for Power System Stability Search*, a special publication of the Power System Dynamic Performance Committee of the IEEE PES, 1999, TP-138-0, pp. 1–3.

stability limits, one has to rely on *steady-state stability*⁶, where concepts such as *stability reserve* and *distance to instability* are introduced naturally and can be unambiguously defined and computed, as shown in the first four chapters of the book.

Another question was whether *controlled approximations* rather than *heuristics* can tame the otherwise complex and computationally intensive stability algorithms and make them suitable for real-time while ensuring the precision and validity of the results. The answer is “yes” and it has been proven in the field, as documented in Chapters 2 through 4.

But what is it meant by “online” and “real-time”? As we see it, in order to qualify for the “real-time” label, the stability software should get input from the most recent state estimate and produce the results *and* visualize them *way before* the start of the next state estimation cycle, so that the operator would have plenty of time to assess the situation and make a decision. In spite of this obvious requirement, some application designers claim that “results are needed typically at every 5–30 minutes”, which would certainly feel like an eternity in a control room where, during a major system event, hundreds of alarms pop-up and critical online operating decisions, e.g., to shed load, have to be made on the spot⁷.

Last on the list of talking points, but not least, is the ease of implementation of the stability software in the control center. From the perspective of a SCADA/EMS designer, the stability software should ideally run on the system servers like any other native application. Solutions that entail multi-computer configurations specifically dedicated to the stability software are cumbersome and further congest the computer rooms and the operator desks, which are already jammed with the system’s own processors and display monitors.

The Book

It might have been tempting to structure this volume in two parts: theory and implementations. We preferred, however, to let the contents flow freely along the lines traditionally recognized in the industry—from steady-state stability, to transient stability and then to voltage stability, followed by trajectory sensitivities and user-interface concepts.

Chapter 1, *Power System Dynamic Equilibrium, Power-Flow, and Steady-State Stability*, by P. W. Sauer and M. A. Pai, establishes a solid theoretical background

⁶ By “steady-state stability” we refer to the *classical concept* as described by: Crary, S. B., *Power System Stability*, General Electric Series, Schenectady, New York, 1945; Kimbark, E. W., *Power System Stability*, Wiley, New York, 1950; IEEE, PES Task Force on Terms and Definitions, *Proposed Terms and Definitions for Power System Stability*, IEEE Transactions on PAS, PAS-101, 7, pp. 1894; and Anderson, P. M., Fouad A. A., *Power System Control and Stability*, The Iowa University Press, Ames, Iowa, 1990, among many others.

⁷ The post-mortem analysis of the July 1977 blackout in New York revealed that the catastrophe could have been avoided if the ConEdison dispatcher would have activated the load shedding button when he was asked to do so by the New York Power Pool system operator.

for steady-state stability. It presents material on the analysis of steady-state equilibrium in electric power systems and reveals the connections between dynamic models, dynamic equilibrium and load-flow analysis, as well as the significance of singularities of Jacobian matrices involved in various computations.

Chapter 2, *Fast Computation of the Steady-State Stability Limit*, by S. C. Savulescu, addresses the theoretical foundation of a field-proven software tool that quickly and reliably quantifies and visualizes the risk of blackout due to steady-state instability. The approach is inspired from Paul Dimeo's REI technology and uses the Bruk-Markovic reactive power stability criterion to determine how far the current system conditions are from a state where voltages may collapse and generators may lose synchronism. Metrics that quantify the distance to instability and to the security margin are also discussed, along with an innovative approach to display essential information that visualizes the risk of blackout.

Chapter 3, *Practical Aspects of Steady-State Stability Assessment in Real-Time*, by J. S. Vergara P., T. A. Thai, N. D. Cuong, H. S. Campeanu and S. C. Savulescu, addresses the: accuracy testing of the approach; tracking of the distance to instability on SCADA trending charts; and the ability to compute the instantaneous voltage and angle stability sensitivities by using PMU data. The validation of the stability reserve computed by the stability software and the trending of the distance to instability are illustrated with actual examples. The use of phasor measurements, which, although conceptually different from the conventional SCADA data model, can help assess the voltage and angle stability sensitivities when large blocks of power are transferred across long transmission lines, is exemplified by a successful experiment conducted in Vietnam. Additional considerations are provided to make the case for deploying steady-state stability tools in real-time.

Chapter 4, *Composite Approach for the Early Detection, Assessment and Visualization of the Risk of Instability in the Control of Smart Transmission Grids*, by R. Eichler, C. O. Heyde and B. O. Stottok, tackles the problem of determining and presenting the relevant information that can assist a power system operator in assessing the risk of blackout due to instability in a timely, efficient and effective manner. Algorithmic approaches and numerical indicators that can help identify the instant status of the degree of operating reliability are also presented. Three concepts to detect, quantify and visualize the risk of blackout are introduced and extensively illustrated with speedometer diagrams, stability trending charts and snapshots taken directly from actual SCADA system user interfaces.

Chapter 5, *Preventive and Emergency Control of Power Systems*, by D. Ruiz-Vega, L. Wehenkel, D. Ernst, A. Pizano-Martínez and C. R. Fuerte-Esquivel describes a general approach to real-time transient stability control, yielding various complementary techniques: pure preventive, open loop emergency and closed loop emergency controls. Recent progress in terms of a global transient stability constrained optimal power flow are presented, yielding in a scalable nonlinear programming formulation which allows to take near-optimal decisions for preventive control with a computing budget corresponding only to a few runs of standard optimal power flow and time-domain simulations. These complementary techniques meet the stringent conditions imposed by the real-life applications.

Chapter 6, *Online Dynamic Security Assessment*, by J. L. Jardim, describes the implementation of an online dynamic security assessment system based on time domain simulation, in which the dynamic models incorporate all the necessary details and are identical to those used offline for planning studies. The foundations of the power flow, continuation power flow, time domain simulation, energy functions, single machine equivalent, and Prony spectral decomposition techniques used by the application are reviewed and their numerical and computational performance is discussed. The utilization of these methods to realize complex security tasks such as dynamic contingency analysis and security region computations is described and illustrated with practical results obtained online and comparisons between online and offline planning cases.

Chapter 7, *Practical Issues for Implementation of Online Dynamic Security Assessment Systems*, by Lei Wang, Xi Lin, Fred Howell and Kip Morison, discusses the issues associated with the successful design and implementation of an online dynamic security assessment system. The need for, the benefits of, and the current application status of such systems are presented. The discussions are primarily focused on the practical issues for implementing an online DSA system, based on the experiences gained from recent applications. Finally, an overview of some future directions on the online DSA technologies is provided.

Chapter 8, *The Case for Using Wide-Area Monitoring and Control to Improve the Resilience and Capacity of the Electric Power Grid*, by Jay Giri, Manu Parashar, Rene Avila-Rosales and Douglas Wilson, explores modern techniques to improve grid reliability by enhancing and extending control center capabilities and substation capabilities. The use of automatic, wide-area protection schemes to mitigate cascading blackouts is examined. Also explored is the use of: wide-area control strategies; new and emerging technologies and communications; software and hardware architectures; and state of the art EMS technologies as the keys to more reliable operations.

T. Van Cutsem and C. Vournas address voltage stability issues in Chapter 9, *Emergency Monitoring and Corrective Control of Voltage Instability*, and Chapter 10, *Online Voltage Security Assessment*. After reviewing the basic voltage instability mechanisms, they describe emergency measures that can be used in order to contain voltage instability and prevent voltage collapse. An actual voltage collapse event in Greece is presented and analyzed. The emergency measures presented include existing or projected controls acting on bulk power delivery transformer load tap changers, as well as direct load shedding. The design and application of a load shedding controller in the Hydro-Quebec system is also addressed. Then, the authors deal with voltage security assessment and its online application. Methods for contingency analysis are briefly reviewed. Methods for preventive security control are outlined. An application of online voltage stability assessment in the control center of a real system is then described and typical results available to operators are presented.

T. B. Nguyen and M. A. Pai, in Chapter 11 *Trajectory Sensitivity Analysis for Dynamic Security Assessment and other Applications in Power Systems*, indicate

that real-time stability evaluation and preventive scheduling in power systems offer many challenges in a stressed power system. Trajectory Sensitivity Analysis (TSA) is a useful tool for this and other applications in the emerging smart grid area. The authors outline the basic approach of TSA, to extract suitable information from the data and develop reliable metrics or indices to evaluate proximity of the system to an unstable condition. Trajectory sensitivities can be used to compute critical power system parameters such as clearing time of circuit breakers, tie-line flow, etc., by developing suitable norms for ease of interpretation. Metrics are developed from these sensitivities. The TSA technique can be extended to perform preventive rescheduling. A brief discussion of other applications of TSA in the placement of distributed generators is also included.

Chapter 12, *Model Predictive Control of Electric Power Systems under Emergency Conditions* is authored by M. Zima and G. Andersson. Model Predictive Control (MPC) is a widely used method in industrial applications for the control of multi-input, multi-output systems. It possesses features that make it attractive for power systems, which exhibit complex characteristics such as mixed continuous and discrete dynamics, nonlinear dynamics and very large size. The MPC optimization computations further increase the challenge, thus the reduction of the computational burden becomes a crucial factor for real-time use. The chapter describes a formulation of MPC for power systems based on trajectory sensitivities and explores application possibilities for MPC in new, previously restricted areas.

Chapter 13, *The Role of Power System Visualization in Enhancing Power System Security*, by T. Overbye, focuses on techniques for the rapid analysis and display of information that can allow operators and engineers to quickly assess the state of a large power grid, and then make effective operating decisions. While the operation of much of the electric power grid is automated, the operators and engineers are still very much “in the loop.” During times of emergency operation, when the system may be close to instability and collapse, having access to timely, pertinent information about a potentially rapidly changing system state could prove crucial in preventing major blackouts.

Prior to starting the work on this *second edition* of our book, we invited all the contributors to the *first* edition to review and edit their original work, remove text that was obsolete or is less important today, and refresh, if needed, their views about the subject matter. They all replied enthusiastically. Large portions of the text were significantly updated, for example the last section in chapter three and the entire chapter eight where the synchrophasor technologies received extensive coverage. New material was also incorporated for the benefit of practically oriented readers (Chapter 4) and to clarify some subtle theoretical aspects of the computational techniques (Chapter 6).

It was our goal to address all the key issues that emerge when designing and implementing applications intended to prevent blackouts. We hope that the second edition of the book *Real-Time Stability in Power Systems* provides answers to many questions and that it will assist practitioners and researchers in their quest for the ultimate real-time stability tool.

Acknowledgments

This book owes its existence to Ms. Tiffany Gasbarrini, Springer's Senior Editor for Energy and Power. She contacted me in late September 2013 to suggest that the first edition of *Real-Time Stability in Power Systems* was "worthy of re-invigorated attention". I took the challenge, Professor Joe H. Chow, Administrative Dean of the School of Engineering at the Rensselaer Polytechnic Institute supported the initiative—and the rest is history. Thank you, Tiffany, and thank you, Joe, for your insight and encouragements!

I am expressing my gratitude to the contributors to the first edition of the book, who accepted without reservation to update their chapters, and to the industry experts who kindly offered to develop additional text. Thank you Ladies and Gentlemen, it was a pleasure working with you!

Many thanks also to Professors M. A. Pai and George Gross from the University of Illinois at Urbana-Champaign for providing valuable comments during the early stages of this project and for reviewing this second edition of the book.

Last, but not least, I would like to acknowledge the assistance received from Ms. Rebecca R. Hytowitz, Springer Science & Business Media Editorial Assistant, during the text editing process.

12 March 2014

Savu C. Savulescu

Energy Consulting International, Inc.

New York, NY, USA

Foreword

Real-time stability assessment has been a goal of power system engineers ever since the North East blackout of 1965. It was realized that fast real-time security analysis tools need to be developed. The industry responded quickly and following the development of reliable state estimation techniques in early 1970s, real-time network analysis also became possible. That was the beginning of static security assessment.

Continued availability of better computer hardware and improved computational algorithms has been a driving force behind much of the advances since then. Research, which began in the 1970s in this area, has resulted in a large amount of analytical and computational techniques.

A further impetus for this effort is now emerging with the development of Wide Area Measurement System (WAMS) based on synchrophasor technology that has been documented well in the literature. Many of the techniques developed in combination with concepts from areas of Control, Communication and Computer Science are now beginning to look like practical tools in addressing the problems of real-time stability evaluation.

The current restructured power system offers a huge challenge in terms of implementation of these tools. Computation of stability margins, available transfer capabilities, congestion management and dynamic visualization are some of the much-needed tools that are now emerging. This requires constant interaction between the practical needs of the industry and the new theoretical advances being made. The ultimate goal in all these efforts is the efficient monitoring and control of the power system as well as having suitable preventive control methodologies in place.

Recognizing this need, Dr. Savu Savulescu has taken the initiative in bringing out this revised edition of his Springer 2005 book. Its purpose is to keep the power engineering community, both industry as well as the academia, informed about the current developments in the field. All the three aspects of stability namely *steady-state*, *transient* and *voltage stability* have been covered in a well-structured way.

Dr. Savulescu has been at the forefront of applications of real-time tools for efficient and reliable operation of power systems since the 1970s. It is therefore a

pleasure to welcome this latest effort by him especially when the power Industry has undergone radical transformation with the impact of WAMS, visualization techniques and closer to real-time stability monitoring tools that are implementable. The present book is therefore a logical sequel to his earlier one in 2005.

15 March 2014

M. A. Pai

Electrical and Computer Engineering,

University of Illinois at Urbana-Champaign, Champaign, USA

Contents

1 Power System Dynamic Equilibrium, Power Flow, and Steady-State Stability	1
Peter W. Sauer and M. A. Pai	
2 Fast Computation of the Steady-State Stability Limit	27
Savu C. Savulescu	
3 Practical Aspects of Steady-State Stability Assessment in Real-Time	63
José Santos Vergara Perez, Tran Anh Thai, Nguyen Duc Cuong, Horia S. Campeanu and Savu C. Savulescu	
4 Composite Approach for the Early Detection, Assessment, and Visualization of the Risk of Instability in the Control of Smart Transmission Grids	97
Roland Eichler, Chris O. Heyde and Bernd O. Stottok	
5 Power System Transient Stability Preventive and Emergency Control	123
Daniel Ruiz-Vega, Louis Wehenkel, Damien Ernst, Alejandro Pizano-Martínez and Claudio R. Fuerte-Esquivel	
6 Online Dynamic Security Assessment	159
Jorge L. Jardim	
7 Practical Issues for Implementation of Online Dynamic Security Assessment Systems	199
Lei Wang, Xi Lin, Fred Howell and Kip Morison	
8 The Case for Using Wide-Area Monitoring and Control to Improve the Resilience and Capacity of the Electric Power Grid	235
Jay Giri, Manu Parashar, Rene Avila-Rosales and Douglas Wilson	

9	Emergency Monitoring and Corrective Control of Voltage Instability	279
	Thierry Van Cutsem and Costas Vournas	
10	Online Voltage Security Assessment	305
	Costas Vournas and Thierry Van Cutsem	
11	Trajectory Sensitivity Analysis for Dynamic Security Assessment and Other Applications in Power Systems	335
	Tony B. Nguyen and M. A. Pai	
12	Model Predictive Real-Time Control of Electric Power Systems Under Emergency Conditions	367
	Marek Zima and Göran Andersson	
13	The Role of Power System Visualization in Enhancing Power System Security	387
	Thomas J. Overbye	
	Index	409

Contributors

Göran Andersson Swiss Federal Institute of Technology, ETH Zurich, Zürich, Switzerland

Rene Avila-Rosales Alstom Grid, Redmond, WA, USA

Horia S. Campeanu ISPE, Bucharest, Romania

Roland Eichler Siemens AG, Nuremberg and Erlangen, Germany

Damien Ernst University of Liège, Liège, Belgium

Claudio R. Fuerte-Esquivel Universidad Michoacana de San Nicolás de Hidalgo, Morelia, Mexico

Jay Giri Alstom Grid, Redmond, WA, USA

Chris O. Heyde Siemens AG, Nuremberg and Erlangen, Germany

Fred Howell Powertech Labs Inc., Surrey, BC, Canada

Jorge L. Jardim High Performance Power System Applications, Rio de Janeiro, Brazil

Xi Lin Powertech Labs Inc., Surrey, BC, Canada

Kip Morison BC Hydro, Vancouver, BC, Canada

Nguyen Duc Coung National Power Transmission Corporation, Hanoi, Vietnam

Tony B Nguyen Pacific Northwest National Laboratory, Richland, WA, USA

Thomas J. Overbye University of Illinois at Urbana-Champaign, Champaign, IL, USA

M. A. Pai University of Illinois at Urbana-Champaign, Champaign, IL, USA

Manu Parashar Alstom Grid, Redmond, WA, USA

Alejandro Pizano-Martínez Universidad de Guanajuato, Salamanca, Mexico

Daniel Ruiz-Vega Instituto Politécnico Nacional, Mexico City, Mexico

Peter W. Sauer University of Illinois at Urbana-Champaign, Champaign, IL, USA

Savu C. Savulescu Energy Consulting International, Inc., New York, NY, USA

Bernd O. Stottok Siemens AG, Nuremberg and Erlangen, Germany

Tran Anh Thai Advanced Technical Systems Co., Ltd., Hanoi, Vietnam

Thierry Van Cutsem Dept. Electrical Engineering and Computer Science, FNRS (Fund for Scientific Research) and University of Liège, Liège, Belgium

José Santos Vergara Perez Empresa de Transmisión Eléctrica, S.A., Panama, USA

Costas Vournas National Technical University of Athens, Athens, Greece

Lei Wang Powertech Labs Inc., Surrey, BC, Canada

Louis Wehenkel University of Liège, Liège, Belgium

Douglas Wilson Psymetrix-Alstom, Edinburgh, UK

Marek Zima Swissgrid, Laufenburg, Switzerland

Chapter 1

Power System Dynamic Equilibrium, Power Flow, and Steady-State Stability

Peter W. Sauer and M. A. Pai

Abstract The material in this chapter focuses on the relationship between power system dynamic equilibrium, power flow, and operating point stability. It addresses issues relating steady-state equilibrium in electric power systems with possible implications about stability of the associated operating point. It presents various connections between dynamic models, dynamic equilibrium, power-flow analysis, and the significance of singularities of Jacobian matrices involved in various computations. It includes advances on earlier work on this subject and provides recent results on computing the equilibrium of “post-contingency” models. These post-contingency models are created to enforce the concept of “constant control inputs” in the steady-state analysis. This impacts subtle things such as post-contingency speed (frequency) and remote voltage regulation. The concepts are illustrated on small system models. Different methods of computation are presented to provide alternatives for possible practical implementation.

Keywords Steady-state stability · Power-flow Jacobian · Power system dynamics · Contingency analysis · Equilibrium · Small-signal stability

1.1 Introduction¹

There are many subtle issues associated with power systems and the viability of mathematical models associated with the physical system. A number of these issues have to do with voltage collapse, voltage instability, and equilibrium conditions. These include the concept of maximum loadability. The issue of load modeling alone raises many questions about the proper modeling techniques and assumptions

¹ Portions of this chapter were previously published with IEEE copyright in the paper by P. W. Sauer and M. A. Pai, “Power System Steady-State Stability and the Load flow Jacobian,” IEEE Transactions on Power Systems, Vol. 5, No. 4, November 1990, pp. 1374–1383, reprinted here with permission from IEEE.

M. A. Pai (✉) · P. W. Sauer
University of Illinois at Urbana-Champaign, Champaign, IL, USA
e-mail: mapai@illinois.edu

P. W. Sauer
e-mail: psauer@illinois.edu

about aggregate behavior. This chapter focuses primarily on equilibrium analysis and information that can be obtained from various types of steady-state analysis. The subjects of voltage collapse and voltage instability have created interest in power-flow Jacobian singularities and their relationship with steady-state stability and voltage collapse.

In 1975, Venikov et al. published a paper that proposed that, under certain conditions, a direct relationship exists between the singularity of the standard power-flow Jacobian and the singularity of the system dynamic state Jacobian (Venikov et al. 1975). This paper has been cited as the primary justification for studying the power-flow Jacobian matrix to determine critical load levels.

In this chapter, we clarify this result in the context of a fairly general dynamic model and show that the result should be considered optimistic for any type of steady-state stability analysis. This chapter includes a tutorial on the role of power flow in dynamic analysis.

1.2 Detailed Dynamic Model Without Stator/Network Transients

This section presents a basic nonlinear multi-machine dynamic model that includes the fundamental features of voltage and frequency control, but assumes that all stator/network transients have been eliminated. The elimination of the stator/network transients leads to algebraic equations that accompany the multi-machine dynamic model as follows:

$$\frac{d\delta_i}{dt} = (\omega_i - \omega_s) \quad i = 1, \dots, m \quad (1.1)$$

$$M_i \frac{d\omega_i}{dt} = T_{Mi} - [E'_{qi} - X'_{di} I_{di}] I_{qi} - [E'_{di} + X'_{qi} I_{qi}] I_{di} - D_i (\omega_i - \omega_s) \quad i = 1, \dots, m \quad (1.2)$$

$$T'_{doi} \frac{dE'_{qi}}{dt} = -E'_{qi} - (X_{di} - X'_{di}) I_{di} + E_{fdi} \quad i = 1, \dots, m \quad (1.3)$$

$$T'_{qoi} \frac{dE'_{di}}{dt} = -E'_{di} + (X_{qi} - X'_{qi}) I_{qi} \quad i = 1, \dots, m \quad (1.4)$$

$$T_{Ei} \frac{dE_{fdi}}{dt} = -\left(K_{Ei} + S_{Ei} (E_{fdi})\right) E_{fdi} + V_{Ri} \quad i = 1, \dots, m \quad (1.5)$$

$$T_{Ai} \frac{dV_{Ri}}{dt} = -V_{Ri} + K_{Ai} R_{fi} - \frac{K_{Ai} K_{Fi}}{T_{Fi}} E_{fdi} + K_{Ai} (V_{refi} - V_i) \quad i = 1, \dots, m \quad (1.6)$$

$$T_{Fi} \frac{dR_{fi}}{dt} = -R_{fi} + \frac{K_{Fi}}{T_{Fi}} E_{fdi} \quad i = 1, \dots, m \quad (1.7)$$

$$T_{RH_i} \frac{dT_{M_i}}{dt} = -T_{M_i} + \left(1 - \frac{K_{HP_i} T_{RH_i}}{T_{CH_i}}\right) P_{CH_i} + \frac{K_{HP_i} T_{RH_i}}{T_{CH_i}} P_{SV_i} \quad i = 1, \dots, m \quad (1.8)$$

$$T_{CH_i} \frac{dP_{CH_i}}{dt} = -P_{CH_i} + P_{SV_i} \quad i = 1, \dots, m \quad (1.9)$$

$$T_{SV_i} \frac{dP_{SV_i}}{dt} = -P_{SV_i} + P_{ci} - \frac{1}{R_i} \left(\frac{\omega_i}{\omega_s} \right) \quad i = 1, \dots, m \quad (1.10)$$

$$0 = V_i e^{j\theta_i} + (R_{si} + jX'_{di}) (I_{di} + jI_{qi}) e^{j(\delta_i - \pi/2)} - \left[E'_{di} + (X'_{qi} - X'_{di}) I_{qi} + jE'_{qi} \right] e^{j(\delta_i - \pi/2)} \quad i = 1, \dots, m \quad (1.11)$$

$$0 = -P_i - jQ_i + V_i e^{j\theta_i} (I_{di} - jI_{qi}) e^{-j(\delta_i - \pi/2)} + P_{Li}(V_i) + jQ_{Li}(V_i) \quad i = 1, \dots, m \quad (1.12)$$

$$0 = -P_i - jQ_i + P_{Li}(V_i) + jQ_{Li}(V_i) \quad i = m+1, \dots, n \quad (1.13)$$

$$0 = -P_i - jQ_i + \sum_{k=1}^n V_i V_k Y_{ik}^{j(\theta_i - \theta_k - \alpha_{ik})} \quad i = 1, \dots, n, \quad (1.14)$$

where the notation is standard for a machine with one damper winding plus field (two-axis model), IEEE type I excitation system, and simplified turbine/governor model (Sauer and Pai 1998). The notation for an m -machine, n -bus system is,

$$V_i e^{j\theta_i} = \text{voltage at bus } i = 1, \dots, n \quad (1.15)$$

$$V_i e^{j\theta_i} = (V_{di} + jV_{qi}) e^{j(\delta_i - \pi/2)} \quad i = 1, \dots, m \quad (1.16)$$

$$I_{Gi} e^{j\gamma_i} = (I_{di} + jI_{qi}) e^{j(\delta_i - \pi/2)} \quad i = 1, \dots, m \quad (1.17)$$

$$Y_{ik} e^{j\alpha_{ik}} = \text{standard power-flow bus admittance matrix entry } i, k = 1, \dots, n \quad (1.18)$$

$$P_i + jQ_i = \text{net injected power into bus from a path not included in the bus admittance matrix } i = 1, \dots, n. \quad (1.19)$$

The algebraic variables P_i and Q_i are introduced so that the standard power-flow equation (1.14) is preserved for any load models (1.12) and (1.13). Note that these equations can be supplemented with algebraic or dynamic models that have an output of $P_{Li}(V_i) + jQ_{Li}(V_i)$. This full dynamic model contains $10m$ dynamic states $(\delta, \omega, E'_q, E'_d, E'_{fd}, V_R, R_f, T_M, P_{CH}, P_{SV})$, $2m + 4n$ real algebraic states

$(I_d, I_q, P, Q, \theta, V)$, and $2m$ inputs (V_{ref}, P_c) . Equation (1.11) is the stator algebraic equation, which is normally expressed either as a phasor diagram or as a quasi-static phasor circuit in the literature (Sauer and Pai 1990). There are $m + 2n$ complex algebraic equations, which should in principle be solved for the $2m + 4n$ real algebraic states as functions of the $10m$ dynamic states.

The machine currents I_d and I_q can easily be eliminated by solving (1.11) and substituting into (1.2)–(1.12). The P and Q algebraic states can easily be eliminated by substituting (1.12) and (1.13) into (1.14), leaving only n complex algebraic equation (1.14) to be solved for the $2n$ real algebraic states θ and V . These remaining algebraic equations cannot normally be solved explicitly.

In the special case of constant impedance loads, it is customary to use an internal generator bus model and include all loads and the machine impedance $R_s + jX'_d$ in the bus admittance matrix (enlarged to $m + n$ buses).

With the additional assumption of $X'_q = X'_d$, all algebraic states can be explicitly eliminated with a reduced ($m \times m$) admittance matrix. For nonlinear load models, the algebraic equations must be retained. This chapter does not introduce internal machine buses.

Wind turbine generators can be included in this model using the basic model of Pulgar and Sauer (2011), where the wind turbine controls add additional dynamic states to the traditional blade rotation and generator electrical transients.

1.3 Standard Power Flow

Standard load flow (or power flow) has been the traditional mechanism for computing a proposed steady-state operating point. For this chapter, we define standard power flow as the following algorithm (Pai 2004):

- Specify bus voltage magnitudes numbered 1 to m
- Specify bus voltage angle number 1 (slack bus)
- Specify net injected real power P_i at buses numbered 2 to m
- Specify load powers P_{Li} and Q_{Li} at all buses numbered 1 to n
- Solve the following equations ((1.13) and (1.14) rewritten) for $\theta_2, \dots, \theta_n, V_{m+1}, \dots, V_n$

$$0 = -P_i + \sum_{k=1}^n V_i V_k Y_{ik} \cos(\theta_i - \theta_k - \alpha_{ik}) \quad i = 2, \dots, m \quad (1.20)$$

(PV buses)

$$0 = -P_{Li} + \sum_{k=1}^n V_i V_k Y_{ik} \cos(\theta_i - \theta_k - \alpha_{ik}) \quad i = m+1, \dots, n \quad (1.21)$$

(PQ buses)

$$0 = -Q_{Li} + \sum_{k=1}^n V_i V_k Y_{ik} \sin(\theta_i - \theta_k - \alpha_{ik}) \quad i = m+1, \dots, n \quad (1.22)$$

(PQ buses)

where

$$P_i (i = 2, \dots, m), V_i (i = 1, \dots, m), P_{Li} (i = m+1, \dots, n), Q_{Li} (i = m+1, \dots, n)$$

and θ_1 are the specified numbers. The standard power-flow Jacobian matrix is the linearization of (1.20)–(1.22) with respect to $\theta_2, \dots, \theta_n$ and V_{m+1}, \dots, V_n . After the power-flow solution, compute

$$P_1 + jQ_1 = \sum_{k=1}^n V_1 V_k Y_{1k} e^{j(\theta_1 - \theta_k - \alpha_{1k})} \quad (1.23)$$

$$Q_i = \sum_{k=1}^n V_i V_k Y_{ik} \sin(\theta_i - \theta_k - \alpha_{ik}) \quad i = 2, \dots, m. \quad (1.24)$$

This standard power flow has many variations, including the addition of other devices such as Tap Changing Under Load (TCUL) transformers, switching Volt–Ampere Reactive (VAR) sources, and High-Voltage Direct Current (HVDC) converters. It can also include inequality constraints on quantities such as Q_i , and can be revised to distribute the slack power between all generators.

We would like to make one important point about power flow. Power flow is normally used to evaluate operation at a specific load level (specified by a given set of powers). For a specified load and generation schedule, the solution is independent of the actual load model. That is, it is certainly possible to evaluate the voltage at a constant impedance load for a specific case where that impedance load consumes a specific amount of power.

Thus, the use of “constant power” in power-flow analysis does not require or even imply that the load is truly a constant power device. It merely gives the voltage at the buses when the loads (any type) consume a specific amount of power. The load characteristic is important when the analyst wants to study the system in response to a change such as contingency analysis or dynamic analysis. For these purposes, standard power flow usually provided the “initial conditions.”

1.4 Initial Conditions for Dynamic Analysis

For any dynamic analysis using (1.1)–(1.14), it is necessary to compute the initial values of all dynamic states and to specify the fixed inputs (V_{ref}, P_c). In the power system dynamic analysis, the fixed inputs and initial conditions are normally found

from a base case power-flow solution. That is, the values of V_{ref} are computed such that the m generator voltages are as specified in the power flow.

The values of P_c are computed such that the m generator real power outputs are as specified and computed in the power flow for rated speed (ω_s). To see how this is done, we assume that a power-flow solution (as defined in Sect. 1.3) has been found. The first step in computing initial conditions is normally the calculation of generator currents from (1.12) and (1.17) as:

$$I_{Gi}e^{j\gamma_i} = \left[(P_i - P_{Li}(V_i)) - j(Q_i - Q_{Li}(V_i)) \right] / (V_i e^{-j\theta_i}) \quad i = 1, \dots, m \quad (1.25)$$

and machine relative rotor angles from the manipulation of (1.11) and the algebraic equation from (1.4)

$$\delta_i = \text{angle of } \left[V_i e^{j\theta_i} + (R_{si} + jX_{qi}) I_{Gi} e^{j\gamma_i} \right] \quad i = 1, \dots, m. \quad (1.26)$$

With these quantities, the remaining dynamic and algebraic states can be found by

$$I_{di} + jI_{qi} = I_{Gi} e^{j(\gamma_i - \delta_i + \pi/2)} \quad i = 1, \dots, m \quad (1.27)$$

$$V_{di} + jV_{qi} = V_i e^{j(\theta_i - \delta_i + \pi/2)} \quad i = 1, \dots, m \quad (1.28)$$

followed by E_{fdi} from (1.3), (1.4), (1.11), and (1.16)

$$E_{fdi} = X_{di} I_{di} + V_{qi} + R_{si} I_{qi} \quad i = 1, \dots, m. \quad (1.29)$$

With this field voltage, R_{fi} , V_{Ri} , and V_{refi} can be found from (1.5)–(1.7) as

$$R_{fi} = \frac{K_{Fi}}{T_{Fi}} E_{fdi} \quad i = 1, \dots, m \quad (1.30)$$

$$V_{Ri} = (K_{Ei} + S_{Ei} (E_{fdi})) E_{fdi} \quad i = 1, \dots, m \quad (1.31)$$

$$V_{refi} = V_i + (V_{Ri} / K_{Ai}) \quad i = 1, \dots, m. \quad (1.32)$$

The initial values of E'_{qi} and E'_{di} are then found from (1.3) and (1.4):

$$E'_{qi} = -(X_{di} - X'_{di}) I_{di} + E_{fdi} \quad i = 1, \dots, m \quad (1.33)$$

$$E'_{di} = -(X_{qi} - X'_{qi}) I_{qi} \quad i = 1, \dots, m. \quad (1.34)$$

Note that, if the machine saturation is included, this calculation for E'_{qi} and E'_{di} may be iterative. The mechanical states and P_c are found from (1.1), (1.2), and (1.8)–(1.10) as:

$$\omega_i = \omega_s \quad i = 1, \dots, m \quad (1.35)$$

$$T_{Mi} = \left[E'_{di} + X'_{qi} I_{qi} \right] I_{qi} + \left[E'_{qi} + X'_{di} I_{di} \right] I_{di} \quad i = 1, \dots, m \quad (1.36)$$

$$P_{CHi} = T_{Mi} \quad i = 1, \dots, m \quad (1.37)$$

$$P_{SVi} = P_{CHi} \quad i = 1, \dots, m \quad (1.38)$$

$$P_{ci} = P_{SVi} + (1/R_i) \quad i = 1, \dots, m. \quad (1.39)$$

This completes the computation of all dynamic state initial conditions and fixed inputs.

For a given disturbance, the inputs remain fixed throughout the simulation. If the disturbance occurs in the algebraic equations, the algebraic states must change instantaneously to satisfy the initial condition of the dynamic states and the new algebraic equations. Thus, it may be necessary to re-solve the algebraic equations with the dynamic states specified at their initial conditions to determine the new initial values of the algebraic states.

From the above description, it is clear that once a standard power-flow solution is found, the remaining dynamic states and inputs can be found in a straightforward way. The machine relative rotor angles δ_i can always be found provided

$$V_i e^{j\theta_i} + (R_{si} + jX_{qi}) I_{Ci} e^{j\gamma_i} \neq 0 \quad i = 1, \dots, m. \quad (1.40)$$

If control limits are enforced, a solution satisfying these limits may not exist. In this case, the state that is limited would need to be fixed at its limiting value, and a corresponding new steady-state solution would have to be found.

This would require a new power-flow solution specifying either different values of generator voltages, different generator real powers, or possibly generator reactive power injections, thus allowing generator voltage to be a part of the power-flow solution. In fact, the use of reactive power limits in power flow can usually be traced back to an attempt to consider excitation system limits or generator capability limits.

1.5 Angle Reference

In any rotational system, the reference for angles is arbitrary. Examination of (1.1)–(1.14) clearly shows that the order of this dynamic system can be reduced from $10m$ to $10m - 1$ by introducing the new relative angles (arbitrarily selecting δ_1 as reference)

$$\delta'_i = \delta_i - \delta_1 \quad i = 1, \dots, m \quad (1.41)$$

$$\theta'_i = \theta_i - \delta_1 \quad i = 1, \dots, m. \quad (1.42)$$

The full system remains exactly the same as (1.1)–(1.14) with each δ_i replaced by δ'_i , each θ_i replaced by θ'_i , and ω_s replaced by δ'_1 in (1.1). During a transient, the angle δ_1 still changes from its initial condition (as found in the last section) as ω_1 changes, so that each original δ_i and θ_i can be easily recovered if needed.

The angle δ'_1 remains at zero for all time. Thus, for dynamic simulation, the differential equation for δ_1 is normally replaced by the algebraic equation which simply states $\delta'_1 = 0$. Notice that θ_1 is normally arbitrarily selected as zero for the power-flow analysis.

This means that the initial value of δ_1 is normally not zero. During a transient, θ'_1 and θ_1 change as all angles except δ'_1 change. If the inertia of machine 1 is set to infinity, ω_1 and δ_1 remain constant for all time.

1.6 Steady-State Stability

The steady-state stability of multi-machine systems is usually evaluated by computing the eigenvalues of the system dynamic state Jacobian matrix that is the linearized version of (1.1)–(1.14) with all algebraic equations eliminated. This dynamic model has one zero eigenvalue corresponding to the angle reference discussed above.

Elimination of δ_1 through the use of (1.41) and (1.42) would eliminate this zero eigenvalue. The system is linearized around a steady-state operating point found using standard power flow. The Jacobian matrix for this standard power flow appears as a sub-matrix in the lower right block and is denoted as J_{LF} below:

$$\begin{bmatrix} \frac{d\Delta y}{dt} \\ 0 \\ 0 \end{bmatrix} = \begin{bmatrix} A & B_1 & B_2 \\ C_1 & D_{11} & D_{12} \\ C_2 & D_{21} & J_{LF} \end{bmatrix} \begin{bmatrix} \Delta y \\ \Delta z \\ \Delta v \end{bmatrix} \quad (1.43)$$

where v contains the power-flow variables $\theta_2, \dots, \theta_n, V_{m+1}, \dots, V_n$. In order to evaluate the stability of the dynamic system, the algebraic equations must be eliminated. This requires the nonsingularity of the algebraic equation Jacobian (J_{AE}):

$$J_{AE} = \begin{pmatrix} D_{11} & D_{12} \\ D_{21} & J_{LF} \end{pmatrix} \quad (1.44)$$

For B equal to the submatrices B_1 and B_2 and C equal to the submatrices C_1 and C_2 , the stability of the steady-state equilibrium point is then determined by the system dynamic state Jacobian:

$$J_{\text{sys}} = A - BJ_{\text{AE}}^{-1}C \quad (1.45)$$

Special cases where the three Jacobians J_{sys} , J_{AE} , and J_{LF} can be more explicitly related are given in the following section.

1.7 Special Cases

There are two special cases where the standard power-flow Jacobian can be directly related to the system dynamic state Jacobian. We do not claim that these are necessarily realistic cases, only that they lead to cases where the three Jacobians can be explicitly related.

a. The first special case makes the following assumptions:

- (a1) Stator resistance of every machine is negligible ($R_{si} = 0$, $i = 1, \dots, m$).
- (a2) Transient reactances of every machine are negligible ($X'_{di} = 0$, $X'_{qi} = 0$, $i = 1, \dots, m$).
- (a3) Field and damper winding time constants for every machine are infinitely large ($E'_{qi} = \text{constant}$, $E'_{di} = \text{constant}$, $i = 1, \dots, m$).
- (a4) Constant mechanical torque to the shaft of each generator ($T_{Mi} = \text{constant}$, $i = 1, \dots, m$).
- (a5) Generator number one has infinite inertia. This together with (a1)–(a3) makes $V_1 = \text{constant}$, $\theta_1 = \text{constant}$ (infinite bus).
- (a6) All loads are constant power ($P_{Li}(V_i) = \text{constant}$, $Q_{Li}(V_i) = \text{constant}$, $i = 1, \dots, n$).

With these assumptions, each δ_i is equal to its corresponding θ_i plus a constant, and each V_i is constant. Choosing ω_1 as ω_s and θ_1 as zero, the dynamic model for this special case (after eliminating P_i and Q_i) is

$$\frac{d\theta_i}{dt} = \omega_i - \omega_s \quad i = 2, \dots, m \quad (1.46)$$

$$M_i \frac{d\omega_i}{dt} = T_{Mi} + P_{Li} - \sum_{k=1}^n V_i V_k Y_{ik} \cos(\theta_i - \theta_k - \alpha_{ik}) - D_i (\omega_i - \omega_s) \quad i = 2, \dots, m \quad (1.47)$$

$$0 = -P_{Li} + \sum_{k=1}^n V_i V_k Y_{ik} \cos(\theta_i - \theta_k - \alpha_{ik}) \quad i = m+1, \dots, n \quad (1.48)$$

$$0 = -Q_{Li} + \sum_{k=1}^n V_i V_k Y_{ik} \sin(\theta_i - \theta_k - \alpha_{ik}) \quad i = m+1, \dots, n \quad (1.49)$$

with

$$T_{Mi} = \text{constant} \quad i = 1, \dots, m \quad (1.50)$$

$$V_i = \text{constant} \quad i = 1, \dots, m \quad (1.51)$$

$$P_{Li} = \text{constant} \quad i = 1, \dots, n \quad (1.52)$$

$$Q_{Li} = \text{constant} \quad i = 1, \dots, n \quad (1.53)$$

$$\theta_1 = 0 \quad (1.54)$$

The linearized form of this model is,

$$\begin{bmatrix} \frac{d\Delta\theta_g}{dt} \\ M \frac{d\Delta\omega_g}{dt} \\ 0 \end{bmatrix} = \begin{bmatrix} 0 & \mathbf{I} & 0 \\ K_1 & -D & K_2 \\ K_3 & 0 & K_4 \end{bmatrix} \begin{bmatrix} \Delta\theta_g \\ \Delta\omega_g \\ \Delta\theta_L V_L \end{bmatrix} \quad (1.55)$$

where $\Delta\theta_L V_L$ is the vector $[\Delta\theta_L \ \Delta V_L]^t$ of incremental load angles and voltages.

For this case (a), the algebraic equation Jacobian ($J_{AE}^{(a)}$) is K_4 . For nonsingular K_4 , the system dynamic state Jacobian for this case (a) is

$$J_{\text{sys}}^{(a)} = \begin{bmatrix} 0 & I \\ M^{-1} (K_1 - K_2 K_4^{-1} K_3) & -M^{-1} D \end{bmatrix} \quad (1.56)$$

The determinant of $J_{\text{sys}}^{(a)}$ is (Sauer and Pai 1990)

$$\det J_{\text{sys}}^{(a)} = \frac{\det(K_1 - K_2 K_4^{-1} K_3)}{\det M} (-1)^{m-1} \quad (1.57)$$

The standard power-flow Jacobian as previously defined can be written in terms of these submatrices as

$$J_{LF} = \begin{bmatrix} -K_1 & -K_2 \\ K_3 & K_4 \end{bmatrix} \quad (1.58)$$

Again, for nonsingular K_4 , the determinant of the power-flow Jacobian is (Sauer and Pai 1990)

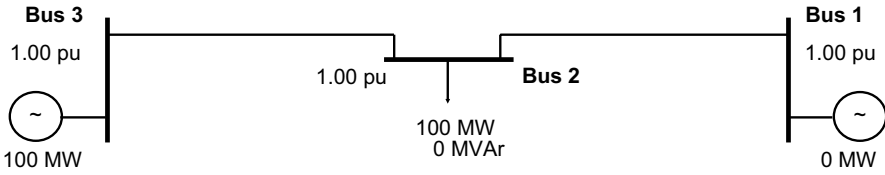


Fig. 1.1 Three-bus power system

$$\det J_{LF} = \det K_4 \det (K_1 - K_2 K_4^{-1} K_3) (-1)^{m-1} \quad (1.59)$$

For this case, a clear relationship between the determinant of the standard power-flow Jacobian and the determinant of the system dynamic state Jacobian exists as

$$\det J_{\text{sys}}^{(a)} = \frac{\det J_{LF}}{\det K_4 \det M} \quad (1.60)$$

This means that under these assumptions, monitoring the power-flow Jacobian determinant can detect a possible dynamic instability. The basic structure of this case (a) is used frequently, but assumptions (a1)–(a3) are slightly different. The same structure of (1.46)–(1.49) can be obtained by assuming a constant voltage behind transient reactance model with the terminal buses eliminated. This leads to a non-standard power-flow Jacobian matrix that includes machine parameters in the bus admittance matrix.

The results of (1.58)–(1.60) above, which were previously published in Sauer and Pai, (Sauer and Pai 1990), were questioned by M. K. Pal, a discussor of Rajagopalan et al. (1992). The question had to do with the assumption of a nonsingular K_4 . A single-machine example was presented by Pal in his discussion to Yorino et al. (1992).

This example had a special structure where the determinant of K_4 was in fact zero at the same condition as $\det J_{LF}$ and $\det J_{\text{sys}}^{(a)}$. However, additional analysis was not done to determine the general validity of the test. Additional testing by Verastegui (Verastegui 2000) indicated that, for more general systems, the power-flow Jacobian and system Jacobian can become zero while maintaining nonsingular K_4 . Figure 1.1 shows a three-bus power system that was used to illustrate the result.

The impedance of the two lines is purely reactive with an impedance of 0.1 pu. The load at bus 3 starts out at 1.0 pu (power base is 100 MW). The two-generator bus voltages are maintained at 1.0 pu. The load at bus 3 remains at unity power factor for the entire example.

For this example, the load at bus 3 is increased from 1 pu while monitoring the values of $\det K_4$, $\det J_{LF}$, and $\det J_{\text{sys}}^{(a)}$. The values of these three quantities as the load is increased are shown in Figs. 1.2, 1.3, 1.4.

- b. A second case where such a relationship can be firmly established was proposed in principle by Venikov et al. (1975). This special case makes the following assumptions:

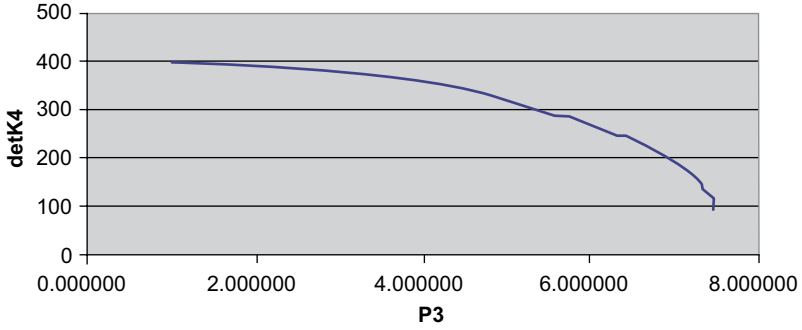


Fig. 1.2 Plot of $\det K_4$ versus load P_3

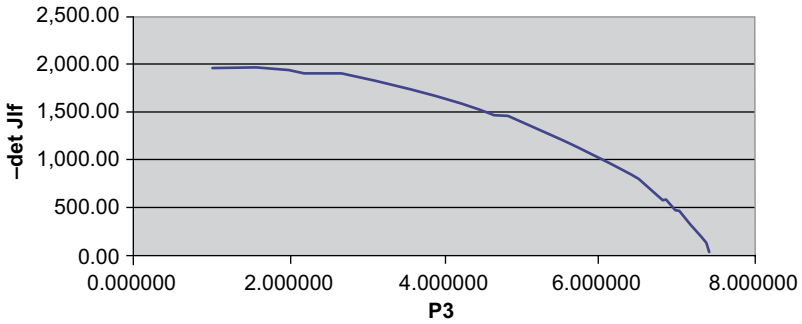


Fig. 1.3 Plot of $-\det J_{LF}$ versus load P_3

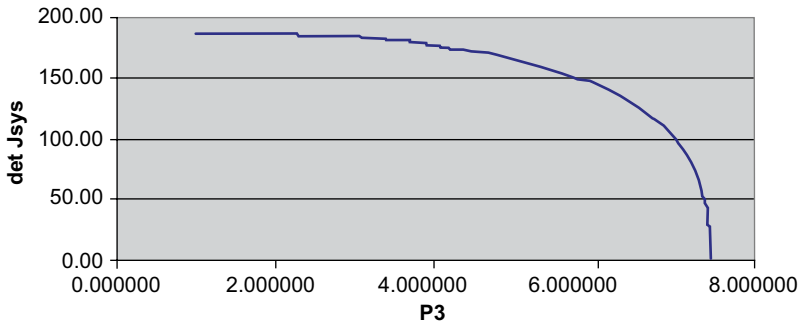


Fig. 1.4 Plot of $\det J_{\text{sys}}^{(a)}$ versus load P_3

(b1) Stator resistance is negligible ($R_{st} = 0, i = 1, \dots, m$)

(b2) No damper windings or speed damping

$$(T'_{qoi} = 0, D_i = 0, i = 1, \dots, m)$$

- (b3) High gain and fast excitation systems so that all generator terminal voltages are constant ($V_i = \text{constant}$, $i = 1, \dots, m$)
 (b4) Constant mechanical torque to the shaft of each generator

$$(T_{Mi} = \text{constant}, i = 1, \dots, m)$$

- (b5) Generator number one has infinite inertia and negligible reactances. This together with (b1)–(b3) makes $V_1 = \text{constant}$ and $\theta_1 = \text{constant}$ (infinite bus)
 (b6) All loads are constant power

$$(P_{Li}(V_i) = \text{constant}, Q_{Li}(V_i) = \text{constant}, i = 1, \dots, n).$$

With these assumptions, the special case dynamic model (after eliminating P_i and Q_i) is

$$\frac{d\delta_i}{dt} = \omega_i - \omega_s \quad i = 2, \dots, m \quad (1.61)$$

$$M_i \frac{d\omega_i}{dt} = T_{Mi} - [E'_{qi} + (X_{qi} - X'_{di})I_{di}]I_{qi} \quad i = 2, \dots, m \quad (1.62)$$

$$0 = V_i e^{j\theta_i} + jX'_{di}(I_{di} + jI_{qi})e^{j(\delta_i - \pi/2)} - [(X_{qi} - X'_{di})I_{qi} + jE'_{qi}]e^{j(\delta_i - \pi/2)} \quad i = 2, \dots, m \quad (1.63)$$

$$0 = -\sum_{k=1}^n V_i V_k Y_{ik} e^{j(\theta_i - \theta_k - \alpha_{ik})} + V_i e^{j\theta_i} (I_{di} - jI_{qi}) e^{-j(\delta_i - \pi/2)} + P_{Li} + jQ_{Li} \quad i = 2, \dots, m \quad (1.64)$$

$$0 = -\sum_{k=1}^n V_i V_k Y_{ik} e^{j(\theta_i - \theta_k - \alpha_{ik})} + P_{Li} + jQ_{Li} \quad i = m+1, \dots, n, \quad (1.65)$$

with

$$T_{Mi} = \text{constant} \quad i = 1, \dots, m \quad (1.66)$$

$$V_i = \text{constant} \quad i = 1, \dots, m \quad (1.67)$$

$$P_{Li} = \text{constant} \quad i = 1, \dots, n \quad (1.68)$$

$$Q_{Li} = \text{constant} \quad i = 1, \dots, n \quad (1.69)$$

$$\theta_1 = 0. \quad (1.70)$$

The $m + n - 2$ complex algebraic equations must be used to eliminate the $2m + 2n - 4$ real algebraic variables E'_{qi}, I_{di}, I_{qi} ($i = 2, \dots, m$), θ_i ($i = 2, \dots, n$), and V_i ($i = m + 1, \dots, n$). We begin by first noting that from (1.63) and (1.64),

$$\left[E'_{qi} + (X_{qi} - X'_{di}) \right] I_{di} I_{qi} = -P_{Li} + \sum_{k=1}^n V_i V_k Y_{ik} \cos(\theta_i - \theta_k - \alpha_{ik}) \quad i = 2, \dots, m. \quad (1.71)$$

This can be substituted into (1.62). Second, we note that (1.63) and (1.64) can be rewritten as

$$X_{qi} I_{qi} = -V_i \sin(\theta_i - \delta_i) \quad i = 2, \dots, m \quad (1.72)$$

$$E'_{qi} - X'_{di} I_{di} = V_i \cos(\theta_i - \delta_i) \quad i = 2, \dots, m \quad (1.73)$$

$$V_i I_{di} = \sum_{k=1}^n V_i V_k Y_{ik} \sin(\delta_i - \theta_k - \alpha_{ik}) + P_{Li} \sin(\theta_i - \delta_i) - Q_{Li} \cos(\theta_i - \delta_i) \quad i = 2, \dots, m \quad (1.74)$$

$$V_i I_{qi} = \sum_{k=1}^n V_i V_k Y_{ik} \cos(\delta_i - \theta_k - \alpha_{ik}) - P_{Li} \cos(\theta_i - \delta_i) - Q_{Li} \sin(\theta_i - \delta_i) \quad i = 2, \dots, m. \quad (1.75)$$

Eliminating E'_{qi}, I_{di} , and I_{qi} (simply equating I_{qi} in (1.72) and (1.75)) gives

$$\begin{aligned} -V_i^2 \sin(\theta_i - \delta_i) &= X_{qi} \sum_{k=1}^n V_i V_k Y_{ik} \cos(\delta_i - \theta_k - \alpha_{ik}) \\ -X_{qi} P_{Li} \cos(\theta_i - \delta_i) - X_{qi} Q_{Li} \sin(\theta_i - \delta_i) & \quad i = 2, \dots, m. \end{aligned} \quad (1.76)$$

Using (1.71), (1.76), and (1.65), this special case dynamic model with E'_{qi}, I_{di} , and I_{qi} ($i = 2, \dots, m$) eliminated is

$$\frac{d\delta_i}{dt} = \omega_i - \omega_s \quad i = 2, \dots, m \quad (1.77)$$

$$M_i \frac{d\omega_i}{dt} = T_{Mi} + P_{Li} - \sum_{k=1}^n V_i V_k Y_{ik} \cos(\theta_i - \theta_k - \alpha_{ik}) \quad i = 2, \dots, m \quad (1.78)$$

$$\begin{aligned} 0 &= V_i^2 \sin(\theta_i - \delta_i) - X_{qi} Q_{Li} \sin(\theta_i - \delta_i) - X_{qi} P_{Li} \cos(\theta_i - \delta_i) \\ &+ X_{qi} \sum_{k=1}^n V_i V_k Y_{ik} \cos(\delta_i - \theta_k - \alpha_{ik}) \quad i = 2, \dots, m \end{aligned} \quad (1.79)$$

$$0 = -P_{Li} + \sum_{k=1}^n V_i V_k Y_{ik} \cos(\theta_i - \theta_k - \alpha_{ik}) \quad i = m+1, \dots, n \quad (1.80)$$

$$0 = -Q_{Li} + \sum_{k=1}^n V_i V_k Y_{ik} \sin(\theta_i - \theta_k - \alpha_{ik}) \quad i = m+1, \dots, n, \quad (1.81)$$

with

$$T_{Mi} = \text{constant} \quad i = 1, \dots, m \quad (1.82)$$

$$V_i = \text{constant} \quad i = 1, \dots, m \quad (1.83)$$

$$P_{Li} = \text{constant} \quad i = 1, \dots, n \quad (1.84)$$

$$Q_{Li} = \text{constant} \quad i = 1, \dots, n \quad (1.85)$$

The linearized form of this dynamic model is

$$\begin{bmatrix} \frac{d\Delta\delta_g}{dt} \\ \frac{d\Delta\omega_g}{dt} \\ 0 \\ 0 \end{bmatrix} = \begin{bmatrix} 0 & I & 0 & 0 \\ 0 & 0 & K_1 & K_2 \\ K_5 & 0 & K_6 & K_7 \\ 0 & 0 & K_3 & K_4 \end{bmatrix} \begin{bmatrix} \Delta\delta_g \\ \Delta\omega_g \\ \Delta\theta_g \\ \Delta\theta_L V_L \end{bmatrix} \quad (1.86)$$

For the case (b), the algebraic equation Jacobian $J_{AE}^{(b)}$ is

$$J_{AE}^{(b)} = \begin{bmatrix} K_6 & K_7 \\ K_3 & K_4 \end{bmatrix} \quad (1.87)$$

Defining B' and C' as

$$B' = [K_1 \quad K_2], C' = \begin{bmatrix} K_5 & 0 \\ 0 & 0 \end{bmatrix} \quad (1.88)$$

for nonsingular $J_{AE}^{(b)}$, the system dynamic state Jacobian for case (b) is

$$J_{\text{sys}}^{(b)} = \begin{bmatrix} 0 & I \\ M^{-1}(-B' J_{AE}^{(b)-1} C') & 0 \end{bmatrix} \quad (1.89)$$

and (Sauer and Pai 1990)

$$\det J_{\text{sys}}^{(b)} = \frac{\det(-B' J_{AE}^{(b)-1} C')}{\det M} (-1)^{m-1} \quad (1.90)$$

Note that the eigenvalues of $J_{\text{sys}}^{(b)}$ will all be either pure imaginary or will include one or more values which are positive real. We will consider the dynamic system case (b) to be stable as long as no eigenvalues are positive real. By rearranging rows and columns of the matrix in (1.86) (Sauer and Pai 1990),

$$\det J_{AE}^{(b)} \det(-B' J_{AE}^{(b)-1} C') = \det K_s \det J_{LF} \quad (1.91)$$

where J_{LF} is as in (1.58). This gives the following relationship between the determinants of the standard power-flow Jacobian, the algebraic equation Jacobian, and the system dynamic state Jacobian:

$$\det J_{\text{sys}}^{(b)} = \frac{\det K_s \det J_{LF}}{\det M \det J_{AE}^{(b)}} \quad (1.92)$$

This means that under these assumptions, monitoring the power-flow Jacobian determinant can detect a possible dynamic instability. This is discussed in the following section.

1.8 Instability and Maximum Loadability

When studying a proposed load or interchange level, a power-flow solution is required before steady-state stability can be analyzed. If a power-flow solution cannot be found, then it is normally assumed that the proposed loading exceeded the “maximum power transfer” capability of the system. This maximum power transfer point is normally assumed to coincide with a zero determinant for the standard power-flow Jacobian.

Using this as a criterion, any load level that produces a zero determinant for the standard power-flow Jacobian is an upper bound and hence an optimistic value of the maximum loadability. It is also important to note that non-convergence of power-flows is also a matter of solution technique. Cases have been cited where Gauss–Seidel routines converge when Newton–Raphson routines do not.

If a standard power-flow solution and associated dynamic system equilibrium point are found (as described in Sects. 1.3 and 1.4), the stability of the point must be determined. In order to do this, the algebraic equation Jacobian must be nonsingular. This matrix is given by (1.44) in general, by K_4 for case (a), and by (1.87) for case (b). Assuming these algebraic equation Jacobians are nonsingular for a given case, steady-state stability must be evaluated from the eigenvalues of the system

dynamic state Jacobian. This matrix is given by (1.45) in general, by (1.56) for case (a), and by (1.89) for case (b).

A system is at a critical point when the real part of one of its eigenvalues is zero. If a real eigenvalue is zero, then the determinant is zero. In the general case of (1.45), the zero eigenvalue due to the angle reference can easily be removed by using a dynamic model reduced in order by 1 (see Sect. 1.5). Clearly, many cases can be found where an equilibrium point can be critically unstable (at least one eigenvalue has a zero real part) and the power-flow Jacobian is nonsingular.

In cases (a) and (b), all detailed model dynamic states have been eliminated by making rather drastic assumptions. In special case (a), as long as $\det M$ and $\det K_4$ are nonzero and bounded, a dynamic equilibrium point exists and has a system dynamic state Jacobian that is singular if and only if the power-flow Jacobian is singular. In special case (b), we need to look at the matrix K_5 . Examination of (1.79) shows that K_5 is diagonal with the i th diagonal entry equal to

$$\begin{aligned} K_{5i} = & -V_i^2 \cos(\theta_i - \delta_i) + X_{qi} Q_{Li} \cos(\theta_i - \delta_i) \\ & - X_{qi} P_{Li} \sin(\theta_i - \delta_i) - X_{qi} \sum_{k=1}^n V_i V_k Y_{ik} \sin(\delta_i - \theta_k - \alpha_{ik}) \quad i = 2, \dots, m \end{aligned} \quad (1.93)$$

From (1.74),

$$K_{5i} = -X_{qi} V_i I_{di} - V_i^2 \cos(\theta_i - \delta_i) \quad i = 2, \dots, m \quad (1.94)$$

and from (1.73),

$$K_{5i} = -V_i \left(E'_{qi} + (X_{qi} - E'_{di}) I_{di} \right) \quad i = 2, \dots, m \quad (1.95)$$

In steady state, (1.4) and (1.11) give (with $R_{si} = 0$)

$$\begin{aligned} 0 = & V_i e^{j\theta_i} + jX_{qi} \left(I_{di} + jI_{qi} \right) e^{j(\delta_i - \pi/2)} \\ & - j \left[E'_{qi} + (X_{qi} - X'_{di}) I_{di} \right] e^{j(\delta_i - \pi/2)} \quad i = 2, \dots, m \end{aligned} \quad (1.96)$$

This means that K_{5i} can be zero (for nonzero V_i) only if (see (1.17))

$$V_i e^{j\theta_i} + jX_{qi} I_{Gi} e^{j\gamma_i} \neq 0 \quad i = 2, \dots, m \quad (1.97)$$

This also shows that K_{5i} is proportional to the magnitude of the voltage behind X_{qi} in steady state. This was discussed in Sect. 1.4 as a condition for the existence of a dynamic equilibrium from a power-flow solution. Thus, if a dynamic equilibrium point exists (Eq. (1.40) is satisfied), then K_5 cannot be singular. Thus, if $\det M$ and $\det J_{AE}^{(b)}$ are nonzero and bounded, then the system dynamic state Jacobian of case (b) is singular if and only if the power-flow Jacobian is singular.

Since $J_{\text{sys}}^{(b)}$ must have all pure imaginary eigenvalues to be stable, $\det J_{\text{sys}}^{(b)}$ must be positive to be stable. Venikov et al. (1975) originally proposed the monitoring of the power-flow Jacobian determinant during power-flow iterations to see if it changed sign between the initial guess and the converged solution. The implication was that if it did, then the case (b) dynamic model would be unstable at that solution, and if it did not then the case (b) dynamic model would be stable (all pure imaginary eigenvalues).

Our interpretation indicates that they did not account for possible values of $\det K_5$ and $\det J_{\text{AE}}^{(b)}$. A change in sign of either of these would affect stability issues. We have shown that $\det K_5$ would probably never change sign, but whether the $\det J_{\text{AE}}^{(b)}$ changes sign or not remains an open question.

1.9 Post-Contingency Equilibrium Analysis

The earlier sections of this chapter presented a method to compute the equilibrium condition based on standard Power-Flow Methods (PFMs) assuming generator voltages and rated frequency. When contingencies occur, the equilibrium immediately following the contingency will be based on the constant control inputs. This section proposes and analyzes several techniques for computing this “post-contingency equilibrium condition.”

Traditional contingency analysis of power systems uses either standard power-flow analysis or full transient simulation. The full transient simulation is normally only used to assess stability information following a hypothetical disturbance. It is rarely used to compute the steady-state equilibrium condition. The reference values fed into the control systems of a generator eventually determine the real power output and some desired bus voltage magnitude (possibly modified by a compensation circuit).

In a dynamic simulation, these control inputs are normally computed from a base case power-flow solution as discussed in Sect. 1.4. If the base case is subjected to a contingency (loss of line), the dynamic model (and therefore presumably also the real system) would respond according to these fixed control inputs until they are changed by an operator or other higher-level control. This means that the post-contingency equilibrium is determined by the fixed controls. This may not produce the same result as a simple power-flow solution modified to reflect a line outage.

This section reports on various techniques to compute the post-contingency equilibrium with fixed control inputs, and compares the results with simple power-flow results. Clearly, running a dynamic solution until steady state is reached (for stable systems) would give the nearly exact post-equilibrium condition and would be considered the benchmark for all other approximate or alternative solution techniques.

The nearly exact post-equilibrium condition should also be computable using analytical methods. However, commercial power-flow programs already solve a

subset of the equilibrium equations and can be utilized to solve for part of the post-contingency equilibrium state. So, rather than creating a completely new Newton-based program to solve the entire problem, an alternative would be to create a new program only for the machine dynamic equilibrium equations and couple this in an iterative fashion with the standard power-flow program.

The potential for decoupling each of the machine equations is also a motivation for pursuing this technique. The remainder of this chapter focuses on these techniques and compares them with the “Time Domain Method” (TDM) and “PFM”.

The basic dynamic model that describes a power system has been given in Sect. 1.1 above. It includes the dynamics of the generator, exciter, and turbine governor along with the algebraic network constraints. The model was changed slightly from above to coincide with the model used in the commercial software known as PSS/E (Power System Simulator for Engineering).

The change included the use of power over per unit speed for the generator mechanical torque, and $-D_i((\omega_i - \omega_s) / \omega_i)$ rather than $-D_i(\omega_i - \omega_s)$ for the damping torque. This was important because the post-contingency generator speeds may not be equal to the nominal rated speed.

The power system equilibrium equations were obtained by setting the time derivatives of the dynamic model to zero. The equations are for an n bus system where the first m buses are connected to a generator. Also, all the machine and bus voltage angles were referenced to the machine angle (δ_1) of the generator at bus number 1 (also the slack bus for the power-flow portion of the analysis). This is denoted by the prime above all the angle variables.

These post-contingency equilibrium equations include the power-flow equations and the steady-state machine equations. The post-contingency equilibrium conditions contain the voltages (magnitude and angle) of a contingency analysis ($2n$ states) plus the states introduced by the machine, referred to as the *reduced machine states* ($5m$ states).

$$\mathbf{x}_m^T = \left[\omega, \delta'_j, I_{di}, I_{qi}, E_{fdi}, P_{Mi} \right] \quad i = 1, \dots, m \quad j = 2, \dots, m \quad (1.98)$$

These are referred to as the *reduced machine states* because the other machine dynamic states have been eliminated by substitution. Their equilibrium values can be recovered by simple substitution at the end if desired. Collectively, there are $5m + 2n$ equations to be solved for the $5m + 2n$ states.

The challenge of post-contingency analysis is to compute the solution of the equilibrium algebraic equations. A solution of these equations by a “Full Newton Method” (FNM) should produce nearly the same post-contingency solution as the full dynamic simulation run to steady-state TDM.

1.9.1 Partitioned Newton Method

In the “partitioned Newton method” (PNM), the equilibrium equations are divided into two sets. The power-flow program is used to solve the power-flow equations. The dependent and independent variables for the power-flow equations are

$$\underline{\mathbf{x}}_{pf}^T = [V_i, \theta'_j] \quad i = m+1, \dots, n \quad j = 2, \dots, n \quad (1.99)$$

$$\underline{\mathbf{u}}_{pf}^T = [V_i, \theta'_1, P_{Gj}, P_{Lk}, Q_{Lk}] \quad i = 1, \dots, m \quad j = 2, \dots, m \quad k = 1, \dots, n \quad (1.100)$$

where P_{Gj} is defined as $P_j - P_{Lj}$. This power-flow step includes the solution of $2n - m - 1$ equations for $2n - m - 1$ states. The remaining $6m + 1$ equations are solved using Newton’s method for the $6m + 1$ states. The dependent and independent variables for this set of machine equations are:

$$\underline{\mathbf{x}}_{mp}^T = [\theta'_1, V_i, \omega, \delta'_j, I_{di}, I_{qi}, E_{fdi}, P_{Mi}] \quad i = 1, \dots, m \quad j = 2, \dots, m \quad (1.101)$$

$$\underline{\mathbf{u}}_{mp}^T = [V_{refi}, P_{ci}, V_l, \theta'_j, \delta'_l, P_{Lk}, Q_{Lk}] \quad \begin{matrix} i = 1, \dots, m & j = 2, \dots, n \\ k = 1, \dots, n & l = m+1, \dots, n \end{matrix} \quad (1.102)$$

The steps for computing the equilibrium condition by the PNM are shown in Fig. 1.5.

Starting from the base case power-flow solution and the reference values of the generators that satisfy this condition, a disturbance in the network is introduced that changes the network topology. The machine equations are then solved using Newton’s method to give a new voltage value of the slack bus generator and a new voltage magnitude and real power output of the Power–Voltage (PV) bus generators.

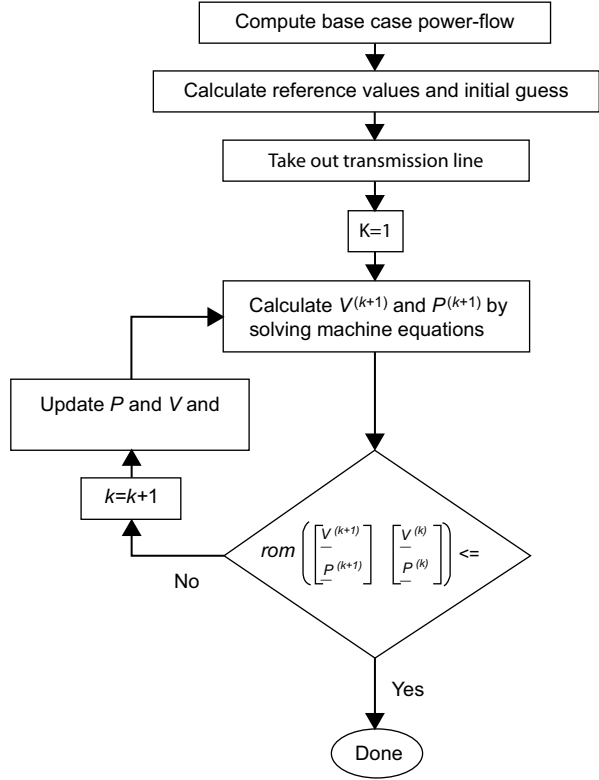
These are the new independent variable values for the power-flow equations. Then the power-flow is solved to provide the new network voltages that are used to solve the machine equations. This loop of updating the independent variables in each equation set is made until the change in the power and voltage values of the generators becomes negligible.

In this technique, the calculation of the power and voltage values of the generators was done by solving all of the machine equations together using Newton’s method. This method alternates between this Newton solution and a standard power-flow solution. It does not exploit the natural decoupling between generator dynamics.

1.9.2 Decoupled Newton Method

All the machines are coupled together by the synchronism of the machine speed at equilibrium. In fact, the speed term ω is the only term that couples the different machines together among the machine states. In the “decoupled Newton method”

Fig. 1.5 Post-contingency equilibrium calculation. (Yeu 2005)



(DNM), the speed term is solved for by only using the power-flow solution and the machine states of the slack bus generator. This decouples the calculation of the power and voltage values of the generators from other generator machine states.

As before in the PNM, the power-flow program is utilized to solve the power-flow equations. Then the slack bus voltage magnitude and angle are calculated by solving the machine equilibrium equations for $i = 1$ using Newton’s method. The dependent and independent variables for this calculation are shown in (1.103) and (1.104). The decoupling of the machines allows the voltage magnitudes and angles of all the other buses, including generator buses, to be independent variables. These voltage values are obtained from the power-flow solution.

$$\underline{x}_{md_1}^T = [\theta'_1, V_1, \omega, I_{d1}, I_{q1}, E_{fd1}, P_{M1}] \tag{1.103}$$

$$\underline{u}_{md_i}^T = [V_{ref1}, P_{c1}, V_k, \theta'_k, \delta'_k, P_{Li}, Q_{Li}] \quad k = 2, \dots, n \quad i = 1, \dots, n \tag{1.104}$$

The slack bus calculation must be made first in the DNM. This is because, while all the voltage magnitude, real power output, and machine speed values of each generator are updated after the calculation is made for all the generators, the slack bus

angle must be updated before the calculation of the next set of power and voltage values of the PV buses.

An update in the slack bus angle along with the other updates would just change the angle reference value of the power flow and would neglect the control of the power output of the slack bus generator driven by the power reference, P_{c1} . The update in the slack bus angle is made before the other updates so that the power and voltage updates of the PV bus generators take into account not only its own control but also the slack bus generator power requirements through the network constraints.

The calculation of the remaining generator voltage and power values can be made in an arbitrary order using Newton's method. The dependent and independent variables for this calculation are shown in (1.105) and (1.106) for $j = 2, \dots, m$.

$$\underline{\mathbf{x}}_{mj}^T = [\delta'_j, V_j, I_{dj}, I_{qj}, E_{fdj}, P_{Mj}] \quad (1.105)$$

$$\underline{\mathbf{u}}_{mj}^T = [V_{refj}, P_{cj}, \omega, V_k, \theta'_i, P_{Li}, Q_{Li}] \quad k = 1, \dots, n \quad i = 1, \dots, n, \quad k \neq j \quad (1.106)$$

The steps of the DNM are similar to those of the PNM. The starting point is the base case power flow. Then power and voltage reference values of the generators are calculated to satisfy the base case condition. After a line is opened, the slack bus voltage magnitude and angle are calculated and the slack bus angle is updated. Then the PV bus generator real power and voltage magnitude values are calculated in arbitrary order or in parallel as previously described.

If the change in the power and voltage values of the generators is within the tolerance range, then the equilibrium solution is reached. Otherwise, the power and voltage values of the generators are updated and used to calculate a new power-flow solution. Another set of power and voltage values of the generators are then calculated using the new power-flow solution and this loop of calculating the updates and calculating the power flow is repeated until the change in the updates is within the tolerance range.

Figure 1.5 with one modification describes these steps. The block for calculating the voltage and power values is replaced by m blocks. The first block represents the calculation of the slack bus voltage values and the update of the slack bus angle, and the remaining blocks represent the voltage and power update of each PV bus generators.

Since the machines are decoupled, the size of the Jacobian used in each of the Newton's methods to calculate the machine states is 7×7 for the slack bus calculation and 6×6 for each of the $m-1$ PV bus calculations.

This is a significant reduction in the size of the Jacobian from the one used in the PNM, which is $(6m+1) \times (6m+1)$. Another advantage of the DNM is that different machine models can be incorporated for the equilibrium analysis easily. This is because of the fact that independent variables for a given machine stay the same for different machine models while the dependent variables are independent from other machine states.

Table 1.1 Maximum pu voltage magnitude difference from TDM (nine-bus case)

Bus	FNM	PNM	DNM	PFM
1	0.0001	0.0001	0.0001	0.0031
2	0.0004	0.0004	0.0004	0.0088
3	0.0002	0.0002	0.0002	0.0131

Table 1.2 Maximum pu real power difference from TDM (nine-bus case)

Bus	FNM	PNM	DNM	PFM
1	0.0052	0.0052	0.0052	0.0311
2	0.0036	0.0036	0.0036	0.0184
3	0.0014	0.0014	0.0014	0.0177

1.9.3 Test Cases

The post-contingency equilibrium analysis was done on two power-system cases using five methods:

- TDM
- FNM
- PNM
- DNM
- PFM

As a benchmark reference, a dynamic simulation using the PSS/E-30 software was run to equilibrium to calculate the post-contingency equilibrium state for the TDM. The next three methods were programmed in Matlab 7.0.1. The Power System Toolbox 2.0 power-flow program was used to solve the power-flow equations in the PNM, DNM, and PFM. The first test case was the so-called Western Electric Coordinating Council (WECC) nine-bus power system (Sauer and Pai 1998). This system contains three machines and nine transmission lines. Only three single line outage cases were stable according to the PSS/E simulations.

Out of these three cases, the maximum per unit differences of the voltage magnitude and real power output from the four methods were compared to the results from the TDM equilibrium analyses with the results shown in Tables 1.1 and 1.2. The maximum differences are shown only for the generator buses.

The second case was the 57-bus test case (Power System Test Case Archive 2014). This system contains 6 machines and 80 transmission lines. All but two single line outage cases were stable.

The maximum per unit differences of the voltage magnitude and real power output from the four methods were compared to the results from the TDM equilibrium analyses with the results shown in Tables 1.3 and 1.4. As before, the maximum differences are only shown for the generator buses.

The results of the post-contingency equilibrium analysis using the FNM, PNM, and DNM and the results from the TDM are basically the same as would be expected. The only explanation we have for the errors shown is the truncation error of

Table 1.3 Maximum pu voltage magnitude difference from TDM (57-bus case)

Bus	FNM	PNM	DNM	PFM
1	0.0001	0.0001	0.0001	0.0054
2	0.0003	0.0003	0.0003	0.0653
3	0.0004	0.0004	0.0004	0.0141
6	0.0002	0.0002	0.0002	0.0162
8	0.0001	0.0001	0.0001	0.0015
9	0.0004	0.0004	0.0004	0.0372
12	0.0002	0.0002	0.0002	0.0058

Table 1.4 Maximum pu real power difference from TDM (57-bus case)

Bus	FNM	PNM	DNM	PFM
1	0.0058	0.0058	0.0058	0.2793
2	0.0027	0.0027	0.0027	0.0442
3	0.0076	0.0076	0.0076	0.0453
6	0.0021	0.0021	0.0021	0.0440
8	0.0045	0.0045	0.0045	0.0532
9	0.0027	0.0027	0.0027	0.0440
12	0.0054	0.0054	0.0054	0.0501

numerical integration to steady state and convergence mismatch of iterative solvers. This shows that the different equilibrium analyses with fixed control inputs accurately characterized the post-contingency equilibrium states.

On the other hand, there are some significant differences between the PSS/E simulation (TDM) and the traditional contingency analysis (PFM). This is also expected since the voltage magnitude and the real power output of a generator do not necessarily stay constant from the base case to the post-contingency equilibrium state as is generally assumed in standard power-flow contingency analysis.

Generally, the voltage and power values did not deviate by a great amount from the base case to the post-contingency state. However, significant deviations such as the 0.06 pu voltage difference on bus 2 for the 57-bus case can occur. Deviations of this magnitude can affect the reliability of a power system considerably and can introduce errors in a contingency analysis.

1.10 Conclusions

Standard power flow is used to find system voltages for a specified level of loading or interchange (regardless of the dynamic load model). It is also the starting point for determining the initial conditions for dynamic analysis. The standard power-flow Jacobian can provide information about the existence of a steady-state equilibrium point for a specified level of loading or interchange. There are two very special cases when the determinant of the standard power-flow Jacobian implies something about the steady-state stability of a dynamic model.

While these two cases have been presented previously, the extensions here illustrate the validity of the basic results. Both of these cases involve very drastic assumptions about the synchronous machines and their control systems. The load level, which produces a singular power-flow Jacobian, should be considered an optimistic upper bound on maximum loadability. The actual upper bound would be either the same or lower since it requires both the existence of a solution *and* stable dynamics.

For voltage collapse and voltage instability analysis, any conclusions based on the singularity of the standard power-flow Jacobian would apply only to the phenomena of voltage behavior near maximum power transfer. Such analysis would not detect any voltage instabilities associated with synchronous machine characteristics or their controls.

This chapter also addressed the issue of post-contingency steady state conditions. New analytical methods of computing the post-contingency equilibrium state of a power system have been described and illustrated. The main observation is that all of the methods provide a solution, which agrees reasonably well with the so-called exact solution of a dynamic simulation run to steady state. The particular illustrations also indicated that there can be substantial error between this true post-contingency equilibrium and standard power-flow contingency analysis.

The FNM is a brute force analytical method requiring an entirely new software program to solve all of the machine and network equations simultaneously. The PNM is an alternative method that divides the solution into two parts—one utilizing a standard power-flow program and another new one for the machine equations—alternating solution updates. The DNM is the most promising method because it exploits the utilization of a standard power-flow program and also decouples the machine equations so that they can be solved by a very low-order iterative program. This also allows the extension to more detailed generator dynamic models that include more complex local dynamics and control actions.

Recent activity in this area has focused on using phasor measurement unit data to detect steady-state stability criteria. This activity is summarized in Reinhard et al. (2013) where Thévenin equivalents are used to represent complete systems on either side of each transmission line. The results propose that as the system approaches a steady-state stability limit, the angle across the entire system approaches 90° (between the two Thévenin equivalents) for at least one line in the system.

Acknowledgments The authors thank Mr. Rodney Yeu for contributing the results from his graduate thesis on computing the post-contingency equilibrium point. Special thanks also to Mr. Tom Moone for providing editorial assistance. This work was supported in part by National Science Foundation grants NSF ECS 87-19055 and NSF EEC 0120153, and in part by the Grainger endowments to the University of Illinois.

References

- Pai MA (2004) *Computer techniques in power system analysis*, 2nd ed, McGraw-Hill, New Delhi
- Power System Test Case Archive (2014) University of Washington College of Engineering, The IEEE 57 bus network model, <http://www.ee.washington.edu/research/pstca/>. Accessed 5 May 2004
- Pulgar-Painemal HA, Sauer Peter W (2011) Reduced-order model of type C wind turbine generators. *Electr Power Syst Res* 81(4):840–845
- Rajagopalan C, Lesieutre B, Sauer PW, Pai MA (1992) Dynamic aspects of voltage/power characteristics. *IEEE Trans Power Syst* 7(3):990–1000
- Reinhard KE, Sauer Peter W, Dominguez-Garcia Alejandro D (2013) On computing power system steady-state stability using synchrophasor data, Proceedings, 46th Hawaiian International Conference on System Science (HICSS), 7–10 Jan 2013, Maui, Hawaii.
- Sauer PW, Pai MA (1990) Power system steady-state stability and the power-flow Jacobian. *IEEE Trans Power Syst* 5(4):1374–1383
- Sauer PW, Pai MA (1998) *Power system dynamics and stability*. Prentice Hall, Upper Saddle River
- Venikov VA, Stroeve VA, Idelchick VI, Tarasov VI (1975) Estimation of electrical power system steady-state stability. *IEEE Trans Power Appar Syst PAS-94*(3):1034–1040
- Verastegui P (2000) Examination of the relationship between power-flow Jacobian singularities and system dynamics Jacobian singularities, special ECE 272 project report, Department of Electrical and Computer Engineering, University of Illinois at Urbana-Champaign
- Yeu R (2005) Postcontingency equilibrium analysis of power systems, MSEE Thesis, Department of Electrical and Computer Engineering, University of Illinois, at Urbana-Champaign, May 2005, pp 1–63
- Yorino N, Sasaki H, Masuda Y, Tamura Y, Kitagawa M, Oshimo A (1992) An investigation of voltage instability problems. *IEEE Trans Power Syst* 7(2):600–611

Chapter 2

Fast Computation of the Steady-State Stability Limit

Savu C. Savulescu

Abstract This chapter addresses the theoretical foundation of a field-proven real-time steady-state stability tool (The commercial name of this tool is *Siemens Spectrum Power QuickStab*. The software is owned by Siemens AG, Germany, and is seamlessly integrated with the Spectrum Power SCADA/EMS platform and SIGUARD® Dynamic Security Assessment suite) that quickly and reliably quantifies and visualizes the risk of blackout due to instability. The approach is inspired from Paul Dimo’s steady-state stability analysis method and uses the Bruk–Markovic reactive power stability criterion in the REI Nets framework to determine how far the power system is from a state where voltages may collapse and generators may lose synchronism. The technique derives its speed and robustness from Dimo’s sound approximations and simplifying assumptions, which are analyzed and substantiated. Metrics that quantify the distance to instability and to the security margin are also discussed, along with innovative tools that extract and visualize essential *information* from the large amount of computational results.

2.1 Introduction

Modern transmission networks must sustain megawatt (MW) transfers that can be quite different from those for which they were planned. This is because energy transactions across multi-area systems may cause parallel flows, excessive network loadings, and low bus voltages. Under certain conditions, such degraded states may lead to blackouts—but how to *quantify* the risk of blackout? How to do it *quickly* in real time, using input from the most recent state estimate and displaying the results before the immediately next state estimation cycle, so that the operator could make *truly online, split-second decisions*? And how to extract *essential* information from large amounts of data and computational results and present it in formats that can be instantly understood and relied upon?

S. C. Savulescu (✉)
Energy Consulting International, Inc., 405 Lexington Avenue, 26th Floor,
New York, NY 10174, USA
e-mail: savu@eciscs.com

The industry has taken for granted concepts such as the Available Transfer Capability (ATC), Total Transfer Capability (TTC), and Transmission Reliability Margin (TRM), but was slow to recognize the need to run real-time stability checks after every single state estimation solution and after each market clearing computation.

According to the North American Electric Reliability Corporation (NERC; NERC 1966), the TTC is given by

$$\text{TTC} = \text{Min} \{ \text{Thermal Limit, Voltage Limit, Stability Limit} \}$$

Thermal and voltage limits can reliably be defined off-line. They are predictable and can even be briefly violated. But how about “stability limits?” NERC’s Policy 9 (NERC 2000) requires reliability coordinators to compute “stability limits” for the current and next-day operation processes to “foresee whether the transmission loading progresses or is projected to progress beyond the operating reliability limit.” This is easier said than done, for detecting thermal and voltage violations is relatively straightforward, whereas defining, quantifying, and computing “stability limits” is an altogether different proposition, especially if it has to be done online.

In order to qualify for real-time deployment, the stability software must, of course, be fast and reliable but, in addition, it should also provide the *ability to identify, quantify, and visualize the stability limits*, as opposed to just assessing whether a given condition is stable or unstable.

Many, if not most, stability tools available until a few years ago, would *not* meet both these requirements. They “determine whether a given condition is stable or unstable, [but] have not been efficient in quickly and automatically determining the stability limits” (Kundur 1999).

Actually, Professor Kundur’s statement was an understatement, in the sense that the term “stability limit” was used without having been explicitly defined or mathematically quantified—not only in this widely quoted reference but also in the literature available at that time. Common sense suggests that if conventional techniques can neither quantify the stability limit, or limits, nor perform split-second computations, an alternate paradigm, perhaps entailing simplifications, should be used—provided that such simplifications would come from sound assumptions and lead to algorithms that are fast and provide dependable answers as well.

Indeed, a method that meets these requirements was developed in Europe in the early 1960s by Paul Dimo (Dimo 1961, 1975) and introduced in the USA in the 1990s (EPRI 1992, 1993; Savulescu et al. 1993; Erwin et al. 1994). It quickly became obvious that, if taken from the drawing board to the real life, this approach does have the potential to overcome the real-time stability challenge. As a result, practical features were incorporated and a commercial-grade stability tool was developed and, then, deployed in actual power system control centers (Gonzalez 2003; Avila-Rosales et al. 2004; Savulescu 2004; Tweedy 2004; Avila-Rosales and Giri 2005; Vergara et al. 2005a; Campeanu et al. 2006; Virmani et al. 2007; Vickovic et al. 2009; Arnold et al. 2009; Eichler et al. 2011; Stottok et al. 2013).

The subsequent sections of this chapter:

- Discuss the general background
- Address the benefit of approaching the real-time stability problem through the steady-state stability prism
- Review the mathematical foundation of Dimo’s steady-state stability analysis method
- Briefly close the gap from theory to implementation and review a set of user-friendly visualization tools inspired from the otherwise cryptic Nodal Images originally introduced by Dimo half a century ago.

2.2 General Background

2.2.1 *In Search of the Stability Limit*

Conceptually, the “stability limit” is a local property of the system state vector: For each new solution of the system of equations that describe the system state, there is a new stability limit. For example, the stability conditions change when static capacitors and shunt reactors are switched. Likewise, transformer tap changes, line outages, load variations, and generator trips affect the distance to instability. To further complicate things, the stability limit also depends upon the path followed to approach it: different search paths may lead to different stability limits.

Simply stated, stability limits exist, are not fixed, and change with the total MW system grid utilization,¹ bus voltage profile, network topology, and the path followed to approach them. It is precisely because of this changing nature of the stability limits that they must be recalculated as often as possible—assuming, of course, that a *metric* has previously been defined so that such stability limits could be *quantified*.

Furthermore, instability develops instantly and leaves no time to react, so, in addition to the need of indices that quantify the distance to instability, the ability must also be provided to rapidly recompute the underlying indices for each new system state, after each state estimate, and after each load flow.

2.2.1.1 Transient and Voltage Stability Limits²

The main directions investigated in the industry during the past two decades point primarily at transient stability and voltage stability. On the *transient stability* venue,

¹ When the system is *importing* power, the total MW system grid utilization is calculated by summing up the total MW generation with the total imported MW; when *exporting* power, the total MW system grid utilization is the total generated MW. In other words, this number shows how many MW are currently “circulating” in the transmission system.

² Portions of this section have been reprinted with permission from Savulescu, S.C. (2004).

much work was done to develop “transient stability indices” aimed at computing the “degree of stability”³ (Kundur 1999).

Regardless of the specific details, these methods follow similar scenarios:

- Start with a base case and a postulated major contingency
- Derive a “severity index” for this contingency
- Compute new power flows for successively degraded states
- Repeat the sequence until either the load flow diverges or an unstable case has been obtained

Their limitations are similar, too:

- Computational burden, which some authors attempted to alleviate by
 - merging all the machines into an equivalent generator, which makes it impossible to identify the dangerous generators and their impact on the system stability conditions
 - using the infinite bus assumption, i.e., implying that voltages are constant, although, in real life, the bus voltages drop when the power system is approaching a state where instability might occur
- Need to examine a huge set of disturbance scenarios, thus further escalating the computational complexity

Voltage stability, also known as load stability (Venikov 1977; Barbier and Barret 1980; Vournas et al. 1996), refers to the maximum MW that can be transferred to a given load bus prior to the occurrence of voltage collapse. But in order to develop a *system-wide* view from such *bus-oriented* calculations, the procedure must be repeated for all the load buses, which becomes computationally expensive for large system simulations.

A more serious limitation comes from the load model. If the load is modeled as constant impedance, the bus MW initially increases up to a maximum, then it gets smaller and *dual power states* (same power at different voltages) are obtained (Ionescu and Ungureanu 1981)—and this is what actually causes the “nose” pattern of the P – V curves. But dual states *cannot* happen in real life, and the validity of any P – V curve drawn on this basis is questionable.

Let us mention en passant the inadequacy of “assessing stability” by running load flows at successively increased load levels and stopping when the load flow diverged. While it is true that Newton–Raphson load flows diverge near instability (Venikov et al. 1975), they may diverge for many reasons. Sauer and Pai (Sauer and Pai 1990) have demonstrated that “for voltage collapse and voltage instability analysis, any conclusions based on the singularity of the load-flow Jacobian would apply only to the voltage behavior near maximum power transfer. Such analysis would not detect any voltage instabilities associated with synchronous machines characteristics and their controls.”

³ With all the respect due to Professor Kundur, this often-quoted paper uses the term “degree of stability” as an a priori concept but neither defines nor quantifies it.

Perhaps the most significant challenge is the representation of generators, which *must* be taken into account (Barbier and Barret 1980; Ionescu and Ungureanu 1981; Sauer and Pai 1990; Kundur and Morison 1993). In the world of continuation load flows, this is a classic catch-22 situation: If the generator reactances *are not* included in the power system model, the ensuing load-flow calculations are meaningless from the point of view of stability; if the machine reactances *are* represented, the values of the generators' internal electromotive force (emf), which are typically much higher than 1.0 pu, would cause the load-flow calculations to diverge.

One way out of this dilemma is to represent the machines in detail, via transfer functions, in which case, much more complex algorithms would have to be deployed (EPRI 1992; Morison et al. 2004), thus significantly increasing the computational burden—or, even better, to change gears entirely and move into the much more promising realm of steady-state stability.

2.2.1.2 The Steady-State Stability Connection

Steady-state stability⁴ is the stability of the system under conditions of gradual or relatively slow changes in load (Crary 1945). Accordingly, the steady-state stability limit (SSSL) of a power system is “a steady-state operating condition for which the power system is steady-state stable but for which an arbitrarily small change in any of the operating quantities in an unfavorable direction causes the power system to lose stability” (IEEE 1982; Navarro-Perez and Prada 1993).

Voltage collapse, units losing synchronism, and instability caused by self-amplifying small-signal oscillations are all forms of steady-state instability. Empirically, the risk of steady-state instability⁵ is associated with low real/reactive power reserves, low voltage levels, and large bus voltage variations in the presence of small load or generation changes.

Recurring “temporary faults” where breakers trip without apparent reason, i.e., are disconnected by protection without being able to identify the fault, might also be indicative of steady-state instability. Breaker trips can happen when loads increase due to “balancing rotors” of generators that trip near instability and then get back in synchronism. In some cases, “the resynchronization happened after the rotor turned 360°, which, in turn, led to lower voltages” (Dimo 1968).

The possibility of operating for a very short time in an unstable operating state and resynchronization due to the action of fast voltage controllers has been known for a long time (Magnien 1964). Also, according to the same report, “any network

⁴ By “steady-state stability,” we refer to the *classical concept* described by Crary (1945), Venikov (1977), IEEE (1982), and Anderson and Fouad (1990), as opposed to “small-signal stability,” as it is understood nowadays (IEEE/CIGRE 2004).

⁵ Throughout the remainder of this chapter and, in general, in the literature that addresses Dimo's concepts and related stability applications, “steady-state instability” actually refers to “aperiodic steady-state instability” and assumes that self-amplifying system oscillations either do not occur or have been prevented by the existence of power system stabilizers.

that meets the steady-state stability conditions can withstand dynamic perturbations and end in a stable operating state” (Magnien 1964).

The SSSL spans a promising landscape. First and foremost, it is *quantifiable*, as shown in the Sect. 3.4.1. Then, it *does* represent an operating limit, in the sense that operating conditions *immediately* below SSSL become unstable if a small change in any of the operating quantities in an unfavorable direction takes place.

Simplicity is another benefit: For a given topology, load and generation conditions, and reactive compensation scenario, the SSSL is simply the total MW grid utilization of the transmission system, including both internal generation and tie-line imports, where voltages may collapse and units may lose synchronism.

Furthermore, although the SSSL depicts an unsafe state, the algorithm used to compute it can be reversed to determine a *security margin*, thus potentially eliminating the need to perform dynamic simulations, if the total base case MW system grid utilization is below such “security margin” (Moraite et al. 1966).

On this basis, a metric of system-wide indices emerges and provides for quantitatively assessing “how far from SSSL” and “how safe” is a given operating state. One pillar of this metric is the *steady-state stability reserve* index; the other one is the *security margin* index. Both these indices change, and need to be computed, for each new system state—and, together, they span the concept of *stability envelope*, as shown in the following section.

2.2.2 *Transient stability limit , total transfer capability, and the Stability Envelope*

A Transient Stability Limit (TSL) also exists (Navarro-Perez and Prada 1993), but, as opposed to SSSL, and because of the computational algorithms and strategy used to detect transient instability, it is not quantifiable through a specific formula. In order to find it, transient stability simulations would have to be performed for each potential fault starting from a base case scenario and continuing with a sequence of successively degraded operating states until the first unstable state has been found.

The intrinsic computational complexity and the large number of credible contingencies render such a problem practically unsolvable.

However, intuition suggests (Fig. 2.1) that:

- For a given set of relay settings, TSL depends, just like the SSSL, upon topology, voltage levels, and total MW system grid utilization.
- For any system state, SSSL and TSL are interrelated and move in the same direction: if SSSL is high, TSL is also high, and vice versa.

In the past, empirical values approximating the *TSL/SSSL ratio* have been used to compute a “safe” MW system grid utilization, referred to as *security margin*, such that, for any system state with a steady-state stability reserve smaller than it, no contingency, no matter how severe, would cause transient instability (Moraite et al. 1966; Dimo et al. 1971).

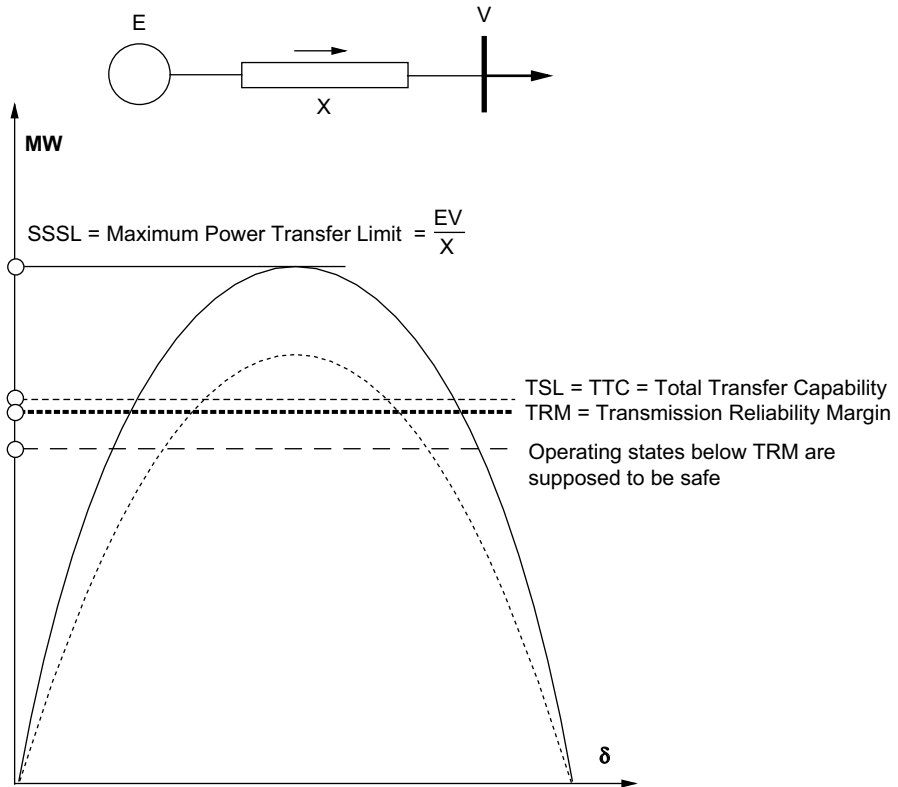


Fig. 2.1 TTC and TRM seen from the steady-state stability perspective

The security margin, which is expressed as a percentage of the steady-state stability reserve, depends upon topology, loads, generators, and reactive compensation. It changes from system to system and, for a particular power system, must be reassessed periodically and for alternate operating scenarios.

For example, extensive studies and operational experience with the Romanian power system, as it was in the 1960s and 1970s, led to setting the security margin at 15% for normal operating conditions and 8% for contingency cases (Dimo et al. 1971).

We do not know if a mathematical formula relating TSL and SSSL can be developed analytically, but the empirical approach described in Vergara et al. (2005a) can be expanded to build the following heuristic:

1. Start with a base case load flow for peak load conditions and compute the SSSL and related security margin.
2. Run an extensive suite of transient stability simulations. If no instability has been detected, go to Step 5. If at least one contingency (fault) case was found to be unstable, go to Step 3.

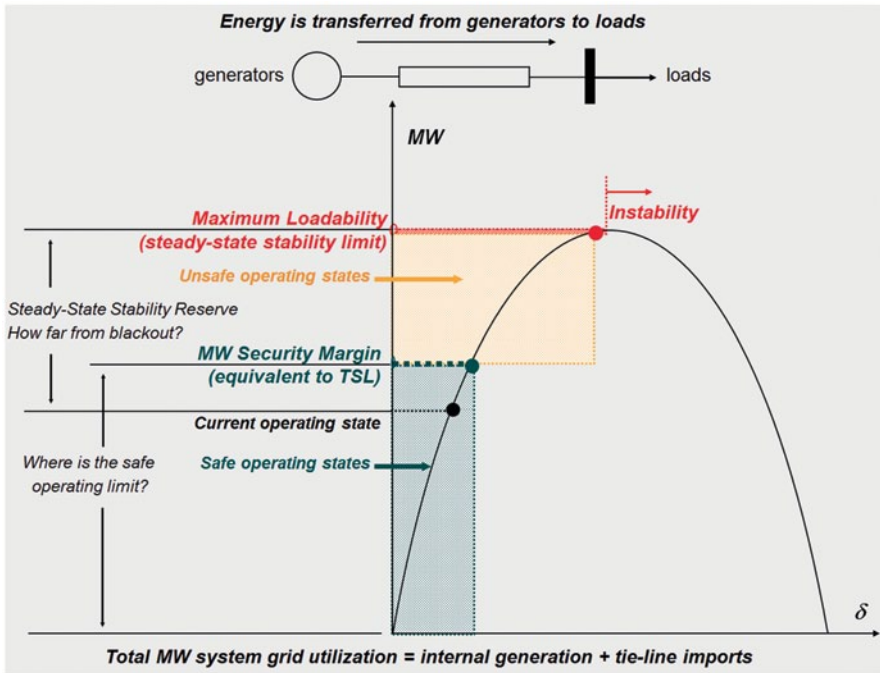


Fig. 2.2 The “stability envelope”

3. Use the security margin MW generation schedules from Step 1 to calculate a new base case load flow.
4. For the load flow computed in Step 3, run an extensive suite of transient stability simulations.
5. If no instability has been detected, repeat Step 4 for successively increased MW levels until at least one contingency causes transient instability. The steady-state stability reserve for the immediately precedent state is the security margin of the system under evaluation.
6. If the Step 4 calculations detected at least one contingency (fault) that would cause instability, build a new load-flow case for a slightly reduced load level and repeat the transient stability checks. If no instability has been detected, recalculate the SSSL and the steady-state stability reserve, which is the security margin of the system under evaluation.

The MW value of the security margin represents a “safe system MW loading limit” that can be interpreted as a *stability envelope* (Fig. 2.2).

Assuming there are no thermal violations, i.e., if the TSL in Fig. 2.2 is the same as NERC’s TTC, the stability envelope corresponds to NERC’s definition of TRM and is obtained as follows:

- *First*: Starting from a state estimate or solved load flow, determine the steady-state stability reserve, i.e., the distance to SSSL.
- *Subsequently*: For a postulated $x\%$ value of the security margin, determine the corresponding safe system MW loading below the SSSL.

The computation of the steady-state stability reserve can be accomplished both by detailed analysis and via approximate methods. Detailed steady-state stability methods have been proposed (Arie et al. 1973) but do not seem to have been actually implemented.

By contrast, approximate methods, if fast and reasonably accurate, are attractive both for real-time and for off-line stability checks. Dimo's technique belongs to this category. At the time when it was introduced, it was used in operations and long-range planning. Its recent extensions improved the computational speed and robustness and, with the newly added visualization capabilities, it has been implemented and successfully used in real time for several years. This topic is addressed in the following section.

2.3 Overview of Paul Dimo's Steady-State Stability Analysis approach

2.3.1 General

Paul Dimo's methodology is predicated on the following major concepts:

- Short-circuit current's network transformation that leads to an REI Net
- Vectorial representation of the short-circuit currents on a Nodal Image
- Use of the reactive power voltage and steady-state stability criterion in conjunction with the Nodal Image
- ase-worsening procedure for computing successively degraded power system states when performing system-wide stability analysis

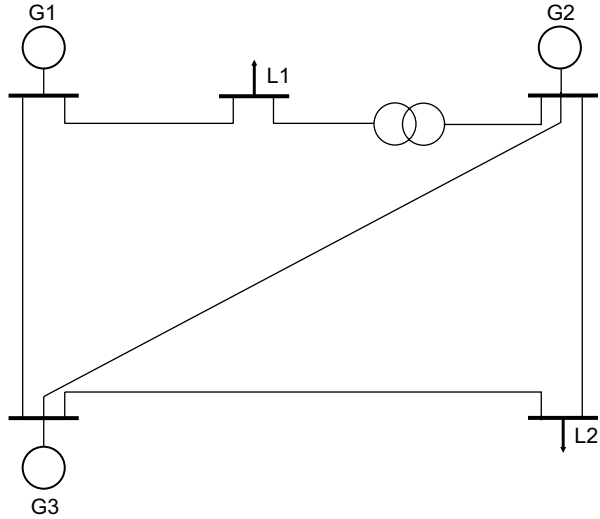
2.3.2 Short-Circuit Currents and REI Nets

Let us consider a typical power system network (Fig. 2.3) and let I , Y and V be the vector of complex injected currents, matrix of complex nodal admittances, and vector of complex bus voltages. The steady-state conditions of this network are given by

$$I = YV \quad (2.1)$$

$$\underline{S}_k = \underline{I}_k^* \underline{V}_k \quad (2.2)$$

Fig. 2.3 Typical power system network



where S_k is the complex power injected into the bus k , I_k^* is the conjugate of the complex current injected into the bus k , and V_k is the complex bus voltage of the bus k . The load buses are numbered sequentially after the generator buses as follows: $1 \dots m \dots G$ generator buses and $i \dots N$ load buses, where, for convenience, $G + 1$ was noted as i .

The standard approach to evaluate the system generators' impact on a specific load bus, let us say the load bus L_1 , is to linearize all the other load buses, i.e., replace the injected currents with constant admittances, include these admittances in the diagonal term of Y , and perform Gauss–Seidel eliminations to reduce the system to a network encompassing only the $1 \dots G$ generator buses and the load bus L_1 . Figure 2.4 shows how the power system network depicted in Fig. 2.3 is “seen” from the load buses L_1 and L_2 .

This process, which allows *seeing* the system generators from any load bus in the power system network, has been used extensively in the voltage stability literature, e.g., (Barbier and Barret 1980) and is known as the *short-circuit currents transformation*. The currents that flow from generators to the load bus in the reduced network are none other than the currents from the bottom equation obtained from Eqn (2.1) after eliminating the linearized buses (Fig. 2.5).

If the bus voltages of the generator nodes are the internal voltages of the generators applied at the ends of their internal reactance (synchronous, transient, etc.), then the two components of the current I_i in Fig. 2.5 are short-circuit currents (permanent, transient, etc.):

- $\Sigma Y_{im} E_{im}$ is the symmetric threephase short-circuit current flowing into the bus i in the case where the voltage $V_i = 0$
- $(\Sigma Y_i + Y_{io})V_i$ is the “no-load short-circuit current” of the bus i and corresponds to the short-circuit current at the bus i if the load current was equal to zero before the short circuit.

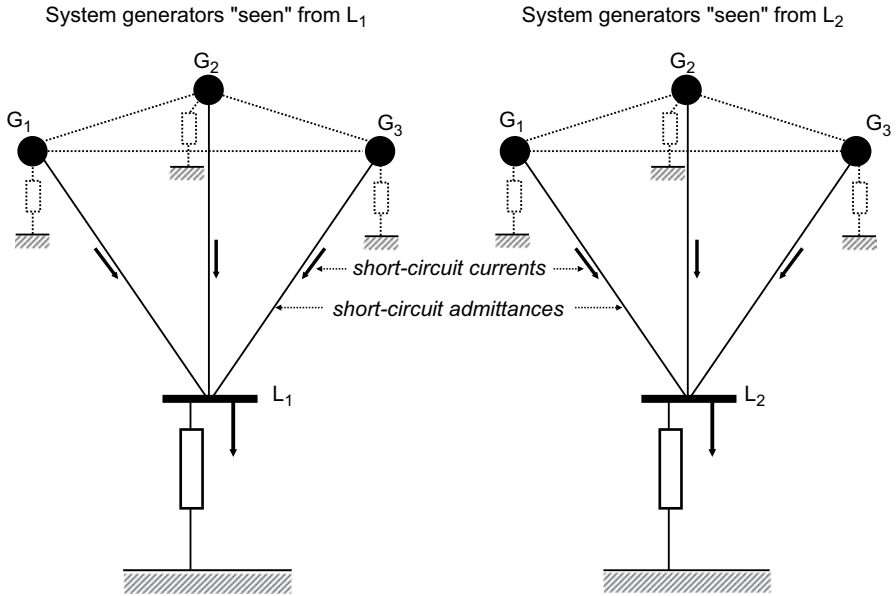
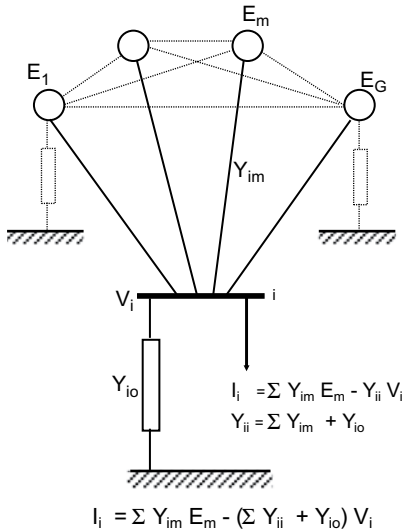


Fig. 2.4 System generators “seen” from load buses

Power system network after retaining only the generators and the study bus i



REI Net representing the generators and the study bus i

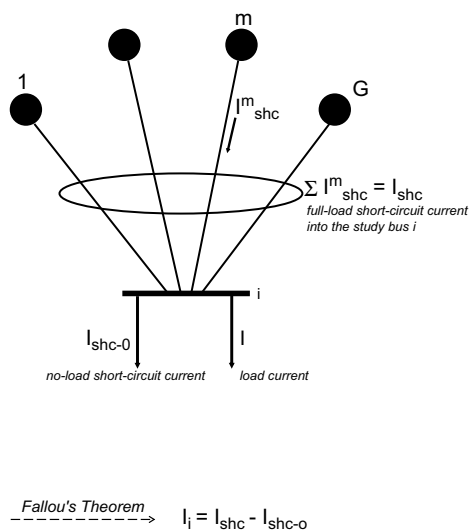


Fig. 2.5 Short-circuit currents and short-circuit admittances. The REI Net

This radial network of short-circuit admittances, or *REI Net*,⁶ in Dimo's terminology (Dimo 1962), is built for a reference state, or base case, for which a load-flow computation has been performed and converged. The base case may depict a peak load case or some other system state involving certain particular features, e.g., high percentage use of hydraulic power, single or multiple line and/or generator contingency, and so on.

The study-bus retained in the model may be actual or fictitious. If it is an *actual load bus* connected *directly* to generators, the machines are "seen" via the short-circuit currents that flow across the actual admittances between generators and load. If the study-bus is an *actual load bus* connected to generators through a typical transmission network, the generator buses are "seen" via short-circuit currents flowing across short-circuit admittances between generators and the load bus.

If the study-bus is a *fictitious load center*, i.e., an equivalent bus where all the system loads have been aggregated by inserting a Zero Power Balance Network and reducing the system to the particular type of REI Equivalent shown in Fig. 2.6, the machines are "seen" via the short-circuit currents that flow across short-circuit admittances between generators and the fictitious load bus.

The generator buses may correspond to either actual synchronous machines or *virtual generators* introduced to model tie-line imports, static VAR compensators (SVCs), Direct Current (DC) injections, etc. It must also be strongly emphasized that in the model built for the purpose of assessing stability, as opposed to a conventional REI Equivalent, *the machines, either real or virtual, must be represented explicitly, and should not be merged into an equivalent generator.*

The REI Net, without introducing any approximations, allows "seeing" the power system network from any bus, either real or fictitious, radially connected with generators via admittances, either actual, i.e., internal generator admittances, or virtual, i.e., short-circuit admittances. As such, it provides a certain amount of information, although rather limited, about the base case for which the short-circuit admittances have been computed.

For example, the module of a short-circuit admittance gives a preliminary indication about the effect of the associated generator on the state of the study-bus. Since, for normal states, the voltages E_m may vary only within a narrow range around the nominal value, it is the short-circuit admittance, i.e., the admittance of the radial branch and the angle across it that have the main impact. Actually, this is a simple way to identify generators and tie-line injections that are negligible when seen from a study bus and to recognize system areas whose impact on the study-bus is significant. The short-circuit admittances' ability to visualize how significant the machines are as seen from a load bus has also been noted by other authors, e.g. Barbier and Barret (1980).

⁶ The REI Net is quite different from the so-called REI Equivalent. The former is a radial network of short-circuit admittances that connect the generators to a specific bus, whereas the latter is a reduced model of the power system where the generators have been aggregated into one or several equivalent generators and the loads have been aggregated into one or several equivalent load centers (Dimo 1968, 1975; Tinney and Powell 1977; DyLiacco et al. 1978; Wu and Narasimhamurti 1979; Oatts et al. 1990; Savulescu 1981).

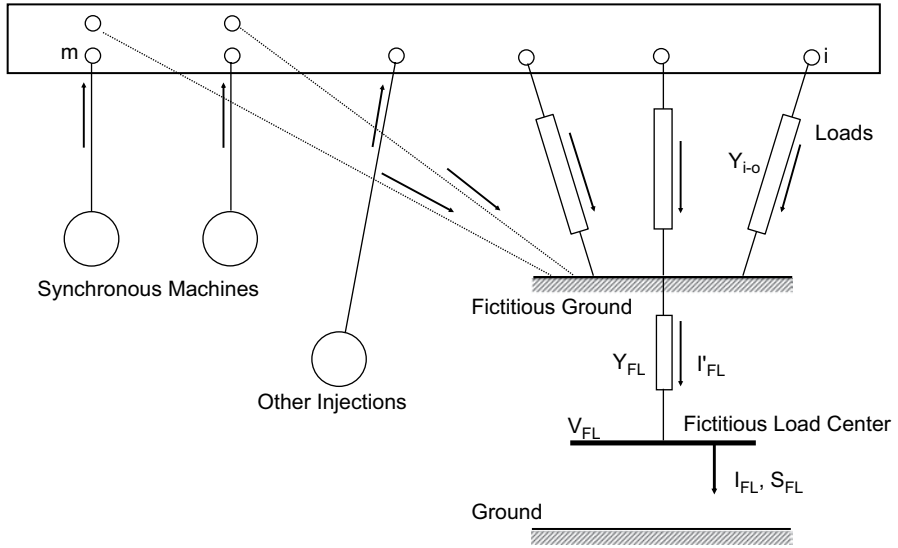


Fig. 2.6 Dimo’s Zero Power Balance Network used to build a fictitious load center

We will return to this topic in Sect. 4.2.2. For the moment, let us just say that the short-circuit admittances can help understand the structure of the transmission system, but not more than that. It is only when the REI Net is associated with its “nodal image” that a large amount of meaningful information can be obtained by simple “visualization.”

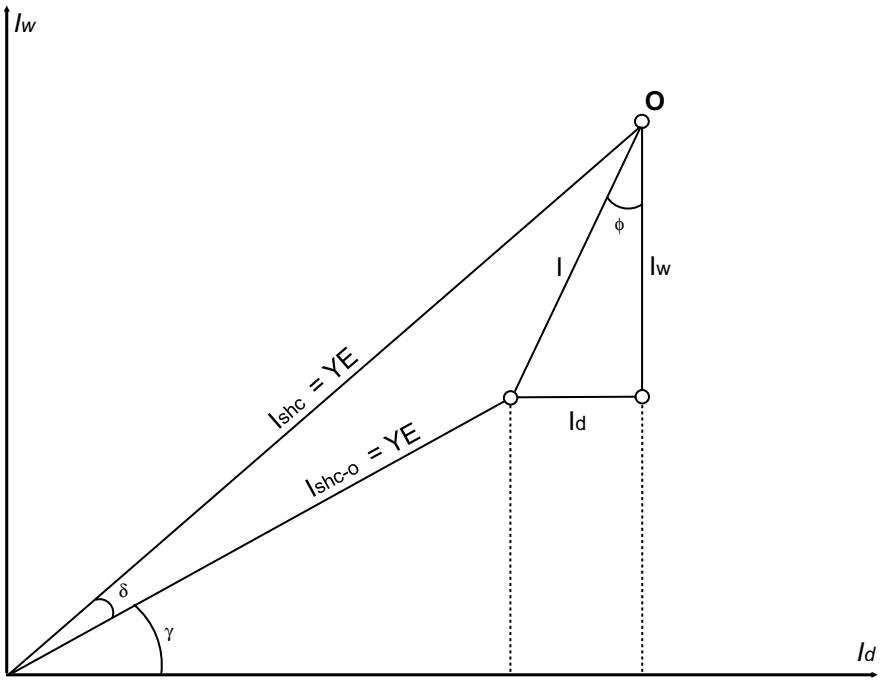
2.3.3 The Nodal Image

The Nodal Image of a bus, either actual or fictitious, is a diagram that shows in detail the short-circuit currents that flow from generators towards that bus across the short-circuit admittances. It is a *vectorial* representation of the short-circuit currents in a system of coordinates defined as follows:

- The ordinate axis is in the direction of the active current I_w .
- The abscissa axis is in the direction of the reactive current I_d .

We will illustrate this concept in two steps—first, an elementary Nodal Image of a synchronous machine connected to a load, then a generalized Nodal Image that can be used to depict the state of any network as “seen” from any actual or fictitious bus.

Let us consider a generator with internal emf and impedance equal to E and Z , respectively, connected at full load to a bus where the voltage has the value V and its phasors are used for reference (Fig. 2.7).



Generator (emf = E) injects the current I into the bus O (bus voltage module = V)

I_{shc} = full-load short-circuit of the generator

I_{shc-0} = no-load short-circuit of the generator

δ = angle between E and V, where V is used as reference

Fig. 2.7 Nodal Image of a synchronous machine connected to a load bus

The symmetric threephase short-circuit current of the generator is given by

$$\underline{I}_{shc} = \frac{E}{Z} = \underline{Y}E \tag{2.3}$$

If the machine was functioning in no-load conditions prior to the short-circuit, its short-circuit current would be given by

$$\underline{I}_{shc-0} = \frac{V}{Z} = \underline{Y}V, \tag{2.4}$$

and with the notation

$$\tan \varphi = \frac{X}{R} \tag{2.5}$$

we have $Z \perp \varphi$ and $Y \perp \varphi$.

By taking V as phase origin and noting with δ the angle between E and V , the full-load current of the machine can be expressed as:

$$\underline{I} = (E \underline{\delta} - V) Y \underline{-\varphi}. \quad (2.6)$$

The complex power on the machine's terminals is given by

$$P + jQ = (E \underline{-\delta} - V) V Y \underline{\varphi} = E V Y \underline{\varphi - \delta} - V^2 Y \underline{\varphi}. \quad (2.7)$$

$$P = Y E V \cos(\varphi - \delta) - Y V^2 \cos \varphi \quad (2.8)$$

$$Q = Y E V \sin(\varphi - \delta) - Y V^2 \sin \varphi. \quad (2.9)$$

With the notations $\gamma = 90^\circ - \varphi$ and $\tan \gamma = \frac{R}{X}$, we get:

$$P = Y E V \sin(\delta + \gamma) - Y V^2 \sin \gamma \quad (2.10)$$

$$Q = Y E V \cos(\delta + \gamma) - Y V^2 \cos \gamma. \quad (2.11)$$

The real, or “watted,” and reactive, or “de-watted,” components of the generator currents are given by

$$I_w = Y E \sin(\delta + \gamma) - Y V \sin \gamma \quad (2.12)$$

$$I_d = Y E \cos(\delta + \gamma) - Y V \cos \gamma, \quad (2.13)$$

respectively, and since YV and YE are the moduli of the of the no-load and full-load short-circuit currents of the generator, respectively, we obtain:

$$I_w = I_{shc} \sin(\delta + \gamma) - I_{shc-0} \sin \gamma \quad (2.14)$$

$$I_d = I_{shc} \cos(\delta + \gamma) - I_{shc-0} \cos \gamma. \quad (2.15)$$

The general case of G generators connected to a load bus, either actual or fictitious, through short-circuit admittances is illustrated in Fig. 2.8.

Simple vectorial algebra manipulations result in the following equations:

$$\Sigma I_{wm} + \Sigma I_{shc-0m} \sin \gamma_m = I_w + \Sigma I_{shc-0m} \sin \gamma_m = \Sigma_{shcm} \sin(\delta_m + \gamma_m) \quad (2.16)$$

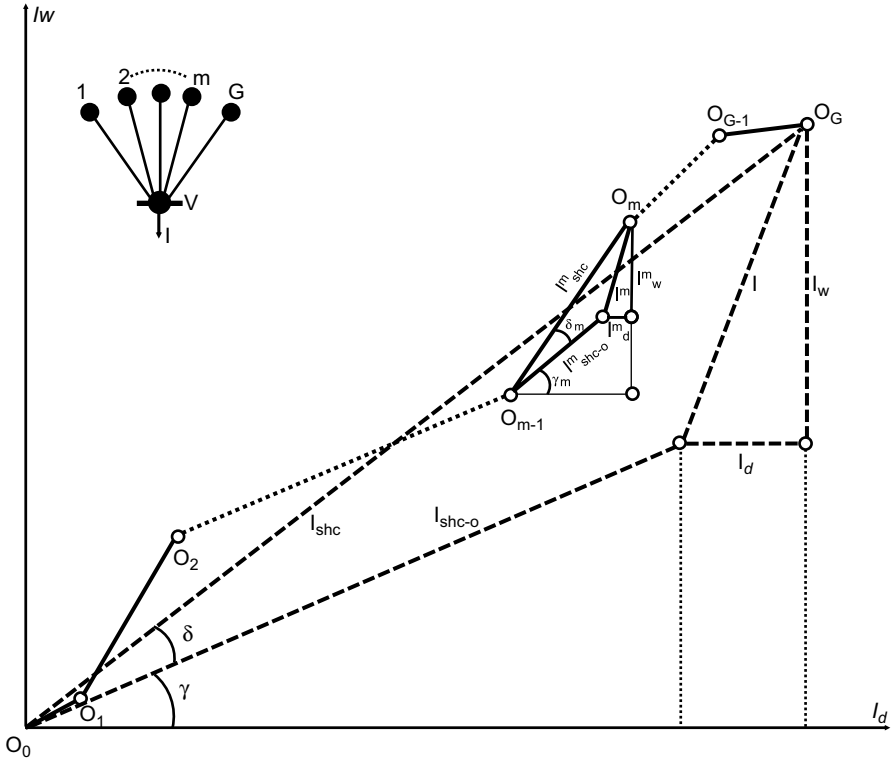


Fig. 2.8 Multiple generators connected to a bus via short-circuit admittances

$$\sum I_{dm} + \sum I_{shc-0m} \cos \gamma_m = I_d + \sum I_{shc-0m} \cos \gamma_m = \sum I_{shcm} \cos(\delta_m + \gamma_m). \quad (2.17)$$

In other words:

- The real component I_w of the total current flowing from generators to the load bus is equal to the sum of the full-load short-circuit currents projections on the ordinate axis minus the sum of the no-load short-circuit currents projections on the ordinate axis.
- The reactive component I_d of the total current flowing from generators to the load bus is equal to the sum of the full-load short-circuit currents projections on the abscissa axis minus the sum of the no-load short-circuit currents projections on the abscissa axis.

With the notations from Fig. 2.8 and remembering that V is the phase origin, the Eqs (16) and (17) can be rewritten as:

$$\underline{I} = \underline{I}_{shc} - \underline{I}_{shc-0} = \sum_m \underline{Y}_m \underline{E}_m - \left(\sum_m \underline{Y}_m + \underline{Y}_0 \right) V. \quad (2.18)$$

In addition to the information about currents and powers, the Nodal Image also provides information about voltages:

- The angles δ_m measure the angle between the phasors E_m and the voltage V , which is used as reference—therefore, the angle differences between the internal voltages of the generators retained in the model can be visualized by simply comparing their full-load short-circuit currents with the no-load short-circuit currents.
- The magnitude of the V voltage is proportional to the projection of the total full-load short-circuit current on the abscissa axis and may be measured by using a conveniently established scale.

Let us note that a generator injection represents an actual current only if the respective branch corresponds to a machine directly connected to the load bus. If this is not the case, the currents calculated with the previous formulae represent the contribution of each machine to the total current injected into the load bus. If similar REI Nets are built for all the load buses, the actual currents injected in generator buses can be calculated by adding the contributions of each generator node to the REI Nets.

Also important is the representation of generators. The base case is obtained from a load-flow calculation by modeling either the high-voltage busbars of the power stations, which is typical in planning studies, or the machine terminals, which is the current practice in real-time and study-mode network analysis as deployed in system operations. But neither approach can represent the *internal admittances* of the generators because, due to the ensuing emf values, which are higher or much higher than 1.0 pu, the load flow would diverge. Stability calculations, however, *must* take into account the behavior of the generators—otherwise, they would be meaningless.

Dimo solved this problem in a simple and elegant way. After the base case has been obtained, but prior to computing the short-circuit currents, the Y matrix is extended with the generators' internal admittances, which may correspond to synchronous reactances or some other reactance.

If synchronous reactances were used, the Nodal Images would give information about permanent short-circuit currents (without regulation) and about the “natural” stability of the system. For steady-state stability studies, where the effect of fast voltage controllers must be reflected, *the generators are represented through transient reactances*. Further details about the representation of generators are provided in the Sect. 3.4.2.

2.3.4 Reactive Power dQ/dV Stability Criterion

2.3.4.1 Exact, Algebraic and Practical Steady-State Stability Criteria

The conventional method of the small oscillations for estimating the steady-state stability (Anderson and Fouad 1990; Sauer and Pai 1990; Venikov 1977) consists of

examining the eigenvalues of the characteristic equation associated with the system of differential equations that describe the free transient processes after a small disturbance takes place in an automatically controlled power system.

The necessary and sufficient condition for steady-state stability is that all the real parts of the eigenvalues be negative (Venikov 1977, p. 216). The analysis encompasses the following steps:

- Describe the transient processes in the form of a system of nonlinear differential equations
- Linearize the equations around the solution point by expanding them into a Taylor series and retaining only the linear (first order) terms
- Calculate the main (characteristics) determinant and its minors and develop the characteristic equation
- Determine the sign of the real roots and the sign of the real part of the complex roots of the characteristic equation.

The approach is laborious and is replaced by determining relationships between the roots and the coefficients of the characteristic equation. Venikov calls these relationships steady-state stability criteria (Venikov 1977, p. 216) and classifies them into *algebraic* (Routh–Hurwitz), *frequency-domain* (Nyquist), and *practical*.

A necessary condition for steady-state stability is derived from the Hurwitz criterion by evaluating the sign of the last term of the characteristic equation, which is the Jacobian determinant D . A change of sign from positive to negative (all Hurwitz determinants are positive) with further loading of the system indicates aperiodic instability. The instability in the form of self-oscillations, however, remains unrevealed by this method (Venikov 1977, p. 138).

If the generators are radially connected to a nodal point, and if, based on practical considerations, it may be assumed that some operating variables are constant, the condition $D=0$ leads to “practical criteria” that are valid within certain limits, for example, the *synchronizing power criterion* $dP/d\delta > 0$, which assumes constant frequency and constant voltage at the nodal point, and the *reactive power voltage and steady-state stability criterion* $dQ/dV < 0$, which assumes that the frequency is constant and the power balance is maintained at the load node (Venikov 1977, p. 138).

At the first sight, the requirement that the network be radial may seem impossible to meet, for power system transmission networks are never radial. However, Dimo recognized that the practical criteria match perfectly with the case of a power system network that has been replaced with an REI Net, which, in fact, is a radial network—not a radial network of physically identifiable admittances, except for the particular case of generators directly supplying a load, but a *radial network of short-circuit admittances connecting the system generators to a central node*. This is the case of both REI Nets built for actual load buses and REI Nets where all the system loads have been aggregated into a fictitious load bus, as shown in Fig. 2.9.

Dimo used the reactive power voltage and steady-state stability criterion $dQ/dV < 0$ in conjunction with the Nodal Image and obtained a simple and efficient

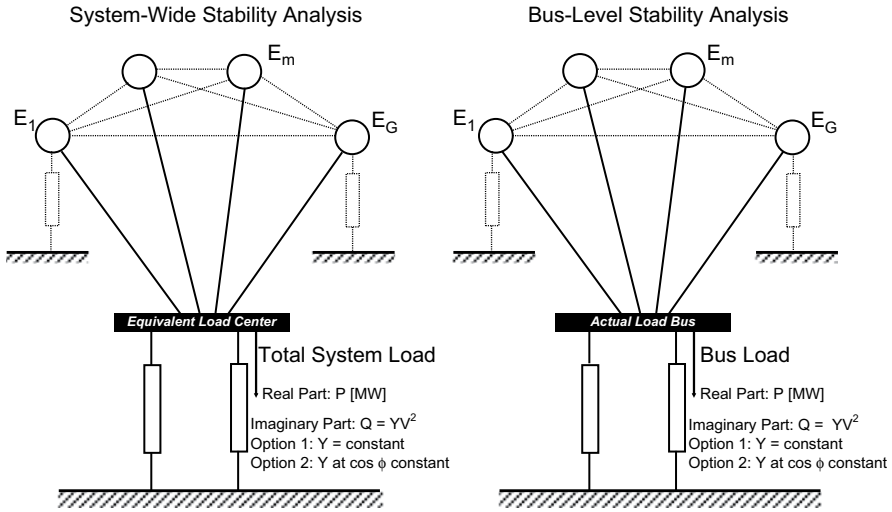


Fig. 2.9 Short-circuit current models for steady-state stability assessment

steady-state stability evaluation algorithm (Dimo 1961, 1975), which is described in detail in Sect. 3.4.4.

But before developing the general expression of Dimo’s formulation of the reactive power voltage and steady-state stability criterion $dQ/dV < 0$, we need to discuss further aspects of generator and load modeling.

2.3.4.2 Modeling the Generators

Two approaches are possible for modeling the machines: representing in detail the excitation control systems, or using approximate models.

In planning studies where system alternatives must be explored in detail, e.g., when simulating past events that have actually occurred, or when developing protection schemes and operating criteria to maintain the power system stability, accurate modeling is necessary and requires detailed generator models. In the initial stages of such studies, though, or in operations planning studies, “simplified models may be adequate for real-time determination of operating limits and for some contingency analysis studies” (IEEE 1990).

The simplest model is the classical model, which consists of a constant voltage $E' = \text{const.}$ behind the transient reactance x'_d (IEEE 1990; Anderson and Fouad 1990; Venikov 1977; Dimo 1975). E' is determined from the pretransient conditions. During the transient condition, the magnitude E' is maintained constant while its angle δ is considered the angle between the rotor position and the voltage V on the machine’s terminals.

As shown by Venikov, machines equipped with forced-action voltage controllers can be modeled as a constant voltage V and $x_{gen} = 0$ (Venikov 1977, pp. 214). Actually, this is how generators are represented, or, rather, *not* represented, in load-flow calculations, where the assumption is implicitly made that the generator bus voltages either at the machine terminals or on the high voltage side of the step-up transformer are and remain constant. In real life, however, these voltages are not constant and some “further constant voltage point must be found, such as the emf behind the synchronous reactance of an alternator” (Barbier and Barret 1980, p. 681).

Taking a more conservative approach, Dimo *always* represents the generators and, depending on how they are modeled, classifies the steady-state stability into “natural stability,” in the absence of voltage regulation, and “artificial stability” if there is voltage regulation (Dimo 1975 p. 129). The natural stability is determined by extending the network with the synchronous reactances, whereas the artificial stability corresponds to the case where the network is extended with the transient reactances of the machines.

Relatively, recent research (Dobson and Liu 1993; Van Cutsem 1993) confirmed these early findings. Accordingly, generators that operate at the reactive power limits under light load conditions will cause the steady-state stability to decrease but not to be destroyed. At sufficiently high loadings, however, encountering the reactive power limits will immediately destabilize the system and precipitate a voltage collapse.

On this basis, an important extension of the original Dimo’s method has been proposed (EPRI 1992/1993; Savulescu et al. 1993) and subsequently incorporated in the fast steady-state stability software documented in (Gonzalez 2003; Avila-Rosales et al. 2004; Savulescu 2004; Tweedy 2004; Avila-Rosales and Giri 2005; Vergara et al. 2005a; Campeanu et al. 2006; Virmani et al. 2007; Vickovic et al. 2009; Arnold et al. 2009; Eichler et al. 2011; Stottok et al. 2013).. It consists of simulating this behavior of the synchronous machine by changing its model from a constant emf E'_d behind the transient reactance x'_d to a constant emf E behind the synchronous reactance x_d when the reactive power at the machine terminals has reached the MVar limit.

2.3.4.3 Modeling the Loads: Voltage Collapse and Dual Power States

Once a steady-state stable power-flow case has been obtained, the next step is to determine *how far* it is from instability. The limit, or critical state, is approached through a series of degraded states where, at each step, the generators produce more power and the bus voltage magnitudes become lower, until the point of voltage collapse is reached.

The results of this system stressing process, which is referred to as “case worsening,” are affected significantly by how the loads have been represented. Three hypotheses can be made about modeling the load: constant admittance; constant P and Q ; and a combination of the two.

Hypothesis 1: Load Modeled as $P=GV^2$ and $Q=BV^2$

Successive load increases cause the real powers flowing from generators into the study-bus to increase until the point of maximum power transfer, while the bus voltage magnitudes get smaller and smaller. Beyond that point, the power supply starts to decrease, the bus voltage continues to drop, and dual power states (same power at different voltages) are obtained. Ionescu and Ungureanu have demonstrated that, in this case, all the states are theoretically feasible, including the dual states, and a steady-state stability limit cannot be obtained (Ionescu and Ungureanu 1981; Ionescu 1993).

Hypothesis 2: Load Modeled as $P=\text{const}$ and $Q=\text{const}$

In this case, the condition stated by the maximum power transfer theorem does correspond to the steady-state stability limit, and the dual states are unstable and have no physical meaning. This hypothesis is rigid and provides conservative results (Ionescu and Ungureanu 1981; Ionescu 1993).

Hypothesis 3: Load Modeled as $P=\text{const}$ and $Q=BV^2$

This hypothesis, which was used extensively by Dimo, implies that the real part of the load does not vary with the bus voltage, and that the reactive component of the load can be represented as a fixed susceptance. This model implies that, while the real power increases, the load's susceptance is maintained constant and a reduction of the bus voltage implies a reduction of the reactive power. In this case, the state associated with the maximum power transfer is critical and occurs when $dQ/dV = 0$.

This model can further be refined by considering that the reactive power of the load varies proportionally with the power factor in the base case. If we note the power factor of the load in the base case with $\tan \varphi_{bc}$, the reactive part of the load for the base case is given by

$$Q_{bc} = P \tan \varphi_{bc} = BV_{bc}^2, \quad (2.19)$$

and the load's susceptance at different values of P [MW] can now be recomputed with formula (20)

$$B = \frac{P \tan \varphi_{bc}}{V_{bc}^2}. \quad (2.20)$$

With the notation, $c_{bc} = \tan \varphi_{bc} / V_{bc}^2$, where c_{bc} is constant, we get:

$$Q = c_{bc} P V^2 \quad (2.21)$$

The formulation (2.21) of Hypothesis 3 corresponds to an average scenario and is well suited for steady-state stability simulations.

2.3.4.4 General Expression of Dimo's Formulation of the Reactive Power Voltage and Steady-State Stability Criterion

As shown in Sect. 3.4.1, the only assumption required to apply the reactive power voltage and steady-state stability criterion to the case of a slow and small variation of the voltage or of the reactive power at a bus connected radially to generators through short-circuit admittances is for the system frequency to be maintained constant (Venikov 1977). In order to build the REI Net and the associated Nodal Image, we start from a solved base case and, then, extend the network with the internal reactances of the generators in accordance with the criteria discussed in Sect. 3.4.2.

When performing a system-wide stability study, all the system loads are aggregated into a single load center as shown in Fig. 2.6. If we perform a bus-level analysis, the study-bus is retained with its actual identity. In either case, the real and reactive parts of the load at the central node of the REI Net are modeled as shown in Fig. 2.9 and in accordance with Hypothesis 3 in Sect. 3.4.3.3.

Dimo derived his version of the dQ/dV criterion for a Nodal Image associated to an REI Net of *reactances*, in which case the angles γ_m in Fig. 2.8 are equal to zero. In the following, we will prove the reactive power voltage and steady-state stability criterion for *the general case*, and then, by substituting $\gamma=0$, we will obtain the original Dimo's formula.

Let us consider an REI Net with n generators. The total real and reactive powers supplied by these machines are:

$$P_g = P_1 + P_2 + \dots + P_n \quad (2.22)$$

$$Q_g = Q_1 + Q_2 + \dots + Q_n, \quad (2.23)$$

and, by using the relationships (10) and (11), the Eqs (2.22) and (2.23) may be written as:

$$P_g = Y_1 E_1 V \sin(\delta_1 + \gamma_1) + Y_2 E_2 V \sin(\delta_2 + \gamma_2) + \dots + Y_n E_n V \sin(\delta_n + \gamma_n) - Y_1 V^2 \sin \gamma_1 - Y_2 V^2 \sin \gamma_2 - \dots - Y_n V^2 \sin \gamma_n \quad (2.24)$$

$$Q_g = Y_1 E_1 V \cos(\delta_1 + \gamma_1) + Y_2 E_2 V \cos(\delta_2 + \gamma_2) + \dots + Y_n E_n V \cos(\delta_n + \gamma_n) - Y_1 V^2 \cos \gamma_1 - Y_2 V^2 \cos \gamma_2 - \dots - Y_n V^2 \cos \gamma_n \quad (2.25)$$

the reactive load being given by

$$Q_l = Y_l V^2. \quad (2.26)$$

Applying the dQ/dV criterion (Venikov 1977, pp. 138–139) to Eqs (2.25) and (2.26), we obtain:

$$\begin{aligned} \frac{dQ}{dV} &= \frac{d(Q_g - Q_i)}{dV} = Y_1 E_1 \cos(\delta_1 + \gamma_1) + Y_2 E_2 \cos(\delta_2 + \gamma_2) + \dots + Y_n E_n \cos(\delta_n + \gamma_n) \\ &\quad - Y_1 E_1 V \sin(\delta_1 + \gamma_1) \frac{\partial \delta_1}{\partial V} - Y_2 E_2 V \sin(\delta_2 + \gamma_2) \frac{\partial \delta_2}{\partial V} - \dots \\ &\quad - Y_n E_n V \sin(\delta_n + \gamma_n) \frac{\partial \delta_n}{\partial V} - 2Y_1 \cos \gamma_1 V - 2Y_2 \cos \gamma_2 V - \dots - 2Y_n \cos \gamma_n V - 2Y_l V. \end{aligned} \quad (2.27)$$

The partial derivatives $\partial \delta_1 / \partial V, \dots, \partial \delta_n / \partial V$ are obtained from Eq (2.10) by considering that the real powers are constant (Hypothesis 3, Sect. 3.4.3.3) and the angles $\gamma_1, \gamma_2, \dots, \gamma_n$ do not depend upon V

$$\frac{dP_1}{dV} = 0 = Y_1 E_1 \sin(\delta_1 + \gamma_1) + Y_1 E_1 V \cos(\delta_1 + \gamma_1) \frac{\partial \delta_1}{\partial V} - 2Y_1 \sin \gamma_1 V \quad (2.28)$$

$$\frac{dP_n}{dV} = 0 = Y_n E_n \sin(\delta_n + \gamma_n) + Y_n E_n V \cos(\delta_n + \gamma_n) \frac{\partial \delta_n}{\partial V} - 2Y_n \sin \gamma_n V, \quad (2.29)$$

whence

$$\frac{\partial \delta_1}{\partial V} = \frac{2V \sin \gamma_1 - E_1 \sin(\delta_1 + \gamma_1)}{E_1 V \cos(\delta_1 + \gamma_1)} \quad (2.30)$$

$$\frac{\partial \delta_n}{\partial V} = \frac{2V \sin \gamma_n - E_n \sin(\delta_n + \gamma_n)}{E_n V \cos(\delta_n + \gamma_n)}. \quad (2.31)$$

By substituting Eqs (2.30) and (2.31) in Eq (2.27), we obtain:

$$\begin{aligned} \frac{dQ}{dV} &= \frac{Y_1 E_1}{\cos(\delta_1 + \gamma_1)} + \frac{Y_2 E_2}{\cos(\delta_2 + \gamma_2)} + \dots + \frac{Y_n E_n}{\cos(\delta_n + \gamma_n)} \\ &\quad - 2 \left[Y_1 \frac{\sin \gamma_1 \sin(\delta_1 + \gamma_1)}{\cos(\delta_1 + \gamma_1)} + \dots + Y_n \frac{\sin \gamma_n \sin(\delta_n + \gamma_n)}{\cos(\delta_n + \gamma_n)} \right] V \\ &\quad - 2(Y_1 \cos \gamma_1 + Y_2 \cos \gamma_2 + \dots + Y_n \cos \gamma_n + Y_l) V, \end{aligned} \quad (2.32)$$

and, with the notation (2.33)

$$Y^Y = Y_1 \sin \gamma_1 \tan(\delta_1 + \gamma_1) + Y_2 \sin \gamma_2 \tan(\delta_2 + \gamma_2) + \dots + Y_n \sin \gamma_n \tan(\delta_n + \gamma_n), \quad (2.33)$$

we obtain the *general expression of Dimo's formulation of the reactive power voltage and steady-state stability criterion*:

$$\frac{dQ}{dV} = \sum_m \frac{Y_m E_m}{\cos(\delta_m + \gamma_m)} - 2 \left(\sum_m Y_m \cos \gamma_m + Y_l + Y^\gamma \right) V. \quad (2.34)$$

If the REI Net branches are approximated through pure reactances, i.e., if $\gamma_1 = \gamma_2 = \dots = \gamma_n = 0$, we get the *original formulation of Dimo's reactive power voltage and steady-state stability criterion* (Dimo 1961., 1977)

$$\frac{dQ}{dV} = \sum_m \frac{Y_m E_m}{\cos \delta_m} - 2 \left(\sum_m Y_m + Y_l \right) V \quad (2.35)$$

2.3.4.5 Distance to Instability: The Case-Worsening Procedure

In voltage and steady-state stability problems, it is *not the base case*, which presumably comes from a fully converged load flow or state estimate, that is of primary importance, since, in most cases, the base case is stable. What really counts is the ability to characterize the system state by its “distance” from an unstable one.

The steady-state stability calculations *per se*, either via simplified techniques such as practical stability criteria or based on detailed simulation, e.g., evaluating the eigenvalues of the Jacobian associated with the system of dynamic equations, would not give such information. In order to find the distance to instability, the steady-state stability calculation must be combined with a “system stressing,” or “case-worsening,” procedure, whereby various system parameters are changed in a direction that is unfavorable to stability.

When using Dimo's methodology, there are several ways to perform case worsening *without* having to recalculate the base case load flow:

- Increase the total generated power to supply successively increased MW load levels—this is achieved by rotating the Nodal Image vectors anticlockwise (trigonometrically) and, as far as the load model is concerned, by considering that the reactive load is modeled by a susceptance that either:
 - has a fixed value, as per Hypothesis 3 in Sect. 3.4.3.3 or
 - varies proportionally with the power factor in the nominal (base) case, as per Eq (21) in Sect. 3.4.3.3.
- Represent the loss of excitation on one or several machines—on the Nodal Image, this is done by reducing the length (module) of the short-circuit currents of the generators.
- Sudden change of the operating conditions of generators that have reached the reactive power limits—if this happens under
 - light load conditions, replacing the transient reactance with the synchronous reactance will cause the steady-state stability to decrease but not to be destroyed.
 - high loadings, the same machine model change may destabilize the system and precipitate a voltage collapse.

Some structural changes can also be simulated on the Nodal Image, for example, adding or removing capacitor banks. But if the network changes are significant, e.g., after single and/or multiple line and/or generator contingencies, a new load-flow solution is required to correctly apply Dimo's technique. Once the new base case has been calculated, the REI Net and the Nodal Image are updated and, then, the steady-state stability index and distance to instability for the new system state are evaluated.

Another situation appears frequently in power systems where, due to specific network topology and load characteristics, significant reactive compensation resources, such as shunt capacitors and MVAR generating units, must be brought on line during peak-load conditions in order to maintain an "adequate" system voltage profile, "adequate" meaning that the bus voltages are sufficiently high to preclude the risk of blackout.

When the same power system operates at medium and light load levels, the reactive compensation goes the other way—capacitors are removed, shunt reactors are reconnected, synchronous condensers and/or units that were running essentially for generating MVARs are taken off-line, and major high-voltage transmission lines are disconnected.

It is obvious that during peak-load conditions, such operating procedures push the network's "maximum loadability," i.e., its steady-state stability limit, at values much higher than the maximum loadability at medium and light load levels. Accordingly, the voltage and steady-state stability calculations should be initiated from different base cases, each one reflecting the structurally different operating scenarios. A fine example that illustrates this situation is described in the reference Vergara et al. (2005).

2.3.4.6 P–V Relationship at the Study Bus

As indicated in Sect. 3.2, the short-circuit current's model has been used extensively in the voltage stability literature to develop power–voltage relationships at load buses. Two references come immediately to mind: the Appendix of Barbier and Barret (1980) and the paper by Ionescu and Ungureanu(1981). The former calculates the critical voltage at the study bus by assuming that the load is modeled as a constant impedance, whereas the later discusses $P = f(V)$ P – V relationship for a network of reactances when the load is represented as per Hypothesis 3 in Sect. 3.4.3.3. In both cases, it is assumed that the voltages at the generator buses are constant, i.e., they correspond to the emf behind some internal generator reactance.

In the following, we will generalize Ionescu and Ungureanu's approach and develop a $P = f(V)$ function for a network of complex admittances with a load $P + jQ$ at the study bus, with Q given by Eq (2.21). In order to simplify the notations, the formula will be initially developed for an elementary REI Net (Fig. 2.7), then it will be extended for the general case.

Let us consider again the Eqs (2.8) and (2.9) and, using (2.21) to express Q as a function of P and V^2 , rewrite them as follows:

$$\frac{P + YV^2 \sin \gamma}{YEV} = \sin(\delta + \gamma) \quad (2.36)$$

$$\frac{c_{bc}V^2P + YV^2 \cos \gamma}{YEV} = \cos(\delta + \gamma). \quad (2.37)$$

By eliminating δ between Eqs (2.36) and (2.37), we obtain:

$$(P + YV^2 \sin \gamma)^2 + (c_{bc}V^2P + YV^2 \cos \gamma)^2 = Y^2E^2V^2, \quad (2.38)$$

then

$$(1 + c_{bc}^2V^4)P^2 + 2P(YV^2 \sin \gamma + c_{bc}YV^4 \cos \gamma) = Y^2E^2V^2 - Y^2V^4. \quad (2.39)$$

With the notations (2.40) and (2.41)

$$A = \frac{YV^2(\sin \gamma + c_{bc}V^2 \cos \gamma)}{1 + c_{bc}^2V^4} \quad (2.40)$$

$$B = \frac{Y^2V^4 \left(\frac{E^2}{V^2} - 1 \right)}{1 + c_{bc}^2V^4}, \quad (2.41)$$

Eq (2.39) can be successively be rewritten as:

$$P^2 + 2PA = B$$

$$P^2 + 2PA + A^2 = B + A^2$$

$$P = -A + \sqrt{B + A^2}.$$

By effecting all the substitutions and algebraic manipulations, we finally obtain the $P = f(V)$ function that expresses the relationship between the power supplied by a generator to a bus and the voltage at that bus

$$P = f(V) = \frac{YV^2}{1 + c_{bc}^2V^4} [-c_{bc}V^2 \cos \gamma - \sin \gamma + \sqrt{(1 + c_{bc}^2V^4) \left(\frac{E^2}{V^2} - 1 \right) + (\sin \gamma + c_{bc}V^2 \cos \gamma)^2}]. \quad (2.42)$$

With the substitution $\gamma=0$, which corresponds to the case of a generator connected to a load through a reactance, e.g., a high-voltage transmission line with resistance practically equal to zero, we obtain the formula developed by Ionescu and Ungureanu in Ionescu and Ungureanu (1981)

$$P = f(V) = \frac{YV^2}{1 + c_{bc}^2 V^4} [-c_{bc} V^2 + \sqrt{\frac{E^2}{V^2} (1 + c_{bc}^2 V^4) - 1}]. \quad (2.43)$$

Formula (2.42) can easily be generalized to relate the voltage V of a bus, where the power P is supplied by $1, \dots, m, \dots, n$ generators with internal voltages $E_1, \dots, E_m, \dots, E_n$ through an REI Net of complex admittances $Y_1 \angle -\varphi_1, \dots, Y_m \angle -\varphi_m, \dots, Y_n \angle -\varphi_n$, with $\gamma_1 = 90^\circ - \varphi_1, \dots, \gamma_m = 90^\circ - \varphi_m, \dots, \gamma_n = 90^\circ - \varphi_n$

$$P_\Sigma = \sum_m \left\{ \frac{Y_m V^2}{1 + c_{bc}^2 V^4} [-c_{bc} V^2 \cos \gamma_m - \sin \gamma_m + \sqrt{(1 + c_{bc}^2 V^4) \left(\frac{E_m^2}{V^2} - 1 \right) + (\sin \gamma_m + c_{bc} V^2 \cos \gamma_m)^2}] \right\}. \quad (2.44)$$

When applying the formula (2.44), it must be remembered that the

- Powers P_m that flow from generators towards the load bus enter the branches of the REI Net *after* the equivalent shunts near the generator buses (Figs. 2.4 and 2.5) and reach the point i (Fig. 2.5) *before* the equivalent shunt $Y_i 0$. In other words, the total power supplied by generators to the study bus covers both the load and whatever shunts resulted after linearizing and eliminating all the other load buses.
- Internal reactances of the generators must be included in the model *after* the load-flow case has been calculated but *before* reducing the system to the REI Net.

2.4 Practical Considerations

2.4.1 Visualization Capabilities of Nodal Images

Dimo used Nodal Images to characterize the power system structure and operating conditions: “Once the network representation has been established, a more general characterization of it can be achieved with the help of the geometry of the resulting Nodal Images. For example, a Nodal Image built for an arbitrary node allows grasping the interdependence between the represented node and every other node retained in the REI Net. The aspect of the vector which appears in the chain composing the vector of the short-circuit current, compared with the resultant vector and with the other component vectors, supplies the necessary indications” (Dimo 1975).

In the following, we will focus on the ability to extract *information* from the results of steady-state stability analysis calculations and, using the Nodal Image analogy, to display the results in graphical formats suitable for use with modern computing technologies.

2.4.2 *Displaying the Results of Steady-State Stability Calculations*

2.4.2.1 **Distance to Instability and Security Margin. Steady-State Stability Reserve**

The search for the steady-state stability limit begins with a Nodal Image for the base case and continues by rotating the chain of vectors in trigonometric sense until dQ/dV becomes positive. The state immediately before instability is called critical state. Once the critical state has been obtained, the security margin is calculated by reversing the case-worsening algorithm and “derotating” the Nodal Image until the system full-load short circuit current vector projection on the ordinate axis becomes equal to, or smaller than, a predefined threshold, e.g. 15% below the critical state.

The angle between the system full-load short circuit current vector in the base case and the system full-load short circuit current vector in the critical state measures the distance to instability. These vectors can be mapped on a *speedometer chart* normalized on a 90°-wide proportional scale where the system state is represented by a *needle* situated between 0°, corresponding to 0 MW, and 90°, which corresponds to instability.

If the security margin MW is also shown on the speedometer, the area between it and the critical MW depicts the set of potentially unsafe operating states, whereas the area to its left corresponds to states where there is no risk of instability.

If the needle’s position maps the value of the dQ/dV derivative rather than the amount of generated MW, a nonproportional scale speedometer is obtained. On this type of speedometer, the needles corresponding to two different system states with the same total MW generation but different dQ/dV values would be shown at different distances from instability. The linear (MW) and nonlinear (dQ/dV) speedometers can be combined on a *two-speedometer* chart, as shown in Fig. 2.10.

This ergonomically powerful representation embodies the *stability envelope* concept illustrated in Fig. 2.2, where the “safe” operating region is shown in green (or blue on the dQ/dV speedometer) and corresponds to system MW grid utilization values smaller than the MW security margin. Let us also note that the red sector does not depict an operating area for the very simple reason that, after instability, a system state would not exist: it is blackout, so there would be no system state any longer.⁷

⁷ Technically speaking, the “red area” should have been just a thin line; however, for ergonomic reasons, it is shown with some depth so that it could be easily identified on the display. Accordingly, for the speedometers in Fig. 2.10, the distance to instability is conveyed by the position of

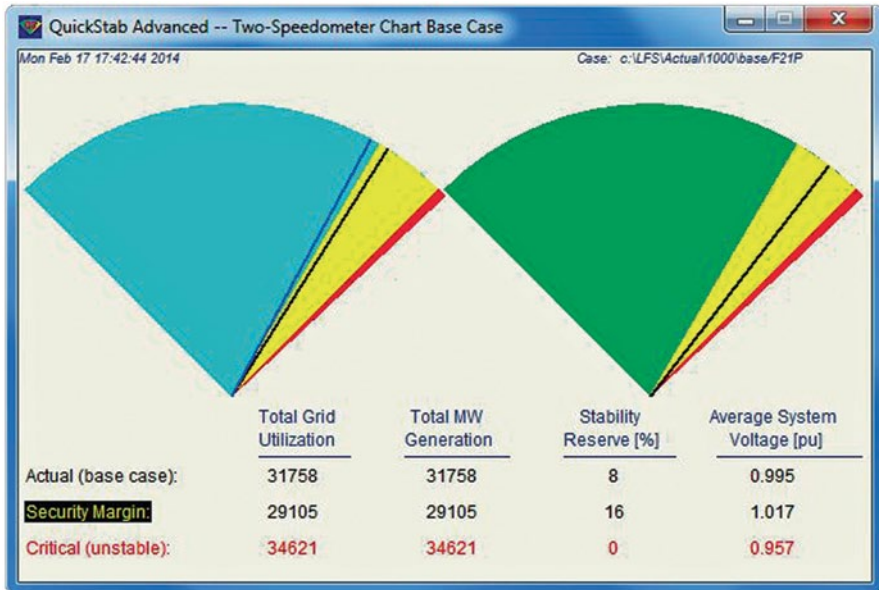


Fig. 2.10 Two-speedometer chart depicting base case system conditions. The *left-hand* speedometer is rated in dQ/dV units whereas the *right-hand* speedometer is rated in MW

Figure 2.11 illustrates a two-speedometer chart where the base case and the worst contingency case, respectively, are represented side by side.

As opposed to the Nodal Image, which requires a thorough familiarity with the theoretical background that substantiates the visualization of system states via short-circuit current vectors, the speedometer charts make it possible to *see*, and instantly evaluate, both how far a system state is from instability and how far it is from the security margin—without reading numbers, and without the need to understand the underlying technology. Furthermore, the speedometer charts facilitate the comparison between different system states and, just through the movement of the needles, allow monitoring the system evolution towards, or away from, instability.

2.4.2.2 Impact of Generators on Steady-State Stability. System-Wide and Bus-Level Unit Ranking

Another capability of the Nodal Image is its ability to show which generators are important and how they impact the steady-state stability of the system, in system-wide analysis, or of the load-bus, in bus-level calculations. For example, a short-circuit current vector that is negligible with respect to the module of the resultant

the needle with respect to the left edge of the red sector and, on the right-hand speedometer, is quantified by the stability reserve below the SSSL.

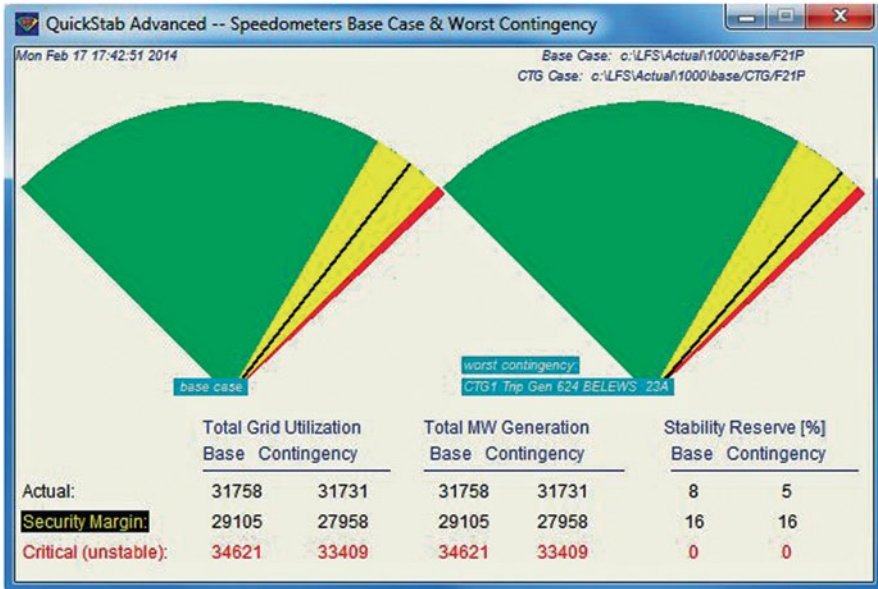


Fig. 2.11 Two-speedometer chart depicting a contingency case developed from the base case conditions shown in Fig. 2.10. Note how the *black needle* has moved to the right, thus indicating that the system’s steady-state stability reserve has decreased

vector and has a small angle corresponds to a machine that has little or no effect upon the bus that is being investigated.

The *unit impact bar chart* illustrated in Fig. 2.12 is built from the information conveyed by the Nodal Image. It depicts the impact of synchronous machines, SVCs, tie-line injections, etc. on the system’s steady-state stability conditions in the *descending order of the normalized values of $Y_m E_m / \cos \delta_m$* .

2.4.3 Real-Time Implementation

At the outset, it is important to define what is actually meant by “real time.” For instance, an application may use real-time input but, due to lengthy calculations, may not be able to converge quickly enough for the results to be used online. This, of course, is not quite ... real-time.

On the other hand, an application that is fast enough to produce real-time results and graphics from real-time input can be implemented in two ways:

- *Seamlessly integrated* with the Supervisory Control And Data Acquisition/Energy Management System (SCADA)/EMS, i.e., executing on the application servers and triggered, automatically, upon event and/or operator request, by the real-time scheduler of the SCADA/EMS system.

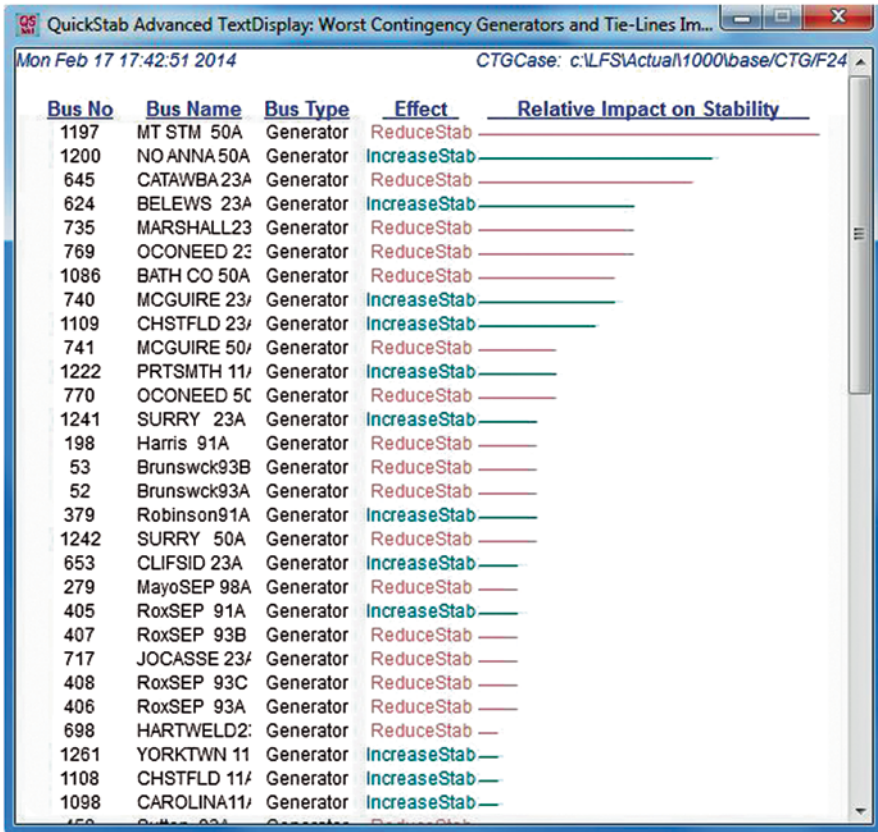


Fig. 2.12 Unit ranking chart. The generators are shown in the order of their impact on the system-wide steady-state stability conditions

- *In parallel* with the real-time system, i.e., using real-time data computed on the SCADA/EMS but running on an off-line processor.

Due to its remarkable solution speed, the steady-state stability assessment technique described in this chapter has been both seamlessly integrated on SCADA/EMS servers and used on off-line processors with state estimation results imported from the real-time system.

Figure 2.13 depicts the early seamless integration of this tool with third-party SCADA/EMS installations. Updated information about the current implementation and use of Siemens Spectrum Power QuickStab is provided in the Chap. 4 of this book (Eichler et al. 2014).

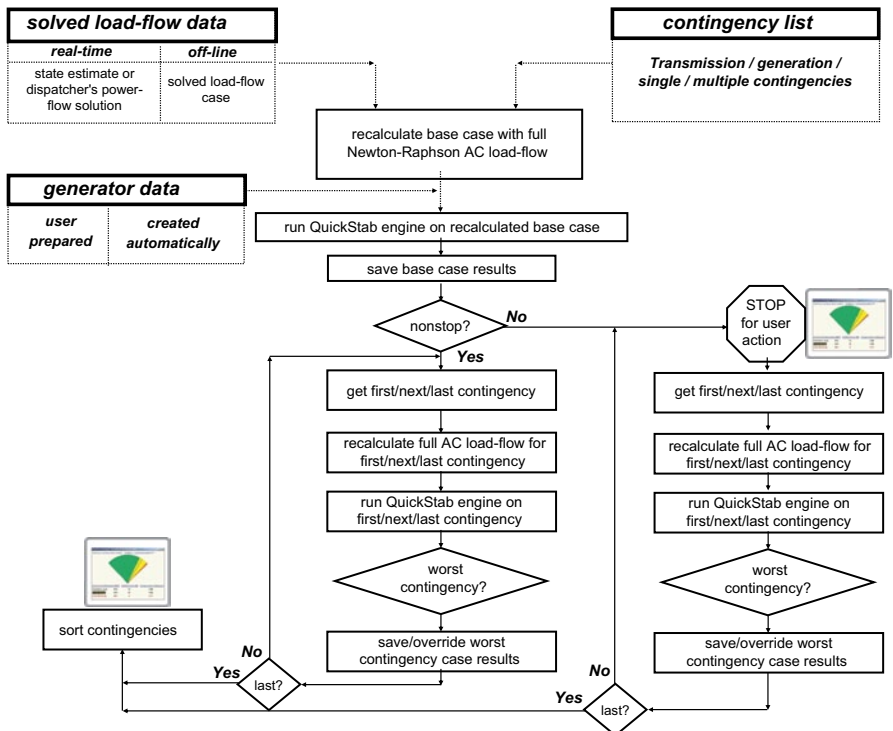


Fig. 2.13 Seamless SCADA/EMS integration of the fast steady-state stability tool

2.5 Conclusions

The main purpose of this chapter was to set the stage for the use of steady-state stability analysis tools to compute the risk of steady-state instability in real time. The approach was illustrated with a field-proven technique that has been successfully deployed in multiple SCADA/EMS installations to assess the power system’s distance to instability both in real time, in conjunction with state estimators, and off-line, with conventional power-flow programs.

The method, inspired from Paul Dimo’s steady-state stability assessment method, determines quickly and reliably how far the transmission network is from a state where voltages may collapse and units may lose synchronism.

The underlying assumptions were extensively analyzed and their validity was substantiated. For the theoretically oriented reader, this chapter also included the detailed development of the generalization of Dimo’s formulation of the reactive power steady-state stability criterion, and an extension of the $P = f(V)$ relationship for the case where the bus loads are modeled as $P + jQ$, rather than constant impedances, and their reactive parts vary proportionally with the power factor in the nominal (base) case.

Both the theoretical analysis and the actual implementation experience, including accuracy and validity tests performed in several control centers, which are summarized in Chap. 3 of this book, point to a mandatory tool for the online computation and monitoring of the distance to instability.

Acknowledgement The display pictures shown in Fig. 2.10 through 2.13 have been provided by and used with permission from Siemens AG, Nuremberg, Germany.

References

- Anderson PM, Fouad AA (1990) Power system control and stability. Iowa University Press, Ames
- Arie E, Pomarleanu M, Bejuscus L, Botgros M (1973) Determinarea Rezervei de Stabilitate Statica a Sistemelor Electroenergetice Complexe, Studii Èi Cercetari de Energetica si Electrotehnica, Tom 23, Nr. 3, pp 709–727, Bucharest, Romania, 1973
- Arnold L, Hajagos J, Manassis SM, Philip A (2009) LIPA implementation of real-time stability monitoring in a CIM compliant environment. In: Savulescu SC (ed) Real-time stability assessment in modern power system control centers. Wiley, New York
- Avila-Rosales R, Giri J (2005) Wide area control for more reliable operation of the power system grid. In: Savulescu SC (ed) Real time stability in power systems. Springer, Norwell
- Avila-Rosales R, Giri J, Lopez R (2004) Extending EMS capabilities to include on-line stability assessment. Paper 04PS0371 presented at the real-time stability challenge panel session, power systems conference and exposition 2004, New York, 10–13 Oct 2004
- Barbier C, Barret JP (1980) An analysis of phenomena of voltage collapse on a transmission system. *Rev Gén Electr* 89(7):3–21
- Campeanu HS, L’Helguen E, Assef Y, Vidal N, Savulescu SC (2006) Real-time stability monitoring at transelectrica. Paper PSCE06–1288 presented at the real-time stability applications in modern SCADA/EMS panel, IEEE power systems conference & exposition 2006 (IEEE PSCE’04), Atlanta, October 29–November 2, 2006
- Crary SB (1945) Power system stability. General Electric Series. Wiley, New York. (Copyright 1945, Third Printing October 1955)
- Dimo P (1961) Etude de la stabilité statique et du réglage de tension. *Rev Gén Electr* 70(11):552–556
- Dimo P (1962) L’Analyse des réseaux d’énergie par la méthode nodale des courants de court-circuit. L’image des noeuds. *Rev Gén Electr* 71:151–175
- Dimo P (1968) Nodal analysis of electrical power systems (Romanian edition), Editura Academiei, Bucharest
- Dimo P (1975) Nodal analysis of power systems. Abacus, Kent
- Dimo P, Manolescu G, Iordanesscu I, Groza L, Ionescu S, Albert H, Moraite G, Ungureanu B (1971) Computation and design of electrical energy systems (Romanian edition), Editura Tehnica, Bucharest, pp 200–201
- Dobson I, L. Liu (1993) Immediate change in stability and voltage collapse when generator reactive power limits are encountered. In: Fink LH (ed) Proceedings of international seminar on bulk power system voltage phenomena II. ECC, Virginia, pp 65–74
- DyLiacco TE, Savulescu SC, Ramarao KV (1978) An on-line topological equivalent for a power system. *IEEE Trans Power Appar Syst* PAS-97(9): 1550–1563
- Eichler R, Krebbs R, Savulescu SC, Wache M (2011) Early detection and mitigation of the risk of blackout (co-author). Paper presented at CIGRE international symposium “The Electric Power System of the Future—Integrating Supergrids and Microgrids in Transmission Grid Operation”, Bologna, Italy, 13–15 Sept 2011

- Eichler R, Heyde CO, Stottok BO (2014) Composite approach for the early detection, assessment and visualization of the risk of instability in the control of smart transmission grids, real-time stability in power systems, 2nd edn. Springer, New York
- EPRI (1992/1993) Power system steady-state stability monitor prototype. Final report EPRI TR-100799, July 1992. and Power system steady-state stability monitor, final report EPRI TR-103169, Dec 1993
- EPRI (1992) VSTAB voltage stability analysis program, final report, RP3040-1, Electric Power Research Institute, Sept 1992
- Erwin SR, Oatts ML, Savulescu SC (1994) Predicting steady-state instability. *IEEE Comput Appl Power* 4(7):15-22
- Gonzalez LA (2003) Post-facto analysis of a near-blackout event, 7th international workshop on power control centers, Orisei, Italy, 26-28 May 2003
- IEEE (1982) PES task force on terms and definitions, proposed terms and definitions for power system stability. *IEEE Trans Power Appar Syst* PAS-101(7):1894
- IEEE (1990) Guide for synchronous generator modeling practices in stability analysis, PES Publication P1110/D11 sponsored by the Joint Working Group on determination and application of synchronous machine models for stability studies, May 1990
- IEEE/CIGRE (2004) IEEE/CIGRE joint task force on stability terms and definitions, definition and classification of power system stability. *IEEE Trans Power Syst* 19(2):1387-1401
- Ionescu S (1993) Discussion of the paper fast steady-state stability assessment for real-time and operations planning. *IEEE Trans Power Syst* 8(4):1557-1569
- Ionescu S, Ungureanu B (1981) The dual power states and voltage collapse phenomena. *Rev Roum Sci Tech, Série Electrotech Energ* 26(4):545-562
- Kundur P (1999) Introduction to techniques for power system stability search. A special publication of the power system dynamic performance committee of the IEEE PES, TP-138-0, pp 1-3
- Kundur P, Morison GK (1993) Classes of stability in today's power systems. *IEEE Trans Power Syst* 8(3):1159-1171
- Magnien M (1964) Rapport spécial du Groupe 32 Conception et Fonctionnement des Réseaux. Conférence Internationale des Grands Réseaux Electriques À Haute Tension, CIGRE Session 1964
- Moraite G, Ionescu S, Feldmann S, Chenzbraun I (1966) Problèmes soulevés par la stabilité statique des réseaux bouclés. Conférence Internationale des Grands Réseaux Electriques À Haute Tension, CIGRE Session 1966
- Morison K, Wang L, Kundur P, Lin Xi Gao W, He C, Xue F, Xu T, Xu J, Xue Y (2004) Critical requirements for successful on-line security assessment. Paper presented at the real-time stability challenge panel session, power systems conference and exposition 2004, New York 10-13 Oct 2004
- Navarro-Perez R, Prada RB (1993) Voltage collapse or steady-state stability limit. In: Fink LH (ed) Proceedings of international seminar on bulk power system voltage phenomena II. ECC, Virginia, pp 75-84
- NERC (1996) Available transfer capability definitions and determination, North American Electric Reliability Council, June 1996
- NERC (2000) Policy 9—Reliability coordinator procedures, Version 2, approved by Board of Trustees, Feb 7, 2000
- Oatts ML, Erwin SR, Hart JL (1990) Application of the REI equivalent for operations planning analysis of interchange schedules. *IEEE Trans Power Appar Syst* PAS-109(5):547-555
- Sauer PW, Pai MA (1990) Power system steady-state stability and the load-flow Jacobian. *IEEE Trans Power Syst* 5(4):1374-1381
- Savulescu SC (1981) Equivalents for security analysis of power systems. *IEEE Trans Power Appar Syst* Pas-100(5):2672-2682
- Savulescu SC (2004) A metric for quantifying the risk of blackout. Paper 04PS0294 presented at the real-time stability challenge panel session, power systems conference and exposition 2004, New York, 10-13 Oct 2004

- Savulescu SC, Oatts ML, Pruitt JG, Williamson F, Adapa R (1993) Fast steady-state stability assessment for real-time and operations planning. *IEEE Trans Power Syst* 8(4):1557–1569
- Stottok BO, Heyde CO, Eichler R, Savulescu SC (2013) Visualizing the risk of blackout in smart transmission grids (co-author). Paper presented at CIGRE international symposium “Smart grids: next generation grids for new energy trends”, Lisbon, Portugal, April 2013
- Tinney WF, Powell WI (1977) The REI approach to power network equivalents, PICA’77 conference, Toronto, Canada, May 1977
- Tweedy J (2004) Assessing stability conditions to evaluate the risk of blackout. A real-time indicator based on field-proven techniques, *Transmission and Distribution*, June 2004, pp. 622–628
- Van Cutsem Th (1993) Voltage collapse mechanisms—a case study. In: Fink LH (ed) *Proceedings of international seminar on bulk power system voltage phenomena II*. ECC, Virginia, pp 85–102
- Venikov VA (1977) *Transient processes in electrical power systems*. Stroyev VA (ed), English Translation, MIR, Moscow
- Venikov VA, Stroev VA, Idelchick VI, Tarasov VI (1975) Estimation of electrical power system steady-state stability. *IEEE Trans Power Appar Syst* 94(3):1034–1041
- Vergara JS, Thai TA, Cuong ND, Nam NT, Campeanu HS, Savulescu SC (2005) Accuracy testing and real-time implementation of Dimo’s stability analysis technique. In: Savulescu SC (ed) *Real-time stability in power systems*. Springer, Norwell
- Vickovic D, Eichler R (2009) Real-time stability monitoring at the independent system operator in Bosnia and Herzegovina. In: Savulescu SC (ed) *Real-time stability assessment in modern power system control centers*. Wiley, New York
- Virmani S, Vickovic D, Savulescu SC (2007) Real-time calculation of power system loadability limit. Paper no. 576 presented at the Powertech 2007 conference, Lausanne, Switzerland, 1–5 July 2007
- Vournas CD, Sauer PW, Pai MA (1996) Relationships between voltage and angle stability of power systems. *Electr Power Energy Sys* 18(8):493–500
- Wu FF, Narasimhamurti N (1979) Necessary conditions for REI reduction to be exact. *IEEE PES winter meeting 1979*, Paper A 79 065–4

Chapter 3

Practical Aspects of Steady-State Stability Assessment in Real-Time

José Santos Vergara Perez, Tran Anh Thai, Nguyen Duc Cuong,
Horia S. Campeanu and Savu C. Savulescu

Abstract Amid the many practical aspects of performing steady-state stability assessment in real time, this chapter addresses the: accuracy testing of the approach, tracking of the distance to instability on Supervisory Control And Data Acquisition (SCADA) trending charts, and the ability to compute the instantaneous voltage and angle stability sensitivities by using Phasor Measurement Unit (PMU) data. The validation of the stability reserve predicted by the stability software and its tracking on SCADA trending charts are illustrated with actual examples taken directly from early QuickStab user sites prior to the June 2010 acquisition of this software by Siemens AG, Nuremberg, Germany. The use of phasor measurements, which, although conceptually different from the conventional SCADA data model, can help assess the voltage and angle stability sensitivities when large blocks of power are transferred across long transmission lines, is exemplified by a successful experiment conducted in Vietnam. Additional considerations are provided to make the case for deploying steady-state stability tools in real time.

S. C. Savulescu (✉)
Energy Consulting International, Inc., 405 Lexington Avenue, 26th Floor,
New York, NY 10174, USA
e-mail: savu@eciscs.com

J. S. V. Perez
Empresa de Transmisión Eléctrica, S.A., Panama, USA

T. A. Thai
Advanced Technical Systems Co., Ltd., Hanoi, Vietnam

N. D. Cuong
National Power Transmission Corporation, Hanoi, Vietnam

H. S. Campeanu
ISPE, Bucharest, Romania

3.1 Introduction

Speed, reliability, and ease of use are key requirements that any software meant to run in a control center must meet. These attributes are even more critical for programs that perform complex algorithms and entail extensive user interaction, e.g., network analysis applications such as load flow and state estimation. Stability assessment is no exception. In order to qualify for being deployed in real time, the stability software must, of course, be fast, reliable, and easy to use—but, unlike other network analysis applications, which fit naturally in a SCADA/EMS, it invites special scrutiny to appraise its ability to identify, quantify, and visualize the *stability limits*, as opposed to just determining whether a given condition is stable or unstable.

Many, if not most, stability programs available until a few years ago, would not pass this test. They “determine whether a given condition is stable or unstable, [but] have not been efficient in quickly and automatically determining the stability limits” (Kundur 1999).

Actually, Professor Kundur’s statement was an understatement, in the sense that the very concept of “stability limit” he was talking about was used loosely and without being quantified not only in this widely quoted reference but also in the vast majority of the papers available at that time and/or published afterwards.

So, then, what *is* “stability limit?”

Theoretically, it is a local property of the system state vector: For each new system state, there are one or several stability limits. Simply stated, “stability limits” exist, are not fixed, and change with the total MegaWatt (MW) system grid utilization,¹ voltages, topology, and the path (trajectory) followed to approach them. Due to their changing nature and assuming that a metric has been defined to quantify them, the “stability limits” need to be recomputed *quickly* and *as often as possible*. This is because, when the system is close to instability, the collapse happens instantly and leaves no time to react.

Therefore, in addition to a *metric* that would *quantify* the stability limits, there is also a need to *rapidly reevaluate* such limits—after each state estimate and after each load flow. In fact, North American Electric Reliability Corporation’s (NERC) Policy 9 (NERC 2000) required that reliability coordinators compute the “stability limits” for the current and next-day operation processes to “foresee whether the transmission loading progresses or is projected to progress beyond the operating reliability limit.”

Was this being done after NERC released its injunction?

The wave of blackouts that affected US, UK, and mainland Europe utilities in 2003 and 2004 suggests that this was not the case, perhaps because detecting thermal and voltage violations was straightforward whereas defining, identifying, and

¹ When the system is importing power, the total MW system grid utilization is calculated by summing up the total MW generation with the total imported MW; when exporting power, the total MW system grid utilization is the total generated MW. In other words, this number shows how many MW are currently “circulating” in the transmission system.

computing stability limits in real time were an altogether different problem that conventional stability methods did not and could not solve. Moreover, since dispatching a power system without knowing its actual stability limit was like walking on thin ice, a “fresh” approach to this difficult challenge was needed.

Actually, such a “fresh” approach had already been at hand since the early 1960s under the umbrella of *steady-state stability*, as this paradigm was understood at that time, and consisted of determining the *stability reserve*, i.e., the distance from any given operating point to the state where voltages may collapse and units may lose synchronism, by alternately evaluating a steady-state stability criterion and computing successively worsened system states. Although the speed, precision, and potential for visualization of this solution technique² were known for a long time (Magnien 1964; Moraite et al. 1966; Dimo 1975), a true production-grade implementation of this technology became available only in 1994 with the advent of QuickStab®.³

At the outset, however, let us make it clear that by “steady-state stability” we refer to the *classical concept* described by Crary (1955), Anderson and Fouad (1990), and IEEE (1982), as opposed to “small-signal stability” as it is understood nowadays (IEEE/CIGRE 2004). The appeal of steady-state stability paradigm is unique. By using the *practical stability criteria* (Venikov 1977) in conjunction with a conveniently designed network equivalencing scheme (Dimo 1975), it allows quantifying the system-wide stability index called *stability reserve*, local sensitivities $\Delta V/\Delta P$ and $\Delta\delta/\Delta P^4$ that apply explicitly, without system reduction, to selected topologies such as long transmission lines that accommodate the transfer of significant blocks of MW power.

In the following, from the myriad of practical issues related to performing steady-state stability assessment in real time, we will address just three important aspects:

- Accuracy testing and validation of the software tool that implements the steady-state stability algorithm, which, in this case, is Dimo’s method.
- Integration of the stability software, in this case QuickStab, with a third-party SCADA/EMS and the real-time tracking of the stability reserve on SCADA displays and trending charts.

² Introduced by Paul Dimo in 1961 (Dimo 1961) and addressed extensively in Savulescu (2005, 2009) and related references.

³ Introduced in 1994 by Savu C. Savulescu, this software was first deployed in real time at Companhia de Transporte de Energia Elétrica de São Paulo (CTEEP) in 1999. Continuously improved solutions followed at OPSIS (Venezuela), ETESA (Panama), Transelectrica (Romania), Independent System Operator in Bosnia and Herzegovina, Transmission System Operator of Serbia, AzerEnerji (Azerbaijan) and LIPA (New York, USA), and were documented in Savulescu (2004, 2009a), Campeanu et al. (2006), Virmani et al. (2007), Arnold and Hajagos (2009), Vickovic and Eichler (2009). This tool is now owned by Siemens and its commercial name is *Siemens Spectrum Power QuickStab*. The software is seamlessly integrated with the Spectrum Power SCADA/EMS platform and SIGUARD® Dynamic Security Assessment suite.

⁴ Not to be confused with the dP/dV and $dP/d\delta$ “practical steady-state stability criteria” (Venikov 1977; Dimo 1975; Savulescu 2005, 2009b).

- Use of the phasor measurements provided by Phasor Measurement Units (PMUs) deployed at both ends of a long transmission line to compute explicitly, without using state estimation results, the steady-state stability of the MW transfer across the line.

3.2 Accuracy Testing and Validation

3.2.1 Background

The very nature of stability applications makes it difficult, if not impossible, to check the accuracy of their predictions: Conceptually, it is not possible to depict instability, which is a system state that does not exist. In the case of QuickStab, further complexities arise if one attempted to compare it with conventional stability applications. This is because QuickStab computes the *distance to instability*, whereas conventional stability programs can only say whether the system is stable or not but *do not quantify* the distance to the state where voltages would collapse and generators would lose synchronism.

Recognizing the need to thoroughly test the application before relying on it, the National Dispatch Center (CND) of Empresa de Transmisión Eléctrica S.A. (ETESA), Panamá, where, in 2002, QuickStab was deployed in real time on the SCADA/EMS by Bailey Network Management, Inc. (today Ventyx-ABB, Inc.), and the National Load Dispatch Center (NLDC) of Vietnam Electricity (EVN), Vietnam, where QuickStab has been used off-line since 2004 in system dispatching and operations planning functions, used a systematic approach to perform accuracy and consistency tests.

3.2.2 Load Flows and Instability

It is well known that near the stability limit of a power system, voltages are low and load flows may diverge (Venikov et al. 1975). However, a nonconverging load flow does not necessarily imply system instability. It was demonstrated that the system load where the load flow diverges is just an upper bound, for one or several units may lose synchronism before that point (Sauer and Pai 1990; Vournas et al. 1996).

The situation is quite interesting. On the one hand, “for voltage collapse and voltage instability analysis, any conclusions based on the singularity of the load-flow Jacobian would apply only to the voltage behavior near the state of maximum power transfer. Such analysis would not detect any voltage instabilities associated with synchronous machines characteristics and their controls” (Sauer and Pai 1990, pp. 1380).

On the other hand, running load flows at increasingly high load levels until divergence is the only way to obtain a base case near the limit of stability, which

then could be used as a starting point by stability assessment tools to perform voltage, steady-state, and/or transient stability checks. This suggests that by alternately performing load-flow calculations and stability checks, one can verify, at least approximately, that the system conditions predicted at, or near, instability correspond to an unsolvable state.

3.2.3 Methodology

The QuickStab accuracy testing procedure, which can be used to validate any type of stability software that has the ability to quantify stability limits, involves using QuickStab in conjunction with a pair of reliable load flow and transient stability programs (in this case, the Siemens PTI PSS/E) as follows.

Given a state estimate or a solved load-flow solution of a power system network, QuickStab computes, in addition to several other indicators, the total MW system grid utilization and the MW generation schedules for the:

- *Critical state* where voltages collapse and units may lose synchronism
- *Security margin* state that corresponds to a user-defined $x\%$ security margin, typically 15% below the critical state

The goal is to demonstrate that critical states are indeed critical, and that the $x\%$ parameter, e.g., 15%, used for the security margin is adequate.

The critical MW is not a fixed, permanent constant. It depends upon the topology, reactive compensation, and voltage schedules in the system state being evaluated. It is larger if the case entails high bus voltages and large amounts of reactive sources, and it is smaller when voltages are lower and the reactive sources are fewer. Therefore, the validation must encompass both normal and contingency system states over a broad range of system load, network topology, bus voltages, and reactive compensation scenarios.

3.2.3.1 Testing the Accuracy of the Critical State Predictions

When running a load-flow calculation with the MW generation schedules computed for the critical state, one of the following mutually exclusive outcomes should be expected:

- a. The load-flow solution converges and either produces a state that QuickStab identifies as being critically stable⁵ or, by slightly further increasing the load, produces an unstable state.
- b. The load-flow solution produces a state that QuickStab finds to be unstable.
- c. The load flow diverges, in which case the generation of MW schedules has to be reduced until a proper solution has been obtained.

⁵ In QuickStab parlance, a state is “critically stable” if its steady-state stability reserve is $< 1\%$.

Therefore, the idea is to compare the stability limits *predicted* for the base case with the stability limits *actually computed* from a load-flow solution that is known to be near instability and to repeat the procedure for different system MW and voltage levels.

Step 1 of the testing procedure entails solving a base caseload flow for peak-load level conditions.

Step 2 consists of running QuickStab for the base case and then retrieving the:

- MW output of the generators for the critical state
- MW output of the generators for the security margin state corresponding to a steady-state stability reserve of 15%

Step 3 entails running a new load flow, called “critical state load flow”, by using the generators’ MW predicted for the critical state in the base case. If the critical state load-flow converges, then:

- Run QuickStab—the expectation is that this case will be found either unstable or critically stable
- Increase the slack-bus generation while maintaining the critical state MW schedules and run new load flow(s) until the load-flow program diverges
- Run QuickStab for the system conditions produced by the most recent converged load flow—this case should be found unstable

If the critical state load flow diverges, reduce the slack-bus generation in small increments until convergence has been reached, then:

- Run QuickStab again—this case should be found either unstable or critically stable.
- Reduce by 1% the total generation and run a new load flow, then execute the stability calculations—this case should be found either critically stable or stable but close to the stability limit.

Since at smaller MW grid utilization levels, which entail less reactive compensation, the stability limits are expected to be lower, the Steps 1 through 3 should be repeated for medium–high and medium–low load levels.

3.2.3.2 Validating the Security Margin

The security margin state corresponds to a *safe* total MW system grid utilization, or *security margin*, such that, for any system state with a stability reserve smaller than this value, no contingency, either single or multiple and no matter how severe, would cause transient instability (Magnien 1964; Moraite et al. 1966; Savulescu 2005). The security margin is related to the stability limit associated with a particular system state and is a by-product of the computations described in Sect. 3.3.1. The accuracy of its prediction can be validated as follows:

- Calculate “security margin load flows” by using the generators’ MW schedules predicted by QuickStab for peak, medium–high, and medium–low load cases.
- Run QuickStab for the “security margin load flows” and compare the results.

Please note that, just like the critical MW system grid utilization, the security margin, expressed as a percentage below the critical MW, is not a universal constant. It depends upon the specific combination of topology, load amounts and locations, generators, and reactive compensation, and must be determined and periodically reassessed for each particular transmission system through extensive transient stability simulations.

The expected outcomes of such transient stability calculations are as follows:

- a. For load-flow cases with total MW system grid utilization levels *higher than the security margin*, at least one fault or contingency should result in transient instability.
- b. For load-flow cases at the *critical MW* level, all the faults and contingencies cases should be unstable.
- c. For load-flow cases where the system MW load is *equal to, or below the security margin*, all the fault and contingency cases should be stable.

However, transient stability calculations are time consuming and require significant effort to prepare the data and set up the study cases. If, for practical reasons, the accuracy testing must be kept to a reasonable level, a shorter computational sequence can be followed as follows:

- Identify a relatively small number of faults and contingencies *known a priori* to correspond to worst-case scenarios.
- Perform transient stability calculations for the base case and the security margin state in the peak-load scenario—skip the critical state because, most probably, all the faults and contingencies would result in transient instability anyway.
- Repeat the procedure for medium–high and medium–low load-level scenarios and run transient stability for the critical states as well.

3.2.3.3 Accuracy Testing for Line Contingency Scenarios

The theory predicts that, during line contingencies, the system gets closer to its stability limit—when lines trip, the overall system equivalent reactance increases and, accordingly, the steady-state stability reserve decreases. If the procedure for testing the accuracy of the critical state predictions was repeated for a contingency case, one should expect that the critical MW in the contingency case would be lower than the critical MW in the base case, i.e., the contingency case would have a smaller steady-state stability reserve and the same should be true for the security margin, too.

Therefore, in order to verify the accuracy of the stability limits predicted for a contingency case, the same validation suite, as executed for a specific load level in the base case, must be repeated by starting at the same load level but from a new

base case that corresponds to a major line contingency. The procedure is then repeated for other contingencies and load-level scenarios.

3.2.4 *The Panamanian Experience*⁶

Until recently, ETESA's CND was equipped with a SCADA/EMS⁷ that incorporated, in addition to an extended array of network analysis functions, a real-time version of QuickStab. The program was seamlessly integrated with the real-time network analysis sequence and was used both in real time and off-line to monitor the risk of blackout caused by instability.

Although the operating reliability measures adopted at CND had prevented major disturbances, nearly critical situations have occurred, as it was the case on August 22, 2002, when the system experienced low voltage conditions. The situation was quickly identified and successfully acted upon by the system operator and security engineers. As shown in Gonzalez (2003) and Vergara et al. (2005), QuickStab was used to assess *post facto* the incident and correctly determined that the system was indeed approaching conditions that could have caused a blackout. With the advent of the coordinated operation in Central America, it was felt that the impact of significant MW transfers in the region would have to be continuously monitored in order to detect and prevent the risk of blackouts. Since operators and security engineers must rely on the predicted distance to instability, CND considered it important to validate the accuracy of the QuickStab computations by comparing their outcome with results from simulations performed with PSS/E.

The calculations were conducted at CND. The power flow modeled the entire interconnected system in Central America but the stability calculations focused only on the actual transmission network of ETESA. The study assumptions were based on the actual operating guidelines adopted at CND, and the QuickStab computational options were set to match the way PSS/E calculates load flows.

3.2.4.1 Load-Level Scenarios

The validation suite used to compare the QuickStab calculation results with PSS/E load-flow computations included the following load-level scenarios:

- *Maximum Expected Demand*: In this scenario, all the shunt capacitors are on-line, the shunt reactors are disconnected, and a small unit that normally is not needed to generate MW is brought in service to generate MVAR. These reactive

⁶ The tables and charts presented in Sect. 2.4 have been reprinted, with permission, from an internal study conducted by the CND.

⁷ At the time of this writing, the ETESA's SCADA/EMS was being replaced with a new system that incorporates a different suite of network analysis applications.

compensation sources help meet the highest possible MW load without risk of voltage collapse.

- *Medium–High Demand:* In this scenario, several steps are taken to reduce the reactive compensation: 15 MVAR in capacitor banks are taken off-line, 40 MVAR in shunt reactors are reconnected, and the machine used to generate MVAR is not activated. These provisions in the load-flow setup emulate the CND operating procedures for lower MW levels where the amount of reactive compensation is reduced to ensure that the system voltages would not violate the higher limits.
- *Medium–Low Demand:* This scenario is similar to the medium–high scenario, but at a further reduced MW load level and 15 MVAR less in capacitor banks.

3.2.4.2 Results of the Accuracy Tests Performed at CND

The detailed numerical outcome of the accuracy testing calculations performed at the CND of ETESA is documented in Table 3.1. In order to facilitate the interpretation of the results, which unequivocally attest the excellent precision of QuickStab, they are summarized on charts and further discussed in the following sections.

Maximum Expected Demand Scenarios

Figure 3.1 depicts the main results of the accuracy testing calculations performed for the maximum expected demand scenario. Five cases were developed and analyzed as follows:

- Case 1: 957 MW base case calculated with PSS/E. The QuickStab application predicted that instability, i.e., the critical state, occurs at 1018 MW, with a security margin of 15 % at 861 MW, and calculated critical MW schedules for the critical state and security margin MW schedules for the security margin state.
- Case 2: PSS/E *diverged* with the critical MW schedules from Case 1. The slack-bus generation was then slowly decreased, while maintaining all the other MW generation schedules unchanged, until convergence was obtained at 1007 MW. The fast voltage and steady-state stability application evaluated this case as unstable. The concept of security margin does not apply when the state is unstable, and, therefore, it was not calculated.
- Case 3: A new PSS/E load flow was executed by reducing the slack-bus generation by 10 MW, i.e., approximately 1 %. The case converged at 995 MW. For this case, QuickStab determined that the system is critically stable with a stability reserve of 0.91 % from the new limit of stability of 1005 MW. The security margin for Case 3 was evaluated at 850 MW.
- Case 4: The MW generation in Case 4 was further reduced by another 1 % to 983 MW. QuickStab determined that the system is stable, with 2 % stability reserve, and predicted that instability occurs at 995 MW. The security margin for Case 4 was evaluated at 842 MW.

Table 3.1 Total MW, average system voltage, and steady-state stability reserve for the maximum expected, medium–high and medium–low demand scenarios

Study case	State	Total MW	Average system voltage	Stability reserve [%]		
Expected maximum demand: Cases 1 through 4	Base case	Actual	957	1.0487	6.07	<i>Stable</i>
		Security margin	861	1.1167	15.34	
		Critical	1018	0.9723	0	
	Critical MW	Actual	1008	1.0177	0	<i>Unstable</i>
		Security margin	n/a	n/a	n/a	
		Critical	1008	1.0177	0	
	Critical MW: 1% less load	Actual	995	1.0406	0.91	<i>Critically stable</i>
		Security margin	850	1.0132	15.34	
		Critical	1005	0.9667	0	
	Critical MW: 2% less load	Actual	983	1.0498	1.12	<i>Stable</i>
		Security margin	842	1.1442	15.79	
		Critical	995	1.0388	0	
Medium high demand: Cases 1 through 4	Base case	Actual	798	1.0567	12.26	<i>Stable</i>
		Security margin	766	1.0377	15.67	
		Critical	909	0.9985	0	
	Critical MW	Actual	906	1.0240	0	<i>Critically stable</i>
		Security margin	765	1.1741	15.52	
		Critical	906	1.0240	0	
	Critical MW raised to divergence	Actual	931	1.0194	0	<i>Unstable</i>
		Security margin	n/a	n/a	n/a	
		Critical	931	1.0194	0	
	Base case+new unit for MVar	Actual	798	1.0567	14.85	<i>Stable</i>
		Security margin	763	1.0338	18.56	
		Critical	937	0.9885	0	
Medium–low demand: Cases 1 through 3	Base case	Actual	742	1.0517	15.75	<i>Stable</i>
		Security margin	742	1.0517	15.75	
		Critical	881	0.9840	0	
	Critical MW	Actual	881	1.0543	0	<i>Critically stable</i>
		Security margin	748	1.1924	15.11	
		Critical	881	1.0543	0	
	Critical MW raised to divergence	Actual	913	1.0175	0	<i>Unstable</i>
		Security margin	n/a	n/a	n/a	
		Critical	913	1.0175	0	

- Case 5: The MW generation in Case 5 was set at 861 MW, which corresponds to the 15% security margin predicted for the Case 1. The steady-state stability limit computed by QuickStab was 997 MW.

Medium–High Demand Scenario

Figure 3.2 illustrates the simulation results for the Medium–High Demand scenario. Three cases were analyzed as follows:

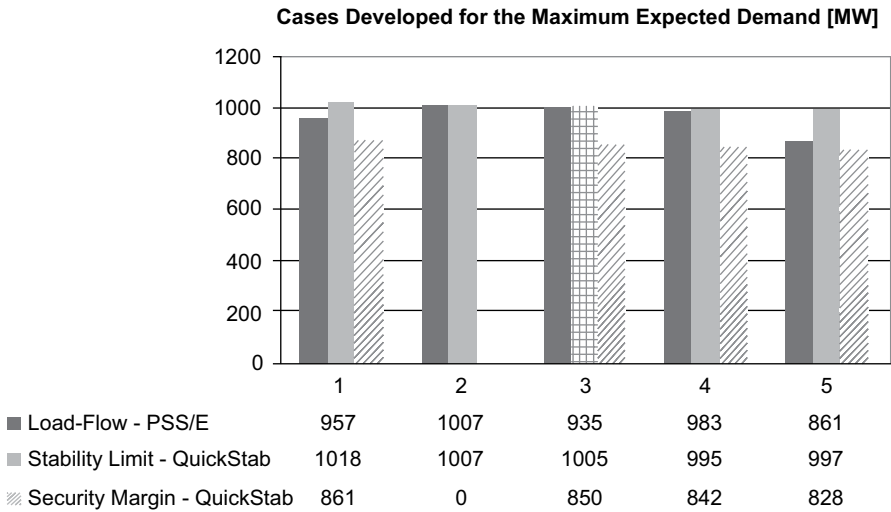


Fig. 3.1 Expected maximum demand cases. All the reactive compensation devices are on line. The system’s maximum transfer capability is at its highest value

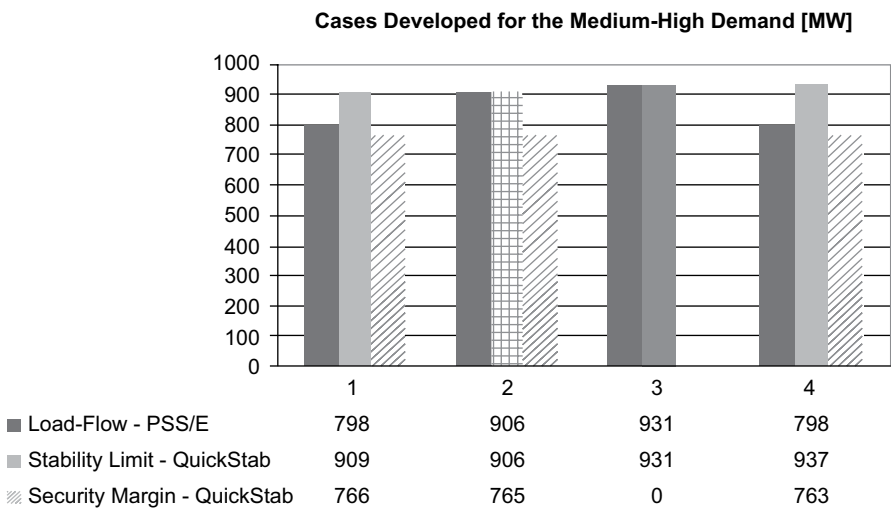


Fig. 3.2 Medium–high demand cases. Fewer reactive compensation devices are on line and, accordingly, the system’s maximum transfer capability is lower, too

- Case 1: 798 MW base case load-flow calculated with PSS/E. QuickStab predicts that instability occurs at 909 MW, with 15% security margin at 766 MW, and calculates the MW generation schedules for both the critical and the security margin states.
- Case 2: The PSS/E load flow was executed with the critical MW schedules predicted by QuickStab in Case 2 and converged at 906 MW. This case was evaluated as critically stable. The security margin of Case 2 was 765 MW.

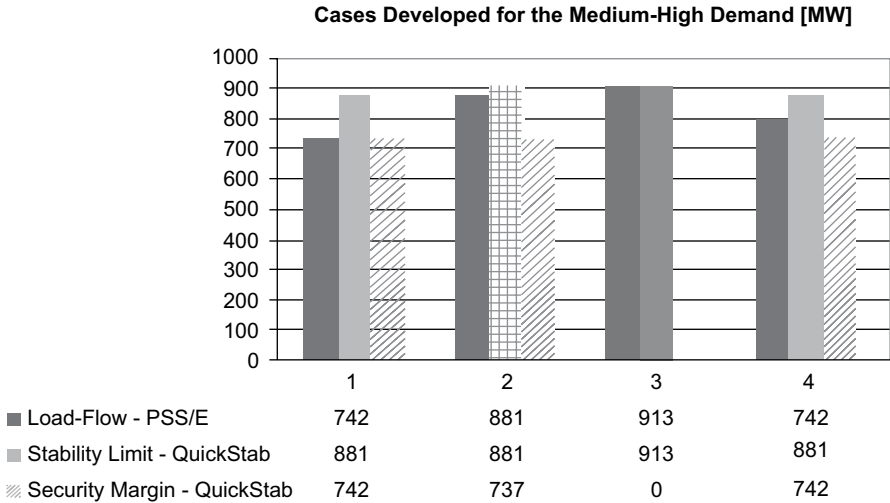


Fig. 3.3 Medium–low demand cases. Most capacitors are disconnected and shunt reactors are on. The system’s steady-state stability limit gets even lower than in the preceding cases

- Case 3: A new PSS/E load flow was executed by increasing the generation in small steps at the slack bus, while maintaining all the other MW schedules unchanged, up to the point where the load flow would diverge. The last converged load flow was obtained at 931 MW and evaluated by QuickStab as unstable.
- Case 4: A special case was derived from the Case 1 by including a small machine that did not generate any MW in the base case but was allowed to pick up some load during the case-worsening calculations performed by QuickStab during the search of the steady-state stability limit.

The purpose of running Case 4 was to simulate the actual operating conditions in Panama where, in order to operate the transmission system at higher load levels, the actual practice is to bring this small generating unit online to generate the MVAR needed for reactive compensation. As shown in Fig. 3.2, starting from a 798 MW case, the fast voltage and steady-state stability application correctly predicted a *higher stability limit*, i.e., 937 MW versus the 909 MW in Case 1.

Medium–Low Demand Scenario

The Medium–Low Demand scenario calculation results are shown in Fig. 3.3. The following cases were analyzed:

- Case 1: 742 MW base case load flow calculated with PSS/E. QuickStab predicts that instability (critical state) occurs at 881 MW, with a security margin of 15% at 742 MW, and calculates the MW generation schedules both for the critical state and for the security margin state.

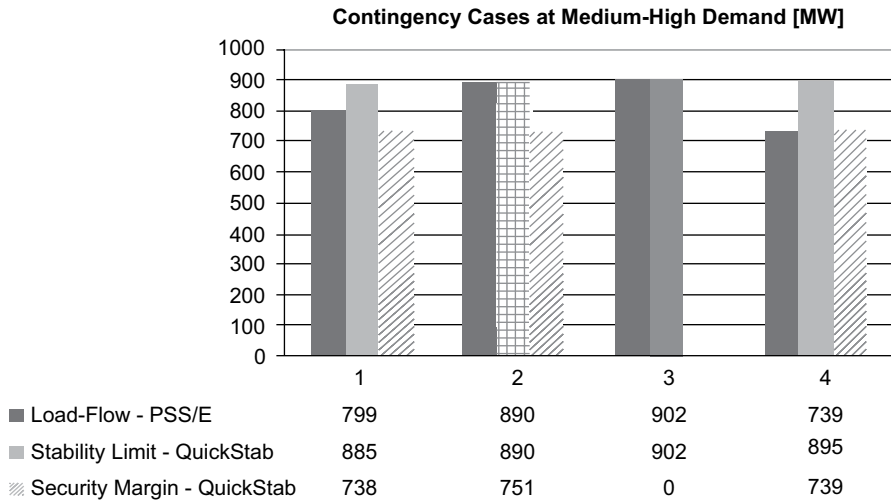


Fig. 3.4 Contingency cases on medium–high demand base case. As expected, the contingency cases have smaller steady-state stability limits when compared with the cases shown in Fig. 3.2

- Case 2: The PSS/E load flow was run with the critical MW schedules predicted by the fast voltage and steady-state stability application in Case 1 and converged at 881 MW. QuickStab evaluated it as critically stable. The security margin was computed at 737 MW.
- Case 3: A new PSS/E load flow was solved by increasing the slack-bus generation in small steps until the load-flow calculations diverged. The last converged solution was at 913 MW and was evaluated as unstable.
- Case 4: This case was supposed to be created with the MW schedules computed for the security margin in Case 1, but since the security margin in Case 1 was already 15%, Case 4 is identical to Case 1 and is shown in Fig. 3.3 for reference only.

Major Line Contingency

Figure 3.4 illustrates the calculation results for a major line contingency case simulated for the medium–high demand scenario.

Four cases were analyzed as follows:

- Case 1: 799 MW base case load flow calculated with PSS/E. The QuickStab application predicts that instability occurs at 885 MW, with 15% security margin at 738 MW, and calculates the MW generation schedules for both the critical and the security margin states.
- Case 2: The PSS/E load flow was executed with the critical MW schedules predicted in Case 2 and converged at 890 MW. QuickStab evaluated this case as critically stable. The security margin of Case 4 was evaluated at 751 MW.

- Case 3: A new PSS/E load flow was run by increasing the generation in small steps at the slack bus, while maintaining all the other MW schedules unchanged, up to the point where the load flow would diverge. The last converged load flow was obtained at 902 MW and was evaluated as unstable. The security margin was not calculated.
- Case 4: This case was built with the MW schedules computed for the security margin in Case 1. An 895 MW stability limit was computed, with a 15% security margin of 739 MW, which was identical to the load-flow case loading.

Transient Stability Simulations

The following transient stability calculation scenarios were evaluated for the Expected Maximum Demand, Medium–High Demand, and Line Contingency Cases:

1. Major generating unit trip in the western area.
2. Major generating unit trip near large load centers.
3. All units of a midsized power plant out of service.
4. Major transmission line contingency.

The results were similar in all the cases and are synthesized as follows:

- *Actual State* (Base Case), corresponding to the “Case 1” conditions described in the previous sections: the system withstood the fault scenarios 1 and 2, but became unstable for the faults scenarios 3 and 4.
- *Security Margin State*, i.e., MW loading 15% lower than the critical MW in the base cases: the system withstood all the fault scenarios.
- *Critical State*, corresponding to the critic MW in the corresponding base cases: all the transient stability simulations resulted in instability.

3.2.4.3 Analysis of CND Cases

In all the scenarios, QuickStab accurately determined the critical state, regardless of how near or how far it was from the base case. As predicted by theory, the peak-load stability limits were higher than those at medium–high and medium–low load levels. Indeed, in system states with less reactive compensation, we expect that the voltage would collapse at MW levels smaller than the maximum MW loadability of the same network where significant amounts of reactive compensation were added.

In all the cases evaluated, the input load-flow model represented the entire Central American interconnection, but the stability calculations were performed only on the area corresponding to ETESA’s transmission network. Accordingly, the program computed MW schedules only for the generators situated in the study area. These MW values were then used in PSS/E to create new load-flow cases, but all the other load-flow data remained the same. The calculations’ accuracy thus confirms the usefulness of the multi-area approach used by the program to assess local stability aspects within large interconnections.

Although the amount and extent of the transient stability simulations were rather limited, they did help getting a good understating of the concept of *security margin*. In all the cases evaluated, the system was stable when the transient stability simulations were executed for the security margin system MW grid utilization, but became unstable in various fault scenarios when the system loading was higher than the security margin MW. Furthermore, for all the transient stability calculations performed at the critical system, MW grid utilization level resulted in instability.

As far as the *computational speed* is concerned, all the simulations performed converged instantly, which was actually expected both because the program is intrinsically fast and because the network area that was evaluated for stability was just a subset of the load-flow model of the Central American interconnected power system.

3.2.5 Validating QuickStab Results in Vietnam⁸

Due to frequent and severe faults that, in some cases, have adversely affected system reliability and security, the NLDC of EVN undertook, in 2003 and early 2004, a series of studies aimed at evaluating the risk of blackout caused by instability. Among several initiatives, NLDC assessed the maximum transfer capability of the transmission system by using the QuickStab software.

The analysis revealed that the power system's steady-state stability margins might be inadequate. The stability reserve indices varied from 6% in the 2005 rainy scenario to 13% in the 2006 rainy scenario, with a relatively better margin in the dry season of 2006.

Since contingencies would certainly push the system even closer to the steady-state stability limit where voltages may collapse and units may lose synchronism, NLDC concluded that the actual operations of the transmission network for the next couple of years will have to be closely and continuously monitored in order to detect and prevent the risk of blackouts.

Accordingly, NLDC expanded the array of network analysis applications with QuickStab,⁹ which, in addition to the then-existing load flow and transient stability programs, was used for some time to support the system dispatching, operations planning, and market clearing functions. The distance to voltage and steady-state instability was calculated three times a day based on the most recent data retrieved from the SCADA/EMS or computed by the market-clearing engine on the Market System.

Since this information had to be relied upon in system and market operations, NLDC developed a series of simulations aimed at validating the accuracy of the QuickStab predictions by following procedures similar to those described in

⁸ The tables and charts presented in Sect. 2.5 have been reprinted, with permission, from an internal study conducted by the NLDC.

⁹ At the time of this writing, the NLDC's SCADA/EMS is being replaced with a new system that incorporates a different suite of network analysis applications.

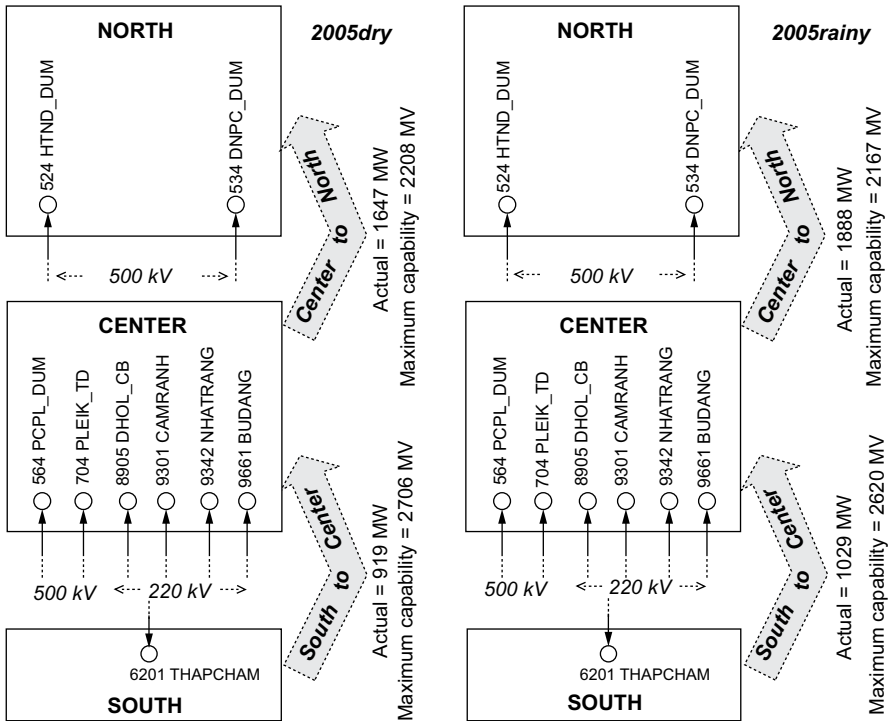


Fig. 3.5 South–North MW transfers in the EVN power transmission network

Sect. 3.3 of this chapter. A brief summary of the most relevant aspects and computational results is provided in the following sections.

3.2.5.1 Testing Scenarios: Simulation Results

The power system of Vietnam has a markedly longitudinal characteristic. It extends over approximately 2000 km and consists of three major subareas, which are loosely interconnected and encompass 220 and 110 kV transmission facilities, attached to an Extra High Voltage (EHV) “backbone” of two 500-kV circuits that go from the extreme south all the way to the northern part of the country (Fig. 3.5).

The operating difficulties that stem from this particular network topology are further worsened by:

- Severe power transfers from the Southern Region to the Northern Region.
- Relatively low load density in the Central Region.
- Large seasonal variations: a *rainy* scenario, where the hydro generation is maximized, and a *dry* scenario, where the generation is primarily thermal.
- Significant MVA injection into the Northern area across the 500 kV lines, disproportionately higher than the flow in the only 220-kV tie-line that interconnects the Northern and Central areas.

Table 3.2 Total MW, average system voltage, and steady-state stability reserve for the dry cases. In sub-scenario A, some generators control voltages at remote buses. In sub-scenario B, all the generators control their own terminals and the overall voltage profile is slightly higher

Study case	State	Total MW	Average system voltage	Stability reserve (%)		
Sub-Scenario A: Cases 1 through 4	Base case	Actual	9516	1.05093	7.17	<i>Stable</i>
		Security margin	8699	1.10416	15.14	
	Critical MW	Critical	10,251	0.9450	0	<i>Stable</i>
		Actual	10,250	1.0222	1.17	
		Security margin	8754	1.1346	15.60	
	Critical MW+1% additional load	Critical	10,372	0.9699	0	<i>Critically stable</i>
		Actual	10,347	1.0178	0.97	
		Security margin	8856	1.1299	15.24	
	Critical MW+2% additional load	Critical	10,449	0.9667	0	<i>Critically stable</i>
		Actual	10,447	1.0078	0.71	
Security margin		8861	1.11357	15.79		
Sub-Scenario B: Cases 5 and 6	Base case	Actual	9494	1.0783	7.8	<i>Stable</i>
		Security margin	8717	1.1246	15.34	
		Critical	10,296	0.9389	0	
	Critical MW	Actual	10,488	1.0402	1.22	<i>Stable</i>
		Security margin	8926	1.1434	15.93	
		Critical	10,617	0.9828	0	

- There are no shunt capacitors: due to insufficient reactive compensation, the generating units are used to hold voltages at remote locations.

Two scenarios were used for performing the accuracy testing: *Dry* and *Rainy*. Both of these scenarios were built for peak load conditions and evaluated under two voltage control assumptions as follows:

- Some generators are allowed to control remote buses.
- All the generators control their own terminal bus voltages.

The results of the simulations performed for the “dry” cases, where two additional cases were run by successively increasing the load in the critical state load-flows by 1%, are shown in Table 3.2 and illustrated in Fig. 3.6.

The results of the calculations performed for the “rainy” cases are shown in Table 3.3 and illustrated in Fig. 3.7.

3.2.5.2 Analysis of NLDC Cases

At the outset, it must be noted that, regardless of the study scenario, it was not possible to obtain converged critical state load flows with voltage profiles similar to the ones predicted for the critical state QuickStab.

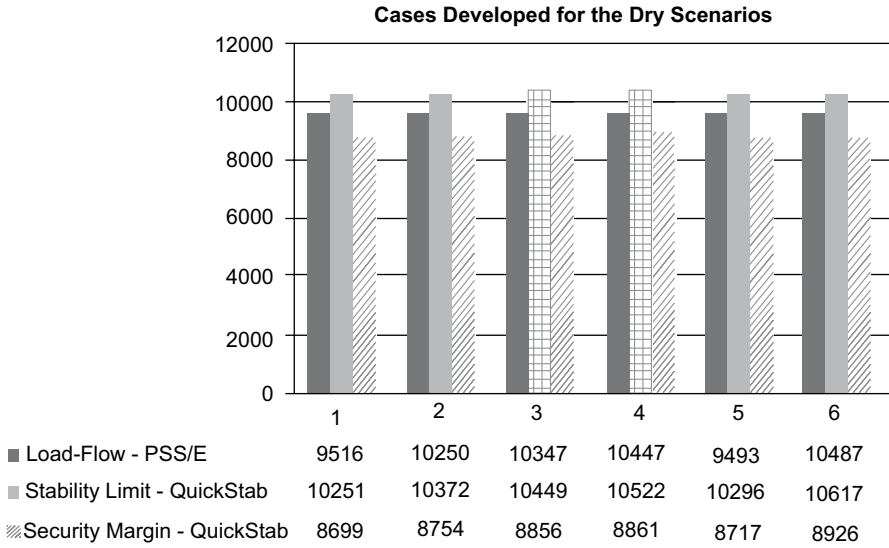


Fig. 3.6 Dry scenario cases

Table 3.3 Total MW, average system voltage, and steady-state stability reserve for the rainy cases. In sub-scenario A, some generators control voltages at remote buses. In sub-scenario B, all the generators control their own terminals and the overall voltage profile is slightly higher

Study case	State	Total MW	Average system voltage	Stability reserve [%]		
Sub-scenario A: Cases 1 and 2	Base case	Actual	9008	1.0857	10.53	<i>Stable</i>
		Security margin	8535	1.1108	15.23	
		Critical	10,068	0.9377	0	
	Critical MW	Actual	10,063	1.0368	1.02	<i>Stable</i>
		Security margin	8546	1.1399	15.95	
		Critical	10,167	1.0234	0	
Sub-scenario B: Cases 3 and 4	Base case	Actual	8983	1.1012	11.87	<i>Stable</i>
		Security margin	8654	1.1081	15.10	
		Critical	10,193	0.9261	0	
	Critical MW	Actual	10,206	1.0344	0.55	<i>Critically stable</i>
		Security margin	8698	1.1371	15.25	
		Critical	10,263	1.0270	0	

Whatever might be the reason(s), the fact that the starting system voltage profile in the critical state load-flow cases was higher suggests that the corresponding maximum transfer capability would also be higher, i.e., the system would still have a small steady-state stability reserve, perhaps close to, or slightly below, 1%, thus qualifying the state as critically stable.

In all the scenarios, QuickStab accurately determined the critical state, regardless of how near or how far it was from the base case. However, the precision was not as good as the accuracy of the Panamanian experiments. A possible explanation,

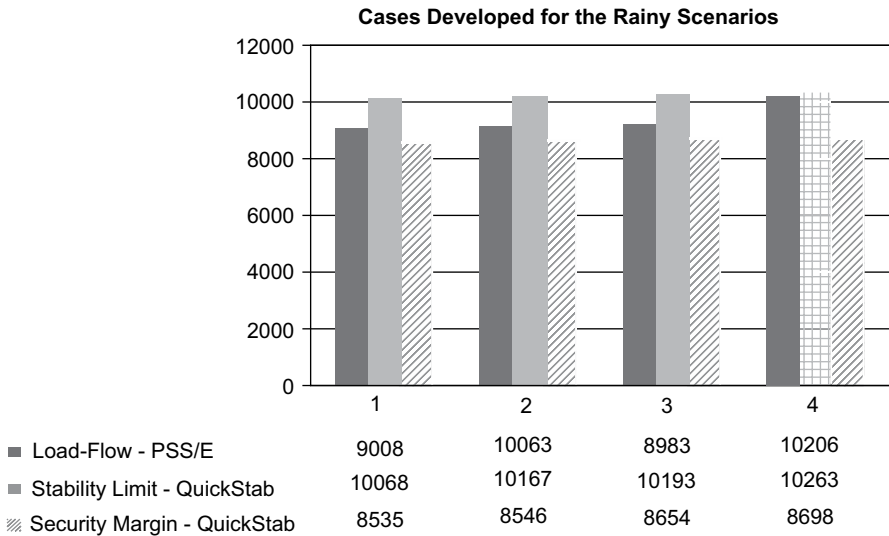


Fig. 3.7 Rainy scenario cases

as suggested in the opening paragraph of this section, might be the fact that in all the “critical MW load flows”, the voltages were higher than the target voltage profile, which obviously should bias the calculation results towards higher stability limits, as predicted by theory.

The load-flow model encompassed the complete interconnected power system of Vietnam, but in order to keep the effort involved in simulations to a reasonable level, only the system-wide cases were considered for testing by running load-flow computations near the stability limits and repeating the voltage and steady-state stability calculations for these new cases.

In real life, however, stability calculations are routinely performed on a subsystem, or area, basis. For the Northern Region, which usually imports a significant amount of power from the Central Region, production grade studies revealed that the MW flows in the 500-kV circuits reach the steady-state stability limits way before getting even close to the thermal limits.

For practical purposes, this means that the system operator should monitor not only the steady-state stability reserve but also, and most importantly, the amount of power being transferred into the Northern Region across the 500-kV interconnection.

For the Southern Region, area-level stability simulations have indicated generation capacity limitations, which means that in the south, for the reactive compensation levels normally considered in operational studies, the system is steady-state stable even if all the generators have reached their maximum MW limits. As far as the Central Region is concerned, the load is relatively low and no stability problems are anticipated.

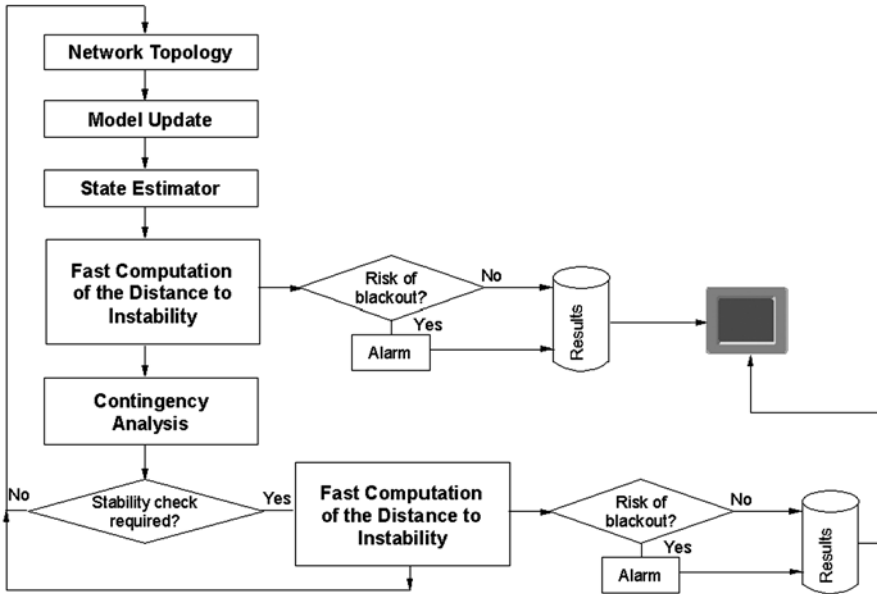


Fig. 3.8 Real-time integration of the fast voltage and steady-state stability analysis computations with the SCADA/EMS state estimator at Transelectrica, Romania

3.3 Tracking the Steady-State Stability Reserve on SCADA Trending Charts

3.3.1 Real-Time Implementation of QuickStab on the SCADA/EMS of Transelectrica

The steady-state stability framework that allows computing and monitoring the distance to instability has been developed, and is well known, in Romania for a very long time (Dimo 1961, 1975), but a true production-grade embodiment of this technology became available only in 2002 when QuickStab was implemented in real time on the SCADA/EMS of Transelectrica,¹⁰ Romania, by Alstom (Avila-Rosales and Giri 2004).

Figure 3.8 illustrates how the QuickStab computational engine that determines the voltage and steady-state stability reserve was seamlessly integrated within the real-time network analysis sequence.

The program is triggered automatically after each successful run of the state estimator and determines both the current value of the system-wide stability reserve

¹⁰ At the time of this writing, QuickStab was being used in real time at the National Dispatch Center (DEN) in Bucharest, Romania, as shown in this section. However, neither the authors of this chapter nor the editor of this book make any implied or explicit assumptions about the continuing use of this application at Transelectrica in the future.

and the steady-state stability reserve for each one of the five critical security cut-sets identified for the Romanian transmission system.

3.3.1.1 Critical Security Cut-Sets

A “security cut-set” identifies a group of transmission lines:

- That form a topological cut-set, i.e., their removal causes the islanding of the transmission network in two disjoint components.
- Whose maximum transfer limit in terms of stability is smaller than the aggregate thermal limit, i.e., may cause voltage and steady-state instability even if the total MW flow across the cut-set has not reached the combined maximum MVA of the lines.

In a sense, the concept of “security cut-set” is similar to the concept of “congestion path” with the difference that the former stems from stability considerations whereas the latter is driven by thermal violations.

Security cut-sets may appear in any multi-area power system where large MW blocks are transferred between areas across relatively weak internal interconnections. This is common in longitudinal transmission networks that span system areas with significant load-generation unbalances, e.g., the Vietnamese power transmission system depicted in Fig. 3.5 where the topologically clustered Northern, Central, and Southern regions are separated by such security cut-sets.

In Romania, where the populated areas and industrial zones are aggregated in concentric areas divided by the Carpathian mountain chain, the security cut-sets are generated by the specific pattern of the MW flows between the center area and the outer ring. The center area is surrounded by mountains and encompasses a dense 110-kV network sustained by a 220–400-kV backbone. Around the central area, there is an outer ring of major power plants that inject their output into a strong 220–400–750-kV transmission system.

The power is transferred primarily from south–southwest towards the center, from south–southeast towards the northeastern part of the outer ring, and from the northern part of the central area towards the northeastern part of the outer ring. DEN has identified five critical security cut-sets. The system subareas circumscribed by these critical security cut-sets are not necessarily disjoint, and some of them overlap. They are not fixed, either, and change depending upon the pattern of load, generating reserves, transmission outages, line flows, voltage levels, and reactive resources.

The configuration of the critical security cut-sets is periodically reassessed off-line with an application developed in-house that identifies, for a given load-flow solution, all the security cut-sets and computes the steady-state stability reserve index for each one of them. The approach is described in Pomarleanu and Savulescu (2009) and combines an REI-Dimo equivalencing procedure (Dimo 1975; Tinney and Powell 1977; Dy Liacco et al. 1978; Oatts et al. 1990; Savulescu 1981), which assigns one REI generator to each side of the security cut-set, with a steady-state

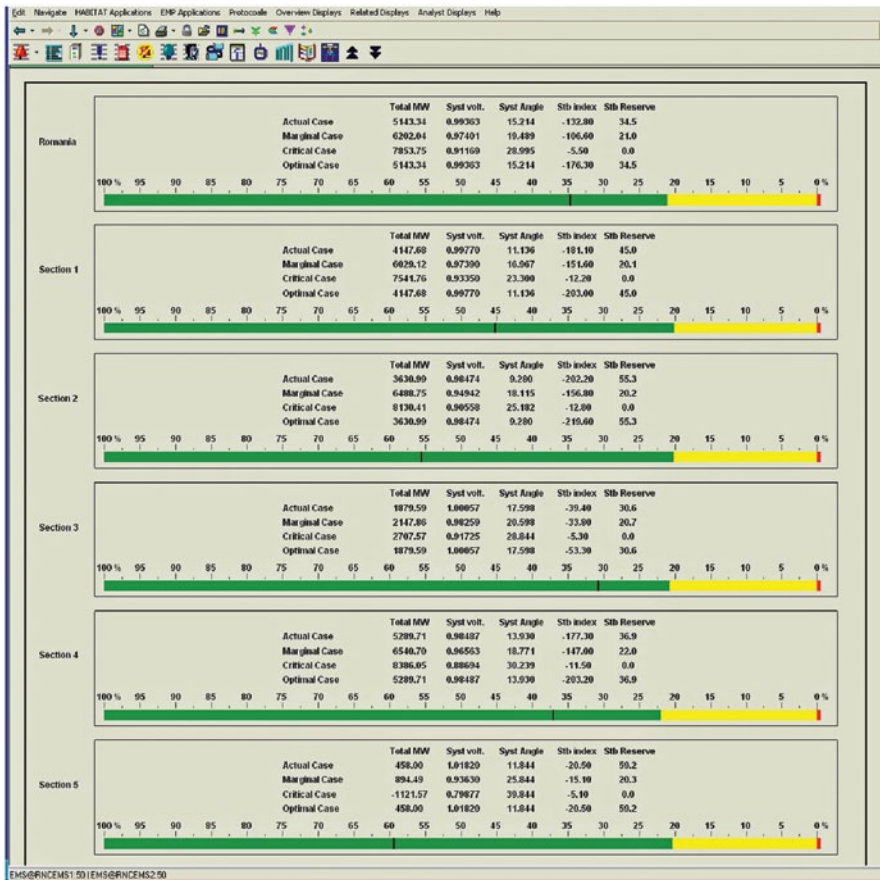


Fig. 3.9 System and security cut-set speedometers. (Reprinted with permission from DEN)

stability calculation for the model consisting of two REI equivalent generators and the link between them.

The security cut-sets are then ranked in the descending order of their steady-state stability reserve and the most critical five are selected. This procedure is executed twice a year. Quite obviously, the actual stability limits across the critical security cut-sets may differ substantially from those computed off-line for the postulated conditions and need to be reassessed continuously based on the actual system conditions as determined by the state estimator. The problem is now solved in real-time QuickStab, which computes the steady-state stability reserves both for the entire system and for each security cut-set. Figure 3.9 shows a real-time display taken directly from the SCADA/EMS, which depicts the current values of the steady-state stability reserves of the system and across the five critical security cut-sets.

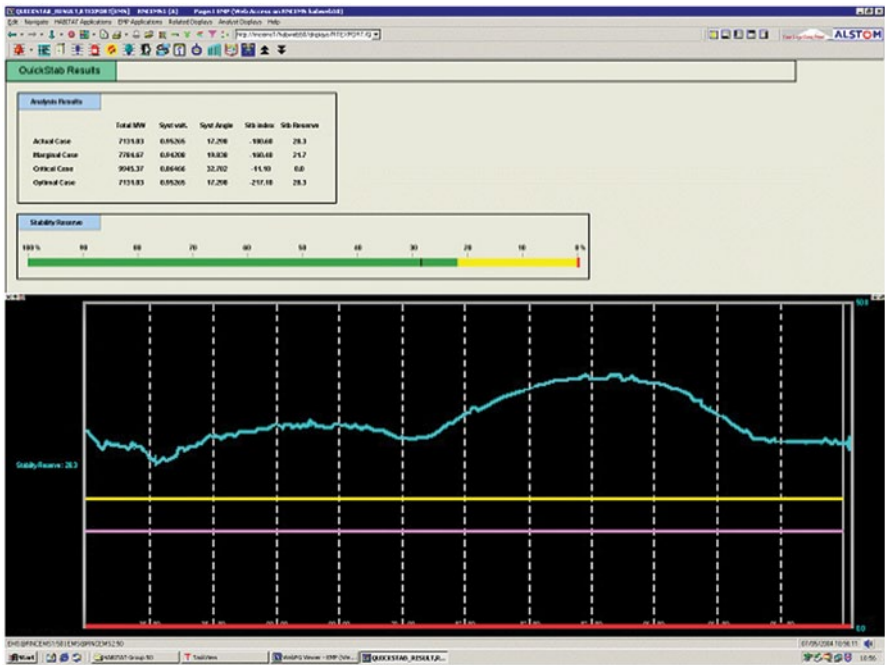


Fig. 3.10 Real-time trending of the distance to steady-state instability on the SCADA/EMS of Transelectrica, Romania. The light color line shows the security margin. The bottom line corresponds to the steady-state stability limit. The gray line in between is the alarm limit. (Reprinted with permission from DEN)

3.3.1.2 Real-Time Trending of the Distance to Instability

The real-time computed values of the system-wide steady-state stability reserve and the steady-state stability reserve of each critical security cut-set is stored in the real-time database and can be subsequently displayed on SCADA trending charts. Figure 3.10 shows a typical trending chart of the system-wide stability reserve over a 24-hour period.

At Transelectrica, Alstom developed an innovative visualization concept, which, on the left side of the monitor, displays the distance to instability for the entire system with each one of the security-cut sets evaluated, and, on the right side, tracks the evolution in time of the stability reserves displayed on the left by using standard SCADA trending charts (Fig. 3.11).

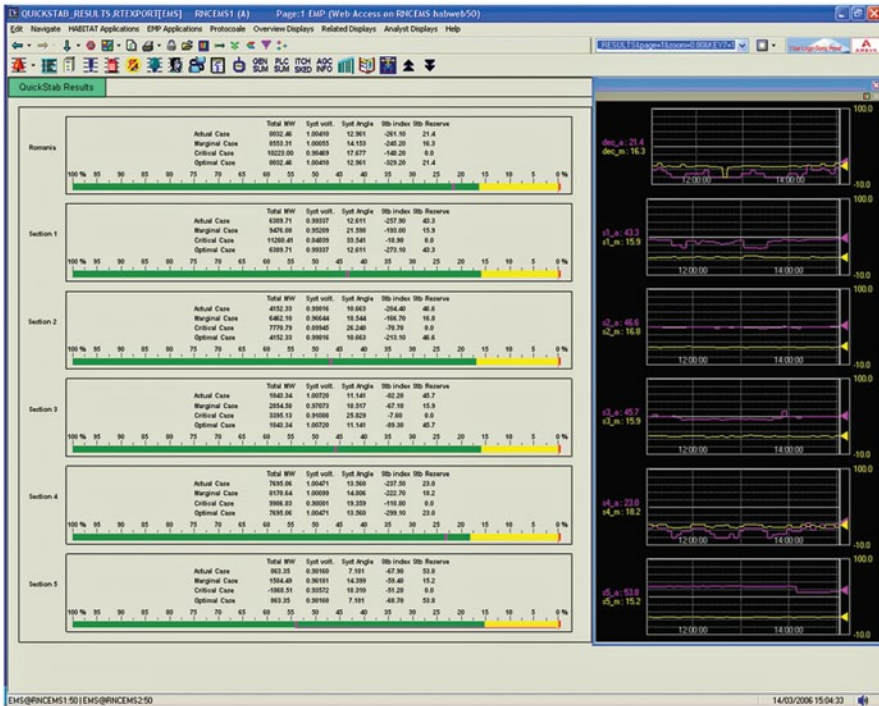


Fig. 3.11 Real-time display from Transeletrica’s SCADA/EMS, which combines the linear speedometers with the trending charts. (Reprinted with permission from DEN)

3.4 Using PMUs to Track Voltage and Angle Stability Sensitivities Across Long Transmission Lines in Vietnam

3.4.1 Introductory Background

The need to increase the power transfers across the existing power system infrastructure, which is characterized by long line distances and large separations between generation and load, and, also, improve the quality of the service, has led EVN to devote significant amounts of talent and resources to the implementation of smart-grid technologies in the country.

In addition to an extended population of Substation Automation Systems (SAS), at the core of this program is the deployment of a vast Wide Area Monitoring System (WAMS) aimed at improving power system performance and reliability.

The plan and scope and the expected applications encompassed by this effort are illustrated in Figs. 3.12 and 3.13, respectively.

This is a two-phase program. The expected WAMS architectures in each one of these phases are illustrated in Figs. 3.14 and 3.15.

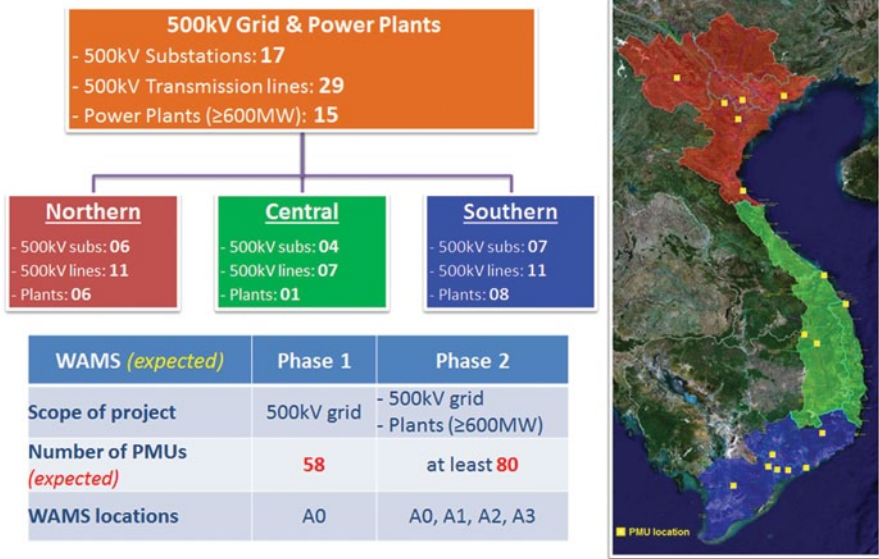


Fig. 3.12 Plan and scope of the expected WAMS model in Vietnam

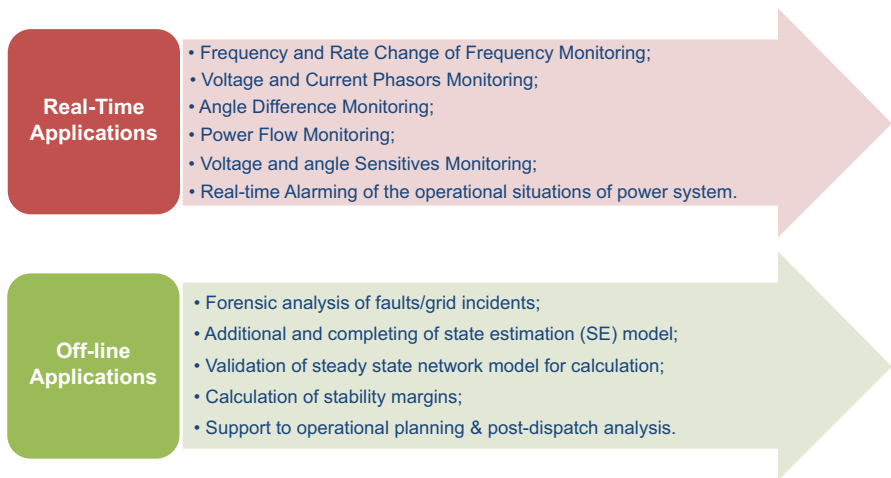
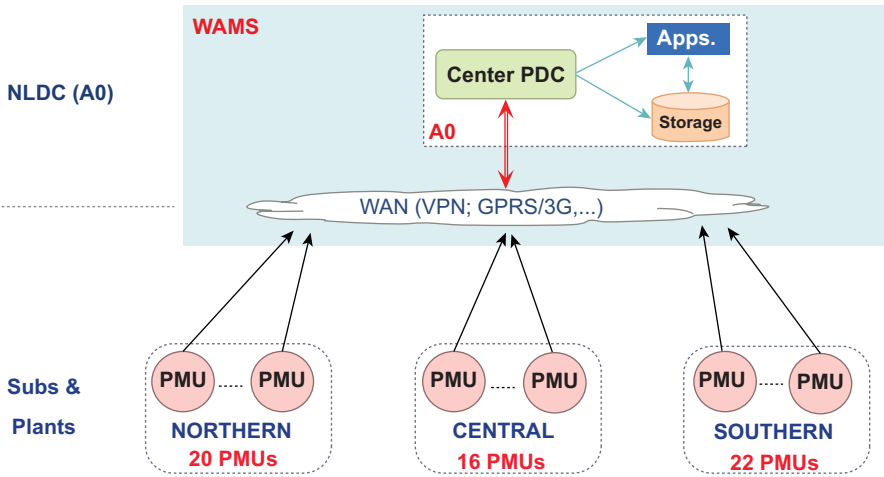


Fig. 3.13 Expected WAMS applications in Vietnam

3.4.2 Real-Time Monitoring of Available Power Transfer Capability Across Long Transmission Corridors

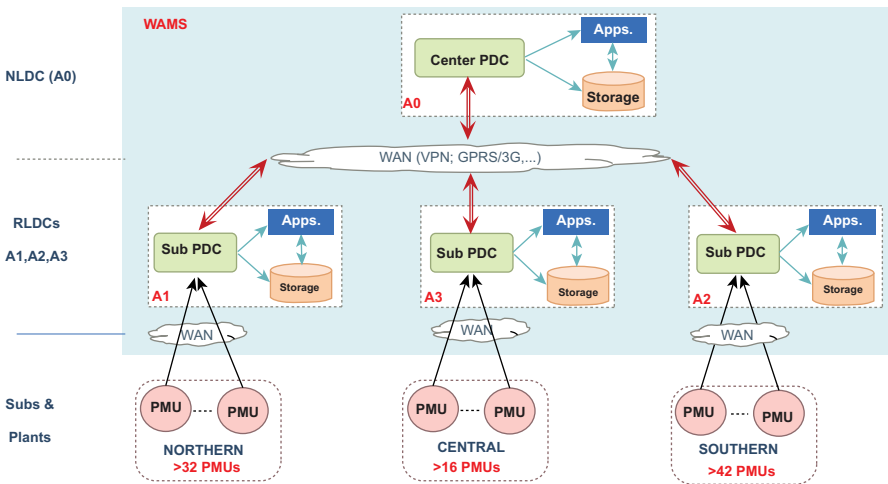
Among the key objectives of the ongoing WAMS effort in Vietnam, which generally aims at improving performance and reliability, is the need to address the fact that one of the primary causes of wide-area disruptions in the current EVN power system is the existence of long transmission corridors that are susceptible to voltage and angle instabilities when major unbalances between load and generation take place.



Phase 1:

- Monitor all 500kV Vietnam Grids (including lines, substations and power plants)
- Number of PMUs (expected): 58

Fig. 3.14 WAMS architecture implementation in Vietnam—Phase 1



Phase 2:

- Monitor all 500kV Vietnam Grids and power plants with the capacity is over 600MW
- Number of PMUs (expected): over 80

Fig. 3.15 WAMS architecture implementation in Vietnam—Phase 2

3.4.2.1 Classical Concepts in the Context of the Synchrophasor Technology

Quoting from the classical steady-state stability theory, the real power transfer across a transmission line between two adjacent network buses is determined by the voltage magnitudes at each bus, the phase angle difference between them, and the line reactance (Crary 1955; Anderson and Fouad 1990; Venikov 1977).

Accordingly, the real power transfer between the two bus terminals of a transmission line, say A and B, is calculated with the following equation:

$$P = \frac{V_A \times V_B}{X_L} \sin \delta,$$

where P is the real power transfer, X_L is the transmission line reactance between the two buses, δ is the phase angle difference across the transmission line, and V_A and V_B are the bus voltage magnitudes at the terminals of the transmission line.

The amount of maximum power that can be transferred across the line, or its total MW transfer capability, is given by

$$P_{\max} = \frac{V_A \times V_B}{X_L},$$

and the line's reserve margin (available transmission capability) $P_{\text{marg}\%}$ of the line is calculated as:

$$P_{\text{marg}\%} = \frac{P_{\max} - P}{P_{\max}} \times 100.$$

From these equations, the total and available transfer capabilities across the transmission line can be computed in real time by using the voltage and current synchrophasor data, respectively, collected at the lines' terminals. Three additional metrics can also be defined as shown in Figs. 3.16, 3.17, 3.18.

3.4.2.2 Demonstration of the Synchrophasor Technology on the Vietnamese 500-kv Transmission System

A demonstration of the synchrophasor technology developed in Vietnam¹¹ was recently conducted at EVN. The functionality, architecture, data flow, and alarm blocks of the application (SmartWAMS) are illustrated schematically in Figs. 3.19, 3.20, 3.21.

The model used for simulation encompassed 17 substations of the Vietnamese 500-kV transmission grid.

¹¹ The synchrophasor technology was introduced in 2012 in Vietnam by Advanced Technical Systems Co. Ltd (ATS) under the trade name SmartWAMS (patent pending).

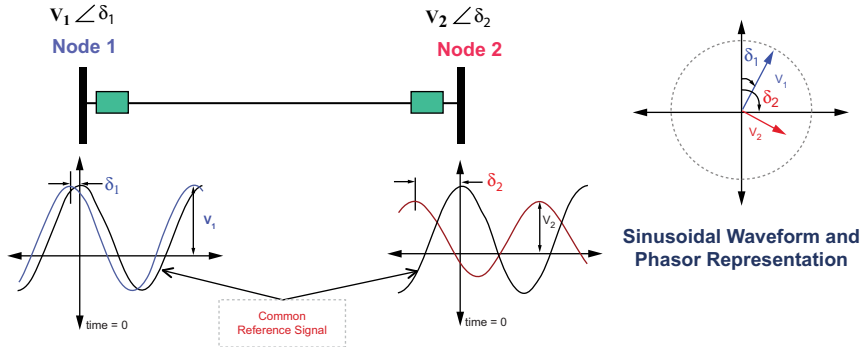
What can cause the bus voltage angle difference to change?

- Transmission line outages or restorations
- Generator trips
- Sudden large load changes, e.g., load crash / load throw off

$$P_{12} = \frac{V_1 V_2}{X_{12}} \sin(\delta_1 - \delta_2)$$

$$\Delta\delta = \delta_1 - \delta_2$$

Knowledge of the angle difference helps synchronization during system restoration



Note: a common reference signal is required to compare the phase angles and to calculate $\Delta\delta$. This common reference signal is available from GPS

Fig. 3.16 Voltage angle difference concept in synchrophasor technology

- $\Delta V/\Delta P$ is the change in voltage as a function of the power flow (MW)
- $\Delta V/\Delta P$ increases as system approaches the collapse region identified as the Nose Point
- Voltage sensitivity allows:
 - Early warning of deteriorating voltage stability
 - Indicate “How far are we from the voltage collapse region?”
 - Determine the voltage stability margin
 - Identify “When a nearby transmission line or substation trips”

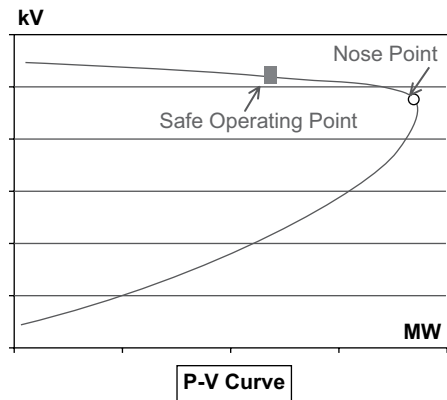


Fig. 3.17 Voltage sensitivity concept

- $\Delta\delta/\Delta P$ is the change in angle as a function of the power flow (MW)
- $\Delta\delta/\Delta P$ increases as system approaches P_{max1} (the maximum power that can be transmitted)
- Angle Sensitivity allows:
 - Early warning of deteriorating angle stability
 - Assessing of the steady state stability
 - Identify "When a nearby transmission line or substation trips"

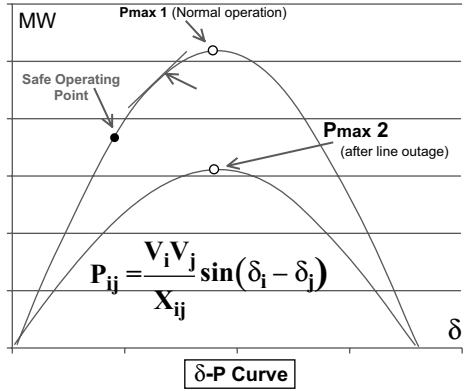


Fig. 3.18 Angle sensitivity concept

Fig. 3.19 SmartWAMS functionality



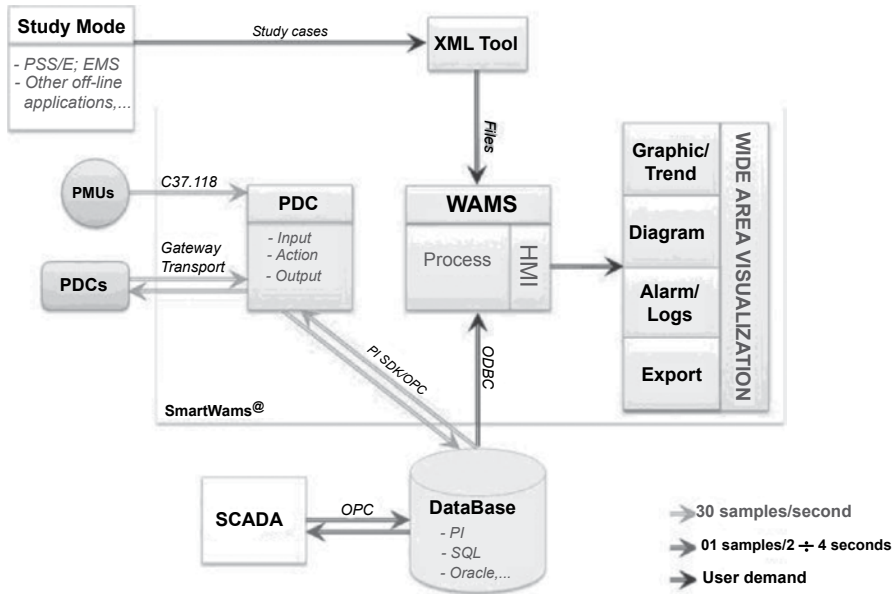
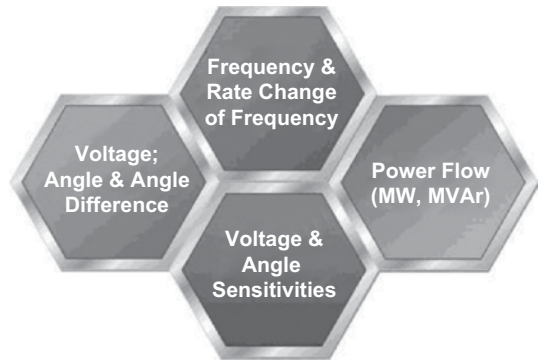


Fig. 3.20 SmartWAMS architecture and dataflow

Fig. 3.21 SmartWAMS visualization alarm blocks



Two demo scenarios were run as follows:

- Scenario 1: running the test with the actual data.
- Scenario 2: running test with solved cases developed with the PSS/E software.

Each scenario included both normal operation conditions (Case 1) and the outage of the 500-kV transmission line PLEIKU—DAKNONG (Case 2).

Some illustrative interfaces and representative results of the simulations are illustrated in Figs. 3.22, 3.23, 3.24, 3.25.

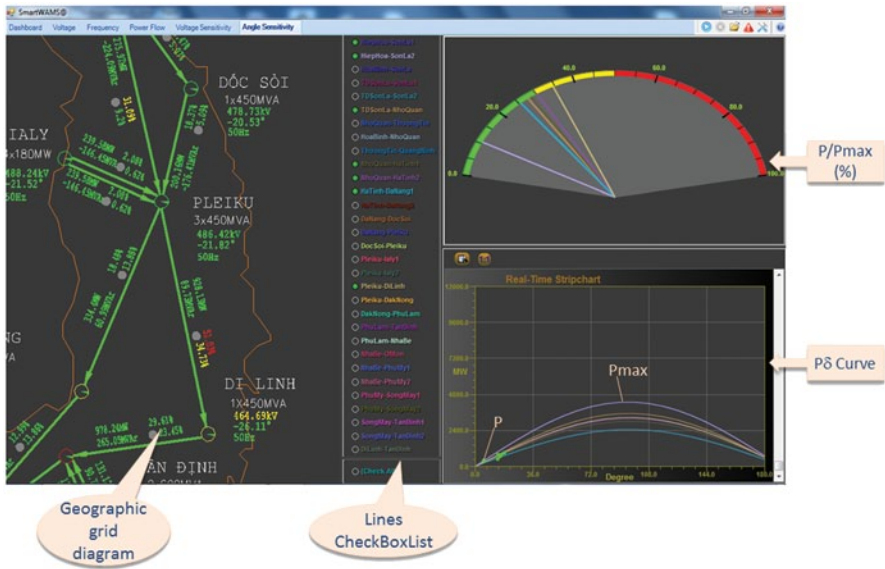


Fig. 3.22 SmartWAMS angle sensitivity displays

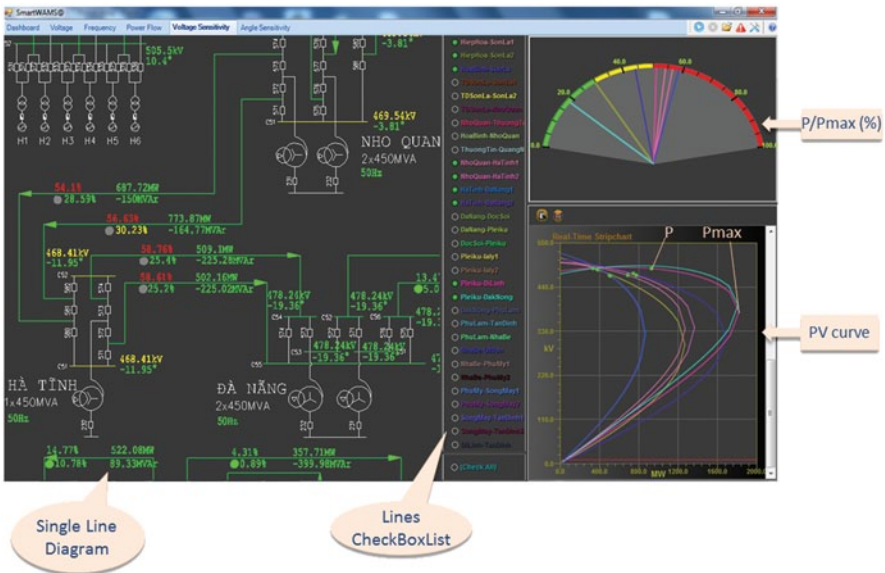


Fig. 3.23 SmartWAMS voltage sensitivity displays

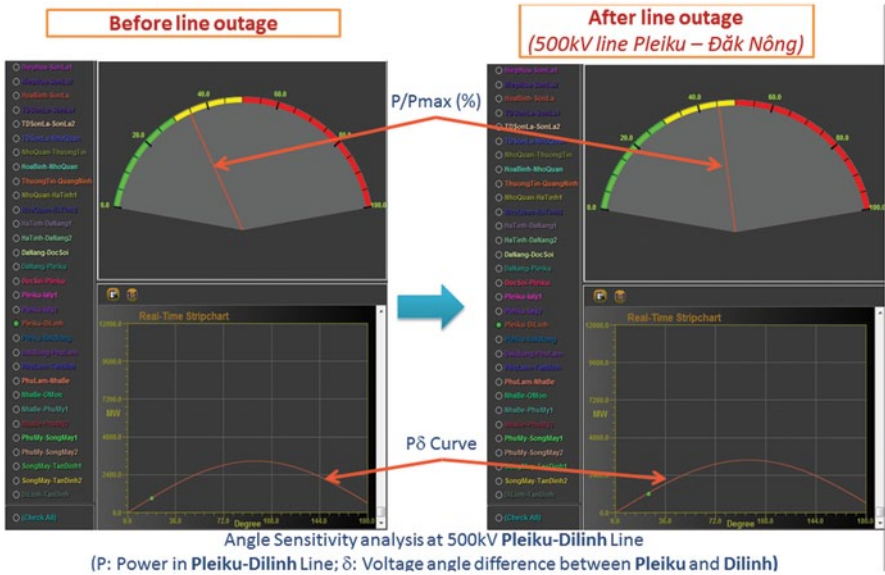


Fig. 3.24 SmartWAMS angle sensitivity displays before and after the outage

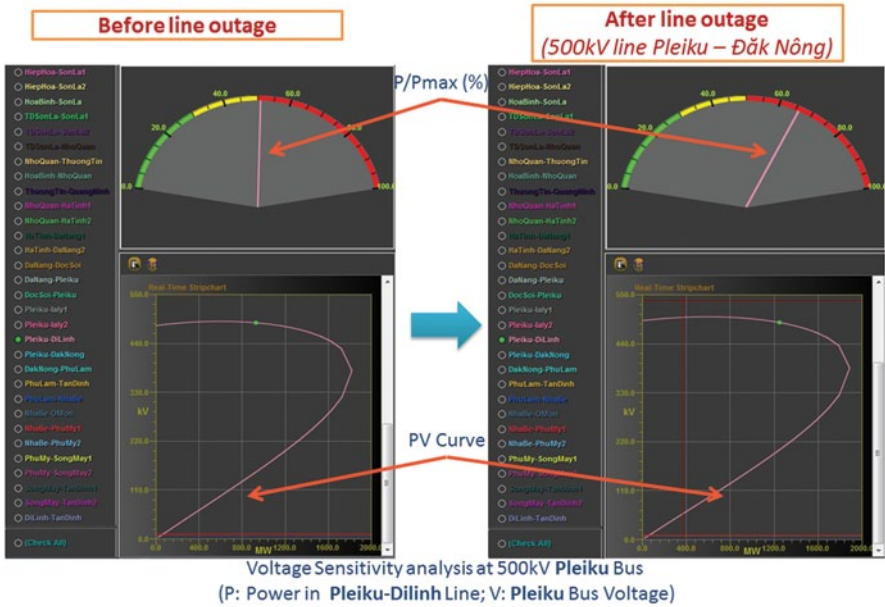


Fig. 3.25 SmartWAMS voltage sensitivity displays before and after the outage

3.5 Conclusions

This chapter addressed several practical aspects of performing steady-state stability assessment in real time. The application validation for accuracy and reliability, which is of paramount importance, has been covered in detail and illustrated with practical experience results obtained by two early users of QuickStab—ETESA, in Panama, and NLDC, in Vietnam. At the time when these tests were performed, ETESA and NLDC were using QuickStab in real time in system dispatching functions and off-line in operations scheduling and market clearing functions. The application validation results confirmed the theory and are consistent with earlier experience with this technology.

The deployment of the steady-state stability assessment in energy control centers was illustrated with an actual example that reflects the benefits of the online monitoring of the risk of blackout via speedometer charts and by trending the distance to instability as it evolves in real time. At the utility site selected for this purpose, the stability computations have been seamlessly integrated with the real-time system by the SCADA/EMS provider.

The potential to use synchrophasor technologies to track voltage and angle stability sensitivities across long transmission lines was also discussed and illustrated with practical results obtained recently in Vietnam. According to the Vietnamese operational experience, the synchronized phasor measurements, which are ideal for monitoring the dynamic power system performance especially during high-stress operating conditions, should be viewed as a complement to, rather than a replacement of, conventional SCADA/EMS tools.

References

- Anderson PM, Fouad AA (1990) Power system control and stability. The Iowa University Press, Ames
- Arnold L, Hajagos J (2009) LIPA implementation of real-time stability monitoring in a CIM compliant environment. Paper PSE-09PSCE0253 presented at the real-time stability assessment in modern power system control centers panel, IEEE power systems conference & exposition 2009 (IEEE PSCE'09), Seattle, WA, March 15–18, 2009
- Avila-Rosales R, Giri J (2004) Extending EMS capabilities to include on-line stability assessment. Paper 04PS0371 presented at the real-time stability challenge panel session, power systems conference and exposition 2004, New York, New York, 10–13 Oct 2004
- Campeanu HS, L'Helguen E, Assef Y, Vidal N, Savulescu SC (2006) Real-time stability monitoring at Transselectrica. Paper PSCE06-1288 presented at the real-time stability applications in modern SCADA/EMS panel, IEEE power systems conference & exposition 2006 (IEEE PSCE'06), Atlanta, GA, Oct 29–Nov 2, 2006
- Crary S (1955) Power System Stability. Steady-State Stability, General Electric Series, Vol. I: third printing, October 1955
- Dimo P (1961) Etude de la stabilité statique et du réglage de tension. Revue Générale de l'Electricité (Paris) 70(11):552–556
- Dimo P (1975) Nodal analysis of power systems. Abacus Press, Kent
- Dy Liacco TE, Savulescu SC, Ramarao KV (1978) An On-line topological equivalent for a power system, IEEE transactions on power systems, PAS-97, pp 1550–1563

- Gonzalez LA (2003) Post-facto analysis of a near-Blackout event. 7th international workshop on power control centers, May 26–28, 2003, Orisei, Italy
- IEEE (1982) IEEE PES task force on terms and definitions, proposed terms and definitions for power system stability, IEEE Transactions on Power Systems, PAS-101, No. 7, July 1982
- IEEE/CIGRE (2004) IEEE/CIGRE joint task force on stability terms and definitions, definition and classification of power system stability. IEEE, transactions on power systems, vol. 19, no. 2, May 2004, pp 1387–1401
- Kundur P (1999) Introduction to techniques for power system stability search. A special publication of the Power System Dynamic Performance Committee of the IEEE PES, TP-138-0, pp 1–3
- Magnien M (1964) Rapport spécial du Groupe 32 Conception et Fonctionnement des Réseaux. Conférence Internationale des Grands Réseaux Electriques à Haute Tension, CIGRE Session 1964
- Moraite G, Ionescu S, Feldmann S, Chenzbraun I (1966) Problèmes soulevés par la stabilité statique des réseaux bouclés. Conférence Internationale des Grands Réseaux Electriques à Haute Tension, CIGRE Session 1966
- NERC (2000) Policy 9—reliability coordinator procedures, version 2. Approved by Board of Trustees 7 Feb2000
- Oatts ML, Erwin SR, Hart JL (1990) Application of the REI equivalent for operations planning analysis of interchange schedules. IEEE transactions on power systems, 5, no. 2, May 1990, pp 547–555
- Pomarleanu M, Savulescu SC (2009) Detection and evaluation of stability constrained transmission paths. In: Real-time stability assessment in modern power system control centers (Savulescu SC ed). Wiley and IEEE Press, New York, New York, Jan 2009
- Sauer PW, Pai MA (1990) Power system steady-state stability and the load-flow Jacobian. IEEE transactions on power systems, 5, T-PWRS-4, pp 1374–1383
- Savulescu SC (1981) Equivalents for security analysis of power systems. IEEE transactions on power systems, PAS-100, pp 2672–2682
- Savulescu SC (2004) A metric for quantifying the risk of blackout. Paper 04PS0294 presented at the real-time stability challenge panel session, power systems conference and exposition 2004, New York, New York, 10–13 Oct 2004
- Savulescu SC (2005) Fast assessment of the distance to instability. Theory and implementation. In: Real time stability in power systems. Springer, Norwell
- Savulescu SC (2009a) Dimo's approach to steady-state stability assessment: methodology overview and algorithm validation (co-author). In: Real-time stability assessment in modern power system control centers (edited by Savulescu SC). Wiley and IEEE Press, New York, NY, USA, pp 320–353
- Savulescu SC (2009b) Real-time stability assessment in modern power system control centers (ed). Wiley and IEEE Press, New York, New York
- Tinney WF, Powell WI (1977) The REI Approach to power network equivalents, PICA'77 conference, May 1977, Toronto, Canada
- Venikov VA (1977) Transient processes in electrical power systems (edited by Stroyev VA, English translation). MIR Publishers, Moscow
- Venikov VA, Stroeve VA, Idelchick VI, Tarasov VI (1975) Estimation of electrical power system steady-state stability. IEEE transactions on power systems, PAS-94, 3, pp 1034–1041
- Vergara JS, Gonzalez LA, Savulescu SC, 2005, Practical experience with Dimo's steady-state stability assessment method in Panama. Energetica 53(9):330–337
- Vickovic D, Eichler R (2009) Real-time stability monitoring at the independent system operator in Bosnia and Herzegovina. In: Real-time stability assessment in modern power system control centers. Wiley and IEEE Press, New York, New York
- Virmani S, Vickovic D, Savulescu SC (2007) Real-time calculation of power system loadability limit. Paper no. 576 presented at the Powertech 2007 conference, July 1–5, 2007, Lausanne, Switzerland
- Vournas CD, Sauer PW, Pai MA (1996) Relationships between voltage and angle stability of power systems. Electr Power Energy Syst 18(8):493–500 (Elsevier Science Ltd.)

Chapter 4

Composite Approach for the Early Detection, Assessment, and Visualization of the Risk of Instability in the Control of Smart Transmission Grids

Roland Eichler, Chris O. Heyde and Bernd O. Stottok

Abstract The present chapter tackles the problem of determining and presenting the relevant information which can assist a power system operator in assessing the risk of blackout due to instability in a timely, efficient, and effective manner. Algorithmic approaches and numerical indicators that can help identify the instant status of the degree of operating reliability are also presented. Three concepts to detect, quantify, and visualize the risk of blackout are introduced and extensively illustrated with speedometer diagrams, stability trending charts, and snapshots taken directly from supervisory control and data acquisition (SCADA) system user interfaces.

4.1 Introduction

The increase of consumption of electric energy during the past decades has led to an expansion of synchronously operated AC systems as well as to higher voltage levels. All around the world, technical and economic advantages of combined operation have brought forth the interconnection of adjoining grids. With a view to needed reduction of CO₂ emissions, there will be a significant change in utilized resources as well as the energy mix. As in the past, transmission and distribution network structures were developed in accordance with the then available generation and load structures – to address the forecasted resources and energy mix, structural and operational changes will have to be applied (Eichler et al. 2012) to move towards the smart grid of the future.

Blackouts do not happen out of the blue and without prior signals of distress. Unplanned transmission outages, decaying voltages, and other events that push a power system towards an unsafe modus operandi usually develop slowly; however, when the unsafe status is reached, the events occur almost instantly within milliseconds and hence do not leave sufficient time for the operator to react. This is the

B. O. Stottok (✉) · C. O. Heyde · R. Eichler
Siemens AG, Nuremberg and Erlangen, Germany
e-mail: bernd.stottok@siemens.com

reason why one needs to detect when the operating conditions of the power system are developing towards a state where a blackout will become unavoidable as early as possible. As the operating conditions are changing continuously, quantifying and posting the risk of instability needs to be performed for every new operating state (Eichler et al. 2011).

Blackouts and large-area outages in America and Europe have confirmed that the interconnection of adjoining networks is beneficial in terms of operation and economy; however, this also bears the risk of uncontrollable, cascading outages (Eichler et al. 2012). This is especially true when grids are operated close to their thermal limits in certain areas, as stability and protection problems will occur (Buchholz et al. 2008). In order to have enough time to take early corrective actions and to prevent approaching states that may be too dangerous, one first needs to detect that the power system is moving in the wrong direction at all. This is also a continuous process which consists of monitoring how the stability conditions change in real time and then issuing appropriate warnings if and when necessary (Eichler et al. 2011).

An important goal of dynamic security assessments is to determine if a power system is able to withstand a series of major contingencies. Another important goal is to evaluate the risk of possible instability if the power system tumbles slowly towards a dangerous state, which could be the result of either a small topology and/or load change together with slow bus voltage changes that might trigger a voltage collapse. Slow load increases may also finally cause one or several generators to lose synchronism. Instability in a power system can also be caused when attempting to transfer large MW blocks to compensate load increases and/or generation outages in certain areas of the power system, thus increasing generation somewhere else. Instability also will take place when units lose synchronism because of self-oscillations (Eichler et al. 2011).

In today's control room environment, there are basically three approaches that in some respect complement each other and help the operator to assess the risk of blackouts successfully. All of them support the operator in monitoring how the stability conditions change in real time and then issue warnings if and when needed (Stottok et al. 2013).

4.2 Supervision and Analysis of Synchrophasors

The use of synchrophasor measurements from Phasor Measurement Units (PMUs) for wide-area monitoring enables the view to dynamic phenomena in the transmission network (Phadke and Thorp 2008). The basic idea is to supply the control center operators with a dynamic and precise real-time view into the voltages, currents, and phase angles of the electric grid by use of a Phasor Data Processing (PDP) system (Styczynski et al. 2009). This enables them to quickly understand the actual stability situation and trend in the system (Eichler et al. 2011). No system topology



Fig. 4.1 Example for frequency measurement with PMU

information is necessary, so the engineering of such a system on the control center side is relatively simple.

However, to observe that a blackout is approaching solely from monitoring PMU data either requires an immense level of expertise or support with further information from additional applications (Stottok et al. 2013). An overview about current and possible future applications for PMU measurements can be found in Novosel (2009). Due to the complexity of the issue, the user interface has to provide operators with the ability to quickly identify and analyze areas of criticality within the power system (Stottok et al. 2013) using components adapted to the various applications. The following applications of synchrophasor measurements can support the system operator in analysis and prediction of system stability:

4.2.1 Frequency Monitoring

Figure 4.1 shows a frequency measurement by a PMU during a scheduled power plant switching at 8:00 pm in the ENTSO-E network in Europe. The east-west-mode (0.2 Hz) can be seen quite well with a small amplitude. Such a frequency curve enables checking of the existing network model and the known power swing modes. Frequency curves from PMUs can indicate upcoming problems such as power swings or active power imbalance.

4.2.2 Phase Angle Monitoring

Phase angle differences indicate the power flow between two locations in the power grid. Increasing phase angle differences indicate increasing power flow between regions. If they differ from the expected load flow, this is an early problem indicator.

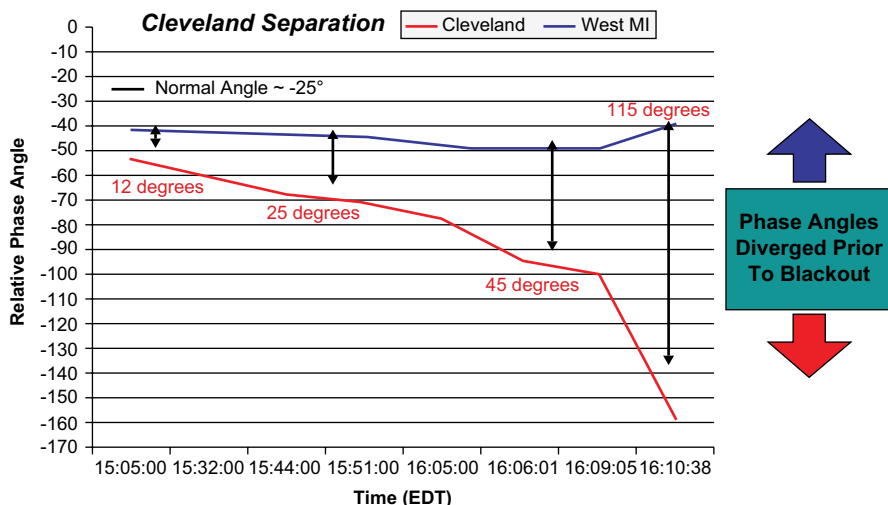


Fig. 4.2 Phase angle during the August 14, 2003, blackout in the USA (taken from www.naspi.org)

The schematic diagram (Fig. 4.2) shows that the upcoming blackout could have been seen in advance if actual phase angle measurements had been available.

Figure 4.3 shows phase angle measurements from PMUs during a switching off of coupling lines between two regions.

The phase angle of the voltage changes immediately and goes with a well-damped oscillation into the new state. These curves show that the system state remains stable. If the phase angle did not trend towards a new constant value, the operator would be immediately made aware that predefined corrective/preventive actions have to be taken.

In a real-life PDP system, the charts window displays time series (Fig. 4.4) and vector diagrams (Fig. 4.5) of individually measured values or calculated values over a time period (Stottok et al. 2013).

4.2.3 Power Swing Recognition

The idea of power swing recognition is to analyze selected measurements continuously to detect power swings. The parameters' damping, amplitude, and frequency (mode) of the power swing determine when an alarm is generated. With the automatic continuous supervision of the measurements, the PDP wide-area monitoring tool provides a reliable, fast indication of critical system states with several visualization possibilities (geographic, alarm, event, and technical data of power swing mode).

To ensure that the operator is made aware of the situation, the power swing is displayed in a geographic overview of the system. The map window (Fig. 4.6) of the PDP shows the network topology of the power supply system. Substation symbols

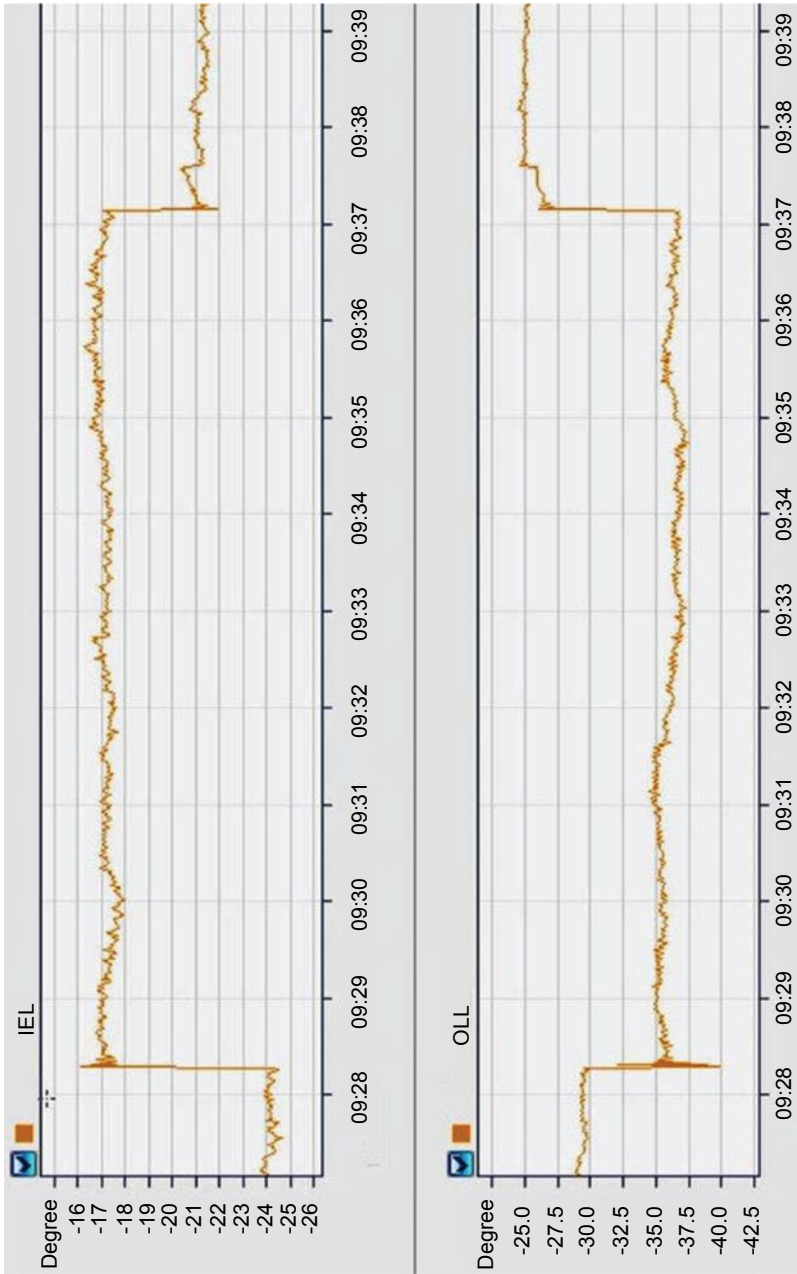


Fig. 4.3 Phase angle on two lines after switch events

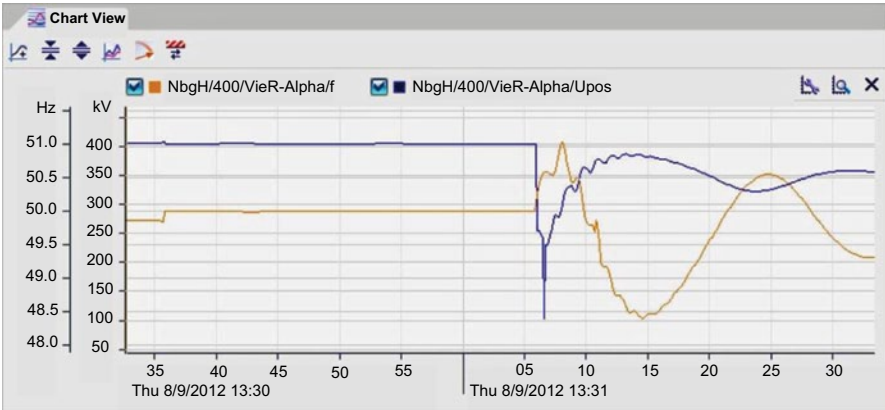


Fig. 4.4 Chart view – display mode of several curves of a time range

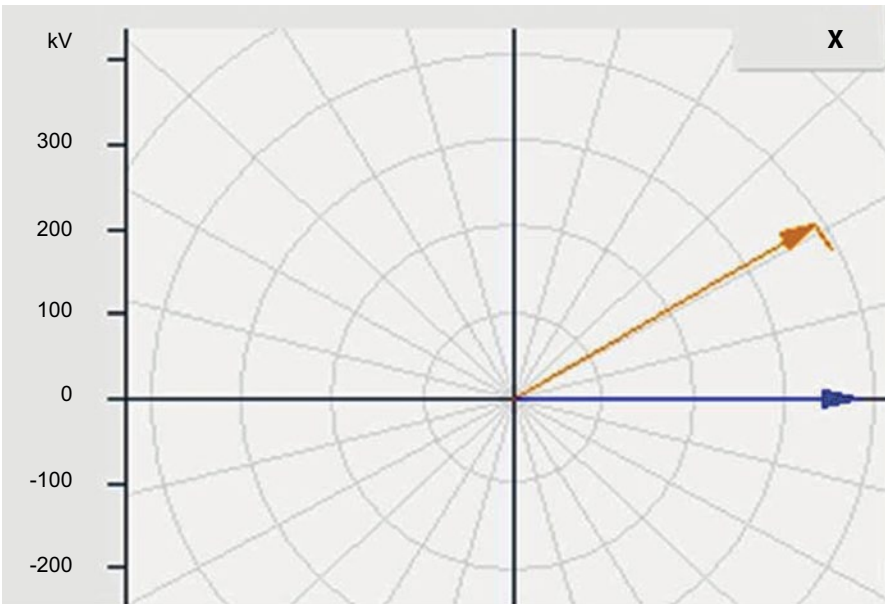


Fig. 4.5 Chart view – vector diagram of two bus voltages

and transmission lines are color coded to indicate whether those objects are in a normal or critical power state. Objects which are colored in blue are normal, yellow objects are approaching a critical state, and red objects have already reached a critical state. A swing detected in the electrical power system is shown in the schematic diagram as colored circular areas around the substations. The circular areas can also be connected by colored rectangular areas, if the swing affects several substations (Stottok et al. 2013).

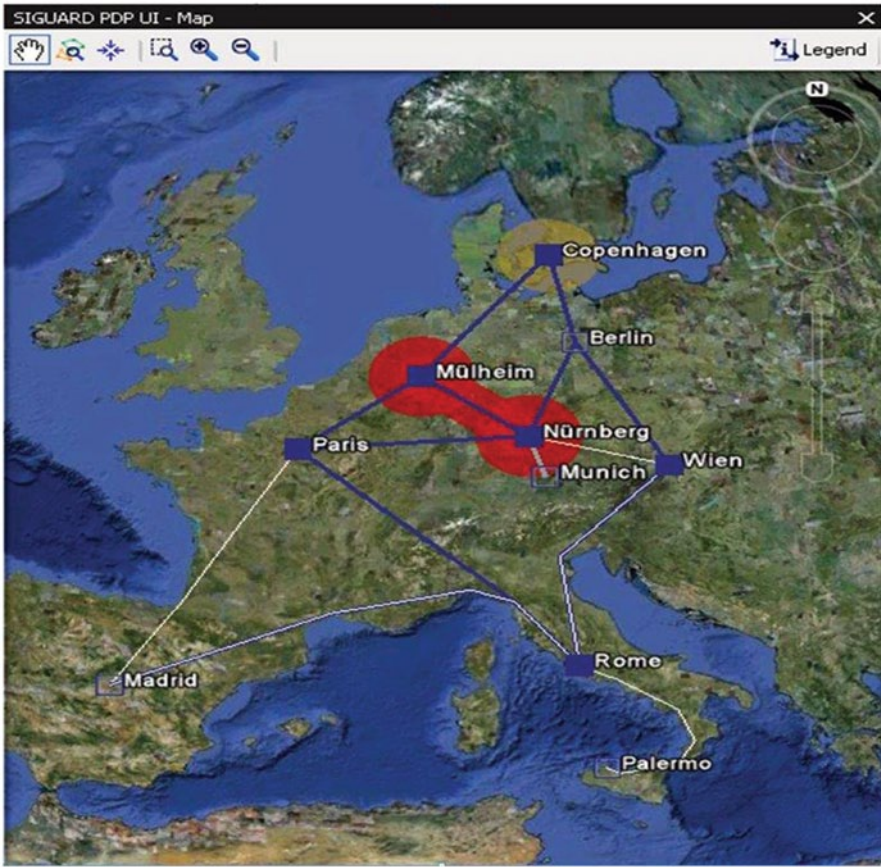


Fig. 4.6 Map-based visualization of power swings and critical equipment states

A further display especially designed for fast interpretation is shown in Fig. 4.7. The diagram indicates all recognized power swings for the current time point as dots in the frequency damping diagram. The colors of the dots visualize the criticality of the swings (red = critical, yellow = dangerous) and are defined based on their damping as well as from the amplitudes of the swings. The dotted lines represent a damping ratio of 3 or 5 %, respectively (Stottok et al. 2013).

4.2.4 Island State Detection

Because every PMU sends a frequency measurement to the wide-area monitoring system, it is possible to compare them. If a difference is detected, this is a hint for a

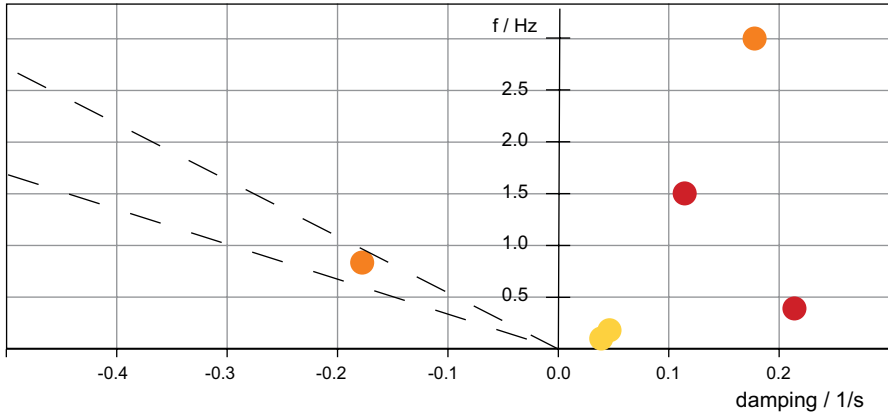


Fig. 4.7 Recognized power swings diagram overview of PMU data or power swings (frequency over damping)

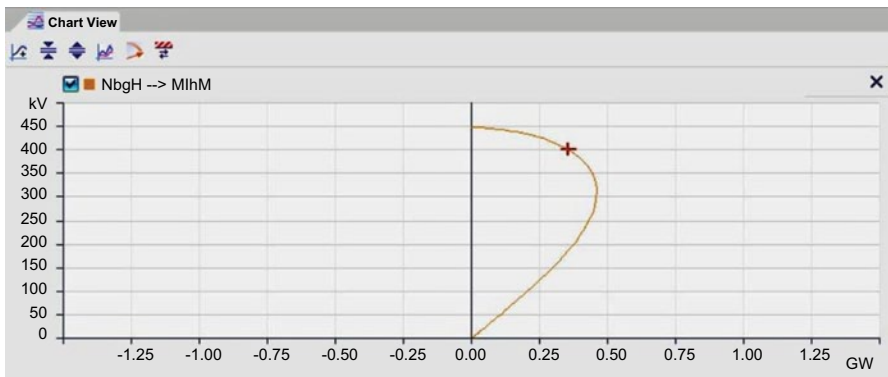


Fig. 4.8 Voltage stability curve of transmission line NbgH-MlhM

system separation which generates an alarm. Additionally, the detected islands can be shown on a geographic map.

4.2.5 Voltage Stability Curve

The voltage stability curve (Fig. 4.8) shows the actual operating point of a line on a voltage–power curve. Two PMUs on both ends of the line supply the application with the actual voltages and currents. With the known impedance of the line, the dynamic difference with respect to the stability limit of the line can be shown in the widespread shape of a PV diagram (“nose curve”).

4.2.6 Line Thermal Estimation

Using the measured current and voltage on a line, it is possible to estimate the line temperature. This gives an impression of actual thermal load and the current reserves on the line. Figure 4.9 shows how the estimated temperature on a line increases where a heavy load is switched on.

4.2.7 Power System Status Curve

The so-called power system status curve, illustrated in Fig. 4.10, actually is not another application that supports the operator's fast comprehension of the power system status; rather it serves as an initial overview visualizing the trend of the power system stability conditions (Stottok et al. 2013).

The power system status curve is calculated using all available measured values for which the limiting values are defined. The user can specify which measured values are to be included in the calculation. The curve is calculated from the weighted distances between the measured values and their limiting values. Critical values of the power supply system are displayed as a red curve in the part of the display above the dotted middle line. The higher the value is represented on the y axis, the more critical it is. In addition, the critical time range is highlighted in light red. Thus, the power system status window provides a single go/no go indication of system health and criticality for both real time and past, e.g., for the past 2 h (Stottok et al. 2013).

4.3 Real-Time Calculation of the Steady-State Stability Limit

Another approach to assessing the risk of blackouts is to run rapid, albeit approximate real-time stability tools with input from the state estimator (SE), i.e., to quickly calculate the power system stability (QuickStab) (Stottok et al. 2013). As opposed to the PDP based approach, QuickStab does not depend on a particular hardware in the field; rather it uses data that are available in a supervisory control and data acquisition/Energy Management System (SCADA/EMS) anyway and it only needs a few pieces of data beyond what is needed for running SE.

A well-suited and field-proven index for power system stability monitoring in real time is the Steady-State Stability Limit (SSSL) (Savulescu 2014). The SSSL of a power system is "a steady-state operating condition for which the power system is steady-state stable but for which an arbitrarily small change in any of the operating quantities in an unfavorable direction causes the power system to lose stability" (IEEE 1982). Known as steady-state stability reserve, this index was introduced in Europe by Paul Dimo (Dimo 1961, 1975). The algorithmic foundation of this technology has been extensively documented elsewhere (e.g. Savulescu 2014). The

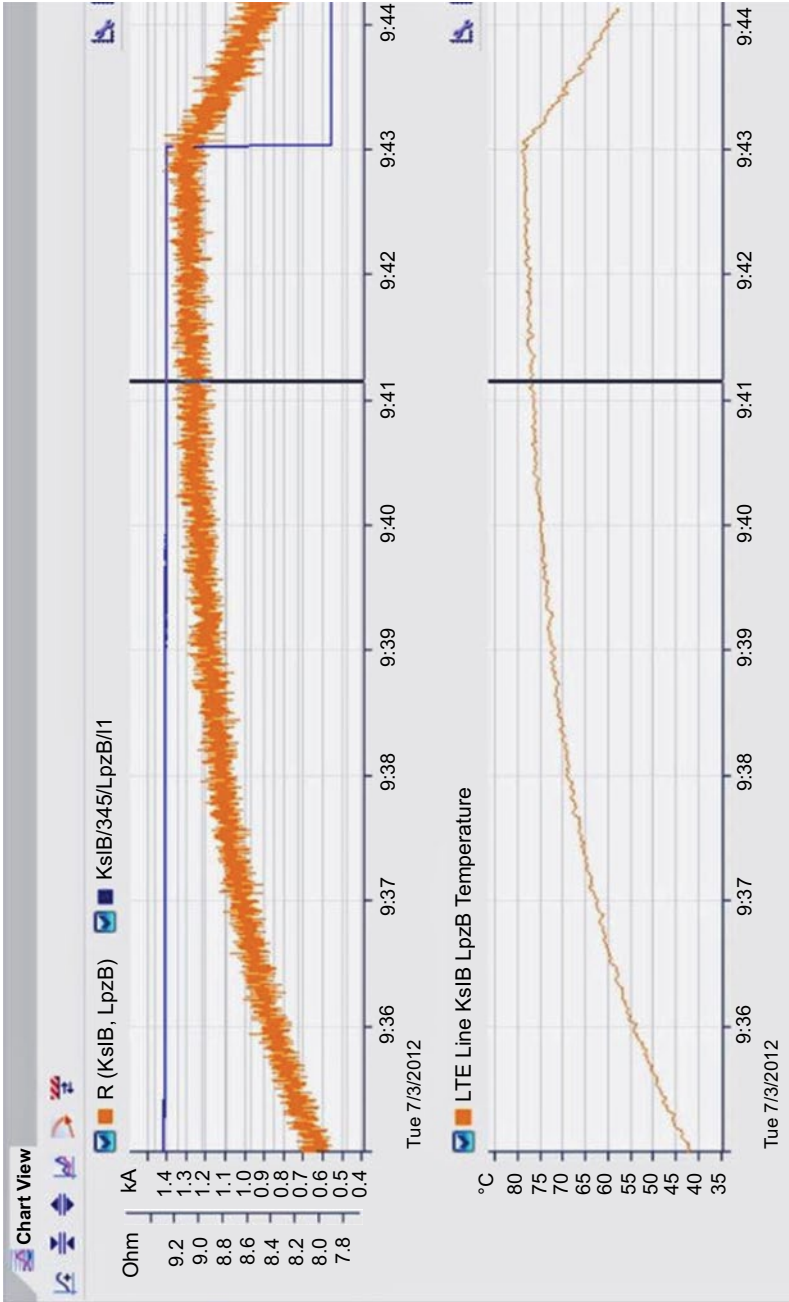
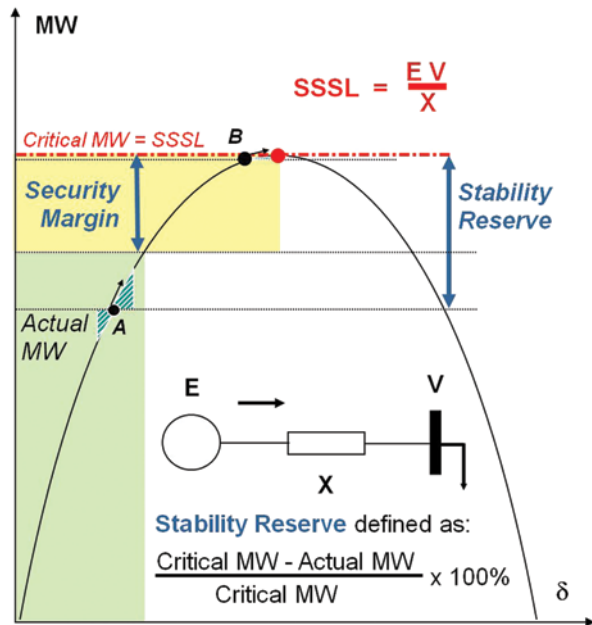


Fig. 4.9 Calculation of line temperature during load switching on a line



Fig. 4.10 Power system status trend curve display of PDP

Fig. 4.11 Simplified visualization of the steady-state stability limit (SSSL)



algorithm combines well-known stability index calculation approaches with inherent characteristics of power system parameters in a way that this calculation can be done in the SE periodicity – even if it includes the consideration of contingency cases as well as some capabilities for providing preventive measures in cases of insufficient stability reserve (Eichler et al. 2011).

The SSSL is mathematically quantifiable, can be computed, and represents an operating limit – albeit one that is local, rather than global, and which is unsafe in the sense that operating states even just below this limit may become quickly, or even instantly unstable (Eichler et al. 2011).

The SSSL can be quantified in terms of the total MW loading of the transmission system, considering both internal generation and tie-line imports (Eichler et al. 2011). Based on this, a metric (Savulescu 2004) can be defined to quantify “how far from SSSL” a given power system operating state is (Eichler et al. 2011). A visualization of the SSSL concept is given in Fig. 4.11. Please note that for sake of

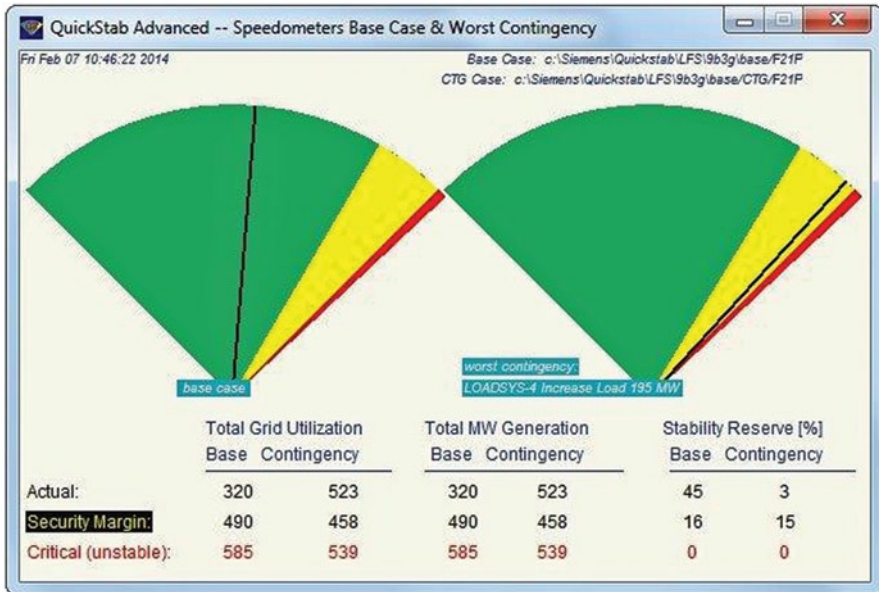


Fig. 4.12 QuickStab Two-Speedometer Chart depicting the distance to instability (*red*) and to the security margin (*yellow*)

easy visualization, a simplification was applied by only illustrating the curve of load MW versus rotor angle for a single-line-single-generator configuration (Eichler et al. 2011).

One of the key displays that are continuously updated on an operator console is the so-called Two-Speedometer Chart depicting side by side the base case, i.e., the current system state as computed during the most recent successful run of the SE, and the worst contingency case (Fig. 4.12).

The left-hand speedometer displays the distance to instability in the base case, i.e., the *current state*. The needle corresponds to the total MW system grid utilization. The *left edge* of the red sector identifies the *critical state*, which is quantified by the SSSL. Several important remarks need to be made:

- The red sector does *not* depict an operating area for the very simple reason that, after instability, the system state does not exist: it is blackout, so there is no system state any longer. Technically speaking, the “red area” should have been just a thin line, but for ergonomic reasons, we chose to build it with some depth so that it could be easily identified on the display.
- The *distance to instability* is conveyed by the position of the needle with respect to the left edge of the red sector and is *quantified* by the stability reserve in [%] below the SSSL.
- The width of the yellow sector is proportional to the percentage value of the security margin.

- This ergonomically powerful representation should be viewed in relation to the “stability envelope” concept illustrated in Fig. 4.11, where the “safe” operating region is shown in green and corresponds to total system MW grid utilizations smaller than the MW security margin (Stottok et al. 2013).
- The speedometer chart *per se* is both intuitively relevant and quantitatively correct: On the one hand, it shows instantly how safe are the system conditions and if there is any risk of blackout; on the other hand, the needle position and the width of the yellow sector are thoroughly recalculated after each state estimation cycle, and so, they truly depict the current power system state as it changes in time. And if, in addition to the “distance” to instability, the operator also wants to know the exact MW amount of the stability reserve and, respectively, the security margin, those numbers are shown at the bottom of the display.

The right-hand speedometer in Fig. 4.12 shows the distance to instability not for the base case but *for the worst contingency* that has been simulated. In the example shown, the worst contingency would reduce the stability reserve from 33% in the base case down to 7% and thus drive the system right into the middle of the yellow area. This indicates to the operator that the power system would be severely at risk once this double branch outage would occur (Stottok et al. 2013).

It is of paramount importance for the system stability indices, e.g., the distance to SSSL, to be continuously updated for the operator. Therefore, their computation and visualization must be connected to the SCADA/EMS of the transmission grid control center. In order to efficiently support the operator monitoring and controlling of a transmission grid facing rapid loading and generation pattern changes, it is important that there are provisions for (Eichler et al. 2011):

- Immediate information for the operator on the distance from instability, periodically as well as after each significant system change, e.g., a circuit breaker tripping;
- Display of the decisive results in the user interface of the SCADA/EMS, especially the trend curve of the “distance to SSSL”;
- Capability to evaluate system instability for perceived situations via the familiar SCADA/EMS study case management and in the same convenient manner as in real time.

The *rending* of the stability reserve is the main display of the SCADA/EMS watched by the control room operator for monitoring the power system stability. Figure 4.13 shows an example from the Transmission System Operator of Bosnia-Herzegovina. The 24 h curve shows significant changes due to some outages that have occurred that day. Phases of decreasing reserve, recovery at a lower level, and again increasing reserves become apparent. The current value of the stability reserve is also shown at a prominent location in the always visible Basic Signaling Display (right in the middle of the upper display part of Fig. 4.13). Additional SCADA/EMS displays showing QuickStab results include a list of generators sorted according to their influence on the stability reserve. This list identifies those generators where

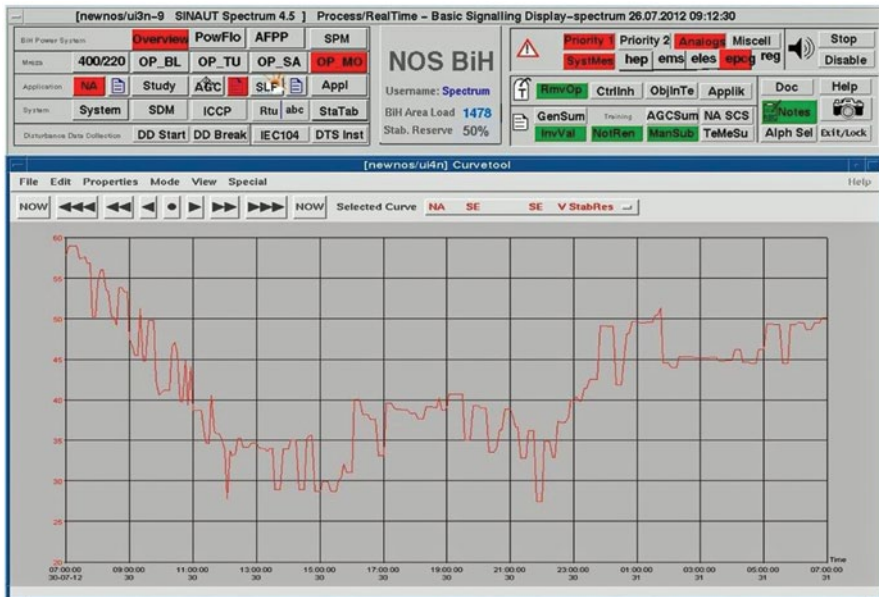


Fig. 4.13 Trend curve of the stability reserve integrated in a SCADA/EMS UI

generation has to be increased (or decreased) in order to enlarge the stability reserve (Stottok et al. 2013).

4.4 Dynamic Stability Assessment

The third approach to increase the situational awareness with respect to power system stability is to perform an online Dynamic Stability Assessment (DSA). This mainly model-based approach uses precise time-domain simulations with an automatic determination of critical situations. Time domain simulations are the most accurate technique; however, they are also the most time consuming. The main procedure of an online DSA application is depicted in Fig. 4.14.

This application needs to work in periodic cycles. Each cycle starts with receiving an SE snapshot and/or system forecasts. This is followed by parallel time-domain contingency simulations on a computation server cluster. The parallelization is done to save time and to be able to process as many contingencies as possible. After the results are available, the system automatically analyzes and ranks and visualizes them to the user. In case stability problems are discovered, an online DSA system must be able to pre-simulate remedial measures in order to propose the most successful corrective steps and actions to the user. The user now decides which action to take and the DSA cycle can start over again.

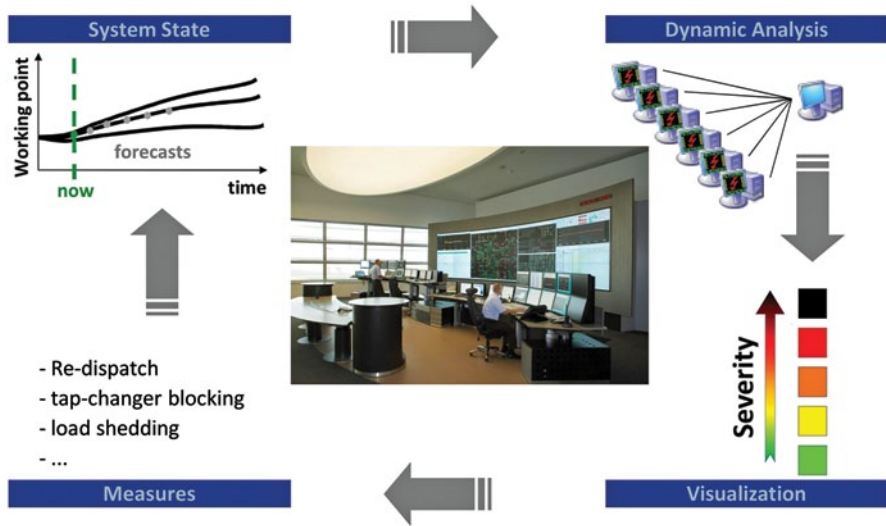


Fig. 4.14 Procedure of online DSA application

In the following, the most important features and benefits an online DSA application should provide are explained on the example of an existing DSA solution.

4.4.1 Technology

DSA is using the power of full time-domain contingency simulations. Similar as in the QuickStab approach, it uses a certain load flow case as the basis for all simulations. Such load flow cases can come from diverse sources such as:

- SCADA/EMS state estimator
- Linear PMU-based state estimator
- Power flow calculation considering short-term forecasts (including, e.g., renewable generation), day-ahead/outage scheduling, and switching plan
- Long-term planning cases

The accuracy of a DSA system is strongly related to the quality of the power system model and the state estimate. Important is the detailed representation of the power system including all devices and controllers affecting its electromechanical behavior. Additionally, modeling the system-relevant protection devices can increase the quality of DSA results. Hence, a modern DSA system should be able to analyze the primary and secondary equipment at the same time, such as (Eichler et al. 2011):

- Generators
- Compensation

- FACTS
- HVDC
- Dynamic loads
- Wires
- Cables
- Transformers
- Distance protection
- Generator protection

Depending on the stability phenomena being studied, simulation time, time steps, and modeling details can vary. For example, for transient and short-term voltage stability studies, a 5-20 s study period is sufficient. Long-term voltage stability studies however require a study period of several minutes. During the simulations, the complete network is observed and in case any stability criteria are violated, the contingency is marked as critical.

The main advantages of using the DSA approach are:

- No model simplification
 - Full topology as in SCADA/EMS and planning model
 - Influence of each power system element can be determined
- All physical stability phenomena as categorized in Kundur (1994) can be analyzed
 - Short- and long-term effects
 - Angle, voltage, frequency and oscillatory stability
- Operational rules compliance can be determined in addition to pure stability
- Definition of contingencies can include sequences of events
 - Subsequent tripping of lines or generators
 - Automatic reclosure cycles
 - Different durations of short circuits
- Inclusion of protection behavior and different special protection schemes
 - Generic function of differential or generator protection devices which are system relevant
 - Load shedding mechanisms or other special protection schemes
- Direct possibility to simulate and validate measures
 - Preventive measures (rescheduling, topology changes, and so forth)
 - Corrective measures (switching, load shedding, and so forth)
 - Automatic corrective measures only armed in critical situations (system integrity schemes, operation tripping, and so forth).

All these advantages have to be paid at the cost of computational power. Twenty years ago, this was a serious problem because CPU power was extremely expensive. The trend however shows that the costs per CPU are constantly decreasing while CPU power is constantly increasing. Due to this fact, together with smart acceleration techniques, DSA can be integrated in the online environment of today's transmission system control rooms.

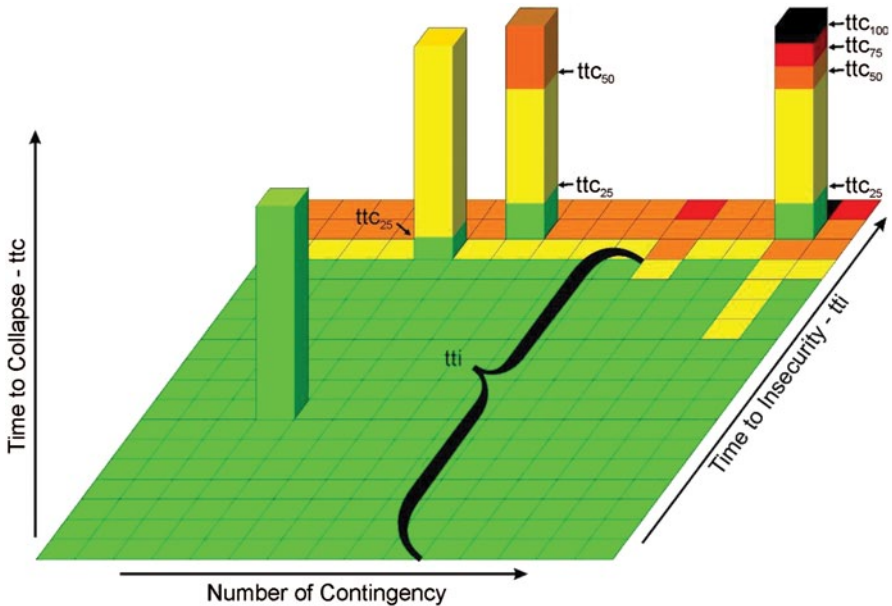


Fig. 4.15 Principle of DSA margin with respect to time

Compared to static stability assessment methods, the purpose of DSA is not to determine the margin to instability in terms of MVA, but it rather gives a qualitative degree of stability. This means that DSA finds all unstable cases where the system collapses and determines cases which are close to instability. However, the DSA approach does not allow for determination of an allowable MVA change up to reach instability. In order to do so, a case degradation would have to be applied during each contingency simulation.

The results from case degradation approaches also strongly depend on the assumed deterioration pattern. By nature, power systems behave in a heavily nonlinear fashion, especially when the system is close to its stability limit. Hence, a small change in that deterioration pattern can cause large changes in the calculated MVA margin. Similarly, this is true for the qualitative degree of stability calculated in a DSA solution. The result “relatively stable” can change to “instable” after small changes have been applied to the base case load flow. To mitigate this drawback, the DSA approach offers the possibility to take into consideration not only theoretical stability criteria but also any other criterion such as sensitivity indices, operational limits, grid-code constraints, and protection induced limits.

Instead of determining the exact MVA margin, the DSA approach rather determines the duration until instability. This is possible by taking into account the most probable system development for the next few hours. If an operator knows that the system is far from instability for the current point in time and for the next 2 h, there is no need to take any action. This concept is depicted more closely (Heyde 2010) in Fig. 4.15, which shows three axes plus the information on the coloring scheme.

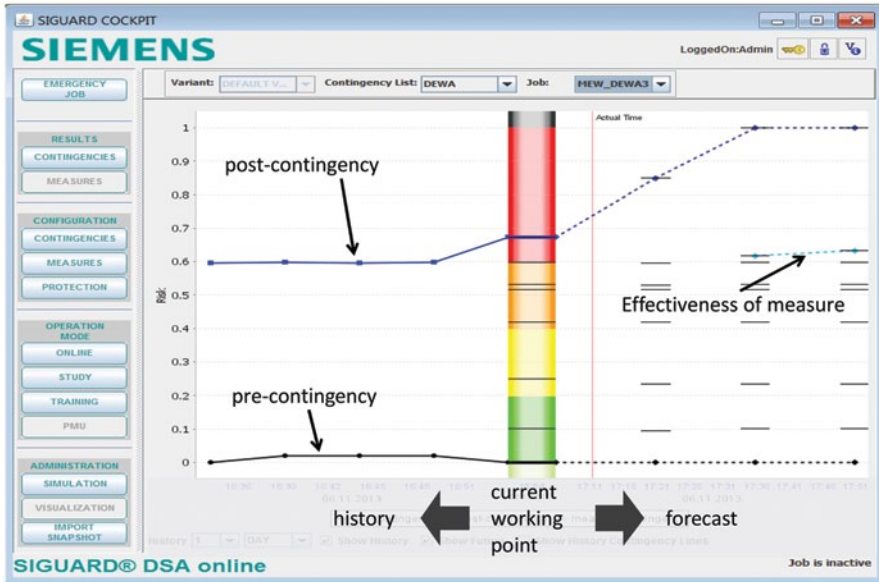


Fig. 4.16 DSA cockpit

The x -axis represents the different contingencies being simulated, for example, events such as short circuits in critical regions or outages of important network elements. The y -axis shows the progress within the time-domain simulations, whether, for example, a voltage collapse will occur 5 s or 5 min after the contingency event. The z -axis (time to insecurity – t_{ti}) shows the forecasting horizon.

The coloring depicts the results of the contingency simulations. Green means that the system is perfectly stable, whereas yellow, orange, red, and black indicate that the system would face stability problems if the contingency actually occurred. In this case, the power system would be in an acceptable state until t_{ti} . When this time is reached, at least one contingency would cause unwanted limit violations (first orange-colored contingency). Please note that for the sake of clarity, only four simulation results are shown completely. In reality, each of the squares in Fig. 4.15 would have an expansion in y -direction.

4.4.2 Visualization

The visualization of the results of dynamic security assessment performed in real time is realized in several levels of details. The very first display should continuously show the risk of blackout in a traffic light fashion to the control center staff. Such a first display is shown in Fig. 4.16 (Stottok et al. 2013).

This diagram shows three curves (black, dark blue, and light blue). The x -axis represents the time from the operator's point of view. It allows viewing of the recent history, the current situation, and the short-term forecast (next few hours). The y -axis represents the severity of possible contingencies. This severity is scaled between 0 and 1, where 1 means high risk and 0 means low risk (Stottok et al. 2013). The coloring in this cockpit corresponds to the coloring in the previous Fig. 4.15.

The black curve indicates the state of the overall power system with respect to stability limits without applying any faults or contingencies (base case or pre-contingency). The risk for this pre-contingency curve is determined from the state estimate-based load flow. Alternatively, this value can also be derived from the evaluation of PMU measurements (Stottok et al. 2013).

The dark blue curve represents the results from the most severe contingency. If this curve reaches a high level, the power system would be insecure because at least one contingency would lead to limit violations. In the case shown, the dark blue curve reaches the value 1 on the right-hand side of the diagram. This means there is one system forecast where instability has been observed. This is the forecast for 1 h from now on. The operator has now 30-45 min left to find successful countermeasures.

A powerful DSA system can also help the operator in finding countermeasures because any measure can be simulated prior to its activation in the field. Possible measures could be among others re-dispatching or topology changes as well as curtailment of renewable generation or loads. Once these measures are known by the DSA system, they can be automatically processed whenever a stability threat is recognized. The results of such measure simulations are exactly the same as for contingency simulations, which is why their effectiveness can easily be displayed in the DSA visualization screens.

In Fig. 4.16, this is done with the light blue curve. In this example, the operator knows from the first view that the system would actually be instable; however, there is a measure available which successfully mitigates the instability.

The advantages of a model-based DSA system can be formulated as follows:

- Preventing blackouts due to increase of situational awareness;
- Higher exploitation of existing assets by lower security margins due to knowledge of actions to take in the unlikely event of a contingency.

The cockpit displayed in Fig. 4.16 is intended to show all relevant information to the operator in the control room. This information can be summarized as follows:

- What is the current risk of a blackout?
- Do the historic or forecasted results show a threatening trend?
- Is my pre-contingency condition already problematic?
- If a high risk of blackout is indicated, how many contingencies are involved?
- If a high risk of blackout is indicated, is a remedial measure available?

In case that high risk has been identified and/or no successful measure could be found automatically, a DSA system must offer the possibility of a detailed analysis of the situation. In conventional planning tasks, the engineer usually focuses on a

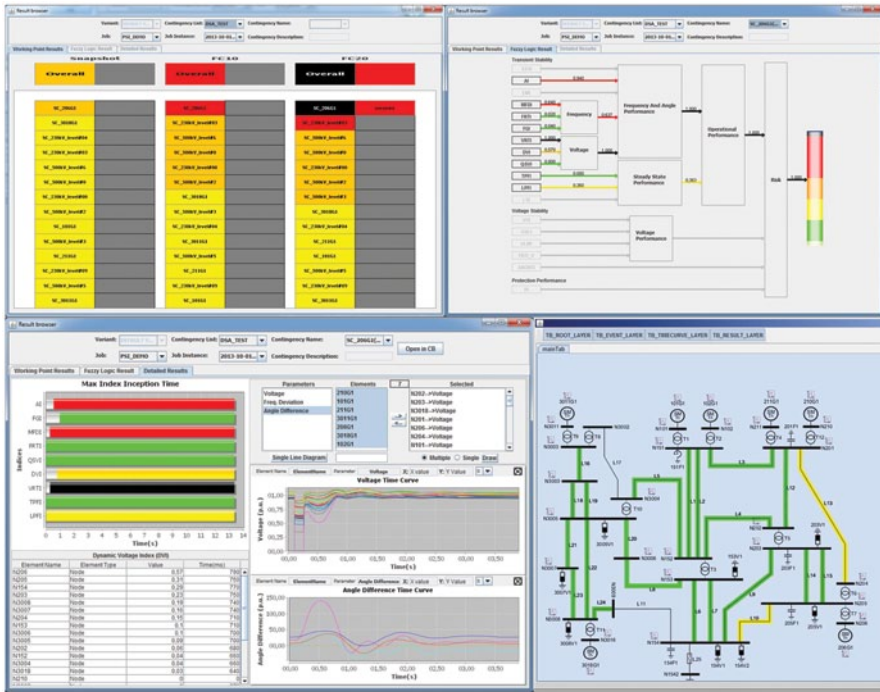


Fig. 4.17 Multilayer visualization with contingency listing (*top left*), data aggregation view (*top right*), expert view (*bottom left*), and single-line diagram (*bottom right*)

selected portion of the power system and performs a limited number of contingency simulations. An online DSA system always has to consider the system as a whole. Hence, the detailed results should be presented to the user in such a way that the following questions can be answered subsequently:

- Which contingency or contingencies caused the problem?
- Which physical phenomena are involved (frequency, angle, or voltage stability)?
- Is the problem local or global?
- What assets are involved?

The DSA system described in this section solves this problem with the multilayer visualization approach. In addition to the cockpit with the most aggregated information (Fig. 4.16), the system uses three layers plus single-line views up to a highly detailed expert view (Fig. 4.17). It depends on the user’s experience if all layers are explored or if, for detailed analysis, the control room staff consults an expert from the planning department to study the security problems and to answer the questions above. In order to collaborate across departmental borders, the DSA system must be designed for multiusers on client-server architecture.

Figure 4.17 gives an overview about the multilayer results visualization. Other than in power system planning tasks, the user of an online DSA system does neither

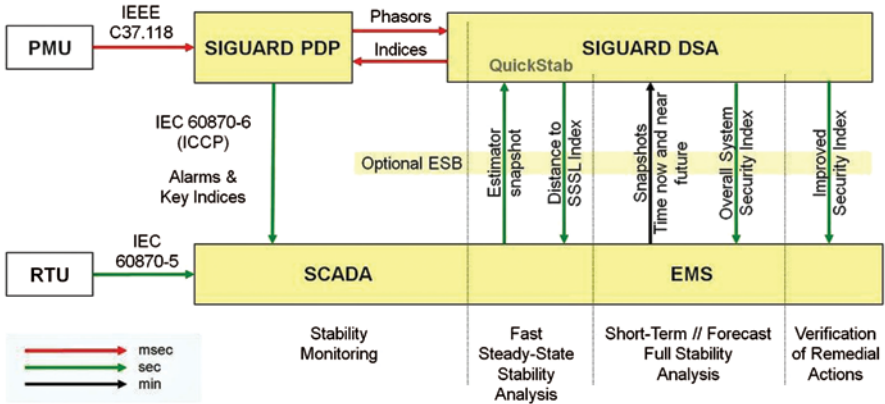


Fig. 4.18 Data flow between blackout prevention modules

have the time nor the knowledge to work through the results of several hundred contingency simulations in order to find the critical ones. Hence, the visualization of an online DSA must at all times find the most important information automatically thus guiding the user through large amounts of data and producing a clear visualized result which is easy to interpret. This is done by ranking of results and by coloring of the graphical user interfaces and single-line diagrams.

4.5 Deployment in SCADA/EMS Environment

4.5.1 Overview

Each of the three tools outlined above brings its particular benefits to the control room operator. Tying them together as shown in Fig. 4.18 allows systematic monitoring of system stability from real time through to the immediate future until hours ahead. Thus, a framework is provided for detecting critical situations on time, *ex-ante* verification of remedial measures, and monitoring of actual observation of stability limits (Eichler et al. 2012).

4.5.2 Modular Set-Up

The framework shown in Fig. 4.18 can be built-up piece by piece with many points to start from. One possibility is to start with the installation of PMUs. A PDP unit as outlined in Sect. 4.2 would continuously analyze the incoming data and detect critical swings, excessive phase angle differences, and so forth at each instant of time.

Additional system relevant analyses are provided by the DSA tool presented in Sect. 4.4. The DSA tool normally applies such algorithms to the simulated contingency states of the power system; however, they can as well be applied to a set of phasor measurements which is transferred from the PDP tool. DSA, in turn, sends additional indices back to the PDP for alarming and displaying in its user interface (Eichler et al. 2012).

In this way, stability monitoring can be done without needing any information from a SCADA system such as network topology. In any case, limit violations and status alarms from applications such as power swing recognition and supervision information of the wide-area monitoring system can be made available to the control center operator by an ICCP communication connection. This allows the operator to focus on the SCADA user interface he/she is used to. If an alarm from the wide-area monitoring system occurs, the operator is notified immediately and can switch to the detailed screens of the PDP module (“Stability monitoring”) (Eichler et al. 2012).

Furthermore, SCADA systems are using unsynchronized system measurements via Remote Terminal Units (RTUs). The measured values are rms values of voltages and currents as well as real and reactive powers that are transmitted to the front end of the EMS in time steps of some seconds. The current load flow situation expressed as magnitudes and angles of voltages and currents is estimated by a so-called SE integrated in the EMS. Robustness and accuracy of this process highly depends on the accuracy of measurements received as well as on the amount of data. The latter defines the “observability”.

The observability of the power system can actually be increased by the use of PMU data. As described in Sect. 4.2, this tremendous amount of data are analyzed and archived in the PDP module; via the ICCP link, the abovementioned snapshots can be transmitted to the EMS in cycles similar to RTUs, e.g., once a second. The EMS thus can use the phasor data to improve the state-estimator results (Eichler et al. 2012).

Another starting point for building up the blackout prevention framework is the EMS part of the control center system. The power system status as calculated by the SE application can be transferred to a module which executes fast steady-state stability index calculation as outlined in Sect. 4.3. The module (in Fig. 4.18 represented by the QuickStab algorithm) may initially be stand-alone and later be extended to the full DSA functionality. Since the calculation is done within seconds (to give an example: the calculation solves 2000-3000 bus systems in even less than a second on regular laptop computers), the distance to SSSL index is sent back to the SCADA/EMS user interface practically in the SE cycle time typically between 30 s and 2 min (“Continuous Steady-State Stability Analysis”) (Eichler et al. 2012).

When the full DSA functionality is available, an Overall System Security Index covering the full range of stability phenomena can be determined and sent back to the SCADA/EMS user interface. However, since the calculation of such indices for the base case as well as for some thousands of contingencies takes some time the application concept is different: regularly, e.g., each 15 min, the most recent SE result is transferred to DSA for full analysis of the current situation (“time now”).

To get an additional view to the future system states, the power flow and forecast components of the EMS calculate the corresponding power system status for near future intervals. For all system states (time now and near future time steps), the DSA calculates all defined contingencies. The stability indices sent back to the SCADA/EMS are updated with each calculation step finalized, thus providing the operator with a virtually continuous stream of information. Latest after 15 min, all calculations are done and the process starts again with the most recent results of SE and forecast power flows (“Short Term and Forecast Full Stability Analysis”). At the same time, the DSA module can provide verification of measures that improve the security index, thus helping the operator to navigate the power system through congestive situations with highest security (“Verification of Remedial Actions”) (Eichler et al. 2012).

4.5.3 Architecture

As can be deduced from the explanations above, the concept is to allow alarming and key index visualization in the SCADA/EMS user interface that is very familiar and always visible to the operator. However, when more detailed information is needed, the genuine specialized user interface of the particular application is used rather than trying to replicate it in the SCADA/EMS environment (Eichler et al. 2012).

Furthermore, the system is modular in a way that the three components which make up the composite approach can be kept entirely separate from a SCADA/EMS. In this case, just industry standard interfaces are used. Tighter integration is an option but not mandatory. The integration of the QuickStab module, for instance, in practice varies from a separate PC running the software and the specialized user interface (Arnold et al. 2009; Savulescu 2014; Vickovic et al. 2007; Vickovic and Eichler 2009) to integrating the QuickStab software completely with the network analysis package of the SCADA/EMS. The latter eliminates the need for a dedicated hardware and makes the real-time calculation of the distance to instability a regular part of the SCADA/EMS functionality such as SE or security analysis (Eichler et al. 2012).

It is obvious that the DSA deployment must have a distributed architecture. The advantage of such architecture is that the system is highly scalable. If, for example, the size of the system model increases and demands for more computational power is augmented, the number of computation servers can be increased without any changes in the rest of the system (Eichler et al. 2012).

4.5.4 Data Communication

The various data communication technologies applied in the proposed architecture are worth analyzing in more detail. Phasor data (red lines in Fig. 4.18) are

communicated at cycles in the order of milliseconds, either based on standardized IEEE C37.118 protocol between PMUs and SIGUARD PDP or using the dedicated SIGUARD Service Interface (SSI) between the PDP and DSA modules. Data at cycles of seconds (green lines) update the SCADA system from both the RTUs and the PDP module by means of standard protocols IEC 60870-5 and IEC 60870-6, respectively. Similarly, resulting information from the DSA module updates the SCADA/EMS user interface a few seconds after a calculation was initiated. The input data for the calculation are transferred at cycles of minutes (full analysis, black line) or fractions thereof (fast steady-state analysis, green line). The technology applied for the latter transfers can be as simple as traditional point-to-point file transfer. A modern SCADA/EMS architecture, however, demands for the use of an Enterprise Service Bus (ESB) and Service-Oriented Architecture (SOA) (CIGRE 2011). Instead of loosely coupling DSA in either way, a fully integrated DSA could use the benefits of SCADA/EMS such as single point of data maintenance and direct access to the network applications database.

4.6 Conclusion

Three approaches have been presented, each of which contributes to the problem of assessing and visualizing the risk of instability in a highly loaded transmission grid. Each of the approaches is suited to considerably support the task of control room operators of today's transmission grid companies. The different characteristics of this support have been discussed in detail in this chapter and need not be repeated here. The different prerequisites however are worth being repeated since absence of any could make a significant difference: collection, monitoring, and analysis of phasor measurement information need investment in field equipment and communication links. However, it should be noted that PMUs tend to become "anyway available" low-cost features of every new protection device installed in a substation.

By investing in sufficient communication infrastructure and PDP software, power system operators will be able to make use of these new, dynamic measurements. As with many emerging technologies, the advantages are obvious but the way to apply them in the current work flow is not directly visible.

A prominent example for this is the Internet which, when first opened to the public was used for a limited number of functions only, for example, e-mails. After some time, people started to use it in their specific ways, by introducing social networks and knowledge bases. The same will happen with PMU measurements because all power networks have their very own topology and are prone to very specific stability problems. Hence, the way PMU measurements and analyses are used to derive operator action will be specific also.

Fast and approximate calculation of the distance to steady-state instability by QuickStab comes with virtually no extra investment in hardware or data, whereas

DSA requires distinguished computation power for its parallel execution plus thoroughly developed data models mirroring the dynamic system behavior. Transmission operators should have the latter available in their planning departments so that the model needs only to be harmonized with the operations department.

As mentioned above, each of the three approaches brings its particular benefits. However, it should be noted that combining the yields of the three methods equates to more benefit than just the sum of the individuals. For instance, extension of DSA with PDP enables the incorporation of additionally calculated indices when assessing the system stability. Adding QuickStab to DSA firstly allows pre-filtering of the list of contingencies thus accelerating the DSA computations and secondly it allows the calculation of a fast – albeit approximate – stability index determination for all contingencies being replaced one by one by accurate DSA results as their computation is in preparation.

From the practical use viewpoint, the modular architecture of the tool set and the use of international communication standards wherever applicable are crucial for the successful use of the tool set in transmission grid control centers.

Furthermore, a workflow-oriented user interface integration of the above described three approaches is decisive for success. As in the control center of the future, all three approaches will exist in parallel to each other and will offer complementary information for the operator, thus supporting him/her in finding answers to the different kind of tasks he/she has to deal with during operation. Such tasks can be related to the actual point of time or they can be of preventive nature, for example, preemptive measures to avoid the risk of a blackout.

The tool set described in this chapter is powerful and pioneering for bringing smarter monitoring and decision tools to the transmission grid control room. However, it is not yet all-encompassing. Adding an online Protection Security Analysis (PSA) module is the next necessary step towards securely controlling continuously changing power systems. PSA will allow the discovery of weak points in the protection scheme as a whole, including main and backup depending on the current network state.

All the above mentioned tools have one thing in common: They are *observing* or *predicting* insecure power system situations which might lead to customer interruptions or even blackouts. They encompass implicit or explicit preventative action proposals that the user still has to activate manually. However, as mentioned earlier, power systems become more dynamic and the manual activation of preventative actions may not be sufficient in some cases.

Therefore, Wide-Area Protection and Control (WAPC) systems have been discussed in the literature for quite some time. WAPC systems are the logical consequences of applying tools to determine the degree of stability. However, these systems are extremely specific for each power network. In order to develop such systems, the knowledge gathered from experience with the help of the three tools described above will be highly beneficial.

References

- Arnold L, Hajagos J, Manassis SM, Philip A (2009) LIPA implementation of real-time stability monitoring in a CIM compliant environment, Real-time stability assessment in modern power system control centers. Wiley and IEEE Press, New York
- Buchholz B-M, Krebs R, Rudion Z, Sassnick Y (2008) Vision 2020—security of network operation today and in future. In: German experiences, Proceedings of the IEEE PES, GM 2008, 20–24 July 2008, Pittsburgh, USA
- CIGRE SC D2 WG D2. 24 (2011) EMS for the 21st century—system requirements. CIGRE, Paris
- Dimo P (1961) Etude de la stabilité statique et du réglage de tension. Rev Gén l'Electr, Paris 70(11):552–556
- Dimo P (1975) Nodal analysis of power systems. Abacus, Kent
- Eichler R, Krebs R, Savulescu SC, Wache M (2011) Early detection and mitigation of the risk of blackout. CIGRE international symposium “The electric power system of the future—integrating supergrids and microgrids in transmission grid operation”, Bologna, Italy, 13–15 September 2011
- Eichler R, Krebs R, Lerch E, Wache M (2012) Mitigating risk of system instability caused by fluctuating renewables with smart transmission grid applications, CEPsi 19th conference on electric power supply industry, Paper A154, Bali, Indonesia, 15–19 October 2012
- Heyde CO (2010) Dynamic voltage security assessment for on-line control room application, MAFO, volume 32, Magdeburg, Germany
- IEEE (1982) PES task force on terms and definitions, proposed terms and definitions for power system stability, IEEE Transactions on PAS, PAS-101, 7, p 1894
- Kundur P (1994) Power system stability and control, EPRI power system engineering series. McGraw-Hill, New York
- Novosel D (2009) Timing the power grid. Presentation at the executive forum. Austin TX, 6 March 2009
- Phadke AG, Thorp JS (2008) Synchronized phasor measurements and their applications. Springer, Norwell
- Savulescu SC (2004) A metric for quantifying the risk of blackout. Paper 04PS0294 presented at the real-time stability challenge panel session, power systems conference and exposition 2004, New York, NY, 10–13 October 2004
- Savulescu SC (2014) Fast computation of the distance to instability. In Real time stability in power systems, 2nd edn. Springer, New York
- Stottok BO, Heyde CO, Eichler R, Savulescu SC (2013) Visualizing the risk of blackout in smart transmission grids (co-author). Paper presented at CIGRE international symposium “Smart grids: next generation grids for new energy trends”, Lisbon, Portugal, April 2013
- Styczynski ZA, Sauvain H, Buchholz BM, Wache M (2009) PMU and wide area measurements in distribution systems. CIGRE, 20th international conference on electricity distribution, Prague, 8–11 June 2009, Round Table 3b
- Vickovic D, Eichler R (2009) Real-time stability monitoring at the independent system operator in Bosnia and Herzegovina. In: Real-time stability assessment in modern power system control centers. Wiley and IEEE Press, New York
- Vickovic D, Eichler R, Savulescu SC (2007) Real-time system stability monitoring in the transmission network of Bosnia and Herzegovina. Paper presented at the Power Grid Europe conference and exhibition, Feria de Madrid, Madrid, Spain, 26–28 June 2007

Chapter 5

Power System Transient Stability Preventive and Emergency Control

Daniel Ruiz-Vega, Louis Wehenkel, Damien Ernst,
Alejandro Pizano-Martínez and Claudio R. Fuerte-Esquivel

Abstract A general approach to real-time transient stability control is described, yielding various complementary techniques: pure preventive, open-loop emergency, and closed-loop emergency controls. Recent progress in terms of a global transient stability-constrained optimal power flow is presented, yielding in a scalable non-linear programming formulation which allows to take near-optimal decisions for preventive control with a computing budget corresponding only to a few runs of standard optimal power flow and time-domain simulations. These complementary techniques meet the stringent conditions imposed by the real-life applications.

5.1 Introduction¹

Power system security is more and more in conflict with economic and environmental requirements. Security control aims at making decisions in different time horizons so as to prevent the system from being in undesired situations, and in particular to avoid large catastrophic outages. Traditionally, security control has been divided into two main categories: preventive and emergency control.

¹ Portions of this chapter have been reprinted, with permission, from L. Wehenkel and M. Pavella 2004, Preventive vs. emergency control of power systems, presented at the *Real-Time Stability Challenge Panel Session, Power Systems Conference and Exposition 2004*, New York, New York, 10–13 October 2004. © 2004 IEEE.

D. Ruiz-Vega (✉)
Instituto Politécnico Nacional, Mexico City, Mexico
e-mail: drv_liege@yahoo.com

L. Wehenkel · D. Ernst
University of Liège, Liège, Belgium

A. Pizano-Martínez
Universidad de Guanajuato, Salamanca, Mexico

C. R. Fuerte-Esquivel
Universidad Michoacana de San Nicolás de Hidalgo, Morelia, Mexico

In preventive security control, the objective is to prepare the system when it is still in normal operation, so as to make it able to face future (uncertain) events in a satisfactory way. In emergency control, the disturbing events have already occurred, and thus the objective becomes to control the dynamics of the system in such a way that consequences are minimized.

Preventive and emergency controls differ in many respects, among which we list the following (Wehenkel 1999).

Types of Control Actions Generation rescheduling, network switching reactive compensation, sometimes load curtailment for preventive control; and direct or indirect load shedding, generation shedding, shunt capacitor or reactor switching, and network splitting for emergency control.

Uncertainty In preventive control, the state of the system is well known but disturbances are uncertain; in emergency control, the disturbance is certain, but the state of the system is often only partially known; in both cases, dynamic behavior is uncertain.

Open Versus Closed Loop Preventive control is generally of the open-loop feed-forward type; emergency control may be closed loop, and hence more robust with respect to uncertainties.

In the past, many utilities have relied on preventive control in order to maintain system security at an acceptable level. In other words, while there are many emergency control schemes installed in reality, the objective has been to prevent these schemes as much as possible from operating, by imposing rather high objectives to preventive security control.

As to any rule, there are exceptions: for example, controlled generation shedding has been used extensively in Northern America to handle transient stability problems; in the same way, corrective control has been used in many systems as an alternative to preventive control in the context of thermal overload mitigation.

Nowadays, where the pressure is to increase trading and competition in the power system field, preventive security control is being considered as an impediment to competition; in turn, this breeds strong incentives to resort less on preventive control and more often on emergency control.

The objective of this chapter is essentially twofold: first, to concentrate on transient stability control, both preventive and emergency, and describe a general methodology able to realize convenient tradeoffs between these two aspects; second, to suggest means of integrated security control, coordinating various types of security (steady-state, voltage, and transient stability).

The general methodology used to design transient stability control techniques relies on the transient stability method called Single-Machine Equivalent (SIME). In what follows, we first describe the fundamentals of SIME and then concentrate on the advocated control techniques.

5.2 A Unified Approach to Transient Stability Assessment and Control

5.2.1 Fundamentals of SIME

SIME is a hybrid direct-temporal transient stability method (Pavella et al. 2000a).

Basically, SIME replaces the dynamics of the multi-machine power system by that of a suitable One-Machine Infinite Bus (OMIB) system. By refreshing continuously the OMIB parameters and by assessing the OMIB stability via the Equal-Area Criterion (EAC), SIME provides an as accurate Transient Stability Assessment (TSA) as the one provided by the multi-machine temporal information and, in addition, stability margins and critical machines.

In other words, SIME preserves the advantages of the temporal description (flexibility with respect to power system modeling, accuracy of TSA, and handling of any type of instability (first or multi-swing, plant, or inter-area mode)), and, in addition, complements them with functionalities of paramount importance.

One of them is generation control (generation rescheduling for preventive control, generation shedding for emergency control), which uses the knowledge of stability margins and critical machines. Indeed, the amount of generation to shift (or shed) depends on the size of the stability margin, and the generators from which to shift (or shed) are the so-called critical machines.

SIME-based preventive control relies on the temporal information (swing curves) provided by a Time-Domain (T-D) simulation program, whereas SIME-based emergency control relies on real-time measurements. Nevertheless, conceptually, the core of the method is the same. In what follows we assume that SIME is fed sequentially by samples of the multi-machine swing curves, no matter whether they are provided by T-D simulations or real-time measurements.

5.2.2 Instability Conditions and Margins

To analyze an unstable case (defined by the pre-fault system operating conditions and the contingency scenario), SIME starts receiving samples of the swing curves as soon as the system enters its post-fault configuration.

At each new sample, SIME transforms the multi-machine swing curve sample into a suitable OMIB equivalent, defined by its angle δ , speed ω , mechanical power P_m , electrical power P_e , and inertia coefficient M . All OMIB parameters are derived from multi-machine system parameters; Pavella et al. 2000a. Further, SIME explores the OMIB dynamics by using the EAC. The procedure stops as soon as the OMIB reaches the EAC *instability conditions* expressed by

$$P_a(t_u) = 0 \text{ and } \dot{P}_a(t_u) > 0, \quad (5.1)$$

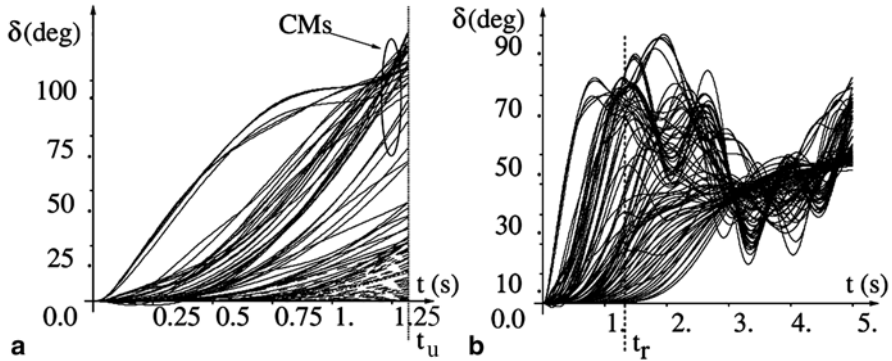


Fig. 5.1 Multi-machine swing curves. **a** Unstable case. **b** Stable case. Critical clearing time, 69 ms; clearing time, 95 ms. (Adapted from Ruiz-Vega 2002)

where P_a is the OMIB accelerating power, difference between P_m and P_e , and t_u is the *time to instability*: At this time, the OMIB system loses synchronism, and the system machines split irrevocably into two groups: the group of “advanced machines” that we will henceforth refer to as the “*Critical Machines*” (CMs), and the remaining ones, called the “*Non-critical Machines*,” (NMs)². Thus, at t_u SIME determines:

- The CMs, responsible of the system loss of synchronism;
- The corresponding unstable margin:

$$\eta_u = A_{\text{dec}} - A_{\text{acc}} = -\frac{1}{2} M \omega_u^2. \quad (5.2)$$

Figures 5.1a to 5.3b illustrate the above definitions on a stability case simulated on the EPRI 88-machine system. More precisely, Fig. 5.1a, b portrays the multi-machine swing curves provided by a T-D program, stopped at “the time to instability”, t_u . The symbol P_C used in the captions denotes the total power of the group of critical machines.

Figure 5.2a, b depicts the equivalent OMIB swing curve, whereas Fig. 5.3a, b represents, in the δ - P plane, the evolution with δ of the OMIB powers P_m and P_e .

² The “advanced machines” are the CMs for upswing instability phenomena, while for backswing phenomena they become NMs.

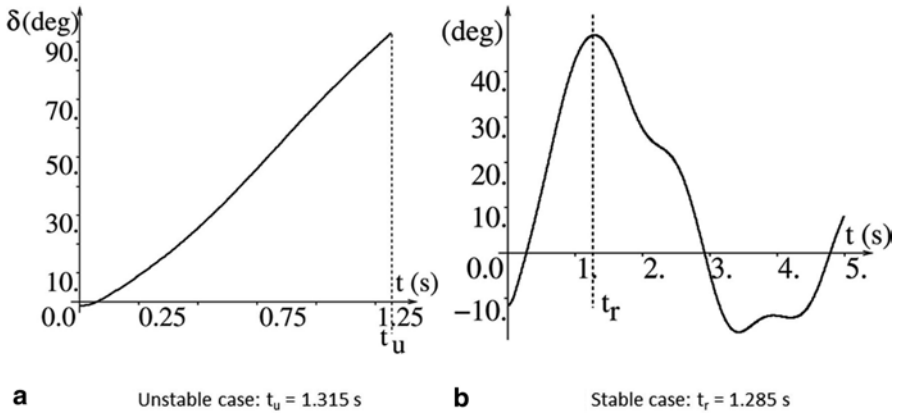


Fig. 5.2 Corresponding OMIB swing curves. **a** Unstable case. **b** Stable case. (Adapted from Ruiz-Vega 2002)

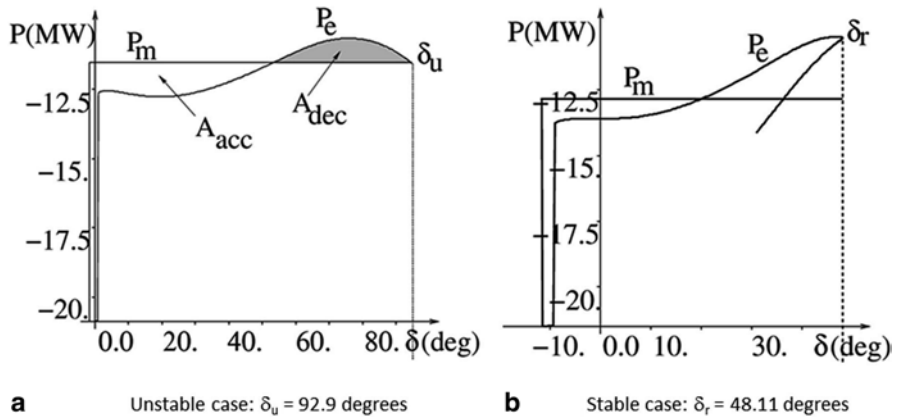


Fig. 5.3 Corresponding OMIB δ - P curves. **a** Unstable case. **b** Stable case. (Adapted from Ruiz-Vega 2002)

5.2.3 Salient Parameters and Properties

1. Calculation of stability margins, identification of the critical machines, and assessment of their degree of criticality (or participation to the instability phenomena) are parameters of paramount importance.
2. The “time to instability,” t_w , is another important factor. It indicates the speed of loss of synchronism and measures its severity.
3. Under very unstable conditions, it may happen that the standard margin does not exist, because the OMIB P_m and P_e curves do not intersect (there is no post-

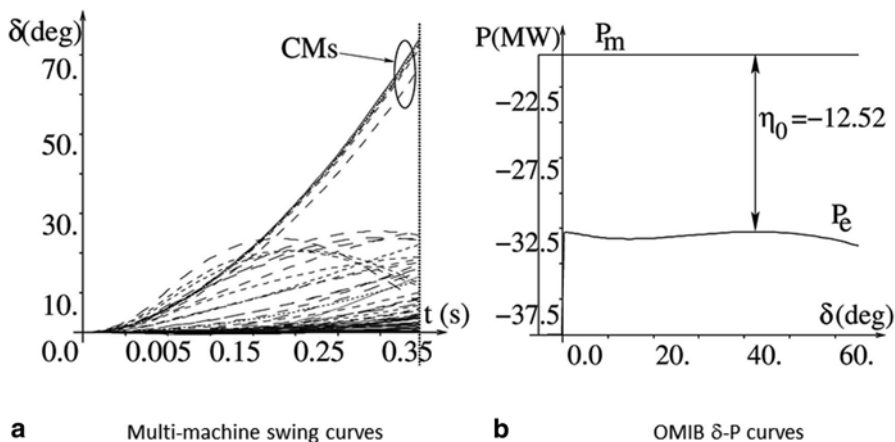


Fig. 5.4 Example of a severely stressed case. **a** Multi-machine swing curves. **b** OMIB δ - P curves. Clearing time=95 ms; $P_c = 5600$ MW. (Adapted from Ruiz-Vega 2002)

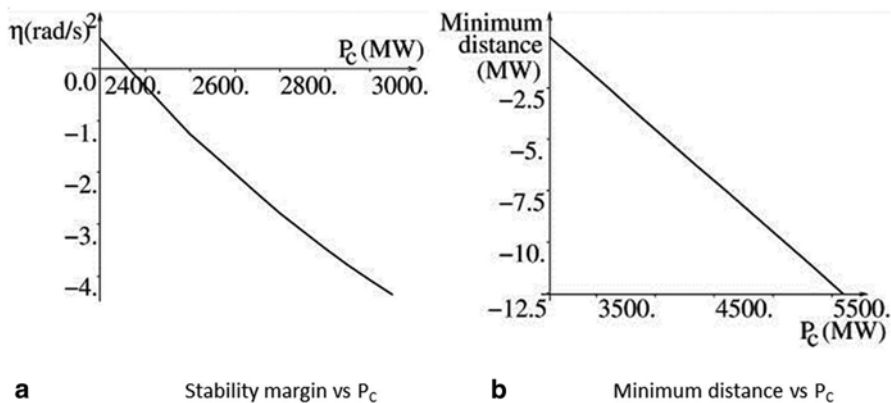


Fig. 5.5 Typical variations of the standard stability margin and of its surrogate with PC. **a** Stability margins versus P_c . **b** Minimum distance versus P_c . (Adapted from Ruiz-Vega 2002)

fault equilibrium solution). A convenient substitute is the “minimum distance” between post-fault P_m and P_c curves. Figure 5.4 illustrates this surrogate margin under particularly stressed conditions Ruiz-Vega and Pavella 2003. Note that here the surrogate to the “time to instability” is the time to reach this minimum distance and to stop the simulation. To simplify, we will still denote it “ t_u ”.

4. A very interesting general property of the instability margins (standard as well as surrogate ones) is that they often vary quasi-linearly with the stability conditions (Pavella et al. 2000a). Figure 5.5 illustrates the margin variation with the total generation power of the group of critical machines, P_c . The proposed control techniques benefit considerably from this property.

5. On stability conditions and margins. Similar to the instability conditions (5.1), stability conditions are defined by (Pavella et al. 2000a)

$$\omega(t_r) = 0 \text{ and } P_a(t_r) < 0, \quad (5.3)$$

where time t_r denotes the *time to stability*: At this time, the OMIB angle reaches its maximum excursion, after which it starts decreasing. At t_r , the first-swing stable margin can be computed by (Pavella et al. 2000a)

$$\eta_{st} = \int_{\delta_s}^{\delta_u} P_a d\delta. \quad (5.4)$$

Figures 5.1b and 5.2b portray, respectively, the multi-machine swing curves provided by an Extended Transient Midterm Stability Program (ETMSP) T-D simulation stopped at the maximum integration period (5 s) and the corresponding OMIB swing curves. Figure 5.3b represents, in the δ - P plane, the evolution with δ of powers P_m and P_e ; to simplify, only part of the evolution of the electrical power P_e has been displayed. Three observations should be made about stability conditions and margins. First, strictly speaking, stable cases do not have an OMIB equivalent (the system does not lose synchronism and its machines do not split into two divergent groups). However, by continuation, one can still use the OMIB corresponding to an unstable case close enough to the stable one. Second, meeting the stability conditions (5.3) does not guarantee that the system will be multi-swing stable. (More precisely, conditions (5.3) met after n swings do not guarantee $(n + 1)$ -swing stability.) Hence, multi-swing stability should be investigated via further exploration of the multi-machine swing curves. Finally, eq. (5.4) is a mere approximate expression of a stable margin, since the angle δ_u is never reached but, rather, assessed approximately.

6. Computational requirements. The above SIME calculations (of the OMIB parameters and resulting transient stability information about critical machines and margins) require virtually negligible computing time (generally, much smaller than 5% of the required T-D simulations).
7. The shape of an OMIB curve may differ significantly from the shape of an actual machine's swing curve. Indeed, the OMIB equivalent does not describe the behavior of an actual machine but, rather, the compressed information about the multi-machine system dynamics.
8. The identification of the group of critical machines is an issue of utmost importance. In some cases, the critical groups can be clearly identified during the whole simulation time. This has caused many researchers to try applying SIME in an incorrect way, in which they run the simulation first, until detecting instability by means of another criterion, like the maximum angular deviation, and then they identify the critical group as it can be observed at the end of the simulation.

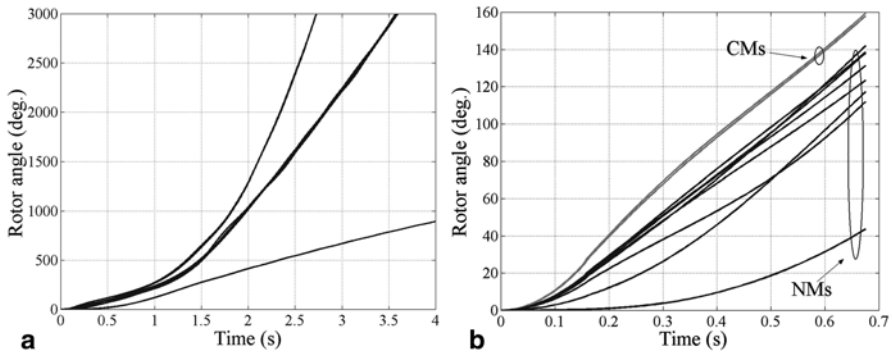


Fig. 5.6 Comparison of the groups of machines at the end of the simulation, and at the time instability conditions are met. **a** Multi-machine swing curves. **b** Identification of the CMs. (Adapted from Ruiz-Vega 2002)

Unfortunately, this procedure is not correct, since the actual critical group cannot always be easily observed at the end of the simulation as shown in *Fig. 5.6*. This case is also interesting because, as can be observed in *Fig. 5.6a*, it shows that the system machines are divided into three groups. Using SIME at each step of the T-D simulation, it is shown in *Fig. 5.6b* that the system machines are initially split into two groups, and that the instability conditions are met at a very early time of the simulation in which the group of machines when the simulation statistics is different from the one at the end of the simulation. This difference in machine groups makes it necessary to apply SIME at each time step of the simulation in order to correctly identify the group of critical machines.

5.2.4 Transient Oscillations Damping

5.2.4.1 Preliminaries

Today, online transient oscillations damping is becoming an issue of great concern, with the trend to include damping techniques as part of a transient stability function. An interesting online damping assessment technique uses the Prony method, where single- or multi-channel algorithms analyze one or several (up to, say, 15) generator swing curves at a time (Ruiz-Vega 2002; Ruiz-Vega et al. 2004). However, the quality of the analysis depends strongly on the number and proper identification of the relevant generator curves, whereas, generally, their number may exceed the algorithmic possibilities, and their identification may be far from obvious.

This may create serious difficulties when dealing with real-world power systems. SIME allows one to circumvent these difficulties by applying single-channel Prony analysis to the OMIB curve. Besides, by identifying the system machines that have a major influence on the oscillatory phenomena, it easily determines the

dominant modes of oscillation. Last but not least, it provides control techniques, able to improve transient oscillations damping as is described in Sect. 5.3.

5.2.4.2 SIME-Based Prony Analysis

For a given contingency, the SIME-based Prony analysis proceeds in the following way:

1. Run SIME to compute the transient stability limit (critical clearing time or power limit), using one stable and one or two unstable cases. The computation of such a limit relies on pair-wise extrapolation (or interpolation) of stability margins (§§ 5.3.2.3 and 5.3.5).
2. On the least unstable case, identify the critical machines and corresponding OMIB. Also, determine the “relative relevance” of each one of the critical machines, defined as the product of its inertia with its angle (absolute or relative to a reference), assessed at time t_u .
3. On the stable OMIB curve corresponding to the stable case in step 1 of this procedure, perform Prony analysis to assess the damping ratio of the OMIB swing curve.

Remarks:

1. The method assesses damping of nearly unstable contingency scenarios, which, generally, are the most interesting ones.
2. The Prony method has to analyze signals close to linear, if a direct comparison with modal analysis is required. This is often the case at the end of the data window, rather than at its inception, where the amplitude of the transients may be large.
3. The use of OMIB improves the Prony accuracy, robustness, and overall performance. Indeed, this second-order dynamic equivalent contains the key dynamics of machines exchanging energy. Besides, unlike other approaches, the OMIB rotor angle inherently captures the nonlinear and nonstationary dynamics of the system and can be used to determine linear and nonlinear attributes of system oscillations. Also, because of its formulation, the OMIB signals are less likely to include other less relevant dynamics, and this greatly facilitates the analysis of the slow dynamics of interest associated with the critical inter-area modes.

5.2.4.3 Sample of Illustrations

Ruiz-Vega et al. (2004) report on simulations performed on two real-world power systems using detailed system models: the EPRI 627-machine (4112-bus, 6091-line) system and the EPRI 88-machine (434-bus, 2357-line) system (Ruiz-Vega 2002; Ruiz-Vega et al. 2004).

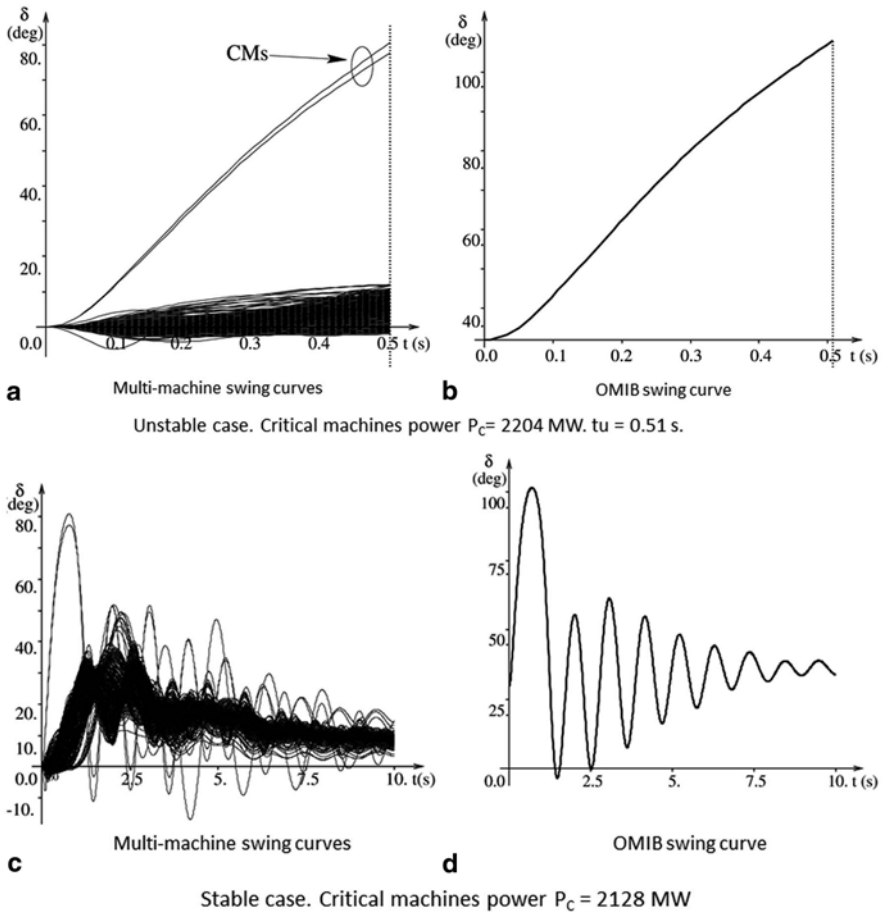


Fig. 5.7 Unstable and stable cases simulated on the EPRI 627-machine system. Unstable case: **a** Multi-machine swing curves, **b** OMIB swing curve; Stable case: **c** Multi-machine swing curves, **d** OMIB swing curve. Clearing time of both cases, 67 ms. (Adapted from Ruiz-Vega 2002)

The contingencies considered yield oscillatory plant modes (on the 627-machine system) and inter-area modes (on the 88-machine system). In all simulations, SIME is coupled with the ETMSP T-D program (EPRI 1994).

Plant Mode Oscillations

The plant-mode oscillations of the 627-machine system involve two critical machines. The resulting multi-machine swing curves of the considered post-fault stable case are displayed in Fig. 5.7c. The Prony analysis is applied to the OMIB swing curve of Fig. 5.7d, whose structure, as mentioned above, was defined on the unstable simulation displayed in Figs. 5.7a and 5.8.

Fig. 5.8 Comparison of the swing curves of the OMIB and the critical machines (Nrs 2075 and 2074) of the stable case simulated on the EPRI 627-machine system. (Adapted from Ruiz-Vega 2002)

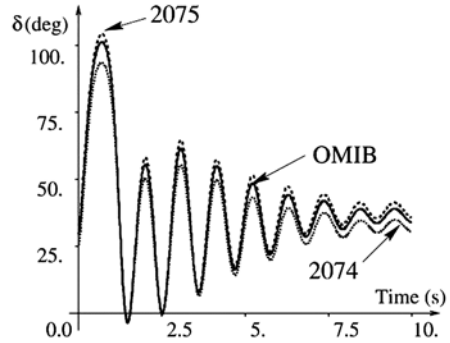


Table 5.1 Results of Prony analysis of the OMIB and the critical machine swing curves on the EPRI 627-machine system. (Adapted from Ruiz-Vega 2002)

α (rad/s)	ω (rad/s)	f (Hz)	ζ (%)	SNR (dB)
<i>OMIB</i>				
-0.483	5.84	0.930	8.23	42.35
<i>Machine # 2075</i>				
-0.509	5.83	0.927	8.7	43.27
<i>Machine # 2074</i>				
-0.474	5.83	0.928	8.0	35.89

Note that the two critical machines, defined on this unstable simulation, are easily identified also on the stable simulation. Hence, in this particular case, the choice of the generators to be analyzed is quite obvious; the SIME method and resulting OMIB are used here to illustrate the approach. Among various observations, we note the following:

1. In Ruiz-Vega et al. (2004), the original OMIB curve and the curve estimated by Prony have been displayed and shown to fit almost perfectly.
2. Also, Prony analysis has been performed on the two relevant machines identified by SIME (labeled #2075 and 2074). The result, displayed in Fig. 5.8, shows that the frequency of these two and of the OMIB curves is almost the same, while the value of the damping ratio of the OMIB lies in between that of machines 2075 and 2074. Table 5.1 gathers their damping features and shows that the numerical results are reflecting well the shapes and relative positions of the three curves.

Inter-Area Mode Oscillations

Application of a severe contingency to the EPRI 88-machine system has created an inter-area mode transient instability in which 36 machines lose synchronism with respect to the remaining 52 system machines. The swing curves of the unstable and stable cases are displayed in Fig. 5.9.

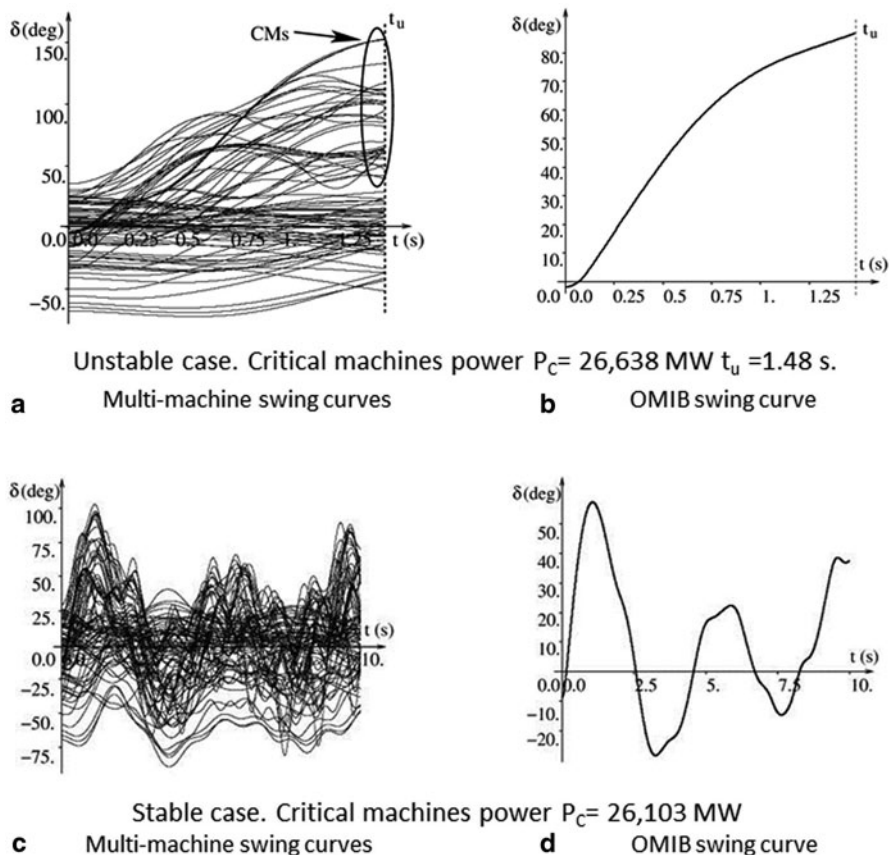


Fig. 5.9 Unstable and stable cases simulated on the EPRI 88-machine system. Unstable case: **a** Multi-machine swing curves, **b** OMIB swing curve; Stable case: **c** Multi-machine swing curves, **d** OMIB swing curve. Clearing time of both cases, 120 ms. (Adapted from Ruiz-Vega 2002)

Table 5.2 Damping assessment by Prony analysis of the OMIB swing curve for the EPRI 88-machine system. (Adapted from Ruiz-Vega 2002)

α (rad/s)	ω (rad/s)	f (Hz)	ζ (%)	SNR (dB)
-0.101	1.5117	0.24	6.6	42.29
0.206	5.5232	0.87	-3.7	

The Prony analysis performed on the stable case provides the results listed in Table 5.2. This table reveals that, actually, there are two dominant modes, and that for the above presumably “stable” case the damping ratio of one of them is negative, which suggests the existence of an unstable oscillation and predicts future system loss of synchronism. Actually, Ruiz-Vega et al. (2004) explain why the T-D simulation did not detect instability, by showing that this instability arises at 11.4 s,

i.e., beyond the preassigned maximum integration period of the simulation (10 s). Further, this reference suggests interesting by-products of this “early instability detection.”

Again, the original OMIB curve and the curve estimated by Prony are shown to fit perfectly (Ruiz-Vega et al. 2004).

5.3 SIME-Based Transient Stability Control Techniques

Various SIME-based control techniques have recently been proposed (Zhang et al. 1997; Pavella et al., 2000a; Ruiz-Vega and Pavella 2003). This section describes three such techniques dealing with preventive control, closed-loop emergency control, and Open-Loop Emergency Control (OLEC); this latter aims at mitigating control actions taken preventively with emergency actions triggered only upon actual occurrence of the threatening event. All three techniques rely on the same principle, described hereafter.

5.3.1 Principle

To stabilize a case, SIME uses the size of instability (margin), the critical machines, and suggestions for stabilization. These suggestions are obtained by the interplay between OMIB–EAC and T-D multi-machine representations as follows: Stabilizing a case consists of modifying the pre- or post-contingency conditions until the stability margin becomes zero. According to EAC, this implies increasing the decelerating area and/or decreasing the accelerating area of the OMIB δ – P representation. In turn, this may be achieved by decreasing the OMIB equivalent generation power. The amount of the OMIB generation decrease required to stabilize the system, ΔP_{OMIB} , is directly related to the margin η (Pavella et al. 2000a; Ruiz-Vega et al. 2003):

$$\eta = f(\Delta P_{\text{OMIB}}). \quad (5.5)$$

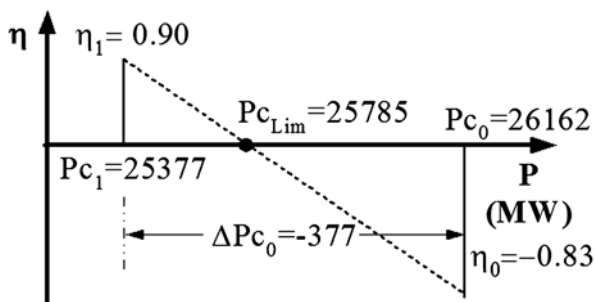
5.3.2 Preventive Control (P-SIME)

5.3.2.1 Iterative Stabilization Procedure

It is shown that to keep the total consumption constant, the following multi-machine condition must be satisfied, when neglecting losses:

$$\Delta P_{\text{OMIB}} = \Delta P_{\text{C}} = \sum_{i \in \text{CMs}} \Delta P_{\text{C}_i} = -\Delta P_{\text{N}} = -\sum_{j \in \text{NMs}} \Delta P_{\text{N}_j}, \quad (5.6)$$

Fig. 5.10 Preventive SIME-based stabilization procedure of a relatively “mild” contingency. Conditions of Figs. 5.1 and 5.2. (Adapted from Ruiz-Vega 2002)



where ΔP_C and ΔP_N are the changes in the total power of the group of critical and noncritical machines, respectively.

Application of eqs. (5.5) and (5.6) provides a first approximate value of ΔP_C that may be refined via a stabilization procedure, which is iterative since the margin variation with stability conditions is not perfectly linear. Nevertheless, in practice, the number of required iterations (margins) seldom exceeds 3 (Pavella et al. 2000a; Ruiz-Vega et al. 2003).

5.3.2.2 Generation Rescheduling Patterns

Expression (5.6) suggests that there exist numerous patterns for distributing the total power change ΔP_N among noncritical machines, and whenever there are many critical machines, numerous patterns for distributing the total ΔP_C as well. The choice among various patterns may be dictated by various objectives, related to market or technical considerations.

In the absence of particular constraints or objectives, the total generation power could be distributed proportionally to the inertias of the noncritical machines. A more interesting solution consists of using an Optimal Power Flow (OPF) program, as discussed below, § 5.3.2.4. Finally, the above procedure may readily be adjusted for stabilizing several harmful contingencies simultaneously (Ruiz-Vega and Pavella 2003).

Remark: The above generation rescheduling procedure can also be used to enhance transient oscillations damping performance.

5.3.2.3 Illustrations

Below we apply the above P-SIME generation rescheduling to two stability scenarios: a relatively “mild” one and a severely stressed one.

Figure 5.10 sketches the simulations performed to stabilize the moderate instability described in Figs. 5.1 and 5.2, concerning a contingency applied to the EPRI 88-machine system and creating instability. More precisely, Figs. 5.1a and 5.2a describe the unstable case, Figs. 5.1b and 5.2b the stabilized case.

On the other hand, Table 5.3 describes the procedure for stabilizing the very severe contingency, which creates the severely stressed case displayed in Fig. 5.4.

Table 5.3 Preventive stabilization of a severe contingency. (Adapted from Ruiz-Vega 2002)

1	2	3	4	5	6
It.	η	Nr of	Pck	Pck + 1	sTDI
#	(rad/s) ²	CMs	(MW)	(MW)	(s)
0	-12.52*	7	5600	5041	0.395
1	-9.70*	7	5041	3431	0.430
2	-1.66*	7	3431	2815	0.605
3	-2.898	7	2815	2731	0.935
4	-2.282	7	2731	2423	1.015
5	0.675	7	2423	2493	5.000

In column 6, sTDI stands for “seconds of time-domain integration.” Recalling that computations of SIME per se are virtually negligible, sTDI is a handy measure of the time required by the T-D program to run a simulation; it therefore makes comparisons of computing performances independent of the computer, system size, and T-D program used

* The asterisk in column 2 indicates a surrogate margin

The asterisk in column 2 indicates a surrogate margin (see item 3 in § 5.2.3 and Fig. 5.4b).

Column 3 indicates that there are 7 critical machines out of the 88 system machines. In such a stressed case, the iterative procedure starts with surrogate margins until curves P_e and P_m intersect, then continues with standard margins. Note that, generally, very severe cases require a larger number of iterations.

Observe that the stabilization of this contingency imposes a generation decrease in the seven critical machines of over 50% of their total initial generation. This countermeasure might be deemed too expensive to apply preventively. The OLEC technique proposed in § 5.3.4 provides an interesting alternative (see the illustration of § 5.3.4.3).

5.3.2.4 Transient Stability-Constrained OPF

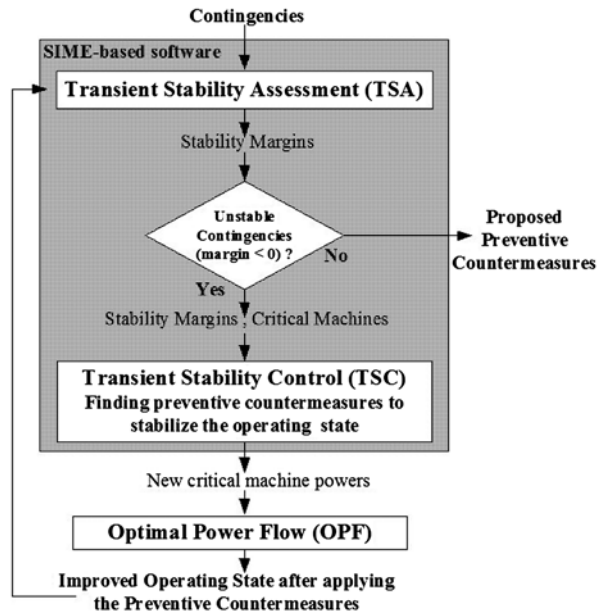
The OPF uses control variables like active and reactive generation powers to achieve a good tradeoff between security and economics. More specifically, this program optimizes the power system operating condition with respect to a prespecified objective (minimum operating cost, maximum power flow), while respecting generator limits and static security constraints (line power flows and bus voltage limits).

Several attempts have been made to imbed transient stability constraints within the OPF. According to the way of handling these constraints, they yielded two different approaches that below we call “global” and “sequential.”

Global Approach A T-D simulation is run. The power system transient stability model is converted into an algebraic set of equations for each time step of this simulation. The set of nonlinear algebraic equations resulting from the whole T-D simulation is then included in the OPF as a stability constraint, forming a (generally huge) single nonlinear programming problem, e.g., see La Scala et al. (1998) and Gan et al. (2000).

Sequential Approach A T-D simulation is run. The transient stability constraints are directly converted into conventional constraints of a standard OPF program, e.g.,

Fig. 5.11 Transient stability-constrained OPF (sequential approach). (Adapted from Ruiz-Vega 2002)



active generation power. Hence, they do not affect the size of the power system model and the complexity of the OPF solution method. They can use any conventional OPF program.

Figure 5.11 illustrates the use of the sequential approach, which, besides the above-mentioned advantages, may easily comply with market requirements thanks to the flexibility of choice among critical machines and noncritical ones on which generation can be re-dispatched.

The main drawback of the sequential approach is that it cannot guarantee optimality. Conceptually, the global approach is therefore more appealing: It is supposed to handle the problem as a whole and, hence, to provide an optimal solution, which would be accepted as the reference by the system operator and the electric market participants. However, its practical feasibility is questionable since it requires very heavy computations due to the huge nonlinear programming model.

5.3.2.5 Online Implementation of the sequential approach

Preventive TSA has been integrated into an online dynamic security assessment platform within the OMASES project funded by the European Commission (EU project OMASES—Open Market Access and Security Assessment System, EU Contract N. ENK6-CT2000-00064, December 2000). Three different operating modes are made available to system operators, i.e., engineering mode, real-time mode, and training mode (Cirio et al. 2005) as follows:

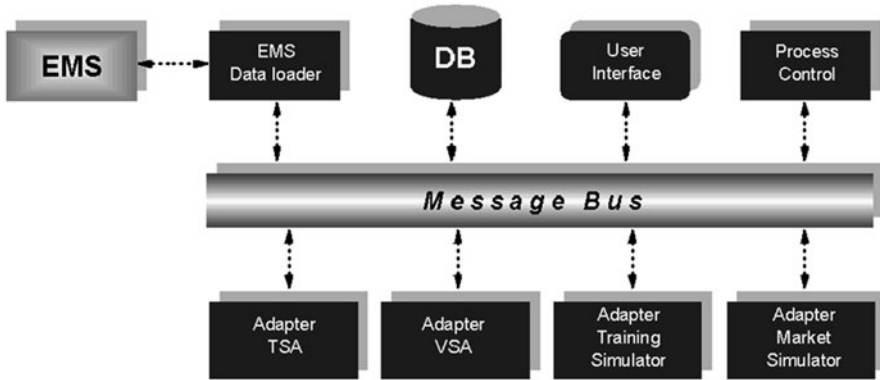


Fig. 5.12 OMASES architecture and application functions. (Taken from Cirio et al. 2005)

1. *Engineering mode*: off-line application of TSA and voltage stability assessment (VSA) studies involving or not the market environment and performed mainly for planning purposes.
2. *Real-time mode*: The Energy Management System (EMS) feeds OMASES with network data and solutions. DSA is synchronized with data transfer and cyclically runs with an overall execution time within 15 min.
3. *Training mode*: The operator gets used with the power system dynamics and DSA tools, and performs analysis (future scenarios, post-event analysis, etc.) of the existing electrical system and/or experiments. Market rules can be used to provide realistic scenarios.

Figure 5.12 depicts the OMASES platform. The EMS data loader transfers the state-estimator online snapshots to a relational database management system, from which the different functions (TSA, VSA, operator training, and market simulators) can access the data.

These latter functions are controlled by the process control module, which launches requests for analyses. The results are then sent back to the user interface via HTML files.

The TSA module of the OMASES platform is based on SIME coupled with the Eurostag T-D simulation software (Bihain et al. 2003). It is composed of a contingency filtering, ranking, and assessment module (called FILTRA (Ruiz-Vega et al. 2001)) and a preventive control module used for generation rescheduling, as described in Sect. 5.3.2.2. A typical screenshot of the FILTRA module's outputs is shown in Fig. 5.13.

Within the OMASES project, the TSA module based on SIME was tested on two real-world systems, namely the Greek extra high voltage (EHV) system (operated by Hellenic Transmission System Operator, HTSO) and the Italian EHV system (operated by Gestore della Rete di Trasmissione Nazionale, GRTN).

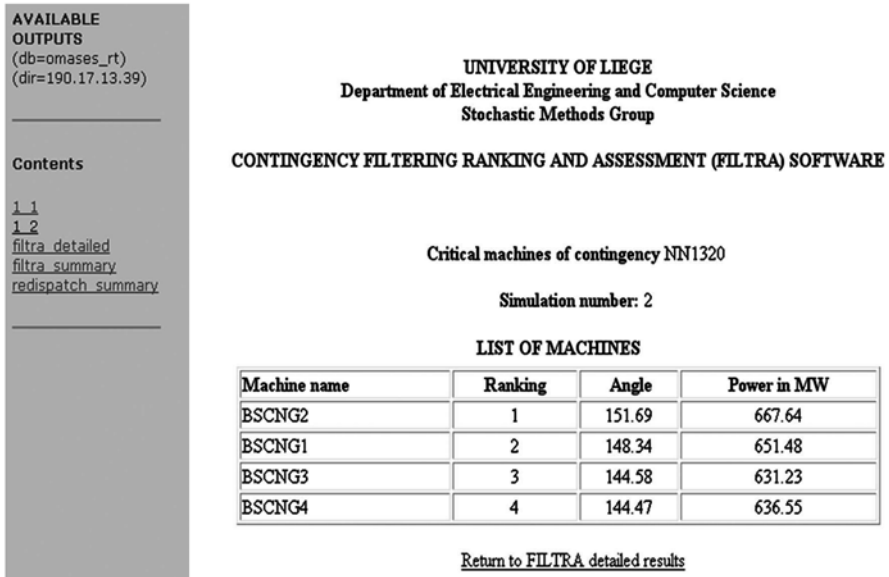


Fig. 5.13 FILTRA results and critical machines of Brindisi power station. (Taken from Cirio et al. 2005)

5.3.2.6 Recent developments concerning the global approach

In recent investigations where SIME is applied to the global approach (Pizano-Martínez 2010; Pizano-Martínez et al. 2010, 2011), many of the drawbacks of this approach were solved, until arriving to a point where its practical feasibility has become a reality. We briefly describe the main ideas which led to this improvement.

Recall that the global approach originally uses two large sets of constraints, additional to the ones of a conventional OPF: the set of transient stability constraints (a set composed by a transient stability inequality constraint for each machine to keep its angle trajectory in a “stable regime”) and the set of dynamic constraints (a typically very large set of nonlinear equality constraints resulting from the discretization of the power system dynamics, namely one subset of constraints for each time step of the considered integration period).

The first improvement proposed in Pizano-Martínez et al. (2010), and called below “Method 4,” proceeds as follows:

1. For an unstable contingency, it first determines t_u and $\delta(t_u)$ of the relevant OMIB dynamics.
2. Next, by reducing the clearing time to the CCT, it determines the corresponding $\delta'(t_u)$ for this marginally stable case.
3. It then uses in the nonlinear program a single stability constraint, which imposes to change the operating point such that $\delta(t_u)$ becomes equal to $\delta'(t_u)$; or slightly smaller).

4. The two above steps are iterated until the resulting operating point becomes indeed stable with respect to the initial contingency and given clearing time.

Notice that this approach already reduces the complexity of the nonlinear programming problem in a significant way, since it replaces the very large number of generator-wise stability constraints imposed over the whole integration period, by a single OMIB stability constraint imposed at a single time step t_u . Furthermore, since the full system dynamics need to be modeled only until t_u to express this stability constraint, this also reduces the number of dynamic constraints. Indeed, in practice, t_u is typically about one order of magnitude smaller than the whole integration period usually used in such transient stability studies.

The work presented in Pizano-Martínez et al. (2011) further builds on the previous ideas in order to reduce the dynamic constraints to the simplest possible expression. The rationale behind their method (called “New Approach,” below) is the following:

1. The authors first notice that once the rotor angles and speeds of all generators are known at some time instant during the integration period, their subsequent dynamics are fully determined over the rest of the integration period (assuming a given fault scenario).
2. In particular, the dynamics thus only depend on the initial values of all rotor angles (since all initial speeds are all equal to zero).
3. Extrapolating this property to the dynamics of the relevant OMIB, they propose to express the stability constraint as an upper bound on the angle of this relevant OMIB at $t=0$. The whole nonlinear programming problem can therefore be formulated by using one single set of equality constraints at $t=0$, plus a single inequality constraint on the OMIB angle at $t=0$.

Building on these ideas, Pizano-Martínez et al. (2011) propose to iteratively force the initial OMIB angle progressively towards its marginally stable value (whose exact value is indeed not known beforehand). Schematically, this works in the following way:

1. For an unstable case, one first determines the relevant OMIB structure and computes its $\delta(t_\rho)$.
2. One then formulates and solves the nonlinear programming problem, so as to compute an operating point under the constraint that the initial angle becomes a bit (say 10%) smaller than $\delta(t_\rho)$.
3. The two above steps are iterated until stability is reached, by exploiting linear extrapolation and linear interpolation as soon as a stable case is found (see Pizano-Martínez et al. 2011, for the details).

The resulting iterative approach turns out to be significantly faster than Method 4, while yielding the same level of accuracy (see below).

In order to have a general idea of the size reduction of the model achieved by this approach, if we denote N_b the number of buses of the system, N_s the number of integration time steps, and N_g the number of generators, the initial global approaches

Table 5.4 Comparison of transient stability-constrained OPF approaches. (Adapted from Pizano-Martínez et al. (2011))

Total power generation cost (\$/h)					
Base OPF	New approach	Method 1	Method 2	Method 3	Method 4
1132.18	1134.71	1191.56	1140.06	1134.01	1135.2

(Gan et al. 2000), using the classical model, require $N_g \times N_s$ additional stability constraints and $(2N_g + 2N_b) \times N_s$ additional dynamic constraints to solve the resulting OPF problem. For a small academic system with three generators and nine buses, considering simulations of 1 s with 0.01 time-step length, the number of additional constraints rises to 300 stability constraints and 2400 dynamic constraints, i.e., 2700 additional constraints. This number of additional constraints, as explained before, increases with system size. On the contrary, using the new approach with the SIME method, the number of additional constraints is the same for any system size and is limited to only one.

An additional advantage of applying SIME in the global approach to transient stability-constrained OPF is that the optimization process is driven by the sensitivity analysis of SIME margins, which makes it possible to reach the exact stability boundary by means of inter-extrapolations and avoid unnecessary T-D simulations, making this approach more efficient in finding a good compromise between economy and security, as discussed below (Pizano-Martínez et al. 2011).

After these important improvements, it was necessary to check if the reduction in the size of the optimization model had not caused a decrease in its performance. Some tests were made comparing the new global approach with other transient stability-constrained OPF approaches, in Pizano-Martínez et al. (2011). The results shown in Table 5.4 highlight that the new global approach, while strongly reducing the size of the nonlinear programming problem, maintains its accuracy in obtaining economic solutions.

The transient stability-constrained OPF methods that are compared in Table 5.4 can be described as follows: Method 1 (Nguyen and Pai 2003) uses a conventional OPF with a generation rescheduling based on a trajectory sensitivity method; Method 2 (Cai et al. 2008) uses a differential evolution global search algorithm, while Method 3 (Zárate-Miñano et al. 2010) and Method 4 (Pizano-Martínez et al. 2010) use the transient stability index based on an OMIB rotor angle to only reduce the number of stability constraints.

As expected, the most economic operating cost is achieved by the conventional OPF (i.e., without any stability constraints). It is important to notice that the approaches that use the SIME method (the new approach and Methods 3 and 4) calculate a similar generation cost. After analyzing the results, it was observed that Methods 1 and 2 had a more expensive final operating condition because they overstabilized the system. This happens because the optimization procedure in both methods is not directly taking into account the real stability boundary, while it is taken into account in all the SIME-based methods. However, regarding the size of the power system model for the optimization process, the new approach, while

reaching the same results as the other SIME-based approaches, only requires adding one single constraint to the conventional OPF model (Pizano-Martínez et al. 2011). Further work is required in order to extend these ideas to the simultaneous treatment of several contingencies.

5.3.3 Closed-Loop Emergency Control

Closed-loop emergency control relies on the “Emergency SIME” method. In short, E-SIME starts acting after a disturbance inception and its clearance. It aims at *predicting* the system transient stability behavior and, if necessary, at deciding and triggering control actions early enough to prevent the loss of synchronism. Further, it aims at continuously monitoring the system in a closed-loop fashion, in order to assess whether the control actions have been sufficient or should be reinforced.

The principle of the control technique remains the same with the preventive SIME, but its application has the following important differences (Zhang et al. 1997; Ernst et al. 1998; Ernst and Pavella 2000; Pavella et al. 2000a):

- The information about the multi-machine system is provided by real-time measurements rather than T-D simulations.
- The generation shift from critical machines is made here by shedding generation that is not compensated by a generation increase on noncritical machines (at least at the very first instants following the control action).
- The system status (unstable margin and critical machines) is *predicted rather than assessed* along the system transient trajectory.
- The resulting practical procedure is summarized below.

5.3.3.1 Predictive Transient Stability Assessment

The prediction relies on real-time measurements, acquired at regular time steps, t_i . The procedure consists of the following steps:

1. *Predicting the OMIB structure*: Use a Taylor series expansion to predict (say, 100 ms ahead) the individual machines’ rotor angles; rank the machines according to their angles, identify the largest angular distance between two successive machines, and declare those above this distance to be the “candidate critical machines,” the remaining ones being the “candidate noncritical machines.” The suitable aggregation of these machines provides the “candidate OMIB.”
2. *Predicting the $P_a - \delta$ curve*: Compute the parameters of this “candidate OMIB,” and in particular its accelerating power and rotor angle, P_a and δ , using three successive data sets acquired for the three different times.
3. *Predicting instability*: Determine whether the OMIB reaches the unstable conditions (1).

If not, repeat steps (a) to (c) using new measurement sets.

If yes, the candidate OMIB is the critical one, for which the method computes successively the unstable angle δ_u , the corresponding time to instability, t_u , and the unstable margin expressed by (2).

4. *Validity test*: Observing that under given stability conditions *the* value of the (negative) margin should be constant, whatever the time step, provides a handy validity test: It consists of pursuing the above computations until reaching an (almost) constant margin value.

5.3.3.2 Salient Features

The method uses real-time measurements acquired at regular time intervals and aims at controlling the system in less than, say, 500 ms after the contingency inception and its clearance. The prediction phase starts after detecting an anomaly (contingency occurrence) and its clearance by means of protective relays. Note that this prediction does not imply identification of the contingency (location, type, etc.). The prediction is possible thanks to the use of the OMIB transformation; predicting the behavior (accelerating power) of all of the system machines would have led to totally unreliable results. There may be a tradeoff between the above-mentioned validation test and time to instability: The shorter this time, the earlier the corrective action should be taken, possibly before complete convergence of the validation test.

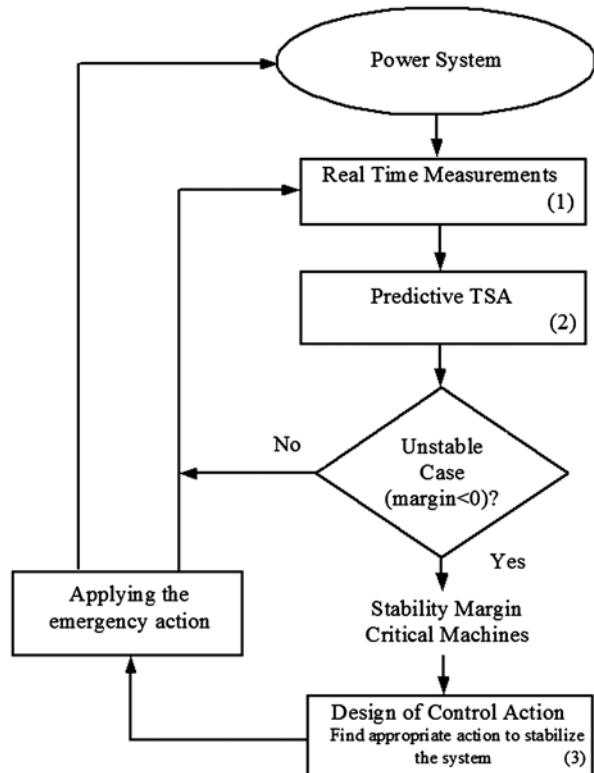
5.3.3.3 Structure of the Emergency Control Scheme

On the basis of real-time measurements taken at the power plants, the method pursues the following main objectives:

- To assess whether the system is stable or it is driven to instability; in the latter case,
- To assess “how much” unstable the system is going to be; accordingly,
- To assess “where” and “how much corrective action” to take (pre-assigned type of corrective action); and
- to continue assessing whether the executed corrective action has been sufficient or whether to proceed further.

Block 2 in Fig. 5.14 covers the two first steps: prediction of instability and its size, and of critical machines. Block 3 handles the control actions and determines the number of units to shed. Note that after the order of triggering the action has been sent, the method continues monitoring and controlling the system in a closed-loop fashion, until reaching stabilization.

Fig. 5.14 Closed-loop transient stability emergency control: general framework. (Taken from Pavella et al. 2000)



5.3.3.4 Real-Time Implementation Concerns

The prediction of the time to (reach) instability may influence the control decision (size of control, time to trigger it, etc.).

The hardware requirements of the emergency control scheme are phasor measurement devices placed at the main power plant stations and communication systems to transmit (centralize–decentralize) this information. Already a few years ago, these requirements seemed to be within reach of technology (Phadke 1995).

The emergency control relies on purely real-time measurements (actually a relatively small number of measurements). This frees the control from uncertainties about power system modeling, parameter values, operating condition, and type and location of the contingency.

Within the EXAMINE project funded by the European Commission (IST 2000 26116), the actual implementation of E-SIME was examined from the viewpoint of designing a real-time measurement and communication system able to cope with the very stringent response-time constraints (Diu and Wehenkel 2002).

In particular, the question of real-time estimation and prediction of rotor angles from synchronized phasor measurements was investigated within the project, e.g., Del Angel et al. (2003).

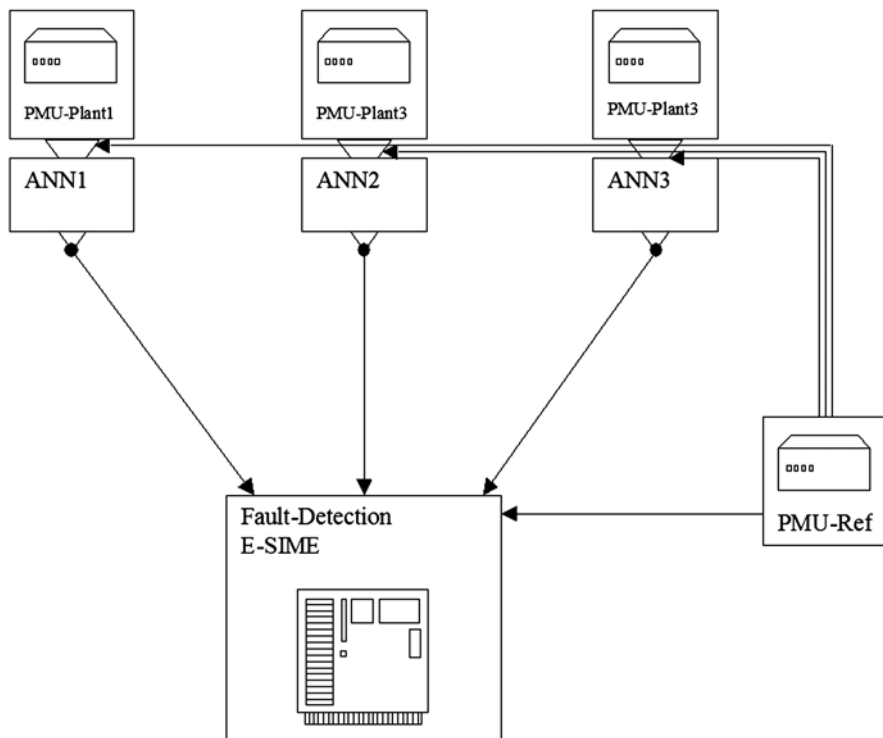


Fig. 5.15 Distributed rotor angle estimation and procedure using one PMU device and one artificial neural network per monitored power plant and one reference PMU

Figure 5.15 shows one of two possible schemes for the E-SIME implementation. This configuration encompasses two types of modules:

- *Distributed Artificial Neural Network (ANN)-based rotor angle estimation and prediction:* Each monitored power plant is equipped with a PMU device measuring the EHV side current and voltage phasors, at a rate of one per each 50-ms interval with respect to a common reference frame synchronized with the nominal frequency. These signals are then put into the actual system frequency reference frame by subtracting the phase signal obtained from a remote system bus (PMU-ref) and fed into the ANN module (three successive values) whose output furnishes an estimate of the current value of the power plant's average rotor angle and its predicted value two time steps ahead (100 ms). The ANN module is trained off-line using a detailed system and PMU model to generate input and output samples.
- *Central monitoring of loss of synchronism and emergency control:* This module receives the estimated and predicted values of rotor angles computed by the devices of the monitored plant, together with the voltage magnitudes of the PMU devices. These signals are monitored in order to detect fault occurrence near one

of the power plants and its clearing. Upon fault clearing, the E-SIME module is armed and starts monitoring the system dynamic behavior. As soon as loss of synchronism is predicted, the tripping signal is computed and sent to the critical power plant. The overall round-trip delay was estimated to be about 300 ms, which led to the conclusion of the feasibility of the E-SIME-based emergency control scheme.

The other implementation scheme that was examined in the EXaMINE project used a centralized version of the rotor angle estimation modules. With respect to the scheme of Fig. 5.15, this latter scheme has higher throughput requirements on the links from the monitored power plants to the central location, but reduces the number of channels from the PMU-Ref location (since this signal does not need to be broadcasted anymore to the individual plant locations).

Note that in both schemes it would be appropriate to introduce redundancy on the different devices and in particular in the common PMU-Ref device. The EXaMINE project led to the installation of six PMU devices on the Italian EHV system.

5.3.4 Open-Loop Emergency Control

5.3.4.1 Principle

This technique is a mixture of the preceding two techniques: From a methodological viewpoint, it is event driven and relies on transient stability simulations, like the preventive control technique, described in § 5.3.2; but its application uses generation tripping, like the emergency control technique, in addition to generation shifting.

The leading idea is to mitigate preventive actions (generation shifting) by complementing them with emergency actions (generation tripping) that would automatically be triggered only if the postulated contingency actually occurs. The technique relies on the assumption that (some of) the critical machines belong to a power plant equipped with a generation tripping scheme; therefore, a certain number of units could be tripped in the emergency mode.

Below, we outline the OLEC procedure in seven steps (Ruiz-Vega 2002; Ruiz-Vega and Pavella 2003).

5.3.4.2 Procedure

1. For an initially unstable scenario (operating condition subject to a predefined harmful contingency and its clearing scheme), compute the corresponding (negative) margin and determine the corresponding critical machines.
2. Assuming that (some of) these machines belong to a power plant equipped with a generation tripping scheme, select the number of units to trip in the emergency mode.

3. Run SIME, starting with the initial scenario up to reaching the assumed delay of generation tripping; at this time, shed the machines selected in step 2, and pursue the simulation until reaching instability or stability conditions (see eq. (5.1) and (5.3)). If stability is met, stop; otherwise, determine the new stability margin and corresponding critical machines (they might have changed from the previous simulation).
4. Run the transient stability control program (see § 5.3.2) to increase to zero this new (negative) margin. To this end, perform generation shifting in the usual way, from the remaining critical machines to noncritical machines. While performing this task, an additional objective may also be pursued, if the OPF software is combined with the transient stability control program.
5. The new, secure operating state results from the combination of the above generation rescheduling taken preventively and the consideration of the critical machines, previously chosen to trip correctively.
6. If there are more than one pattern of critical machines to trip, repeat steps 1–5 with each one of them, until getting an operating condition as close as possible to what is considered to be the “optimum” one (Ruiz-Vega and Pavella 2003).
7. After the number of machines to trip is determined, the settings of the special protection activating the generation tripping scheme in the plant is adapted so as to automatically disconnect these machines in the event of the contingency occurrence.

5.3.4.3 Illustration

Consider again the severe contingency that has been stabilized in the preventive mode in § 5.3.2.3. Recall that the corresponding stability case has seven critical machines, belonging to the same power plant, and having a total generation of 5600 MW in the transient stability-unconstrained pre-fault operating condition (Ruiz-Vega et al. 2003). Recall also that stabilizing this contingency in the purely preventive mode requires decreasing this generation to 2423 MW (see Table 5.1). Below, we consider again this contingency and stabilize it by OLEC, using the following parameters:

- Number of critical machines to trip: two; their stability-unconstrained pre-fault generation is $5600 - 4010 = 1590$ MW (see columns 4 of Tables 5.3 and 5.5).
- Time delay for tripping these critical machines: 150 ms.

Accordingly, the OLEC preventive generation rescheduling concerns the remaining five critical machines, whose stability-unconstrained pre-fault generation is 4010 MW.

The design of the control action follows the procedure of § 5.3.4.2. First, it is found that, because the case is very unstable, tripping two critical machines 150 ms after the fault inception would not be sufficient to stabilize it. Figure 5.16 describes the dynamics of the stability case, respectively before (Fig. 5.16a, b) and after tripping the two critical machines (Fig. 5.16c, d).

Table 5.5 OLEC stabilization of a very severe contingency (two machines tripped). (Adapted from Ruiz-Vega 2002)

1	2	3	4	5	6
It. #	η (rad/s) ² (or MW)	Nr of CMs	P_{c_k} (MW)	$P_{c_{k+1}}$ (MW)	sTDI (s)
0	-7.83*	5	4010	3609	0.421
1	-4.83*	5	3609	3260	0.461
2	-2.35*	5	3260	2662	0.506
3	-1.964	5	2662	2583	0.771
4	-1.265	5	2583	2440	0.856
5	-0.086	5	2440	2430	1.146
6	-0.036	5	2430	2415	1.216
7	0.028	5	2415	2422	5.000

* The asterisk in column 2 indicates a surrogate margin

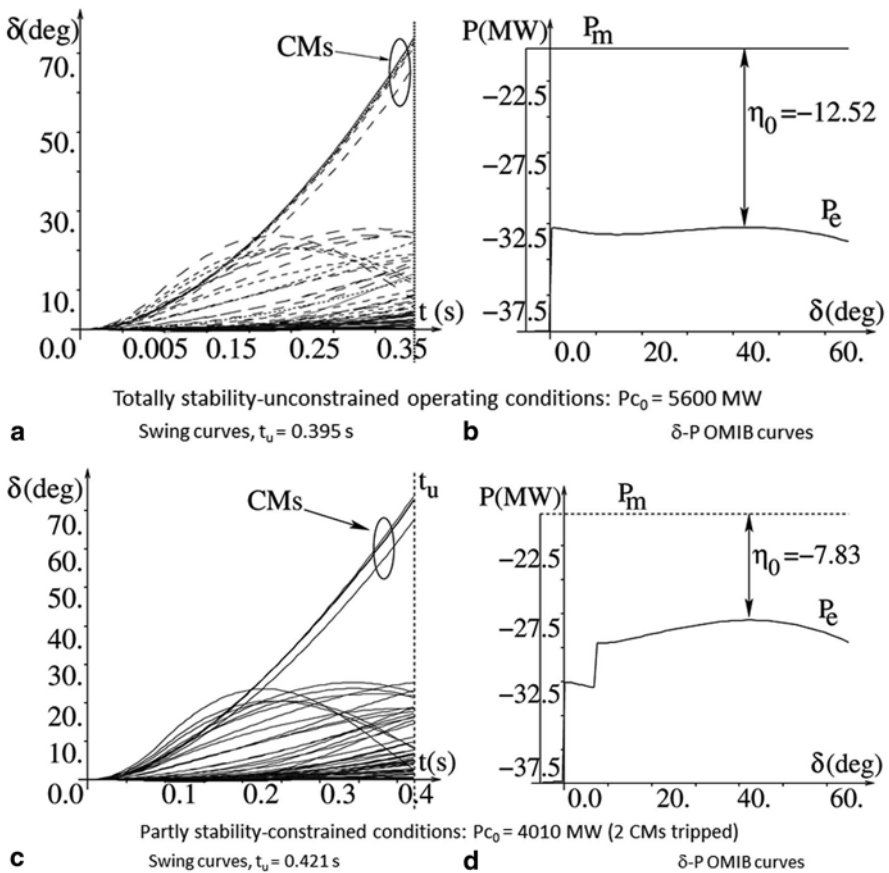


Fig. 5.16 Multi-machine swing curves and δ -P OMIB curves of two unstable cases. Totally stability-unconstrained operating conditions: **a** Swing curves, **b** δ -P OMIB curves; Partly stability-constrained conditions: **c** Swing curves, **d** δ -P OMIB curves. (Adapted from Ruiz-Vega 2002)

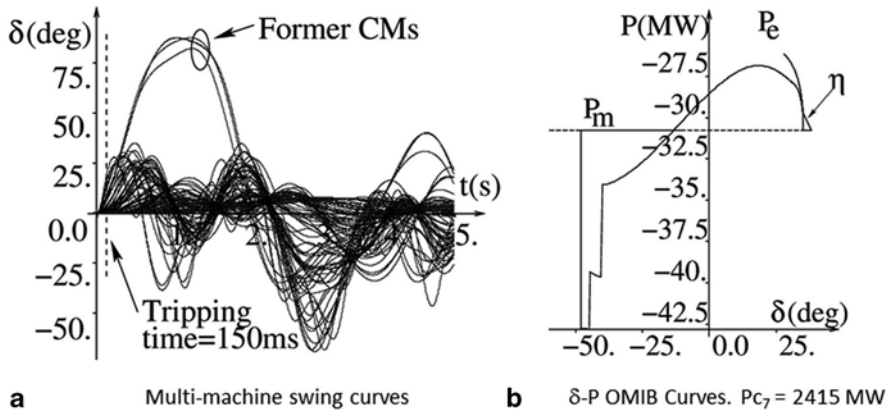


Fig. 5.17 Multi-machine swing curves and δ - P OMIB curves of the stabilized case. Two generators are automatically tripped if the contingency actually occurs. (Adapted from Ruiz-Vega 2002)

More precisely, Figs. 5.16a, b portray, respectively, the multi-machine swing curves and the δ - P OMIB curves of the totally stability-unconstrained system.

Fig. 5.16c, d portray the curves corresponding to the partly controlled case, obtained by tripping two critical machines 150 ms after the contingency inception.

Comparing Fig. 5.16a, c suggests that the partly stability-constrained system is hardly less unstable than the unconstrained one: Compare the slope of their swing curves as well as their times to instability (395 ms vs. 421 ms). Similarly, comparing Fig. 5.16b, d shows that after the generation tripping (corresponding to $\delta_i = 7.34^\circ$) the OMIB P_e curve gets somewhat closer to the P_m one, without, however, crossing it (their minimum “distance” decreases from 12.52 to 7.83 MW).

Since the emergency action is insufficient to stabilize the case, the procedure of § 5.3.4.2 continues with step 3: The new surrogate margin is computed and the appropriate preventive generation rescheduling is decided in order to stabilize the operating conditions.

The iterative procedure of rescheduling the five remaining machines is described in Table 5.5. The asterisk in column 2 indicates minimum distances between P_e and P_m OMIB curves, in MW, whereas “standard” margins are expressed in $(\text{rad/s})^2$.

See, for example, in row 0 of Table 5.5 and in Fig. 5.16d the margin of -7.83 MW. Row 7, column 4 of Table 5.5 provides the final result of the preventive stabilization procedure of the system with five critical machines; it indicates that their generation should be reduced to 2415 MW.

Figure 5.17 displays the multi-machine and OMIB δ - P curves corresponding to this stabilized case. They clearly show the effectiveness of the combined action of generation shifting (preventive) and generation tripping (emergency) controls. In particular, Fig. 5.17b shows that the OMIB equivalent power decreases from its initial value (-20.1 MW, see Fig. 5.16d) to its secure value (-30.7 MW), creating a decelerating area and making the system able to dissipate the kinetic energy gained by the five critical machines in the during-fault period.

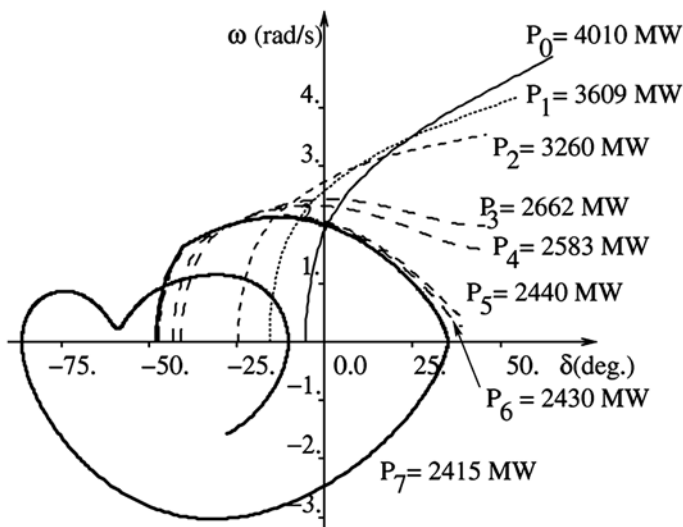


Fig. 5.18 OMIB phase plane representation of the seven simulations described in Table 5.5. Two generators tripped if the contingency actually occurs. (Adapted from Ruiz-Vega 2002)

A synopsis of the seven simulations listed in Table 5.5 is given in Fig. 5.18, plotting the OMIB phase plane. Incidentally, observe how clearly this plot describes the system dynamics under the various conditions.

In summary, to stabilize the considered severe contingency by OLEC, one should decrease preventively the pre-fault generation of the five critical machines (CMs) from 4010 to 2415 MW, under the assumption that the other two CMs would be tripped correctly, after the contingency inception.

Once the conditions of the stabilization process are obtained, the special protection activating the generation tripping in the plant is armed to *automatically* disconnect the selected plants in case the contingency *actually occurs*. The remaining five machines are rescheduled to their new values.

The pre-fault power of the plant, however, has been improved, with respect to the results presented in Table 5.3 ($2415 + 1590 = 4005$ MW by OLEC vs. 2423 MW by P-SIME in purely preventive mode).

5.3.5 Limit Search

Stability margins computed by SIME may be readily exploited to accelerate the computation of transient stability-constrained power flow limits and TTC/ATC calculations. Typically, the calculation of a power flow limit by dichotomy search requires about eight to ten runs (each run is composed of a power flow calculation and a T-D simulation for each contingency). By exploiting the stability margins one can

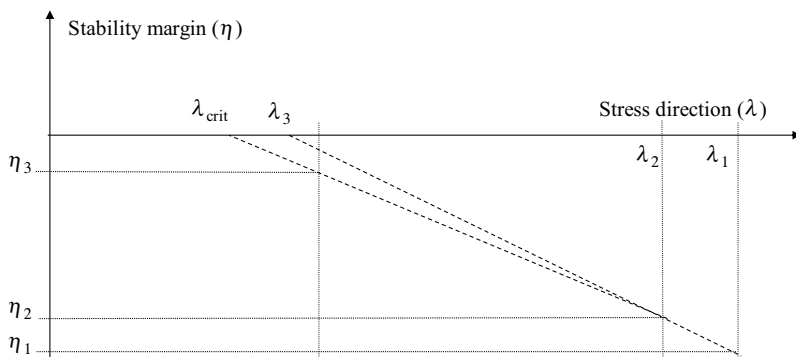


Fig. 5.19 Acceleration of limit search by SIME

use extrapolation or interpolation in order to reduce this number to three (Pavella et al. 2000b; Ruiz-Vega et al. 2002).

Figure 5.19 illustrates this idea graphically. The first simulation corresponds to the upper bound of the search interval (λ_1 , the most stressed base case, for the given stress direction, yielding the margin η_1). The second simulation corresponds to a 10% reduction of the stress parameter, leading in the illustrated case to a second unstable simulation (λ_2, η_2).

The two unstable margins are then exploited to estimate by linear extrapolation the critical value of the stress parameter. If this value is far from the second value (as depicted in Fig. 5.19), a third and last simulation is carried with a slightly higher value (λ_3 on Fig. 5.19) to improve accuracy. The final estimate of the critical value (λ_{crit}) is obtained from the two smaller, in absolute value, unstable margins.

5.4 Discussion

5.4.1 A Pragmatic Approach to Integrated Security Control

5.4.1.1 Preventive Mode Security Control

Preventive mode security assessment and control methods and software tools have been developed separately for static security, transient stability, and voltage stability. In principle, these tools are able to identify harmful contingencies and preventive control actions to alleviate insecurities from each point of view. However, each method concentrates only on part of the overall security control problem and hence its recommendations are generally not fully satisfactory from a global point of view.

It is thus necessary to incorporate these methods into a single decision support tool for secure online operation. Such a tool would ensure at the same time static

and dynamic security with respect to a list of potentially harmful contingencies identified during the analysis stage. We propose to use the optimal power flow formulation as a generic approach to handle this problem.

More specifically, let CL-SS be a list of potentially harmful contingencies from the viewpoint of static security, CL-TS a list of such contingencies from the viewpoint of transient stability, and CL-VS a list of potentially harmful contingencies from the viewpoint of voltage stability.

Then, we can formulate an optimization problem incorporating the following constraints:

1. *Operating (i.e., preventive mode) constraints*: pre-contingency power flow equations, and equality and inequality constraints (voltage magnitudes in normal range and branch flows below steady-state limit, operating limits, transactions, etc.).
2. *Static security constraints*: for each element in CL-SS a set of post-contingency power flow equations, and equality and inequality constraints (voltage magnitudes in emergency range and branch flows below emergency state limit).
3. *Transient stability constraints*: for each element in CL-TS a constraint on the total normal mode generation of the corresponding set of critical generators (note that such constraints can be derived by P-SIME).
4. *Voltage stability constraints*: for each element in CL-VS one (or several) constraints on the normal mode active and reactive power injections ensuring voltage stability with respect to that contingency (e.g., see Carpentier et al. 2001; Capitanescu and Van Cutsem 2002; and Bihain et al. 2003, for an approach yielding such information).

For a given objective function (e.g., minimal deviation, minimal cost of reschedule), the solution of such an optimization problem can be computed by a conventional security-constrained OPF. As long as the number of elements of CL-SS remains small, the CPU time required by a single run of such a tool remains compatible with online requirements.

Nevertheless, there is no guarantee that the resulting rescheduled operating point exists (feasibility) and is simultaneously secure with respect to all three security criteria. Thus, in principle, it would be necessary to iterate the above resolution scheme according to the same principle as the one given in Fig. 5.10.

Note also that there is no absolute guarantee that such an iterative process would converge in a reasonable number of iterations, and if yes, that the resulting new operating point would indeed be optimal. Nevertheless, we believe that such an integrated preventive security control framework is feasible and would be of value to online operation under stressed conditions.

We notice that the approach proposed relies on the availability of DSA tools able to express approximations to dynamic security regions in terms of pre-contingency parameters. The more accurate these approximations are, the better the resulting optimization will be. In particular, we believe that the proposed scheme is reasonable when combined with methods such as P-SIME and VSA.

5.4.1.2 Emergency Mode Security Control

While in preventive mode it is necessary to combine into a single coherent decision-making strategy the handling of all security constraints (because they may be conflicting), in emergency mode security control one can generally take advantage of the temporal decoupling of the different phenomena, since thermal problems are typically significantly slower than voltage collapses which in turn are typically much slower than loss of synchronism. Hence, the different emergency control schemes can operate independently from each other.

5.4.2 Limitations and Further Research Needs

5.4.2.1 Arbitration between Preventive and Emergency Control

A first limitation of the current security control approaches lies in the fact that they are not able to arbitrate between preventive and emergency control. More precisely, the current approach supposes that the contingencies and phenomena that must be treated in a preventive way are given a priori in the form of a list of “credible” contingencies and a set of static and dynamic constraints. Preventive security control then tries to change the operating conditions so that these constraints are satisfied for all contingencies. Emergency control is supposed to handle all other, non-credible, disturbances.

However, from a rational point of view the fact that a certain security problem (or constraint) should be treated in preventive or in emergency mode actually depends on operating conditions (electrical ones, economic ones, and meteorological ones as well).

For example, if a certain N-2 contingency becomes very likely (e.g., because of changing weather conditions), or if the cost of treating it in preventive mode is low (e.g., because there is cheap load curtailment available), then it could make sense to handle it in preventive mode, rather than in emergency mode.

Thus, in principle, the arbitration between preventive and emergency mode security control should be an output of (and not an input to) the security control decision support tools. However, there are intrinsic difficulties in achieving this objective mainly because of lack of data on probabilities of contingencies (as a function of real-time conditions) and difficulties to model the costs of interruptions, both of which would be required to allow a better coordination of preventive and emergency mode security control (Wehenkel 1999).

5.4.2.2 New Control Devices

New control devices such as variable series compensation, as well as more systematic use of interruptible load, can potentially make it easier to handle security

in online operation. However, the analytical methods developed today, like SIME, VSA, etc., do not take into account these possibilities. Thus, further adaptations are needed in order to develop tools able to suggest how to use such devices.

5.4.2.3 Uncertainties

A major problem in large-scale systems is that of real-time information concerning the status of neighbor systems and the incorporation of this information into appropriate dynamic equivalents needed to carry out meaningful simulations and DSA computations in real time.

The unavailability of this information translates into modeling uncertainties, which should be taken into account in a conservative way. Here also, research and developments are necessary in order to reduce the amount of arbitrariness of security control (Diu and Wehenkel 2002).

The addition of new generating plants based on renewable energies (wind and solar power plants mainly) have also increased the uncertainty in predicting the power system operating state, since their power output can change, in large amounts, in a very short period of time, due to faults or weather conditions. This is an additional difficulty to apply both preventive and emergency control.

5.4.2.4 Inter-Area and Inter-Temporal Coordination

In large power system interconnections, the security control of the overall system is presently organized in a distributed multi-area fashion. Each area is controlled by a system operator, responsible for the security in his/her area. One can show that bad coordination of these control agents can lead to quite suboptimal operation in each area of the system (Zima and Ernst 2005).

Also, the overall security of the system strongly relies on the quality of the exchange of information between different areas, in the form of static and dynamic equivalents as well as threatening disturbances.

To circumvent these difficulties, the trend has been in the USA to create MEGA System Operators responsible for the overall security, leading to the necessity to handle huge supervisory control and data acquisition (SCADA)/EMS databases and the explosion of computational requirements for security assessment and control software.

In other places and, particularly, in Europe, the trend has been to attempt to improve data exchange and coordination between the different existing system operators. In both cases, however, a sound-distributed security assessment and control approach, defining in a systematic and transparent way appropriate coordination schemes among areas, would be of great value.

In a similar fashion, a better coordination of security control decisions over different time horizons, i.e., operation planning, day ahead, real time, next hour, next day, etc., could help improve security and at the same time reduce costs. This would

lead to state security control as a sequential decision problem, which could be tackled in the framework of stochastic or dynamic programming (Wehenkel 2004).

5.4.2.5 Wide-Area Transient Stability Emergency Control

The networks of synchrophasors that are already installed in some countries can be used to develop a wide-area transient stability emergency control that monitors the system state in order to verify if the action of other preventive controls, and/or fast event-based emergency controls, has been able to stabilize the system. This system would act “in extremis,” as a backup control, in case an additional control action would be required to stabilize the system.

This type of control is a new application of the emergency SIME method in the following aspects: It would not be applied to analyze a power plant but it would consider the stability of the whole power system; in addition, the critical machines could change along with the operating conditions and the actual fault. One advantage of this application of E-SIME is that it will have more time to act, since preventive control and the fast event-based controls had already been applied, giving, in this way, more time for applying the method in case the system would require an additional control action.

5.5 Conclusion

The present chapter has pursued a twofold objective. On the one hand, it has addressed the issue of real-time transient stability control, which has long been considered to be extremely problematic if at all feasible. Three different schemes have been advocated, able to encounter a variety of specific needs, depending on power systems specifics.

It was shown that preventive control and its variant, the OLEC, are mature enough and ready for implementation. Closed-loop emergency control, on the other hand, is very much dependent on today’s high tech; its implementation requires strong incentives so as to foster the necessary investment in modernized communication infrastructure and monitoring equipment.

The second objective was an attempt towards integrated security control techniques, able to cover all dynamic and steady-state security aspects. It appeared that the software tools available today are able to achieve such integrated approaches.

Nevertheless, while from a theoretical viewpoint the above-advocated approaches are within reach, their realization depends on information about the system configuration, including generation status that the liberalized electricity markets seem reluctant to provide. And although such issues have not been addressed in this chapter, these authors feel that blackouts will continue threatening the power systems, unless such information is made available, under the pressure of regulatory bodies in the USA, Europe, and other continents.

Acknowledgments Prof. Mania Pavella contributed to the first version of this chapter (Wehenkel et al. 2005). The authors gratefully acknowledge her scientific work, encouragement, and support for developing this updated version.

References

- Bihain A, Cirio D, Fiorina M, Lopez R, Lucarella D, Massucco S, Ruiz-Vega D, Vournas CD, Van Cutsem T, Wehenkel L (2003) Omases—a dynamic security assessment tool for the new market environment. In: Proceedings of IEEE Bologna power tech
- Cai HR, Chung CY, Wong KP (2008) Application of differential evolution algorithm for transient stability constrained optimal power flow. *IEEE Trans Power Syst* 23(2):719–728
- Capitanescu F, Van Cutsem T (2002) Preventive control of voltage security: a multi-contingency sensitivity-based approach. *IEEE Trans Power Syst* 17:358–364
- Carpentier J et al (2001) Application of a new security concept in optimal power flows to congestion management. In: Proceedings of the 6th international workshop on electric power system control centers, Opio, France, June 10–13
- Cirio D, Lucarella D, Vimercati G, Morini A, Massucco S, Silvestro F, Ernst D, Wehenkel L, Pavella M (2005) Application of an advanced transient stability assessment and control method to a realistic power system. To appear in Proceedings of PSCC05
- Del Angel A, Glavic M, Wehenkel L (2003) Using artificial neural networks to estimate rotor angles and speeds from phasor measurement. In: Proceedings of intelligent systems applications to power systems, ISAP03
- Diu A, Wehenkel L (2002) EXaMINE—experimentation of a monitoring and control system for managing vulnerabilities of the European infrastructure for electrical power exchange. In: Proceedings of IEEE PES summer meeting
- EPRI (1994) Extended transient midterm stability program version 3.1 user’s manual. Final Report EPRI TR-102004, Projects 1208-11-12-13
- Ernst D, Pavella M (2000) Closed-loop transient stability emergency control. In: Proceedings of IEEE/PES winter meeting, Singapore
- Ernst D, Bettiol A, Zhang Y, Wehenkel L, Pavella M (1998) Real time transient stability emergency control of the south-southeast Brazilian system. In: Proceedings of SEPOPE, Salvador, Brazil, (invited paper, IP044)
- Gan D, Thomas RJ, Zimmerman RD (2000) Stability-constrained optimal power flow. *IEEE Trans PWRS* 15(2):535–540
- La Scala M, Trovato M, Antonelli C (1998) On-line dynamic preventive control: an algorithm for transient security dispatch. *IEEE Trans PWRS* 13(2):601–610
- Nguyen TB, Pai MA (2003) Dynamic security-constrained rescheduling of power systems using trajectory sensitivities. *IEEE Trans Power Syst* 18(2):848–854
- Pavella M, Ernst D, Ruiz-Vega D (2000a) Transient stability of power systems: a unified approach to assessment and control. Kluwer, The Netherlands
- Pavella M, Wehenkel L, Bettiol A, Ernst D (2000b) An approach to real-time transient stability assessment and control. Techniques for power system stability limits search—IEEE special publication no TP-138-0
- Phadke AG (1995) Synchronized phasor measurements in power systems. *IEEE Comput Appl Power* 6(2):10–15
- Pizano-Martínez A (2010) Determination of steady-state and transiently stable optimal equilibrium points in electric power systems. PhD Thesis, Universidad Michoacana de San Nicolás de Hidalgo, Morelia, Michoacán, México
- Pizano-Martínez A, Fuerte-Esquivel CR, Ruiz-Vega D (2010) Global transient stability-constrained optimal power flow using an OMIB reference trajectory. *IEEE Trans Power Syst* 25(1):392–403

- Pizano-Martínez A, Fuerte-Esquivel CR, Ruiz-Vega D (2011) A new practical approach to transient stability-constrained optimal power flow. *IEEE Trans Power Syst* 26(3):1686–1696
- Ruiz-Vega D (2002) Dynamic security assessment and control: transient and small signal stability. PhD Thesis, University of Liège
- Ruiz-Vega D, Pavella M (2003) A comprehensive approach to transient stability control. Part I: near optimal preventive control. Part II: open loop emergency control. *IEEE Trans Power Syst* 18(4):1446–1460
- Ruiz-Vega D, Pavella M, Hirsch P, Sobajic D, Ernst D (2001) A unified approach to transient stability contingency filtering, ranking and assessment. *IEEE Trans Power Syst* 16(3):435–443
- Ruiz-Vega D, Olguín Salinas D, Pavella M (2002) Simultaneous optimization of transient stability-constrained transfer limits of multi-area power systems. In: *Proceedings of med power 2002 conference*, Athens
- Ruiz-Vega D, Messina A, Pavella M (2004) Online assessment and control of transient oscillation damping. *IEEE Trans Power Syst* 14(2):1038–1047
- Wehenkel L (1999) Emergency control and its strategies. In: *Proceedings of PSCC99*, vol 1, pp 35–48, Trondheim
- Wehenkel L (2004) Whither dynamic congestion management? *Proceedings of bulk power system dynamics and control—VI, IREP04*, 2 pages
- Wehenkel L, Ruiz-Vega D, Ernst D, Pavella M (2005) Preventive and emergency control of power systems. In: *Real time stability in power systems*. Springer, Norwell
- Zárate-Miñano R, Van Cutsem T, Milano F, Conejo AJ (2010) Securing transient stability using time-domain simulations within an optimal power flow. *IEEE Trans Power Syst* 25(1):243–253
- Zhang Y, Wehenkel L, Pavella M (1997) A method for real-time transient stability emergency control. In: *Proceedings of CPSPP97, IFAC/CIGRE symposium on control of power systems and power plants*, Beijing, pp 673–678
- Zima M, Ernst D (2005) On multi-area control of electric power systems, PSCC, Paper 2 in Session 9, Liege, Belgium, August 2005, Liège

Chapter 6

Online Dynamic Security Assessment

Jorge L. Jardim

Abstract This chapter describes an implementation of an online dynamic security assessment system based on time-domain simulation, in which dynamic models are the same as those used offline for planning studies with all necessary details. It contains a review of the adopted methods and algorithms (power flow, continuation power flow, time-domain simulation, energy functions, single machine equivalent, and Prony spectral decomposition) focusing on the main issues related to their numerical and computational performance. The utilization of these methods to execute complex security tasks such as dynamic contingency analysis and security region computations is described. Aspects of high-performance computation (fine- and coarse-grain parallelization) are discussed. Some practical results obtained online and comparisons of online with offline planning cases are shown.

6.1 Introduction

Power system security limits are typically computed offline and stored as nomograms and tables to be monitored by system operators in the real-time environment. Several uncertainties exist during such computations and consequently reasonable security margins must be taken into account in the final limits. Despite this, unplanned outages may cause operational conditions not considered at planning stages and consequently system operators are left with no proper security information under such circumstances. Online security assessment has been proposed as an additional line of defense in which security limits can be computed based on the actual power system state, which eliminates most of the uncertainties, thus providing more accurate limits (Debs and Benson 1975; Dy Liacco 1968; Hayashi 1969; Limmer 1966). Of course, this approach assumes that reasonably accurate online data are available.

Power system security may, and typically does, require evaluation of several different aspects such as thermal limits, steady-state and transient voltage levels, transient stability, etc. The steady-state aspects are generally evaluated through

J. L. Jardim (✉)
High Performance Power System Applications, Rio de Janeiro, Brazil
e-mail: jljardim@live.com

power flow contingency analysis, which, for the currently available computational resources, can be easily done online, even for very large networks. The transient aspects are traditionally evaluated by visual inspection of time-domain simulation trajectories. In this case, two major difficulties exist in doing it online. One is that the computational costs of these simulations are normally several orders higher than those of steady-state analysis, i.e., the problem presents a much higher computational complexity, in particular for large systems. Therefore, efficient simulation methods and parallel processing are required. The other is that the evaluation cannot depend on visual inspection as typically done in offline studies. However, this difficulty can be circumvented with post-processing algorithms to derive the essential information from monitored time-simulation trajectories.

Basically, two main lines of research have been proposed in the literature and applied in the industry to deal with the computational complexity. One is to simplify the problem by using reduced network and/or dynamic models and computing stability indices based on faster calculations. In some cases, heuristics are used to further simplify the problem. Such indices are not expected to be quite accurate, but just provide a degree of proximity to transient instability. Several different approaches have been developed in this line, such as Transient Energy Functions (TEF; Pai 1989), single machine equivalent (Pavella et al. 2000), and steady-state stability indices (Molina et al. 2009).

The other line of research is to use full time-domain simulations with detailed models, efficient simulation algorithms, and parallel processing (Jardim 2000; Jardim et al. 2004; Jardim et al. 2006; Jardim 2009). Detailed models are used at least for the main area of interest, but when necessary external network and dynamic equivalents can be used. Some advantages of this kind of approach are the following:

- Close compatibility with limits computed offline
- Quite accurate assessment
- Not only transient stability but also all other dynamic security aspects can be evaluated; and
- Easier validation of online assessments

The online security assessment can be done for the (real-time) operating point only or additionally for a region around this point. An operating point is said to be secure if no predefined contingency causes violation of the security criteria. Time-domain simulations can tell whether the system is transiently stable or not, but do not provide a quantifiable degree of stability/instability. For example, if the system is stable, how close is it to be unstable? Additional methods, such as energy function methods, can be embedded in the time simulation to estimate stability margins and answer these types of questions. These estimates cannot be very accurate due to the nonlinear nature of models and phenomena involved. On the other hand, by successively stressing the system in a particular fashion and reprocessing contingencies, it is possible to obtain more accurate limits for such conditions, but at the expense of much more computation. In practice, this is the approach used offline for computing security limits (nomograms).

The main disadvantage of time-domain simulations, in particular when detailed models are used, is the inherently high computational cost. Therefore, the adoption of quite efficient numerical integration methods can make a huge difference in performance for this type of application.

This chapter presents the main aspects of an online Static And Dynamic Security Assessment System (SDSA) that is based on time-domain simulation with detailed models and is able to calculate security regions (nomograms). Essentially, it is an automation of offline procedures, and therefore its relevant characteristics are in the details of the adopted algorithms, the automation process, and the methods used to verify all security aspects. SDSA has been online for several years in the control centers of the Brazilian National Operator (ONS).

6.2 Simulation Methods

Whenever there is a numerical failure in offline simulations, the analyst can normally circumvent the problem by examining its results, changing parameters, and trying it again. For example, if a power flow does not converge, it is possible to change the starting procedure, change or block specific controls, etc. In the case of time-domain simulation with fixed time step, reducing the step or changing the load characteristics during a fast transient may overcome a numerical instability.

As online processes are not supervised by an analyst, they demand careful choice of the numerical methods and of procedures for circumventing failures. In this section, the traditional simulation methods are revisited with focus on aspects to improve their performance and to avoid numerical problems. Nevertheless, it is always important to remember that despite the importance of the methods and their implementation, any online power system application based on detail modeling depends fundamentally on good data and models, not only for the accuracy of the results but also for the software performance.

6.2.1 Power Flow

Power flow calculation is the most basic method used in a security assessment system. For online SDSA, the power flow is used for computing the initial system condition with reasonable accuracy and steady-state contingency analysis. Theoretically speaking, the solved power flow case retrieved from the Energy Management System (EMS) should be fully converged and ready to be used by the security assessment; in practice, though, this may not be true due to differences in tolerance and/or inaccuracies that might have been introduced by data truncation, depending on the data exchange format. Also, and more important, the power flow calculation is the engine for steady-state contingency analysis.

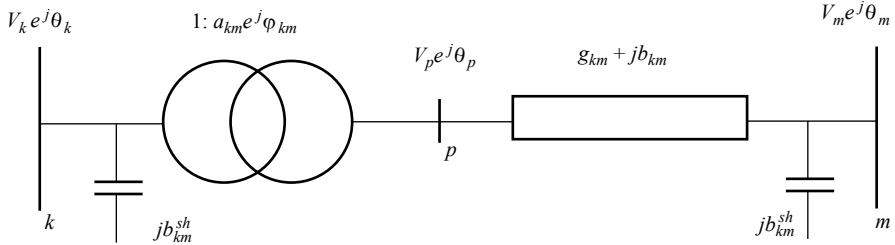


Fig. 6.1 Generic branch model

The power flow formulation is well known (Stott 1974), largely described in textbooks, e. g., Monticelli (1999) and is summarized in the following.

A network branch can be modeled as in Fig. 6.1, where for a transmission line $a_{km} = 1$ and $\varphi_{km} = 0$, for an in-phase transformer $\varphi_{km} = 0$, and $b_{km}^{sh} = 0$ for transformers.

The general power flow equations for this generic branch are given by

$$P_{km} = a_{km}^2 V_k^2 g_{km} - a_{km} V_k V_m (g_{km} \cos(\theta_{km} - \varphi_{km}) + b_{km} \sin(\theta_{km} + \varphi_{km})) \quad (6.1)$$

$$Q_{km} = -a_{km}^2 V_k^2 (b_{km} + b_{km}^{sh}) + a_{km} V_k V_m (b_{km} \cos(\theta_{km} + \varphi_{km}) - g_{km} \sin(\theta_{km} + \varphi_{km})) \quad (6.2)$$

and

$$P_{mk} = V_m^2 g_{km} - a_{km} V_k V_m (g_{km} \cos(\theta_{km} + \varphi_{km}) - b_{km} \sin(\theta_{km} + \varphi_{km})) \quad (6.3)$$

$$Q_{mk} = -V_k^2 (b_{km} + b_{km}^{sh}) + a_{km} V_k V_m (b_{km} \cos(\theta_{km} + \varphi_{km}) + g_{km} \sin(\theta_{km} + \varphi_{km})). \quad (6.4)$$

The power flow formulation is obtained by applying Kirchoff's nodal law to all nodes of the network, which results in the following reciprocal power equations:

$$0 = -Pg_k + Pl_k + \sum_{m \in \Omega_k} P_{km} \quad (6.5)$$

$$0 = -Qg_k + Ql_k + \sum_{m \in \Omega_k} Q_{km} \quad (6.6)$$

for $k=1, \dots, n$, where n is the number of buses in the system

Pg_k and Qg_k are respectively the active and reactive generation at bus k , and Pl_k and Ql_k are the active and reactive load at bus k , respectively. Loads can be constant power or voltage dependent.

The solution of the set of equations (6.5 and 6.6) requires at least one reference voltage and one reference angle, which are normally set at a specific bus, called swing or slack bus. Considering, for example, that the injected power for all

remaining buses is known, the problem consists of solving a set of $2n-2$ nonlinear equations with $2n-2$ variables (V, θ), typically by the Newton–Raphson method. By the nature of the problem, the load imbalance (generation—load—losses) is allocated to the slack bus. Therefore, for some uses of power flow calculation, such as in contingency analysis, it may be desirable to distribute the imbalance among some or all generators in the system.

Generators, switchable shunts, FACTS, and Tap Changing Under Load (TCUL) transformer taps are set to control terminal or remote buses, and phase shifters and FACTS can be set to control power flow. Possible formulations for each control are the suppression of one variable, making it constant, and one equation. Alternatively, an equation specifying the control logic and the respective control variable can be added. Also, additional equations must be included when multiple devices (e. g., generators) control the same variable (e. g., bus voltage) to define the participation of each control and avoid multiple solutions. For example, if generators at buses i and j control the same bus voltage, an additional equation establishing how they will participate in the control can be defined as

$$K_i Q_i - K_j Q_j = 0,$$

where Q and K are the generator MVA_r output and participation factor.

Of course, control limits must be enforced and it is imperative that they are correctly specified. Controls must be able to back-off limits whenever possible.

DC Links are represented by additional power injections in (6.5, 6.6; Smed et al. 1991).

The set of equations (6.5, 6.6) and additional control equations can be represented in a simplified form as:

$$0 = f(x), \tag{6.7}$$

where $f(x)$ is a vector function of independent variables x (typically, V, θ, a, ϕ).

The Newton method solves iteratively (6.7) approximated by a first-order truncated Taylor series, i.e.,

$$f(x^v + \Delta x^v) \cong f(x^v) + f'(x^v) \Delta x^v, \tag{6.8}$$

where $f'(x)$ is the Jacobian matrix and v is the iteration number.

At a solution point $\Delta x=0$ and $f(x)=0$ which leads to the following iterative process:

$$\Delta x^v = -[J(x^v)]^{-1} f(x^v) \tag{6.9}$$

$$x^{v+1} = x^v + \alpha \Delta x^v \tag{6.10}$$

until $\Delta x^v < \varepsilon$ or $f(x) < \varepsilon$, where ε is a small tolerance.

Although the power flow problem is relatively simple, some practical considerations must be observed to minimize the possibility of failure, as follows:

- The full Newton–Raphson method, in which all variables are solved simultaneously, is the preferred solution algorithm because of its better convergence properties. The alternate approach where some variables (e.g., taps and phase shifts) are solved between iterations of the Newton method generates interface errors that can be amplified or sustained, thus preventing convergence. The fast decoupled algorithms were very attractive with respect to computational speed when computer power was quite limited, but, due to its inferior convergence properties when compared with the full Newton, unless for specific applications, there is no reason to adopt it today. Again, reliable algorithms should be the primary concern in the implementation of online applications
- It is critical to scale the update by a factor α to improve convergence, as shown in (6.10). For ill-conditioned cases, some of the elements in Δx can be very high, thus violating the assumption in (6.8), i.e., that Δx is small. Of course, for well-behaved situations α can be set to 1 without causing any problem. Several methods have been proposed to find a suitable α , including one-dimension minimization methods (Braz et al. 2000)
- It is well known that the Newton–Raphson method has a very good local convergence, but may fail for initial conditions far from the solution. This should not be critical for online base cases as long as the state estimator is able to deliver a converged power flow. For offline applications, a cold start procedure, such as DC power flow combined or not with one iteration of the fast decoupled method can be quite useful
- It is important to remember that a solution to the power flow problem may not be, and normally is not, unique. To make a long discussion around this subject short and assuming the problem can be solved, if only continuous controls and constant power loads are represented, there should be one useful solution and several nonrealistic ones, but if dead-band controls are represented there may be several useful solutions. The possibility of finding nonrealistic solutions also emphasizes the need of starting close to the solution. Of course, the concern is related to unrealistic solutions that may yield false security violations. For online applications, starting too far away from the solution can be a problem in contingency analysis and when re-dispatching generation to stress the operating condition. Thus, it is useful to implement methods to move smoothly between two different operating points. The continuation power flow method is quite effective in dealing with this problem and should be the preferred choice whenever possible
- A problem frequently observed in solved power flow cases consists of conflicting or wrongly defined controls. There are several situations in which this may happen. A few examples are the following: (a) two parallel tap-controlled transformers controlling voltages at opposite sides; (b) a voltage control device controlling the voltage of a very remote bus or a bus in a different electrical island; (c) two voltage control devices controlling the same bus, but at different voltage levels; (d) a tap controlled transformer with no voltage source device on the low voltage side trying to control the voltage of a high voltage side bus; etc. Such situations may occur because of data errors or due to a topological network

change caused by a contingency. Then, it is important to implement routines to verify and correct or disable controls, if necessary, at the data input level and during the iterative process.

6.3 Continuation Power Flow

For the reasons explained in the previous section, moving as smooth as possible between different power flow solutions helps power flow convergence and avoids convergence to unrealistic solutions. The Continuation Power Flow (CPF) method is very effective and efficient for this, and it is used in SDSA for the process of searching security boundaries, i.e., stressing the system pre-contingency operating condition in a given direction. Also, although it is not the rule, there may be situations in which the security boundary is not affected by the specified contingencies, but instead it is found on the pre-contingency case. For these cases, for example, the CPF can provide the maximum loadability point with good accuracy whereas the regular power flow is likely to fail at lower stress/load level.

The efficiency of the CPF method comes from the fact that it allows larger steps when moving the operating point in a particular direction. Also, the prediction phase, with the cost of one power flow iteration, saves more than one iteration in the corrector phase.

The tangent vector method approach (Ajjarapu and Christy 1991; Seydel 1994) is adopted in SDSA. It consists of two phases, linked through a continuation parameter. In the first phase, called *predictor*, the power flow equations are parameterized and sensitivities of the power flow variables with respect to the parameters are computed. These sensitivities are used to estimate a new operating point, given a uniform change in the parameters. Then, in the second phase, called *corrector*, the Newton–Raphson method is used to find the solution with a good accuracy, considering one of the variables, called *continuation parameter*, fixed. The predictor–corrector cycle is repeated until the desired solution (target operating point or maximum loadability) is obtained.

6.3.1 Tangent Vector Method

The following description of the method assumes that generations and loads will be re-dispatched according to a given pattern (direction) defined by changing factors. The parameterization is set as

$$\begin{aligned} Pg &= Pg_0 + \lambda Kp_g \\ Pl &= Pl_0 + \lambda Kp_l \\ Qg &= Qg_0 + \lambda Kq_g \\ Ql &= Ql_0 + \lambda Kq_l \end{aligned}$$

where λ is the generation/load increment variable applied to all buses of the system, Pg_0 , Pl_0 , Qg_0 and Ql_0 are the generation and load values at the initial operating point, and Kp_g , Kp_l , Kq_g , and Kq_l are the generation/load change factor or parameters, defined for each bus in the system.

Considering $\lambda=0$, the set of nonlinear equations system defined in (6.7) becomes:

$$f(x, \lambda) = 0. \quad (6.11)$$

Linearizing (6.11) at a solution, one gets

$$\begin{aligned} f(x + \Delta x, \lambda + \Delta \lambda) &\cong f(x, \lambda) + f'(x, \lambda)(\Delta x, \Delta \lambda)^T \\ &= f'(x, \lambda)(\Delta x, \Delta \lambda)^T = 0 \end{aligned} \quad (6.12)$$

From (6.12), the sensitivity of the state variables with respect to λ can be computed and then prediction of these variables for a step increase/decrease of λ can be calculated.

The predicted values, supposedly close to the final solution are used as initial condition for a slightly modified power flow calculation. In this process, one of the variables (called continuation parameter) in (6.11) is kept constant. The predictor–corrector cycle is repeated until the solution (target point or maximum loadability) is obtained.

The continuation parameter may be the increment variable, lambda, or the voltage at one bus. The decision is based on which one has the highest sensitivity, which is computed in predictor phase. Figure 6.2 illustrates the process. In practice, voltage is selected only near maximum loadability points (nose tip).

The first task in the prediction process is to calculate the tangent vector. This tangent calculation is derived by the augmented Jacobian matrix, which has one extra column, associated with the additional unknown variable lambda (λ). One additional equation must be added to match the number of variables. This can be done by considering the sensitivity of the variables to a step change (increase or decrease) in the increment variable, i.e.

$$\partial \lambda = \pm 1.$$

The set of equations then becomes

$$\begin{pmatrix} f'(x, \lambda) \\ e_\lambda \end{pmatrix} \begin{pmatrix} \partial x \\ \partial \lambda \end{pmatrix} = \begin{pmatrix} 0 \\ \pm 1 \end{pmatrix}, \quad (6.13)$$

Where e_λ is a row vector with all elements equal to zero except in λ position, which is one.

Once the (sensitivity) tangent vector $t = (\partial x, \partial \lambda)$ has been found, the step size should be chosen so that the predicted solution is within the radius of convergence of the corrector. A possible choice is the inverse of the norm of the tangent vector, as follows:

$$\begin{pmatrix} \Delta x \\ \Delta \lambda \end{pmatrix} = \alpha \|t\|^{-1} \begin{pmatrix} \partial x \\ \partial \lambda \end{pmatrix}, \quad (6.14)$$

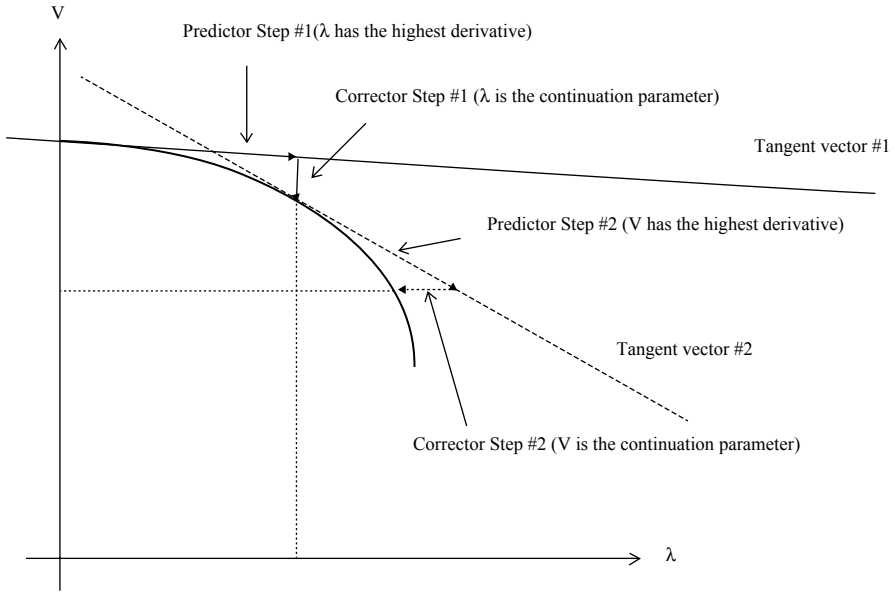


Fig. 6.2 Example of two predictor–corrector cycles with different continuation parameters

where α can be adjusted to reach specific points, or guarantee that the initial condition will be sufficiently close to the solution.

The corrector step solves (6.11) using the Newton power flow method, but forcing the continuation parameter at the specified value. The continuation parameter can be either voltage at a specific bus or lambda. Considering that η is the specified value for the continuation parameter (V_k or λ) the new system to be solved can be expressed as:

$$\begin{bmatrix} f(x, \lambda) \\ V_k - \eta \end{bmatrix} = [0]$$

or

$$\begin{bmatrix} f(x, \lambda) \\ \lambda - \eta \end{bmatrix} = [0].$$

6.4 Time-Domain Simulation

The most computationally expensive task in a detailed modeling approach for dynamic security assessment is that performed by the time-domain simulation engine. Consequently, overall performance is very much affected by the numerical integration methods adopted.

Most of the existing time-domain simulation programs use numerical integration based on fixed time step and alternate solution of control and network equations (Arrillaga et al. 1983). This kind of technology was acceptable, and possibly a good choice, for computers with low memory, nonstiff system of equations (only synchronous machines with relatively large time constants), and offline studies performed much ahead of real time. For those cases, computational speed was not a critical factor.

However, adapting these programs for online applications is not a good choice now because computer memory is not a limitation anymore, power electronic devices are increasingly being represented in dynamic studies, which stiffen equations, security assessment requires huge amount of fast computation, and there are much better and well-recognized methods for numerical integration.

Despite the fact that more advanced methods have been recommended for quite some time (Stott 1979), the majority of the commercial software still have not adopted them.

The time-domain simulation in SDSA is based on the Adams–Bashforth–Moulton and Backward Differentiation Formulas (ABM–BDF) numerical integration method (Astic et al. 1994, Brenan et al. 1989, Lambert 1991) associated with the Variable-Step-Variable-Order (VSVO) approach and the simultaneous solution of the algebraic and differential equations.

These techniques yield high numerical stability and improved performance (several times faster) compared with more traditional nonsimultaneous fixed-time-step approaches. The shortcomings of the latter are explained as follows. To avoid numerical instability (Lambert 1991), the fixed step alternated solution methods have to use very small integration time steps. Roughly speaking, their step size should not be greater than the smallest time constant in the dynamic models. But under stiff numerical conditions, even smaller time steps may be required to avoid numerical instability. Obviously, the impact on the performance is severe, particularly when fast acting control devices such as static VAR compensators or DC links need to be represented.

By contrast, in a simultaneous solution approach, the size of the time step is bounded by the accuracy of the simulation rather than its numerical stability. In practical terms, the desired accuracy can be met with small-time steps during fast transients and larger time steps on smoother trajectories. The time step size is optimized by a dynamic adjustment mechanism as described below.

The differential and algebraic equations describing a power system model are represented by the following equations:

$$\dot{y} = f(y, x, t) \quad (6.15)$$

$$0 = g(y, x, t), \quad (6.16)$$

where:

$y \in R^n$ is the vector of the state variables (or phase variables) that represent the dynamic models of control components such as synchronous machines, voltage regulators, DC links, etc.

$x \in R^m$ is the vector of algebraic variables, which are basically network voltages, current injections, and some control variables.

The ABM and BDF can be represented as

$$\sum_{i=0}^j \alpha_i y_{n+i} = h \sum_{i=0}^j \beta_i f_{n+i}, \quad (6.17)$$

where:

α_i and β_i are parameters dependent on the specific integration method, j is the number of steps of the method, and h is the time step.

Using the appropriate parameters, the first-order ABM and BDF methods correspond to the Euler method:

$$y_{n+1} = y_n + hf_n \quad (\text{predictor}) \quad (6.18)$$

$$y_{n+1} = y_n + hf_{n+1} \quad (\text{corrector}) \quad (6.19)$$

The second order ABM is usually known as the Trapezoidal method:

$$y_{n+1} = y_n + 0.5h(3f_n - f_{n-1}) \quad (\text{predictor}) \quad (6.20)$$

$$y_{n+1} = y_n + 0.5h(f_{n+1} + f_n) \quad (\text{corrector}) \quad (6.21)$$

The second order BDF is given by

$$y_{n+1} = 2y_n - 3y_{n-1} + y_{n-2} \quad (\text{predictor}) \quad (6.22)$$

$$y_{n+1} = \frac{4}{3}y_n - \frac{1}{3}y_{n-1} + \frac{2}{3}f_{n+1} \quad (\text{corrector}) \quad (6.23)$$

The ABM method is used for most of the differential equations, whereas the BDF method is used for algebraic equations and differential equations with very small time constants (< 10 ms). For improved efficiency, the current and past information are stored in Nordsieck (Lambert 1991) vector form.

By applying the numerical integration formulae (6.18–6.23) to the model equations (6.15–6.16), the following set of algebraic equations is obtained:

$$0 = y_{n+1} - \beta_{n+1} hf(y_{n+1}, x_{n+1}) - C, \quad (6.24)$$

$$0 = g(y_{n+1}, x_{n+1}) \quad (6.25)$$

where:

C is the weight sum of y_n and \dot{y}_n terms

β_{n+1} is the constant that multiplies f_{n+1} in the integration formulae (6.18–6.23).

The solution of this set of equations is obtained by a “dishonest Newton method,” in which the Jacobian matrix is updated only if: there is a time step change, or the algorithm does not converge, or if a large hard discontinuity occurs. Typically, two to three iterations are needed to converge at a time step.

The mechanism to change the time step is based on the estimation of the Local Truncation Error (LTE) at the end of each time step. If the LTE is smaller than the required tolerance, the current step is accepted and the possibility of increasing its size is evaluated. If the LTE is above the tolerance, the current step is rejected and the step size is sufficiently reduced to bring the error to half of the tolerance.

The LTE estimation is based on the first neglected term of the Taylor series:

$$E_k = \frac{h^{k+1} y^{k+1}}{k+1},$$

where k is the current integration order (1 or 2). The maximum time step \bar{h} is calculated by considering the truncation error equal to the tolerance

$$\bar{h} \approx h \left[\frac{\tau}{E_k} \right]^{\frac{1}{k+1}},$$

where τ is the tolerance. Considering that there is no error margin in this estimation, a conservative approach is adopted for the next step, say half of the estimated value.

Whenever the time step is changed, the best order is also evaluated. The criterion to choose the best order is the decreasing pattern of the truncated Taylor terms. Thus, the Taylor series expansion behaves as expected for the second order if the magnitude of the third-order terms form a decreasing sequence. Otherwise, first-order integration is used (Brenan et al. 1989).

A difficult problem in time-domain simulation is the treatment of discontinuities. The one-step (self-starting) methods can handle this better, but are generally less efficient as they require smaller time steps when compared to higher order methods. The multistep methods need step size and order changes to deal effectively with such situations. Re-initialization with first-order integration is one of the possible approaches.

This implementation deals with discontinuities in different ways depending on their types. The main sources of discontinuities are network and control switching and state variable nonlinearity. Switching operations can be specified by the users (e.g., in the contingency definition) or are automatically activated by controls such as excitation limiters, or protection systems such as line tripping. Depending on the

severity of the switching operation, the program re-initializes the numerical integration process by zeroing the time step. The severity is measured by the norm of the first-order derivative of the state variables. The re-initialization of the integration process nullifies the past (previous steps) information and the integration order is set to one. If necessary, the time step is reduced so that a switching operation occurs at the specified time.

The severity of the effect of nonlinearity on state variables, such as integrator saturation, is taken into account at the end of the step. If the LTE is greater than the tolerance, the step is rejected and decreased.

6.5 Diagnostic Methods

Assessing security through time-domain simulation without visual inspection of trajectories requires specific functions for monitoring the security criteria. Some of the most frequently adopted criteria include transient stability (or stability margin), electromechanical oscillation damping, transient voltage behavior, and frequency limits. Computing stability margins is not trivial and typically requires energy function methods. Computing oscillation damping also requires special algorithms (e.g., Prony analysis), but it is a simpler problem. Practically, all the other criteria can be assessed by trivial procedures.

The classical TEF methods are based on simplified dynamic models (e.g., classical synchronous generator models) with the purpose of estimating stability margins. For SDSA, which is based on a detailed modeling approach, a much more suitable technique, single machine equivalent (SIME; Pavella et al. 2000) is adopted, as it does not impose restriction on the models, can be easily embedded in time-domain simulation programs, and has a negligible computational cost. But some key concepts of the TEF methodology (Pai 1989) are adopted in SDSA to detect instability and early terminate simulations, support some of the SIME features, and select generators for modal spectral analysis.

6.5.1 Energy Functions

SDSA uses numerical energy functions and a modified version of the SIME method for energy/power margin computation, instability detection, and identification of oscillatory machines.

System stability can be detected via the following dot product (Pai 1989):

$$f_{ip} = P_{ac}^T \Delta \theta, \quad (6.26)$$

where:

$$\begin{aligned}
 P_{ac}^T &= (pac_1, pac_2, \dots, pac_{ng}) \\
 \Delta\theta &= (\Delta\theta_1, \Delta\theta_2, \dots, \Delta\theta_{ng}) \\
 \theta_i &= \delta_i - \theta_{coi} \\
 \theta_{coi} &= \frac{1}{M_t} \sum_{i=1}^{ng} M_i \delta_i \\
 pac_i - pm_i - pe_i - \frac{M_i}{M_t} pcoi \quad i &= 1, 2, \dots, ng \\
 pcoi &= \sum_{i=1}^{ng} (pm_i - pe_i) \\
 M_t &= \sum_{i=1}^{ng} M_i
 \end{aligned}$$

where M_i , δ_i , pe_i , pm_i and pac_i are, respectively, the inertia constant, rotor angle, electrical output, mechanical power, and accelerating power of machine i ; ng is the number of synchronous generators; θ_i is rotor angle of machine i referred to the center of inertia θ_{coi} ; and P_{ac} and $\Delta\theta$ are the vectors of generator accelerating power and angle deviation respectively. Both quantities are referred to the center of inertia.

For classical synchronous machine models, system instability is detected when $f_{ip} < 0$. For higher-order synchronous machine models, a lower level is used, i.e., $f_{ip} < \tau$, $\tau < 0$.

Individual energy functions are also computed to determine machines with low damping. The potential energy function is given by

$$Vpe_i = \int pac_i d\theta,$$

the kinetic energy function by

$$Vke_i = \frac{1}{2} M_i \omega_i^2,$$

and the total energy is

$$Vt_i = Vpe_i + Vke_i.$$

The rate of decay of Vt_i indicates those machines with lower damping. These are selected for Prony decomposition analysis.

6.5.2 Modified SIME Method

The SIME method can be used to estimate security margins at a given operating point. In the following implementation, it can also be used for contingency filtering. A brief review of the SIME method (Pavella et al. 2000) in both the original and the modified versions is presented as follows.

6.5.3 Original SIME Method

It is well known that a power system transient instability is caused initially by the separation of only two generation areas. Certainly, cascading effects may lead to further separations, but the interest is obviously to avoid the initial separation, which is caused by a power imbalance in which generators of one area accelerate (or decelerate) with respect to the others. This leads to the concept of two coherent groups of generators, denominated critical and noncritical clusters. By definition here, the critical cluster is the one with smaller inertia. If the critical cluster accelerates with respect to the noncritical cluster, it is said that it swings *forward*, if it decelerates then it swings *backward*.

The critical cluster is composed of the generators with angle increasing (decreasing) with respect of the Center Of Angle (COA) of an electrical island, if it swings forward (backward). It is important to know whether the critical cluster mode is forward or backward because the corrective measure will be to reduce or to increase respectively its generation.

The determination of the critical cluster can be done by selecting several candidate sets and testing for the one with lowest margin. The original SIME method proposes the use of the most advanced angles (large angle excursions) to classify machines in candidate sets. Rotor speeds are also a good measure for this classification. In SDSA, and for stable cases, the identification of critical clusters occurs only when the total kinetic energy reaches a minimum, which correspond to a point of maximum separation between critical and noncritical clusters.

Given the critical and noncritical groups, the respective machines are aggregated into their respective COA and then the COAs are replaced by a One-Machine Infinite Bus (OMIB) equivalent, as follows.

Compute the quantities of the aggregated groups

$$\delta_c(t) = \frac{1}{M_c} \sum_{k \in C} M_k \delta_k(t) \quad (6.27)$$

$$\delta_n(t) = \frac{1}{M_n} \sum_{j \in N} M_j \delta_j(t) \quad (6.28)$$

$$M_c = \sum_{k \in C} M_k \quad (6.29)$$

$$M_N = \sum_{k \in N} M_k \quad (6.30)$$

$$\omega_C(t) = \frac{1}{M_C} \sum_{k \in C} M_k \omega_k(t) \quad (6.31)$$

$$\omega_N(t) = \frac{1}{M_N} \sum_{j \in N} M_j \omega_j(t) \quad (6.32)$$

$$Pe_C(t) = \frac{1}{M_C} \sum_{k \in C} Pe_k(t) \quad (6.33)$$

$$Pm_C(t) = \frac{1}{M_C} \sum_{k \in C} Pm_k(t) \quad (6.34)$$

$$Pe_N(t) = \frac{1}{M_N} \sum_{j \in N} Pe_j(t) \quad (6.35)$$

$$Pm_N(t) = \frac{1}{M_N} \sum_{j \in N} Pm_j(t), \quad (6.36)$$

where the subscript C denotes the group of critical machines and N the noncritical machines.

Compute the equivalent OMIB

$$\delta(t) = \delta_C(t) - \delta_N(t) \quad (6.37)$$

$$\omega(t) = \omega_C(t) - \omega_N(t) \quad (6.38)$$

$$Pm(t) = M(Pm_C(t) - Pm_N(t)) \quad (6.39)$$

$$Pe(t) = M(Pe_C(t) - Pe_N(t)) \quad (6.40)$$

$$Pa(t) = Pm(t) - Pe(t) \quad (6.41)$$

$$M = \frac{M_C \times M_N}{M_C + M_N} \quad (6.42)$$

Equations (6.37–6.42) represent the mapping of a multi-machine system into an OMIB system, which allow us to apply the principle of the Equal Area Criterion (EAC).

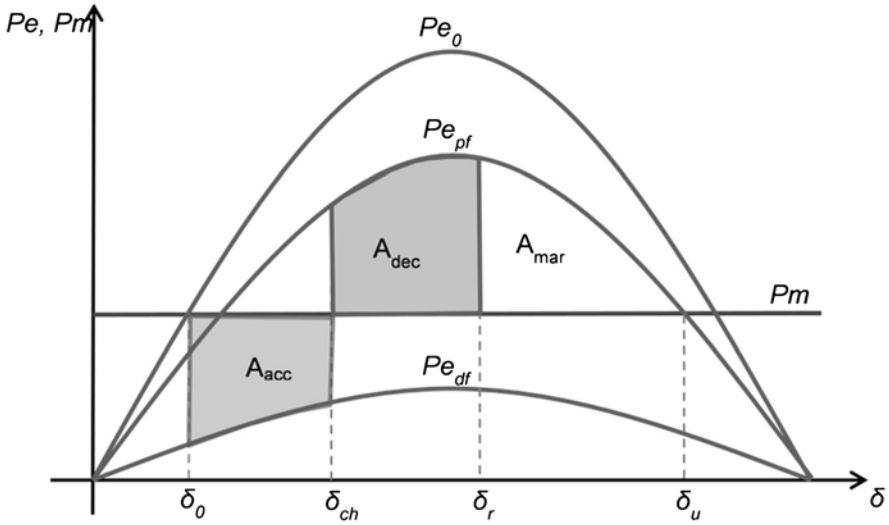


Fig. 6.3 Equal area criterion

Figure 6.3 illustrates the EAC concept, where Pe_0 , Pe_{df} , and Pe_{pf} are the OMIB power transfer characteristics for pre-fault, during the fault, and post-fault conditions, respectively, δ_0 is the pre-fault rotor angle, δ_{ch} is the post-fault rotor angle in which the accelerating power changes from positive to negative, δ_r is the angle of return, i.e., the maximum angular excursion for a stable scenario, δ_u is the unstable equilibrium point, A_{acc} is the acceleration area ($Pm > Pe$), A_{dec} is de deceleration area ($Pe > Pm$), and A_{mar} is the margin area, i.e., the energy margin of the system for the particular fault. To simplify the analysis, Pm is considered constant. The sum ($A_{dec} + A_{mar}$) is the total potential energy available to absorb the kinetic energy introduced into the system by the fault. Computation of A_{mar} requires that the function of Pe_{pf} versus angle is known (or estimated with good accuracy).

During the fault, the machine accelerates because the accelerating power ($Pac = Pm - Pe$) is positive. At the point in which the accelerating power becomes negative (most of the time it is the fault clearing time), the machine speed is maximum and it starts decelerating.

The total energy gained by the system can be determined as the kinetic energy at this point, as follows:

$$A_{acc} = \frac{1}{2} M \omega_{ch}^2 \tag{6.43}$$

The condition for the system to be transiently stable is that the decelerating area A_{dec} must be greater than A_{acc} . In other words, the angle of return δ_r must be smaller than the unstable angle δ_u .

Instability is detected by the crossing of the unstable equilibrium point, which is characterized by the accelerating power changing from negative to positive and by the derivative of the angle being positive. At this point, the remaining energy in the system, not dissipated in the decelerating area, is the negative energy margin and can be accurately computed by

$$\eta_u = \frac{1}{2} M \omega_u^2, \quad (6.44)$$

where ω_u is the equivalent machine speed at the crossing point.

A key aspect on the accuracy of the SIME method is the computation of the positive margin A_{mar} for stable cases. In Pavella et al. (2000), two methods are proposed to estimate this margin. The first approach consists of the triangle approximation, formulated as:

$$A_{mar} = \frac{1}{2} (Pe_{pf}(\delta_r) - Pm)(\delta_u - \delta_r). \quad (6.45)$$

Obviously, this requires the knowledge of the unstable angle δ_u , but this angle is not known if the system is stable. In practice, repeated simulations with increasing stress are necessary to find the unstable angle. This makes the triangle approximation inefficient and of little interest.

The other suggested approach is to approximate the $Pe_{pf}(\delta)$ as follows:

$$Pe(\delta) = A\delta^2 + B\delta + C, \quad (6.46)$$

where a , b , and c are computed through weighted least-square approximation using three or more successive time steps. In practice, $Pe_{pf}(\delta)$ is not as well behaved as in Fig. 6.1 and, for stable scenarios with large margins, the points may not be representative of the real characteristic. Additionally, if the case is quite stable the angle excursion is small and the available points for the curve fitting may be insufficient. Consequently, large errors can occur. Again, to use this method effectively it would be necessary to run successive simulations with increasing stress level to find a good approximation, which is again quite inefficient.

6.5.4 Modified SIME Method

An improved, meaning faster and more accurate, method for computing positive margins is crucial to the SIME approach in order to obtain a reliable and quick assessment of the system stability. The objective is to be able to estimate the energy margin (positive or negative) a few milliseconds, for example, 200 ms, after the fault is cleared.

The central idea is to approximate the $Pe_{pp}(\delta)$ characteristic by the power transfer function of the OMIB system:

$$Pe(\delta) = \frac{E_m(\delta)E_\infty}{X_e} \sin \delta + P_0, \quad (6.47)$$

where E_m is the equivalent machine voltage behind its transient reactance, which is modeled as a function of the rotor angle, E_∞ is the infinite bus voltage, which is assumed to be constant, δ is the equivalent machine rotor angle, and P_0 represents a local power referred to the OMIB equivalent. To use this approximation, E_m , E_∞ , and X_e need to be estimated. If this is possible, P_0 can be calculated to fit the equation at a particular point.

Remark The approximation $Pe(\delta) = P_{12} \sin \delta + P_0$ was also tried, where P_{12} is a constant, and P_{12} and P_0 are computed using values at successive time steps. But this leads to the same problems of the weight least-square approximation of (6.46). Also considering P_{12} constant is a source of error as generator excitation can change significantly from nonstressed to stressed scenarios.

$E_m(\delta)$ is estimated in the adopted approach as the average of the critical cluster voltages behind the transient reactance:

$$E_m(\delta) = \frac{1}{nc} \sum_{k \in C} E_k(\delta). \quad (6.48)$$

where nc is the number of generators in the critical cluster. E_∞ is estimated in the same fashion for the noncritical cluster, but in the tests performed so far, it has been estimated at the returning angle and left constant, i.e., it is not considered as a function of the angle displacement.

X_e is estimated in the proposed approach as the weighted average of the external impedance seen by each generator plus its own transient reactance.

$$X_e = \frac{1}{M_C} \sum_{k \in C} M_k (xe_k + xd'_k), \quad (6.49)$$

where xd'_k and xe_k are the transient reactance and the external impedance seen by generator k , respectively. Thus, the missing piece of information to complete the proposed approximation is the external impedance seen by each generator.

One way of finding this information is by the explicit computation of the Thévenin impedance seen by each generator in the cluster, considering the other generators of the cluster as open circuit, but depending on the number of generators in the critical cluster, this computation can be quite expensive. Then the following alternative approach was used.

Assuming that the interconnection between the critical and noncritical clusters is through a reactance and that the machines in the cluster oscillate coherently, one can write

$$\bar{V}_{mk}(t) = j(xe_k) \bar{I}_k(t) + \bar{E}_\infty \quad (6.50)$$

where $\bar{V}_{mk}(t)$ and x_{e_k} are the terminal voltage of and external impedance seen by machine k , respectively. Considering also that \bar{E}_∞ is constant (infinite bus), one can write

$$|x_{e_k}| = \left| \frac{\frac{d\bar{V}_{mk}(t)}{dt}}{\frac{d\bar{I}_k(t)}{dt}} \right| \quad (6.51)$$

Remark The approximations in this model are quite reasonable compared with the overall approximation of the SIME model. Generally, there is no infinite bus, but in a multi-machine system for a single machine the rest of the system typically behaves as an infinite bus. Also, the interconnection between critical and noncritical clusters is not purely reactive but typically the resistive component is relatively small.

The external impedance seen from each individual machine x_{e_k} can be computed at any post-fault time step, but in the current implementation it is being computed as an average over a time range.

Note that the external impedance can be theoretically estimated immediately after the fault is cleared. Consequently, the entire decelerating area can be readily estimated. The maximum kinetic energy (accelerating area) is known, as mentioned above, as soon as the accelerating power changes from positive to negative.

For not very stressed conditions, this occurs at fault clearance; for stressed conditions, it can take a few milliseconds after fault clearance, and for very stressed conditions it may not happen at all. But this last case can be easily flagged as a severe condition without requiring too long time simulation. Then for the other two conditions, the energy margin (total decelerating area minus the accelerating area) can be estimated at most a few milliseconds after fault clearance, which results in a very fast approach for contingency ranking and simulation early termination.

The form of implementation of the SIME algorithm depends on the purpose of its use. For example, for contingency screening it is desirable to estimate the stability margin just few milliseconds after fault clearance, but for the diagnostic of a full time-domain simulation the urgency is not needed and the estimation can be more conveniently performed at returning angles or instability detection.

The following implementation strategy was used for diagnosis of time-domain simulation:

1. Start the time-domain simulation.
2. For the post-fault system condition, check for instability or angle of return (minimum kinetic energy) at each time step.
3. If instability is detected, determine the critical cluster and the negative energy margin and stop the simulation.
4. If a point of return is found, determine the critical cluster and compute the positive energy margin.

For contingency ranking, the strategy used is the following:

1. Start the time-domain simulation.
2. If the system is in post-fault condition and instability is detected, compute the negative energy margin and stop the simulation.
3. If the system has been simulated for a minimum time interval (few milliseconds) in post-fault condition and the kinetic energy has reached a maximum, compute the positive (or negative) energy margin and stop the simulation.

6.5.5 Prony Analysis

The Prony method (Castanié 2011; Hauer 1991) is used for spectral analysis (damping assessment) of synchronous machine angle trajectories. The objective is to compute the following spectral decomposition for a given signal, say rotor angle, $\hat{y}(t) = \hat{\delta}(t)$:

$$y(t) = \sum_{i=1}^n R_i e^{\lambda_i t} \quad (6.52)$$

or in the discrete time

$$\begin{aligned} \hat{y}_k &= \sum_{i=1}^n R_i z_i^k \\ z_i &= e^{\alpha_i \tau} \quad , \\ t &= k \tau \end{aligned} \quad (6.53)$$

where $y(t)$ approximates $\hat{y}(t)$, $R_i \in C$ is the residue for pole $\lambda_i \in C$. The objective is to identify residues, poles, and the order n of the model to minimize the least square of $y(t)$.

Assuming that $y(k)$ can be described by a combination of n past values

$$y(k) = a_1 y(k-1) + a_2 y(k-2) + \dots + a_n y(k-n) \quad (6.54)$$

Let the set of sample vectors $\{\bar{y}_i\}, i = 1, \dots, n+1$, where

$$\bar{y}_i = [y(i), y(i+1), \dots, y(i+N-n-1)]^T. \quad (6.55)$$

By repeatedly applying (6.28), the following system of linear equations is formed:

$$\begin{aligned} Y \bar{a} &= [\bar{y}_n, \bar{y}_{n-1}, \dots, \bar{y}_1] \bar{a} = \bar{y}_{n+1} \\ \bar{a} &= [a_1, a_2, \dots, a_n]^T \end{aligned} \quad (6.56)$$

Y is a Toeplitz matrix that can be solved with $2n$ data samples. From (6.53) and (6.54), and considering $k=n$, $\{z_i\}$ represent the roots of the characteristic polynomial

$$C(z) = z^n - a_1 z^{n-1} \dots - a_n = 0 \text{ and } \lambda_i = \ln(z_i) / \tau \quad (6.57)$$

Then the residues $\{R_i\}$ can be found by

$$Z \bar{R} = \bar{y}_i, \quad (6.58)$$

where

$$Z = \begin{bmatrix} 1 & 1 & \dots & 1 \\ z_1 & z_2 & \dots & z_n \\ \vdots & \vdots & \vdots & \vdots \\ z_1^{N-1} & z_2^{N-1} & \dots & z_n^{N-1} \end{bmatrix} \text{ and } R = [R_1, R_2, \dots, R_n]^T.$$

The algorithm can be summarized as follows:

1. Given a sampled signal y_p , $i = 0, 1, \dots, m$, determine the coefficients a_i of the characteristic polynomial by fitting a linear prediction model.
2. Using the a_i 's, compute the discrete-time eigenvalues by solving for the roots of the characteristic polynomial z_i 's.
3. Compute the R_i 's by solving (6.58).
4. Calculate the continuous time eigenvalues λ_i 's using $z_i = e^{\lambda_i \tau}$.

The cost of computing this spectral decomposition to all generator rotor angles is very high and must be avoided. In SDSA, just the least damped rotor angles are selected based on the rate of decay of the machine total energy.

6.6 Security Functions

The automation of any security assessment process is dependent on the operation planning practices of the relevant utility or system operator entity. In the present SDSA case, three basic assessment functions apply:

- Contingency analysis at the operating point (is the operating point secure?)
- Maximum transfer (interchange) between two subsystems
- Maximum security region or transfer nomogram for three subsystems

In addition, functions are provided for recommending preventive actions on the basis of such assessments. Preventive action is needed when one or more contingencies will bring the system state to a condition in which at least one security criterion is violated. This action, such as generation re-dispatch, moves the system state to a new secure operating point.

6.6.1 Contingency Analysis at an Operating Point

This is the most basic component of the SDSA system. Contingency analysis is normally performed for both the steady and dynamic states.

In steady-state contingency analysis, the critical aspect is the robustness of the power flow engine. For example, if a solvable contingency fails to converge, the interpretation might be that the operating point is beyond the maximum loadability limit. This can wrongly trigger an uneconomical preventive re-dispatch. Therefore, the care with respect to the implementation of power flow solutions, as pointed out in Sect. 6.2 must be observed.

In dynamic contingency analysis, a stability diagnosis may not be produced at all if the numerical integration algorithm fails to converge. Again, it is critical to avoid numerical problems, in particular when fast controls are represented in the model. The simultaneous solution of differential and algebraic equations associated with variable time step is key to avoid this problem, as discussed in Sect. 6.4.

In addition, the ability of changing the time step has two fundamental advantages. One of course is to increase it, whenever possible, to speed up the simulation. Thus the computation, depending on the stiffness of the equations, can be one or two orders faster. The other advantage is to reduce the time step below regular values whenever a difficult numerical condition occurs. This can significantly slow down the simulation, but prevents the worst scenario, i.e., the computation failure.

If the number of contingencies is large, screening methods can be applied to improve performance. For steady-state analysis, this is usually not necessary for today's computer power. For dynamic analysis, the key technique is to terminate as early as possible those simulations that are estimated to be "quite" stable. As presented in Sect. 6.5, SDSA adopts early termination for unstable cases and provides stability indices based on the modified SIME method that allows filtering contingencies on the fly.

However, it is important to remember that most, if not all, of the screening methods proposed so far deal only with the transient stability aspect. It is then assumed that if the system is "quite" stable, it should comply with all other criteria. This is hard to prove, of course, and care should be taken. In practice, power system analysts know the set of contingencies that can cause any harm to the system. Today's operational planning is based on such knowledge. This may not be possible in the steady-state analysis where contingencies all over the network can cause some security violation, such as thermal or voltage limit violation. On the other hand, the dynamic problems are invariably associated with transmission bottlenecks (relatively weak interconnections), with location well known by planners. These locations can change over time as system topology changes, but it is still possible to predefine effective contingency sets. Thus, the "blind" approach, typically advocated and used for steady-state contingency screening, should be avoided or not used at all in online dynamic security assessments because it is an unnecessary waste of computer resources and the proposed techniques do not cover all security criteria.

6.6.2 *Import–Export Transfer Capacity*

This SDSA function is useful for assessing the maximum secure transfer between two interconnected areas. It basically consists of performing contingency analysis at successively increasing/decreasing power transfer levels between two areas. The pre-contingency operating point at which a security criterion becomes violated defines the maximum transfer capacity for that specific criterion. To identify this transfer level with relatively good accuracy, a binary search is used.

To speed up this search, specific quantities (voltages, flows, etc.) and indices (MW stability margin, damping, etc.) are stored along the one-dimensional search and are used to estimate the violation point by interpolation and extrapolation. The search stops when two consecutive estimated points are sufficiently close to each other.

The changes in transfer level are effected by re-dispatching generation in the exporting and importing areas. All other generation and loads in the system remain constant. Then, neglecting changes in losses, the security region per criterion is defined by sets of points (line segments) belonging to the line $Pa + Pb = K$, where Pa and Pb are the respective generations in each area, and K is constant. The direction of search from the operating point is given by $\Delta Pa + \Delta Pb = 0$.

This function demands much more computation than the single contingency analysis at the operating point as the contingencies will be simulated at various operating points. On the other hand, the number of contingencies simulated for this kind of function is typically small, since only those that affect the transfer between the two areas are of interest. The function is useful for monitoring critical transmission corridors and it automatically provides the security margins for the current operating point, which is very desirable information at real time.

The operating point change in the direction of search is implemented with the CPF, Sect. 6.3. For steady-state transfer capacity assessment, the contingencies are computed by the Newton power flow with care to restart and approach the solution “slowly” if the first direct attempt fails. For dynamic transfer capacity assessment, contingencies are simulated with the methods presented in Sect. 6.4.

6.6.3 *Security Regions*

Situations arise where transfer limits are highly dependent on the generation patterns in three areas. Therefore, re-dispatching generation in only two of them may provide inaccurate transfer limit estimates. At this point, the objective is to find secure regions in the two-dimensional surface defined by $Pa + Pb + Pc = K$, where Pa , Pb , and Pc are the respective generations in the three areas and K is constant, if changes in losses are neglected. This surface is embedded in three-dimensional space and it is bounded by the generation limits in each area. Alternatively, it is also possible to replace one of the generations (Pa , Pb , or Pc) by a load set. In this case,

the security region is embedded in the surface defined by $Pa + Pb - L = K$, where L is the total load of the set.

The display of the security surface in a three-dimensional space is possible, but it has been found that it is better visualized by its projections on a two-generation subspace. For example, Fig. 6.1 shows the projections relative to three generation groups named Paranaíba (Pa), Grande (Pb), and Parana (Pc).

This figure shows three superimposed regions. The green region is secure. The yellow region represents post-contingency thermal limit violation and the red region is unstable or inaccessible due to generation limits. The operating point is a gray dot inside the green region. Instability means that if the system is operating at any point in the red region, at least one of the evaluated contingencies will cause system transient stability.

The violation of any other monitored criterion (oscillation damping, transient overvoltage, frequency limit, etc.) can similarly be depicted by a contour. For example, the blue contour in Fig. 6.4 shows violation of after fault voltage drop. Whenever the operating point approaches a contour, some preventive actions may be need. For example, these actions could entail generation re-dispatch to keep a security margin or energizing a shunt device to avoid undesired post-contingency voltages.

The process of finding the boundary in a particular direction is similar to that used for the import–export transfer capacity, but now the directions of search are given by $\Delta Pa + \Delta Pb + \Delta Pc = 0$. These are radial directions from the operating point.

Finding the boundary as in the import–export method, i.e., by binary search, is a brute-force approach. Based on a huge number of simulated cases so far, it has been observed that the contours are convex. Irregularities on the border may occur only as a result of a numerical problem, typically power flow data errors. This convexity characteristic can be exploited to significantly reduce the number of contingencies in the search of contour boundaries. For example, pre-contingency operating points may be targeted near the expected boundary, avoiding several unnecessary simulations, once two adjacent directions have been completed.

Also, and very useful, is to filter contingencies in a particular direction if two relatively close directions have been completed and found that these contingencies do not present threat to the system, i.e., their stability margins are high all over the adjacent directions. The performance gain with this and other heuristic approaches vary from case to case, but can be huge.

To achieve a good plotting contour, it is important to maintain a straight-line direction of search, keeping the ratios $\Delta Pa/\Delta Pb$ and $\Delta Pb/\Delta Pc$ constant. As the operating point moves along this direction, contingencies are processed and evaluated. The final contours represent the intersection of all violations resulting from all contingencies.

The number of directions used for each contour plot determines the precision of the contour. But as this number increases, more computation is required and, given limited computational resources, consequently performance decreases. Thus, a good compromise is required for online applications.

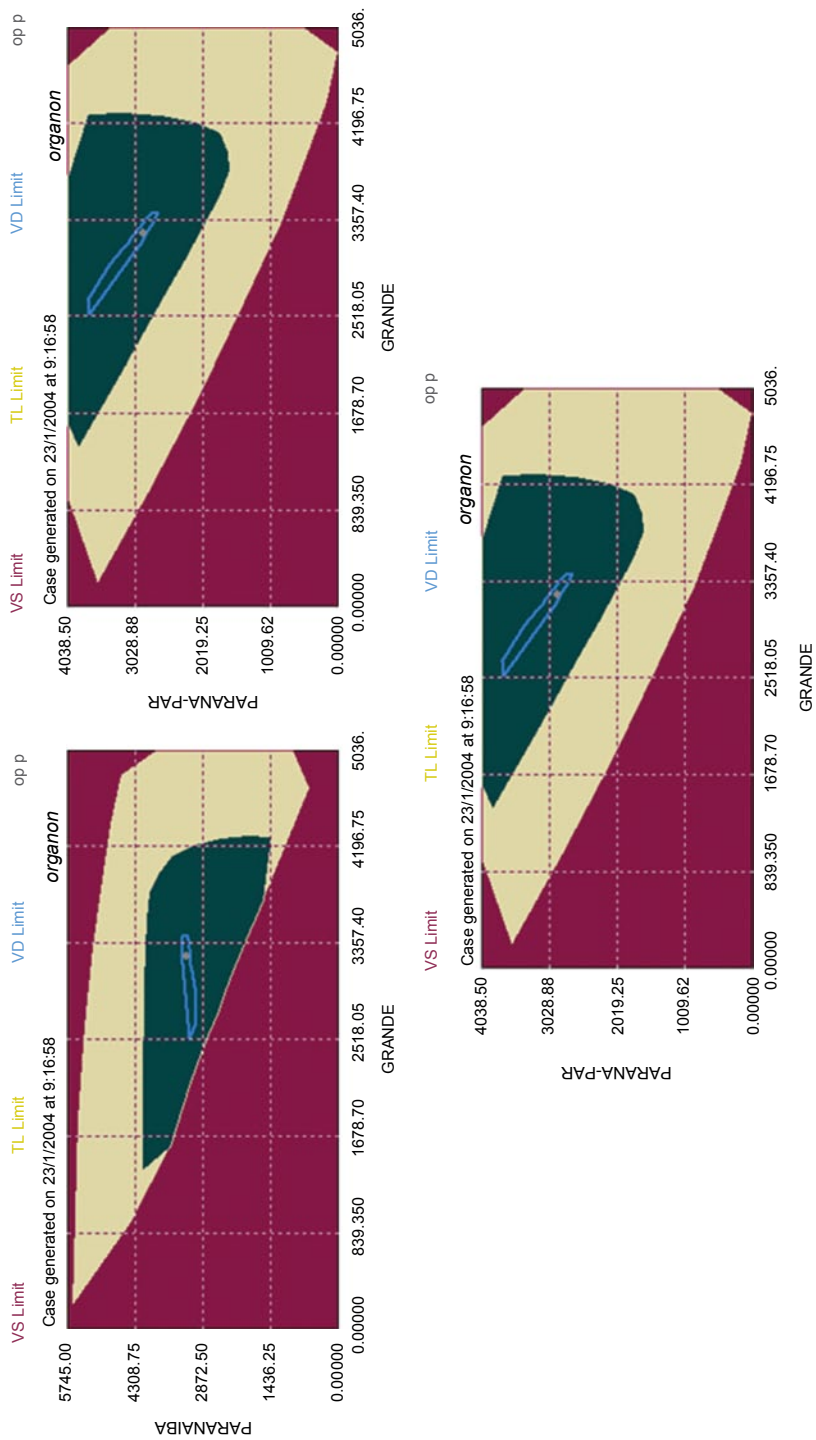


Fig. 6.4 Security region projected on two-generation subspaces

If better accuracy in defining the security border is required, the generation units may be allowed to switch on and off along the re-dispatch direction to keep the spinning reserve within a realistic range (excessive spinning reserve would lead to optimistic security margins, since the total inertia and MVar margin would be bigger than expected in practice).

Before re-dispatching the generation, the spinning reserve at the new operating point is checked against the range and adjusted if possible. This feature has been used more frequently for operational planning. For online security assessment, this is not used because the focus is on what are the security boundaries for the current state and energized devices. In this case, committing generation units can artificially extend the boundaries.

The complexity of the security region calculation is obviously greater than that for import–export transfer capacity, but only a small set of contingencies is typically required. The security region computation for a transmission corridor typically requires only a few dozen contingencies. Thus, for example, for a case with 10 contingencies, 20 radial directions, and an average of 7 contingencies checks on each direction, approximately 1400 contingencies are computed.

One of the main benefits of computing and displaying a security region is the powerful and immediate insight that it provides to system operators. For example, if the operating point lies outside in the insecure (red) region, the required generation re-dispatch (where and how much) to correct the problem can directly be retrieved from the region display. Each line segment of a contour is associated with the contingency that caused the violation. This information is available in tables, with full report for each line search, and on the region via mouse hovering on contour boundaries. It is also possible to retrieve the pre-contingency operating point at any point in the security region to be analyzed in study mode or to be displayed on the operator's one-line diagrams. The process is simple and requires just a few mouse clicks.

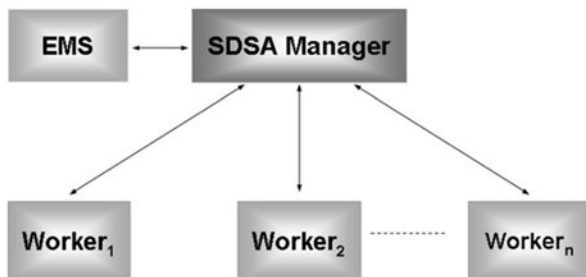
A security region is focused in a specific transmission bottleneck. For a large system, it may be necessary to monitor several bottlenecks. This is done by multiple instances implementation of SDSA. The instances run concurrently, using the same real-time information, but with a different set of contingencies and different generation areas. For the Brazilian system implementation, each of its four control centers currently monitors four different transmission bottlenecks, totaling 16 different security regions.

6.7 Solution Architecture

6.7.1 Parallelization

In order to meet stringent performance requirements, the SDSA adopts parallel processing techniques in a manager/worker (master/slave) configuration, as shown in Fig. 6.5.

Fig. 6.5 Manager–worker distributed processing environment

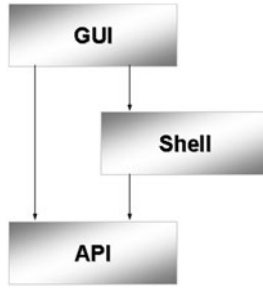


The manager process contains the high-level instructions to perform the security assessment functions. Most of the calculations (power flow, time-domain simulation, etc.) are done in the worker processes. The manager is responsible for generating base cases, distributing tasks among servers, collecting the respective reports, communicating with the supervisory control and data acquisition (SCADA)/EMS, managing distributed resources, and storing/displaying results and plots. Workers receive tasks from the manager on a first-to-ask-first-to-get basis, process them using the task-specified power system simulation tool, send the respective results back to the manager, and ask for another task. The workload per processor tends to be well balanced as the number of tasks increase. This is certainly the case for security region calculation and contingency analysis with a large number of contingencies. The idle time per processor is relatively small and occurs only at the end of an assessment cycle when some have finished their tasks and there is no additional work to be done. Depending on the number of processes (workers), initial data (operating point base case) broadcasting from manager to workers may have a nonnegligible effect on performance.

This effect can be minimized by broadcasting only data changes from the previous assessment. For example, dynamic models do not change and can remain in memory over subsequent assessments. It has been observed that in up to 48 processes, the data exchange (task assignment and report) between workers and the manager during the calculations does not cause significant overhead. If more processes are necessary, the parallelization strategy can be modified to decentralize the manager role and balance the workload. Worker processes can run in silent mode or be attached to a console. The manager can run in silent mode, attached to a console or the graphical user interface (GUI).

This level of parallelization is implemented via the Message Passing Interface (MPI) mechanism (Gropp et al. 2000). The initial data are broadcasted to workers. Task assignments and diagnosis reports for security regions are implemented via send/receive communication with the tasks assigned in a first-to-ask-first-to-get order. For contingency analysis, tasks are assigned in chunks and results are gathered at the end of the assessment. The send/receive strategy adopted for security regions was found to be more convenient because the manager process can take decisions on the fly to terminate processes based on results achieved by other processes.

In addition to MPI parallelization, the software can also be compiled with loop-level and working share (Chandra 2001) directives for lower granularity

Fig. 6.6 Software layers

parallelization, allowing improved performance in multiple core architectures. This type of parallelization can provide significant speed up of a time-domain simulation because the most costly tasks in this type of simulation are the computation of the vector functions (6.15 and 6.16), which can be shared among processes/threads.

However, for computing a large number of contingencies with limited computational resources the best overall performance is obtained with large granularity parallelization only. This observation can be explained by the fact that there is no data interdependence for coarse granularity parallelization (contingency simulations), whereas significant interdependence in fine-grain parallelization (loop parallelization within a contingency simulation), which adds a significant overhead to the total computation, and more importantly, for fine-grain parallelization there are significant parts of the codes that have to be executed sequentially.

Moreover, the need for improving the performance of a time-domain simulation is not so critical when using variable time step, as this can be several orders faster than fixed-time-step approaches. Therefore, if a limited number of cores are available, the loop-level parallelization would be only recommended for very large networks and few contingencies to be simulated.

6.7.2 Software Layers

Internally, the software is organized in layers as shown in Fig. 6.6, where the arrows indicate the data dependence relationship. The (GUI) can be removed if not desired. The shell consists of input/output interfaces.

The API communicates with the security assessment functions as well as allowing direct access to their analytical engines, such as power flow, contingency analysis, etc. This design facilitates different levels of both SCADA/EMS integration and the offline use of the software.

6.7.3 Integration with SCADA/EMS

The general design for SDSA hardware integration with the SCADA/EMS systems is shown in Fig. 6.7.

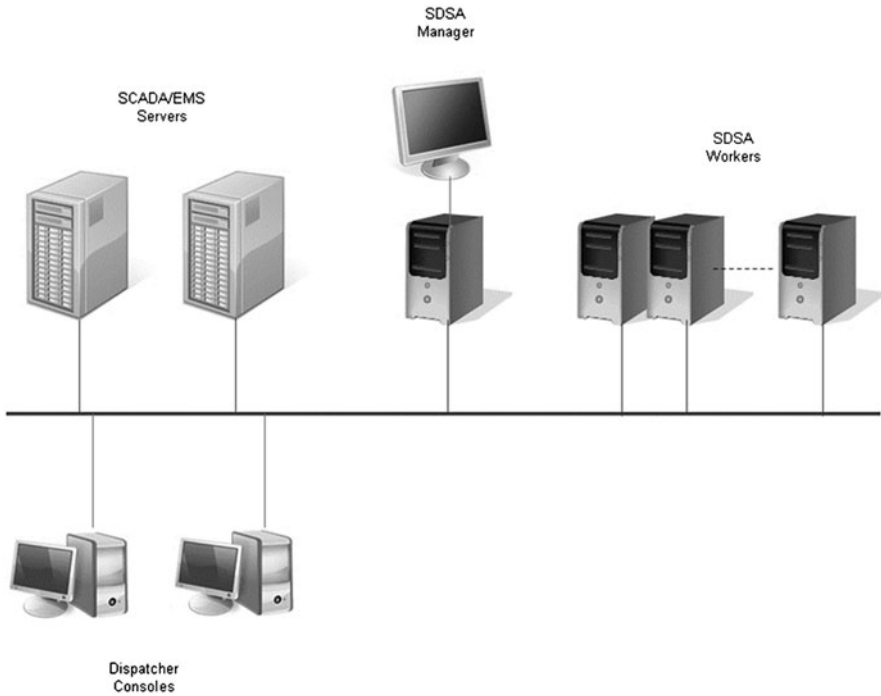


Fig. 6.7 SCADA/EMS network for SDSA

In a loose integration approach, the base cases generated by the SCADA/EMS real-time network analysis subsystem are saved in the form of flat files and are retrieved by the SDSA periodically but asynchronously. The security assessment results are displayed in the SDSA GUI. They can also be either viewed on dispatcher consoles or projected on the control room displays. This kind of integration is relatively simple to implement. The SDSA can also periodically retrieve base cases and be used in study mode.

In tight software integration mode, the SCADA/EMS servers and SDSA servers are in the same local network, as shown in Fig. 6.7. Any of the nodes dedicated to SDSA can be the manager process. There is no communication between the SCADA/EMS and SDSA workers.

A failover procedure can be implemented. The general idea is the following. Failure of a worker process can be detected by the manager process, which reassigns the task to another process. A monitor process in the SCADA/EMS detects failures of the manager process and restarts the SDSA, reallocating the manager process to another node if necessary.

The sequence of events for security assessment is as follows:

- The SCADA/EMS generates a bus-branch model based on the state estimation output.
- The SCADA/EMS sends a message to the SDSA to start a new assessment cycle.

- The SCADA/EMS sends the data and calculation parameters to the SDSA.
- The SDSA performs the assessment and sends the results back to the SCADA/EMS to be stored in its database.

Results are displayed on the dispatcher's consoles and control room projection board. As most of the time the system operates with sufficient security margin, it may not be necessary to display nomograms and other results permanently. One way of circumventing this dilemma is to generate alarms whenever the system operating condition approaches one of the security boundaries.

SDSA can be implemented in multiple instances, i.e., when several different assessments run concurrently, e. g., two instances with online nomograms for different transmission corridors and one instance running system-wide contingencies.

SDSA can also be used to monitor near real-time operating conditions. For this, it is important to be able to generate base cases that represent the near future operating condition with reasonable accuracy. It is necessary to access databases with information regarding generation scheduling, load forecast, and outage schedule. A combination of power flow and CPF methods can be used to solve the problem or, preferably, an optimal power flow method (Granville 1994).

6.7.4 Performance

It is difficult to establish accurate performance figures given that it depends on several factors such as:

- a. Network size and number of dynamic models represented
- b. Complexity of the model (e. g., representation of several remedial action or special protection schemes) that can extend transient periods
- c. Stiffness of equations (e. g., representation of DC links, series controlled compensators, static VAR compensators, etc.
- d. Number of available CPUs
- e. Number of contingencies
- f. Type of assessment (operating point or security region)

It is desired that the response time for an online security assessment system should not be >5 min and preferably around 2 min. This can be achieved by properly dimensioning the computer resources.

An SDSA performance example, using the same number of contingencies (brute force) and different number of cores is shown in Table 6.1.

The simulation conditions for this example are as follows:

- *Model characteristics:* It consists of the computation of a security region for the 500/765 kV south-southeastern corridor of the Brazilian Grid. The network comprises 5306 buses, 7604 branches, and 1173 generators in service. As most of the power plants are hydro with several similar units operating in parallel, the respective generator models are trivially aggregated resulting in 867

Table 6.1 SDSA performance for different number of CPUs

Number of instances	Number of CPUs	Total time (s)	Effective time per contingency (s)
2	32	189	0.166
3	48	141	0.124
4	60	126	0.111

generation buses. The case represents a heavy load condition with approximately 78,000 MW. The dynamic model includes two LCC HVDC (six monopoles) links, four TCSC, several SVCs, out-of-step protection systems, and a highly complex generation shedding protection scheme

- *Contingencies and stiffness*: The five most severe N–1 contingencies in this corridor are considered. The simulation time for each contingency is 20 s. Several of these contingencies result in commutation failure and/or generation shedding. Consequently, the respective simulations are computationally demanding because of several hard discontinuities and fast transients to which the system is subjected. Whenever there is a discontinuity, the time step reduces significantly and remains low for the duration of the fast transient. Thus, more steps per simulation are necessary, which decrease the performance. (Note: The effect of stiffness on simulations based on fixed time step is even worse, as it may force the time step to be quite small for the total duration of the simulation to avoid numerical instability.)
- *Computational effort*: The security region was computed with 20 boundary search direction and required a total of 1137 time-domain simulations, which correspond to an average of 56.85 simulations per searching direction, or 11.37 simulations per searching direction per contingency. Only brute-force approach, i.e., binary search method, was used in this process to obtain a worst-case scenario (as explained in Sect. 6.6, more intelligent heuristic methods can be used to significantly speed up the process). Loop-level parallelization was not used.
- *Security Criteria*: In addition to the traditional criteria (transient stability margin, minimum acceptable damping, transient voltage levels and duration, thermal limits, and frequency levels), transient impedance trajectories seen by out-of-step relays are also monitored. If a trajectory approaches the relay’s tripping threshold by a given margin, the criterion is violated.
- *Platform*: Instances of Amazon cloud (virtual) cluster cc2.8xlarge with two processors ES-2670 (physical 8 cores each), which means a total of 16 physical cores per instance.

It was assigned one SDSA process per CPU. Even using a brute-force approach it is possible, in this case, to meet the requirements with only two instances. If optional heuristic methods are used, some of the simulations are avoided, speeding up the assessment. However, the performance gain can change from case to case and would be better quantified by statistical methods.

6.8 Practical Implementation Aspects

6.8.1 Bus Numbering

The regular bus-branch network model used in planning studies needs to be adapted for online dynamic security assessment. The locations of the dynamic models are usually specified by bus numbers, but these numbers are not fixed in real-time models. Therefore, mapping is necessary. To help with this, a bus identification scheme was implemented. It consists of extending the bus number by adding the section number. For example, bus section 1 of bus 100 can be represented by 100.1. If there is only one section in this bus, it is represented by 100 as usual without section information. This also helps to model bus split/merge events in contingencies without losing the original bus number identity.

6.8.2 Network Size and Observability

For small- to mid-sized network models, say $< 10,000$ buses, network reduction can help improve performance, but it is not critical for today's computational capacity. However, for very large networks, model reduction can be necessary to achieve online response requirements, in particular for dynamic security assessment. Also, for situations in which there is no real-time observability of external networks, the use of external equivalents is necessary. Several effective methods to reduce networks and derive external equivalents have already been proposed (Monticelli et al. 1979; Savulescu 1981). SDSA currently adopts the Ward method (Monticelli et al. 1979) with flexibility to allow some of its variants. For steady-state contingency analysis, it can yield very accurate results with neglectful computational cost. The issue is how to couple the external equivalent with the network model that has been observed online. If the EMS allows, this can be done during the state estimation process using pseudo-measurements. Otherwise, it can be done externally via a similar process or, as in SDSA, via nonlinear programming (Granville 1994).

The network reduction must take into account important aspects for dynamic security analyses. Depending on the network size, a simple and effective practice is to retain in the network equivalent all or most of the generation buses. For very large systems, quite remote generation buses can be aggregated and simplified dynamic models adopted for the aggregated generator. For the Brazilian network, for example, the real-time network is smaller than the used for planned studies because some portions of the low voltage grid (under 138 kV) are not represented, but dynamic models are the same in both cases.

6.8.3 *Contingency Set*

For transfer capacity and security region studies, the set of contingencies to be simulated is relatively small, since the contingencies are restricted to the transmission path of interest. The contingencies are predefined by planning engineers based on their experience and can be enabled/disabled by operators on line.

Security assessment by contingency analysis for the entire network demands a relatively large set of contingencies. In this case, a screening process can significantly improve the performance. Considering the quite efficient time-domain simulation, as described in Sect. 6.4, there may be no need for screening or the screening can be performed on the fly. The modified SIME method, as described earlier in this chapter, is quite suitable for this. However, it is important to remember as noted Sect. 6.6 that:

- The proposed screening methods generally estimate only energy margins, consequently do not assess other security criteria.
- These methods are devised for simple simulations where the fault is removed after a few milliseconds along some equipment. For more complex simulation patterns and models with automatic action of protection relays or schemes, subsequent events can be triggered invalidating the screening.

6.8.4 *Real-Time Data*

Real-time data with reasonable quality must be available for online security assessment, of course. Among the well-known prerequisites are sufficient observability of the internal system, robust state estimation, and a carefully maintained database. When used to initialize security assessment, a state estimator's requirements are much higher than merely providing correct values for voltages and flows. The estimator needs to produce a solved model that is valid for power flow solutions including all controls. For example, it is not uncommon to see real-time cases with the following problems:

- Unrealistic MVar injections in neighboring buses, sometimes canceling each other
- Generators with MW outputs significantly above their specified maximum capacities
- Generators with unbounded (very high) capacity
- Generators, shunts or on-load tap changing transformers controlling extremely remote buses, etc.

Some of these problems originate from the state estimation process and some are related to errors in the database. At the cost of some extra computation, various conflicting control problems can be intercepted and resolved by extensive input data-checking functions of the security assessment software itself. This is preferably

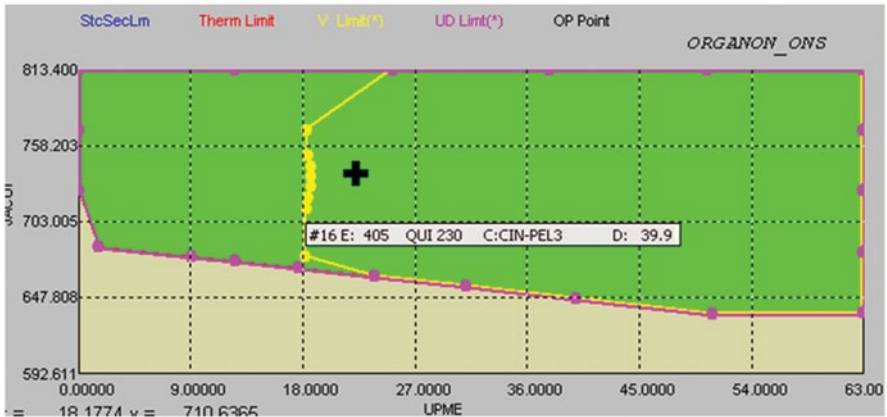


Fig. 6.8 Operating point near voltage limit contour

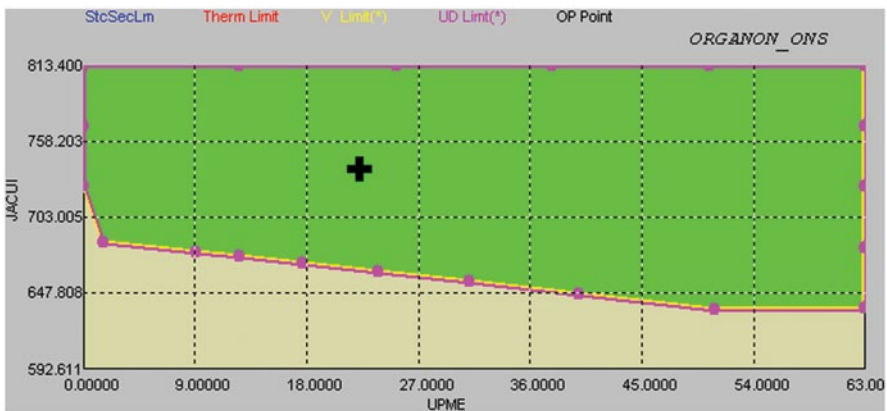


Fig. 6.9 Assessment after preventive action (capacitor switching)

done offline, of course. Problems of poor observability (generally, an inadequate measurement set) are more difficult to solve and, depending on the required accuracy, may be a major barrier for the online implementation.

6.9 Examples

Figure 6.8 shows an example where the real-time operating point (black cross), monitored by one of ONS control centers, was approaching a (yellow) contour indicating violation of voltage limit.

In Fig. 6.9, the same operating condition of Fig. 6.8 is assessed, but after switching on a capacitor bank. If contingencies had only been computed at the operating point, the proximity to violation would have passed unnoticed.

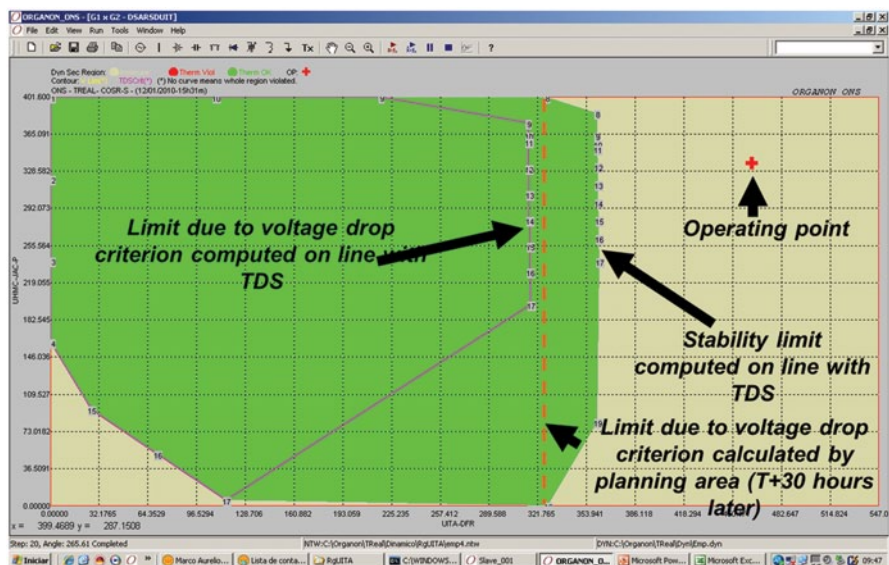


Fig. 6.10 Unsecure operating point for not planned condition

Figure 6.10 shows the real-time operating point outside the security region due to an N-2 condition for which no security limits had been computed offline. System operators were able to correct the problem based on online nomogram computation, i.e., the generation was re-dispatched to correct the violation. The online case was saved and after the fact (T+30 h) studies confirmed the online calculations.

Figure 6.11 shows a security region validation (online vs offline) for one of the most important transmission corridors in the south-southeastern part of Brazil.

Figure 6.11a presents the security region computed online with no generation commitment. Figure 6.11b shows results computed offline for the same transmission bottleneck with the base case data adjusted for conditions quite close to the online case and allowing generation commitment to keep reasonable spinning reserve.

Figure 6.11c shows the online results superposing the offline results. The light green contour represents voltage drop limitation and the red contour represents the operation of out-of-step relays. In Fig. 6.11c, it is noticeable that the stability regions (nonred regions) in the upper right corner are very close in both cases.

The limiting factors are the proximity of out-of-step triggering and voltage drop (A and B in Fig. 6.11c), which are practically the same in both cases. The extended lower boundary in the offline security region, depicted by C in Fig. 6.11c, is because unit commitment is enable in this case.

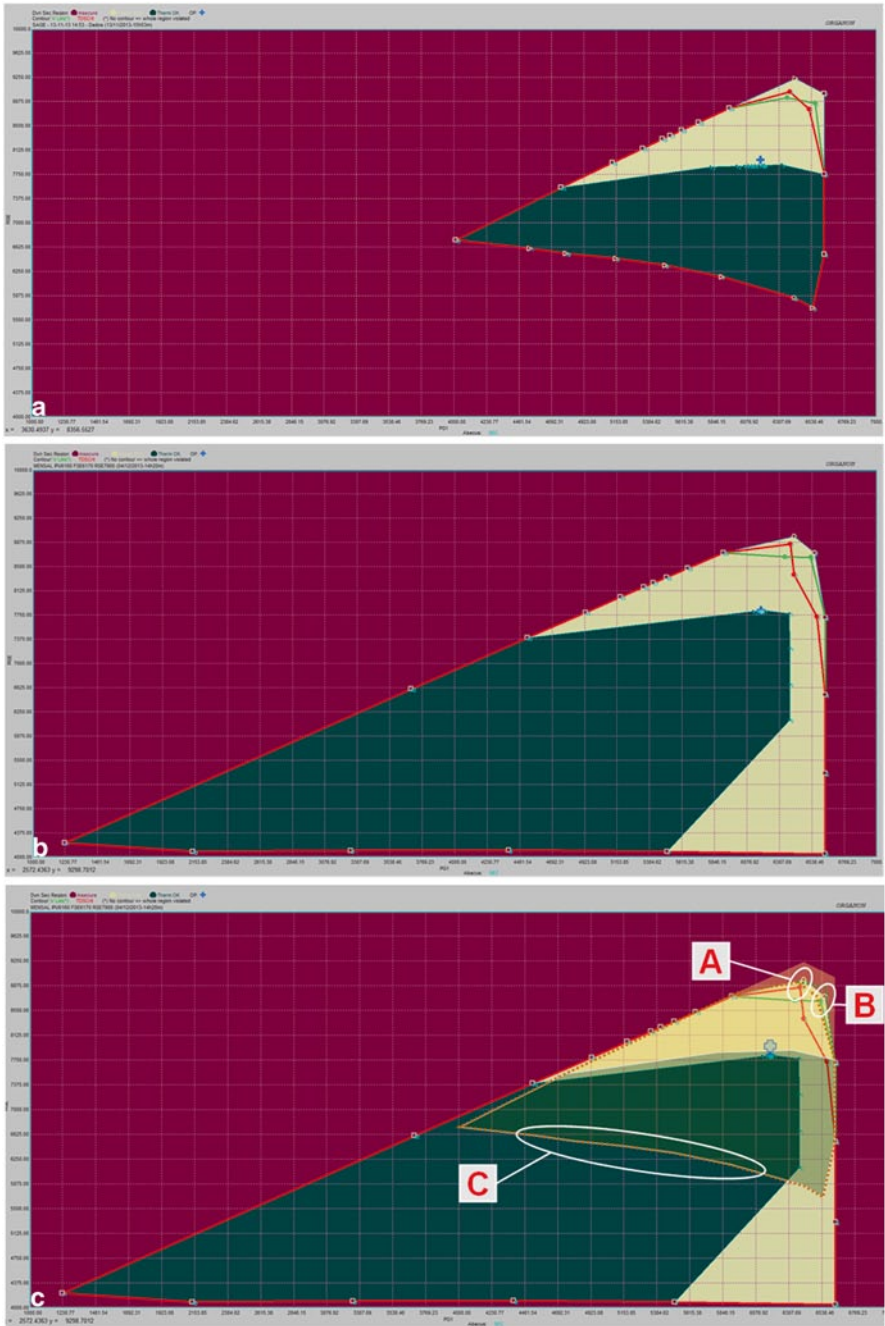


Fig. 6.11 Security regions: a using real-time data, b using offline planning data, c real-time results superimposed on planning results

6.10 Conclusions

This chapter has described an online security assessment system whose development was dominated, particularly on the dynamics side, by the need for consistent and solid analytical methods, process automation, and high-performance computing. The system is able to perform detail and sufficiently fast security assessments. The full detail time-domain simulation approach keeps close compatibility with offline studies, provides accurate assessments, and can be easily validated. It can also be combined with faster simplified methods to reduce the computational burden and improve response time under fast changing operating conditions.

In summary, until recently it was very difficult, if not impossible, to implement online dynamic security assessment for medium-sized to large power systems because the analytical methods for security margin estimation were not mature enough and low-cost computing power was not available, either. These barriers no longer exist. Today, the state of the technology allows us to perform huge numbers of detailed simulations in a few minutes. This is of use not only for online security assessment, but also for power system planning. It is a change in paradigm, which brings benefits to all areas of power system analysis.

6.11 Acknowledgments

The author is grateful to ONS, in particular to Dr. Luiz Claudio de A. Ferreira and Dr. Carlos Alberto da S. Neto for providing examples of SDSA application and performance figures. Portions of this chapter have been reprinted, with permission, from Jardim, J, 2009, Online Security Assessment for the Brazilian System—A Detailed Modeling Approach, in *Real-Time Stability Assessment in Modern Power System Control Centers*, IEEE Press and John Wiley & Sons, Inc., Hoboken, NJ, 2009, ©2009 IEEE.

References

- Ajjarapu V, Christy C (1991) The continuation power flow: a tool for steady state voltage stability analysis, IEEE PICA conference proceedings, May 1991, pp 304–311
- Arrillaga J, Arnold CP, Harker BJ (1983) Computer modelling of electrical power systems. Wiley, London
- Astic JY, Bihain A, Jerosolimski M (1994) The mixed Adams—BDF variable step size algorithm to simulate transient and long term phenomena in power systems. IEEE Trans Power Syst 9(2):929–935
- Braz LMC, Castro CA, Murati CAF (2000) A critical evaluation of step size optimization based load flow methods. IEEE Trans Power Syst 15(1):202–207
- Brenan KE, Campbell SL, Petzold LR (1989) Numerical solution of initial-value problems in differential-algebraic equations. SIAM Classics in Applied Mathematics, North-Holland, New York

- Castanié F (2011) *Digital spectral analysis: parametric, non-parametric and advanced methods*. Wiley, Hoboken
- Chandra R (2001) *Parallel programming in OpenMP*. Academic, San Diego
- Debs AS, Benson AR (1975) *Security Assessment of Power Systems*. In: *Proceedings of system engineering for power: status and prospects*, Henniker, NH
- Dy Liacco TE (1968) *Control of power systems via the multi-level concept*, Case Western Reserve University System Research Center, Report no SRC-68-19, June 1968
- Granville S (1994) Optimal reactive dispatch through interior point methods. *IEEE Trans Power Syst* 9(1):136–146
- Gropp W et al (2000) *MPI: the complete reference*. MIT Press, Cambridge
- Hauer JF (1991) Application of Prony analysis to the determination of modal content and equivalent models for measured power system response. *Proceedings of the IEEE winter meeting*, 215-4 PWRS
- Hayashi S (1969) Power system security assessing by digital computer simulation—basis control. In: *Proceedings of PICA conference*, Denver, Colorado, 18–21 May 1969
- Jardim JL (2000) Online dynamic security assessment: implementation problems and potential use of artificial intelligence. *Proceedings of IEEE power engineering society summer meeting*, vol 1, 16–20 July 2000
- Jardim J (2009) Online security assessment for the Brazilian system—a detailed modeling approach. In: Savulescu SC (ed) *Real-time stability assessment in modern power system control centers*. IEEE Press and Wiley, Hoboken
- Jardim JL, Neto CS, Kwasnicki WT (2004) Design features of a dynamic security assessment system. *Proceedings of IEEE power system conference and exhibition*, New York, 13–16 Oct 2004
- Jardim JL, Neto C, Santos MG (2006) Brazilian system operator online security assessment system. *Proceedings of IEEE power system conference and exhibition*, Atlanta, GA, 30 Oct–02 Nov 2006
- Lambert JD (1991) *Numerical methods for ordinary differential systems: the initial value problem*. Wiley, New York
- Limmer HD (1966) *Security applications of on-line digital computers*. Second power systems computation conference, Stockholm, 27 June 1966
- Molina RDM, Cassano M, Savulescu SC (2009) Dimo’s approach to steady-state stability assessment: methodology overview, numerical example, and algorithm validation. In: Savulescu SC (ed) *Real-time stability assessment in modern power system control centers*. IEEE Press and Wiley, Hoboken
- Monticelli A (1999) *State estimation in electric power systems: a generalized approach*. Kluwer, Norwell
- Monticelli A, Deckmann S, Garcia A, Stott B (1979) Real-time external equivalents for static security analysis. *IEEE Trans Power Syst* 98(2):498–508 (PAS)
- Pai MA (1989) *Energy function analysis for power system stability*. Kluwer, Norwell
- Pavella M, Ernst D, Ruiz-Vega D (2000) *Transient stability of power systems: a unified approach to assessment and control*. Kluwer, Norwell
- Savulescu SC (1981) Equivalents for security analysis of power systems. *IEEE Trans Power Syst* 100(5):2672–2682 (PAS)
- Seydel R (1994) *Practical bifurcation and stability analysis: from equilibrium to chaos*. Springer-Verlag, New York
- Smed T, Andersson G, Sheblé GB, Grigsby LL (1991) A new approach to AC/DC power flow. *IEEE Trans Power Syst* 6(3):1238–1244
- Stott B (1979) Power system dynamic response calculations. *Proc IEEE* 67(2):219–241
- Stott B (1974) Review of load flow calculation methods. *Proc IEEE* 62:916–929

Chapter 7

Practical Issues for Implementation of Online Dynamic Security Assessment Systems

Lei Wang, Xi Lin, Fred Howell and Kip Morison

Abstract This chapter discusses the issues associated with the successful design and implementation of an online dynamic security assessment system. The need for, the benefits of, and the current application status of such systems are presented. The discussions are primarily focused on the practical issues for implementing an online Dynamic Security Assessment (DSA) system, based on the experiences gained from recent applications. Finally, an overview of some future directions on the online DSA technologies is provided.

7.1 Introduction

Security refers to the degree of risk in a power system's ability to survive imminent disturbances (contingencies) without interruption to customer service. It relates to robustness of the system to disturbances and, hence, depends on the system's operating condition as well as the contingent probability of disturbances (IEEE/CIGRE 2003).

Historically, ensuring secure operation has always been of paramount importance in the safe and economic operation of power systems. When a system has an insufficient degree of security, it becomes exposed to severe, and in some cases catastrophic, system failures of the types observed recently in various power grids around the world (US-Canada Power System Outage Task Force 2004; FERC and NERC 2012), events that have enormous economic costs and may even lead to loss of life.

During the times of regulated and vertically integrated power systems with traditional generation and transmission technologies, systems tended to be more secure for a number of reasons. Firstly, power systems were designed, built, and operated by monopolies (usually government bodies and public utilities) through which inte-

L. Wang (✉) · X. Lin · F. Howell
Powertech Labs Inc., 12388 88 Ave, BC V3W 7R7 Surrey, Canada
e-mail: Lei.Wang@powertechlabs.com

K. Morison
BC Hydro, 333 Dunsmuir, BC V6B 5R3 Vancouver, Canada

S. C. Savulescu (ed.), *Real-Time Stability in Power Systems*,
Power Electronics and Power Systems, DOI 10.1007/978-3-319-06680-6_7,
© Springer International Publishing - Switzerland 2014

grated planning ensured that generation and transmission facilities kept in pace with the load growth, thereby limiting overloading and equipment failures that could lead to system disturbances.

Also, costs tended to be less constrained and opposition (public and regulatory) to new infrastructure build-out tended to be less than it is today—making it easier to enhance the grid. The result was systems that could be built to inherently have more margin than is generally possible today.

Maintenance programs were also, in general, more rigorous than they are today. From an operation perspective, forecasting system conditions was simpler, since there were fewer generation and transmission owners, and limited renewable generation resources, such as wind, that currently contribute to greater operational uncertainty. Even if a potentially threatening event occurred, it was typically easier to identify an effective and practical mitigation solution.

As a result, the systems were operating in a carefully planned and cooperative manner. However, the evolution of the electric power industry toward open markets and adoption of renewable resources have introduced a number of factors that have increased the possible sources for system disturbances, reduced the robustness of systems, and lowered the predictability of operation.

Some of these factors are described in Table 7.2. On the other hand, recent development in the smart grid technologies provides the strategies and tools with which such issues can be addressed.

To ensure that a power system is sufficiently *reliable*, that is, that there is an acceptable probability of it operating satisfactorily over the long run, the system must be (a) properly *designed* with security as a primary consideration and (b) monitored during *operation* to ensure sufficient security margin exists at all times (since actual operating conditions and/or contingencies are usually different from those planned for).

The success of achieving these goals relies heavily on the application of good engineering, which in turn includes a growing reliance on the application of *power system analysis tools*.

The changes that have occurred in the new environment have both heightened the need for more rigorous power system security assessment and changed the requirements for the capabilities of power system analysis tools (Table 7.1).

7.2 Online Dynamic Security Assessment

Dynamic Security Assessment (*DSA*) refers to the analysis required to determine whether or not a power system can meet specified reliability and security criteria in both steady-state and dynamic time frames for all credible contingencies (Kundur 1994). In the operating environment, a secure system is one in which operating criteria is respected at both pre-contingency and post-contingency conditions.

Table 7.1 Acronyms

CA	Contingency analysis
CIM	Common information model
DSA	Dynamic security assessment
DTS	Dispatcher training simulator
ED	Economic dispatch
EMS	Energy management system
GPU	Graphics processing unit
HVDC	High-voltage direct current
ISO	Independent system operator
NERC	North American electric reliability corporation
PCM	Preventive control measure
PMU	Phasor measurement unit
PSS	Power system stabilizer
PV	Power–voltage
RAS	Remedial action scheme
RMT	Reserve management tool
RTU	Remote terminal unit
SCADA	Supervisory control and data acquisition
SE	State estimation
SPS	Special protection system
STATCOM	Static synchronous compensator
SVC	Static VAr compensator
TTC	Total transfer capacity
WAMS	Wide area measurement system
WECC	Western electricity coordinating council
WSAT	Wind security assessment tool

This implies that analyses must be performed to assess all aspects of security, including the thermal loading of system elements, voltage, and frequency variations (both steady-state and transient), and all forms of stability. The computations needed to accurately assess the security of a single defined system condition are technically rigorous and require considerable effort. As a result, security assessment has been historically conducted in an off-line operation-planning environment in which the steady-state and dynamic performance of the forecasted or planned system conditions are exhaustively determined using tools such as power-flow and time–domain simulations.

Because of the engineering and computational efforts needed for the more complex assessments, such as those required for stability assessment, it was necessary to compute system operating limits well in advance of the time in which they were expected to occur. In this approach, all planned conditions and contingencies had to be examined even though most would never actually occur.

In the new competitive environment, the uncertainty of predicting future operating conditions has created a need for a new approach to security assessment: *Online Dynamic Security Assessment (DSA)* (CIGRE 2007; Zhang et al. 2010). In this approach, the system stability for the current operating condition is computed as it occurs, and with sufficient speed to either trigger an automatic control action or to allow time for the operator to react, if a contingency analyzed is shown to

Table 7.2 Factors influencing modern power systems

Characteristic	Potential impact
Aging transmission infrastructures	Increased probability of component failures and malfunction leading to system disturbances
Lack of new transmission facilities	Overloading of transmission facilities leading to protection operation or contributing to phenomena such as voltage collapse Bottlenecks in key transmission corridors leading to congestion
Cutbacks in system maintenance	Component failures and disturbances such as flashovers to trees
Increased dependence on controls and special protection systems	Increased probability of inadvertent/incorrect operation of protections Increased unpredictability of cascading events
Large numbers of small and distributed generators	Increased difficulty in adequate system design due to uncertainty in generation plans. Uncertainty in dispatch
Large-scale integration of renewable resources such as wind and solar	Unpredictable and uncertain behaviors posing challenges for system planning and operation Additional requirement, such as frequency regulation, during disturbances
Market-driven transactions	Unpredictable power-flows and system usage leading to congestion and/or poor dynamic behavior New forms of stability problems such as voltage and small-signal stability
Increased dependence on communications and computer systems	Software/hardware failures may leave large portion of the system unobservable to operators, leading to inappropriate, or lack of, control actions during disturbances
Limited integrated system planning	Insufficient/improper generation and transmission resources
Trend toward interconnection	Exposure to cascading disturbances brought on by events in neighboring systems New forms of stability problems such as small-signal stability
New technologies such as PMU, energy storage, etc.	Advanced analysis capability to support the applications of such technologies
Increased regulatory demand on situational awareness in system operation	Need of the appropriate applications and the associated analysis capabilities to meet the requirements
Aging and downsized workforces	Lack of experienced personnel that may lead to the inability to deal appropriately with emergency conditions Increased use of automated solutions such as online DSA

be potentially insecure. Since this approach performs analyses on a snapshot of the current system condition, the uncertainty embedded in off-line analysis using forecasted condition is largely eliminated. This approach provides a radar-like mechanism that continually sweeps the system for potential problems that may result should a contingency occur ($n-1$ or any type of $n-x$ contingency included in the analysis).

While it is uncertain if online DSA could have prevented recent events such as the August 14, 2003 blackout in Northeast USA/Canada (US-Canada Power System Outage Task Force 2004) and the September 8, 2011 blackout in Southern California (FERC and NERC 2012), it is very likely that such assessments would provide operators with early indications of pending trouble and the opportunity to take remedial actions. In fact, the *US-Canada Power System Outage Task Force's Final Report* (US-Canada Power System Outage Task Force 2004) on the August 14, 2003 blackout includes a number of recommendations (particularly Recommendations 13 and 22) related to the research, evaluation, and adaptation of reliability-related tools and technologies, aiming at establishing guidelines for real-time operating tools. Similar recommendations were made in FERC and NERC (2012) for the September 8, 2011 blackout in Southern California.

The main functional components of an online DSA system are shown in Fig. 7.1. The system takes measurements of the actual system-operating condition with which a set of models is assembled for the required security assessment. Various types of security analyses are performed in near real-time in the DSA computation engine; the results are then passed to the operator or directly on to control systems to arm/trigger the required remedial actions. Some auxiliary functions are usually available to assist the operation of an online DSA system.

The following sections give more information on each of the main functional components in an online DSA system.

7.2.1 Measurements

System measurements can be obtained from a number of sources including traditional Supervisory Control and Data Acquisition (SCADA) systems using Remote Terminal Unit (RTU) as the measurement units, wide-area measurement systems (WAMS) - using Phasor Measurement Units (PMUs) as the measurement units, and additional disturbance monitors.

The measurements obtained are used for three primary purposes, as follows:

- Input to State Estimation (SE) where network models (power-flows) will be developed
- Direct input to security computation engines for the purpose of setting real-time equipment status, customizing contingencies and other data, etc.
- Benchmarking of SE results or computational results

All power systems have SCADA systems. SCADA data are updated at reasonably fast rate that can meet the data assembly requirements of online DSA systems.

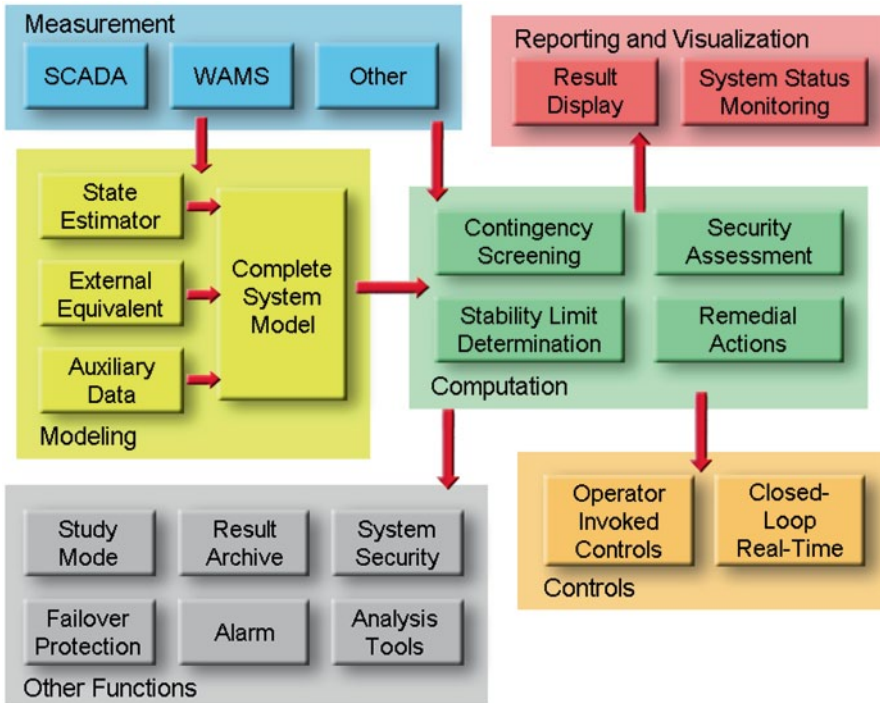


Fig. 7.1 Components of an online dynamic security assessment system

On the other hand, PMUs in WAMS have substantial advantages in that they can provide accurate, continuous, and time-synchronized data at very fast sampling rate for both magnitudes and phases of virtually any quantities in the system. This helps improve the quality of system models (for example, by enhancing the SE function) for the online DSA applications.

7.2.2 Modeling

When detailed analyses are to be performed for online DSA, high-quality models of the interconnected system are needed. In fact, since all analyses are dependent on the quality of the system models, it is perhaps the most important component in an online DSA system. Conventional SE is the main source for the power-flow models, which must be supplemented with other data such as dynamic models. Development of these models requires not only comprehensive technical capabilities but also an in-depth understanding of the requirements for the intended applications for the online DSA system. Generally speaking, the model development effort is focused on the following:

- Accuracy. The models must appropriately represent the characteristics of the physical phenomena to be studied.
- Completeness. Different aspects of the modeling must be addressed consistently to ensure the adequacy of the entire set of models for the problems to be solved.
- Flexibility. Sufficient degree of freedom should be left in the models so that they can be used for a wide variety of problems, with proper customization, if necessary.

Some of the modeling issues specific to the online DSA applications are further discussed in Sect. 7.4.

7.2.3 Computation

The types of methods used for dynamic security assessment are widely varied, the predominant being a class of the so-called model-based approaches in which the response of the power system is assessed using detailed models of the steady-state and dynamic characteristics of the system. Contingencies are applied and the responses computed using techniques such as time-domain simulations. The selection of a suitable computational method is based on a balance of the requirements described below.

7.2.3.1 Computation Capabilities

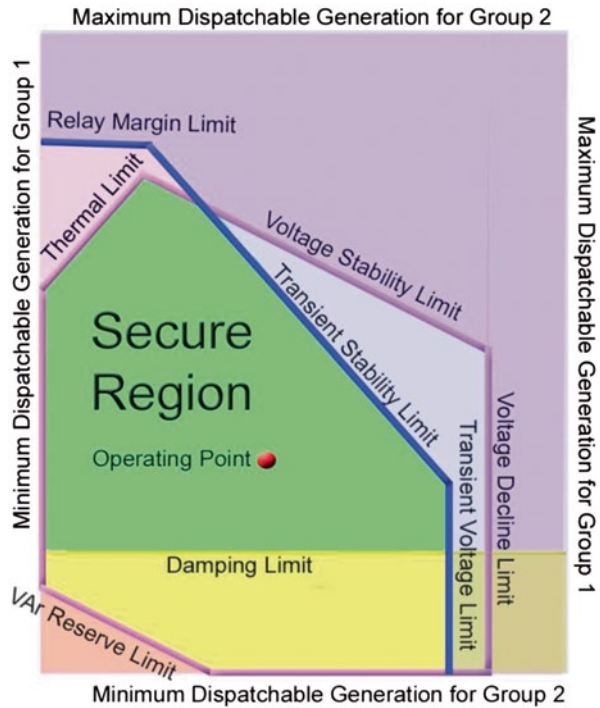
What operators need to know at any instant of time is (a) how secure is the current system state, (b) how secure will the system be if it is maneuvered, in the studied time frame, from the current state to a different state, and (c) if the degree of system security is unacceptable, what measures can be taken to make it acceptable?

In essence, the primary challenge is to verify the security of the current state and find the *secure region* within which the system can be maneuvered. This secure region can be visualized in nomograms as illustrated in Fig. 7.2 and is defined by boundaries set with respect to limits representing various security criteria including:

- Thermal overloading of transmission elements
- Steady-state voltage and frequency excursions
- Transient voltage dip/rise
- Transient stability
- Small-signal stability
- Voltage stability
- Frequency stability
- Other

The assessment of security limits associated with these items can be done using either full simulations or using approximate methods. Examples of full simulation methods include full power-flow solution of Power-Voltage (PV) curves for volt-

Fig. 7.2 Security nomogram



age security, time-domain simulations for transient security, and eigenvalue analysis for small-signal stability assessment.

Approximate methods include techniques such as sensitivity methods for voltage security assessment and direct energy methods for transient stability assessment. Although the approximate methods may offer some speed advantages, the full simulation methods provide the most accurate assessment of security and eliminate the question of the suitability of the assumptions made in approximate methods under changing system conditions.

7.2.3.2 Automation and Reliability

Online DSA systems must be highly automated and be capable of completing all tasks, repetitively, under varying conditions with little or no human intervention. This demands not only high standard on the DSA software but also functionalities with certain intelligence in order to provide the required results.

For example, determination of appropriate remedial actions may need the assessment of additional contingencies and/or system scenarios depending on the security assessment results. Reliability is another important issue for an online DSA system. As illustrated in the blackout of August 14, 2003, the potential consequences of the unavailability of mission-critical software applications can be devastating. In

addition to ensuring the deployment of high-quality software and hardware for an online DSA system, techniques such as redundancy and self-healing should be considered to meet the reliability requirements.

7.2.4 Reporting and Visualization

The ability to display the results of the security assessment in a simple, consolidated, and meaningful manner is critical to the success of online applications. DSA results must clearly report on key findings such as critical contingencies, potential criteria violations, affected elements (or region), security margins (nomograms), system conditions at the least acceptable security level, and required remedial actions. If deployed as a mission-critical application, additional visualization effect, such as alarm, may need to be issued upon detection of severe system conditions.

Reporting and visualization is an evolving topic and significant effort has been spent to improve this. Some of the current trends are further described in Sect. 7.4.

7.2.5 Control

If an online DSA system determines that a specific contingency may lead the system to an insecure situation, or a specific system condition does not have sufficient security margin for a foreseeable dispatch in the system, remedial measures must be determined. Remedial measures can be either preventative or corrective actions and could include such actions as capacitor switching, generator rescheduling, transformer tap-setting adjustment, or arming of special protection systems such as generation rejection or load shedding.

These controls can either be invoked by the operator as recommended by the online DSA system or automatically invoked by the system. In this manner, the online DSA system can become an integral part of special protection systems. An application of such a closed-loop control scheme is discussed in Sect. 7.4.

7.2.6 Other Functions

A number of additional important requirements for an online DSA system include:

- *Study mode (and other operation modes)*: The system should allow the operators or engineers to study any scenarios of interest in a “study mode” environment using base data taken from the live system (or archive). Other operational modes may be as important, as further described in Sect. 7.4.
- *Archive*: The system should be able to periodically and selectively store cases studied and corresponding output results for use in the study mode or for

postmortem analyses. Selected critical results may also need to be saved in Energy Management System (EMS) data historian for display on EMS.

- *System monitoring, diagnostics, and maintenance functions*: As a component of the real-time applications, it is important that the performance of the online DSA system is monitored continuously and any indication of operational irregularity should be detected and reported for diagnostics and maintenance.

7.3 Applications and Benefits

Tremendous accomplishments have been made in recent years toward the development and implementation of the online DSA technologies (Morison et al. 2004a; Wang and Morison 2006). The latest generation of sophisticated, highly automated, and reliable software tools have, combined with the seemingly endless improvements in computer hardware, led to the implementation of online DSA systems at many sites worldwide.

In North America, the majority of Independent System Operators (ISO) have adopted online DSA technologies, including the Electric Reliability Council of Texas (ERCOT; Avila-Rosales et al. 2003); PJM (Tong and Wang 2006; Wang et al. 2012); Midcontinent ISO (MISO); California ISO (CAISO; Rahman et al. 2013); ISO New England; Independent Electricity System Operation (IESO) in Ontario; and Alberta Electric System Operator (AESO; Wang et al. 2008b).

Also moving to this technology are large utilities such as BC Hydro (Atanackovic et al. 2013) and Southern Company Services (Viikinsalo et al. 2006). Internationally, this trend continues, with applications found in UK (Moore et al. 2013), Ireland (Dudurych et al. 2012), Brazil (Neto et al. 2010), China (Morison et al. 2004), Korea (Choi et al. 2014), and New Zealand (Nair et al. 2013), just to name a few.

These online DSA systems are often implemented with different objectives, and may result in significant benefits in many different forms, as described below.

7.3.1 Monitor System Security

This is the basic function with which an online DSA system checks the security status of the current system condition for all specified credible contingencies. A wide range of security criteria (as described earlier) may be applied to monitor system security.

The operator is alerted for appropriate actions, should any defined security criteria be violated. This function is particularly useful when the system is operating in region not studied off-line. Other chapters of this book include operational experiences indicating potential unstable system conditions that were not known to the operator.

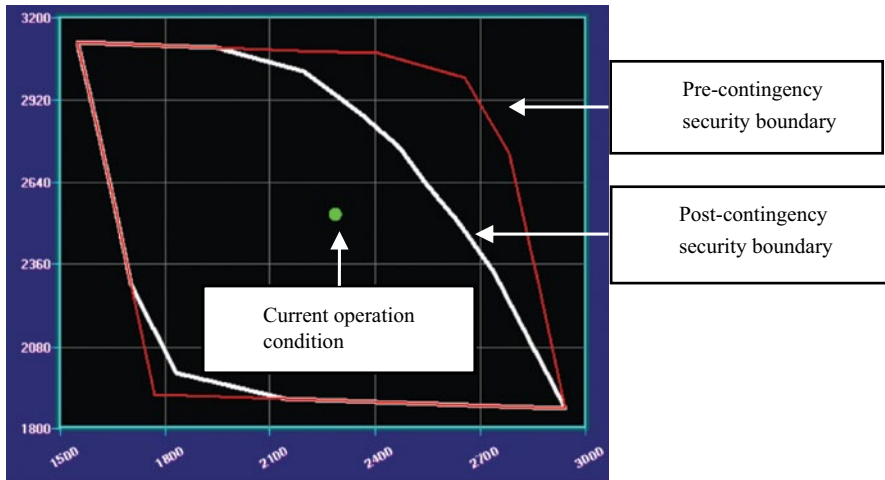


Fig. 7.3 A two-dimensional security nomogram

7.3.2 Determine Stability Limits

Determination of stability limits is a common task in the operation of power systems in which power transfers are limited by stability. Stability limits form the feasible region within which the system can be safely dispatched to meet load and market demand, and they also show the security margin available for the current operating condition. Conventionally, such limits are calculated off-line using planning system models and augmented with sufficient margin to ensure system security. It is well known that such an approach is often overly conservative, resulting in lost transfer capacity.

Limits calculated by online DSA, using real-time data, are much more accurate and reliable to use. For example, the two-dimensional nomogram shown in Fig. 7.3 indicates security limits measured by flows on key interfaces, from the current operation point subject to the specified security criteria and a set of contingencies. It can be determined easily from this diagram how much increase for the MW flow on Interface 1 or Interface 2 or any combinations, without loss of security.

Figure 7.4 shows a comparison for the security limits obtained from an ISO in North America.

The graph shows the security limits measured in terms of the MW flow on a key interface over a period of 24 h from the planning models (using off-line studies) and real-time models (using online DSA). Note that the results from the planning models indicate much lower security margin than those from the real-time models. This is typical as the planning models often represent the so-called worst-case condition, and thus the limits so obtained are usually very conservative.

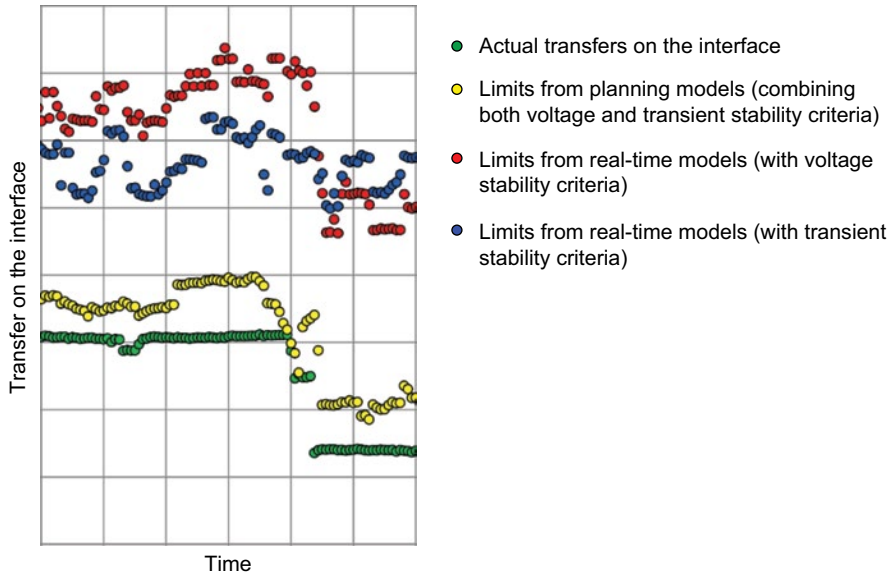


Fig. 7.4 Comparison of security limits from planning and real-time models

7.3.3 Recommend Remedial Control Actions

When a system is insecure, or does not have sufficient security margin, or is not able to transfer the required power due to security constraints, remedial control actions (preventive and/or corrective wherever available) should be taken to mitigate the problems. Online DSA is ideal for such tasks and its results are usually better than those obtained from the lookup tables prepared off-line.

The following example illustrates the effectiveness of such a function. This case was obtained from an actual online DSA system which includes a Preventive Control Measure (PCM) module. This case concerns the stability assessment of a power plant (Plant X) shown in Fig. 7.5. Plant X has three units. At the real-time system condition assessed:

- Unit #1 was out of service.
- Units #2 and #3 were in service and their MW generation was close to their rated outputs.

The contingency applied was a single-phase-to-ground fault at the Plant X end on line Y with a breaker (A) failure. This led to loss of both line Y and transformer D after the fault was cleared. Simulation showed that the system was unstable for this contingency.

The PCM module was activated to investigate this problem. This involved the determination of a quasi-optimal generator dispatch scheme that had the smallest amount of generation dispatch but could help maintain system stability for the

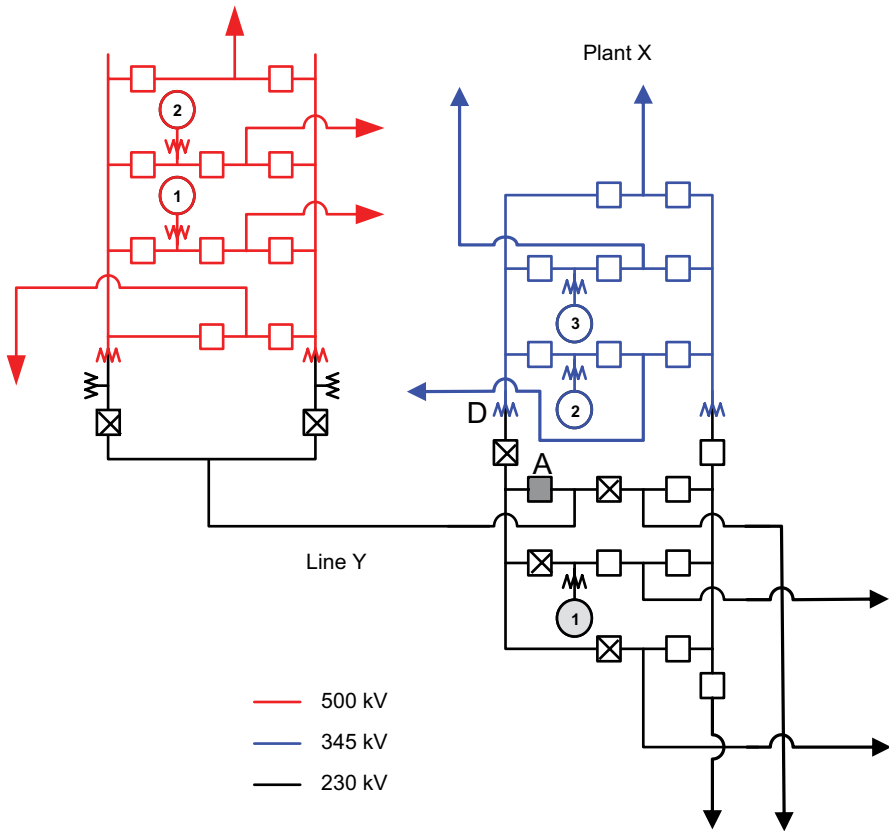


Fig. 7.5 An example for PCM application

contingency. A solution was successfully found for this real-time case: simply reducing the total outputs of units #2 and #3 by 28 MW which was a small adjustment. Figure 7.6 shows the simulation verification. This example clearly indicates the effectiveness and practicality of the identified PCM action. Such PCM solutions are presented to the operator for possible dispatch actions.

7.3.4 Manage Renewable Resources

Renewable resources, such as wind and solar, have become increasingly popular as a form of clean energy. Although advantageous to the environment, systems with high penetration of such generation may be difficult to operate due to a number of unique characteristics:

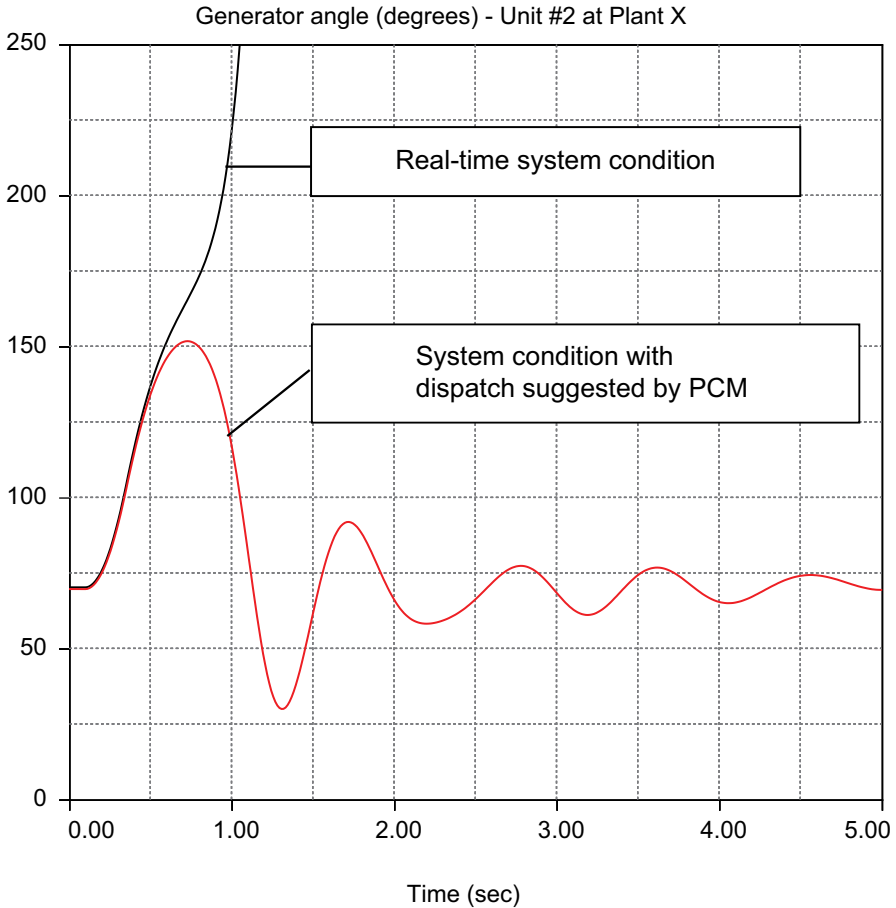


Fig. 7.6 Simulation verification for PCM

- Renewables are often located in unpopulated remote region requiring long transmission.
- Outputs may be unpredictable (e.g., due to sudden drop of wind speed).
- New generation technologies are adopted, which may be nonsynchronous, even nonrotary.
- Little voltage and frequency regulation capabilities are usually available.
- The operation of these units may be very sensitive to certain system conditions, such as low voltages.

These can raise the concerns from system operators on the highest amount of such generation that can be allowed at any given time without compromising system security. The solution to these concerns is to perform very quick assessment of system conditions in order to determine the optimal (or maximum) dispatch of this type of

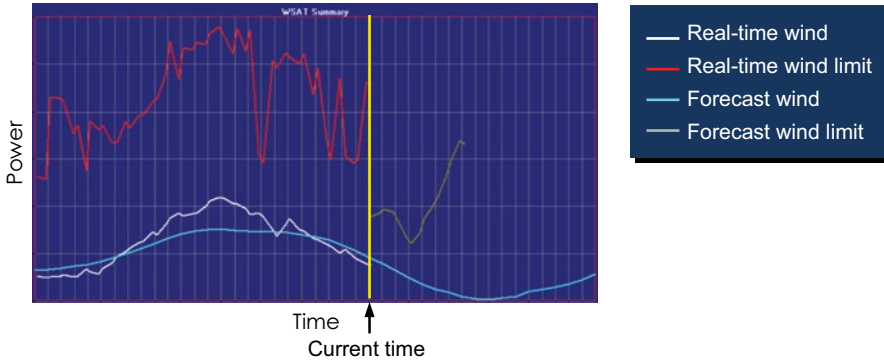


Fig. 7.7 Security limits from real-time and forecast wind levels

generation. Online DSA is able to perform such analysis with the turnout speed in the order of minutes.

An example of such applications is the Wind Security Assessment Tool (WSAT) implemented and operational at Irish national grid company (EirGrid; Dudurych et al. 2012). WSAT addresses high wind generation penetration concerns by ensuring satisfactory system performances for power transfers between wind and conventional generation for the base $N-1$ and credible $N-n$ system conditions for criteria including thermal loading, steady-state voltage levels, voltage stability, transient stability, and frequency deviations. It operates in two modes, a *real-time* mode and a *forecast* mode. For any given time, WSAT can tell system operators the real-time and forecast wind limits (Fig. 7.7). This information gives the operators clear guidance on the security margin available.

7.3.5 Determine/Verify Special Protection Systems

Special Protection Systems (SPS) are designed to protect a system for losing stability for severe contingencies (Pai and Sun 2008). Although the design of an SPS should consider all possible system conditions under which it will operate, practically only a limited number of scenarios are typically used. After the SPS is in service, unexpected system conditions may occur, which may lead to SPS malfunction. Inclusion of SPS models in online DSA (Wang et al. 2008) can put these SPS under constant testing, thus verifying their functions and ensuring their correct actions during various system conditions. For complex SPS whose arming logic, triggering logic, and output actions all depend on system conditions, it is possible to optimize the SPS operation based on real-time data by using online DSA.

An example of verifying SPS and updating SPS operational lookup table with online DSA is illustrated in Sect. 7.4.

7.3.6 Mitigate Congestion in a Power Market

One of the problems to be solved in operating a power market is to settle power transaction requests; this must be done very quickly with all security criteria respected. Online DSA certainly is an ideal tool in achieving such a goal, since it can be fully included in the market settlement cycle to automatically perform such a function. As mentioned earlier, transfer limits computed using real-time data are not only more accurate but also usually higher than those obtained using conservative off-line planning models. This can result in less transfer congestion and thus reduce possible congestion payment. As an example, the monthly congestion management credit paid by IESO averaged \$ 11.7 million during 2003–2007 (Ghasemi and Ahmed Maria 2008). Therefore, even a small fraction of reduction in this payment due to increased transfer limits would represent significant financial benefits. Such benefits have been more and more recognized by market operators, as in the case of ERCOT (Avila-Rosales et al. 2003), CAISO (Rahman et al. 2013), and a few others.

7.3.7 Determine Active and Reactive Power Reserves

For some systems, the determination of active and reactive power reserves can be critical. In small systems, for example, frequency fluctuations can be significant when a large unit is tripped; therefore, maintaining proper active power reserve is important to ensure frequency stability of the system. In this case, online DSA can play a critical role in optimizing the active power reserve while respecting frequency criteria set for the system.

Such an application is best illustrated by the reserve management problem shown in Prince-Pike et al. (2012) for the New Zealand power grid. For this application, a simplified real-time Reserve Management Tool (RMT) capable of determining the appropriate active power reserve requirement subject to certain defined risks is used in New Zealand's power market settlement. Due to the importance of this tool, a full-scale online DSA solution is being developed to replace the current RMT to provide a better solution for this function.

7.3.8 Help in Scheduling Equipment Maintenance

Equipment maintenance represents an unusual system operation condition, and if such maintenance is to occur in a stressed system condition, care must be taken to ensure system security. Outage scheduling is traditionally done using planning models and, as is the case for stability limit determination, often results in overly conservative conclusions. Online DSA provides a much better alternative, in which a real-time system condition is extracted and modified to reflect the maintenance requirements. This not only gives more accurate results but also makes the studies more efficient.

7.3.9 Calibrate and Validate Power System Models

One of the continued pursuits of power system engineers is to develop system models that can accurately capture the system characteristics for studies. Unfortunately, this is not always achieved easily. Typical examples include the postmortem analysis following the 1996 and 2003 North America blackouts, in which original system models assembled after the incidents were found to be unable to replicate the system responses recorded. This prompted programs to improve the quality of system models, such as the Western Electricity Coordinating Council (WECC) generator model testing and validation initiative. Online DSA provides a great way to calibrate and validate such models by comparing the computer simulation results with field measurements (say from PMUs). In fact, model validation has been one of the strong motivations behind the implementation of some of the recent online DSA projects in North America.

7.3.10 Prepare Models for System Studies

Traditionally, power system studies performed off-line use data prepared from system planning. It is increasingly recognized that such models do not give good representation of the practical system conditions, particularly when used to perform short-term operational planning studies. One way to overcome this problem is to start such studies with the real-time models assembled by online DSA. This approach is getting serious attention by some of the online DSA users, and initial results are encouraging.

7.3.11 Perform System Restoration

When a system is in an emergency state with loss of many elements, restoration tasks must be performed. The system in this form of state is usually not studied using off-line models, and therefore little guidance is available with regard to the security during the system restoration. Online DSA can play a vital role in this process, as shown in the experience for the system restoration effort after the Hurricane Katrina documented in Viikinsalo et al. (2006).

7.3.12 Perform Postmortem Analysis of Incidents

When an incident does occur in a power system that results in a significant impact, it is inevitable that a postmortem analysis will be required. An online DSA system is usually capable of archiving system conditions periodically, together with all necessary auxiliary data, to perform stability analysis. Such archived data can provide an

excellent starting point for a postmortem analysis. Wang et al. (2012) share such an example for investigating an oscillation event recorded in the PJM footprint, with a real-time archived stability case.

7.4 Trends and Issues

Although tremendous progress has been achieved in the development and implementation of online DSA over the last decade or so, this technology continues to advance rapidly in both technical capabilities and applications. The modern power system is constantly facing new operational challenges including the introduction of new generation technologies, the use of advanced wide-area control systems, the heightened need for more efficient and reliable operations, and changing customer expectations.

In this section, a few current trends and issues are discussed for the online DSA technology with comments on the progress made or the possible directions to go.

7.4.1 Coordinated Applications of Online DSA

Online DSA was proposed as a simple, independent application that performs stability analysis using real-time captured system data. This concept may not be able to meet the demand for the overall security assessment of the system.

A more comprehensive approach involves a highly coordinated deployment of online DSA systems at different levels of the operational system.

7.4.1.1 Real-Time Systems

Real-time systems refer to those that *must* complete a computation cycle within a specified period of time. Such systems are often used to:

- Assess the general security status of the real-time system conditions (“real-time DSA”). In each computation cycle, the analysis is performed with SCADA/SE model. Results are required typically at every 5–30 min. Real-time DSA forms the backbone of an enterprise online DSA solution.
- Provide short-term forecast on the system security (“forecast DSA”). In each computation cycle, the analysis is performed with a forecast system operation condition (30 min to a few hours ahead of the real time) which is superimposed to the current network model provided by SCADA/SE. Results are usually required at the same cycle as the real-time DSA. The forecast DSA is important for systems whose short-term operation cannot be reasonably well scheduled (for example, due to high penetration of wind generation).

- Manage the security constraints in power market (“market DSA”). The analyses are performed with market model and the computation speed must comply with the market settlement requirements (it might even be possible that several DSA calls are made within one market settlement cycle). Common computational tasks are determination of transfer limit nomograms, active/reactive reserve requirements, etc. Market DSA must be integrated with the market system, and thus high customization is usually required for such systems.

Real-time systems are increasingly being considered as mission-critical applications. Hence, such systems are often deployed with dedicated hardware, advanced computational architecture (such as distributed computations), and failover schemes to meet the computation speed and robustness requirements.

7.4.1.2 Off-line Systems

These are systems that run for specific tasks or run only when triggered by users. They usually require rich and complex analysis features but do not have strict requirements for fast computation cycling time. These systems are typically designed to:

- Analyze mid- to long-term system security (“look-ahead DSA”), such as Total Transfer Capacity (TTC) calculation for the next day, week, etc. It is often allowed that such a task be completed in longer time period (in terms of hours); however, because of the massive amount of computations involved (e.g., TTC calculations for several transfers at every hour for the next week), advanced computational techniques must be utilized.
- Perform studies for specified system conditions (“study DSA”). This has turned out to be one of the most useful functions in an enterprise online DSA solution. A study DSA can further have two possible operation modes:
 - Study mode for historical scenarios: In this mode, the starting point is an archived case from real-time DSA, and the user can implement the required modifications for the case and then perform studies. The objective is usually to investigate an incident, a reported insecure case, the impact of new models (such as an SPS), a case with bad data, or a what-if scenario to provide insight on system responses.
 - Study mode for future scenarios: In this mode, the starting point is a future time for the study scope specified by the user. The corresponding system model is then assembled with information extracted from the EMS, such as load forecast, generation plan, outage scheduling, as well as possible manual changes made by the user. The objective is to check the system security for the specified future time and study condition, for example, for purpose of equipment maintenance scheduling
- Provide training to operators (“training DSA”). This is a straightforward requirement as online DSA becomes part of the advanced solutions in EMS. Integra-

tion of a training DSA option in Dispatcher Training Simulator (DTS) helps the operators understand the online DSA results and learn the actions necessary to handle the security issues identified.

- Serve as a testing platform (“testing DSA”). This is necessary as a platform to test new models, new software release, different computational configurations, system performance, etc.

The performance requirements for non-real-time systems are not as demanding as real-time systems; however, greater flexibilities are the key, in terms of modeling, system configuration, result processing, etc.

7.4.1.3 Coordination and Integration

The coordination and integration of different online DSA systems are critical in order to ensure they are able to continuously operate smoothly for the intended functions. A few key issues:

- **Model sharing:** This is probably one of the most important issues when several online DSA systems operate under the same roof. It is almost certain that such systems will share some common models (for example, dynamic models, transfer definitions, etc.). Sharing of such models is an effective way of not only ensuring computational efficiency but also achieving result consistency. This requires that the data in each DSA system be flexibly defined, from a common share, from a private definition, or even a combination of these two.
- **Resource sharing:** resources (e.g., computer servers) required by different online DSA systems may be different since the computational burden and performance requirements may be quite different for each system. It is therefore quite common that different resources are assigned to them. What is making this more complicated is that the resource requirements for some systems may vary, so the resource assignment may not be a one-time static task. For instance, if a large study is to be performed for a period of time using a study DSA, more servers may need to be added to this system to help meet the performance requirements. Fortunately, with the multiple-core servers and virtualization, seamless and scalable resource reassignment is possible. The DSA computation engine should, of course, be able to take advantage of such dynamic resource assignment.
- **System synchronization:** All operational DSA systems should have exactly the same version, with the same patches, if applicable. This is obviously necessary in order to ensure consistency of results. In addition to good and clear procedures to follow during the software installation, there should also be capability built in the systems to self-validate this requirement.
- **Configuration synchronization:** In case that a model or parameter of one online DSA system needs to be shared by another system, a process is required to populate this to other systems. This is referred to as a configuration synchronization process and is important to maintain online DSA systems. A typical application scenario is when updating models (for example, when adding a new power plant

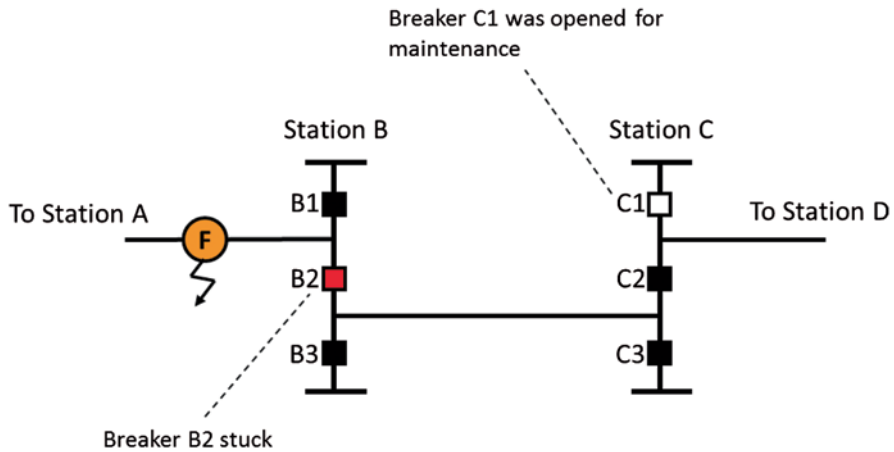


Fig. 7.8 Illustration of a stuck breaker contingency

to the system model). The model would be first added to the testing DSA where necessary testing is done to validate the model. After that, the model can be pushed to all other online DSA systems using this synchronization process.

7.4.2 Adoption of Node/Breaker Modeling Approach

In off-line planning studies, bus-branch models are commonly used to represent a power system. In such models, the bus bars (nodes) at each nominal voltage level in a substation are typically represented by a single *bus*, with the breakers and switches connecting them aggregated and thus not explicitly modeled. It is based on the assumption that the bus bars are connected by breakers/switches in the designed way that a single element (line, transformer, generator, etc.) outage would not cause other elements to trip.

However, in real-time system operations, the breakers and switches are constantly opened/closed, which makes the topology of a substation different from the designed “normal” topology. Depending on the substation real-time topology, a single element outage may cause consequent outages (sympathetic actions). For example, in Fig. 7.8, a fault on the line between substation A and substation B and a stuck breaker B2 would cause three transmission lines to be tripped.

To accurately analyze the contingencies and possible SPS/Remedial Action Scheme (RAS) actions in an online DSA system, the real-time station topology, i.e., the detailed node/breaker status information, is needed. Such information is available in SCADA/WAMS and they should be integrated into online DSA. The following are some of the practical considerations in adopting the node/breaker modeling for online DSA:

- The format in which the node/breaker data are passed to DSA: Common Information Model (CIM) is an apparent choice. Other vendor specific formats may have advantages, for example, compact data size and flexibilities for handling system specific issues.
- Study engineers are familiar with planning tools which are in the bus/branch model. Further, when studying future system conditions in study DSA, bus/branch modeling approach is probably sufficient since the future node/breaker topology is difficult to predict. In some situations, node/breaker information may not even be available, for example, in the equivalized model for the external system (refer to Sect. 7.4.3 for details). It would therefore be ideal that an online DSA system can handle a hybrid modeling representation, i.e., for substations or areas where node/breaker information is available, node/breaker representation is used, for other substations or areas, and bus/branch representation can still be used. Such a hybrid approach can also help greatly reduce the data transfer and processing requirements.
- An automatic topology analyzer needs to be implemented in the online DSA system when adopting the node/breaker modeling approach. From an initial event (a fault considered in a contingency or a RAS/SPS action), the topology analyzer will search for the breakers which need to be opened in order to clear the fault or to operate the associated elements. In the example shown in Fig. 7.8, the user just needs to specify a fault on line between substations A and B and the stuck breaker B2. Other breakers and elements to be opened or outaged will be determined by the topology analyzer based on the real-time node/breaker information.
- With the topology analyzer, the online DSA system can automatically build the full contingency sequence based on an initial event specified by the user. During this process, however, additional information may be required, which may not be available in EMS and which is usually defined manually in the contingency sequence when the bus/branch model is used. This includes settings of the associated relays, breaker time, sequence network data, etc.

7.4.3 External System Equivalencing

Some interconnected power systems have grown very large in size, and as a result, their “full simulation” models have correspondingly expanded in dimension. The North American Electric Reliability Corporation (NERC) planning models for the North American eastern interconnection, for example, have now more than 65,000 buses and some state estimator models (which are intended to approximate the full system representation) for this region have approximately 40,000 buses.

In general, it is necessary to model large portions of the power system in on-line DSA systems since some limiting phenomena, particularly small-signal stability, can involve wide areas of the system. SCADA data (or other source of system measurements) and the resulting state estimator output, on the other hand, may be limited to a specific region of observability (such as a specific portion of the

interconnected system, usually corresponding to a control area). It is therefore necessary to include representation of the external system (possibly in the form of equivalents) prior to conducting analyses. This can be achieved by either appending the state estimator model with an external representation developed “off-line” or merging several state estimator models from different parts of the interconnected system. These approaches are still evolving and there currently does not appear to be a universally adopted method.

Chow (2013) describes some of the techniques in performing system model equivalencing. A case study was given in this reference, in which a reduced power system model was created from a full model of 16,330 buses, for the purpose of running online DSA. The reduced model contains an unreduced study area of 4875 buses, which is observable to the control area, and an external reduced area of 2335 buses. The entire reduced model is thus only 44% of the full model; however, its performance for both steady-state and transient analyses is very close to the full model, even when the system condition is dispatched to some of the operational extremes.

7.4.4 Real-Time System Data Reconditioning

The state estimation results (system snapshots) from SCADA or WAMS are the primary sources of data to be used as input to online DSA systems. A system snapshot comes in the form of a solved power-flow case, and it provides the online DSA system with the real-time system-operating condition.

A state estimation model generally could be more detailed than the power-flow models used in planning studies, for example, with the inclusion of node/breaker topology information. However, it has been found in many online DSA system implementations that state estimation models may also not necessarily represent the physical reality accurately enough for online DSA applications:

- Traditional EMS applications such as Contingency Analysis (CA) and Economic Dispatch (ED) often use simplified steady-state analysis algorithms, and hence the models may be simplified.
- In power market applications, generating units might be represented based on their ownership or bidding block prices for convenience.

Due to the limitations in state estimation models, real-time system data reconditionings are often needed for online DSA implementations. When an online DSA system receives a system snapshot, certain user-specified modifications are applied to the snapshot, and a new power-flow is generated for the security analyses. Some of the typical common modifications required include:

- Generator grouping and de-grouping: When a generator is represented in the snapshot with multiple units, these units need to be combined as one generator. In some cases, multiple generators in one plant are modeled as one generator, for example, all units in a wind farm may be represented by one unit. If this

wind farm consists of different types of wind generators, the unit needs to be de-grouped (split) into multiple units to match different stability models.

- Insertion of station service load and/or step-up transformer: Generators in the state estimation model are often represented by their net injections to the network, so the station service loads and/or step-up transformers are not represented. This introduces inaccuracies in stability analyses. In the reconditioning process, the service loads and/or step-up transformers can be added to the plant, and the outputs of the generators are increased to match the actual unit outputs.
- Addition of High-Voltage Direct Current (HVDC) links: For simplicity, HVDC links are often modeled as decoupled injections (loads/generators) to the Alternate Current (AC) network in the state estimation model. However, in stability analyses, HVDC links need to be modeled in detail in the power-flow. DC converters, DC lines/cables, and DC buses are added to the power-flow to replace the dummy loads/generators. The HVDC power-flow equations and matching dynamic models will then be used in stability analyses.
- Addition of Static Var Compensator (SVC)/Static Synchronous Compensator (STATCOM): It is a common practice to model an SVC/STATCOM as a generator in the state estimation model. This could introduce significant inaccuracy in stability analyses. The data reconditioning process will need to replace the generator with the actual SVC/STATCOM model.

7.4.5 Special Modeling Requirements

One of the major differences in performing online DSA as compared with off-line planning studies is the modeling requirements. While the basic model requirements between these two forms of the analyses are similar, some of the modeling details may vary. Traditional planning studies tend to ignore or assume certain aspects of modeling details, in most cases, because such details are not available. In the online analyses, however, availability of information or the nature of the studies determines that such details shall be included. Some of these are discussed below.

7.4.5.1 Modeling of RAS/SPS

RAS/SPS are widely used in power systems to provide protection against severe system conditions or severe disturbances. Models of these devices are usually not included or included with simplification in planning studies. Such a modeling practice may be changed in the future as recommended by the report for the September 8, 2011 Southern California blackout (FERC and NERC 2012).

For online applications, full RAS/SPS models shall be considered. Wang et al. (2008) proposed a framework for representing such models in transient analysis which are fully user-definable and thus very flexible to apply. As a simple example,

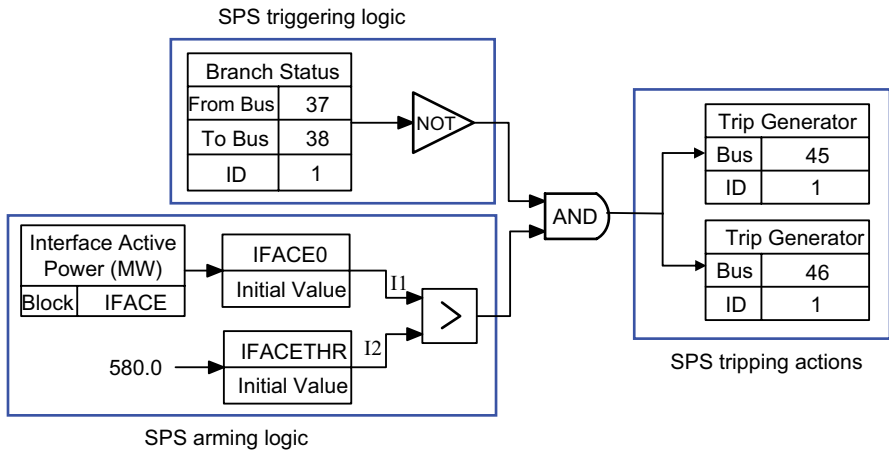


Fig. 7.9 A sample SPS model

Fig. 7.9 shows an SPS scheme built using this approach. The SPS is armed when the defined interface flow (IFACE) at the initial condition is greater than 580 MW. The SPS triggering condition is the loss of a circuit (37-38-1) which leads to the tripping of two generators (45-1 and 46-1). This model can be included in the study case and the generators are tripped only if both arming and triggering conditions are met.

The above approach has been used to model RAS/SPS in a number of online DSA systems, including those reported in reference Rahman et al. (2013).

7.4.5.2 Combined-Cycle Power Plants

Combined-cycle (CC) power plants are common in many systems. The unique physical connection between gas and steam turbines in each CC set of units requires that the output of these units follow certain rules in power-flow dispatches, or in other words, the MW output of the units in a CC set cannot be randomly set. This is important in transfer analysis when generation is dispatched as either source or sink. Separate CC dispatch rules must be defined and respected.

7.4.5.3 Real-Time Wind Generation Capacity

Wind modeling is getting more and more attention for different types of studies. There has been significant progress on the modeling of individual wind turbines. However, one assumption remains on the modeling of a wind farm.

The standard way to represent a wind farm is to aggregate *all* turbines to one or a few equivalent generators and represent these equivalents in a study case. During planning studies, the total Mega Volt Ampere (MVA) rating of these equivalents is

kept the same, i.e., all wind turbines are assumed to be in service. This is an acceptable assumption for planning studies, since this obviously is the most reasonable scenario to study. For online studies, however, there is no reason to make such an assumption. The exact wind turbine operation status at a given time is known; therefore, the corresponding real-time case should represent such operation condition by adjusting the MVA rating for the aggregated wind generation. The study results using such a model will be certainly better.

7.4.5.4 Real-Time Equipment Status

Equipment in a system may not always be in service. A simple example is a generator whose status (in or out of service) is always included in the power-flow case since it is too important to ignore for any study. For other equipment, however, the operation status may not be considered in planning studies. This cannot be taken for granted in online applications. The typical situation is that some devices, such as Power System Stabilizer (PSS) and RAS/SPS, may be taken out of service for a period of time for maintenance. In case of RAS/SPS, there may be more reasons to consider its operation status. Consider a load-shedding model as an example in which the location of load to be shed may depend on the time of the tripping action. This is to achieve a level of fairness to the customers. Thus, the actual models for a real-time study case must be adjusted based on the real-time information on the equipment status, passed to the online DSA system.

7.4.6 Real-Time Closed-Loop Control

The real-time security status and secure operating region of a system are determined by a few factors: real-time operating condition, security criteria, credible contingencies, and in some systems, SPS.

For many SPS, the settings and arming conditions are more or less static, i.e., they do not change frequently with system-operating conditions. For such SPS, the settings and arming conditions can be determined by off-line studies. Once implemented, they will be used for all system-operating conditions. Such settings and arming conditions will only be updated infrequently (monthly, seasonally, annually, or even as needed).

For some power systems (such as BC Hydro; Pai and Sun 2008), the SPS arming conditions may need to be updated frequently. An example is the generation-shedding scheme implemented at BC Hydro. The operation of this SPS combines the results of off-line studies and an online pattern matching technique. First, a large amount of predicted system-operating conditions are created and studied off-line. The major system attributes (loads, flows, outages, etc.) extracted from these power-flows and the associated amount of generation to be shed to maintain system stability are then stored in a database. In real-time, system snapshots from EMS are

periodically compared with this database to obtain the right match for the generation-shedding amount which is finally used to arm the SPS. In less complex SPS, lookup tables may be used in SPS operation, which are created using off-line studies, and SPS arming conditions are selected in real time by matching a few power-flow parameters with the lookup table.

Both of the above approaches are based on off-line studies and they have similar drawbacks:

- As system complexity increases, the number of possible conditions and contingencies to be studied becomes unmanageable.
- Most study results are never used, which results in high wastage.
- Off-line studies are often conservative, which may result in overactions. This could lead to other issues. This is especially true when the SPS involves load/generator shedding.
- Exact system state is rarely accurately captured by forecast; hence, incorrect or inaccurate SPS arming may occur.

Application of the online DSA technology to the SPS-arming process is a superior solution to such problems. This needs a real-time closed-loop control scheme. In such a scheme, the SPS settings and/or arming conditions and other automatic controls are periodically updated based on the online DSA results.

To implement such a closed-loop control scheme, the requirements to the online DSA system are more rigorous. First, since the online DSA system is in a closed control loop, and its results will directly affect the performance of the power system, the reliability of the online DSA system must be high. It is expected that such a system would continuously generate reliable results, and would properly handle any exceptions.

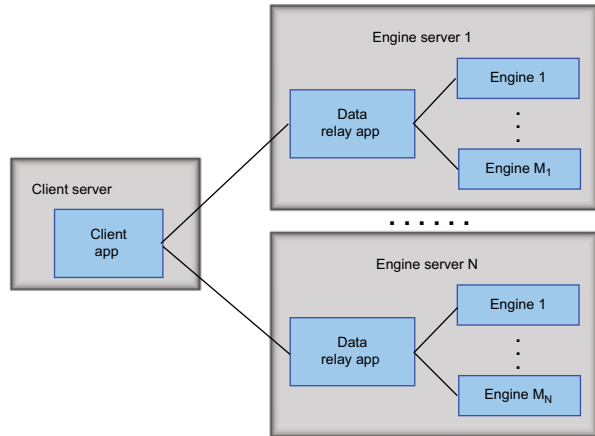
Second, unlike conventional online DSA systems, in which straightforward contingency analysis and transfer analysis may be performed, an online DSA system included in the closed control loop evaluates the effectiveness of different SPS settings and arming conditions. This may require optimization of its operations, and special customization would usually be needed.

Third, the computation speed is also an important consideration. To put online DSA in a closed control loop usually means a shorter computation cycle. For example, arming of the generation-shedding SPS implemented at BC Hydro is updated every 4 min. So, all computations required to obtain the arming parameters in an online DSA system must be completed within this time.

7.4.7 High-Performance Computation

Although detailed simulations are recognized as providing the most accurate security assessments, speed of computation remains a challenge, particularly with the complex models required in analyzing large interconnected systems. The typical computation cycle for an online DSA system is 5–30 min, that is to say that a

Fig. 7.10 A distributed computations scheme



complete security assessment (both the base case and transfer analyses) must be completed within such a period from the time the snapshot is taken from the system to the time the results are made available.

Since security assessment must determine the security for *critical* contingencies, a common approach to speed up online DSA is to screen contingencies. This refers to using a fast algorithm to select the contingencies which must be analyzed in detail. While numerous methods have been proposed and applied for this task, there remains a balance between speed and accuracy. Screening methods for thermal overloading or steady-state system behavior may be much easier to apply when compared with those for dynamic behavior, in which complex dynamics and nonlinearities of the system may render simplified screening methods unreliable. This may be coupled with additional burdens for special requirements in security assessment, such as the need to consider RAS/SPS actions, or applications of oscillatory and frequency criteria, in which cases full time-domain simulations are required without compromise in modeling and computational techniques. However, research in this field is ongoing.

Another approach in dealing with computational speed issue is to increase the computing power of an online DSA system. Two possible schemes have been proposed: parallel computations (Tomim et al. 2009; Huang et al. 2007) and distributed computations (Wang 2012) achieved using multiple servers, multiple Central Processing Unit (CPU) cores, or Graphics Processing Unit (GPU), which are very popular and affordable. Parallel computations are more attractive for obvious reason; however, it is more technically challenging and there has been no production code available to deal with power system models without simplification. Distributed computations, on the other hand, have been successfully implemented and applied for a number of online DSA systems. The following is a brief description on how this technique is applied and benefits.

In a distributed computation scheme, the contingencies for a case are sent to multiple computation engines which run in separate servers (or separate CPU cores). Figure 7.10 shows an implementation of this scheme.

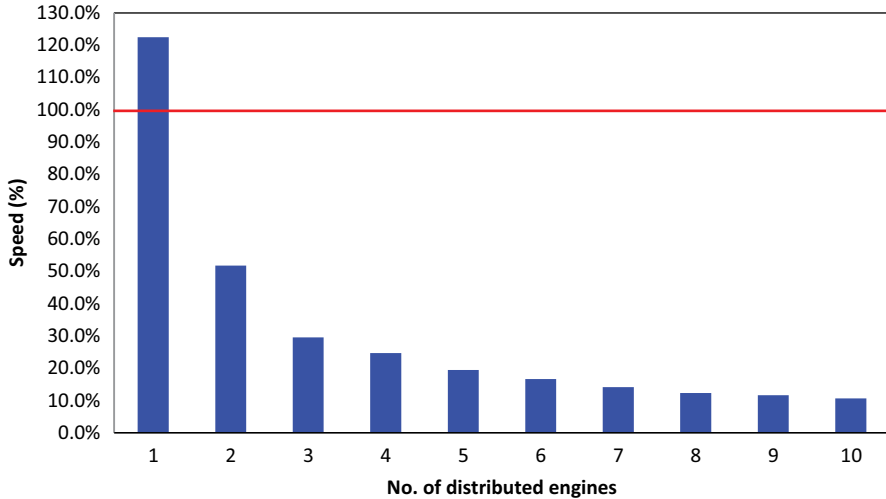


Fig. 7.11 Computational efficiency for the distributed computations

This scheme uses one Client Server and N Engine Servers (each of the engine servers has multiple CPU cores). A complete study case is assembled by the Client App residing in the Client Server. The contingencies to be processed are then evenly split according to the total number of available cores. The case data plus the split contingency sets are sent to each Engine Server where the Data Relay App creates the actual simulation cases to be run by individual engines in the Engine Server. The computation results from each engine are sent back to the Client Server where they are consolidated so that the full results can be presented to the user. This scheme is very effective in dealing with large systems with many contingencies to be processed and it also minimizes the data communication requirements. Figure 7.11 shows the speed improvement that can be achieved for time-domain simulations of a 6620-bus system with 400 contingencies. The line at 100% in the figure represents the benchmarking speed when no distributed computation is used. When there is only one distributed engine, the computation speed is slower than the benchmarking as expected, due to data communications required. However, as the number of computation engines increases, the time required to complete the entire case decreases almost linearly.

7.4.8 Output Visualization

Result visualization is the last step in an online DSA cycle, but it is probably the one that has the most need and potential to be improved. The requirements on visualization can also be conflicting, from a simple high-level summary for operators to logically arranged full details for support and study engineers. Therefore, visualization may need to be organized or customized for different users.

Cont. No.	Transient Stability Index	Damping Index (%)	Voltage Duration Index Drop (sec) Rise (sec)	Frequency Duration Index Drop (sec) Rise (sec)	Relay Margin Index Zone 1 (%) Zone 2 (%)	Status	Contingency Description
3	-66.92	99.00	0.067 0.000	0.000 1.200	100.0 100.0	Insecure	3 phase fault at 7042; tripping of 7042-7269-99
1	-65.50	99.00	0.567 0.000	0.003 0.900	100.0 100.0	Insecure	3 phase fault at 7011; tripping of 7011-7060-99
10	-40.51	99.00	0.000 0.000	0.000 0.583	100.0 100.0	Insecure	3 phase fault at 7106; tripping of 7106-7108-0
7	43.22	1.84	0.000 0.000	0.000 0.000	100.0 100.0	Insecure	3 phase fault at 7192; tripping of 7192-7199-99
2	43.96	12.22	0.000 0.000	0.000 0.000	100.0 100.0	Secure	3 phase fault at 7032; tripping of 7032-7036-99
9	44.52	11.94	0.000 0.000	0.000 0.000	100.0 100.0	Secure	3 phase fault at 7225; tripping of 7225-7231-99
5	44.80	9.95	0.000 0.000	0.000 0.000	100.0 100.0	Secure	3 phase fault at 7125; tripping of 7125-7129-1
8	45.06	-2.44	0.000 0.000	0.000 0.000	100.0 100.0	Insecure	3 phase fault at 7218; tripping of 7218-7235-4
6	46.41	12.74	0.000 0.000	0.000 0.000	100.0 100.0	Secure	3 phase fault at 7183; tripping of 7183-7184-1
4	49.24	53.93	0.000 0.000	0.000 0.000	100.0 100.0	Secure	3 phase fault at 7110; tripping of 7110-7134-99

Fig. 7.12 Table with contingency analysis results

A few effective ways of displaying DSA results include:

- Security summary tables. A security summary table is best suited for summarizing results of contingency analysis. Figure 7.12 shows such a table for displaying transient security assessment results, in which each row reports on the results of simulation of one contingency and each column provides a summary of an applied criterion (red indicates a criterion violation).
- Geographical displays. When the security analysis results shall be interpreted with geographical information, such a display works the best. A typical example is the understanding of a mode shape for an inter-area oscillatory mode as provided by an eigenvalue/eigenvector pair. Figure 7.13 displays such a mode shape geographically. The oscillation pattern of the mode is very clear from this diagram.
- Security bars and nomograms. When presenting results of transfer analysis, the common approach is to use security bars (Fig. 7.14) for one-dimensional (1D) transfers and nomograms (Fig. 7.13) for 2D transfers. These graphics show the base operating point, quantities by which the transfers are measured (source, sink, or specific interface flows), and the limits constrained by various security criterion violations.
- Security meters. For greater simplicity and clarity, security meters can be used to show the relative “distance” (for example, in terms of percentage) of a system to insecurity. Figure 7.15 is one example. These meters show whether the system is safe (green), cautious (yellow), or close to insecure (red), by user-defined rules.
- Transfer limit histograms. One of the benefits from an online DSA system is the ability to continuously monitor and follow the security of the power system. This means that a large amount of history data are available on system security, and transfer limit histogram can be used to explore the security trend of the system. Figures 7.16 and 7.17 show the histograms of 1D and 2D transfer limits.

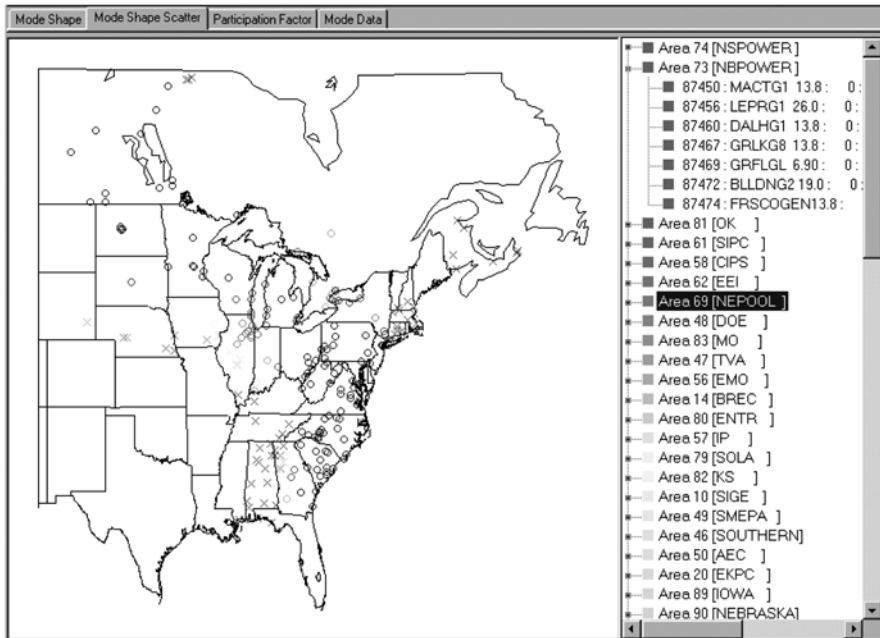


Fig. 7.13 A mode shape diagram

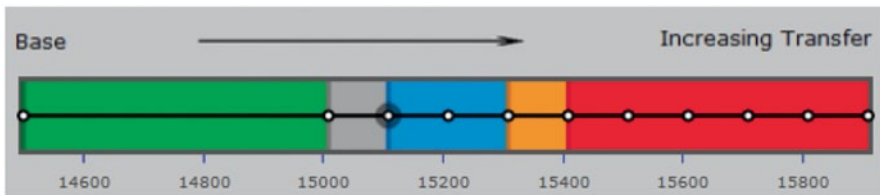


Fig. 7.14 A security bar for 1D transfer

Other visualization ideas include web-based result browsing and sharing, apps on mobile devices, interfaces with other databases in the EMS, and inclusion of analysis functions such as data mining, trending, prediction, statistical analyses, etc.

7.5 Looking Forward

Online DSA is still an evolving technology that will embrace new concepts, methods, and applications in its migration of becoming a common component for power system operation. This is especially true when new technologies, for example, those



Fig. 7.15 Security meters

in measurements, analysis, and IT, are becoming commercially available. Some potentially interesting applications of such technologies to online DSA are discussed in this section.

7.5.1 PMU Technologies

PMUs are not new, and they have been widely used in utilities to provide real-time monitoring and situational awareness functions. With the wide-scale deployment of PMUs in locations such as the USA and with the cost of such technology continuing to drop, the use of PMU technology in many aspects of power system planning and operation is expected to grow significantly. Online DSA has also benefited from this technology with one of the earliest applications in using PMU data to improve the quality of state estimation. There are other areas in which online DSA and PMU applications can be more tightly integrated:

- Wide-area monitoring and control: PMU is best for understanding the current system condition and online DSA for future system conditions. It is thus conceivable that together they can offer much better monitoring and control functions for power systems. Giri (2013) presents a vision in which PMU and online DSA are applied in a complementary way to provide the complete solution for grid security assessment.

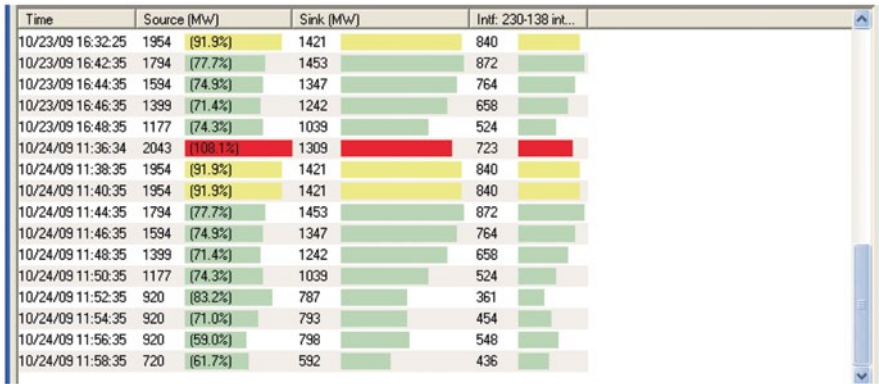


Fig. 7.16 1-d transfer limit histogram

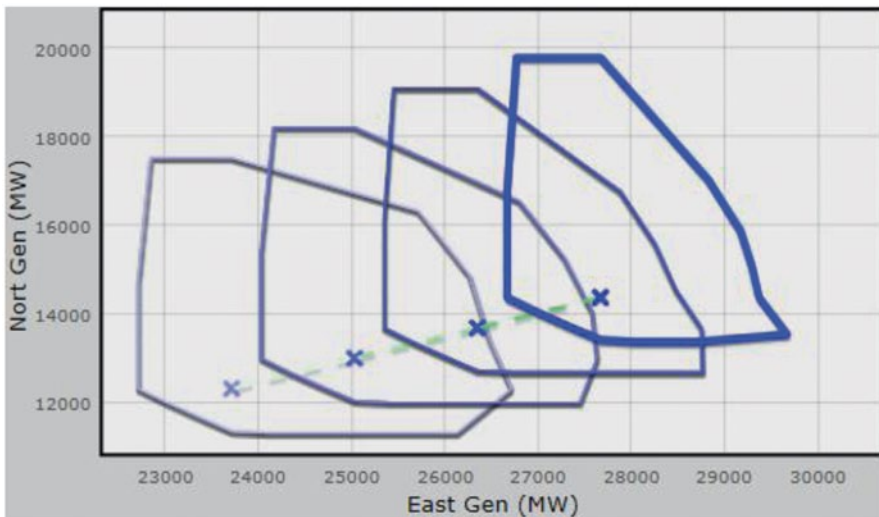


Fig. 7.17 2D transfer limit histogram

- Model validation: PMU can faithfully record system responses after a disturbance and this provides a great opportunity to validate system models that are critical for online DSA applications. Such a measurement-validation approach can be made as a process to self-tune system models so as to continuously improve the quality of such models and ultimately the security assessment results from online DSA systems. Kosterev and Davies (2010) describes the WECC’s practices in model validation.
- Dispatcher training: As PMU is becoming a mainstream technology in control rooms, there is a requirement to introduce emulated PMU signals in DTS to

allow the training of PMU-based applications for system operators. Conventional DTS however includes only simulation engines capable of producing quasi-dynamic system responses at resolutions of seconds, which would not be sufficient for PMU applications. Simulated system responses at the PMU resolution are possible using the online DSA technology, although some fine details need to be settled for practical uses, for example, fixed sampling rate, time synchronization, inclusion of required features (for training purposes) in the simulated results, interface with other DTS modules, etc. Haut et al. (2012) describes such an application and research in this area is active.

7.5.2 Risk-Based System Security Assessment Method

Online DSA systems currently in operation generally rely on deterministic analysis methods and, therefore, have to exhaustively examine many contingencies and search for security limits using a rigorous approach. While this approach provides very accurate results, it is computationally burdensome and therefore time consuming. Moreover, since all contingencies are considered with equal weight, system operation is often limited by contingencies with small probability, resulting in lost market opportunities and reduced financial return.

To cope with such limitations, risk-based security assessment can be used in which security and economics are coordinated to provide the operation limits with least risk. There is already rich literature in the research community for this approach—for example, Ming et al. (2003). This is a very promising direction for the online DSA technologies to grow.

7.5.3 Cloud Computing

The distributed computation scheme mentioned in Sect. 7.4.7 for high-performance computing appears to be suitable for cloud computing, which is becoming increasingly powerful and cost-effective. There are already attempts at utilizing such an advanced computation platform for power system analysis (Huang 2010). Further research is required to take full advantage of the possibilities that can be offered by cloud computing for online DSA.

7.6 In Summary

Ensuring security requires the use of advanced power system analysis tools capable of comprehensive security assessment with due consideration to practical operating criteria. These tools must be able to model the system appropriately, compute security limits in a fast and accurate manner, recommend appropriate remedial or control

actions if required, and provide meaningful displays to system operators. Technologies are currently available to achieve these goals and are being implemented in many sites worldwide.

Such systems are of relatively low cost and are becoming easy to implement, as EMS vendors act to integrate these tools into their native products. Online dynamic security assessment can provide the first line of defense against widespread system disturbances by quickly scanning the system for potential problems and providing operators with actionable results. With the development of emerging technologies such as wide-area phasor measurements and high-performance computing power, online DSA is expected to become a dominant weapon against system blackouts.

Acknowledgments Dr. Prabha Kundur contributed to the first version of this chapter and his effort is greatly appreciated.

References

- Atanackovic D, Yao M, Vinnakota R, Wang L, Lin X (2013) Modeling of cascading events of power systems for dynamic security assessment (DSA). Presented at the IEEE PES general meeting, July 21–25, 2013, Vancouver, Canada
- Avila-Rosales R, Sadjadpour A, Gibescu M, Morison K, Hamadani H, Wang L (July 2003) ERCOT's implementation of online dynamic security assessment. Panel session of the IEEE PES 2003 general meeting, Toronto, Canada
- Choi Y, Shin Y, Wang L, Lee B (2014) Development of on-line dynamic security assessment system for energy management system in Korean power grid. Presented at ICEE 2014, June 15–19, 2014, Jeju, Korea
- Chow J (ed) (2013) Power system coherency and model reduction. Springer, London
- CIGRE (2007) CIGRE technical brochure on review of on-line dynamic security assessment tools and techniques. CIGRE Working Group 4.6. 01, 2007
- Dudurych IM, Rogers A, Aherne R, Wang L, Howell F, Lin X (2012) Safety in numbers. IEEE Power Energy Mag March/April 2012 62–70
- FERC and NERC (2012) Arizona-Southern California outages on September 8, 2011: causes and recommendations, April 2012
- Ghasemi H, Ahmed Maria M (2008) Benefits of employing an online security limit derivation tool in electricity markets. Presented at IEEE PES general meeting, July 20–24, 2008, Pittsburgh, Pennsylvania, USA
- Giri J (2013) Synchrophasor PMU solutions for grid operations. Presented at the IEEE PES general meeting, July 21–25, 2013, Vancouver, Canada
- Haut B, Bouchez F, Villella F (2012) Improved real-time computation engine for a dispatcher training center of the European transmission network. High performance computing, networking, storage and analysis (SCC), November 10–16, 2012, Salt Lake City USA
- Huang Z, Guttromson R, Nieplocha J, Pratt R (2007) Transforming power grid operations. *Sci Comput* 24(5):22–27
- Huang Q, Zhou M, Zhang Y, Wu Z (2010) Exploiting cloud computing for power system analysis. Presented at POWERCON 2010, October 24–28, 2010, Hangzhou, China
- IEEE/CIGRE (2003) IEEE/CIGRE joint task force on stability terms and definitions, definition and classification of power system stability. CIGRE Technical Brochure No. 231, 2003
- Kosterev DN, Davies D (2010) System model validation studies in WECC. Presented at the IEEE PES general meeting, July 24–29, 2010, Detroit, USA
- Kundur P (1994) Power system stability and control. McGraw-Hill, New York

- Ming N, McCalley JD, Vittal V, Tayyib T (2003) Online risk-based security assessment. *IEEE Trans Power Syst* 18(1):258–265
- Moore J, Laojavachakul S, Zhao G, Howell F, Li F, Magnago F (2013) Real-time operational stability analysis including fault clearing scenarios. Presented at the IEEE PES general meeting, July 21–25, 2013, Vancouver, Canada
- Morison K, Wang L, Kundur P (2004a) Power system security assessment. *IEEE Power Energy Mag* Sept/Oct:30–39
- Morison K, Wang L, Kundur P, Lin X, Gao W, He C, Xue F, Xu J, Xu T, Xue I (2004b) Critical requirements for successful on-line security assessment. Paper presented at the real-time stability challenge panel, IEEE power systems conference & exposition 2004 (IEEE PSCE'04), 10–13 October 2004, New York, NY
- Nair NKC, Naik P, Chakrabarti B, Goodwin D (2013) Managing transmission system operation in New Zealand with high renewable penetration. Presented at the IEEE PES general meeting, July 21–25, 2013, Vancouver, Canada
- Neto CAS, Quadros MA, Santos MG, Jardim J (2010) Brazilian system operator online security assessment system. Paper presented at a panel session at the IEEE PES general meeting, July 2010, Minneapolis, USA
- Pai SC, Sun J (2008) BCTC's experience towards a smarter grid—increasing limits and reliability with centralized intelligence remedial action schemes. In: *Proceedings of IEEE Canada electrical power and energy conference*, October 6–7, 2008, Vancouver, Canada
- Prince-Pike A, Wilson D, Ilieva I, Li A, Phethean M (2012) Maintaining New Zealand's electrical reserve management tool. Presented at IPEC 2012, December 12–13, 2012, Ho Chi Minh City, Vietnam
- Rahman KA, Subakti D, Wu J, Haq E, Howell F, Wang L (2013) Online transient stability analysis for system operation at CAISO. Presented at the IEEE PES general meeting, July 21–25, 2013, Vancouver, Canada
- Tomim MA, Martí JR, Wang L (2009) Parallel solution of large power system networks using the multi-area Thévenin equivalents (MATE) algorithm. *Int J Electr Power Energy Syst* 31(9):497–503
- Tong J, Wang L (2006) Design of a DSA tool for real time system operations. Presented at POWERCON 2006, October 22–26, 2006, Chongqing, China
- US-Canada Power System Outage Task Force (2004) Final report on the August 14, 2003 blackout in the United States and Canada: causes and recommendations, April 2004
- Viikinsalo J, Martin A, Morison K, Wang L, Howell F (2006) Transient security assessment in real-time at southern company. Paper presented at the real-time stability applications in modern SCADA/EMS Panel, IEEE power systems conference & exposition 2006 (IEEE PSCE'04), October 29–November 2, 2006, Atlanta, GA
- Wang L (2012) Techniques for high performance analysis of transient stability. Presented at the IEEE PES general meeting, July 23–26, 2012, San Diego, USA
- Wang L, Morison K (2006) Implementation of online security assessment. *IEEE Power Energy Mag* Sept/Oct:47–59
- Wang L, Howell F, Morison K (2008a) A framework for special protection system modeling for dynamic security assessment of power systems. *POWERCON* conference, October 12–15, 2008, New Delhi, India
- Wang L, Howell F, Moshref A, Mueller M, Viray E, Yang C, Qiu J (2008b) A real-time voltage security assessment system (VSAS) at Alberta electric system operator. *CIGRÉ Canada Conference on Power Systems*, October 19–21, 2008, Winnipeg, Canada
- Wang L, Tong J, Li H (2012) An application example for on-line DSA systems. Presented at POWERCON 2012, October 30–November 2, 2012, Auckland, New Zealand
- Zhang P, Li F, Bhatt N (2010) Next-generation monitoring, analysis, and control for the future smart control center. *IEEE Trans Smart Grid* 1(2):186–192

Chapter 8

The Case for Using Wide-Area Monitoring and Control to Improve the Resilience and Capacity of the Electric Power Grid

Jay Giri, Manu Parashar, Rene Avila-Rosales and Douglas Wilson

Abstract It is important for power grids to become flexible to accommodate diverse technologies such as intermittent renewables and power electronic conversion sources, while conventional generation resources are becoming more volatile with market forces and political directions. Environmentally, building new transmission is challenging. With smart grid technologies, there is a great deal of potential to control the power system using many widely distributed resources, but there is a considerable challenge in making use of the control capabilities in a novel way. This nascent volatility versus reliability demand makes operational decision-making and execution more challenging than in any other time in history. This chapter will explore modern techniques to improve grid reliability by enhancing and extending control center capabilities and substation capabilities. The use of automatic, wide-area protection schemes to mitigate cascading blackouts will be examined. Also explored will be the use of: wide-area control strategies, new and emerging technologies and communications, software and hardware architectures, and state-of-the art Energy Management System (EMS) technologies as the keys to more reliable operations. Additional focus will be placed on the positive impacts of synchronized phasor measurements.

8.1 Introduction

The high-voltage electric power grid was designed to operate in a stable condition. And, historically, that is how the grid has been typically operated. As per its intended design, the grid uses high-voltage transmission lines to transport electricity across thousands of miles. The power starts at various geographically dispersed generating units and is moved to numerous substations across the grid. The substations

J. Giri (✉) · M. Parashar · R. Avila-Rosales
Alstom Grid, Redmond, WA, USA
e-mail: jay.giri@alstom.com

D. Wilson
Psymetrix-Alstom, Edinburgh, UK

S. C. Savulescu (ed.), *Real-Time Stability in Power Systems*,
Power Electronics and Power Systems, DOI 10.1007/978-3-319-06680-6_8,
© Springer International Publishing - Switzerland 2014

transform the high-voltage energy to lower voltages, which are suitable for transfer by distribution networks to the customers.

The grid typically has sufficient capacity to transfer energy to every customer 24 h/day, 7 h/week. Scheduled maintenance may temporarily take some of the grid components (generating units, transmission lines, transformers, etc.) out of service. Additionally, unexpected failures, due to acts of nature or other causes, may take components out of service. In order to maximize safety, mitigate systems damage, and minimize downtimes to customers, the grid has established a set of stability limits.

When components of the grid are disabled, the grid's transfer capacity is reduced and the grid operates on a thin capacity margin. This means that the likelihood the grid will exceed its stability limits is greatly increased.

There are many different types of stability limits including:

- Transmission line thermal overloads
- High or low voltages, and Voltage Stability (VS)
- Transient angle stability
- Damping of oscillations

Conventional protection is designed to isolate elements of the grid that may be damaged as a fault occurs. However, designing conventional protection to address wide-area stability issues can be challenging and conservative, and constraint levels can be conservative to ensure the integrity of the power system. In order to be effective, the relay protection schemes, which are deployed all across the grid, need to be coordinated.

Responsibility for monitoring power system conditions across the grid lies with the Energy Management System (EMS) operator. The EMS receives new data every 2–4 s and sounds alarms when violations are detected. The EMS also performs a variety of network analyses and calculations to help the operator assess and manage the stability of the grid. While this human/machine team is usually capable of handling anything that arises, there are infrequent circumstances when the grid becomes unstable and some areas lose power.

Many companies have implemented remedial action schemes or special protection schemes in order to protect equipment when certain predetermined conditions are encountered. These automatic preventive control actions include reconfiguring the topology of the grid or even blacking out a portion of the grid in order to prevent the spread of a blackout across the entire grid. These schemes tend to be conservative since they are based on heuristics and off-line assumptions that have to span a wide range of power system operating conditions.

This chapter focuses on a wide-area grid control approach that is based on real-time power system operating conditions. Automated schemes that use current conditions to deploy the most rapid and effective strategies will be discussed. The primary objective of wide-area control is to protect the interconnected power grid from uncontrolled widespread failure.

The August 14, 2003 blackout and other similar critical grid failures around the world have driven the industry to develop more automatic and adaptive control

systems to prevent future catastrophes. Postmortem analyses and other investigative reports have concluded that the power system planner and the EMS operator must both be provided with the data and means to avoid system-wide power failures caused by unexpected events.

Now, more than ever, electric utility companies are facing a wide range of problems. It is becoming more and more difficult to operate the power system in a stable and reliable manner. Some of the issues forcing the utilities to emphasize improved grid stability include:

- Unexpected adverse weather conditions
- Shifting of load distribution and load management
- Dispersed and intermittent generation resources
- Electricity market system initiatives that cause the grid to be utilized in a more dynamic and less predictable manner
- Generation company decisions since they have been separated from the transmission companies
- Transmission stability decisions that are based on assumptions of load forecasts, generation capacities, and margins
- Stability margin concerns, since the system is operating closer to its limits

In order to cope with these issues, companies are focusing on new technologies and techniques to take full advantage of:

- Early problem detection and warning signals identified by synchronized measurements
- Recorded data analysis
- Wide-area visualization
- Wide-area closed-loop control

It is very clear that the use of EMS applications needs to be extended in order to improve the reliability and accuracy of system condition estimation (state estimation), the reliability and accuracy of relay coordination and relay settings, the implementation of utility practices and new regulations (Giri and Avila-Rosales 2002), and the defense plans against disturbances (Avila-Rosales et al. 2004). In addition, all of these new power system operational challenges have resulted in a new set of engineering challenges.

8.2 Engineering Challenges

Nowadays, electric utilities are deploying grid stability analysis tools in their EMS architectures for power system model structures of unprecedented size. Today 50,000 bus systems are not uncommon. These deployments impose major computational challenges related to model data collection and accuracy, solution techniques, visualization of the results, and the systems architecture.

In order to be effective, the EMS needs the capability to model and simulate the behaviors of extremely large transmission systems over a wide range of time domains, frequency domains, and topological designs.

Accurate tools for transient (angular) conditions and voltage stability (VS) are required, in order to assess and simulate all sorts of scenarios for the current time and immediate future. Quick methods are needed to reduce the computational burden associated with dynamic analysis and quasi-dynamic simulations to evaluate cascading events for preventive/corrective actions. The “prediction of dangerous states” by look-ahead simulation is becoming a new requirement in the industry.

The challenges go from modeling to accurate results of simulation and monitoring tools in the EMS and market applications.

8.2.1 Accurate Modeling and Data Quality

Some of the problems in the current EMS deployments are linked to modeling errors (Meliopoulous et al. 2001) and parameters that are improperly migrated from planning models to operational databases. The operational model is a bus-branch oriented model, although almost all Supervisory Control and Data Acquisition (SCADA) information is available at the substation level. Making matters worse is the fact that not all of the SCADA information is passed to the operational model; the node-circuit breaker models are not fully considered.

The EMS therefore relies on the State Estimator (SE) to pinpoint and identify topology errors as well as parameter problems. Unfortunately, the identification of the topology problem is combinatorial in nature. The estimation algorithm can pinpoint where the problems are but a system for the fast determination of the actual status of branches, switches, and breakers has not been properly implemented yet.

To compensate, the EMS operators usually communicate with their neighbors whenever unusual behaviors are identified. External network topology errors continue to be an issue and are adjusted manually (or according to schedule) to minimize the impact on the internal part of the power system. Synchronized phasor measurements are currently in place to correct some of these modeling errors. Still, there is a lot of room in this area for research and development towards improving wide-area operations.

Special protection schemes and load shedding schemes are based on predefined scenarios with the support of off-line applications. These applications also suffer from incorrect modeling. For this reason, the planning offices spend a lot of time identifying potential problems and system conditions. They basically create problem scenarios in order to specify schemes to mitigate them.

To reduce the analysis burden, and to get realistic information, the planning engineers are studying available modes to retrieve information from real-time events and create snapshots that deserve further analysis via “what-if?” conditions.

Still, the following problems need to be addressed, spanning the time frames from planning to operations preparation, to operations, to real-time analysis and control:

- Inadequate network modeling
- Incorrect static and dynamic parameters
- Unreliable limits
- Improper protection settings
- Measurement calibration errors

These issues must be addressed as soon as they are identified and as early as possible in the implementation phases of wide-area system information technologies.

8.2.2 Very Large Simulation Models

Electricity markets span very large geographical regions and are not necessarily constrained by utility company jurisdictional boundaries. This has resulted in the need to simulate very large-scale network models that represent a larger portion of the power grid.

A 32,000 bus State Estimator was deployed in 2005 by a company in the USA and continues to be in real-time operation now. Recently, requirements for 50,000 bus models have also been proposed.

Fortunately, modern SE and network analysis software packages are readily scalable to handle tasks of these sizes. Additionally, computer-processing power has increased dramatically allowing these very large equations to be solved in 30–45 s on average.

These large-scale SE solutions pose challenges for:

- Accurate and consistent input data
- Voluminous output data, which need to be quickly summarized as decision-making information for the operator

8.2.3 Accurate State Estimation

SE is considered a fundamental component of the modern EMS capabilities. As a matter of course, SE is periodically executed in order to calculate and provide a consistent and reliable state of the system based on SCADA, synchronized measurements, and other relevant information. SE is expected to calculate very large models, and with a higher frequency rate of execution, impose hard-performance requirements on existing algorithmic methods.

SE nowadays takes full advantage of distributed/parallel processing, given the advancements in available computer technologies. The steady-state estimation must also provide a valid, accurate, and robust solution under a wide variety of normal and emergency conditions.

Market applications and deregulation practices are aggressively requiring much faster, more precise, and more accurate results from SE. In the market context, financial settlements are based on sensitivities obtained from SE. If these sensitivities

are incorrect, or unavailable, they translate into significant errors in the settling of market transactions.

Under severe emergency conditions, the estimation process should rely on all vital data available including historical data, recent recordings, and recent results. In this way, it is possible to monitor the grid backbone and adapt automatically. The operators have a critical reliance on SE under these circumstances to provide meaningful results under stressed conditions.

Furthermore, SE is the foundation of all subsequent network analyses such as N-1 Contingency Analysis (CA), optimal power flow calculations, stability enhancement assessments, etc. If SE fails to provide a valid solution, the rest of the network analysis cannot run.

8.2.4 Fast Stability Assessment

Near-real-time stability assessments are extremely desirable at major transmission companies (Avila-Rosales et al. 2003), particularly for wide-area control-room applications. These applications are executed based on current snapshots of the power system from the SE and the latest Phasor Measurement Unit (PMU) measurements. The results of the stability assessment flag the system as operating normally, alarmed, or under emergency conditions. The following types of limits determine these states of operational condition:

- Thermal condition
- Voltage Stability
- Angular stability
- Frequency stability
- Steady-state stability
- Available Transfer Capacity (ATC)
- Market congestion

Multiprocessing applications and appropriate hardware architecture can reduce calculation time to simulate stability problems accurately (Avila-Rosales et al. 2004). Master/slave multilayered configurations are appropriate to handle hundreds of events. There is still room, however, to reduce the burden by using information such as recent violations and an adaptive, up-to-date list of contingencies based on violation histories.

8.2.5 A Comprehensive View of EMS and Stability Results

Most operator information is based on alarms, EMS applications displays, and map board information. There is a vast amount of data available, yet there is often no easy way to provide useful information in a meaningful way to the operator. There

is an urgent need for all operators to have better ways to visualize voltages, frequencies, contingency violations due to transactions, and early stability warnings. Under the pressures of cascading outages, rapid frequency changes, and voltage deterioration, an operator will sometimes rely more on instincts and past experiences than on data streams. Needless to say, this is not the optimal way to assess anomalies, fix problems, and prevent imminent catastrophes.

All operators need an easy-to-use, intuitive, geographic visualization system for both steady-state and dynamic stability assessments. Such a system should incorporate all types of warning signals and system violations. Advanced EMS applications are also needed to identify problems more quickly and to propose control actions to mitigate imminent catastrophes. Along with the visualization, operational procedures and use-case scenarios are critical to empower an operator to take a well-informed response to an emerging critical situation.

Some utilities are already using advanced visualization technologies in their control rooms, where they can see at a glance shaded voltage clusters, coloring, and pie charts fed with live SCADA data. This is certainly an area where the EMS applications can improve operations. Visualizing a stability trend is invaluable. Also, showing the operator the grid's immediate history and imminent future conditions can truly help. Advanced visualization is an enabling technology with a significant potential for developing advisory control techniques that would eventually move towards automated closed-loop control in the field.

Some visualization techniques show two-dimensional stability regions where all of the dynamic and thermal readings are displayed. These are continually updated as the system evolves. Going forward, the utilities define what specific data and monitoring information would be beneficial to them in order to improve system stability.

Many consortia have been formed to address specific grid stability operational issues and improved information visualization. These consortia are comprised of utilities, universities, software vendors, and hardware vendors.

8.3 Recent Technology Advances

8.3.1 Faster and More Economical Computer Power

Computer processor speeds and parallelization techniques, along with reducing costs, lead to much greater computer power accessible to utilities. As a result, these centers can perform more complex and computationally intensive tasks.

Distributed processing is now being utilized at control centers to speed up the solution process of certain computationally intensive functions such as CA and Dynamic Stability Analysis (DSA).

8.3.2 Substation Automation: Decentralized Processing

Another ongoing trend is to add more processing capability and intelligence at the substations (Apostolov 2004). Data from these processors can be used locally to optimize substation operations. This information can also be used to improve system-wide optimization and operator decision-making by providing more consistent and valid data for analysis at the control center.

Many utilities are now deploying PC-based SCADA systems at major substations. In addition to basic SCADA-type functions, new applications are being added to improve monitoring and control locally.

8.3.2.1 Substation-Based State Estimation

Current substation technologies already have infrastructure to handle the PMU work. This is done through relays in feeders and devices connected to the high sides and low sides of the transformers. PMU technologies can be integrated with other systems in order to provide operators with a wide range of network applications and data correction methods.

The use of substation technologies will change the way that the Regional Transmission Organization (RTO) business is modeled. A lot of data filtering and data cleanup can take place before the final data are actually used at the transmission level. The whole configuration, including switches, breakers, flows, etc., can be monitored and recorded. The local control and coordination of protection tasks during load shed is one of the most important operations during emergency conditions and there is a lot that can be done at this level.

8.3.3 State Estimation Robustness

Nowadays, SE is becoming a critical function at the control center. Market settlements and revenue calculations are based on subtle details and key data from the SE systems. The newer, very large models have also been focusing on improved SE functions. Furthermore, SE is the foundation of all subsequent network analysis calculations. All network-oriented applications (steady-state and dynamic) need the initial conditions as the starting point.

Therefore, if the SE fails, the rest of the network sequence does not have a valid base number. These technical drivers have resulted in a closer scrutiny of SE methodologies and algorithms. They have also resulted in the development of a more accurate, efficient, and reliable SE application at the control center. In the end, the SE solution must be guaranteed by any means necessary, either by using approximated solutions or by reducing the scope through utilizing new measurements and algorithms.

8.3.3.1 Wide-Area State Estimation

The possibility of running SE at the scan-rate level (substation level) and less-than-a-minute level (wide-area level) is one of the most exciting lines of power grid research today. The ability to take advantage of the existing substation infrastructure in order to identify and correct problems for more accurate readings at the wide-area level can now be implemented.

One reason for this progress could be the fact that the RTO business lacks detailed models in some areas (breaker node). Other areas like the substation level, however, provide all of the necessary details. The usual error problems in the vicinity of failures could be avoided through the use of substation-based applications. Topology problems could also be quickly identified.

8.3.4 Improvements in Visualization Techniques

Experience of blackouts globally emphasizes the need for improving control center capabilities for better “situational awareness.” This means that the operators need to constantly be aware of current system conditions. The information needs to be presented rapidly, reliably, and meaningfully so that decision-making is expedited. Accompanying situational awareness is the need for operational response guidance that defines the actions that would relieve wide-area stress and dynamic threats. Specific guidance is key to taking real-time action in response to an alarm.

8.3.5 Globally Synchronized Phasor Measurements

Synchrophasor (or phasor) measurement involves deriving a phasor representation of measured waveform, referenced to an ideal 50- or 60-Hz sine wave with peaks on precisely timed second boundaries (Fig. 8.1). The ability to represent a voltage or current waveform concisely as a magnitude and angle means that the measurements can be streamed from the substation to a central unit where geographically separate measurements can be time-aligned and compared.

Phasor measurements are increasingly being deployed across power grids worldwide. In North America, under the Smart Grid Investment Grants (SGIG), the number of PMU installations has grown fivefold over the past 4 years. Since 2004, 1200 PMUs have been installed on the US grid. This trend has energized the industry—the next large-scale deployments of PMUs are expected to happen in India and Brazil. India is committed to deploying more than 1700 PMUs across the entire country beginning in 2014.

Each PMU typically monitors 6–36 phasor quantities, digitals, frequency, and frequency rate-of-change, and all of the data are time-tagged using the Global

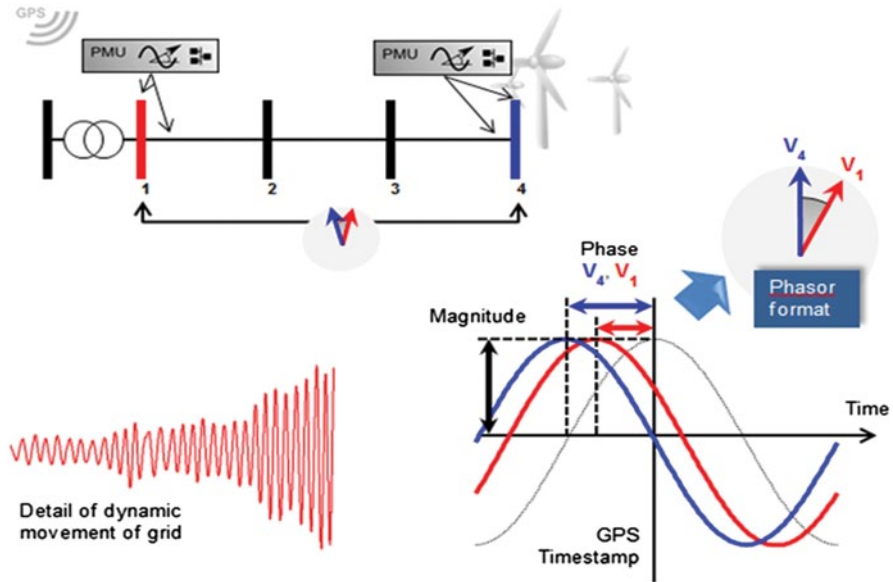


Fig. 8.1 Phasor measurement units (PMUs) and synchrophasors

Positioning System (GPS) to insert a global time stamp. There is also a growing trend of incorporating synchrophasor capability into relays and other IEDs. These synchronized phasor measurements are transmitted at very fast rates: from 10 to 120 samples per second. The information is captured at the millisecond time frame, and includes voltage, current, and frequency values.

8.3.5.1 PMU Instrumentation

Timely, synchronized PMU measurements are available to operators nowadays. Most utilities worldwide have some form of PMU project, in either research or commercial application. As illustrated above, PMU devices measure synchronized voltage and current, and transmit data to a central location where they are compared, analyzed, and processed. The PMU hardware is normally based on platforms built for disturbance recording or protection relays, and are equipped with a GPS receiver and Inter-Range Instrumentation Group-B (IRIG-B) time-code generator. While GPS is currently used exclusively as the time source, there is an industry direction to reduce dependence on continuous GPS availability through the use of Institute of Electrical and Electronics Engineers (IEEE) 1588 Point-to-Point time protocol and highly stable master clocks.

The ability of PMUs to provide synchronized information offers operators a lot of advantages, like dynamic trending. This facilitates the prediction of frequency behaviors, active load changes, and reactive power changes immediately after dis-

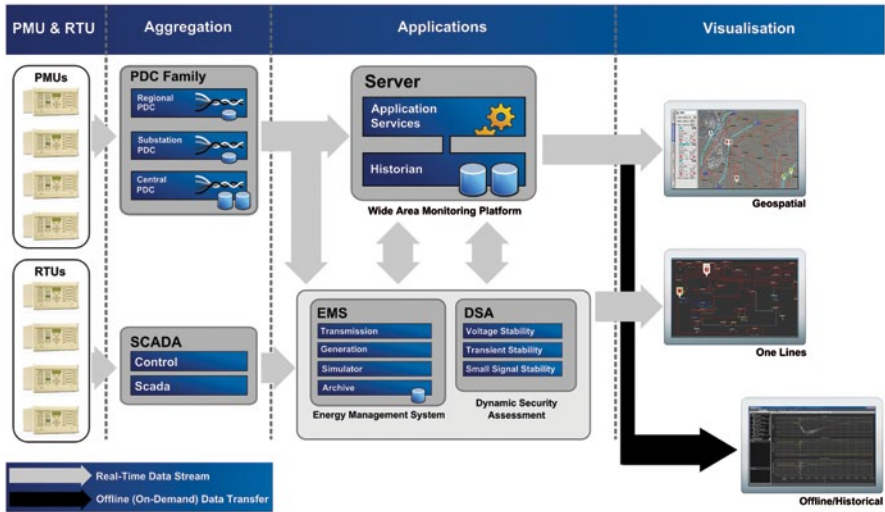


Fig. 8.2 PMU–PDC and application integration layers

turbances. This gives the operators a better chance to accurately assess both grid stability and overall stability.

Most utilities are currently considering the following integration layers for monitoring:

- *Measurements*: This may consist of a set of PMUs from different vendors and Intelligent Electronic Devices (IEDs) passing information to a Phasor Data Concentrator (PDC) at the substation level.
- *Data processing*: This involves analysis algorithms applied to incoming data to extract information such as oscillation frequency and damping, and disturbance event occurrence and impact. The information is displayed and stored by the WAMS Datacenter, and can be forwarded to the EMS or other clients.
- *Data management*: This consists of information being accessed normally via dedicated communications using a variety of protocols to exchange information between several databases, data archiving systems, planning model validation programs, SCADA systems, and SE systems.

The accuracy of PMU data has been considered in some detail, relating to the PMU processing itself and the instrumentation channels. While the hardware solution is not being completely discarded, there are software alternatives now under consideration in the North American Synchrophasor Project (NASPI) consortium. A lot has been learned from the off-line applications experiences in the PMU/PDC environments. This can be seen as the first step towards online applications.

Figure 8.2 details the different integration layers and the data management tools available to the EMS.

8.3.5.2 Emerging PMU Standards

As PMUs become mainstream technology, there is a need for industry standards around performance and data exchange to ensure measurement accuracy and interoperability across different manufacturer offerings. Since 2005, IEEE C37.118 had been the de facto standard for real-time synchrophasor data exchange between PMUs, PDCs, data management systems, and applications. The standard was updated in 2011, and its component parts C37.118.1 and C37.118.2 now dictate the requirements for synchrophasors.

In particular, the C37.118.1-2011 addresses the measurement aspects for phasor, frequency, and rate-of-change of frequency (ROCOF)—it retains the steady-state requirements from the 2005 standard, and adds performance requirements for dynamic conditions. Additionally, it distinguishes these requirements between “M-class” (i.e., analytic applications that could be adversely effected by aliased signals and do not require the fastest reporting speed) and “P-class” (i.e., protection applications requiring fast response). The C37.118.2 addresses the communication aspects for synchrophasor data exchange.

Similarly, the recently developed IEC 61850-90-5 report on Routed Generic Object Oriented Substation Event (GOOSE) and Sample Value (SV) datasets is an upgrade to the IEC 61850 GOOSE and SV profiles respectively to accommodate synchrophasor measurements. The GOOSE is a user-defined dataset that is sent primarily on detection of a change of any value in the dataset. SV is also a user-defined dataset; however, the data are streamed at a user-defined rate (e.g., the reporting rate of the synchrophasors). The new profile takes either a GOOSE or SV dataset and wraps it in a UDP/Multi-cast IP wrapper. Security is a key element in any communication system. To this end, the 90-5 profile implements authentication of a transmitted message and optional encryption of the same message (Parashar et al. 2012).

8.3.5.3 PMU Allocation, Redundancy, and Communication Cost

As utilities transition from Research and Development (R&D)-grade PMU installations to production-grade deployments, some issues that need to be addressed include:

- Resource allocation
- System redundancy
- Data quality
- High-speed communication facilities
- PMU–PDC communication backup for failures

For wide-area control, a redundant set of measurements is desirable so that, in the event of the failure of one PMU, other adjacent PMUs and information from connected devices can provide reasonable results.

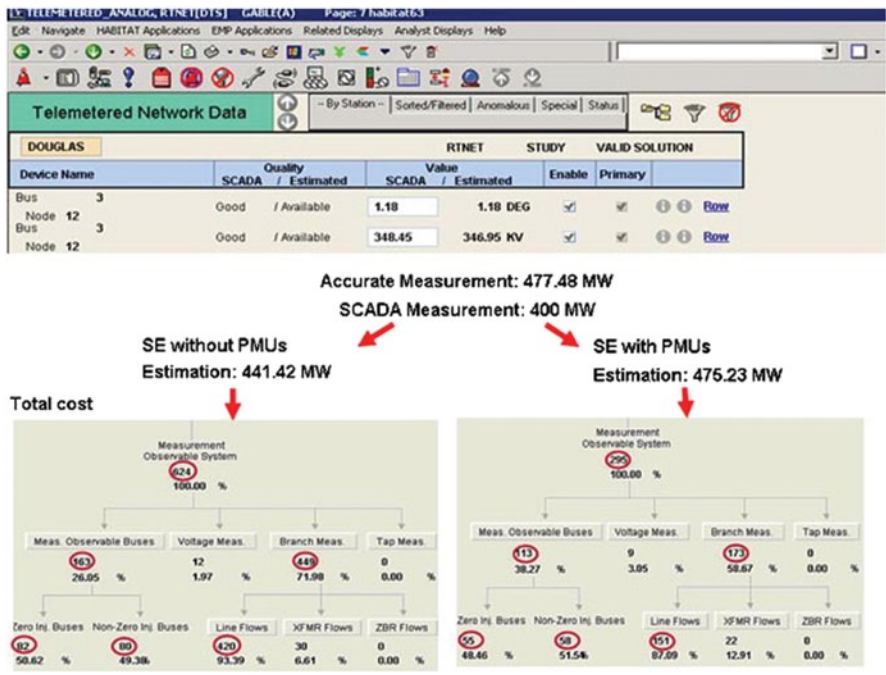


Fig. 8.3 PMU impact on state estimation

The PMU allocation problem is being analyzed in order to determine a meaningful allocation standard. Such a standard will seek to minimize the costs of communications while maximizing the ability to leverage the EMS applications particularly the SE. Some of the allocation tests seek to find a baseline through graph theory, observability (Baldwin et al. 1993; Nuqui and Phadke 2002; Xu and Abur 2004), and the costs of communication. Other utilities focus on oscillation patterns to improve the system damping as part of the wide-area stabilization process.

Regardless of the scope of the work, there is a tendency now to allocate the devices as if they were building blocks that will remain in the same place along the installation plan. In the end, however, PMU allocation will likely be constrained by the installation and communications cost.

Several studies have been conducted and the findings are under consideration to evaluate the benefit of the synchronized measurements in SE. The study results are very positive and as the number of PMUs increases a better accuracy of SE results are expected. Figure 8.3 shows a sample of a process during the benefit analysis of SE with and without PMU devices.

8.4 Techniques for Improving the Reliability of Power Grid Operations

8.4.1 *Direct Stability Measurements and PMU-Based Analytics*

The advent and growth of PMU data at the control center has spawned a new suite of purely measurement-based synchrophasor analytics. This paves the path to being able to monitor and analyze grid behavior at a sub-second rate, which in turn makes online grid stability analysis a practical reality. Furthermore, these applications do not have the overhead burden of the large network model (along with uncertainties in the model data and SCADA data), but rather are based on digital signal processing techniques to characterize the power grid's dynamic behavior. Operational benefits of adding synchrophasor applications at the control center include:

- Maximizing utilization of existing transmission capacity by confidently operating the grid closer to its actual, “true” operating limit
- Providing an early warning system to quickly identify grid disturbances to guard against blackouts
- Monitoring for undesirable grid dynamics and oscillations
- Identifying islanding conditions
- Enabling efficient forensic post-disturbance analysis to find out what just happened, where, and why

Some of the emerging PMU-based analytics are discussed below.

8.4.1.1 Phase Angle Separation to Assess Steady-State Stress

Using “phase angle differences” within an expression of stability margins (as opposed to just megawatt, MW, flows) is a more direct indicator of grid stress between key source and sink regions, for two reasons. Firstly, because it not just monitors MW flow problems but also encapsulates impedance changes due to line outages which weaken the transmission paths. Secondly, noting that stability-constrained corridors are not simple impedances, but include loads and power injections along the length of the corridor, the angle difference is a useful indication of the overall loading of the corridor and the effect of this loading on the physical stability limit. In practice, it can be beneficial to introduce angle difference limits in combination with power limits, so that the power limit can be exceeded if the angle is within the boundary (Fig. 8.4).

A scenario that has been studied for power-angle constraints is related to a Transient Stability (TS) constraint in a corridor that has a large infeed of low-inertia renewable energy that contributes to power flow without participating in the TS problem. Some indicative results suggest 10–12% uplift in the TS limit could be achieved through the use of the power-angle constraint (Wang et al. 2014).

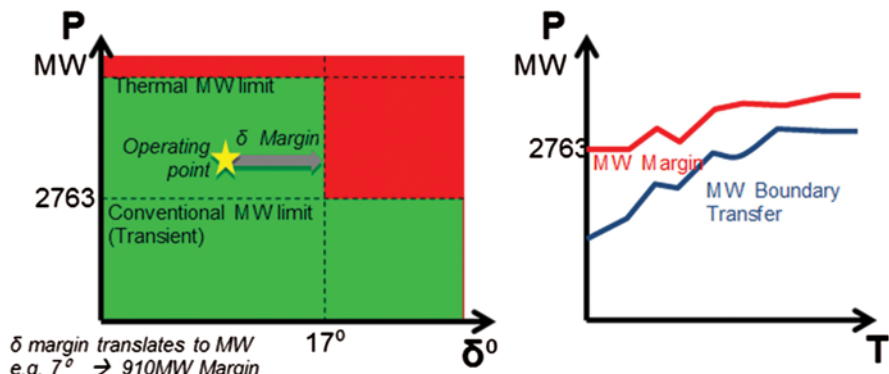


Fig. 8.4 Operating constraints based on angle difference and power, showing *operating point* and *margins*

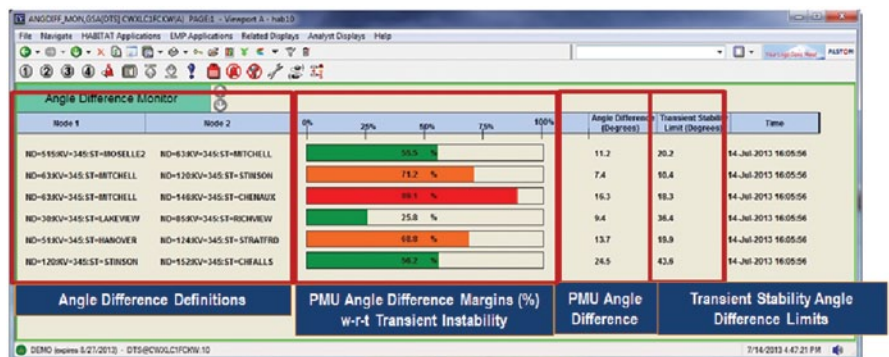


Fig. 8.5 Angle difference monitoring: against the EMS transient stability limits

Increased MW flows or weakening of transmission paths both result in greater stress on the grid. Additionally, since topology changes are reflected in the monitored angle differences themselves, the angle limit will tend to be more constant than the limit based on summation of MW flows. The traditional approach of prorating the MW limits to account for outages on the grid is therefore no longer necessary when moving to an “angle difference” approach; this is a significant benefit to managing and operating the grid more reliably and effectively (Fig. 8.5).

8.4.1.2 Oscillation Monitoring

The power grid experiences a variety of power oscillations, including:

- Slow-power oscillations related to governors or improperly tuned AGC bias (typically 10–100 s period, or 0.01–0.1 Hz)

- Inter-area electromechanical power oscillations (typically 1–5 s period, or 0.2–1.0 Hz)
- Power plant and individual generator oscillations
- Wind turbine torsional oscillations (usually about 1.5–2.5 Hz)
- Control issues in generator, SVC, and High-Voltage Direct Current (HVDC) systems
- Steam generator torsional oscillations (about 5–50 Hz, etc.)

Grid oscillations are always present. If the system is stable, normal power imbalances excite oscillations that are damped and return to a steady state. However, oscillations can become negatively damped and grow in amplitude. The growing oscillations can result from power system stress, unusual operating conditions, or failed controllers (PSS, excitation, etc.), or unintended control interactions between devices in the network. Also, cyclical mechanical power or local control instability can inject a forced oscillations into the grid, which can be amplified through the network if it coincides with a network oscillation.

Growing power oscillations can cause line opening and generator tripping, and in the worst case, lead to cascading power blackouts. Another risk is that the interactions between oscillations can lead to major equipment damage. One interaction phenomenon is sub-synchronous resonance when a generator torsional oscillation resonates with the LC circuit natural frequency of series compensated lines, and there is a risk of breaking a generator shaft or causing large over-voltages on the transmission system. Recently, a similar interaction between wind farm control and series compensated lines was observed, known as sub-synchronous control interaction. Higher-frequency phenomena can be added to a WAMS system, but may require adapted measurements.

With PMU measurements, it is possible to characterize the stability of the various oscillatory modes in real time based on the reaction of the power grid to random perturbations in loads or generation (Fig. 8.6). The information provided by such a measurement-based application is analogous to eigenvalue analysis of dynamic models and includes:

- Mode frequency, amplitude (energy), and damping trends (which are useful indicators of power-system stress, usually declining with increased load or reduced grid capacity)
- Mode shape information, typically presented on a geographic display (to identify observability of that mode across the power grid)

The lower-frequency dynamics, typically up to 10 Hz phenomena, can be extracted from standard PMU measurements. Also, the sources contributing to poor damping can be found from measurements (Arango et al. 2010; Al-Ashwal et al. 2014).

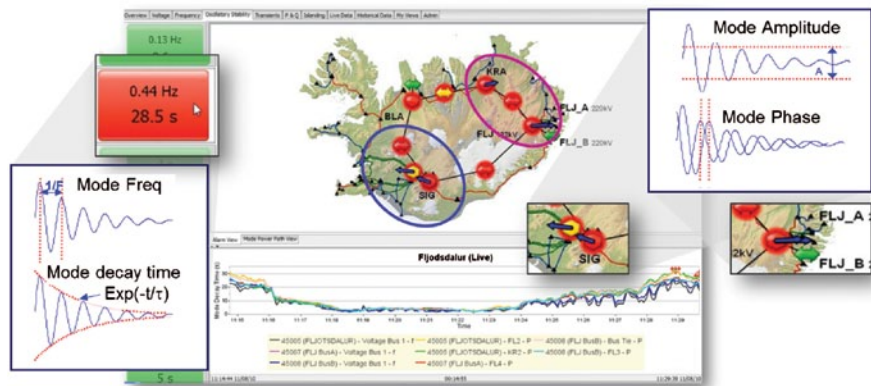


Fig. 8.6 Oscillatory stability monitoring and visualization in the control room

8.4.1.3 Islanding Detection, Resynchronization, and Blackstart

The cardinal symptoms of electrical separation of parts of a power system include: (1) a sustained difference in the frequency across the system and (2) freely rotating phase angles.

PMU-based voltage phasor measurements, together with frequency measurements, can provide an immediate indication of the separation of a system into two or more electrical islands. They can also provide valuable information for operators to prepare the system for resynchronization and supervise the process of synchronizing the system and subsequent network strengthening. It is very useful for operators to have a supervisory indication of the frequency and angle so that islands can be balanced before a resynchronization is attempted. It is also useful for immediate diagnosis if the check-sync relay fails to close, or if the breaker reopens.

This PMU-based geographic view of the system is also useful in the blackstart process. A blackstart plan normally involves energizing the system from a few generators at strategic positions in the grid, then re-energizing the network islands around the generators and finally reconnecting the islands. The network can be quite insecure during this process, and view of the stability of frequency and angle in real time is valuable (Fig. 8.7).

8.4.1.4 System Disturbance Detection and Characterization

PMU measurements make it possible to promptly detect sudden disturbances on the grid and to identify the nearest points of measurement to the source of the disturbance. Such a disturbance could be a trip of a major generator, loss of a major load, or a line trip. Because of the inertia of rotating machines, angles of generators

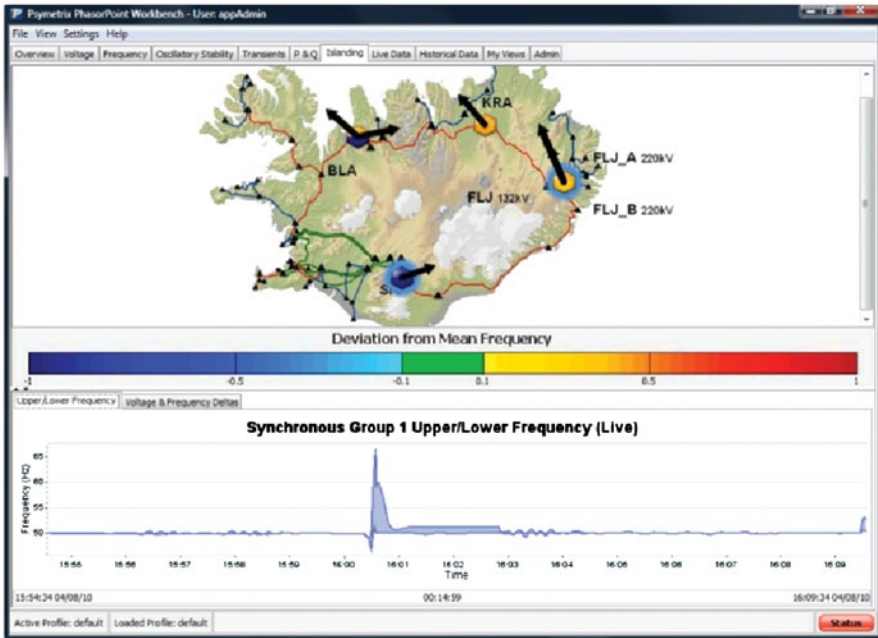


Fig. 8.7 Islanding visualization in the control room

cannot change instantaneously, and the angles and instantaneous frequency will change more rapidly close to the source of a problem than at a distant location.

Furthermore, based on the emerging frequency and phase angle patterns following the disturbance, it is possible to characterize it as a line trip or a generator/load loss. In the case of generator trip or load loss, it is also possible to quantify the MW amount based on drop in frequency shortly after the event. Such applications are also capable of triggering event data captures with a user-defined pre- and post-event period, which are automatically stored in the long-term event storage archive for post-disturbance analysis.

Even if such disturbances may occur outside the utility’s jurisdictional footprint, since the grid is interconnected, the impact is felt across the entire power system. Hence, such a PMU-based application is especially valuable to grid operators as it provides observability across the larger system, for which traditional SCADA measurements may not be available.

8.4.1.5 Voltage Stability (VS) Monitoring

A wide variety of purely PMU-based VS indices that serve as a measure of the proximity to the voltage instability (degree of system stability) have been proposed. In principle, such a stability index maps the current system state into a single (usually

scalar) value with a predictable shape that can be monitored as system operating conditions and parameters change (Parniani et al. 2006). Some of these approaches include:

- Monitoring voltage magnitudes at critical locations (i.e., key load center and bulk transmission buses): This is the simplest approach and consists of monitoring voltage magnitudes at critical locations and their comparison with predetermined thresholds. Voltage magnitude is not a good indicator of the security margin available at an operating point. However, when the system enters an emergency situation low voltage of the affected buses is the first indication of an approaching collapse.
- Sensitivity-based VS indices: These indices relate changes in some system quantities to the changes in others, such as a change in voltage magnitude per change in MW/MVAr flows, which can directly be computed by tracking the PMU measurements.
- VS indices derived from Thévenin impedance matching condition (Vu et al. 1999): They measure stability degree of individual load buses (or a transmission corridor) by monitoring the equivalent Thévenin impedance of the system and equivalent impedance of local load (magnitude of these values are equal at the voltage instability point). Furthermore, stability degree can be expressed in terms of local voltage magnitude and voltage drop across the transmission path as well as in terms of power margin (MW or MVA). The use of these indices must in some way address contingencies, as the impedance can instantaneously change by nearby generation or voltage support tripping.
- Reactive power reserve monitoring: A considerable decrease in reactive power reserves of system's key generators is a good indicator of system stress. Computation of reactive power reserves requires placement of measurement devices at several locations, does not require system model, and in principle can make use of both SCADA and PMU-based measurements (Bao et al. 2003).
- Singular Value Decomposition (SVD) applied to a measurement matrix: This approach focuses on computing and tracking the largest singular value of the matrix. Measurement matrix is constructed from PMU measurements such that each column is a stacked vector of the available PMU measurements over a time window (two to three times the number of available PMUs; Overbye et al. 2010).

8.4.2 Positive Impacts of PMUs on the EMS

Integration of the new synchrophasor solutions with modern-day EMS analytics is our best promise for implementing a practical production-grade online stability solution at the EMS.

In Fig. 8.8, on the left, we have the traditional EMS analytics (SCADA, State Estimator, etc.) that have been developed over the past 5 decades. More recently, we have integrated “model-based” stability analytics which use the network model and the State Estimator solution to run dynamic stability studies. These are called Dy-

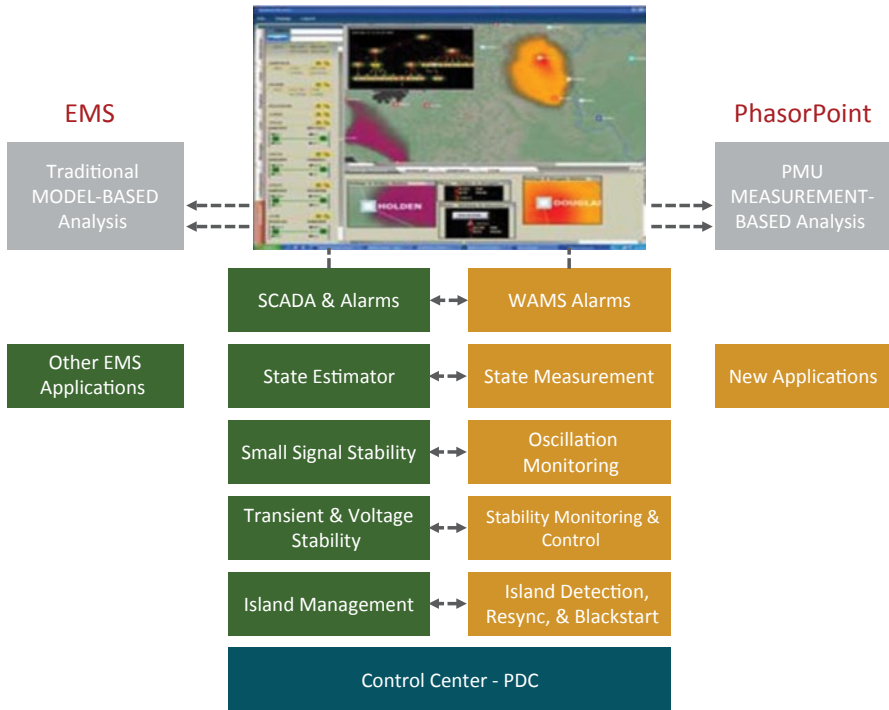


Fig. 8.8 The next-generation energy management system

dynamic Security Assessment (DSA) and include assessments of Small-Signal Stability (SSS), VS, and TS. These have traditionally been off-line planning functions since they are computationally very intensive. More recently, with faster computing processors, algorithmic approach changes and DSA software performance enhancements, these functions have migrated into the online EMS and can now run in “close to real time,” with the advantage of assessing stability risks and constraints based on the actual operating conditions rather than conservative planning assumptions.

8.4.2.1 PMUs in State Estimation

The most immediate benefit of combining PMUs with model-based applications is the use of the PMU data to improve the accuracy of existing topologies and State Estimators (SEs). This benefit can be used as a migration path towards more comprehensive installations. The operators see the benefits at the monitoring levels so they wish to use the information as much as possible to get better solutions. SE is capable of running at the scan rate at the substation level and less frequently at the wide-area control center level. This is done in order to assess the stability of the grid with the latest information from the field. PMU technology has the potential for a positive impact on SE in a number of key areas including:

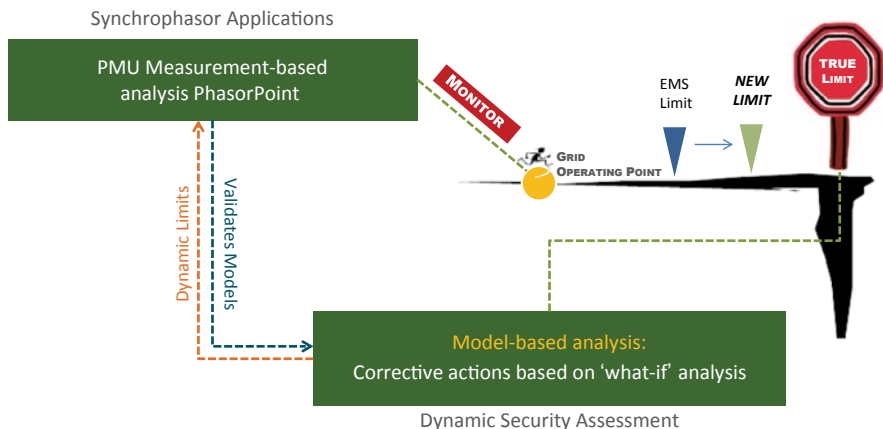


Fig. 8.9 Integrating PMU measurement-based analysis with model-based DSA applications

- Increased observability
- Improved solution accuracy
- Improved convergence
- Improved detection of bad data

More recently, a purely PMU-based State Estimator has been implemented for entities that have complete PMU observability for all or a portion of their transmission network. Since this is a linear problem, this Linear State Estimator (LSE) can operate at sub-second rate of the incoming PMU data and towards dynamic state estimation.

8.4.2.2 Integrated PMU Measurement-Based and Model-Based Stability Analysis

Figure 8.9 illustrates how the model-based and measurement-based analytics work together for congestion management. The synchrophasor applications tell you what the current operating state is and track its changing behavior at sub-second rates. The operator wants to know how far the current state is from the edge of the cliff or the limit at which the grid would collapse—this is called the “true limit.” This “true limit” typically reflects the post-contingency operating conditions (i.e., N-1 scenario), and is therefore determined by the EMS model-based DSA tools since they are based on a network model and can perform what-if studies to increase loading and stress on the grid till its point of collapse. Traditionally, estimates of the “true limit” have come from off-line planning studies and on “worse-case scenarios” to accommodate a wide range of conceivable operating conditions and system contingencies. Furthermore, a safety margin is required to establish the “EMS limit” since the model which was used to calculate the limit has inaccuracies and uses

conservative assumptions. For these very reasons, these operating limits tend to be overly conservative which only means that existing transmission assets are not being utilized at their full capabilities.

By running the DSA tools in real time based on the most recent “State Estimator” solution (i.e., current operating conditions), we are able to eliminate some of the uncertainties, and therefore imply less conservative limits.

The new limit based on real-time measurements combined with real-time model-based analysis can be less conservative for a number of reasons:

- The DSA limits are based on a real-time stability assessment (as opposed to an off-line planning study) and reflect the current operating condition.
- The measurement is more directly related to the physical phenomenon, such as angle measurements being a more direct measure of TS than MW.
- The dynamics analysis extracted from measurements relate to the actual dynamic condition of the grid and reduce uncertainties implicit in the model (e.g., whether equipment and control is operating correctly, nature of the load model, etc.).
- Actions can be defined that respond to emerging threats at an early stage, while conventional systems require a longer time frame to design a response. A shorter look-ahead time period means less conservatism in the volatility assumed between the study time and real time.

The ultimate goal is closed-loop wide-area control and protection of the grid. Current grid stability applications estimate the control signals and send them to the devices that are very far apart geographically. This type of operation can be problematic. As an alternative, it may be more efficient to concentrate on reduced portions of the network and extend the findings to wide-area implementations, at least until better and faster communication facilities are available.

8.4.2.3 Monitoring the System State

The proper use of early warning signals (Bhargava et al. 2004), dynamic simulations, and visualizations will permit operators to quickly take actions to prevent and/or correct imminent systems problems.

The following modes are suggested for wide-area systems analysis time horizons:

- On-line wide-area monitoring of current states
- System state predictions
- Planning analyses

8.4.2.3.1 Online Wide-Area Monitoring of Current States

The ability to model and simulate grid behavior over a wide range of time domains, frequency domains, and topological resolutions needs to be developed.

The applications comprise fast, dynamic tools for transient (angle) variations, VS changes, and long-term dynamics to simulate all sorts of power plants and nonlinear devices on the grid. The consideration of fast-time domain techniques, such as quasi-dynamic simulations, may help to evaluate cascading and islanding during a system recovery. The EMS will take periodic grid snapshots to update the network topology and provide information for dynamic simulation and assessment.

The extent of the network topology to be modeled needs to be adapted to handle a wide range of structures, such as RTOs, stability coordinators, transmission operators, and others. The proper identification of events and conditions in the system should trigger the right time frame over which the appropriate dynamic simulation and modeling are needed. The use of synchronized information and processing is synonymous with wide-area monitoring.

8.4.2.3.2 System State Predictions

There is definitely a need to be able to predict where the system will go before the control actions are deployed (Khatib et al. 2004). A simulation environment should be available using real-time information from the EMS in addition to historical data recordings that can be fed into the dynamic simulation. The accuracy of the system state prediction simulation environment depends on how reliable the schedules and limits are in the short-term time frame. Under catastrophic conditions, a few minutes in advance may help to significantly reduce the risks of system failure.

For fast-state prediction simulation, a change of simulation scope and region of interest may help. The state prediction could be triggered automatically or on demand to assess control movements and reconfiguration plans during disturbances. In this way, a lot of potential problems can be identified. For emergency situations, a model including only the measurements that can be delivered to the control center in the shortest possible time is required. These measurements may include items such as:

- Important generator outputs
- Frequency and voltage measurements
- Important flow measurements
- Important new measurements (angle measurements)
- Information and recent recordings

One of the goals of the system prediction environment is to estimate where the system is heading and what the stability level is going to be (Samuel et al. 1994; Savulescu 2004) when it gets there. If the events that created the condition (energy imbalance) are known, the angular and VS assessment simulation could be used to avoid further cascading (that otherwise could drive the system to total collapse). The purpose of the state prediction is to assess the long-time condition (within approximately one hour or so) before the system would reach a state where voltages might collapse and generators might lose synchronism.

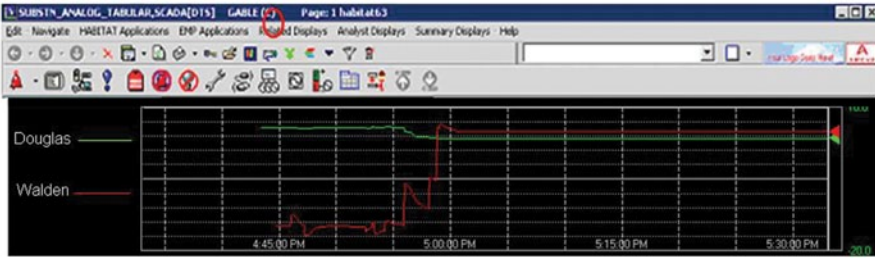


Fig. 8.10 System prediction information

Dangerous states could trigger alarms in advance. Recent SE snapshots combined with time-domain analysis and historical information could provide a good opportunity to exploit consecutive snapshots and identify any system trends. After the system prediction is done, the operator would be in a position to identify:

- Grid stability after large disturbances
- Grid movements towards unstable conditions

Figure 8.10 provides the look of the angular trend between two selected points (PMU) after the occurrence of an unanticipated outage (prediction) while the grid is experiencing heavy traffic. The substations and monitored points can be selected in advance.

8.4.2.3.3 Planning Analyses

Analytical applications run in study-mode environments and can be used as stand-alone models or incorporated into network sequence studies. The study tool is used to prepare cases, perform validations, and update the bus-branch model based on “what-if” conditions from the latest power flow results.

The study mode can be initialized from real-time snapshots or previous cases, as long as the models are consistent; otherwise, the validation task will reject the execution. The planning horizon studies are prepared using the corresponding time-point models and topologies in the study network sequences. Then a number of executions are performed and the corresponding output results are saved back to the EMS.

PMUs are of immense benefit to the planners as well. Specifically, the dynamic observability they provide along with the precise time synchronization is very valuable for after-the-fact postmortem analysis of system disturbances to identify sequence of events and associated root causes, as well as assesses power system performance and response following the events.

The synchrophasor-based observations during such disturbances are equally useful for dynamic model validation, as they offer valuable feedback to validate and fine-tune the dynamic models such that the model-based reconstructions of



Fig. 8.11 Dynamic model validation using synchrophasor measurements (left), along with simulated reconstructions (right)

these system events closely match the actual grid performance captured by PMUs. Figure 8.11 shows how synchrophasor measurements, along with simulated reconstructions of the disturbance, can be utilized in an off-line mode to verify the dynamic models.

When there is a clear discrepancy in the time domain, a modal decomposition is useful in identifying the particular mode(s) contributing to the mismatch, and the associated mode shape is helpful in identifying a particular power system element that needs validation. For example, in Fig. 8.11, the discrepancy shown can be attributed to a 1.07-Hz local mode where a positive damping (5.59%) has been identified from the measurement recording, while a negative damping (−0.73%) is indicated from the corresponding simulations.

8.4.2.4 Dynamic Stability State Assessment

PMU data can be analyzed and preprocessed to notify the operator about rapid changes in any of the measured electrical variables. These rapid changes could trigger recording devices to start capturing data at a faster rate and the EMS applications could be engaged. This would provide the operator with recommendations for preventive/corrective actions (Pavella et al. 1999).

The following warning signals are available at specific PMU locations:

- Sustained frequency oscillations
- Excessive angular deviations between pairs of nodes on the grid
- Slow voltage decline
- Sudden voltage dip

- Sudden current change
- Sudden current dip
- Fast frequency decline and rate
- Sudden change of active/reactive flows

8.4.2.5 Automated System Restoration

Automated system restoration has been an objective of many utilities in the past, and very recently (since the August 2003 blackout) it has been the focus of studies to avoid cascading events and even total system collapses. System recovery depends very much on the topological structure. Modern short-term, mid-term, and long-term applications provide enough simulation to support intelligent grid control actions and to avoid cascading incidents, although, again, the communications component is really the big issue in the wide-area context.

8.4.3 Online Dynamic Stability Assessment Techniques

Today's VS and TS tools (Giri and Avila-Rosales 2000; Kundur et al. 1999) are designed for online as well as off-line applications.

The voltage tools perform stability assessments using static analysis techniques. For any number of given scenarios, they determine the VS of the base case (operating point), for the given contingencies, solution/control parameters, and stability criteria (stability margin, voltage profile, and volt-amperes reactive (VAR) reserve). In addition, for each scenario that includes a transaction (power transfer from a source to a sink) it can determine the VS limit of the transaction's increase or decrease. Contingency screening and remedial action capabilities are also available.

The transient application performs stability assessments via nonlinear time-domain simulation techniques (Avila-Rosales et al. 2000). In addition, a number of post-simulation analyses can be carried out to assess the various forms of TS, including angle stability, damping, transient voltage and frequency stability, and relay margins. It can even process multiple contingencies and multiple study scenarios in a single session. Similar to its voltage counterpart, power transfer limits in defined transactions can be determined automatically. Further, these determinations comply with all forms of stability requirements.

Dynamic applications are designed to provide the operator a set of stability indices to assess the overall system stability and to provide early warnings of problems. These are all based on fast and accurate time-domain simulations (Kundur et al. 1998).

Under normal conditions, angular and voltage transient simulations provide the stability margin for a set of energy transactions and flow gates ("from and to" locations on the grid). The margins are used to determine control recommendations to maximize grid stability, while ensuring market rule compliance and maintaining sufficient active/reactive power reserves.

Small-signal analysis contributes with measurements taken to identify oscillation problems and parameter tuning to increase the system damping for certain contingencies (Kundur and Wang 2002). These early warnings help the operator to:

- Measure the impact of any event and the current stability status (sort of red, yellow, blue, and green light indicators)
- Evaluate the overall thermal, transient, voltage, and frequency limits and provide recommendations to reduce the risks of operation

8.4.3.1 Wide-Area Stability Modes

Dynamic stability assessment has always played an important role in systems operations. It has also been one of the most computationally intensive calculations in any control center. Utilities are now demanding tools that can address the challenges of competitive markets, while providing the same reliable operations as a full EMS. Specifically, utilities are requiring tools to address static and dynamic stability power system challenges. The advent of independent power producers (IPPs), multiparty energy transactions, increased transaction volumes, and new energy routing routines requires system operators to put a great emphasis on voltage control and stability changes.

The analysis of the current operating condition, immediate future, and several time points in advance for large systems is becoming more of an issue every day. This level of work imposes additional computational challenges, which are affected by model accuracy, solution techniques, and systems architecture. There is clearly a need for three frames of analysis to assess stability, and they are usually defined as modes of operation.

All modes depend on efficient communication and data transfer from the EMS hardware to all of the other platforms and machines. Each mode requires the validation and input/output data processing between the EMS and dedicated machines for stability; the following are some of the features:

- Data validation
- Data exchange between all dynamic engines and the EMS
- Output results and visualizations
- User interfaces and operations
- Multiprocessing system configurations

The triggering and data exchange operations between the dynamic engines and the EMS are controlled and coordinated by applications. All input data for voltage and TS are sent automatically (or upon request) to the selected dynamic parties for evaluation. A function constantly checks the availability of the results in order to retrieve the proper information from the dynamic machines. The coordinator ships the network snapshots and specific data once a validation process is executed. Multiuser capabilities can be performed since there is a unique relation between the coordinator and the corresponding dynamic instances. The coordinator knows what to send to whom and when to get the results back to the EMS.

8.4.3.2 Online Dynamic Triggering

A real-time version of the dynamic coordinator is available as part of the EMS' on-line sequence. This execution can be enabled or disabled from the real-time network analysis control panel. It executes on a schedule (which can be defined by the user) provided that the SE solution is valid. A function has been added to the coordinator for the purpose of exporting a bus-branch model to all dynamic engines, since the EMS is based on a node-breaker model.

The latest topology changes are reflected on the exported network snapshot. The use of web-based user interface tools (and the viewer tools available on the dynamic side) reduces the amount of data transferred back to the EMS since they are maintained until the next online execution takes place. The operating horizon, which starts in the next hour, covers the immediate short term. The planning horizon starts after the operating horizon and continues into the future. The coordinator does not allow entries from the user unless a new network model is put online.

8.4.3.3 Dynamic Stability System Configuration

The dynamic client/server configuration allows for distributed computing of any number of scenarios on any number of CPUs. The clients communicate with the EMS to receive the data and return the results. The clients also coordinate the servers for the parallel processing of scenarios received from the EMS. The overhead for distributed processing is very small and additional server machines/CPU's can be easily added to the cluster for increased computational speed.

8.4.3.4 Dynamic Stability Validation

Dynamic applications require a network model, monitored elements, selected outputs (units, branches, and buses), and transaction specification (source and sink definition, step, type, and load options). In addition, certain specific data are required for each application.

Before the dynamic applications are executed, there is a full validation that takes place to make sure the dynamic parameters and allocations are updated with the latest topology changes. The validation function validates the content of the entire dataset against the existing network contingency and translation table to maintain user-oriented descriptions. The translation table, which is automatically updated during every run, maps the EMS node-breaker model to the bus-branch model used by the dynamic engines.

Since no dynamic data are maintained on the EMS side, the bus, unit, and load sections of the translation tables must be such that the locations of the buses, the generators, and the other dynamic devices match with the numbers used in the dynamic data files.

8.4.3.5 Data Exchange Between Dynamic Analysis and the EMS

The data exchange function sends the dynamic oriented data, the network snapshots (created by either SE or power flow), the contingency data, and the translation tables in the format specified by the dynamic engines.

A shared space is used as the central location from where the EMS and the dynamic engines can exchange information; each dynamic task is tied to a PC on which the dynamic client programs run. When the dynamic executions are triggered, the clients coordinate the computation of the scenarios on available servers. A user-friendly configuration setup avoids concurrency problems. The data exchange function consists of tasks for the creation of the dynamic related files and the shipment of all files and the network snapshots to the selected systems.

8.4.3.6 Data Retrieval and Saved Scenarios

Data retrieval (or copy) is possible from real time or any other system as long as the model is the same. In particular, network data, contingency data, dynamic scenario data, and translation data can be copied from other EMS applications. Once the user executes a scenario, that user can create a saved scenario for further analysis or simply to share the information with others.

8.4.3.7 Data Exchange Definition

Data exchange is defined as the description of the current scenario, dynamic data, PC where the dynamic engine is running, and some parameters associated with waiting (and timeouts) to get results back from the dynamic tasks and out to the EMS.

8.4.3.8 Preventive/Corrective Control Recommendations

The dynamic results are posted to EMS displays with the latest status and execution flags, times of the latest executions, and plans for preventive and corrective actions based on sensitivity calculations. Most of the information can be viewed on the dynamic boxes from the EMS. The most important results are available on the dynamic machine's main windows. Output results and specific data can be transferred on request from the EMS.

8.4.3.9 Steady-State Stability Assessment

For a recent EMS project, a real-time steady-state stability analysis tool has been integrated into the online EMS environment (Avila-Rosales et al. 2004; Savulescu

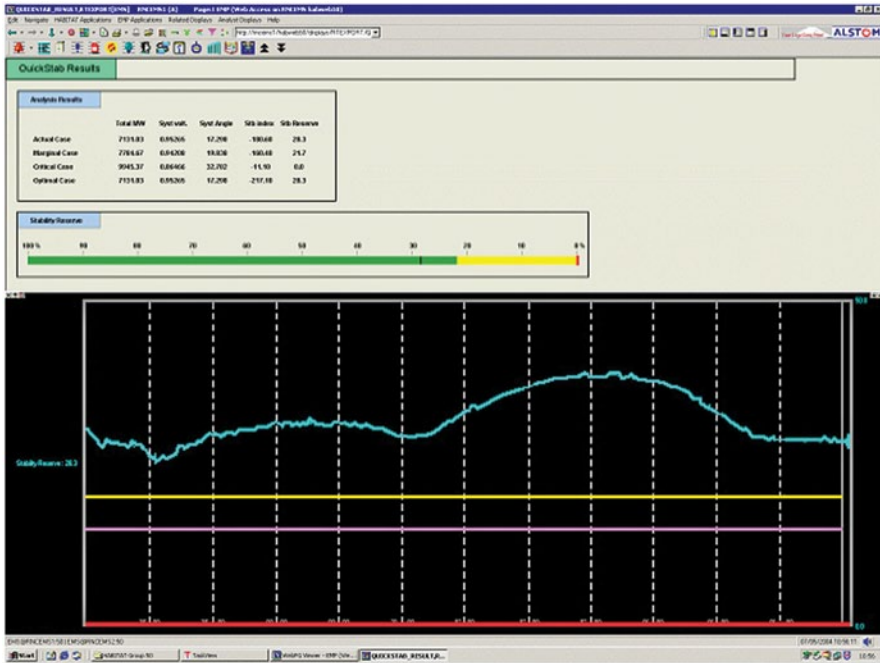


Fig. 8.12 Real-time trending of the steady-state stability margin

2004). This analysis gives the operator information on how far the system is from the critical state and also calculates a stability reserve index in percentages.

After a successful SE execution, a snapshot file in a standard format (PSS/E) is created. This file together with a local dynamic data file for generator characteristics is used as input data for the steady-state stability application. This application predicts the maximum power transfer (or MW load-ability) of the transmission network and computes the distance to the critical state where steady-state instability occurs. The distances to the stability margin state (user specified margin) and the optimal state (re-dispatching of generation to maximize the distance to critical state) are also evaluated.

Relevant information for the EMS operator is summarized in a results table display and in a bar chart providing a graphical indication of the current stability reserve as displayed in Fig. 8.12. A trend of the stability indices over several hours is also provided and provides very useful information about the stability evolution over time. This allows operators to anticipate critical systems instability conditions. Furthermore, after each analysis an alarm is sounded if the stability reserve percentage is below a user-specified danger level.

8.4.4 Wide-Area Protection and Control

During normal operations, the focus is always on the economics of the system. However, during an emergency (particularly with cascading conditions), the focus is on control shifts in order to guarantee grid stability. When an abnormal condition/failure is not mitigated or repaired, it can spread and lead to catastrophic conditions. The power system should be prepared to deal with the conditions created by:

- Volatility created by market rules and restructuring
- Uncertainty due to high penetration of intermittent renewables
- Power system operation very close to limits
- Transmission congestion and stressed conditions
- Weak connections
- Unexpected events
- Stability threats
- Hidden failures in protection systems

Any of the above conditions could trigger a catastrophic event, and assuming the system behaves properly the following actions will be taken:

- Monitoring will identify the location of a catastrophic failure.
- Applications will initialize and readjust controls to stop the exacerbation of the failure.
- Special protections will react to reduce the risks to operations.
- Load shedding will commence to maintain acceptable line frequency.

If the power system continues behaving in an unpredictable fashion, dynamic islanding will isolate the troubled area to avoid further grid deterioration

8.4.4.1 Special Protection Systems

The actions taken by these systems are intended to provide uninterrupted power supply by the use of “last defense” methods that should not be initiated under normal conditions. The objective is to maintain power system stability with regard to local conditions and wide-area conditions. These contingencies use data from several locations with a wide-area orientation to handle disturbances.

These systems are designed for the following purposes:

- Detect abnormal contingency system conditions
- Initiate preplanned corrective actions to mitigate the problems
- Provide acceptable system performance

The SPS controllers have some or all of the following characteristics:

- They can be armed/disarmed depending on the system conditions.
- They employ discrete controls and feed forward control laws.

- The control actions are normally predetermined.
- Some form of communication is involved in the control action.

Still, excessive reliance on these schemes may result in stability risks due to:

- Failure to respond
- Unwanted overlap with other protection systems
- Accidental operation

8.4.4.2 Wide-Area Protection and Control with PMUs

Some of the disadvantages of the current SPS systems are the fact that they work only for predefined events. This is where synchrophasor measurements provide a very useful addition to the capability to control the system to operate close to its physical limits, and also to defend the system against separation. They largely allow us to move away from predefined “event-driven” approach towards a “response-driven” approach.

The use of synchrophasor measurement in control and protection application is an expanding field and is likely to play a key role in emerging smart grid solutions.

The basic characteristics that make synchrophasor measurements attractive for protection and control solutions are as follows:

- They form a summary measure of system stress, responding to the loading and impedance between the measured points. This means that control to maintain the operation within its capability can be implemented with much fewer measurement points and communication channels than the alternatives, leading to greater robustness of the scheme.
- Angle measurements are directly related to the angular stability of the power system and its ability to remain in synchronism. The progression of a system separation can clearly be observed using synchrophasor measurements, and an automated response taken to avoid the separation. A particular benefit of using synchrophasors for angular stability, rather than more conventional event-based inter-tripping is that the synchrophasor approach is more general and can respond to unpredictable and complex event sequences.
- Since synchrophasor measurements can be streamed in real time at a rate that reflects the dynamic movement of the power system, it can be useful in improving the transient and oscillatory performance of the power system.

The applications of synchrophasor measurements apply in many different conditions to a wide range of issues. This includes both transmission and distribution applications, and distributed microgrids. Depending on the associated timescales of the grid phenomena (Fig. 8.13), the control scheme can be the following:

- Localized protection (< 200 ms) at the substation where all information is captured at the substation level and is used for local control. These local actions include adjusting equipment settings, taps, power flow controllers, and more.

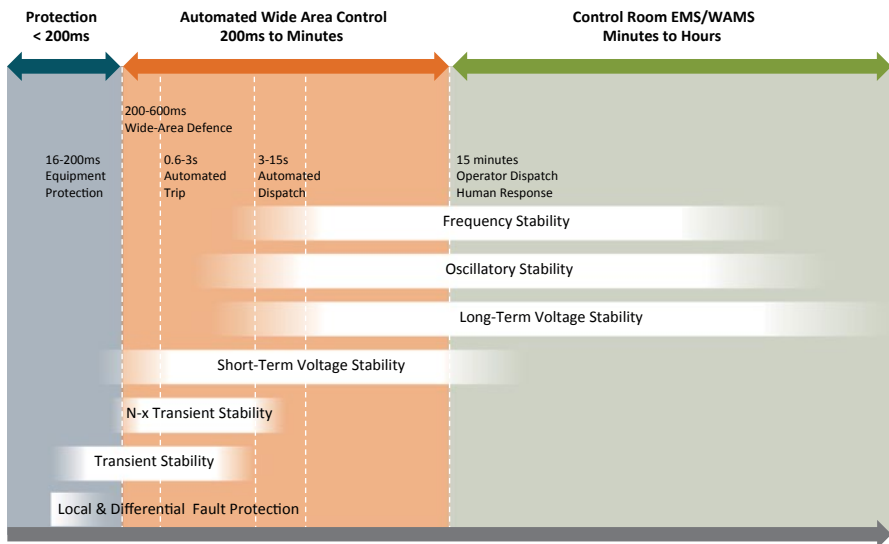


Fig. 8.13 Dynamic grid stability phenomena

- Decentralized synchrophasor-based automated wide-area control scheme (200 ms to minutes) that leverages the time synchronization property of the measurements in combination with fast processing and high speed communication between the substations to assess when a control action is needed.
- Centralized scheme that combines EMS software (including its network model-based analysis capabilities) alongside PMU information to optimize the control action. The dynamic engines are fast enough to assess the stability risks and control action evaluations for a few minutes. Operator or human intervention is likely to be part of such a centralized control scheme with minutes to hours to respond. Examples include re-dispatch to alleviate transmission congestion and/or corrective actions when the power system is operating close to its limits.

The types of control and protection mechanism include slow-speed loading optimization, high-speed stability defense, continuous control process, or discrete triggering. The options for actuation of the control include conventional or renewable generation tripping or continuous control, FACTS/SVC control, HVDC control, and voltage support.

In the various domains in which synchrophasors can be applied to control and protection, it is useful to categorize the problem in terms of:

- Defining the boundary limit: providing an expression of the capability of the relevant corridor that may be a simple angle difference, or a combined expression of measurements that best represents the limiting condition.

- Controlling to the limit: determining the control action applied at the equipment that is available to control, to operate the system up to the boundary limit. This will typically be a relatively slow control.
- Extending the limit: applying discrete or continuous control to manage the outcome of critical events such that the system can be operated beyond the N-1 limit that would apply if the control scheme was not present.

In this section, a number of examples of applications of synchrophasors in control and protection are considered.

8.4.4.2.1 Next Generation of System Integrity Protection Systems

The ability of a power system to return to a stable steady-state condition after a fault is essentially a question of angle stability. The loss of angular stability involves loss of synchronism between areas, typically resulting in an out-of-step condition followed by electrical separation between the areas. Out-of-step operation puts a great deal of stress on the network, as large cycles of electromechanical torque on generators and large voltage swing cycles. Separation across a loaded boundary leads to significant power imbalance in the areas and a risk that the areas affected will black out.

TS limits between areas of the grid is a complex problem, but a parallel can be drawn with a simple case of a single plant losing synchronism with the system. In the case of a single plant, a fault causes acceleration of the plant, and the stability criterion requires that the acceleration and angle difference between the plant to the nearest “strong” part of the network does not exceed the network’s capability to extract the excess kinetic energy of the plant. The plant-to-system case is similar to the classical (but idealized) Equal Area Criterion.

The diagrams in Fig. 8.14 illustrate the basic TS problem, showing that the energy represented by Area A1 that accelerates the rotor during the fault must be less than the energy represented by Area A2 than the network can export following the fault; otherwise the system will lose synchronism. In Fig. 8.14b, the influence of generation inter-tripping is shown, increasing the energy for deceleration of the fast region.

The area-to-area loss of synchronism across several lines is more complex than the plant-to-system case, as the acceleration and angle differences immediately after the fault is cleared are different throughout the group of generators. The dynamics between the generators within the group are important for the system to return to a stable condition.

Although the process can be complex, some key influences on the TS of the boundary are:

- The accelerating energy during the fault-on period, determined by the mechanical power of generators at or close to the critical fault, and the nature of the fault
- The inertia of the area in question
- The pre-fault angle difference between the areas

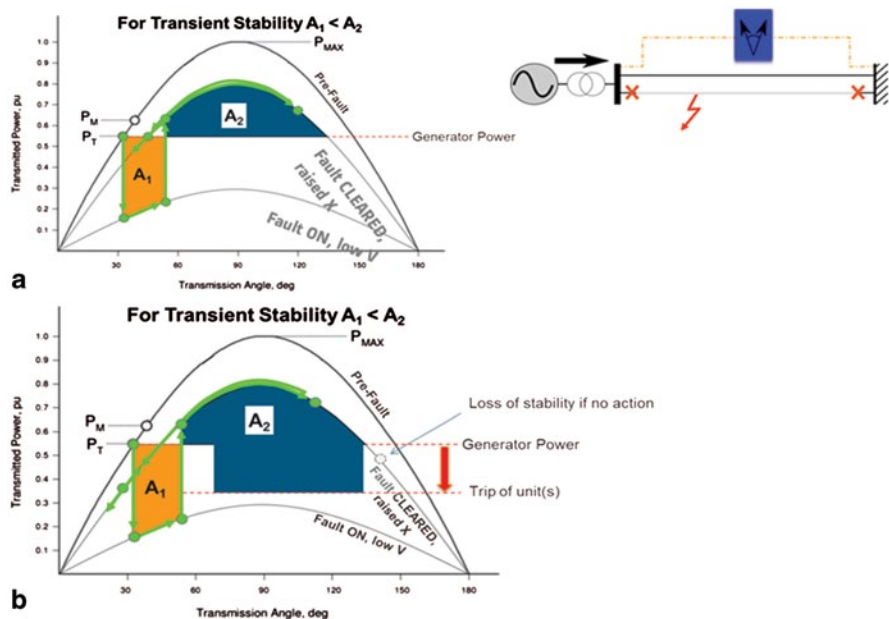


Fig. 8.14 Basic transient stability problem a) without generation shedding and b) with generation shedding

The change in the generation portfolio influences the inertia of the area. With low-inertia renewable generation capacity taking an increasing share of the operational generation mix, there may be less synchronous generation within the area to counteract the acceleration of a generator close to a critical fault. Thus, the rotor angle swings in response to a fault may be greater, and the TS constraint could become more limiting. Thus, the stability characteristics of grids are changing, and transient response is an important consideration.

8.4.4.2.2 Response-Driven Control of TS

As mentioned above, the stability of a system can be improved by inter-tripping generation in the exporting region of the grid. This has the effect of increasing the capability of the network to decelerate the exporting region and therefore pull the area back into synchronism. This is currently achieved through the use of fast-acting inter-tripping mechanisms based on predefined fault criteria. While such schemes have been successfully implemented, there are drawbacks, for example:

- Conventional inter-tripping will be over-responsive, as the worst-case fault scenario must be assumed. Practical faults will almost always be higher impedance than the defining faults which are typically three-phase short circuit at or near large generation. Thus, the scheme will trigger more generation shedding than

actually necessary, and this creates a larger overall disturbance (and therefore risk) to the network.

- Conventional inter-tripping is designed for predefined fault scenarios. However, experience of large-scale disturbances shows that there are often multiple events and complex behavior, and the inter-tripping may not cover all scenarios.

8.4.4.2.3 Response-Driven Versus Event-Driven System Integrity Protection Schemes

In general, System Integrity Protection Schemes (SIPS) can be categorized as event-driven or response-driven. Event-driven action responds to a change of status in the system, such as a breaker opening, and initiates a predefined action. By contrast, a response-driven scheme creates an action that is based on the observed movement of the power system, and the action can be proportionate to the power system response.

To date, SIPS schemes have only been response-driven for relatively slow phenomena such as thermal overload. Stability problems have exclusively been event-driven in order to achieve the speed of response required to avoid separation. The response time for inter-tripping schemes, including the entire time budget from detection of initial triggering event through to the completion of breaker opening, is often required to be <200 ms. It should be noted, however, that loss of synchronism through TS is not always fast, and examples exist of the angular separation occurring 5 s after the fault.

Due to the speed of synchrophasor measurement and the direct representation of a stability problem, it introduces the possibility of response-driven action for stability. A response-driven action is slower than an event-driven action because of the finite time taken by the power system to show an angular separation (because of inertia) and the time window required for sufficiently accurate derivation of a phasor measurement. This means that there is an engineering trade-off between the speed of response achievable by an event-driven scheme and the proportionate response achievable by a response-driven scheme. A practical example of a response-driven stability SIPS is reported in Iceland (Wilson et al. 2013).

It is likely that in future, a new generation of SIPS schemes will emerge that generate a fast-acting initial event-driven response, supplemented by a response-driven component. This hybrid approach would combine the benefits of speed of response and proportionality.

8.4.4.2.4 HVDC Stability Control

There is an increasing trend to deploy HVDC links to augment a constrained Alternating Current (AC) corridor flow. Given the need for more transmission capacity and public resistance to large-scale transmission building, the greater capability of Direct Current (DC) transmission relative to AC transmission for similar visual impact, the choice of HVDC transmission embedded in the AC network can often

be viable. Thus, HVDC transmission is quite frequently located across stability-constrained corridors.

HVDC technology is inherently capable of producing a fast controlled response, and is therefore capable of improving the stability characteristics of the AC system. Thus, the capacity of the AC corridor can be increased through control of the DC link, increasing the total capacity of the corridor.

A stability control capability in an HVDC corridor responds to an acceleration of the exporting region by rapidly increasing power flow from the exporting to the importing region. This has the effect of counteracting the angle difference swing between the regions. Since the critical period in a TS problem is the first swing, occurring typically within a second or two, the short-term rating of the HVDC transmission system would accommodate a substantial control capability.

Synchrophasor measurement is attractive for implementing HVDC stability control because it provides observability of the angle difference across the corridor and can be used to differentiate angle difference swings from local effects. Also, wide-area measurement can be used to introduce a continuous control that not only improves first-swing stability but also improves the damping of subsequent oscillations.

One of the benefits of using HVDC control for TS improvement above generation inter-tripping is that the control does not cause any net change in the power balance of the system. It therefore does not impact the global system frequency. By contrast, an equivalent generator inter-tripping approach results in a frequency drop, and the combination of initial disturbance and inter-trip response must be within the limits of the dimensioning generation loss that the system is designed to withstand.

8.4.4.2.5 Generation Output Control for a Transmission Boundary

Conventionally, a transmission constraint is managed by operational dispatch from the control room. This works well where the changes to load and generation are relatively slow, and there is time for an operator to take a response. However, as the penetration of intermittent renewable generation increases, the changes in power generation can be rapid. Without automated control, it is necessary for the system operator to use a safety margin that accounts for changes that may occur during the time horizon that the operator is not able to respond. Typically, an operational response initiated by an operator can take around 20 min. Thus, the constraint level of a transmission boundary must be de-rated by the extent of volatility that can occur within around 20 min.

A controlled response may be applied such that the renewable generation volatility is contained such that the power transfer is clipped as it reaches the boundary limit. The boundary transfer can be dispatched much closer to the actual boundary capability, with much less need for a safety margin for generation volatility. As long as the limit can be effectively defined, and a control mechanism is in place to clip the power flow in the corridor, then greater renewable generation

can be accommodated. It may be noted that the curtailment may be applied at conventional or renewable generation, and may be shared across a number of plants.

As described elsewhere in this chapter, there are advantages to defining a boundary constraint with the use of angle information. Compared with the use of a MW level to define the limit, the use of angles in the constraint definition reduces the variability of the level with respect to changes in low-inertia renewable generation and network topology changes. An angle-based constraint provides a practical approach to boundary management without the need for frequent operational updates.

8.4.4.2.6 Continuous Damping Control

Wide-area damping control can be an effective method of improving the performance of the power system, particularly for inter-area oscillations. In order for a mode of oscillation to be effectively damped, it is necessary for the mode to be both observable and controllable. Using wide-area angle monitoring as an input to damping control enables a choice of measurement inputs that emphasize inter-area oscillations that may not be strongly observed in local signals. The effectiveness of a conventional stabilizer using local measurements may be limited by the relative amplitude of low-frequency governor and local electromechanical modes. Using remote phasor input compared with a local phasor increases the stabilizer's response to the inter-area mode.

8.4.4.3 Centralized Wide-Area Control Using Dynamic Analysis Triggers in EMS

Depending on the timescales available to respond to a potential or emerging stability problem, it may be feasible to centrally optimize the corrective actions to mitigate the situation. This is especially true when operating in a preventive security control mode so as to make it able to face future events in a satisfactory way. Dynamic engines these days are fast enough to assess the stability risks and control action evaluations for a few minutes. The dynamic applications in current EMS can be triggered periodically and under specific topology conditions or scenarios prepared in advance. With the use of the latest PMU information, and considering the closed-loop operation, the applications can be triggered automatically by the following events:

- Frequency oscillations
- Slow voltage decline
- Frequency decline and rate
- Margin stability decline
- Sudden outages

The appropriate dynamic application will execute itself so that the proper control actions are recommended. There is, however, a post-processing task to coordinate and organize the set of actions to solve the specific problem.

For the same event, there will be a plan to deal with reactive issues and another to deal with frequency issues. A control could have conflicting values depending on the type of plan. Right now the operator can select the problem he or she would like to address, but for closed-loop operation the system needs to react automatically, which is one of the challenges of wide-area control.

The final recommendations will be deployed as one or more of the following defense plans:

- Protection triggering and SPS deployment (including arming of PMU-based SIPS)
- Control shifts
- Islanding protocols

The dynamic applications must be highly automated and capable of completing the tasks under varying conditions with little help (or none) from the operator.

The global and local information is available at the control center so the following triggers are possible for wide-area control:

- *Voltage decline or load level*: If this is the case, VS will execute to provide the proper set of switching/control actions considering a ~ 10 -s time frame.
- *Phase angle separation, frequency decline, and/or rate of frequency*: Global warning signals such as considerable angle difference and global and local frequency information can trigger TS wherein time frame ranges at the millisecond level. The decision to arm the PMU-based SPS could be an outcome of the TS analysis.
- *Oscillations*: If poor damping levels for the inter-area oscillatory modes are detected, they can be addressed by the small-signal applications (e.g., dispatch to reduce stressed conditions) and/or rely on the PMU-based SPS.
- *Stability margin*: If reactive reserve is the issue, the VS engine can assess the problem. If the margin is expressed in terms of angular stability then TS will address the problem.
- *Cascading*: With the help of trending, unwanted outages and cascading can be detected so the system prediction can be initialized with the most recent real-time snapshot and disconnected equipment status. The focus is on conducting a ~ 10 -minute-ahead simulation to detect dangerous conditions.

Figure 8.15 addresses the implementation of the dynamic applications, PMUs, PDCs, and warning signals to trigger the execution of advanced analytics.

8.4.4.4 Dynamic Adaptive Islanding

If all lines of defense are exhausted, there is another possibility: Separate the network into small f - V -controllable islands. The control actions should be highly automated and they should be deployed with enough intelligence to figure out the

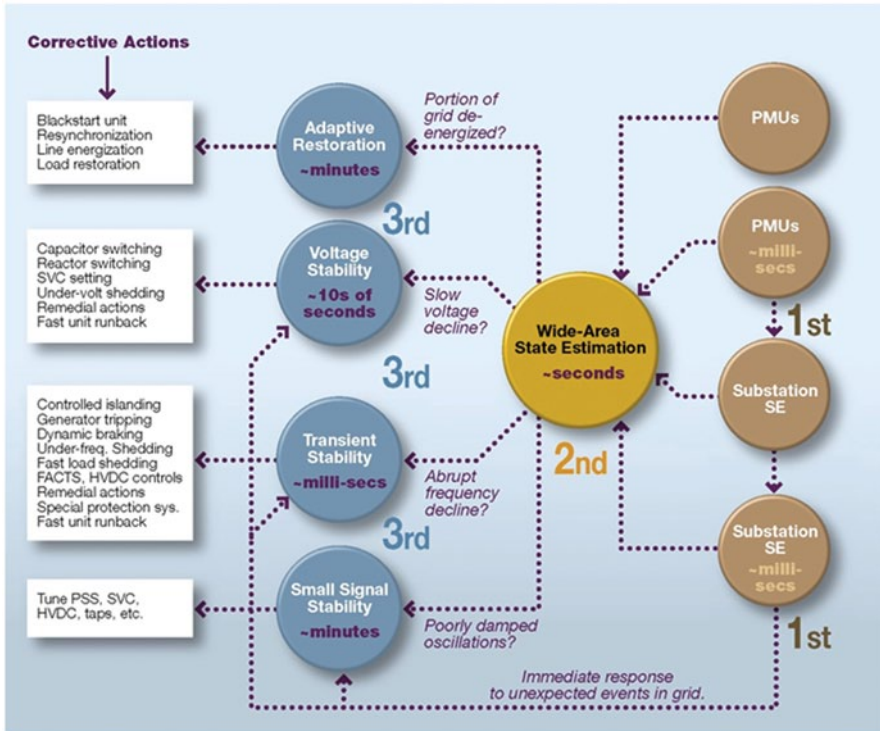


Fig. 8.15 Dynamic applications triggering and coordination

right set of alternatives to safely split the system (Vittal et al. 1998). There is a list of steps before this recommendation is ready. The steps include monitoring, trends, and finally smart network partitioning and restoration strategies. In the event that an event takes place, the following sections describe steps for dynamic islanding.

8.4.4.4.1 System Drift

The event begins and the system drifts and the generators react to it depending on its nature. They share the frequency tendency and rate of change; oscillating units are detected and grouped into critical sets. The applications process the critical datasets and provide the list of potential cut sets linking oscillating groups. System controllability and restoration guidelines are imposed to help decision making.

8.4.4.5 Trends and Triggers

The need to use recent and previous wide-area information to determine the trending of selected electrical variables (or composite indices) to identify potential problems

(frequency rate, voltage rate, increased oscillations, angle and VS margins, etc.) is very important for islanding. The analysis of all PDC information will confirm or caution the operator about potential problems.

8.4.4.6 Network Partitioning

The oscillating groups define the points where the system is weak and propose where to make splits. When making grid splits, both the frequency impact and reactive impact of the various split options must be evaluated. The best choice will be the one that reduces the active power imbalance, based on the smallest generation-load imbalance to avoid further cascading. In order to be effective, the islands must be easy to restore and synchronize with the rest of the system. Optimization functions will guarantee enough active/reactive control capability to push the frequency ranges and voltages back to their nominal values.

8.4.4.7 Resynchronization

The restorative condition of the system is a state that is allowed momentarily to avoid further deterioration of the grid. Still, it is desirable to minimize the time of restoration and resynchronization. So as part of the selection for the best plan to separate the system into small islands, there is a need to consider the availability of reactive controls and sufficient resources to return the control center to a normal condition.

8.4.4.8 Infrastructure Requirements for Control and Protection Applications

It is necessary to address scheme design consideration when using synchrophasor measurements in control applications. Compared with monitoring applications, there will generally be more stringent requirements on data availability and latency. It is noted that the present IEEE C37.118 standard, both in the 2005 and 2011 versions, use Internet Protocol communication; hence, latency may require special attention for the faster requirements (Fig 8.16). The design of a protection or control scheme should account for:

- Defining the overall time budget that is available for the application to run successfully
- Ensuring that the latency at all stages including the measurement process, processing delay, communication, and actuation is within the time budget
- Defining a graceful degradation process, if required
- Identifying the need for redundancy and the implementation
- Ensuring that the static and dynamic signal qualities are appropriate for the application

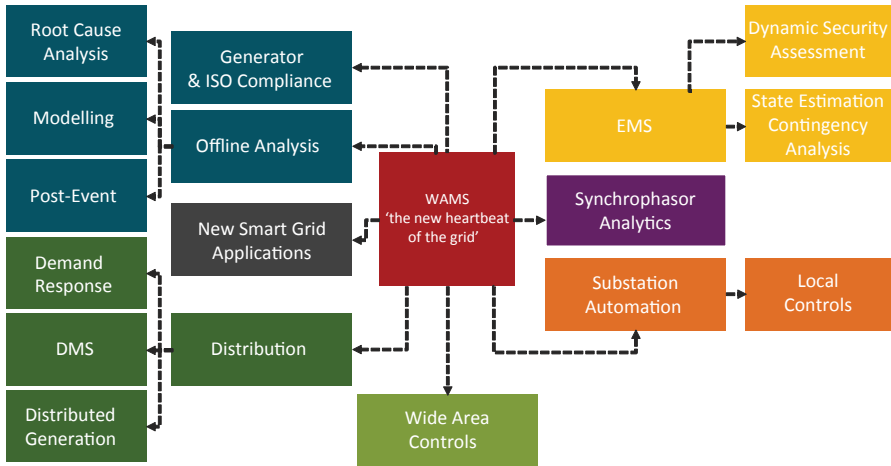


Fig. 8.16 The evolution of grid monitoring and control solutions. Illustrates how the growth of synchrophasor PMU data will facilitate a Wide-Area Monitoring System (WAMS) that becomes a rich source of fast, accurate, grid monitoring data that will drive the EMS as well as other smart grid analytics, to facilitate prompt regional, local, and wide-area controls

8.5 Conclusion

This chapter has described a high-level plan to implement a wide-area control system in an EMS. Such a system would improve power system grid stability and make recoveries easier. The primary intent of the wide-area control system is to extend the operational boundaries of the system, while protecting the electrical interconnections from a widespread collapse. In some cases, the appropriate action would be islanding and blacking out a portion of the grid in order to prevent widespread collapse.

A key element is to evaluate the optimal approach towards using PMU data in the EMS steady-state and dynamic applications. SE is the obvious first application to be leveraged, since PMUs can improve SE observability, reliability, and accuracy. Furthermore, SE forms the basis and foundation of all model-based steady-state or DSA.

PMU data are received much faster (milliseconds) than traditional SCADA data (2–4 s). This allows for faster detection of signatures of potential system problems (such as transient or oscillatory instability) and could be used to trigger dynamic analysis simulations. The dynamic simulation engines could also be deployed to directly utilize PMU data, along with the latest state-of-the-art communications and hardware to respond quickly to mitigate the spread of a system disturbance.

This approach entails analysis, prediction, and determining the appropriate wide-area control actions. Finally, communications is a challenge that needs to be addressed in order to deploy fast, automated closed-loop operations on the electric power grid.

References

- Apostolov AP (2004) Requirements for automation event analysis in substation automation systems. IEEE paper 0-7803-8465-2/04, pp 1–6
- Avila-Rosales R, Giri J, Ruiz-Vega D, Ernst D, Pavella M (2000) Online transient stability ATC calculations. IEEE PES 2000 summer meeting, Seattle, WA, July 2000
- Avila-Rosales R, Sadjadpour A, Gibescu M, Morison K, Hamadanizadeh H, Wang L (2003) ER-COT's implementation of online dynamic security assessment. IEEE PES summer meeting, Toronto, ON, July 2003
- Avila-Rosales R, Giri J, Lopez R (2004) Extending EMS capabilities to include online stability assessment. IEEE PSCE 2004, New York, October 2004
- Baldwin TL, Mili L, Boisen MB, Adapa R (1993) Power system observability with minimal phasor measurement placement. IEEE Trans Power Syst 8(2):707–715
- Bao L, Huang Z, Xu W (2003) Online voltage stability monitoring using VAr reserves. IEEE Trans Power Syst 18(4):1461–1469
- Bhargava B, Rodriguez GD, Salazar A (2004) Use of synchronized phasor measurement system for enhancing power system transmission reliability. EIPP Meeting, Columbus, OH, 21 Sept, pp 1–7
- Giri J, Avila-Rosales R (2000) Transient stability assessment integration with EMS and control center requirements. IEEE PES winter meeting, Singapore, Jan 2000
- Giri J, Avila-Rosales R (2002) Security assessment in the electricity market environment. IEEE PES summer meeting, Chicago, IL, July 2002
- Khatib AR, Nuqui RF, Ingram MR, Phadke AG (2004) Real-time estimation of security from voltage collapse using synchronized phasor measurements. IEEE paper 0-7803-8465-2/04
- Kundur P, Wang L (2002) Small signal stability analysis: experiences, achievements and challenges. IEEE paper 0-7803-7459-2/02, pp 6–12
- Kundur P, Morison GK, Wang L, Hamadanizadeh H (1998) Power system control: requirements and trends in the new utility environment. Bulk power system dynamics and control IV-restructuring, Santorini, Greece, Aug 1998
- Kundur P, Morison GK, Wang L, Hamadanizadeh H (1999) Online dynamic security assessment of power systems. 5th International workshop on electric power control centers, Heviz, Hungary, 13 June
- Meliopolous SAP, Fardanesh B, Zelingher S (2001) Power system state estimation: modeling error effects and impact on system operation. Proceedings of the 34th Hawaii International Conference on system sciences, pp 1–9
- Nuqui RF, Phadke AG (2002) Phasor measurement unit placement based on incomplete observability. IEEE paper 0-7803-7519-X/02, pp 888–893
- Overbye T, Sauer P, DeMarco C, Lesieutre B, Venkatasubramanian M (2010) Using PMU data to increase situational awareness, PSERC Report 10-16. Parashar M, Dyer J, Bilke T, EIPP Real-time dynamics monitoring system, HICCS, Hawaii, 2006
- Parashar M et al (2012) Wide area monitoring and situational awareness. In: Grigsby LL (ed) Power system stability and control, 3rd edn. Electric Power Engineering Handbook, Chapter 15. CRC Press, New York
- Parniani M, Chow JH, Vanfretti L, Bhargava B, Salazar A (2006) Voltage stability analysis of a multiple-infeed load center using phasor measurement data. Proceedings of 2006 IEEE Power System Conference and Exposition, Atlanta, GA
- Pavella M, Ruiz-Vega D, Giri J, Avila-Rosales R (1999) An integrated scheme for online static and transient stability constrained ATC calculations. IEEE PES summer meeting, Alberta, CA
- Savulescu SC (2004) Real-time detection of the risk of blackout. Invited paper 04GM0484, presented at the "Control Center Issues", IEEE PES general meeting, Denver, CO, 9 June, pp 1–2
- Vittal V, Kliemann W, Chapman DG, Silk AD, Ni Y-X, Sobajic DJ (1998) Determination of generator groupings for an islanding scheme using the method of normal forms. IEEE Trans Power Syst 13(4):1345–1351

- Vu K, Begovic MM, Novosel D, Saha MM (1999) Use of local measurements to estimate voltage stability margin. *IEEE Trans Power Syst* 14(3):1029–1035
- Wang D, Wilson DH, Clark S (2014) Defining constraint thresholds by angles in a stability constrained corridor with high wind, *IEEE T&D*, Chicago, IL
- Wilson DH, Al-Ashwal N, Halldorsson H, Boroczky S (2013) *Discrete Control for Transient Stability and Oscillations: Applications and Case Studies*. IEEE PES General Meeting, Vancouver, Canada
- Xu B, Abur A (2004) Observability analysis and measurement placement for systems with PMUs. *IEEE paper 0-7803-8718-X/04*, pp 1–4

Chapter 9

Emergency Monitoring and Corrective Control of Voltage Instability

Thierry Van Cutsem and Costas Vournas

Abstract After reviewing the basic voltage instability mechanisms, this chapter describes emergency measures that can be used in order to contain voltage instability and prevent a voltage collapse leading to a blackout. A real case of such a voltage collapse in the Hellenic system is presented and analyzed. Emergency measures presented include existing or projected controls acting on bulk power delivery transformer load tap changers, as well as direct load shedding. An actual design and application of a load-shedding controller in the Hydro-Quebec system is presented.

9.1 Introduction

Power system instability may take on the form of angle, frequency, or voltage instability (Kundur et al. 2004). This chapter and the next one focus on voltage stability, which deals with the ability of maintaining voltage magnitudes near their nominal values when the system is subject to disturbances.

Simply stated, voltage instability results from the inability of the combined transmission and generation system to deliver the power requested by loads. It is a dynamic phenomenon largely driven by the load response to voltage changes. In a voltage-unstable situation, the voltage drops caused by power transfers across the network are no longer in the order of a few percents (as in normal operating conditions) but undergo a dramatic, generally monotonic decline in the seconds or minutes following a disturbance. When this decrease is too pronounced, the system integrity is endangered mainly due to protecting devices that trip generation, transmission, or load equipment, not to mention the nuisance caused to customers by sustained voltage sags. This disruption process may eventually lead to a blackout in the form of a voltage collapse.

T. Van Cutsem (✉)
Dept. Electrical Engineering and Computer Science, FNRS (Fund for Scientific Research)
and University of Liège, Sart Tilman, B37-B4000 Liège, Belgium
e-mail: t.vancutsem@ulg.ac.be

C. Vournas
National Technical University of Athens, Athens, Greece
e-mail: vournas@power.ece.ntua.gr

S. C. Savulescu (ed.), *Real-Time Stability in Power Systems*,
Power Electronics and Power Systems, DOI 10.1007/978-3-319-06680-6_9,
© Springer International Publishing - Switzerland 2014

Voltage instability is much better understood today (Taylor 1994; Van Cutsem and Vournas 1998) than it used to be few decades ago, in the mid 1980s. However, several of the theoretical and practical difficulties associated with the subject still remain. Let us quote, non-exhaustively, the:

- Inherent nonlinearity of the phenomenon, that introduces a nontrivial mathematical complexity even for small power system models
- Strong coupling of active power flows and voltages (at load buses) near a voltage stability limit, which defies the stereotype linking voltage to reactive power alone, valid for a moderately loaded system operating near its nominal voltages
- Multiplicity of the time scales involved
- Possible spread of a local but uncontrolled voltage collapse, while a relatively small corrective action may stop the system degradation, if applied at the right place and time
- Need for a sufficiently detailed representation of major components even when geographically remote from the most disturbed area
- Uncertainty of load behavior, especially when subjected to large voltage changes

In many power systems throughout the world, voltage instability is still considered a major cause of blackout, as important as thermal overloads and the associated risk of cascaded line tripping. There are two lines of defense against incidents likely to trigger such instability: preventive and corrective controls.

Preventively, security margins must be evaluated with respect to contingencies and appropriate preventive actions must be taken to restore sufficient margins, where needed. Preventive enhancement of security may lead the Transmission System Operator (TSO) to decrease the posted available transfer capabilities, to reschedule generation, to request some units to be kept in operation for voltage support, and, as the last resort, to shed load.

All these actions have a cost. Furthermore, in the prevailing open market environment, such decisions have to be taken in a transparent way. Hence, appropriate decision tools should support them.

However, it would be extremely expensive, and most likely impossible, to protect a power system against any disturbance. As a trade-off between reliability and economy, power systems are usually operated in such a way that they can survive credible contingencies, i.e., incidents with a reasonable probability of occurrence, while for more severe incidents the TSO relies on corrective controls. The latter should take on the form of automatic emergency actions, through *System Protection Schemes* (SPS), aimed at preserving operation of the largest possible part of the system by isolating the unstable part (Karlsson 2001; Van Cutsem and Vournas 2007). Corrective actions usually affect generators and/or loads and hence are acceptable only in the presence of severe disturbances.

The objectives of this chapter are to briefly review the voltage instability mechanisms and corrective countermeasures, describe an actual voltage-instability-induced blackout, and discuss the implementation of some effective emergency

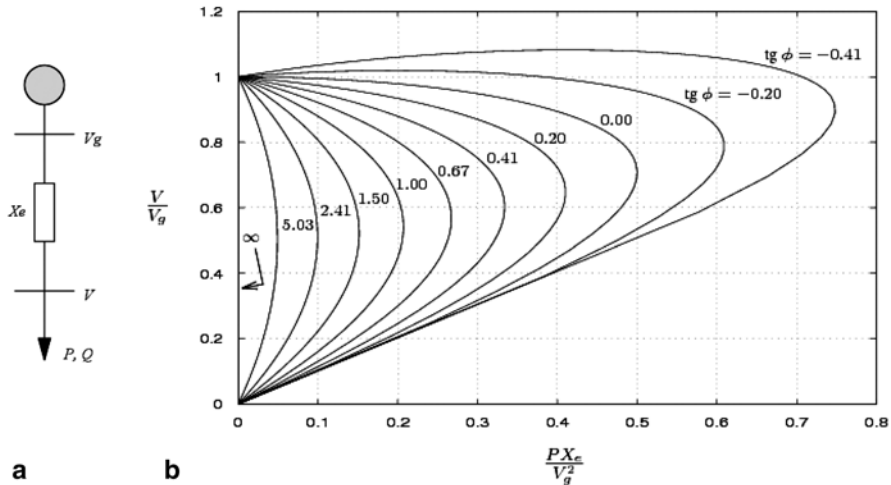


Fig. 9.1 One-generator one-load system and PV curves

controls. The system considered in the example will be further considered in the next chapter, in the framework of online Voltage Security Assessment, which can help operators in taking preventive countermeasures.

Several options exist for emergency controls that will help protect the system against voltage collapse. Reactive shunt element switching and fast generation re-scheduling have no impact on consumers and will be normally the first to be utilized if available. In this chapter, we concentrate on emergency controls that have a direct or indirect impact on consumed power. The former involves load shedding, while the latter category comprises several emergency controls of Load Tap Changers (LTCs). A practical application of load shedding in a real power system is included in the chapter.

9.2 Voltage Instability Mechanisms

9.2.1 PV Curves and Maximum Load Power

One of the primary causes of voltage instability is the large transfer of power from generation to load centers. The salient features of such a transfer are captured by the simple one-generator one-load example of Fig. 9.1a, where a constant voltage source is initially assumed.

It is common in both theoretical reasoning and industry practice to consider the curves that relate the voltage V to the active (respectively reactive) power P (respectively Q) of the load. Such curves, usually referred to as PV curves, or “nose” curves, are shown in Fig. 9.1b. In this figure, each curve corresponds to a given load

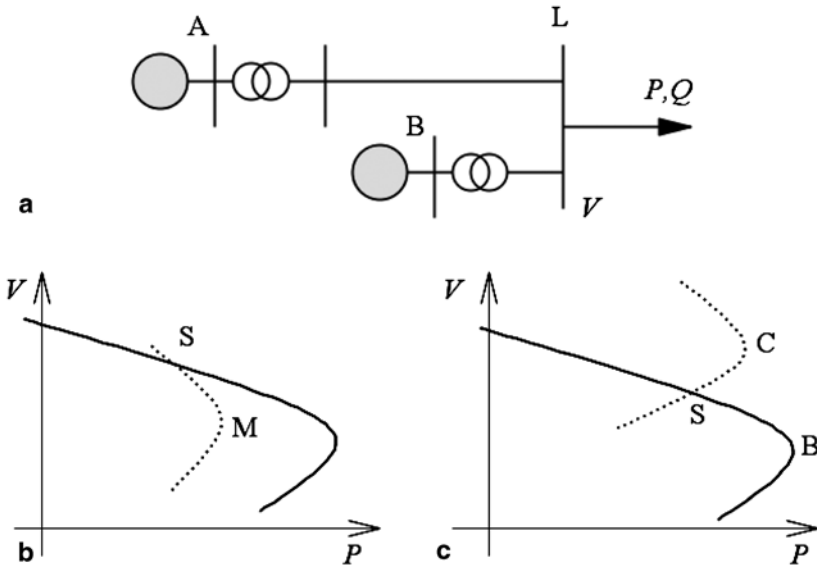


Fig. 9.2 Two-generator one-load system and PV curves

power factor, i.e., $Q = tg \phi P$ for all points. Similarly, one may consider QV curves under constant power factor, under constant P , etc. For a given power, normal operation is on the upper part of each PV curve.

The PV curves confirm the existence of a maximum load power, well known from circuit theory. Simply stated, voltage instability results from the attempt to operate beyond maximum load power. This may result from a severe demand increase or from a large disturbance that increases the transmission impedance and/or decreases the generator voltage to the extent that the pre-disturbance load demand can no longer be satisfied. In the latter case, instability is driven by internal mechanisms of loads that tend to restore the consumed power to (almost) its pre-disturbance level. This *load power restoration* process is present at different time scales in induction motors, in loads fed by LTCs and in thermostatically controlled loads.

Synchronous generators are not pure voltage sources. Besides some voltage droop under Automatic Voltage Regulator (AVR) control, field, and armature current limits must be obeyed. The former are imposed by Overexcitation Limiters (OEL) and the latter by armature current limiters or (most often) by plant operators. These limits have a strong impact on maximum load power, as recalled hereafter.

Consider the slightly more realistic example of Fig. 9.2a, where active power is transferred from the generator of bus A to the load of bus L, the generator of bus B being used for local voltage support. Being electrically closer to the load, generator B supplies most of the reactive demand, as well as part of the increasing reactive losses in the A–L transmission. At some point, generator B switches under field current limit and does no longer control the voltage at bus B. For further load increases, only a little additional reactive power can be obtained from generator B and

the voltage drop at the load bus will be more pronounced. The corresponding PV curve is shown in Fig. 9.2b, where the solid (respectively dotted) line refers to generator B under AVR (respectively OEL) control. Once the generator is limited (point S), the load can still be increased, though at the expense of a more pronounced voltage drop, until the maximum is reached at point M. Note that, in some cases, the PV curves may appear as in Fig. 9.2c (Dobson and Lu 1992; Van Cutsem and Vournas 1998). Here, no further load increase is possible beyond point S, since along path SB (assuming AVR control) the generator would be overexcited, while along path SC (assuming OEL control), the AVR would regain control. The maximum load power is thus reached at point S.

Maximum load power is significantly reduced by generator reactive power limits and is usually reached at a higher voltage. The latter aspect means that in voltage stability limited systems, operating at normal voltages is no guarantee of security. Any analysis technique that overlooks the effect of these limits is of little practical use for most systems.

9.2.2 Time-Scale Decomposition

In stability studies, the general dynamic model of a power system takes on the form:

$$\mathbf{0} = \mathbf{g}(\mathbf{x}, \mathbf{y}, \mathbf{z}) \quad (9.1)$$

$$\dot{\mathbf{x}} = \mathbf{f}(\mathbf{x}, \mathbf{y}, \mathbf{z}) \quad (9.2)$$

$$\mathbf{z}(t_k^+) = \mathbf{h}(\mathbf{x}, \mathbf{y}, \mathbf{z}(t_k^-)). \quad (9.3)$$

The algebraic Eq. (9.1) represent the network equations. Electromagnetic transients being neglected, and the quasi-sinusoidal (or time-varying phasor) approximation being adopted, its response is assumed instantaneous.

The differential Eq. (9.2) relate to a wide variety of phenomena and controls that can be classified into:

- *Short-term dynamics* of generators, turbines, governors, AVRs, Static VAr Compensators (SVCs), induction motors, High-Voltage Direct Current (HVDC) links, etc. lasting typically from 1 to several seconds
- *Long-term dynamics* of secondary frequency and voltage control, load self-restoration, etc. lasting typically several minutes, if not more
- In practice, the short- and long-term dynamics are fairly well decoupled so that (9.2) can be further decomposed into

$$\dot{\mathbf{x}}_1 = \mathbf{f}_1(\mathbf{x}_1, \mathbf{x}_2, \mathbf{y}, \mathbf{z}) \quad (9.4)$$

$$\dot{\mathbf{x}}_2 = \mathbf{f}_2(\mathbf{x}_1, \mathbf{x}_2, \mathbf{y}, \mathbf{z}) \quad (9.5)$$

where \mathbf{x}_1 (respectively \mathbf{x}_2) is the fast (respectively slow) component of \mathbf{x} , and correspondingly for the state equations.

The discrete-time Eq. (9.3) capture discrete events that stem from:

- Controllers acting with various delays on shunt compensation, generator set points, LTCs, etc
- Equipment protections such as OELs, etc
- SPS acting on loads and/or generators

The corresponding (shunt susceptance, transformer ratio, etc.) variables are grouped into \mathbf{z} , which undergoes step changes from $\mathbf{z}(t_k^-)$ to $\mathbf{z}(t_k^+)$ at some times t_k . We assume that the discrete dynamics belongs to the long-term category.

The above time decoupling allows to categorize voltage instability phenomena and to derive faster analysis tools, as described in the sequel (Van Cutsem and Vournas 1998).

9.2.3 Short-Term Voltage Instability

When a power system is subject to a disturbance, the short-term dynamics are excited first. Over a period of a few seconds, the long-term variables \mathbf{x}_2 and \mathbf{z} do not respond yet and can be considered as constant parameters in (9.1), (9.4).

The short-term time scale is the time frame of angle instability, i.e., the loss of synchronism between generators. It is also the time frame of *short-term voltage instability*, which is linked to fast load recovery by induction motors and possibly HVDC systems.

When an induction motor is subject to a voltage drop, the electromagnetic torque initially decreases as the square of voltage. As a result, the motor decelerates, i.e., the slip increases, until this increase causes the electromagnetic torque to restore to the value of the mechanical one. After these slip changes have taken place, the active and reactive powers take the values given by the curves of Fig. 9.3a, b, respectively, where S is the *stalling point*, below which the induction motor cannot operate.

The following are scenarios of short-term voltage instability caused by induction motors:

1. The outage of transmission equipment causes the maximum deliverable power to become smaller than the power the motor tends to restore (see Fig. 9.3a). The electromagnetic torque cannot reach the value of the mechanical one, thus the motor stalls, which causes the voltage to drop and a high current to flow in the armature.
2. A short-circuit near the motor causes the latter to decelerate. If the fault is not cleared fast enough, the motor is unable to reaccelerate and thus it stalls, with the same outcome as in Case 1.

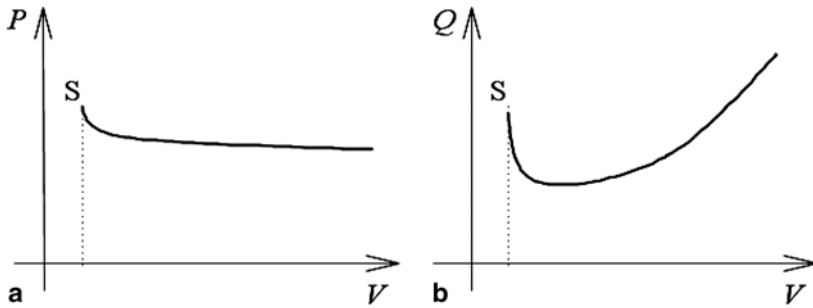


Fig. 9.3 Induction motor: steady-state active and reactive power variations with voltage

In the first case, the system has no post-disturbance equilibrium, while in the second case the long-lasting fault makes it escape from the region of attraction of its post-disturbance equilibrium.

9.2.4 Long-Term Voltage Instability

Let us assume that the system has survived the short-term period following the disturbance. From there on, it is driven by the long-term dynamics (9.3), (9.5). *Long-term voltage instability* is associated with these slower dynamics. LTCs and OELs play an important role. A typical long-term instability scenario is as follows.

The triggering event is the outage of generation and/or transmission equipment reducing the maximum power deliverable to loads and causing transmission voltages to drop (although moderately at first) and generators to increase their excitation under AVR action. After some intentional delay time, LTCs start trying to restore the voltages of distribution networks by adjusting the ratios of the transformers feeding them. Bringing the distribution voltages back to the LTC set points (in practice, close to them, due to deadband effects) would mean restoring load powers to their pre-disturbance value. Tap changes and load power recovery depress voltages on the transmission side. This further draws on the reactive reserves and activates some OELs, which contribute to further reducing the maximum power deliverable to loads (see Fig. 9.2). If the latter becomes smaller than what the LTCs tend to restore, instability follows in the form of useless tap changes (that will eventually depress distribution voltages) and dramatic transmission voltage drops.

In this scenario, the system loses its long-term equilibrium: With reference to Figs. 9.1 and 9.2, the post-disturbance network PV curve no longer crosses the vertical line representing the long-term constant power behavior of LTC-controlled loads.

In the best case, the process stops when LTCs hit their limits, yielding pseudo-stabilization. However, it is also possible that the long-term system degradation triggers instability of the short-term dynamics (assumed stable up to now). This may take on the form of:

- Field current-limited generators losing synchronism
- Motors stalling due to low-voltage conditions
- Oscillatory angle instability due to OELs bypassing power system stabilizers
- Finally, the situation may be aggravated by protections tripping:
- Lines due to thermal overload or zone-3 relay activation
- Field current-limited generators owing to low terminal voltage or armature thermal overload

Long-term instability may also be driven by thermostatically controlled loads, which exhibit similar recovery behavior.

9.3 Anatomy of a Voltage Instability Incident

The following system description and blackout analysis are based on the work already published by Vournas et al. (2000, 2007).

9.3.1 *The Hellenic Interconnected System*

The Hellenic Interconnected System includes the generation and transmission systems of mainland Greece and some adjacent islands. The main production center is located in the northwest part of the country close to the lignite mines, which is the basic fuel source, while the main center of consumption lies in the southern part including the metropolitan area of Athens (see Fig. 9.4).

The installed generation capacity of the interconnected system in 2004 was about 10,700 MW with 48% lignite, 29% hydro, 14% natural gas, 7% oil, and 2% renewable. The generation capacity in the southern part of the country was close to 2860 MW, installed mainly at the power plants of Lavrio, Ag. Georgios (both near Athens), Aliveri in Central Greece, and Megalopolis (in Peloponnese).

The transmission system operates mainly at the levels of 400 and 150 kV. In 2004, there were five Alternating Current (AC) interconnection lines with the neighboring countries in the north and a Direct Current (DC) interconnection with Italy via a submarine cable (with a maximum capacity of 500 MW). Depending on topology, the system consists on the average of 800 buses, 1100 branches, and 70 generators.

As already mentioned, the geographical imbalance between generation and consumption leads to heavy power transmission in the north–south direction. This transfer continuously increased up to 2009 due to the high increase of the yearly peak loads mainly in the south; such peaks occur during the summer period and they are mainly due to air-conditioning and other cooling devices. After 2010, the economic recession curbed the load increase, which is expected to ramp up again only after economic recovery. The delays in the implementation of planned transmission projects (mainly due to public protest) deteriorated further the transfer capacity.



Fig. 9.4 Map of Hellenic Interconnected System with the north-south split of July 12, 2004

Thus, occasionally, the Hellenic system faced critical operational conditions regarding voltage stability. Such incidents have been experienced since 1996. The most severe disruption occurred on July 12, 2004, when the southern part of the country suffered a blackout lasting for 2 h. This event is briefly described below.

9.3.2 *The Blackout of July 12, 2004*

This incident happened just before the commissioning of some crucial transmission projects, which had been planned to reinforce the transmission system in order to improve voltage stability and increase the transfer capacity from north to south. These reinforcements included the installation of additional autotransformers at Extra High Voltage/High Voltage (EHV/HV) substations in the metropolitan area

of Athens and the adjacent area of Central Greece, the installation of mechanically switched capacitor banks at some crucial substations (totally 400 MVar) on medium voltage, as well as 150 kV buses, and the reinforcement of the 150-kV network in the Athens region. These transmission projects had been considered necessary since Athens was the host of the 2004 Summer Olympic Games. The deadline for the commissioning of these projects was the 15th of July.

Also, a crash program was tendered by the Hellenic Transmission System Operator (HTSO) to install gas turbines (140 MW) in the south at the new thermal power plant of Heron, under a special contract, to be used during peaks for voltage support. The official commissioning date of this plant was the end of June, but the project was delayed for about a month due to licensing problems.

The sequence of events leading to the blackout was the following.

From the previous day (July 11), one 125 MW generating unit in Peloponnese (Megalopoli) and one generating unit in Northern Greece were out of service. The effect of the Megalopoli unit loss was that a small amount of power (close to 80 MW) was flowing via Athens to Peloponnese. This was further stressing the Athens grid.

At time 07:08 of July 12, unit 2 (rated 300 MW) of the Lavrio power station in the Athens area was lost due to auxiliaries UPS failure. The failure was repaired, but due to further problems occurring during start-up the unit was only synchronized at 12:01. At that point, load had peaked to 9160 MW and voltages in the Athens area were constantly dropping, reaching 90% of the nominal value. Voltage decline stopped as soon as Lavrio-2 synchronized and started generating.

However, at 12:12 unit Lavrio-2, still being in the process of achieving its technical minimum, and consequently on manual control, was lost again due to high drum level. This brought the system to an emergency state.

At 12:25, a load shedding of 100 MW was requested by the HTSO Control Center. At 12:30, a disconnection of 80 MW was achieved manually. This, however, was not enough to stop the voltage decline, so a further shedding action of 200 MW was requested at 12:35. At that time, load had reached 9320 MW.

The second load-shedding command did not have the time to be executed. At 12:37, unit 3 of Aliveri power station serving the weak area of Central Greece tripped automatically. It is unclear which event initiated this critical tripping. At 12:38, the remaining unit in Aliveri was manually tripped. After that, voltages were collapsing and the system was split in two at 12:39.

The splitting of the system (shown in Fig. 9.4) was initiated by the opening of the north-south 400 kV lines, due to the “switch-onto-fault” function of the protection relays. After splitting, the remaining generators in the areas of Athens and Peloponnese were disconnected by undervoltage protection leading to the blackout.

The split of the system saved the north and western parts of the Hellenic system, which remained interconnected, even though the resulting surplus of power created a severe disturbance in the neighboring systems of the second Union for the Coordination of Transmission of Electricity (UCTE) synchronous zone, which was then operating isolated from the main UCTE interconnection, but has since been re-synchronized.

The total excess generation was about 2000 MW changing the flow at the north interconnections from import of 900 MW to export 1100 MW. The interconnection with FYROM was overloaded and tripped, and the Bulgarian interconnection received the total flow of 1100 MW. The frequency increased to 50.75 Hz. The DC cable to Italy continued importing according to its program (250 MW).

The restoration of the south system started at 12:45. With the generating units of the north and west in operation, the restoration was relatively fast following simultaneously two different directions: from the west to the lignite plants in Peloponnese, and from the center down to the power plants in the area of Athens. In half an hour (13:15), all the main substations of the south were energized. In 1 h and 15 min (14:00), 1900 MW had been supplied. The supply to the rest of the load was restricted, to avoid a new occurrence of instability, since the units involved in the blackout continued to be out of operation. The Aliveri units were synchronized at 15:05 and Lavrio 2 unit at 22:42. All the consumers were fully supplied by 17:30.

Immediately after the occurrence of the blackout, a committee was formed by the Minister of Development of Greece to investigate the causes of the blackout and estimate the security of the system for the then upcoming Athens Olympics of August 2004. The first postmortem analysis was based on the 12:35 State Estimator solution of the HTSO Energy Management System, as obtained through the data transfer utilities of the online Voltage Security Assessment (VSA) application that will be described in the next chapter. A more detailed analysis followed later, so as to validate the generator and system data. Generator aspects were investigated closely. The investigation concerned initially the accuracy of generator reactance and saturation data, which have a direct effect in the representation of the overall generator performance during stressed system conditions, determining mainly their reactive capability.

Starting from the generator short-circuit and open-circuit characteristics, provided by HTSO for the thermal plants with a dominant role during the incident (units in the Athens and Central Greece areas), the direct-axis synchronous reactance was checked and the saturation coefficients were calculated. After that, the maximum allowable continuous excitation current was adjusted to a new value based on the rated generation data and calculated taking into account the saturation of the generator. This led to a better approximation of the generator reactive production during system simulation.

Armature current limitation was also considered for the generators in the Athens and Central Greece areas. Under normal voltage, the rotor current limit is more restrictive than the armature current limit at loading levels below the rated active power. However, once field current limiters acted on generators located in the most affected areas, the continuous decrease in their terminal voltages led to excessive armature currents. In the Hellenic system, there is no automatic limiter to adjust the stator current; thus, the model adopted for the simulation tried to duplicate the suggested generator operator practice, in order to avoid stator overheating and the loss of the unit. In some other cases, where plant equipment was upgraded (turbine efficiency improvement by retrofit and/or new rotor installation), generator

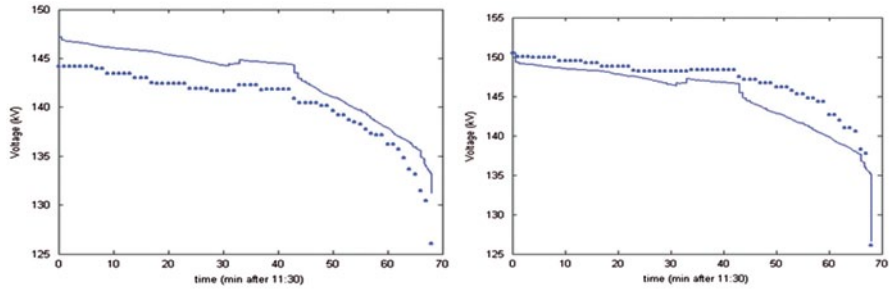


Fig. 9.5 Typical simulated (*solid lines*) and measured (*dots*) voltage responses

dynamic data and rated outputs were updated. In addition, all data were compared and checked carefully.

A simulation of the system response with the corrected data was carried out using again the WPSTAB software of National Technical University of Athens (NTUA; Fig. 9.5) and relies on the quasi-steady-state technique explained in Chap. 11.

The simulation starts from the 11:30 snapshot of July 12, which together with that of 12:00, proved more reliable and consistent than that of 12:35, even though the state estimation errors still persisted. A ramp was imposed on system load demand with a rate that matched the total load consumption at 12:00 with that of the corresponding control center snapshot. Negative reactive loads were removed from the ramp increase, as they were attributed to non-modeled capacitor banks.

All changes in the active generation of the units close to Athens were duplicated in the simulation, as was the active and reactive contribution of Lavrio-2 unit between 12:00 and 12:15. Both rotor and stator current limits were imposed in the simulation. All generators were assumed to control voltage up to the point of reaching their rotor current limits except from cases where the measurements showed that a generator was operating on constant reactive power mode, in which case the simulation model was corrected.

Two typical voltage responses simulated (continuous lines) and measured (dots) are plotted in Fig. 9.5. These correspond to transmission buses close to power stations in the Athens region. One can see that the simulated voltage response is similar to the one exhibited by the actual system, since the general trend is followed.

The simulation seems more accurate up to the point where the unit Lavrio-2 synchronized and tripped. After 12:15, the slope of the simulation differs slightly from that of the actual voltage decline. Based upon the simulation agreement with the measurements, which is demonstrated in Fig. 9.5, one can claim with some confidence that the numerical representation of the system used in the online VSA application to be described in Chap. 10 is close enough to actual system behavior.

9.4 LTC Emergency Control

Automatic LTCs on bulk power delivery transformers constitute a prime source of load restoration and are thus a driving force for voltage instability. Emergency LTC control measures have been proposed in the literature (among the recent references, let us quote Larsson 2000; Otomega et al. 2003; Vournas et al. 2004) for containing voltage instability and avoiding an imminent voltage collapse.

In this section, LTC emergency control methods are briefly reviewed and compared. Also, some possible combinations of these measures that could improve protection against voltage collapse are proposed. All measures are compared using a simple system involving one restorative load behind an LTC.

9.4.1 LTC Emergency Control Schemes

All measures discussed in this section can be activated when transmission side voltage drops below a threshold, which we will denote as V_L . The following emergency controls are considered:

- *Tap blocking* is the simplest countermeasure involving emergency LTC control. It consists simply of deactivating the control mechanism that is normally restoring the secondary (distribution side) voltage of the power delivery transformer. In this way, load restoration is cancelled or, in the worst case, delayed.
- *Voltage set-point reduction* consists of lowering the reference voltage and associated deadband of the distribution side voltage. The LTC is left to control this voltage in the normal way.
- *Tap locking* is the action of assigning a specific tap position, where the LTC will move and then lock.
- *Tap reversing* consists in changing the control logic, so that the LTC controls the transmission-side voltage instead of the distribution side. The reference for the primary voltage is taken as $V_L + e$, where e is either zero or positive. Thus, the control mechanism will start regulating the transmission-side voltage (primary) as soon as it falls below the threshold and will try to restore it to the value $V_L + e$.

From the above controls, tap blocking, voltage set-point reduction, and tap locking are easily implemented, since they are supported by most of the existing LTC controller hardware. On the other hand, tap reversing requires some further development and a special design to coordinate taps. As will be seen, tap reversing can yield similar effects to load shedding, but up to now it has been considered less cost-effective than direct partial load disconnection.

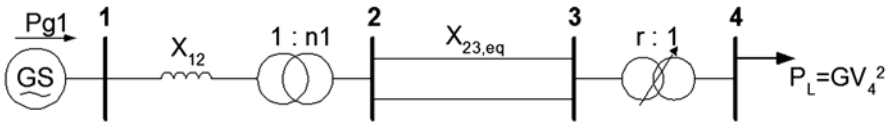


Fig. 9.6 Generator: single load system

9.4.2 Comparison of Methods

9.4.2.1 Test System Description

Fig 9.6 shows the one-line diagram of a small power system used to compare the performance of the above emergency measures. The system consists of an isolated generator feeding a restorative load through a double-circuit transmission line and an LTC transformer with ratio r . The LTC has fixed time delays of 30 s (for the first step) and 10 s (for the subsequent steps).

One important aspect in emergency protection against voltage collapse is the possible existence of load restoration mechanisms acting behind the LTC. Such mechanisms include thermostatically controlled loads, distribution system voltage regulators, etc.

To account for this behavior, a slow load restoration is implied for the load at bus 4, which is modeled as a variable conductance obeying the differential equation

$$T_L \dot{G} = P_o - GV_4^2, \tag{9.6}$$

Thus, the load is constant admittance initially, but it is attempting to restore to constant power in the long run. The generator on bus 1 is modeled with an AVR and an OEL. The OEL is activated 40 s after the rotor current exceeds its limit and is enforcing this limit by keeping the generator on constant excitation, equal to its maximum allowed for continuous operation.

The contingency considered in order to simulate a case of voltage collapse is the loss of one of the two circuits between buses 2 and 3.

9.4.2.2 Simulation of Countermeasures

After the line loss, the generator becomes overexcited and can no longer maintain the power demand P_o . Therefore, (9.6) has no longer an equilibrium point and this leads to a collapse.

This is illustrated in Fig. 9.7 showing the post-contingency $P-V_3$ curve, where it is evident that the long-term load demand characteristic corresponding to $P = P_o$ (vertical dashed line) is beyond the maximum power point C.

Following the loss of the long-term equilibrium point, the system is voltage unstable, so that increased load admittance results in decreased power consumption. The time evolution of the power P_L under the combined effect of LTC and load

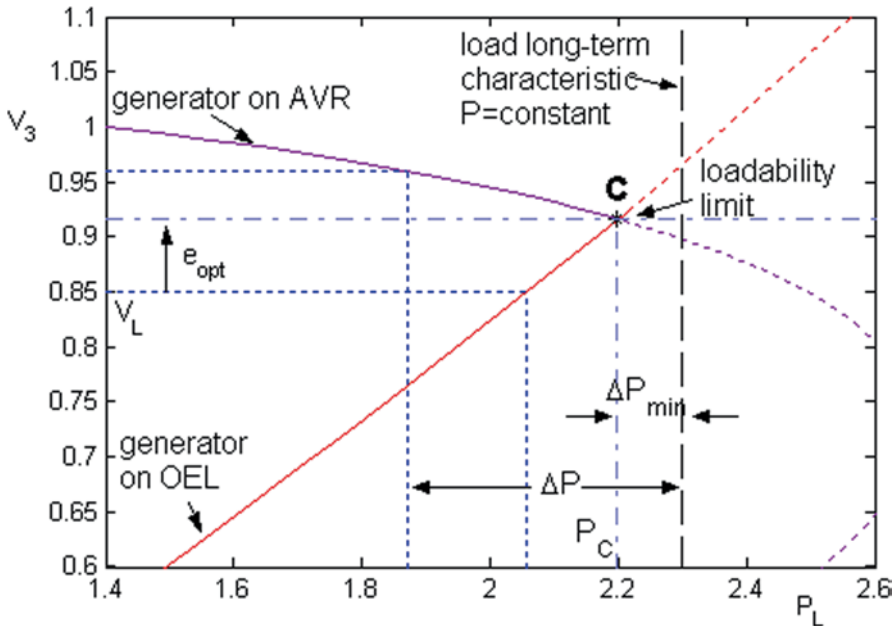


Fig. 9.7 PV curves for the simple system of Fig. 10.6

restoration is shown in Fig. 9.8 (curve marked “no emergency control”). As is clearly seen, the load drops fast until the point where the LTC reaches the limits of its control range (r_{min}). From this point, the slope of voltage drop is slower, due to load self-restoration only. Fig 9.9 shows the corresponding evolution of distribution side voltage V_4 . The voltage instability is evident, when no countermeasures are taken: The voltage falls close to 80% when the LTC tap positions are exhausted and even further as the load restoration continues.

In Figs. 9.8 and 9.9, the four LTC emergency control methods mentioned above are compared to each other and to load shedding.

Starting from the left, the one less efficient is clearly the tap blocking. As seen, this type of emergency control does not introduce any actual relief for the system; it simply changes the slope of decline. However, the time thus gained may be valuable, especially if load self-restoration is not in effect. Note also that tap blocking is more effective when applied preventively, i.e., before the transmission voltage drops due to load pickup or a contingency.

Distribution voltage set-point reduction is more efficient as a countermeasure, since it forces the LTC to operate in favor of the transmission-side voltage. As seen in Fig. 9.9, the LTC is able to keep V_4 within its new deadband for some time. However, as a long-term equilibrium has not been restored, load self-recovery will eventually pull the system to the lower side of the PV curve (once the generator gets limited). Note that while the LTC is able to keep V_4 within the deadband, load consumption is increased thanks to the load self-restoration.

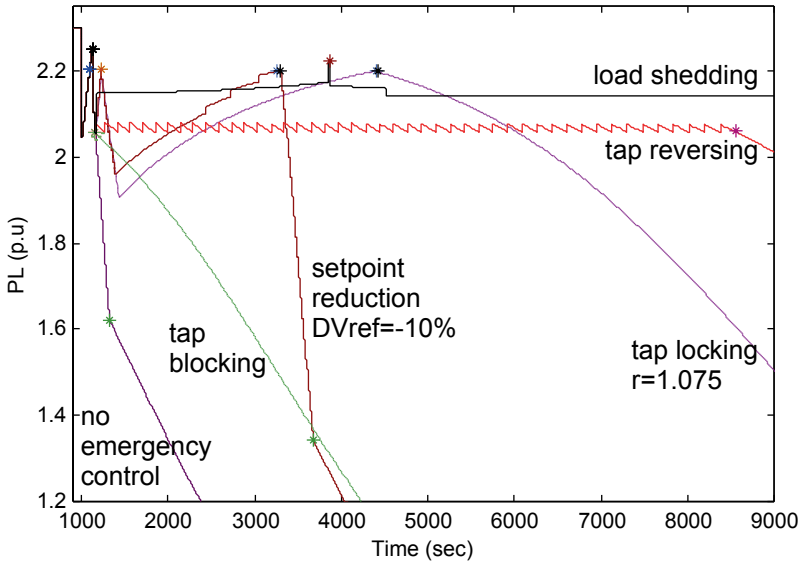


Fig. 9.8 Test system simulation: load consumption versus time

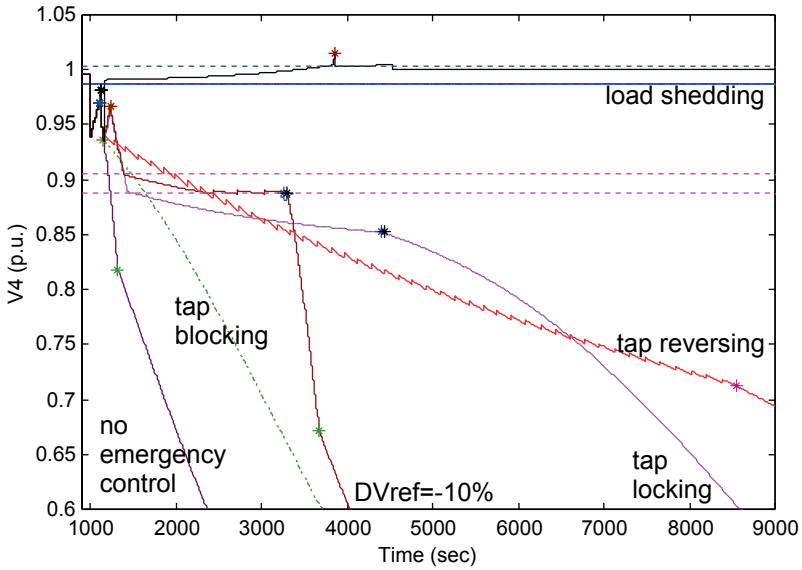


Fig. 9.9 Test system simulation: distribution voltage versus time

The third method illustrated in Figs. 9.8 and 9.9 is LTC locking at a prespecified tap (in this case, $r=1.075$). This countermeasure combines the benefits of the two previous ones: It provides a temporary relief to the system by tapping in favor of the transmission-side voltage, and it avoids the LTC instability.

On the other hand, the disadvantage of tap locking is that the secondary voltage is not regulated and, as seen in Fig. 9.9, it drops below even the reduced deadband of the previous method.

The fourth method is that of tap reversing. The curves shown for comparison in Figs. 9.8 and 9.9 refer to the case with $e=0$. As seen in the figures, tap reversing is the most effective of all LTC emergency measures, as it allows operation with almost constant load and transmission voltage for as long as the LTC is within its control range.

During this time, the admittance seen from the primary

$$G_1 = G / r^2 \quad (9.7)$$

is kept almost constant as the tap ratio increases to compensate for load conductance increase. In this way, voltages and load consumption are kept almost constant.

Note from Fig. 9.8 that tap reversing is essentially dynamic load reduction. This can be explained by observing the PV curve of Fig. 9.7. As the voltage V_3 is brought to its specified value ($V_L + e$), the power absorbed from the network is also determined. Note also that the voltage correction (e_{opt}) providing the minimum load reduction (ΔP_{min}) is that corresponding to the maximum loadability point C. It can be easily shown that in this case tap reversing is also able to remain longer in effect, i.e., the LTC range is exhausted later.

As seen from all the above measures, only load shedding is able to restore the long-term system equilibrium in the presence of load self-restoration. Thus, in serious contingencies, a system cannot be efficiently restored without some form of direct load shedding. In the next section, the question of designing an efficient load-shedding scheme is considered.

9.5 Undervoltage Load Shedding

While used in the last resort, load shedding is an effective countermeasure against voltage instability (Taylor 1992) especially when the system undergoes a severe initial voltage drop that cannot be tolerated for a long time. This section describes the load-shedding scheme implemented by Hydro-Quebec (H-Q) to protect its system against long-term voltage instability.

As for any SPS, the design of automatic load shedding is a challenging task in terms of number of protection settings and scenarios to consider. Even study engineers with a very good knowledge of their system face this huge complexity problem. We describe how combinatorial optimization has been used to choose the most appropriate settings of the above-mentioned load-shedding scheme.

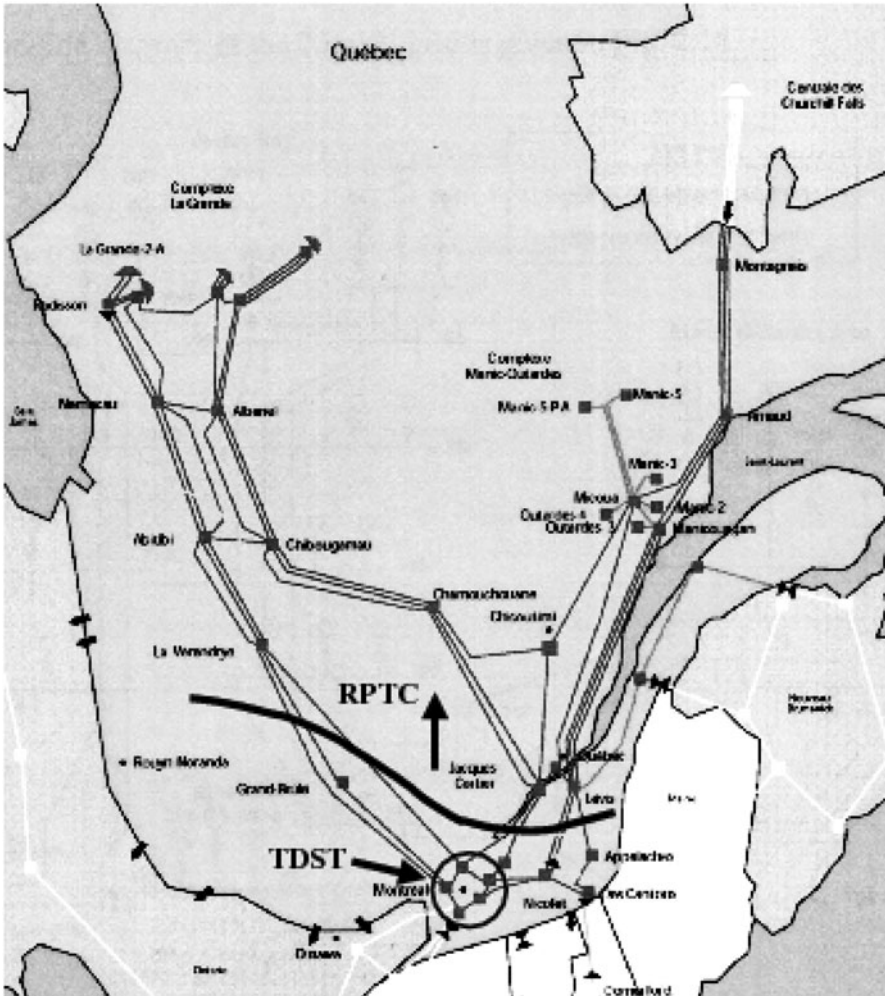


Fig. 9.10 H-Q system and its SPS

The material of this section is largely borrowed from Moors et al. (2000), Van Cutsem et al. (2002), Moors (2002), and Lefebvre et al. (2003, 2004) in which the interested reader may find additional information.

9.5.1 Undervoltage Load Shedding in the H-Q System

With its long transmission corridors between the hydro generation areas in the north and the main load centers in the southern part of the province (see Fig. 9.10), the H-Q system is exposed to angle, frequency, and voltage stability problems.

Besides static VAR compensators and synchronous condensers, the automatic shunt reactor switching devices—named MAIS—play an important role in voltage control (Bernard et al. 1996). These devices, in operation since early 1997, are now available in 22 735-kV substations and control a large part of the total 25,500 MVAR shunt compensation. Each MAIS device relies on the local voltage, the coordination between substations being performed through the switching delays. While fast-acting MAIS can improve transient angle stability, slower MAIS significantly contribute to voltage stability. MAIS devices react to voltage drops but also prevent overvoltages by reconnecting shunt reactors when needed.

In order to upgrade the reliability of its transmission system, H-Q has developed over the recent years an extensive defense plan against major disturbances. Besides traditional underfrequency load-shedding measures, an extensive generation rejection and remote load-shedding scheme—named RPTC (Trudel et al. 1999)—has been installed to face transient angle stability problems. The next step of this deployment has been the undervoltage load-shedding scheme—named TDST (see Fig. 9.10).

While RPTC is an *event-based* SPS (due to the speed of angle instability phenomena), TDST will be *response-based* (owing to the nature of long-term voltage instability), relying on five transmission voltages measured in the Montreal area. More precisely, local voltages will be measured (with a sampling rate of 0.1 s) in five 735-kV substations equipped with MAIS devices and validated through the data acquisition chains of the latter. The average \bar{V} of these local voltages will then be considered, provided that three valid values out of the five have been received. The protection will rely on \bar{V} not only to allow bad data rejection but also to better identify dangerous disturbances. Indeed, while an N-1 contingency (for which no load shedding is allowed) can affect one of the local voltages, it will have little effect on the average \bar{V} . Conversely, a significant drop of \bar{V} is an indication that an N-2 or more severe disturbance has occurred.

TDST can act in a predefined “load basin”, of which it will be allowed to shed at most a certain percentage. The remote load-shedding controller present in RPTC knows which distribution circuit breakers can be opened.

9.5.2 The Load-Shedding Logic

The load-shedding controller relies on the following:

- Three rules, each allowed to act *once*:

$$R_1 : \text{if } \bar{V} < V_1^{\min} \text{ during } d_1 \text{ seconds, shed } \Delta P_1 \text{ MW} \quad (9.8)$$

$$R_2 : \text{if } \bar{V} < V_2^{\min} \text{ during } d_2 \text{ seconds, shed } \Delta P_2 \text{ MW}$$

$$R_3 : \text{if } \bar{V} < V_3^{\min} \text{ during } d_3 \text{ seconds, shed } \Delta P_3 \text{ MW}$$

- One rule allowed to act several times, provided that (at least) one of the above has been already activated:

R_l : if $\bar{V} < V_l^{\min}$ during d_l seconds, shed ΔP_l MW, where the larger $V_l^{\min} - \bar{V}$, the larger ΔP_l .

Rules R_1 to R_3 aim at making the voltage promptly recover once it has dropped below an unacceptable level (for instance, from the customer viewpoint). The V_1^{\min} parameter is set at this level, while the other voltage thresholds are such that

$$V_3^{\min} < V_2^{\min} < V_1^{\min}. \quad (9.9)$$

Each rule corresponds to a different level of severity. Correspondingly, the load-shedding amounts and delays are chosen so that the deeper the voltage drop, the larger the shedding and the shorter the delay:

$$\Delta P_3 > \Delta P_2 > \Delta P_1 \text{ and } d_3 < d_2 < d_1 \quad (9.10)$$

Alternative choices may be thought of. For instance, there might be less or more rules, although in the latter case, the computational effort of the optimization should be kept in mind. Also, the inequalities (9.10) are not mandatory but they have been found to work well. The idea behind rule R_l is to set up a controller adjusting its action to the severity of the situation. The latter is assessed through the average voltage drop over the time interval d_l . To this purpose, the load-shedding step is taken as

$$\Delta P_l = k \Delta V_{avg} \text{ with } \Delta P_l^{\min} \leq \Delta P_l \leq \Delta P_l^{\max} \quad (9.11)$$

where ΔV_{avg} is the average voltage drop,

$$\Delta V_{avg} = \frac{1}{d_l} \int_{t_o}^{t_o+d_l} (V_l^{\min} - \bar{V}) dt, \quad (9.12)$$

and t_o is the time at which \bar{V} falls below V_l^{\min} . Clearly, the larger $V_l^{\min} - \bar{V}$, the larger ΔP_l . Finally, ΔP_l is discretized to take into account that loads are shed by blocks (when opening distribution feeders). While the main purpose of rules R_1 to R_3 is to react to a severe voltage drop, the role of R_l is the final stabilization of the system. In this respect, the thresholds of R_1 and R_l are such that

$$V_1^{\min} < V_l^{\min}. \quad (9.13)$$

With V_l^{\min} set to a higher value, the risk increases of an undue load shedding following a large system transient. On the basis of simulations, it is possible to tune the protection parameters to avoid such false operation; however, the uncertainty affecting the simulation models must be considered as well. Therefore, to increase the protection security, H-Q has decided to condition the application of R_l to the previous triggering of (at least) one of the rules R_1 to R_3 .

Rules R_1 to R_3 are “concurrent” in the sense that any of them can be applied irrespective of the others. However, each rule may be triggered only once. On the

other hand, R_i is conditioned to the other rules, as explained above, but can be applied repetitively. This yields a *closed-loop* design since the protection may act several times, each action being based on the measured result of the previously taken actions, and adjusted in amplitude to the system evolution. This closed-loop design guarantees a higher SPS robustness against modeling uncertainties at the design stage. Note finally that by adjusting its action to the severity of the situation, the controller minimizes the risk of overfrequency (and thermal unit tripping) due to excessive load shedding.

9.5.3 Optimization of the Load-Shedding Controller

The methodology used to adjust the settings of TDST consists of two steps (Moors 2002). In the first step, a set of training scenarios is built, and each unstable scenario of this set is analyzed to determine the minimal load shedding needed. In the second step, the protection parameters are adjusted in order to match as closely as possible the optimal shedding signals computed in the first step, over the whole set of scenarios. A combinatorial optimization method is used to this purpose.

9.5.3.1 Scenario Analysis

The first step thus consists in setting up a set of s training scenarios, corresponding to various topologies, load levels, generation schemes, contingencies, etc. Given the load basin that TDST will control, for each scenario we determine P_i^* ($i = 1, \dots, s$), the minimal amount of load to shed *at a single point in time*, in order to stabilize the system.

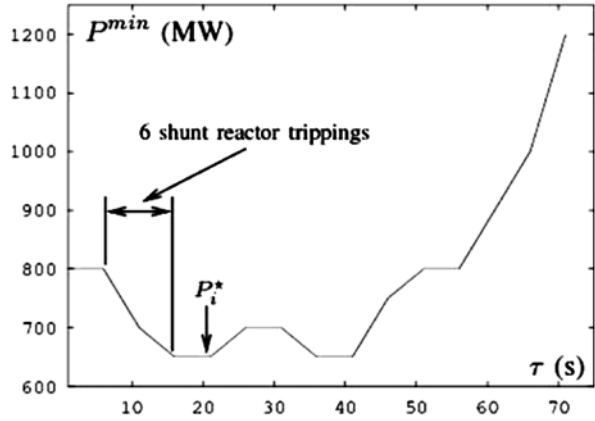
To this purpose, for a given shedding delay τ , the minimal amount P_i^{\min} of load to shed is determined iteratively by incremental or binary search (Moors 2002). This determination is repeated for various values of τ . P_i^* is then taken as the minimum of the $P_i^{\min}(\tau)$ curve. An example is given in Fig. 9.11 for the H-Q system. For the scenario of concern, the best time to shed load is 15–20 s (or 35–40) after the disturbance. This delay allows the MAIS to trip shunt reactors and hence to increase the network transmission capability, thereby reducing the amount of load to shed. Shedding earlier resets the MAIS by increasing the transmission voltages monitored by these devices. The value of P_i^* is 650 MW in this case.

9.5.3.2 The Optimization Problem

Let us denote by \mathbf{x} the vector of all parameters that appear in the rules and have to be adjusted:

$$\mathbf{x} = \left[\Delta P_1 \Delta P_2 \Delta P_3 d_1 d_2 d_3 V_2^{\min} V_3^{\min} k \Delta P_l^{\min} \Delta P_l^{\max} V_l^{\min} d_l \right]. \quad (9.14)$$

Fig. 9.11 Minimal load shedding as a function of shedding delay



Given the s training scenarios, the problem is to determine \mathbf{x} such that the following requirements are met:

- The amount of load shedding must be as close as possible to the ideal value P_i^* determined in the first step.
- All unstable scenarios must be saved (dependability).
- No load must be shed in a stable scenario (security).
- The average voltage \bar{v} must not stay below V_1^{\min} for more than some time.

This can be translated into an optimization problem: Minimize either the L_1 objective,

$$\frac{1}{s} \sum_{i=1}^s [P_i^{sh}(\mathbf{x}) - P_i^* + p_i(\mathbf{x})], \tag{9.15}$$

or the L_∞ objective,

$$\max_i [P_i^{sh}(\mathbf{x}) - P_i^* + p_i(\mathbf{x})] \tag{9.16}$$

where, in the i -th scenario, $P_i^{sh}(\mathbf{x})$ is the total load power shed by the controller and $p_i(\mathbf{x})$ is a penalty term accounting for the violation of the above requirements (Van Cutsem et al. 2002; Moors 2002). In (9.15) or (9.16), the sum or the maximum extends over all the unstable scenarios. The expression within brackets is expected to be positive since the penalties are taken positive and

$$P_i^{sh}(\mathbf{x}) > P_i^*, \tag{9.17}$$

since more load has to be dropped when shedding in several steps (as the controller does) rather than a single one (as assumed when computing P_i^*). This assertion has been verified in all our simulations.

The above optimization problem is complex. Indeed, both $P_i^{sh}(\mathbf{x})$ and $p_i(\mathbf{x})$ must be determined from time-domain simulations and, hence, explicit analytical expressions cannot be established. Moreover, they vary with \mathbf{x} in a discontinuous manner, which prevents from using mathematical programming methods. Finally, multiple local minima are expected. For these reasons, it has been chosen to resort to combinatorial optimization. To this purpose, each component of \mathbf{x} is discretized in a finite number of possible values. The discretization steps are chosen in accordance with the engineering knowledge of the problem.

Evaluating the L_1 or L_∞ objectives for a given protection setting requires to simulate the s scenarios (in order to compute the terms within brackets in (9.15) or (9.16)). This time-consuming step precludes a brute-force enumeration of all the discrete instances of \mathbf{x} . Instead, a method inspired of the branch-and-bound principle has been used with success. The interested reader will find detailed information in the already quoted references, which also provide detailed simulation results.

9.5.4 Examples

We briefly illustrate the operation of the load-shedding controller in two representative scenarios taken from the training set. Both relate to severe double line trips. Figs 9.12 and 9.13 show the post-disturbance time evolutions of \bar{V} (average of five 735-kV bus voltages) under the effect of LTCs, MAIS devices, and load shedding.

The minimal load shedding P_i^* found in the analysis phase was 1450 MW for the case of Fig. 9.12, and 650 MW for that of Fig. 9.13. The disturbance is applied at $t=5$ s. In the scenario of Fig. 9.12, the behavior is typical of a “traditional” undervoltage load-shedding scheme. In the first seconds following the disturbance occurrence, several rules are activated to shed an important amount of load, which brings \bar{V} back above 0.94 pu. The final stabilization is then guaranteed by both MAIS devices and the R_i rule.

The situation is different in Fig. 9.13: Although \bar{V} falls below V_1^{\min} and V_2^{\min} just after the disturbance, the controller takes advantage of the MAIS devices, which make \bar{V} recover above 0.94 pu. Once the voltage decrease resumes, the controller has to wait for rule R_1 to shed 400 MW; then, it relies on rule R_i to adjust its action to the severity of the situation. This allows the total load shed (700 MW) to be very close to the target value ($P_i^* = 650$ MW).

9.6 Recent Advances in Voltage Stability Monitoring and Protection

This section summarizes the more recent research conducted by the authors of this chapter concerning voltage instability monitoring and system protection against voltage collapse.

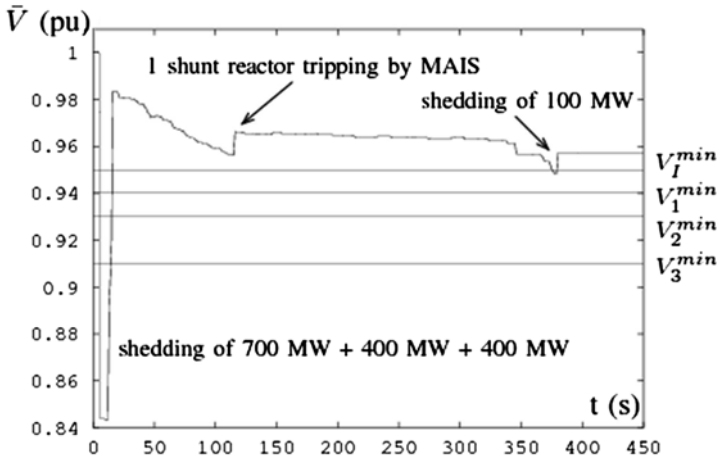


Fig. 9.12 Post-disturbance evolution of voltage (first example)

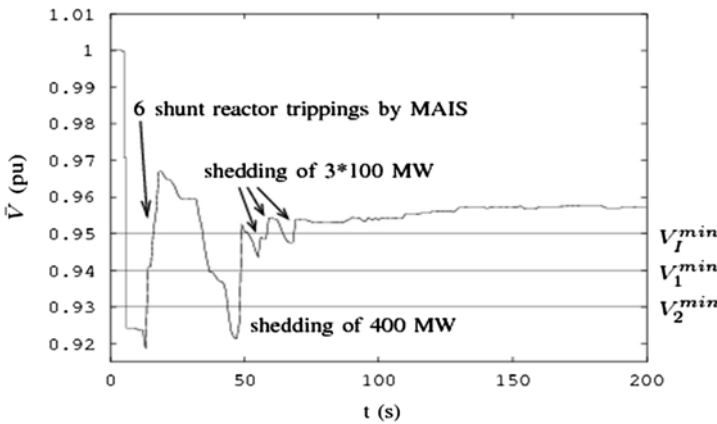


Fig. 9.13 Post-disturbance evolution of voltage (second example)

Concerning voltage stability monitoring, the failure of the LTC to restore the controlled voltage after a severe drop due to a contingency can serve as a voltage instability indicator. This feature is exploited in the method called Local Identification of Voltage Emergency Situations (LIVES) described in Vournas and Sakellariadis (2008) and Vournas and Van Cutsem (2008). An autonomous voltage stability protection system based on LIVES method was proposed (Vournas et al. 2010) and was compared to a minimum load-shedding scheme based on wide-area Phasor Measurement Unit (PMU) measurements (Glavic and Van Cutsem 2009a, 2009b).

Further research has been conducted on early detection of impending voltage instability after a large disturbance. An overview of voltage instability detection methods is offered in Glavic and Van Cutsem (2011). The use of voltage and cur-

rent synchrophasor measurements appears to be promising (Glavic and Van Cutsem 2009a, 2009b) although the challenge is to exploit a limited number of such measurements (Glavic and Van Cutsem 2012).

Various forms of emergency control involving load shedding and its proper combination with LTC emergency controls are reported in Otomega et al. (2007, 2013), Capitanescu et al. (2009), and Otomega and Van Cutsem (2011).

References

- Bernard S, Trudel G, Scott G (1996) A 735-kV shunt reactors automatic switching system for Hydro-Quebec network. *IEEE Trans Power Syst* 11:2024–2030
- Capitanescu F, Otomega B, Lefebvre H, Sermanson V, Van Cutsem T (2009) Decentralized tap changer blocking and load shedding against voltage instability: prospective tests on the RTE system. *Int J Electr Power Energy Syst* 31(9):570–576
- Dobson I, Lu L (1992) Immediate change in stability and voltage collapse when generator reactive power limits are encountered. *IEEE Trans Circuits Syst I* 39(9):762–766
- Glavic M, Van Cutsem T (2009a) Wide-area detection of voltage instability from synchronized phasor measurements. Part I: principle. *IEEE Trans Power Syst* 24(3):1408–1416
- Glavic M, Van Cutsem T (2009b) Wide-area detection of voltage instability from synchronized phasor measurements. Part II: simulation results. *IEEE Trans Power Syst* 24(3):1417–1425
- Glavic M, Van Cutsem T (2011) A short survey of methods for voltage instability detection. In: *Proceedings of the IEEE PES general meeting*, IEEE, Pittsburgh
- Glavic M, Van Cutsem T (2012) State reconstruction from a limited number of synchronized phasor measurements: application to voltage instability detection. In: *Proceedings of the IEEE PES general meeting*, IEEE, San Diego
- Karlsson D (convener) (2001) CIGRE TF 38.02.19: system protection schemes in power networks. CIGRE Brochure 2001
- Kundur P (convener), Paserba J (secretary), Ajarapu V, Andersson G, Bose A, Canizares C, Hatziargyriou N, Hill D, Stankovic A, Taylor C, Van Cutsem T, Vittal V (2004) Definition and classification of power system stability. *IEEE Trans Power Syst* 19:1387–1401
- Larsson M (2000) Coordinated voltage control in electric power systems, Ph. D. Dissertation, Dept. of Industrial Electrical Engineering and Automation, Lund University, Lund
- Lefebvre D, Moors C, Van Cutsem T (2003) Design of an undervoltage load shedding scheme for the Hydro-Quebec system. *Proceedings of IEEE PES general meeting*, IEEE, Toronto
- Lefebvre D, Bernard S, Van Cutsem T (2004) Undervoltage load shedding scheme for the Hydro-Quebec system. *Proceedings of the IEEE PES general meeting*, IEEE, Denver
- Moors C (2002) On the design of load shedding schemes against voltage instability in electric power systems, PhD thesis. University of Liège, Faculty of Applied Sciences
- Moors C, Lefebvre D, Van Cutsem T (2000) Design of load shedding schemes against voltage instability. *Proceedings of IEEE PES winter meeting*, IEEE, Singapore
- Otomega B, Van Cutsem T (2011) A load shedding scheme against both short- and long-term voltage instabilities in the presence of induction motors. *Proceedings of the IEEE PES Power Tech*, Trondheim, IEEE, Norway, June 2011
- Otomega B, Sermanson V, Van Cutsem T (2003) Reverse-logic control of load tap changers in emergency voltage conditions. *Proceedings of the IEEE Power Tech*, IEEE, Bologna
- Otomega B, Glavic M, Van Cutsem T (2007) Distributed undervoltage load shedding. *IEEE Trans Power Syst* 22(4):2283–2284
- Otomega B, Glavic M, Van Cutsem T (2013) A two-level emergency control scheme against power system voltage instability. *Control Eng Pract* (in press) (available online: 10.1016/j.coneng-prac.2013.10.007)

- Trudel G, Bernard S, Scott G (1999) Hydro-Quebec's defense plan against extreme contingencies. *IEEE Trans on Power Syst* 14:958–965
- Taylor C (1992) Concepts of undervoltage load shedding for voltage stability. *IEEE Trans Power Syst* 7:480–488
- Taylor C (1994) *Power system voltage stability*. EPRI/Mc Graw-Hill, New York
- Van Cutsem T, Vournas C (1998) *Voltage stability of electric power system*. Kluwer, Boston
- Van Cutsem T, Vournas C (2007) Emergency voltage stability controls: an overview. *Proceedings of the IEEE PES general meeting, IEEE, Tampa, June 2007*
- Van Cutsem T, Moors C, Lefebvre D (2002) Design of load shedding schemes against voltage instability using combinatorial optimization. *Proceedings of the IEEE PES winter meeting, IEEE, New York*
- Vournas C, Sakellariadis NG (2008) Problems and solutions for local identification of voltage instability and emergency control. *Proceedings of the IEEE PES general meeting, IEEE, Pittsburgh, July 2008*
- Vournas C, Van Cutsem T (2008) Local identification of voltage emergency situations. *IEEE Trans Power Syst* 23(3):1239–1248
- Vournas C, Manos G, Kabouris J, Van Cutsem T (2000) Analysis of a voltage instability incident in the Greek power system. *Proceedings of the IEEE PES winter meeting, IEEE, Jan 2000*, pp 1483–1488
- Vournas CD, Metsiou A, Kotlida M, Nikolaidis V, Karystianos M (2004) Comparison and combination of emergency control methods for voltage stability. *Proceedings of the IEEE PES general meeting, IEEE, Denver, June 2004*
- Vournas CD, Nikolaidis VC, Tassoulis A (2007) Post-mortem analysis and data validation in the wake of the 2004 Athens blackout. *IEEE Trans Power Syst* 21(3):1331–1339
- Vournas C, Lambrou C, Glavic M, Van Cutsem T (2010) An integrated autonomous protection system against voltage instability based on load tap changers. *Proceedings of the 2010 IREP symposium—bulk power system dynamics and control—VIII, Buzios, Brazil, Aug 2010*

Chapter 10

Online Voltage Security Assessment

Costas Vournas and Thierry Van Cutsem

Abstract This chapter deals with Voltage Security Assessment (VSA) and its online application. Methods for contingency analysis are briefly reviewed. The associated concepts of transfer capability, loadability limit, and secure operation margin are explored in some detail. Methods for preventive security control are outlined. An application of online VSA in the control center of a real system is then described and typical results available to operators are presented.

10.1 Introduction

Power system security in general refers to the ability of a system operating in a particular condition (operating point) to withstand any disturbance out of a pre-specified set. These disturbances (such as relay tripping, etc.) are usually referred to as contingencies. In the case of voltage security, we examine in particular voltage stability after a contingency.

In this sense, an operating point is voltage secure, if following any contingency of the specified set voltage stability is maintained and a new stable operating point is reached in each case. Usually only long-term voltage stability is examined, but in some cases, where induction machines are dominating, the analysis can be extended to short-term voltage stability as well (see Chap. 9).

Since Voltage Security Assessment (VSA) deals with voltage stability, it is part of Dynamic Security Assessment (DSA) and is thus different from Static Security Assessment (SSA), which concentrates on verifying that post-contingency voltages are within some limits and line currents below thermal capacity. However, it is relatively easy to combine VSA and SSA since the tools for the former are also able to analyze the latter.

C. Vournas (✉)
National Technical University of Athens, Athens, Greece
e-mail: vournas@power.ece.ntua.gr

T. Van Cutsem
Dept. Electrical Engineering and Computer Science, FNRS (Fund for Scientific Research)
and University of Liège, Sart Tilman, B37 - B4000 Liège, Belgium
e-mail: t.vancutsem@ulg.ac.be

The contingencies that are relevant to VSA are in general equipment outages, such as generator, transformer, or transmission line tripping. All single contingencies are usually included in the specified contingency set, which is then referred to as *N-1 security* set. An exception is made for radial links, whose opening will obviously result in an isolated bus.

Apart from single contingencies, a number of selected credible double or even triple contingencies may be included in the specified contingency set. These contingencies are determined by considering common cause events, based upon the experience of the VSA user and the knowledge of system structure.

This chapter concentrates on the methods used by the authors in a number of VSA applications in collaboration with industrial partners (Van Cutsem et al. 1995; Van Cutsem and Mailhot 1997; Vournas 1999). In particular, the application of on-line VSA in the National Control Center (NCC) of the Hellenic interconnected system is described (Van Cutsem et al. 2005a). The voltage stability problems to which this system is exposed have already been described in Chap. 9. Use of the VSA tools presented in this chapter for preventive control, as well as for off-line assessment of countermeasures and system upgrades, is also discussed.

10.2 Voltage Stability Analysis Methods

10.2.1 Classification of Methods

The following are the main categories of computations performed for voltage stability analysis purposes:

1. *Contingency analysis* consists of checking the system response to large disturbances, at a given operating point. As discussed in the introduction, the contingencies of interest for long-term voltage stability are outages of transmission or generation facilities; the sequence of events leading to such outages does not really matter. According to the N-1 criterion, the system must be able to withstand any single transmission or generation outage with the sole help of post-contingency controls that do not prevent load power restoration (Load Tap Changer (LTC) blocking and load shedding, described in the previous chapter, are thus not allowed). For short-term voltage stability, the system responses to short circuits are investigated, but only the transient limitation of generator excitation is included in the model.
2. *Security margins* provide a deeper look at security. Voltage stability margins are most often assessed in terms of admissible load demand increase. Generation is increased in a remote area, which leads to increasing power flows on the transmission system. Available Transfer Capabilities (ATCs) are particular cases of security margins. According to the grid codes in effect in most electricity markets, Transmission System Operators (TSOs) have to post ATC values in order

for the market participants to reserve capacity for their transactions. ATCs must take into account, among other factors, the voltage security of the system.

3. *Preventive control* aims at determining the optimal adjustment of pre-contingency parameters so that the system response to the disturbance or load increase is improved.
4. As for SSA, *contingency filtering* is of high practical importance, when extensive lists of contingencies have to be considered.

In the remainder of this section, several of the above methods will be briefly reviewed. A more extensive (and somewhat more exhaustive) analysis of methods can be found in Van Cutsem and Vournas (1998).

10.2.2 Contingency Analysis Methods

Before describing the methods used for contingency analysis, a brief overview of the power system model is introduced, as well as a note on static versus time-domain methods of analysis.

10.2.2.1 Review of Power System Model

For the ease of the reader, and to make the chapter self-supporting, we briefly recall hereafter the set of equations that make up the long-term model of a power system (further details in Sect. 9.2.2 of Chap. 9):

- Network equations:

$$\mathbf{0} = \mathbf{g}(\mathbf{x}, \mathbf{y}, \mathbf{z}) \quad (10.1)$$

- Short-term continuous dynamics:

$$\dot{\mathbf{x}}_1 = \mathbf{f}_1(\mathbf{x}_1, \mathbf{x}_2, \mathbf{y}, \mathbf{z}) \quad (10.2)$$

- Long-term continuous dynamics:

$$\dot{\mathbf{x}}_2 = \mathbf{f}_2(\mathbf{x}_1, \mathbf{x}_2, \mathbf{y}, \mathbf{z}) \quad (10.3)$$

- Long-term discrete dynamics:

$$\mathbf{z}(t_k^+) = \mathbf{h}(\mathbf{x}, \mathbf{y}, \mathbf{z}(t_k^-)) \quad (10.4)$$

10.2.2.2 Static Versus Time-Domain Methods

As recalled in Sect. 9.2.4 of Chap. 9, the main cause of long-term voltage stability is the loss of long-term equilibrium. Static methods focus on the existence of such equilibrium and therefore rely on algebraic equations derived more or less accurately from the equilibrium conditions of the dynamic model (10.1)–(10.4). Most often, the power system model at equilibrium is approximated by its standard load-flow equations, in which:

- Loads are represented as constant power. This is justified inasmuch as they are controlled by LTCs and the latter do not get limited. Neglecting the LTC dead-bands involves some approximation.
- Generators are represented as either constant voltage or constant reactive power sources. This neglects the voltage droop under automatic voltage regulator (AVR) control, as well as variations of reactive power with voltages under field—and even more armature—current limit; in all cases, it is absolutely essential to represent the Q limit as a function of active generation P and preferably also of terminal voltage V .
- Following any power imbalance, all generator active powers should be rescheduled (e.g., according to frequency control), so that the slack bus is not unrealistically loaded.

Static methods are usually very efficient but, expectedly, they cannot account for post-contingency controls that depend on the system evolution nor capture more involved instability mechanisms (such as lack of attraction towards an existing equilibrium).

Time-domain methods, on the other hand, are generally computationally demanding but offer higher accuracy and better interpretability of results (e.g., with respect to the sequence of events).

10.2.2.3 Post-Contingency Load flows

Starting from the static methods, the most widely used tool for contingency analysis is the post-contingency load flow. When the load-flow program converges to a solution after a contingency, this demonstrates the existence of a long-term equilibrium of the system. The divergence of the load-flow program, on the other hand, may reveal the loss of a long-term equilibrium and, hence, a long-term voltage instability problem. However, a load flow may diverge for numerical reasons, especially when many controls have to be adjusted and/or many generators switch under reactive power limits. In addition, in the case of divergence due to real instability, one is left without information on possible causes and/or remedies.

Several modifications to the standard Newton method have been proposed (e.g., Iwamoto and Tamura 1981; Overbye 1995) to increase reliability in cases of difficult convergence and provide information on the location of the problem (whatever the size of the system, even a single, erroneously loaded, radial appendix may cause divergence!).

10.2.2.4 Multiple Time-Scale Simulation

Short-term voltage stability simulation requires the numerical integration of the differential-algebraic model (10.1, 10.2). This is basically the model used in conventional transient or small signal (angle) stability studies, but with proper account for load behavior, especially of induction machines.

Long-term voltage stability studies require simulating the whole model (10.1–10.4). This model is stiff, involving both fast and slow components. A number of approaches are used by the industry:

- The full system response is computed with a constant, small step size needed for accurate simulation of the short-term dynamics. This is a simple but brute-force approach resulting generally in long computing times.
- A variable step size is introduced that increases after the short-term transients have died out in order to filter out the fast transients when no longer significant.
- The step size is automatically adjusted to the system behavior: shorter when fast transients are excited and longer when only slow transients are present.

The last two approaches require a numerically robust integration scheme, in practice an implicit method, such as the trapezoidal rule for instance. Several criteria are available to adjust the step size.

In long-term voltage simulations, the numerous discrete-type devices (10.4) give rise to frequent discrete transitions, which are an obstacle to large step size increases. Indeed, the transition times have to be determined with a reasonable accuracy and the fast dynamics induced by the transitions may cause the step size to decrease very often. To avoid those discontinuities, a continuous-time approximation of the LTC model or a generic model of load power restoration can be used.

In spite of the significant speedup brought by variable step size integration, multi-time-scale simulation remains heavy in terms of computing times, data maintenance, and output processing. However, some more recent advances, briefly summarized in Sect. 10.4, tend to change this picture quite drastically.

10.2.2.5 Quasi-Steady-State Time Simulation

The Quasi-Steady-State (QSS) approximation of the long-term dynamics extends the idea of filtering out the fast dynamics in long-term simulation. This method consists of neglecting the short-term dynamics, which are replaced by their equilibrium conditions. Thus, the differential equations (10.2) of generators, motors, compensators, etc. are formally replaced by the algebraic equations:

$$\mathbf{0} = \mathbf{f}_1(\mathbf{x}_1, \mathbf{x}_2, \mathbf{y}, \mathbf{z}), \quad (10.5)$$

which are solved together with the set of network equations (10.1).

In practice, three equations of the type (10.5) are sufficient to accurately represent each synchronous machine, taking into account saturation, AVR voltage regulation,

and speed governor regulation, respectively. The corresponding variables in \mathbf{x}_1 are the Electromotive Force (EMF) proportional to field current, the EMF behind saturated synchronous reactances, and the internal rotor (or load) angle. System frequency is an additional algebraic variable of the type \mathbf{x}_1 , the changes in active power production being automatically shared by generators according to permanent speed droops, or another mechanism.

The resulting QSS model (10.1, 10.3–10.5) is easily simulated. Short-term dynamics being neglected, there is no point in identifying very accurately the time t_k of each transition in (10.4); rather, the various discrete devices are checked “synchronously” at multiples of the time step h , which is in the order of several seconds, depending on the system. Hence, $t_k = kh$ in (10.4).

To integrate the long-term dynamics, a partitioned scheme is preferred, i.e., the algebraic equations (10.1, 10.5) and the differential equations (10.3) are solved alternately. This allows using a single Jacobian matrix to both integrate the long-term dynamics and solve the numerous discontinuities (10.4). This Jacobian is kept constant as long as possible. In some systems, it is possible that the model includes no differential equation (10.3); the QSS evolution is then a succession of short-term equilibria dictated by the discrete transitions (10.4).

The QSS technique has been extensively tested by the authors, in a wide variety of applications and systems. It greatly reduces the computational complexity of long-term simulation, provides the computational efficiency required for real-time applications, and is a good compromise between the efficiency of static methods and the advantages of time-domain methods.

10.2.2.6 Combining Detailed and QSS Simulation

The QSS approximation is appropriate for checking voltage security with respect to “normal” (typically N-1) contingencies (Van Cutsem and Mailhot 1997). When dealing with severe disturbances, expectedly the QSS model meets some limitations.

The first limitation lies in the implicit assumption that the neglected short-term dynamics are stable. After a large disturbance, the system may lose stability in the short-term time frame (within—say—the first 10 s after the disturbance) and hence never enter the long-term phase simulated under the QSS approximation.

The second limitation is linked to the discrete events represented by (10.4). A large disturbance may trigger controls with great impact on the system long-term evolution (e.g., shunt compensation switching, underfrequency or undervoltage load shedding, etc.). Since the sequence of controls depend on the continuous dynamics, it might not be correctly identified from the simplified QSS model.

To deal with the above situations, a coupling between detailed and QSS simulation has been proposed in Van Cutsem et al. (2005b). Detailed time simulation is used to analyze the short-term period following the simulated disturbance, detect possible instability, and identify the discrete controls triggered. Next, QSS simulation is used

to simulate the same time interval with the discrete controls imposed as external events before letting the system evolve as usual in the long term. Successful results have been obtained on the Hydro-Quebec system (presented in Chap. 9).

10.2.3 Total Transfer Capability and System Stress

As explained in Sect. 10.2.1, TSOs are required to post ATCs in various directions. ATC is usually obtained by computing the Total Transfer Capability (TTC) between specified sets of sources (where generation is increased) and sinks (where generation is reduced, or load increased), and subtracting the base case value of the corresponding power transfer as well as a reliability margin accounting for uncertainties.

10.2.3.1 Types of Limit Computation

Within the context of long-term voltage security, there are basically two approaches to compute TTC:

- In *loadability limit* computations, the system is progressively stressed until it reaches instability or unacceptable operating conditions. Loadability limits can be computed in the current (no contingency, or “N”) configuration of the system. However, since many voltage instability incidents were triggered by disturbances, it is of interest to compute *Post-Contingency Loadability Limits (PCLL)*. The latter indicate how much the system can be stressed *after* a contingency has taken place
- In *Secure Operation Limit (SOL)* computations, the system is progressively stressed in its pre-contingency configuration, until its response to the contingency becomes unacceptable. SOLs are more meaningful for real-time operation where they refer to parameters that operators either observe or control. Also, the computational procedure allows accounting for both pre-contingency actions/controls taken in reaction to the increased power transfer and post-contingency controls taken in response to the disturbance.

Sections 10.2.4 and 10.2.5 summarize methods for determining loadability and SOLs, respectively.

10.2.3.2 Definition of Stress Direction

Both loadability and SOLs, and hence TTCs and ATCs, rely on a specified direction of system *stress*. The stress is a change in load and generation, which makes the system weaker by increasing power transfer over relatively long distances and/or drawing on reactive power reserves. A system stress is characterized by its *direction*,

i.e., by the participation of each load active and reactive power to the overall load demand increase and also the participation of each generator active power production to the necessary overall generation adjustment. This can be written as:

$$P_i^d = P_i^{do} + a_i \Delta P^d \quad (10.6)$$

$$Q_i^d = Q_i^{do} + b_i \Delta Q^d \quad (10.7)$$

$$P_k^g = P_k^{go} + c_k \Delta P^g, \quad (10.8)$$

where

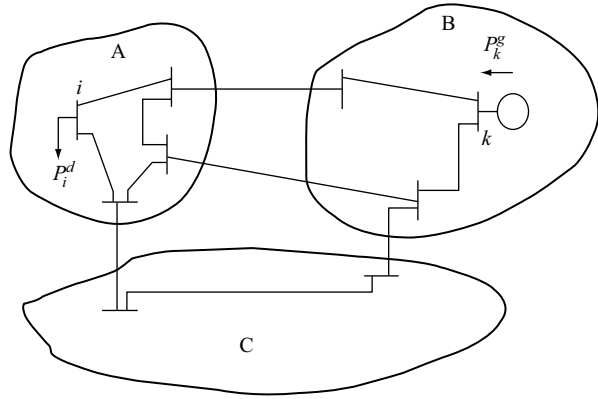
$P_i^d(Q_i^d)$	is the active (reactive) load demand at bus i ;
$P_i^{do}(Q_i^{do})$	the initial (base-case) active (reactive) load demand at bus i
$\Delta P^d(\Delta Q^d)$	the total active (reactive) load demand increase
P_k^g	the active power generation at bus k
P_k^{go}	the corresponding initial generation at bus k
ΔP^g	the total active power generation increase
a_i, b_i and c_k	dimensionless participation factors.

Most often, the reactive power increase ΔQ_d is taken to be proportional to the active power increase ΔP^d and the generation change ΔP^g proportional to ΔP^d (with a ratio slightly larger than 1, in order to account for losses). Hence, all power injection changes can be rewritten as proportional to a single parameter, denoted μ in the sequel. This is essential in order for the resulting security margin to be uniquely determined. With this notation, the system long-term equilibrium equations can be written in compact form as:

$$\mathbf{F}(\mathbf{u}, \mathbf{p}^o + \mu \mathbf{d}) = \mathbf{0}, \quad (10.9)$$

where \mathbf{u} is a vector of state variables, \mathbf{p}^o is the vector of initial parameters P^{do} , Q^{do} , P^{go} , and \mathbf{d} defines the direction of stress. Note that in (10.9) the reactive power (or excitation current) limits are implicitly included. An inequality formulation is also possible to ensure this (Van Cutsem and Vournas 1998).

For instance, in the example system of Fig. 10.1, one might be interested in assessing the TTC from area B to area A. One stress direction to assess this capability is a load increase in area A and a generation increase in area B, which corresponds to $a_i = 0$ in area B and $c_k = 0$ in area A. Alternatively, the stress direction may consist of generation decrease in A and generation increase in B. In this case, $c_k < 0$ in area A and $c_k > 0$ in area B whereas ΔP^g is the amount of generation rescheduling and $\Delta P^d = 0$. Note that each stress direction will result in a different limit, due to the highly nonlinear nature of the system equations.

Fig. 10.1 Three-area system

10.2.4 Computation of Loadability Limits

Various methods have been devised to compute loadability limits:

- *Continuation power flows* (Iba et al. 1991; Ajarapu and Christy 1992; Cañizares and Alvarado 1993) aim at tracing solution paths of (10.9) for varying μ up to the loadability limit and back, using a change of continuation parameter to deal with the loss of solvability near the limit.
- *QV curves* (Mansour et al. 1994) express the relationship between the reactive power at a given bus and the voltage at this bus. They provide the loadability limit with respect to a single bus reactive load increase.
- *Optimization methods*, including *Optimal Power Flow (OPF)*, (Austria et al. 1991; Van Cutsem 1991; Cañizares and Alvarado 1993; Granville et al. 1996; Irisarri et al. 1997), can directly provide the loadability limit as corresponding to the maximum value of μ in the presence of the equality constraints (10.9) and taking into account the switching of generators under reactive power limits.

Thus, a loadability limit can be defined as the solution of the following optimization problem:

$$\max_{\mu, \mathbf{u}} \{ \mu : \mathbf{F}(\mathbf{u}, \mathbf{p}^o + \mu \mathbf{d}) = \mathbf{0} \}, \quad (10.10)$$

where \mathbf{F} includes the appropriate set of generator equations as discussed above. This problem can be solved directly with one of the above quoted methods. It can also be solved indirectly with the help of a time-domain method by simulating the response of the system to a ramp increase in μ . The rate of increase must be slow enough to allow the system to evolve through a succession of steady states, but fast enough to save computing time.

The method applies either to the full dynamic model (10.1–10.4) or its QSS approximation (10.1, 10.3–10.5), which is particularly appropriate for simulating

smooth changes in parameters. It should be noted that during simulation the system is not at equilibrium. However, for a slow enough ramp, each step in the simulation can be considered as a steady state corresponding to a modified set of parameters (e.g., LTC deadbands could be fictitiously modified to include the value of controlled voltage, so as to be at equilibrium).

This method allows using more detailed load models, typically voltage-dependent active and reactive powers behind active LTCs. For instance, a widely used load representation is the exponential model:

$$P_i = P_i^d \left(\frac{V_i}{V_{oi}} \right)^\alpha \quad Q_i = Q_i^d \left(\frac{V_i}{V_{oi}} \right)^\beta, \quad (10.11)$$

where $P_i(Q_i)$ is the active (reactive) consumption and V_{oi} the reference voltage. The ramp is applied to P_i^d and Q_i^d . If load buses are not controlled by LTCs, the total load consumption is smaller than the demand due to voltage drops. When load voltages are controlled by LTCs, this difference becomes smaller, but still remains, due to the effect of LTC deadbands. This does no longer hold when LTCs hit their limits and obviously when the system becomes long-term unstable.

During the demand increase, the imbalances between load and generation due to losses and the discrepancy between load demand and consumption is typically covered by generator governor control.

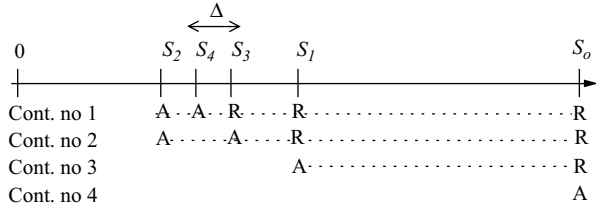
Time simulation can be coupled to sensitivity analysis to stop the simulation after the loadability limit has been crossed (Van Cutsem et al. 1995). At this point, sensitivities based on the inverse of the (long-term) Jacobian matrix change sign through infinity. Sensitivities of the (total) reactive power production to (individual) load reactive powers are very convenient.

10.2.5 Determination of SOLs

10.2.5.1 Binary Search Techniques

For a given direction of stress, the SOL corresponds to the most stressed operating point, such that the system can withstand any contingency in the specified set. Unlike a post-contingency loadability limit, the SOL refers to the pre-contingency configuration of the system. In the SOL computation, the stressed system states are obtained from a pre-contingency load-flow computation, while the effect of a contingency is assessed using one of the methods of Sect. 10.2.2, for instance, time simulation initialized at the load-flow solution. Thus, the pre-contingency stress assumes full load recovery ($P_i = P_i^d$ and $Q_i = Q_i^d$). The reactive power generations are rescheduled by letting the machines under AVR control, unless their reactive capabilities are reached.

Fig. 10.2 Example of simultaneous binary search; post-contingency evolution: *A* Accepted, *R* Refused



The SOLs are determined by *binary search*. This simple and robust method consists of building smaller and smaller intervals of stress values such that the lower limit of each interval corresponds to an acceptable post-contingency evolution, while the upper limit to an unacceptable one. At each step, the interval is divided in two equal parts; if the midpoint is found acceptable (unacceptable), it is taken as the new lower (upper) bound. The procedure is repeated until the interval becomes smaller than a specified tolerance Δ .

To preserve computational efficiency in the presence of multiple contingencies, one should avoid repeating pre-contingency load-flow computations relative to the same stress level. The number of load flows can be minimized by performing a *simultaneous binary search*, which handles as many contingencies as possible at a given stress level. At a given step of this procedure, the unacceptable contingencies remaining from the previous step are simulated. If at least one of them is unacceptable, the acceptable ones are discarded (since their limits are higher than the current stress) and the search proceeds with the unacceptable ones only. For the most severe contingency(ies), the SOL is computed with the desired accuracy, while for the others, a lower bound on the SOL is obtained.

A simple example with four contingencies is shown in Fig. 10.2. The sequence of tested stresses is S_o, S_1, S_2, S_3, S_4 . Five pre-contingency load flows are thus performed in the course of this simultaneous binary search. The SOL corresponds to S_4 and relates to contingency no. 1. Contingency no. 4 is discarded at stress S_o , contingency no. 3 at S_1 , and contingency no. 2 at S_3 .

10.2.5.2 Limits in Load Power Space

It is clear from the above description that the notion of “margin” in multi-load systems may have different interpretations depending upon the method used, as well as upon the way loads are grouped together. Figures 10.3 and 10.4 sketch the difference between SOL and PCLL using a typical sequence of events as seen in the load power space for a hypothetical system.

In particular, the vertical axis corresponds to the power consumption of the area mostly affected by the contingency of concern, while the horizontal axis shows the power consumed in the rest of the system.

Figure 10.3 relates to SOL computation. Point A corresponds to the base case operating point of the system, where security margins are assessed. The dashed line

Fig. 10.3 SOL in load power space

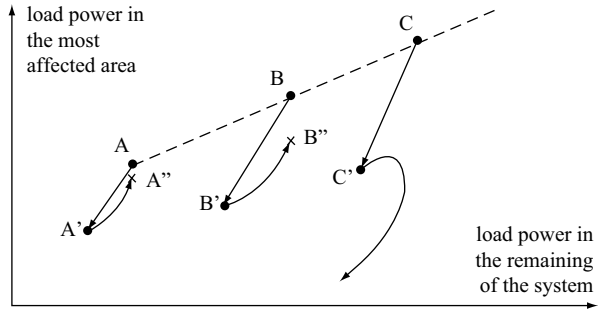
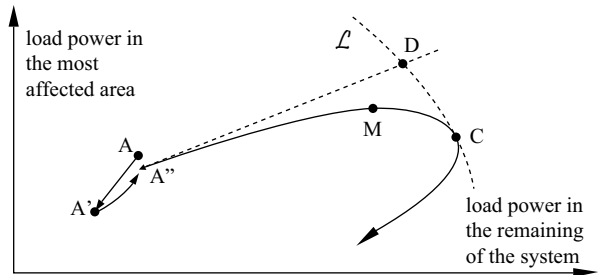


Fig. 10.4 PCLL in load power space



indicates the chosen direction of stress. Points B and C are stressed pre-contingency operating points, at which the system response to the contingency is checked during the binary search for the SOL.

Consider, for instance, system operation at point A. Due to load sensitivity to voltage, under the effect of the contingency, the power consumed by loads drops and the system operating point moves from A to A'. From there on, load restoration mechanisms such as LTCs bring the system back to operating point A'' close to point A, but not exactly, due to LTC deadband effects. In stressed situations, it is possible that some taps reach their limits in the area affected by the contingency, in which case the corresponding load power will not be restored, as suggested by point B'' in the same figure. Clearly, the SOL lies between points B and C of Fig. 10.3.

Figure 10.4 relates to PCLL computation. Again, point A denotes the base case operating point. Following the contingency and the load restoration, the new operating point is A'', which differs from A for already mentioned reasons. From there on, a smooth ramp is imposed on the demand of voltage sensitive loads to bring the system to its loadability limit, and the LTCs are left to act. Under the effect of LTC deadbands, the system trajectory diverts from a straight line. Moreover, the figure refers to the situation where the LTCs in the affected area hit their limits. Under this effect, the distortion of stress direction becomes more pronounced, leaving the affected area with low distribution voltages.

The loadability surface consists of all points where maximum power transfer conditions hold in the post-contingency configuration of the system, i.e., all solutions of (10.10) for various values of \mathbf{d} . The post-contingency trajectory hits the

loadability surface at point C, which may significantly differ from point D, the loadability limit under a linear load increase.

Note that along the post-contingency trajectory the power consumed in the affected area is maximum at point M, which is not literally a loadability limit. At point M, load restoration is still possible, but it is not achieved due to the combined effect of limited LTCs in the affected area and the continuing increase of the load in the rest of the system. The tip of the PV curve referring to this area will correspond to point M and demonstrates how far the load of the affected area will be able to restore following the contingency and assuming the specific stress direction.

It is clear that SOLs and PCLLs give different information and call for different interpretations. SOL is better suited to quantify the “distance to insecurity” in terms of total system load. Along the pre-contingency stress, we have normal operating points similar to those operators are used to observe.

10.2.6 Contingency Filtering

Contingency filtering is an important step of any online security assessment application.

Within the context of SOL computation, a form of filtering takes place at the first step of the simultaneous binary search (at stress S_o in Fig. 10.2), when discarding the contingencies that yield an acceptable system response at maximum stress. However, in spite of the QSS simulation speed, it may take too long to simulate the system response to each contingency of a long list. An additional pre-filtering may be needed before the binary search is launched.

In a majority of systems, post-contingency load flows can be advantageously used to this purpose. The significance of post-contingency load flow in the context of voltage stability has been recalled in Sect. 10.2.2.3. Note, however, that this technique may be inappropriate in systems with strong post-contingency controls (such as the Hydro-Quebec system described in Sect. 9.5.1 of Chap. 9 in this book).

As explained in Sect. 10.2.2.3, load-flow divergence may result from purely numerical problems and some dynamic controls that help stability cannot be accounted for in the static load-flow calculation. Conversely, some system dynamics may be responsible for an instability not detected by the load flow.

Keeping in mind the above conflicting aspects, the filtering consists of:

- Performing detailed simulation of a subset of contingencies labeled potentially harmful
- Identifying the latter as the contingencies that cause the load flow to diverge, or some voltages to drop by more than a threshold ΔV

The value of ΔV must be taken to be large enough to filter out as many harmless contingencies as possible, but not too large to avoid missing a dangerous contingency.

Furthermore, for filtering purposes, accurate post-contingency voltages need not be computed: Estimates obtained from linearized load-flow equations may be

appropriate to filter out the harmless contingencies. If needed, the threshold ΔV can be adjusted to account for the approximation. Otomega and Van Cutsem (2005) report on the successful use of linear estimates of the post-contingency voltage drops obtained by:

- First solving a sparse system to update the phase angles
- Then, assuming constant active power flows in branches, solving a second sparse system to update the voltage magnitudes

This technique yields better accuracy than a single iteration of the full Newton–Raphson method, while retaining the sparse structure of a decoupled formulation.

10.2.7 Preventive Control

Besides security margin computation, it is important to determine which are the best actions to restore a given level of security. As will be illustrated in the next section, some side products of the SOL and PCLL computations can help engineers and trained operators to take preventive actions in the area prone to voltage instability. However, it may be desirable to further assess the merit of candidate control actions, especially in an open market environment. To this purpose, sensitivity analysis is very useful to rank the candidate remedial actions according to their relative efficiency to strengthen the system.

The next step towards control is the incorporation of voltage security constraints into an optimization problem, that can be solved for instance by an OPF, aimed at changing the system operating point in the best possible way.

10.2.7.1 Sensitivity Analysis

Sensitivities computed from the Jacobian matrix of the load flow (Peschon et al. 1968) or long-term equilibrium (Van Cutsem et al. 1995) equations have been used for a long time. Within the VSA context, sensitivities have been proposed as voltage stability indicators (see, for instance, Cañizares 2002, although in practice the latter are not likely to be as meaningful as the power margins provided by ATCs). They have been proposed also to detect the crossing of a loadability limit, as mentioned in Sect. 10.2.4.

A central contribution to sensitivity analysis has been provided by Dobson (1992), where a general formula is obtained for the sensitivity of a loadability margin to parameters. It involves the left eigenvector relative to the zero eigenvalue of the Jacobian matrix computed at a saddle-node bifurcation point. This formula was derived within the context of loadability limit computation. An extension to the analysis of post-contingency unstable scenarios was proposed in Van Cutsem et al. (1995), which involves the computation of sensitivities along the system trajectory and eigenvector at the so-called *critical point*.

Another early approach to the diagnosis of voltage instability relies on the modal analysis of the reduced Jacobian of reactive power with respect to voltages (Gao et al. 1992). Information is retrieved from eigenvectors or participation factors relative to real dominant eigenvalues. This approach can suggest instability modes at normal operating points. However, owing to nonlinearities, the analysis has to be performed at the saddle-node bifurcation or at the critical point (Morison et al. 1993), where the Jacobian has an (almost) zero eigenvalue. The corresponding eigenvector is included in the eigenvector of the unreduced Jacobian, which is preferred in order to exploit matrix sparsity.

The above two approaches identify the best remedial actions from the eigenvector of an (almost) zero eigenvalue. This, however, may suffer from two drawbacks.

First, dominant eigenvalue computation methods may experience problems when the initial estimate of the dominant eigenvalue is not accurate enough. This is especially true when the loadability limit corresponds to a *switching point*, where a generator field current limit is imposed, as illustrated in Fig. 9.2c of Chap. 9 in this book, in which case the real dominant eigenvalue jumps from a negative to a large positive value (Van Cutsem and Vournas 1998). Further references on switching loadability limits are summarized in Sect. 10.4.

Second, in practice, voltages are often requested to stay above some thresholds (corresponding for instance to undervoltage tripping of equipment). In some cases, these minimum voltage limits can be more constraining than voltage stability limits. If so, the system response will be already unacceptable before the loadability limit is reached. At the last acceptable operating point, voltages are low but stable and the Jacobian eigenvalues are still on the stable side; hence, the eigenvector computation does not apply.

A unified approach that encompasses the low voltage, the zero eigenvalue, and the switching loadability limits described above has been proposed in Capitanescu and Van Cutsem (2005), where it is proposed to replace the eigenvector computation by a simple sensitivity calculation which provides very close results, but is non-iterative and can still be computed when the system reaches low but stable voltages. This method is combined to time simulation and consists of:

- Identifying bus ℓ that experiences the largest voltage drop (due to the load increase when computing loadability limits, or the contingency when performing contingency analysis)
- Computing the sensitivities of the V_ℓ voltage at that bus with respect to the candidate controls \mathbf{p} (which are most often bus power injections):

$$\frac{\partial V_\ell}{\partial \mathbf{p}} = \left[\frac{\partial V_\ell}{\partial p_1} \dots \frac{\partial V_\ell}{\partial p_n} \right]^T \quad (10.12)$$

- Evaluating these sensitivities:
 - In voltage-unstable situations: at the point of the trajectory where a Jacobian eigenvalue passes through zero (this is easily detected through sensitivities changing sign through infinity)
 - In low voltage situations: at the final point of the system evolution

It can be shown that in voltage-unstable cases, the proposed sensitivities computed near the loadability limit or the critical point yield practically the same control ranking as the eigenvector-based formula (Dobson 1992) and can be substituted to the eigenvector to compute the sensitivity of the power margin to \mathbf{p} . In low but stable voltage cases, the information carried by sensitivities is also meaningful. Last but not least, the method is simple and reliable, since it is noniterative and requires solving a single sparse linear system only.

10.2.7.2 Security Constraints

An OPF can be used to optimally modify the controls \mathbf{p} so as to restore power margins to a desired value M_d . Denoting by $M(\mathbf{p}^o)$ the margin corresponding to the current value \mathbf{p}^o of \mathbf{p} , the following inequality constraint can be embedded in an OPF:

$$\sum_{j=1}^n S_j \Delta p_j \geq M_d - M(\mathbf{p}^o), \quad (10.13)$$

where the sensitivities S_j are computed as outlined in the previous section and $\Delta p_j = p_j - p_j^o$ is the change in the j th control variable. A constraint (10.13) is considered for each contingency with a margin below of somewhat above the threshold M_d . Further details and examples can be found in Capitanescu and Van Cutsem (2002). A similar formulation has been applied for the optimization of network autotransformer taps in order to maximize loadability margins in the presence of switching loadability limits (Vournas and Karystianos 2004).

10.3 Online VSA in the Hellenic System

10.3.1 Application of Online VSA

As seen in Chap. 9, the Hellenic Interconnected System is under a constant threat of voltage instability. In order to monitor closely the voltage security of this system, an online VSA tool has been installed at the NCC of the Hellenic Transmission System Operator (HTSO), now Independent Power Transmission Operator (IPTO). This online VSA tool has been developed by the National Technical University of Athens and the University of Liège within the framework of the OMASES project (coordinated by ALSTOM) and sponsored by the European Union (Bihain et al. 2002; Van Cutsem et al. 2005a). It was in online operation until June of 2003, when the OMASES project ended. In the fall of 2004, online VSA has been reactivated with the implementation of user-recommended modifications and it is used since as an online and study tool at the Hellenic System NCC.

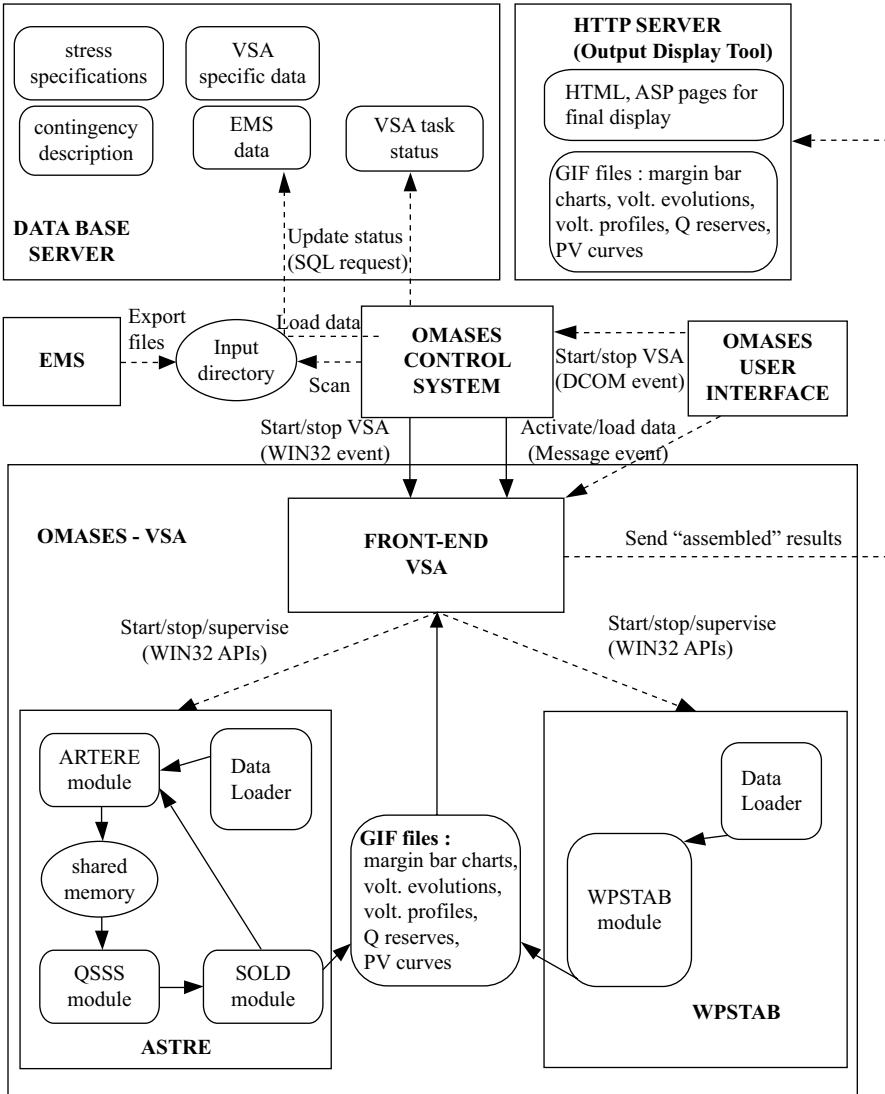


Fig. 10.5 Architecture of the VSA application

The OMASES project included development of DSA, training simulator, and market operation tools, with an on-site experimentation at the NCC. The general architecture of the online application within the OMASES platform is shown in Fig. 10.5.

The online VSA tool is fed with system data from either the real-time state estimator or the study power flow program available at the NCC. The scope of VSA is the analysis of the impact of significant contingencies and the determination of

security margins in terms of power transfers or power consumption in load areas. More precisely, the application involves:

1. Contingency filtering according to the technique of Sect. 10.2.6
2. Determining SOLs using the technique of Sect. 10.2.5.1
3. Computing the system pre-contingency loadability limit, using the method of Sect. 10.2.4
4. Computing PCLL, by the same method, for the dangerous contingencies identified at item 2.

The main outcome of the loadability limit computations is a set of PV curves showing voltages at key buses versus (regional or system) load.

The QSS approach of Sect. 10.2.2.5 is used to determine the system response to both contingencies and the load demand increase.

10.3.2 Implementation Aspects

The online VSA application runs on a Windows-XP server connected through a Local Area Network (LAN) under the TCP/IP protocol. This server is separate from the mainframe computer, which hosts the Energy Management System (EMS) platform and hierarchical databases. The communication with the EMS is accomplished with text files loaded by the EMS host onto the Windows server.

An EMS process periodically creates 14 text files containing the latest network solution computed by the state estimator. Each file is a description of a class of EMS components (e.g., substations, nodes, buses, lines, transformers, generators, loads, etc.). These files are sent by the same EMS process to a predefined real-time entry directory, which triggers the VSA computation cycle.

The role of the OMASES control system is to queue and dispatch messages to the VSA application, detect the presence of new EMS files, load them into the database, active, and synchronize and supervise the VSA task automatically. The platform is controlled and the results are displayed through a web interface.

The VSA software itself is made up of two packages, developed prior to the project. The SOL computation and contingency filtering rely on the ASTRE software developed at the University of Liège (Van Cutsem et al. 1995, 2005b; Van Cutsem and Mailhot 1997, Van Cutsem and Vournas 1998). ASTRE itself is made up of a load-flow module used for stressing the system and filtering contingencies, a QSS simulator for simulating contingencies, both driven by a “conductor” module implementing the binary searches. The former two executables communicate through a shared memory for the data and through files for the outputs. The computation of PCLLs and the preparation of PV curves rely on the WPSTAB software developed at the National Technical University of Athens (Vournas 1999).

Data loaders connect (through Structured Query Language (SQL) requests) to the relational database containing the EMS data, the VSA dynamic data, the stress specification, and the contingency description. They produce the American Stan-

Table 10.1 Secure Operation limits

No.	Contingency name	Margin (MW)
254	LINE_CON_KEPK2-KEPK1.1	0
312	LINE_CON_MEΣOΓΓ-KEPK2.1	0
296	LINE_CON_MOYPT-MEΣOΓ.1	0
299	LINE_CON_KARD-ELBA400.1	0
228	LINE_CON_KΘΕΣ-ΣΧΟΛΑΡ.1	0
61	GEN_CON_K_ΛΑΥΠΙΟ.GFIC.UN	40
51	GEN_CON_ΛΑΥΠΙΟ.GFIC.GEN2.UN	79
	All other contingencies	>316

ard Code for Information Interchange (ASCII) files needed by ASTRE and WPSTAB, respectively.

A “front-end” program prepares, manages, and removes dynamically the working environment of a new VSA session, communicates (through messages) with the remaining of the OMASES environment, launches the data loaders, calls sequentially, and supervises the ASTRE and WPSTAB programs. It also collects the figures produced (in GIF format) by these two software and assembles them into HTML pages, together with Active Server Page (ASP) scripts, for web-based display by the HTTP server.

10.3.3 Description of Online VSA Results

10.3.3.1 Secure Operation Limits

The contingencies resulting in the most constraining SOLs are listed in a table format as seen in Table 10.1, together with the corresponding margins (computed with a tolerance $\Delta=10$ MW). Note that the first five contingencies of Table 10.1 have a zero margin, meaning that the occurrence of any of these at the specific time that the snapshot was taken would result in unacceptable post-contingency conditions. However, as will be seen, all these contingencies have very local effects and refer to areas of the system where transmission upgrades were already under way. In particular, the first three contingencies refer to breaking the loop of cables feeding the island of Kerkyra resulting in an abnormally long radial path to a relatively large load and, hence, in an excessive voltage drop. The nature of the other local problems is similar. Note that all these local problems have long been eliminated following successful network upgrades.

The first contingency with really serious system-wide effect is no. 61 referring to the loss of a combined cycle plant in Lavrio. A similar loss of generating units in Lavrio is contingency no. 51, with slightly larger margin. All other contingencies have margins above 316 MW.

The snapshot of Table 10.1 corresponds to a snapshot during the winter of 2003 where one natural-gas power station (Ag. Georgios) in the Athens area was not in

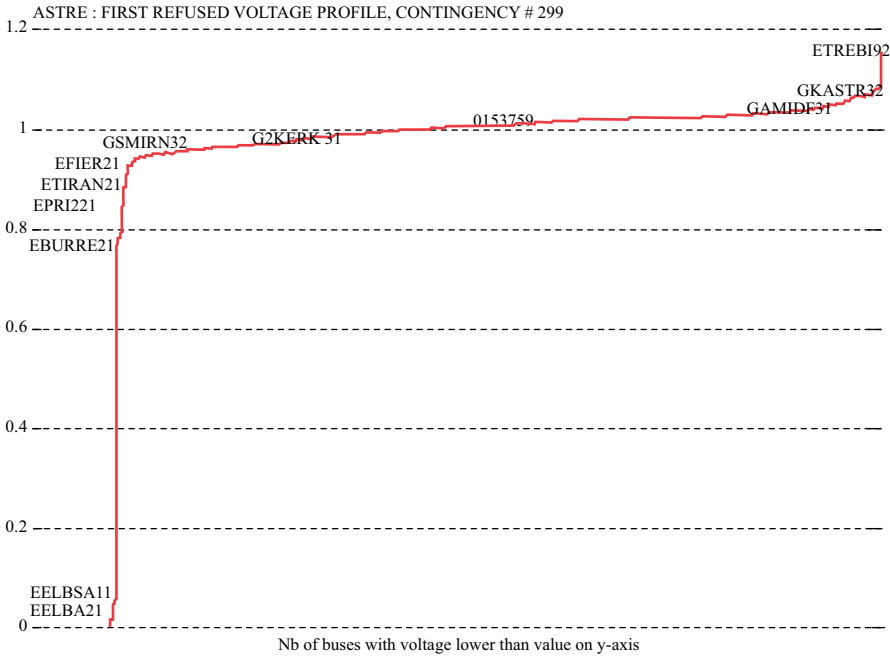


Fig. 10.6 Voltage profile for a contingency with local effect

operation, which left the region with little reactive support. Although the total load was quite light at the time, contingency no. 61 has a very small margin of 40 MW. This is a typical case where the system operator should ask the missing unit to start (if available) for security reasons.

As seen, the contingencies with small margin are not all equally dangerous. The extent of the problems caused to the system by an unacceptable contingency is easily assessed from the “voltage profiles” automatically produced by the SOL computation and described in the sequel.

10.3.3.2 Voltage Profiles

A voltage profile shows the number of buses with voltages below a certain level. The voltages correspond to a snapshot of the collapsing system at the marginally refused level of stress during SOL computation. The affected area is identified from the names of typical buses. For instance, Fig. 10.6 shows the voltage profile corresponding to a contingency with very localized effect (no. 299 of Table 10.1). As can be seen, very few buses with very low voltages exist in this case, while almost all buses remain above 0.9 pu voltage. By examining such voltage profiles, it is easily seen that all contingencies with zero margin in Table 10.1 result in local problems.

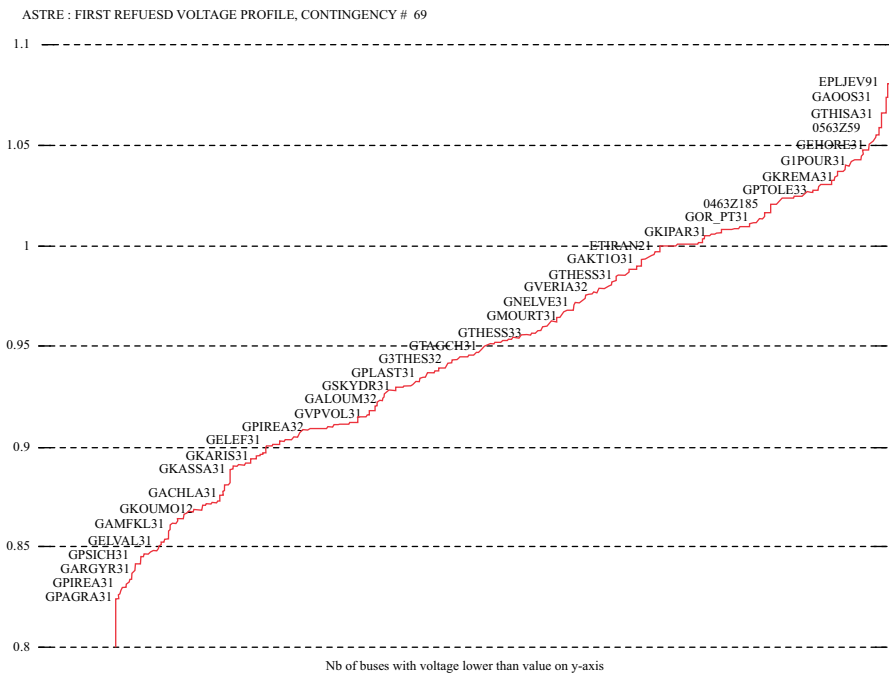


Fig. 10.7 Voltage profile for a contingency with system-wide impact

In contrast, Fig. 10.7 shows the voltage profile of a system-wide dangerous contingency. As can be seen, the disturbance is widely spread, even though the focal point (lowest voltages) can be located in a specific area, namely Central Greece, just to the north of the Athens metropolitan region. This picture is typical of the South system instability mode, which is endemic in the Hellenic system.

10.3.3.3 Voltage Evolutions

Another output readily available for interpreting results is the post-contingency time evolution of the lowest transmission voltage. This is displayed at the marginally accepted and marginally refused stress levels of SOL computation. The final voltages are compared to a lower acceptable value, typical of a voltage collapse, to decide whether the system evolution is acceptable or not.

Figure 10.8 shows the voltage evolution for a case of unacceptably low voltage. As can be seen, the marginally refused simulation does not correspond to a voltage instability, but merely to final voltages that are a little below the assumed 0.7 pu threshold. Hence, for this contingency, the SOL should not be interpreted strictly as a voltage stability limit.

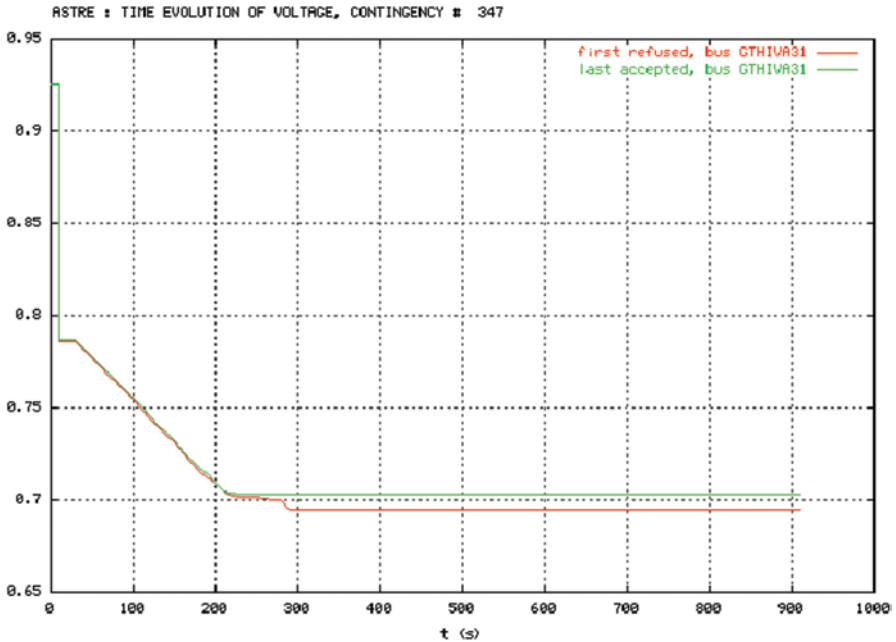


Fig. 10.8 Post-contingency voltage evolutions: low but stable voltages

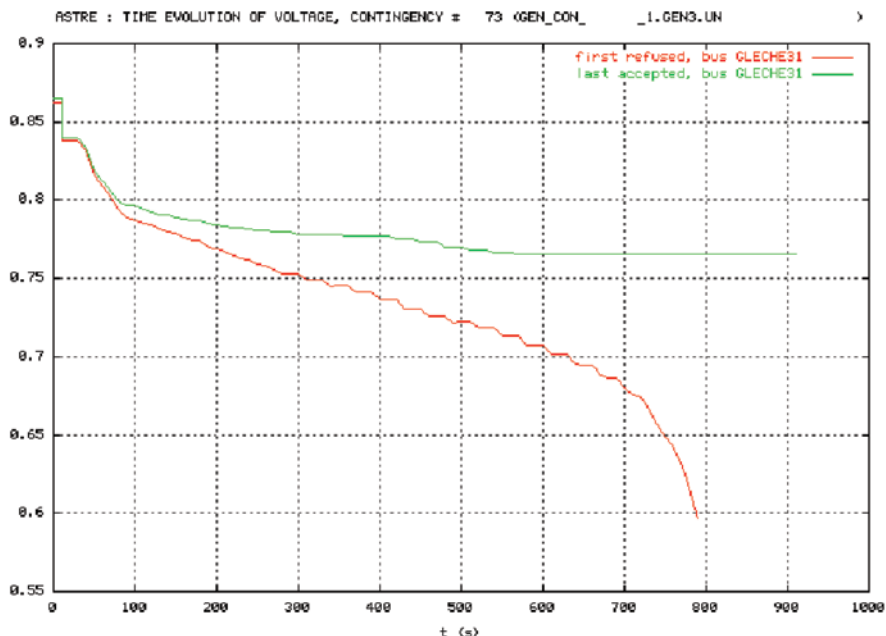
A quite different situation is shown in Fig. 10.9, which shows the voltage evolution corresponding to a contingency leading to a voltage instability and collapse. Here, the marginally unstable simulation ends up in a collapse and loss of synchronism at $t=880$ s.

This evolution is clearly very different from the one of Fig. 10.8. The final collapse shown in Fig. 10.9 can be explained as a loss of synchronism occurring at the Aliveri power station. In order to demonstrate this, the post-contingency loadability limit for this contingency is computed and, for this run, the simulated rotor angle curves of the two generators of Aliveri station are plotted in Fig. 10.10, together with that of a generator in Northern Greece, for comparison purposes (even though this is a different simulation from that in Fig. 10.9, the contingency being the same, the same outcome is reasonably expected).

Figures 10.6–10.9 illustrate the type of information that can be retrieved from unstable post-contingency system evolutions obtained by QSS simulation. In the case of Fig. 10.9, for instance, a standard load flow would have merely diverged, providing no further information.

10.3.3.4 Regional and National PV Curves

The regional *PV* curves are plots of the simulated voltage of a critical bus in each area as a function of the total system load actually consumed in the area, whereas



Thu Oct 31 14:24:26 2002

Fig. 10.9 Post-contingency voltage evolutions near a stability limit

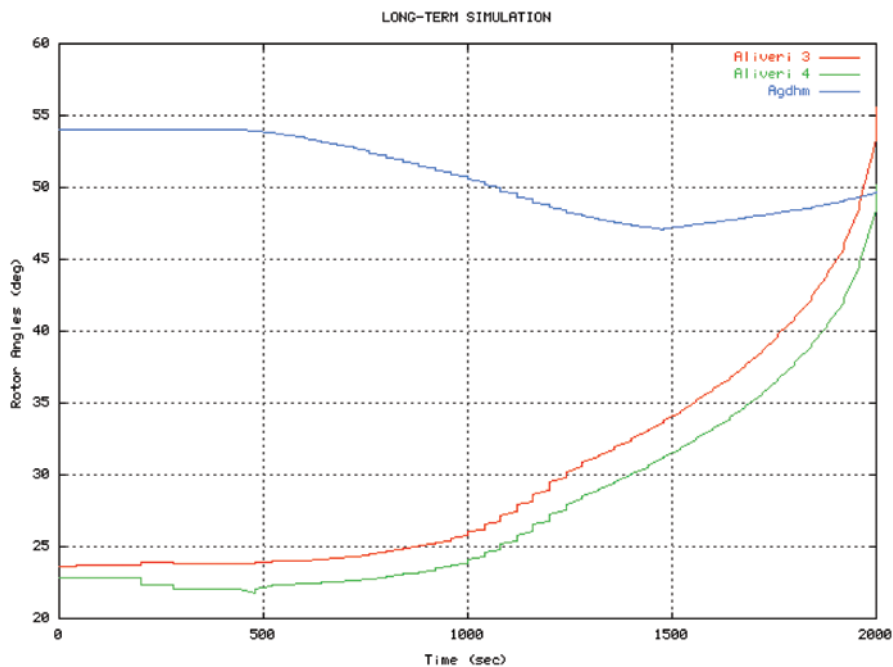


Fig. 10.10 Rotor angles of Aliveri and Ag. Demetrios generators

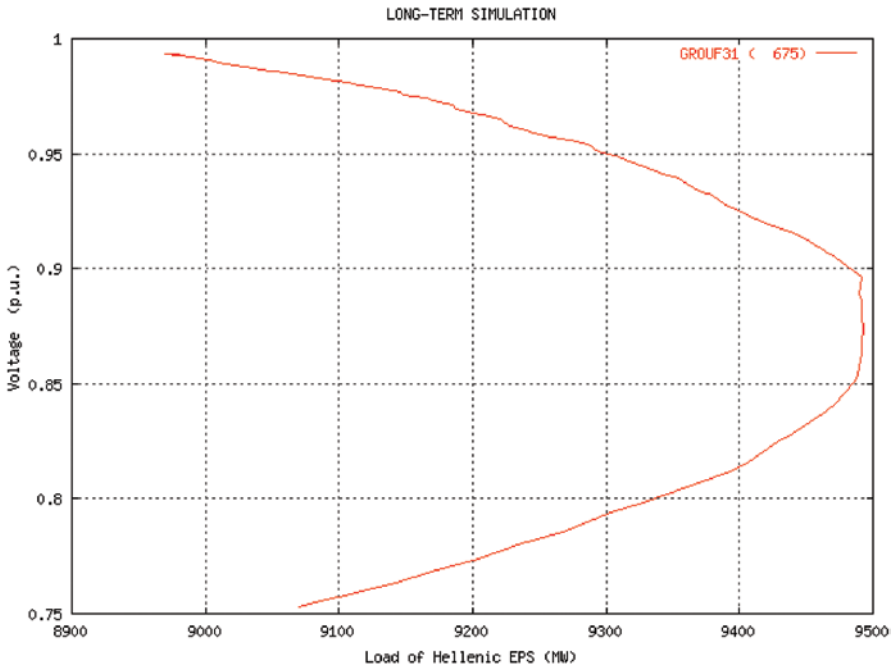


Fig. 10.11 National PV curve without contingency

the national PV curve shows the total load consumed in the system versus the voltage of a representative 150-kV bus located in Athens. In the absence of any contingency, PV curves are obtained through QSS simulation of a ramp increase in demand, as already mentioned. An example of a national PV curve without any contingency is shown in Fig. 10.11. This result tells the operator how far the system could go without incident. In this example, the load could increase by >500 MW with an acceptable voltage level.

PV curves relative to a post-contingency situation, on the other hand, include the effect of the contingency followed by the demand increase. Figure 10.12 shows the national PV curve corresponding to a very severe contingency, namely the loss of a large combined cycle plant at the Lavrio power station.

As seen in Fig. 10.11, the total load is barely able to restore to its pre-contingency consumption even after the demand ramp. This is due to the exhaustion of the regulating range of the LTCs in the affected area, where the power received by consumers is reduced due to low distribution voltages. Note that due to the non-restoration of load, the PCLL implied in Fig. 10.12 should not be compared to the SOL margin, for which the stress is applied prior to the contingency assuming full restoration of load power.

The regional PV curve of the area of Central Greece is shown in Fig. 10.13. Clearly, in this case, the load power is severely reduced after the contingency and the demand increase cannot lead to increased consumption. Inspecting the various

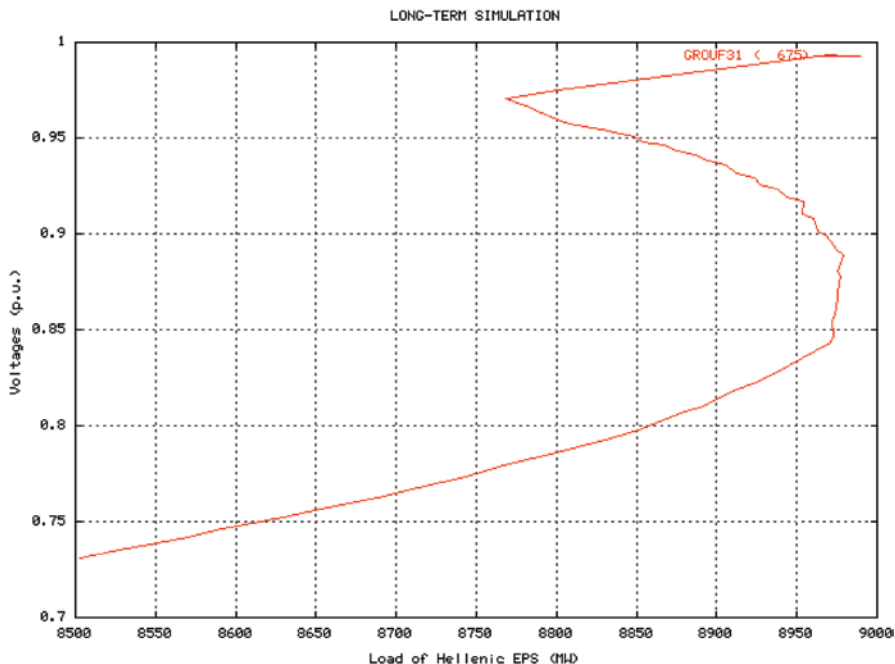


Fig. 10.12 National PV curve after severe contingency

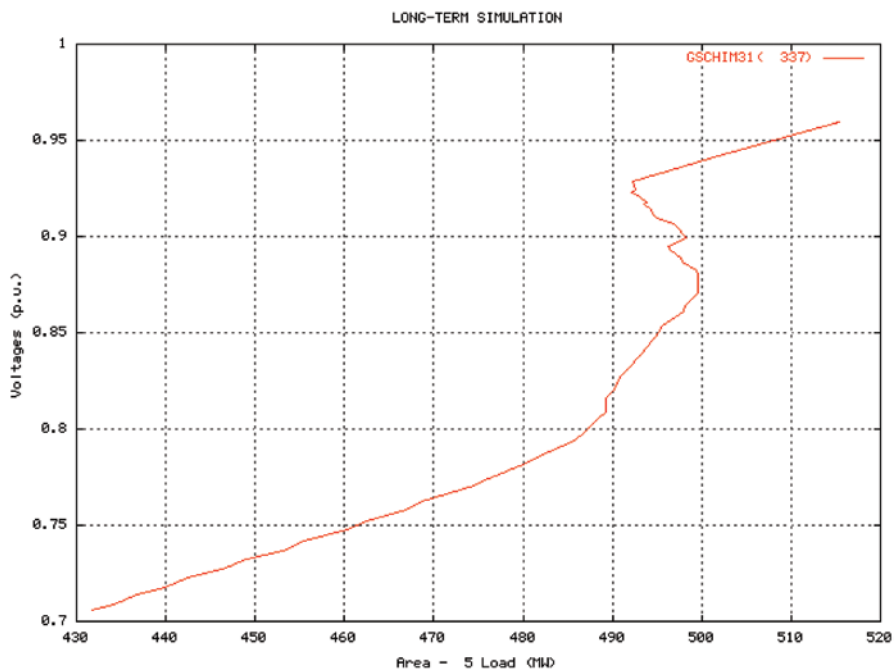


Fig. 10.13 Central Greece regional PV curve after severe contingency

Table 10.2 Secure operation limits for load level of 8884 MW

Contingency	Case 1	Case 2	Case 3
LAVRION.CC3.GEN2	0	77	555
LAVRION.CC4	0	77	491
LAVRION.CC3	318	385	>826
LAVRION.GEN2	374	461	>826
MEGALOPOLIS.GEN4	261	385	529
MEGALOPOLIS.GEN3	>598	>615	>826

PV curves clearly demonstrates that the most affected region by the specific contingency is Central Greece. Customer service in this area will greatly suffer, if such a contingency occurs in the considered operating condition.

10.3.3.5 Assessment of System Upgrades

The online VSA tool can be also used in study mode, in order to assess the effect of various changes in the system. In this context, it was used in the above-described HTSO implementation to quantify the improvements made in the Hellenic system since the summer of 2004 (several transmission upgrades, autotransformer tap optimization, new generating station in the south, etc.; Christoforidis et al. 2005). Indicative results of these studies are shown in Table 10.2, where SOLs are presented for three cases, all with the same load of 8884 MW, which corresponds to July 9, 2004, i.e., the Friday before the blackout. The three cases are:

- *Case 1* is the actual July 9 snapshot retrieved from the EMS real-time state estimator.
- *Case 2* refers to the same system, but with optimized Extra High-Voltage/High-Voltage (EHV/HV) autotransformer tap ratios obtained as described in Christoforidis et al. (2005).
- *Case 3* was constructed using as basis the snapshot of September 2, 2004, that includes the complete reinforced network and applying a uniform load increase in each area, so as to match the load of the other cases.

These results show a clear increase in the margins from 70 to 120 MW by optimizing autotransformer tap ratios. With the reinforced network, the increase achieved in margins ranges from 260 to 500 MW. The national *PV* curves for the three cases described above and for the most severe contingency (LAVRION.CC4) are given in Fig. 10.14.

10.4 Outline of Recent Research

As stated in Sect. 10.2.2.4, the advance of computer power in the past 10 years, as well as the progress made in computational techniques, has now allowed for much faster response of full multi-time-scale simulation. Recently applied techniques and relevant results are reported in Aristidou et al. (2013) and Fabozzi et al. (2013).

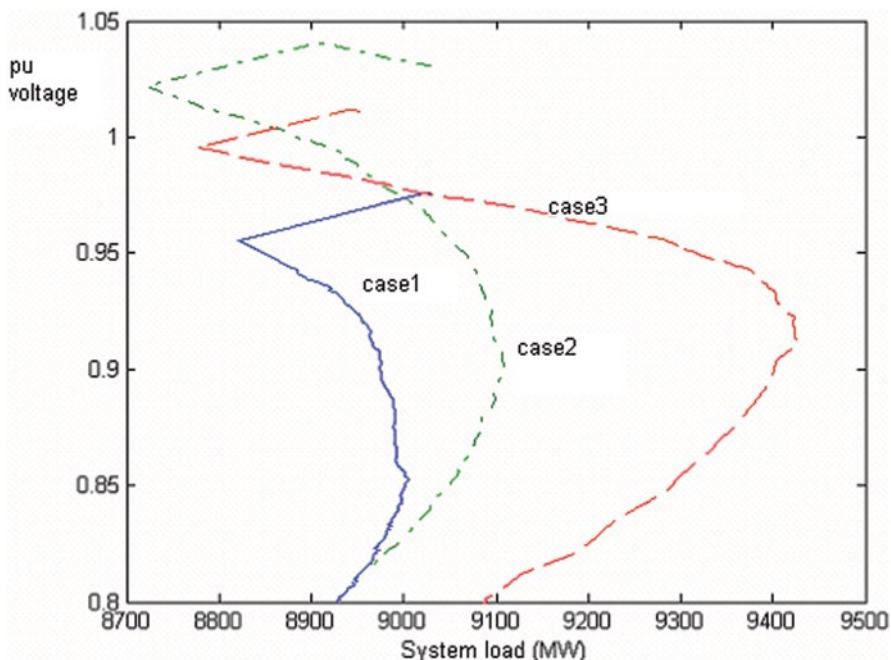


Fig. 10.14 National PV curves for contingency LAVRION.CC4

Regarding the security awareness in a power system, recent developments in the PMU applications allow a closer monitoring of power system state close to real time. Recent results dealing with voltage stability can be found in Glavic and Van Cutsem (2012, 2013).

Further research on loadability limits involving inequality constraints is reported in Karystianos et al. (2007). More recent results on the voltage stability of the Hellenic Interconnected System can be found in Lambrou et al. (2013).

References

- Ajjarapu V, Christy C (1992) The continuation power flow: a tool for steady-state voltage stability Analysis. *IEEE Trans Power Syst* 7:416–423
- Aristidou P, Fabozzi D, Van Cutsem T (2013) Dynamic simulation of large-scale power systems using a parallel Schur-complement-based decomposition method. *IEEE Trans Parallel Distrib Syst* (in press)
- Austria RR, Reppen ND, Uhrin JA, Patel MC, Galatic A (1991) Applications of the optimal power flow to analysis of voltage collapse limited power transfer. In: *Bulk power system voltage phenomena II—voltage stability and security*, Deep Creek Lake, pp 311–319
- Bihain A, Burt G, Casamata F, Koronides T, Lopez R, Massucco S, Ruiz-Vega D, Vournas C (2002) Advance perspectives and implementation of dynamic security assessment in the open market environment, paper 39–101, CIGRE 2002

- Cañizares C (ed) (2002) Voltage stability assessment: concepts, practices and tools, special publication of the IEEE Power System Stability Subcommittee, 2002, ISBN 0780378695
- Cañizares CA, Alvarado FL (1993) Point of collapse and continuation methods for large ac/dc systems. *IEEE Trans Power Syst* 8:1–8
- Capitanescu F, Van Cutsem T (2002) Preventive control of voltage security: a multi-contingency sensitivity-based approach. *IEEE Trans Power Syst* 17:358–364
- Capitanescu F, Van Cutsem T (2005) Unified sensitivity analysis of unstable or low voltages caused by load increases or contingencies. *IEEE Trans Power Syst* 20:321–329
- Christoforidis G, Kabouris J, Vournas C, Van Cutsem T (2005) Investigation of parameters affecting voltage security of the Hellenic interconnected system. In: *Proceedings of the 15th PSCC, Liege (Belgium)*
- Dobson I (1992) Observations on the geometry of saddle-node bifurcation and voltage collapse in electric power systems. *IEEE Trans Circuits Syst-I* 39(3):240–243
- Fabozzi D, Chieh A, Haut B, Van Cutsem T (2013) Accelerated and localized Newton schemes for faster dynamic simulation of large power systems. *IEEE Trans Power Syst* 28(4):4936–4947
- Gao B, Morison GK, Kundur P (1992) Voltage stability evaluation using modal analysis. *IEEE Trans Power Syst* 7:1529–1542
- Glavic M, Van Cutsem T (2012) State reconstruction from a limited number of synchronized phasor measurements: application to voltage instability detection. In: *Proceedings of the IEEE PES General Meeting, San Diego, 2012*
- Glavic M, Van Cutsem T (2013) Reconstructing and tracking network state from a limited number of synchrophasor measurements. *IEEE Trans Power Syst* 28(2):1921–1929
- Granville S, Mello JCO, Melo ACG (1996) Application of interior point methods to power flow unsolvability. *IEEE Trans Power Syst* 11:1096–1104
- Iba K, Suzuki H, Egawa M, Watanabe T (1991) Calculation of critical loading condition with nose curve using homotopy method. *IEEE Trans Power Syst* 6:584–593
- Irisarri GD, Wang X, Tong J, Mokhtari S (1997) Maximum loadability of power systems using interior point nonlinear optimization method. *IEEE Trans Power Syst* 12:162–172
- Iwamoto S, Tamura Y (1981) A load flow calculation method for ill-conditioned power systems. *IEEE Trans Power App Syst* 100:1736–1743
- Karystianos ME, Maratos NG, Vournas CD (2007) Maximizing power system loadability in the presence of multiple binding complementarity constraints. *IEEE Trans Circuits Syst-I* 54:1775–1787
- Lambrou C, Vournas C, Christoforidis G, Kambouris J (2013) Voltage stability monitoring and control studies in the hellenic interconnected system. In: *Proceedings of IEEE power tech conference, Grenoble, France*
- Mansour Y, Alvarado F, Rinzin C, Xu W (1994) SVC placement using critical modes of voltage instability. *IEEE Trans Power Syst* 9:757–763
- Morison GK, Gao B, Kundur P (1993) Voltage stability analysis using static and dynamic approaches. *IEEE Trans Power Syst* 8:1159–1171
- Otomega B, Van Cutsem T (2005) Fast contingency filtering based on linear voltage drop estimates. In: *Proceedings of IEEE power tech conference, St Petersburg, Russia*
- Overbye TJ (1995) Computation of a practical method to restore power flow solvability. *IEEE Trans Power Syst* 10:280–287
- Peschon J, Piercy DS, Tinney WF, Tveit OJ (1968) Sensitivity in power systems. *IEEE Trans Power App Syst* PAS-87:1687–1696
- Van Cutsem T (1991) A method to compute reactive power margins with respect to voltage collapse. *IEEE Trans Power Syst* 6:145–156
- Van Cutsem T, Mailhot R (1997) Validation of a fast voltage stability analysis method on the Hydro-Quebec system. *IEEE Trans Power Syst* 12:282–292
- Van Cutsem T, Vournas C (1998) Voltage stability of electric power system. Kluwer, Boston
- Van Cutsem T, Jacquemart Y, Marquet J-N, Pruvot P (1995) A comprehensive analysis of mid-term voltage stability. *IEEE Trans Power Syst* 10:1173–1182

- Van Cutsem T, Kabouris J, Christoforidis G, Vournas CD (2005a) Application of real-time voltage security assessment to the Hellenic interconnected system. *IEE Proc Gener Transm Distrib* 152(1):123–131
- Van Cutsem T, Grenier M-E, Lefebvre D (2005b) Combined detailed and quasi steady-state time simulations for large-disturbance analysis. In: *Proceedings of the 15th PSCC, Liège, Belgium*
- Vournas C (scientific coordinator) (1999) Software development for voltage stability analysis. Project 96 SYN 95 Report, NTUA, Athens
- Vournas C, Karystianos M (2004) Load tap changers in emergency and preventive voltage stability control. *IEEE Trans Power Syst* 19:492–498

Chapter 11

Trajectory Sensitivity Analysis for Dynamic Security Assessment and Other Applications in Power Systems

Tony B. Nguyen and M. A. Pai

Abstract Real-time stability evaluation and preventive scheduling in power systems offer many challenges in a stressed power system. Trajectory Sensitivity Analysis (TSA) is a useful tool for this and other applications in the emerging smart grid area. In this chapter, we outline the basic approach of TSA, to extract suitable information from the data and develop reliable metrics or indices to evaluate proximity of the system to an unstable condition. Trajectory sensitivities can be used to compute critical parameters such as clearing time of circuit breakers, tie-line flow, etc. in a power system by developing suitable norms for ease of interpretation. The TSA technique has the advantage that model complexity is not a limitation, and the sensitivities can be computed numerically. Suitable metrics are developed from these sensitivities. The TSA technique can be extended to do preventive rescheduling. A brief discussion of other applications of TSA in placement of distributed generation is indicated.

11.1 Introduction

Online reliability evaluation of power systems has come a long way with Phasor Measurement Unit (PMU)-based Wide-Area Measurement System (WAMS). The early work in this area (Alsac and Stott 1974; Athay et al. 1979; Fouad 1988; Kumar et al. 1987; Ruiz-Vega and Pavella 2003; Yuan et al. 2003; La Scala et al. 1998; Shubhanga and Kulkarni 2004; Padiyar and Krishna 2001; Vittal et al. 2005) is now being augmented by the WAMS-based tools (Monticelli 2000; Abur and Exposito 2004; Monticelli 2007; Ahmad 2012). Although simulation in real time is the ultimate solution, there are many ways to extract suitable information from the limited online simulations or PMU data to develop reliable metrics or indices to evaluate proximity of the system to an unstable condition for a given set of contingencies.

T. B. Nguyen (✉)

Pacific Northwest National Laboratory, Richland, WA, USA

e-mail: Tony.Nguyen@pnnl.gov

M. A. Pai

University of Illinois at Urbana-Champaign, Champaign, IL, USA

The currently available technique of Transient Energy Function (TEF; Pai 1981, 1989; Fouad and Vittal 1991; Pavella and Murthy 1994; Pavella et al. 2000) is sometimes limited by its inability to handle complex models.

Sensitivity analysis is a technique used in all branches of engineering. In linear systems, eigenvalue sensitivity, sensitivity to parameter variations, or its application in parameter identification is widely reported in the control literature. Trajectory sensitivity, on the other hand, has not found many applications although it was proposed in the 1960s (Tomovic 1963; Tomovic and Vukobratovic 1972; Kokotovic and Rutman 1973; Laughton 1964; Frank 1978; Eslami 1994).

We first motivate its use directly in the preventive rescheduling situation when the system is identified as being close to being insecure for a given set of contingencies (Nguyen and Pai 2003). The next application (Nguyen et al. 2002) of the trajectory sensitivity analysis (TSA) technique is in computing critical parameters of the power system by developing suitable metrics to translate the trajectory sensitivities into some scalar indices. Critical values of the clearing time are computed by treating clearing time itself as a parameter by proposing a suitable norm as a metric. The motivation for using this metric is provided through a Single-Machine Infinite Bus (SMIB) example. In this approach, computation at two points is necessarily followed by an extrapolation. Extension to include tie-line power as a parameter is included. Critical generators are also identified.

More applications of TSA for real-time stability such as identification of critical relays and electrical centers in the event of system separation are briefly discussed. Thus, a comprehensive overview of the topic is presented. Adaptation of TSA in the field of WAMS is a wide area for open research, and this chapter may lead to further topics for investigation.

11.2 Current State of the Art in Dynamic Security Assessment

Power system security is concerned with the evolution of a system when a disturbance results in a change in system condition. System security is generally concerned with large changes, which are called *contingencies*. These may be faults caused by tripping of lines, lightning flashover, failure of a major piece of equipment, etc. Such events cause relays to operate and result in a change in system configuration, such as loss of a component or in rare cases, cascaded tripping of lines.

The mathematical analysis involving computation of the dynamic response and evaluating it for possible instability is called *Dynamic Security Assessment* (DSA). DSA has also been formally defined as an evaluation of the ability of a certain power system to withstand a defined set of contingencies and to survive the transition dynamically to an acceptable steady-state condition.

In the current environment, the existing transmission system often operates at its limit because of congestion on transmission lines and multilateral transactions. In addition, power systems must be operated to satisfy the transient stability

constraints for a set of contingencies. In these situations, DSA plays a crucial role. The aim of online DSA is to assess the stability of the system for a set of pre-defined contingencies. These contingencies are user specified or are chosen automatically through some filtering process. Filtering of contingencies is done so that they are separated into critical and noncritical ones. The critical ones are saved for further study, and the noncritical ones are discarded to reduce the computational burden. For each contingency if the system is stable, DSA can also provide a security margin based on the technique used.

For instance, if critical clearing time is computed, then the difference between the critical clearing time and the actual clearing time, $t_{cr} - t_{cl}$, is the margin. On the other hand, if the TEF is used, then the difference between the critical energy and the energy at clearing, $V_{cr} - V_{cl}$, is the margin. The security margin is used to provide the operators with guidelines to improve system operation while at the same time maintaining economic operation. This is known as *security-constrained optimization*. The literature on preventive control is focused on enhancing the stability margin as defined by $V_{cr} - V_{cl}$ in the TEF method (Pai 1989; Fouad and Vittal 1991) and $t_{cr} - t_{cl}$ in the case of the SIME method (Pavella et al. 2000). These methods, however, suffer from the fundamental drawbacks of model limitation and the need to compute the controlling unstable equilibrium point (u.e.p.).

The technique based on trajectory sensitivities (Nguyen and Pai 2003; Nguyen et al. 2002; Laufenberg and Pai 1998; Zima and Andersson 2003; Hiskens and Pai 2000) has been proposed for both DSA and preventive control. This technique has several advantages over all the other techniques:

1. There is no restriction on complexity of the model.
2. Extension to systems with discrete events is possible.
3. Information other than mere stability can be obtained.
4. Limits to any parameter in the system that affect stability can be studied.
5. Identification of weak links in the transmission network is possible.
6. Preventive strategies can be incorporated easily.

However, the above advantages are obtained at the expense of increased computational time. As an alternative, phasor measurements can be used.

11.3 Mathematical Background: System and Sensitivity Model

In simulating disturbances, switching actions take place at certain time instants. At these time instants, the algebraic equations change, resulting in discontinuities of the algebraic variables. In general, the power system can be cast in the form of a differential-algebraic discrete model incorporating discrete events, as in Hiskens and Pai (2000). A special case is the model described by *Differential-Algebraic Equations* (DAE) of the form

$$\dot{x} = f(x, y, \lambda). \quad (11.1)$$

$$0 = \begin{cases} g^-(x, y, \lambda) & s(x, y, \lambda) < 0 \\ g^+(x, y, \lambda) & s(x, y, \lambda) > 0. \end{cases} \quad (11.2)$$

A switching occurs when the switching function $s(x, y, \lambda) = 0$. For example, if a device is switched into service at time $t = t_{sw}$, then the switching function in this case can simply be defined as $s(x, y, \lambda) = t - t_{sw}$.

In the above model, x represents the dynamic state variables such as machine angles, velocities, etc.; y represents the algebraic variables such as load bus voltage magnitudes and angles; and λ represents the system parameters such as line reactances, generator mechanical input power, or fault clearing time. Note that the state variables x are continuous, while the algebraic variables can undergo step changes at switching instants.

The initial conditions for Eqs. (11.1) and (11.2) are given by

$$x(t_0) = x_0, y(t_0) = y_0. \quad (11.3)$$

where y_0 satisfies the equation

$$g(x_0, y_0, \lambda) = 0. \quad (11.4)$$

For compactness of notation, the following definitions are used:

$$\underline{x} = \begin{bmatrix} x \\ \lambda \end{bmatrix}, \underline{f} = \begin{bmatrix} f \\ 0 \end{bmatrix}.$$

With these definitions, Eqs. (11.1) and (11.2) are written in a compact form as

$$\dot{\underline{x}} = \underline{f}(\underline{x}, y) \quad (11.5)$$

$$0 = \begin{cases} g^-(\underline{x}, y) & s(\underline{x}, y) < 0 \\ g^+(\underline{x}, y) & s(\underline{x}, y) > 0. \end{cases} \quad (11.6)$$

Note that the parameters are absorbed in the differential equations as state variables where their derivatives are equal to zero.

The initial conditions for Eqs. (11.5) and (11.6) are

$$\underline{x}(t_0) = \underline{x}_0, y(t_0) = y_0. \quad (11.7)$$

Trajectory sensitivity analysis studies the variations of the system variables with respect to the small variations in initial conditions x_0 and parameters λ (or equivalently \underline{x}_0).

Away from discontinuities, the differential-algebraic system can be written in the form

$$\dot{\underline{x}} = f(\underline{x}, y) \quad (11.8)$$

$$0 = g(\underline{x}, y). \quad (11.9)$$

Differentiating Eqs. (11.8) and (11.9) with respect to the initial conditions \underline{x}_0 yields

$$\dot{\underline{x}}_{\underline{x}_0} = \underline{f}_{\underline{x}}(t)\underline{x}_{\underline{x}_0} + \underline{f}_y(t)y_{\underline{x}_0} \quad (11.10)$$

$$0 = \underline{g}_{\underline{x}}(t)\underline{x}_{\underline{x}_0} + \underline{g}_y(t)y_{\underline{x}_0}, \quad (11.11)$$

where $\underline{f}_{\underline{x}}$, \underline{f}_y , $\underline{g}_{\underline{x}}$, and \underline{g}_y are time-varying matrices and are calculated along the system trajectories. $\underline{x}_{\underline{x}_0}(t)$ and $y_{\underline{x}_0}(t)$ are the trajectory sensitivities.

Initial conditions for $\underline{x}_{\underline{x}_0}$ are obtained by differentiating Eq. (11.7) with respect to \underline{x}_0 as

$$\underline{x}_{\underline{x}_0}(t_0) = I, \quad (11.12)$$

where I is the identity matrix.

Using Eq. (11.12) and assuming that $\underline{g}_y(t_0)$ is nonsingular along the trajectories, initial conditions for $y_{\underline{x}_0}$ can be calculated from Eq. (11.11) as

$$y_{\underline{x}_0}(t_0) = -[\underline{g}_y(t_0)]^{-1} \underline{g}_{\underline{x}}(t_0). \quad (11.13)$$

Therefore, the trajectory sensitivities can be obtained by solving Eqs. (11.10) and (11.11) simultaneously with Eqs. (11.8) and (11.9) using Eqs. (11.7), (11.12), and (11.13) as the initial conditions. At the discontinuity where $s(\underline{x}, y) = 0$, the trajectory sensitivities $\underline{x}_{\underline{x}_0}$, $y_{\underline{x}_0}$ typically undergo a jump. Computation of these jump conditions is discussed in detail in Hiskens and Pai (2000).

For a small change in initial conditions, the sensitivities with respect to initial conditions can be numerically approximated as

$$\underline{x}_{\underline{x}_0}(t) = \frac{\partial \underline{x}(t)}{\partial \underline{x}_0} \approx \frac{\Delta \underline{x}(t)}{\Delta \underline{x}_0} \quad (11.14)$$

$$y_{\underline{x}_0}(t) = \frac{\partial y(t)}{\partial \underline{x}_0} \approx \frac{\Delta y(t)}{\Delta \underline{x}_0}. \quad (11.15)$$

11.4 Dynamic Security-Constrained Rescheduling of Power Systems Using Trajectory Sensitivities

We first review the use of trajectory sensitivities through its straightforward application to preventive control. The theoretical development closely follows Nguyen and Pai (2003) with minor modifications. The Stability-Constrained Optimal Power Flow Formulation (SCOPF) is now discussed.

11.4.1 Problem Formulation

The standard OPF problem is (Gan et al. 2000)

$$\text{Minimize the cost function } C(P_g) \quad (11.16)$$

subjected to

$$P_g - P_L - P(V, \theta) = 0 \quad (11.17)$$

$$Q_g - Q_L - Q(V, \theta) = 0 \quad (11.18)$$

$$S(V, \theta) - S^M \leq 0 \quad (11.19)$$

$$V^m \leq V \leq V^M \quad (11.20)$$

$$P_g^m \leq P_g \leq P_g^M \quad (11.21)$$

$$Q_g^m \leq Q_g \leq Q_g^M. \quad (11.22)$$

Equations (11.17) and (11.18) are the active and reactive power balance equations, respectively; P_g, Q_g are the vectors of generator active and reactive power injections, respectively; P_L, Q_L are the vectors of real and reactive load, respectively; V and θ are the vectors of bus voltage magnitudes and angles, respectively; $P_g^m, P_g^M, Q_g^m, Q_g^M, V^m, V^M$ are the vectors of lower and upper limits of generator real, reactive power outputs, and bus voltage magnitudes, respectively; $S(V, \theta)$ is the vector of apparent power flowing across the transmission lines; and S^M is the vector of thermal limits of those lines. Note that the variables in this problem are P_g, Q_g, V , and θ .

The relative rotor angles are used to detect the system stability/instability. To check the stability of the system for a credible contingency, relative rotor angles are

monitored at each time step during dynamic simulation. The sensitivities of rotor angles with respect to generator power P_m are also computed at the same time.

Although sensitivity computation requires extensive computational effort, an efficient method to compute sensitivities is available by making effective use of the Jacobian, which is common to both the system and sensitivity equations (Chaniotis et al. 2001).

It is proposed that when the relative rotor angle $\delta_{ij} = \delta_i - \delta_j > \pi$ for a given contingency, the system is considered as unstable. This is an extreme case, as pointed out in Gan et al. (2000), and one can choose an angle difference less than π depending on the system. Here, i and j refer to the most and the least advanced generators, respectively.

The sensitivities of the rotor angles at this instant are used to compute the amount of power needed to be shifted from the most advanced generator (generator i) to the least advanced one (generator j) according to the following formulae:

$$\Delta P_{i,j} = \frac{\delta_{ij} - \delta_{ij}^0}{\frac{\partial \delta_{ij}}{\partial P_i} - \frac{\partial \delta_{ij}}{\partial P_j}} \bigg|_{\max \delta_{ij} = \pi} \quad (11.23)$$

$$P_i^{\text{new}} = P_i^0 - \Delta P_{i,j} \quad \text{and} \quad P_j^{\text{new}} = P_j^0 + \Delta P_{i,j}, \quad (11.24)$$

where P_i^0, P_j^0 and δ_{ij}^0 are the base loading of generators i and j , and the relative rotor angle of the two at the solution of the OPF problem stated in Eqs. (11.16)–(11.22); $\frac{\partial \delta_{ij}}{\partial P_i}$ and $\frac{\partial \delta_{ij}}{\partial P_j}$ are the sensitivities of relative rotor angle with respect to the output of the i th and j th generators; and P_i and P_j are components of the parameter λ discussed in the mathematical background section of this chapter.

After shifting the power from generator i to generator j according to Eqs. (11.23) and (11.24), the system is secure for that contingency but it is not an optimal schedule. New power constraints introduced into the OPF formulation to improve the optimality are proposed, as discussed in the next section.

The OPF problem with the new constraints is then resolved to obtain the new operating point for the system. Thus, we retain the DAE and the sensitivity model, and replace the original constraints by the new constraints. The methodology and algorithm are discussed next.

11.4.2 Stability Constrained Optimal Power Flow Solution Methodology

The steps to solve the dynamic security constrained OPF are shown in the flow chart of Fig. 11.1. The steps are as follows (Nguyen and Pai 2003):

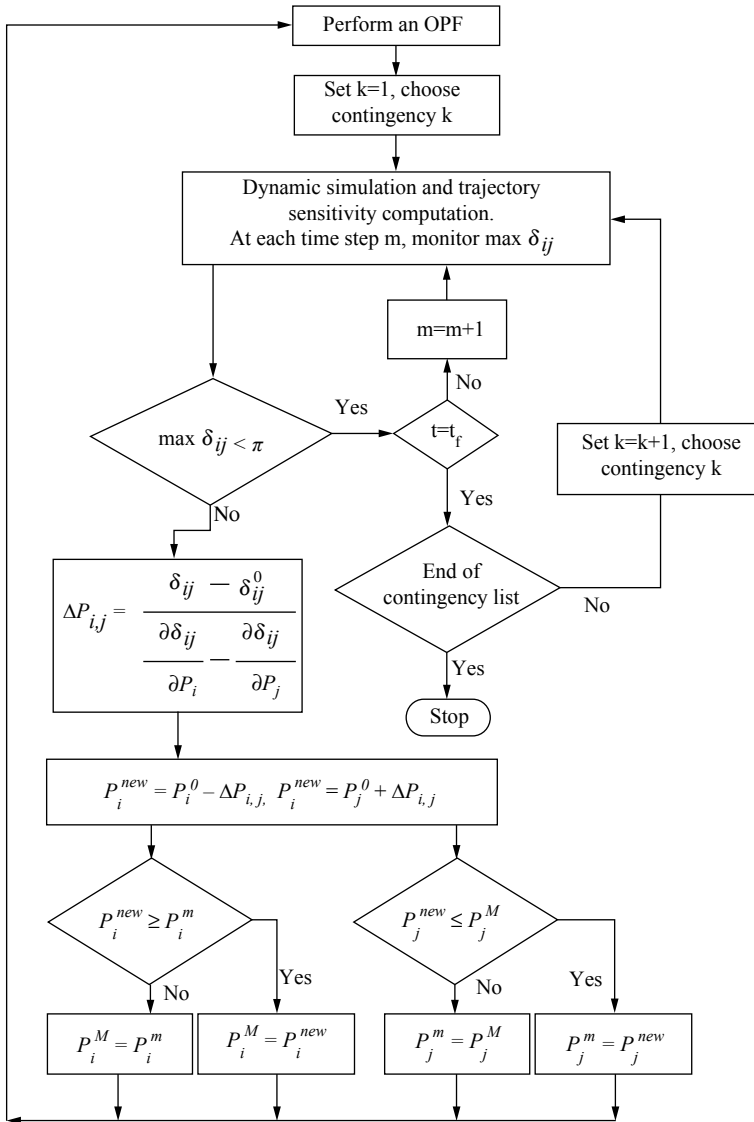


Fig. 11.1 Flow chart for dynamic security-constrained OPF. (Adapted from Nguyen and Pai 2003)

1. Perform the OPF to obtain the optimal operating point according to Eqs. (11.16)–(11.22). Set $k = 1$.
2. Apply contingency k from the specified list of credible contingencies.
3. Perform a dynamic simulation and compute the trajectory sensitivities using models specified by Eqs. (11.8)–(11.11), and monitor the maximum of relative rotor angles at each time step.

4. If $\max(\delta_{ij}) < \pi$ for entire simulation interval t_f ,
 If not at the end of the contingency list, set $k=k+1$, and go to step 2.
 Else, stop.
 Else, go to step 5.
5. Calculate the power shift needed from the i th-generator to the j th-generator, P_i^{new} , and P_j^{new} Eqs. (11.23) and (11.24).
6. If $P_i^{\text{new}} \geq P_i^m$, then set $P_i^M = P_i^{\text{new}}$; else, set $P_i^M = P_i^m$. If $P_j^{\text{new}} \leq P_j^M$, then set $P_j^m = P_j^{\text{new}}$; else, set $P_j^m = P_j^M$.
7. Go back to step 1.

Note that in step 6, if one generator hits its output limit and the other does not as a result of the shift, there will be a mismatch between generations and loads after the shift. This mismatch will be taken care of by the result of the OPF in the rescheduling. Also, in step 6, if the least advanced generator j is at its maximum limit, the shift will be carried out from generator i to the next-to-least advanced generator instead.

Note also that Eq. (11.23) is still computed at $\max \delta_{ij} = \pi$. If a solution obtained by applying the proposed algorithm exists, this solution is the globally secure one and is the optimal dispatch over the specified set of contingencies. Of course, there is no guarantee about the existence of the globally secure solution. There may be situations where this solution does not exist. If this is the case, the system loads need to be studied further. Then the system operator will have appropriate actions to take if contingencies were to occur.

If there is more than one advanced generator crossing the threshold at the same time, then one of them can be chosen in the power shift to start the algorithm. But different choices of generators to start the shift will have different impacts on the system in terms of cost and computational time. In this case, the operator's decision for the selection, which is incorporated in the algorithm, is very important to effectively keep the system in the secure operating condition at minimum cost, both economically and from a computational point of view.

11.4.3 Illustrative Examples

The three-machine, nine-bus system (Sauer and Pai 1998) is discussed in detail to illustrate the algorithm stated in Sect. 11.3. The two-axis model is used for synchronous machines with the Institute of Electrical and Electronics Engineers (IEEE) type-1 exciter and constant mechanical input. Loads are modeled as constant-impedance type. Results of the OPF are obtained by using the MATPOWER package (Zimmerman and Gan 2005).

Fig. 11.2 The three-machine, nine-bus system

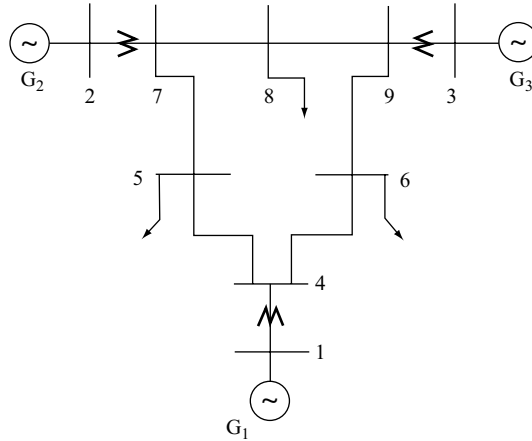


Table 11.1 Generator data and the optimal schedule for the base case

Generators	Rating (MW)	Cost function (\$/h)	Optimal loading (MVA)	Total cost (\$/h)
1	200	$0.0060P^2 + 2.0P + 140$	$106.19 + j24.26$	1132.59
2	150	$0.0075P^2 + 1.5P + 120$	$112.96 + j0.37$	
3	100	$0.0070P^2 + 1.8P + 80$	$99.20 - j11.62$	

11.4.3.1 The Three-Machine, Nine-Bus System

A single line diagram of this system is shown in Fig. 11.2. The OPF is performed for the base case and the optimal schedule is shown in Table 11.1 along with the cost functions for generators and their ratings.

1. *Contingency CI*: Fault at bus 7

The fault is simulated at bus 7 and cleared by tripping line 7-5 at $t_{cl}=0.35$ s, which is greater than the critical clearing time. The critical generators are G2 and G3, so the algorithm can be first applied to either G2 or G3. Two cases will be considered here as follows:

Case A: Shifting output power from generator 2 to generator 1. Using Eq. (11.23), the amount of power needed to be shifted is found to be $\Delta P_{2,1} = 49.53$ MW. Applying the algorithm of Sect. 11.4.2, the new schedule for the generators is G1, $155.72 + j25.73$ MVA; G2, $63.43 - j0.80$ MVA; and G3, $98.64 - j10.65$ MVA. The total cost for this case is US \$ 1167.90. The system is dynamically stable in this loading condition for the same fault. The relative rotor angles after the shift are shown in Fig. 11.3.

Case B: Shifting output power from generator 3 to generator 1. Applying the algorithm of Sect. 11.4.2, the new schedule for the generators is G1, $173.20 + j26.95$ MVA; G2, $73.55 - j0.52$ MVA; and G3, $70.98 - j10.88$ MVA. The total cost for

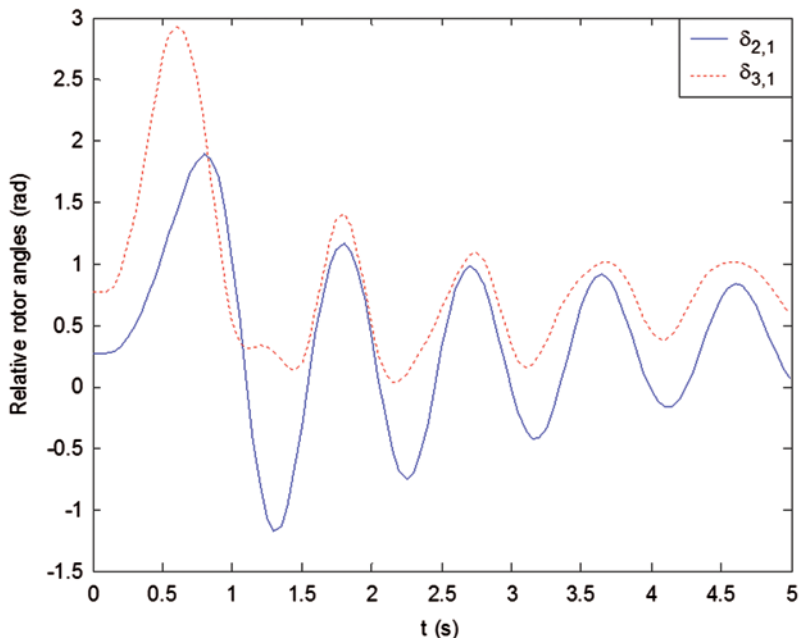


Fig. 11.3 Relative rotor angles for Case A

this case is US \$ 1180.33. With this loading condition, the system withstands the contingency dynamically if it were to occur. Note that unlike case A where the system is stable after only one shift (from G2 to G1), the system in this case is still unstable after the shift from G3 to G1. After this shift, only generator 2 is found to be unstable. Equation (11.23) is used again to compute the power to shift from G2 to G1. As a result, the system is dynamically stable after the second shift. The relative rotor angles for this case are shown in Fig. 11.4.

From the results of Case A and Case B, it can be seen that when there is more than one generator crossing the threshold at nearly the same time, more than one option for shifting power can be used in step 5 of the algorithm. The most effective option will save computation time and minimize the cost increase associated with the shift (Case A). On the other hand, other options can be used at step 5 with the possibility of more computation time and higher cost (Case B). Therefore, operators' knowledge about the system plays a crucial role in choosing the most effective option that can be implemented in the algorithm for preventive rescheduling.

2. Contingency C2: Fault at bus 9

The fault is simulated at bus 9 and cleared by tripping line 9-6 at $t_{cl}=0.30$ s, which is greater than the critical clearing time. The critical generator is G3 and the least advanced one is G1.

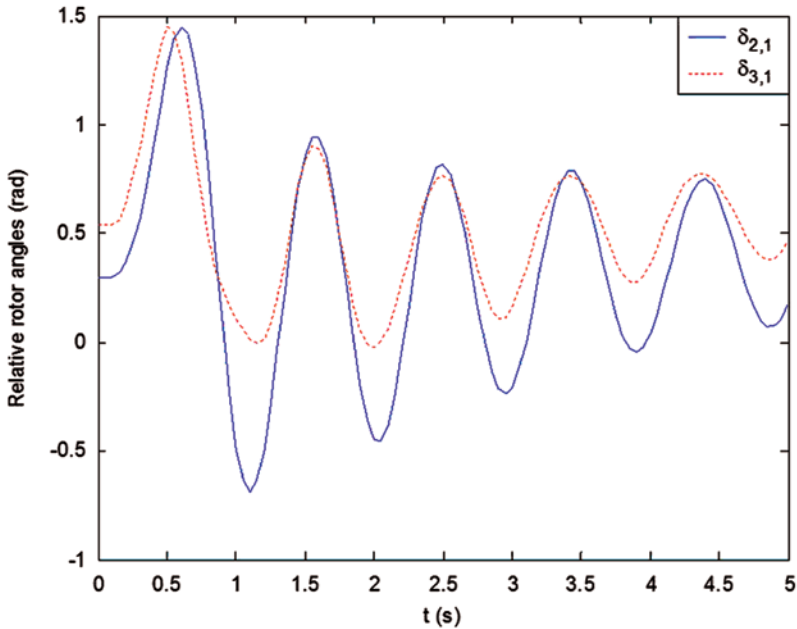


Fig. 11.4 Relative rotor angles for Case B

Case C: Shifting output power from generator 3 to generator 1. The amount to shift is $\Delta P_{3,1} = 51.75\text{MW}$, obtained by using Eq. (11.23). The new loading in this case is G1, $157.94+j25.36$; G2, $112.39+j0.70$; and G3, $47.45-j11.13$; and the system is dynamically stable. The total cost is US \$ 1170.04. With this loading condition, the relative rotor angles are shown in Fig. 11.5.

3. Contingency set comprising C1 and C2

Case AC: Now the set of contingencies, which comprises contingencies C1 and C2 as in cases A and C, is considered. The globally secure and optimal schedule obtained by applying the algorithm of Sect. 11.4.2 is G1, $200+j30.74$ MVA; G2, $69.33+j0.68$ MVA; and G3, $48.77-j9.18$ MVA. The cost in this case is US \$ 1224.49. With this loading condition, the system will be dynamically stable for either contingency C1 or C2, as shown in Figs. 11.6 and 11.7.

The optimal loadings for the base case, the constrained cases A, B, C, and AC, and the total cost in each case are summarized in Table 11.2. Note that the cost for the dynamically constrained cases is always higher than for the base case, as expected. The highest cost is in case AC, where the globally secure optimal schedule, which will survive both contingencies, is obtained.

For larger system validation, see Nguyen and Pai (2003).

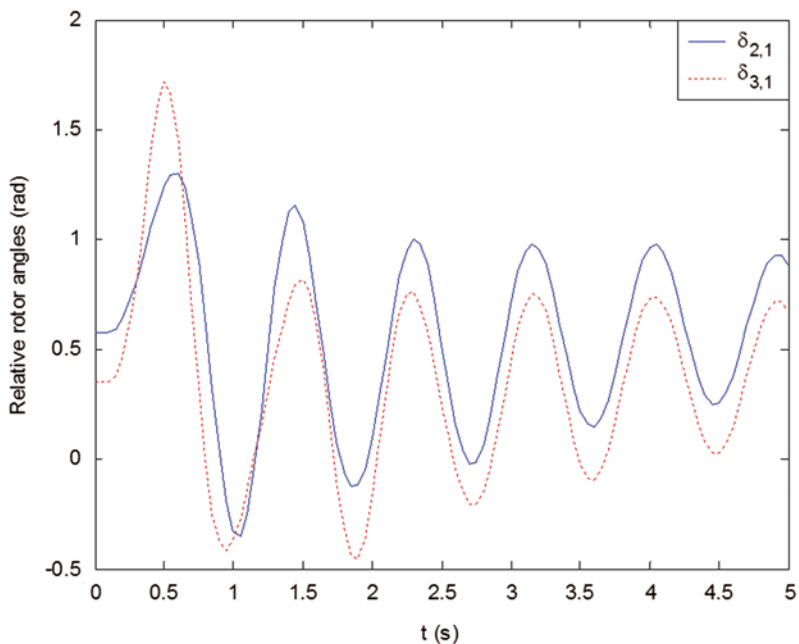


Fig. 11.5 Relative rotor angles for case C

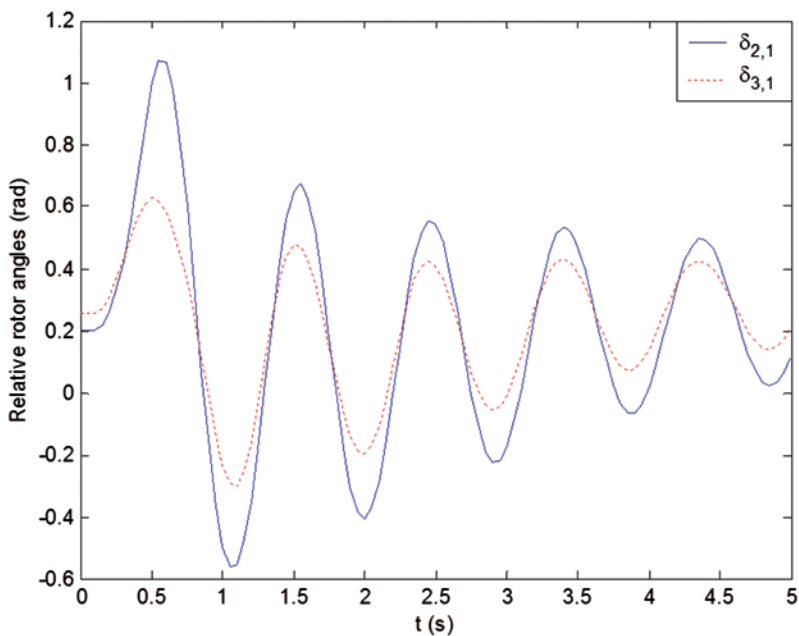


Fig. 11.6 Relative rotor angles for case AC, fault at bus 7

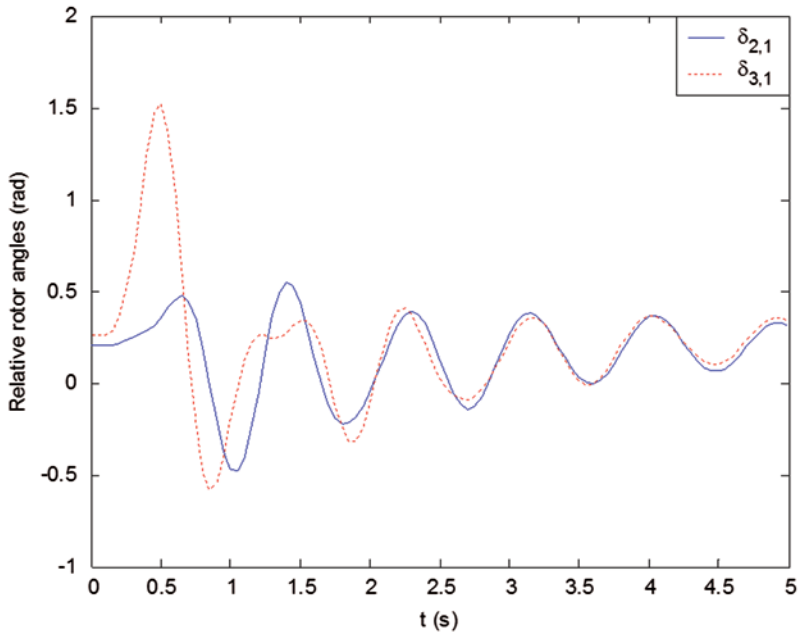


Fig. 11.7 Relative rotor angles for case AC, fault at bus 9

Table 11.2 Optimal schedules for the base case and the four cases A, B, C, and AC

Case	Optimal schedule			Cost (\$/h)
	G1 (MVA)	G2 (MVA)	G3 (MVA)	
BASE	106.19+j24.26	112.96+j0.37	99.20-j11.62	1132.59
A	155.72+j25.73	63.43-j0.80	98.64-j10.65	1167.90
B	173.20+j26.95	73.55-jj0.52	70.98-j10.88	1180.33
C	157.94+j25.36	112.39+j0.70	47.45-j11.13	1170.04
AC	200.00+j30.74	69.33+j0.68	48.77-j9.18	1224.49

11.5 Trajectory Sensitivity Norm and its Use in Computing the Critical Clearing Time

In this section, we outline an approach using trajectory sensitivity information *directly* to estimate the critical clearing time (Nguyen 2002). To motivate this approach, let us consider a SMIB system described by

$$\begin{aligned}
 M\ddot{\delta} + D\dot{\delta} &= P_M & 0 < t \leq t_{cl} & , \delta(0) = \delta_0, \dot{\delta}(0) = 0. \\
 M\ddot{\delta} + D\dot{\delta} &= P_M - P_{em} \sin \delta & t > t_{cl} &
 \end{aligned}
 \tag{11.25}$$

The corresponding sensitivity equations are

$$\begin{aligned} M\ddot{u} + D\dot{u} &= 0 & 0 < t \leq t_{cl} \\ M\ddot{u} + D\dot{u} &= (-P_{em} \cos \delta)u & t > t_{cl} \end{aligned}, u(0) = 0, \dot{u}(0) = 0, \quad (11.26)$$

where $u = \frac{\partial \delta}{\partial t_{cl}}$.

Equation (11.25) can be written in a DAE form by augmenting the parameter t_{cl} and the time variable t into the state vector, resulting in

$$\begin{aligned} \dot{x}_1 &= x_2 \\ \dot{x}_2 &= \frac{1}{M}(P_M - y_2 P_{em} \sin x_1 - D x_2) \\ \dot{x}_3 &= 0 \\ \dot{x}_4 &= 1 \end{aligned} \quad (11.27)$$

$$0 = \begin{cases} g^- = \begin{bmatrix} x_4 - x_3 - y_1 \\ y_2 \end{bmatrix} & y_1 \leq 0 \\ g^+ = \begin{bmatrix} x_4 - x_3 - y_1 \\ y_2 - 1 \end{bmatrix} & y_1 > 0 \end{cases}$$

with the initial conditions

$$\begin{aligned} x_1(0) &= \delta_0 \\ x_2(0) &= 0 \\ x_3(0) &= t_{cl} \\ x_4(0) &= 0 \end{aligned} \quad (11.28)$$

and

$$\begin{aligned} y_1(0) &= -t_{cl} \\ y_2(0) &= 0, \end{aligned} \quad (11.29)$$

where $x_1 = \delta$, $x_2 = \dot{\delta}$, $x_3 = t_{cl}$, and $x_4 = t$. Note that Eq. (11.29) is obtained by solving

$$0 = g^-(x, y).$$

The corresponding sensitivity system of Eq. (11.27) is obtained as

$$\dot{x}_{x_0} = f_x(t)x_{x_0} + f_y(t)y_{x_0} \quad (11.30)$$

$$0 = g_x(t)x_{x_0} + g_y(t)y_{x_0} \quad (11.31)$$

where

$$\underline{f}_{\underline{x}} = \begin{bmatrix} 0 & 1 & 0 & 0 \\ -\frac{y_2}{M} P_{em} \cos \underline{x}_1 & -\frac{D}{M} & 0 & 0 \\ 0 & 0 & 0 & 0 \\ 0 & 0 & 0 & 0 \end{bmatrix}$$

$$\underline{f}_y = \begin{bmatrix} 0 & 0 \\ 0 & -\frac{P_{em}}{M} \sin \underline{x}_1 \\ 0 & 0 \\ 0 & 0 \end{bmatrix}$$

$$\underline{g}_{\underline{x}} = \underline{g}_{\underline{x}}^- = \underline{g}_{\underline{x}}^+ = \begin{bmatrix} 0 & 0 & -1 & 1 \\ 0 & 0 & 0 & 0 \end{bmatrix}$$

$$\underline{g}_y = \underline{g}_y^- = \underline{g}_y^+ = \begin{bmatrix} -1 & 0 \\ 0 & 1 \end{bmatrix}.$$

The initial conditions for Eqs. (11.30) and (11.31) are

$$\underline{x}_{\underline{x}_0}(0) = \begin{bmatrix} 1 & 0 & 0 & 0 \\ 0 & 1 & 0 & 0 \\ 0 & 0 & 1 & 0 \\ 0 & 0 & 0 & 1 \end{bmatrix} = I \quad \text{and} \quad y_{\underline{x}_0}(0) = -\underline{g}_y^{-1}(0) \underline{g}_{\underline{x}}(0) = \begin{bmatrix} 0 & 0 & -1 & 1 \\ 0 & 0 & 0 & 0 \end{bmatrix}.$$

The phase plane portraits in the (δ, ω) plane of the system for two values of t_{cl} , one small and the other close to t_{cr} , are shown in Figs. 11.8 and 11.9.

The corresponding behaviors of sensitivities in the (u, \dot{u}) plane are shown in Figs. 11.10 and 11.11. From this, it is seen that the sensitivity magnitudes increase much more rapidly as t_{cl} approaches t_{cr} . Also, the trajectories in the (u, \dot{u}) plane can cross each other because the system (11.26) is time varying, whereas that is not the case for the system (11.25), which is an autonomous system.

Qualitatively, both trajectories in the (δ, ω) plane and the (u, \dot{u}) plane give the same information about the stability of the system, but the sensitivities seem to be stronger indicators because of their rapid changes in magnitude as t_{cl} increases. Hence, we can associate sensitivity information with the stability level of the system for a particular clearing time.

When the system is very close to instability, the sensitivity reflects this situation much more quickly, as seen in Fig. 11.12, for a three-machine test system. This qualitative relationship was discussed for the general nonlinear dynamic systems by

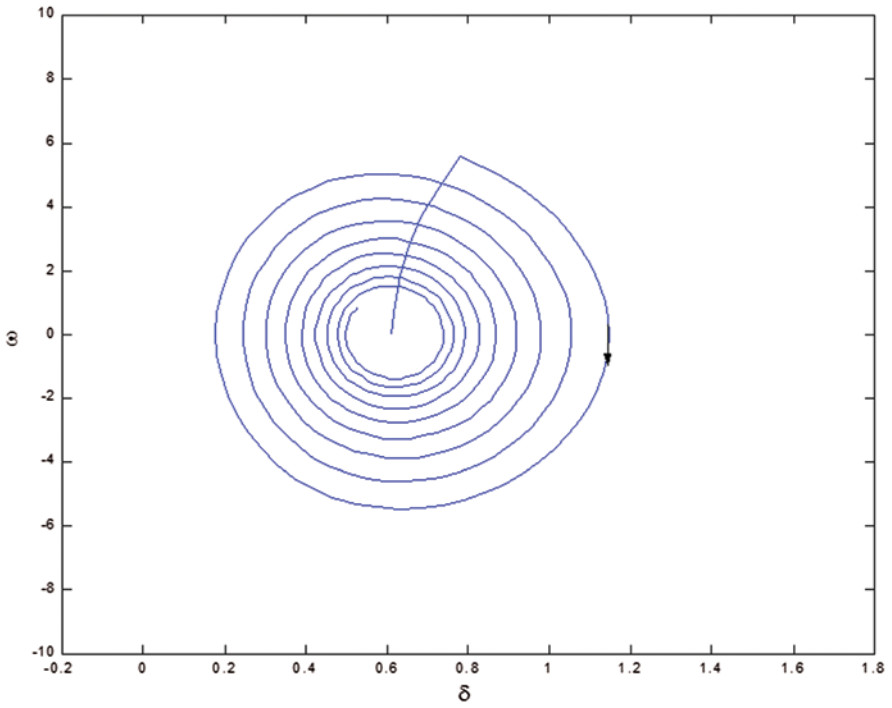


Fig. 11.8 Phase plane behavior for small t_{cl} ($\approx 50\%$ of t_{cr})

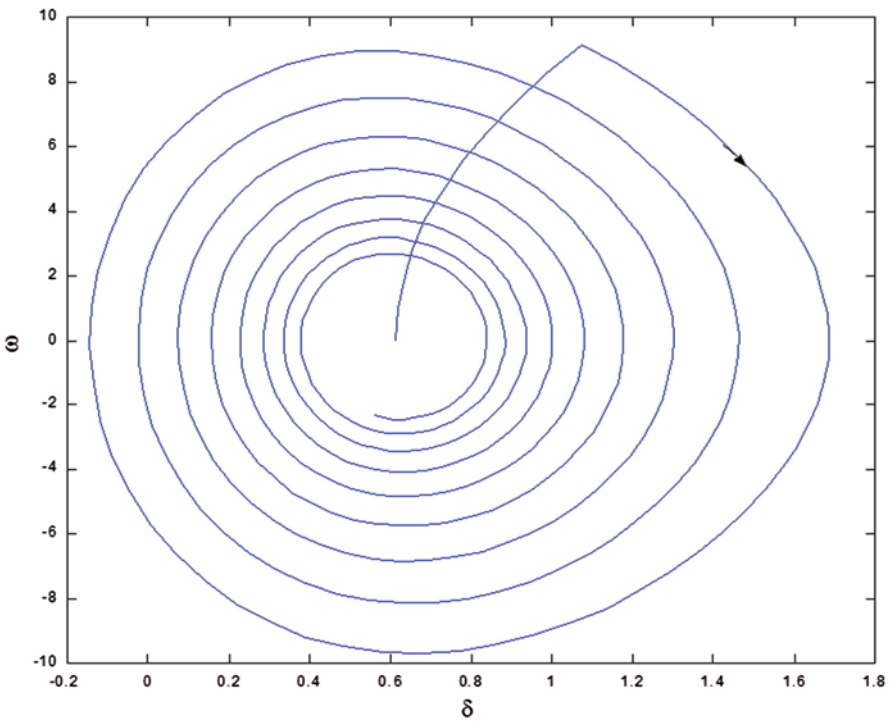


Fig. 11.9 Phase plane behavior for t_{cl} close to t_{cr} ($\approx 80\%$ of t_{cr})

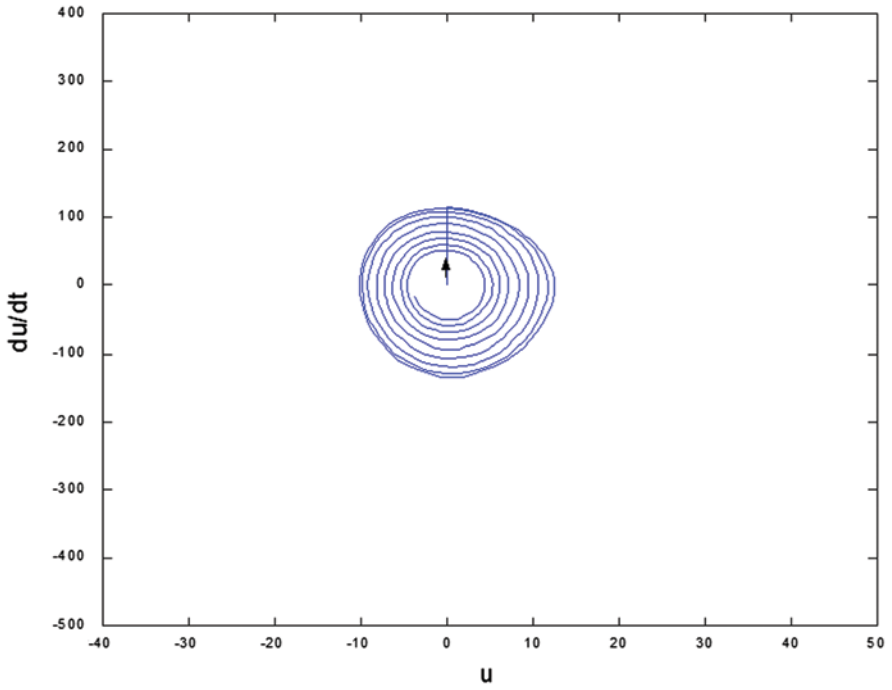


Fig. 11.10 Sensitivity plane behavior for small t_{cl} ($\approx 50\%$ of t_{cr})

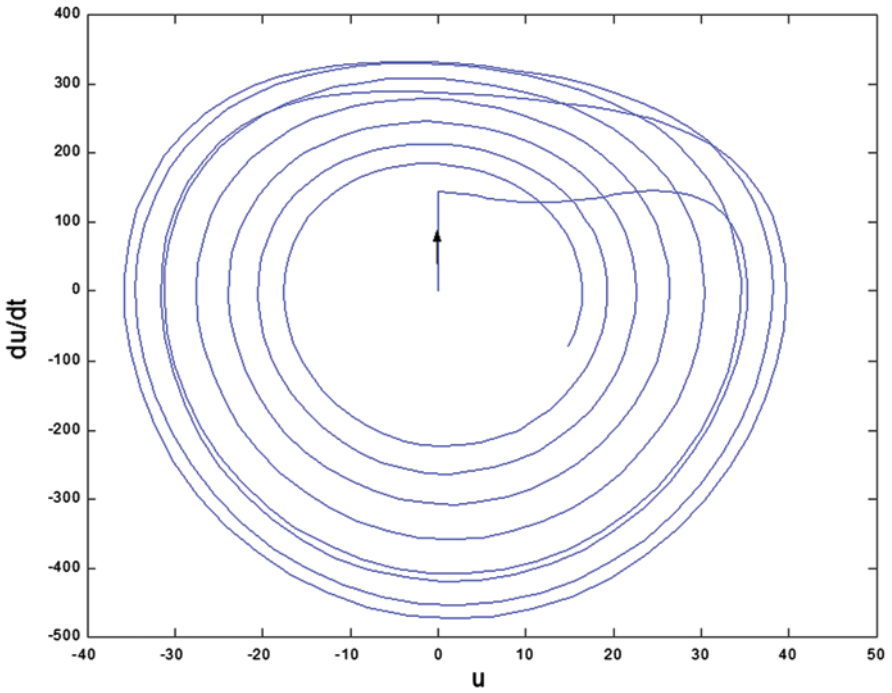


Fig. 11.11 Sensitivity plane behavior for t_{cl} close to t_{cr} ($\approx 80\%$ of t_{cr})

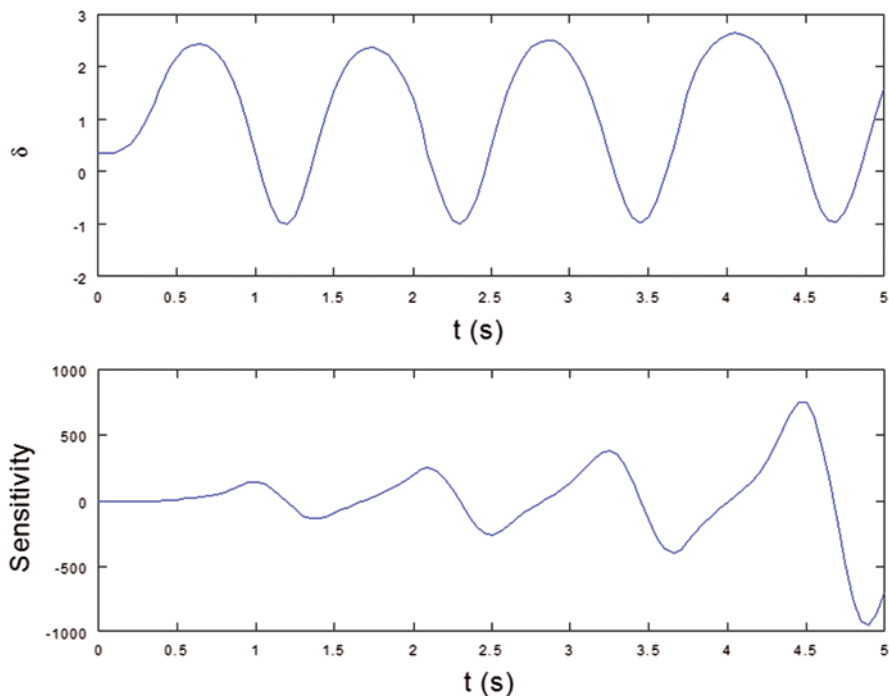


Fig. 11.12 Rotor angle (*top*) and its sensitivity (*bottom*) for t_{cl} very close to t_{cr} for three-machine system

Tomovic (1963). One possible measure of proximity to instability may be through some norm of the sensitivity vector. The Euclidean norm is one such possibility.

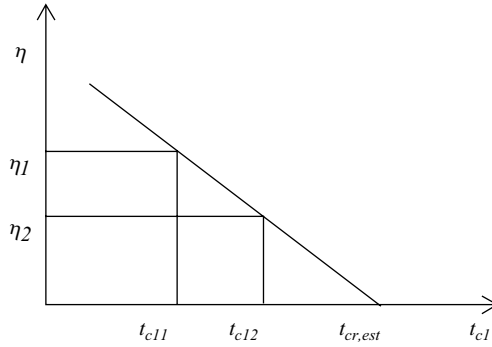
The sensitivity norm S_N is computed for two different values of t_{cl} , which are chosen to be less than t_{cr} . Because we are computing only first-order trajectory sensitivities, the two values of t_{cl} must be less than t_{cr} by at most 20%. This might appear to be a limitation of the method. However, extensive experience with the system generally will give us a good estimate of t_{cr} . Because the system under consideration is stable, the sensitivity S_N will display larger excursions for larger t_{cl} . Because sensitivities generally increase rapidly with increases in t_{cl} , we plot the reciprocal of the maximum of S_N over the post-fault period as

$$\eta = \frac{1}{\max(S_N)}$$

A straight line is then constructed through the two points (t_{cl1}, η_1) and (t_{cl2}, η_2) . The estimated critical clearing time $t_{cr, est}$ is the intersection of the constructed straight line with the time axis in the (t_{cl}, η) plane, as shown in Fig. 11.13.

As discussed later, this linearity is valid for a small region around t_{cr} . The sensitivity norm for an m -machine system is defined as

Fig. 11.13 Estimate of t_{cr}



$$S_N = \sqrt{\sum_{i=1}^m \left(\left(\frac{\partial \delta_i}{\partial t_{cl}} - \frac{\partial \delta_j}{\partial t_{cl}} \right)^2 + \left(\frac{\partial \omega_i}{\partial t_{cl}} \right)^2 \right)}$$

where the j th machine is chosen as the reference machine.

If other parameters of interest are chosen instead, the technique will give an estimate of critical values of those parameters.

Since this technique only uses sensitivity information that has no modeling limitation, it can be applied to power systems without any restriction on system modeling or complexity. This is a major advantage of this technique.

11.5.1 Numerical Examples

For the three-machine system (Fig. 11.2), a self-clearing fault is simulated at bus 5 and cleared at two different values of t_{cl} less than t_{cr} . The corresponding values of η discussed in Sect. 11.5 are computed, and the results are shown in Fig. 11.14.

The procedure is repeated for the same system by simulating the fault at bus 8. The estimated critical clearing time and the actual value obtained for both the cases are shown in Table 11.3. Hence, the values of t_{cr} obtained from the proposed technique are very close to the actual value.

11.5.2 Computation of Other Critical Parameters Using Sensitivity Norm

11.5.2.1 Critical Loading of a Generator

The sensitivity norm technique is used to estimate the critical value of generator loading, or equivalently, the mechanical input power P_M . Two simulations for two values of P_M are carried out. The change from normal operating values in P_M is

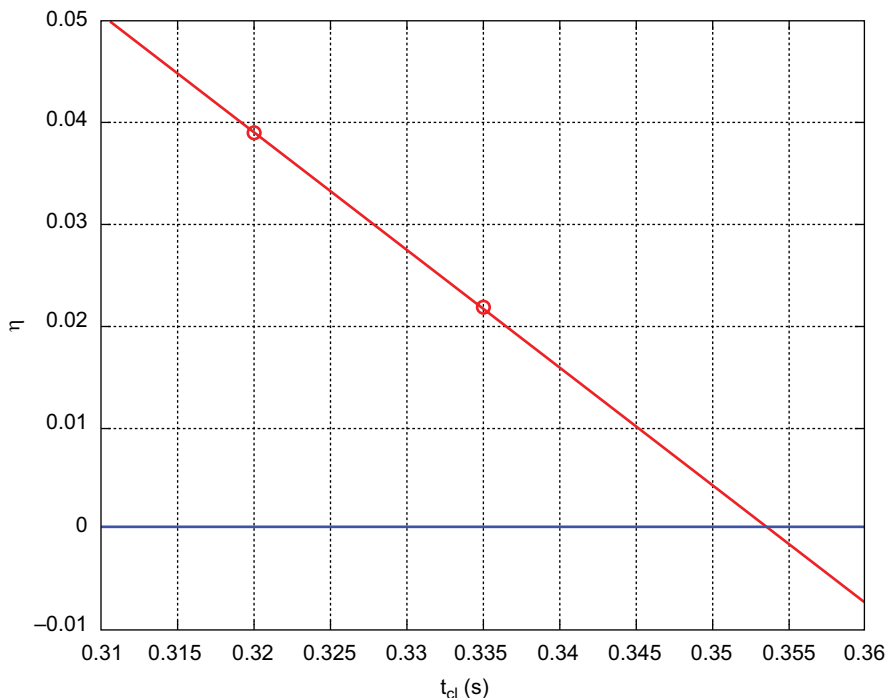


Fig. 11.14 Estimate t_{cr} for fault at bus 5 using sensitivity norm

Table 11.3 Estimate t_{cr} using sensitivity norm for three-machine system

Faulted bus	Sensitivity norm	Actual
	$t_{cr,est}$ (s)	t_{cr} (s)
5	0.354	0.352
8	0.333	0.334

distributed uniformly among all loads in the system, so that the loading of the rest of the generators is unchanged. The sensitivity norm is calculated for the two specified values of P_M and then extrapolated to obtain the estimated value of the critical P_M for the chosen generator.

The fifty-machine system (Fouad and Vittal, 1991) is used as an illustrative example. A self-clearing fault is simulated at bus 58 and cleared at $t_{cl}=0.15$ s. Applying the proposed technique, the following result is obtained and shown in Table 11.4. To validate the results, it was verified that with the critical value of P_M , the system goes unstable.

11.5.2.2 Critical Impedance of a Transmission Line

The sensitivity norm technique can also be used to estimate the critical value of a line reactance. The three-machine system (Fig. 11.2) is used to illustrate the

Table 11.4 Estimated value of critical input power P_M versus the actual value

Machine number	Sensitivity Norm $P_{M,est}$ (pu)	Actual $P_{M,act}$ (pu)
4	22.9	22.3
5	17.0	16.5
7	4.3	4.2
12	10.0	9.6

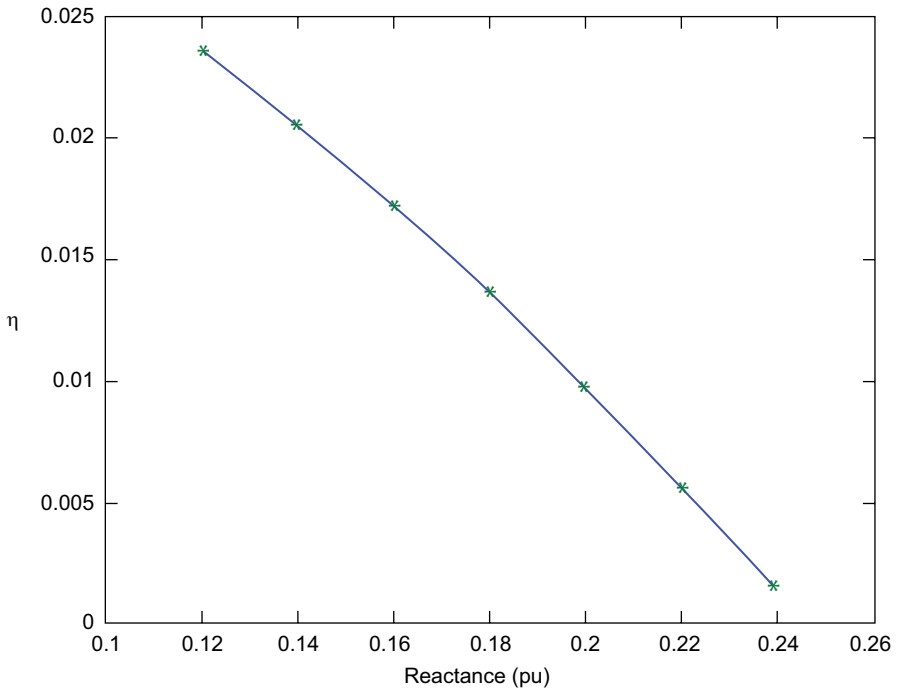


Fig. 11.15 Estimate critical value of the reactance of the line 8-9

technique. A fault is simulated at bus 7 and cleared at $t_{cl}=0.08$ s by tripping the line 5-7. Figure 11.15 shows the corresponding values of η for different values of reactance of the line 8-9. The critical value of the reactance of line 8-9 is 0.246 pu. It can be seen from Fig. 11.15 that the estimated value of the critical reactance is quite accurate if the two values of the line reactance are picked in the close range of the actual critical value.

Knowing the critical value of a line reactance is very important in controlling power flow path in the system by the variable impedance devices. Such devices belong to a type of devices called Flexible AC Transmission Systems (FACTS), which can be very useful in controlling the stability of power systems (Hingorani and Gyu Gyi 2000).

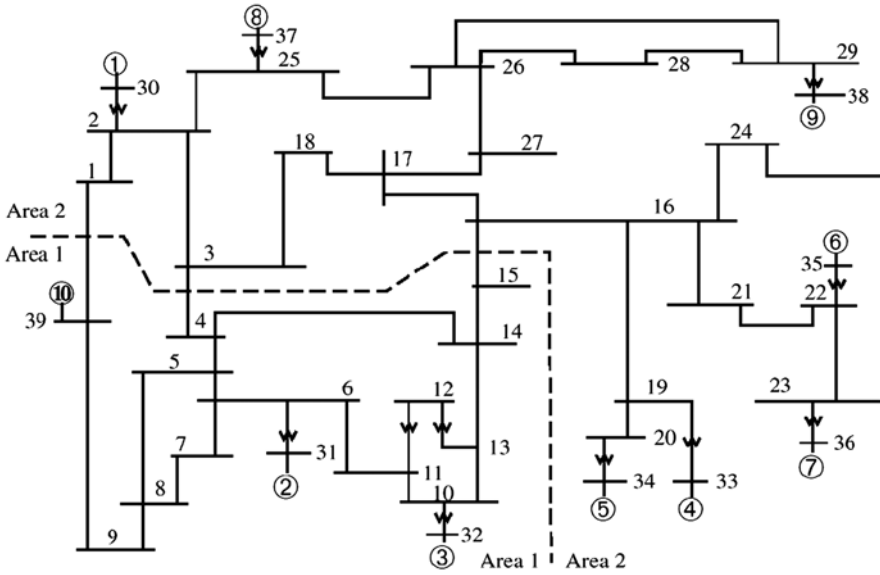


Fig. 11.16 The 10-machine, 39-bus system

11.6 Other Applications of Trajectory Sensitivities

11.6.1 Sensitivity of Tie-Line Power

The 10-machine, 39-bus system is used to illustrate the procedure and is shown in Fig. 11.16. It is divided into two areas. For a pre-defined set of contingencies in each area, the sensitivities of tie-line power transfers between areas with respect to generation at each machine are computed using the numerical approach. The sensitivity information is used to directly identify and rank the contingencies that have an important impact on the power transfer between areas (Hiskens et al. 1999).

The numerical sensitivities are calculated approximately by the following procedure:

1. For a given load, perform an economic dispatch to obtain $P_{Gi}^0, i=1, \dots, 10$.
2. Using P_{Gi}^0 of step 1, perform dynamic simulation for a particular contingency and obtain $P_{tie}^0(t)$ for $t \geq 0$.
3. To calculate the sensitivity of tie-line power with respect to the input power at generator $i, i=1, \dots, 10$, increase P_{Gi}^0 by 2%, i.e., $P_{Gi}^1 = 1.02P_{Gi}^0$, and keep the other $P_{Gj}^0, j \neq i$, unchanged. With this new loading condition, repeat step 2 for the same contingency and calculate $P_{tie}^1(t)$.
4. The trajectory sensitivity of tie-line power with respect to input power at generator i is approximated by

$$S_i(t) = \frac{P_{tie}^1(t) - P_{tie}^0(t)}{P_{Gi}^1 - P_{Gi}^0}, i = 1, \dots, 10.$$

Table 11.5 Peak-to-peak sensitivities of tie-line powers with respect to generation for various t_{cl} ($t_{cr}=0.17$ s)

Generator number	Tie-line	t_{cl} (s)			
		0.05	0.10	0.15	0.162
2	39-1	0.50	1.34	5.62	13.21
	4-3	0.11	0.35	1.94	9.34
	15-16	0.37	0.98	4.09	8.05
3	39-1	0.66	1.75	7.52	18.76
	4-3	0.15	0.46	2.70	14.21
	15-16	0.47	1.25	5.37	11.19
5	39-1	1.60	4.34	14.29	31.81
	4-3	0.31	0.95	5.92	26.55
	15-16	1.19	3.40	11.31	20.10
6	39-1	1.72	4.66	18.23	55.08
	4-3	0.34	1.07	7.00	46.73
	15-16	1.26	3.23	11.58	29.17
8	39-1	0.58	1.53	5.88	12.00
	4-3	0.14	0.38	2.04	6.95
	15-16	0.42	1.09	4.16	7.93
9	39-1	3.80	11.77	79.60	∞
	4-3	1.00	4.03	52.69	∞
	15-16	2.78	7.89	45.75	∞

Depending on the maximum excursion of the sensitivities, the severity of the contingencies can be ranked, and the most sensitive generators can also be detected.

The maximum peak-to-peak sensitivity deviations for several clearing times are tabulated in Table 11.5. The sensitivities with respect to generators 1, 4, and 7 are small and are not shown here. A number of observations can be made from these results. First, the flow on tie-line 39-1 is more sensitive than the other tie-line flows in all cases. It means that changes in tie-line flows induced by generation rescheduling should be such as to decrease the sensitivities in line 39-1. This higher sensitivity indicates that line 39-1 has a larger impact on system stability than the other tie-lines.

Therefore, system security could be improved by reducing the flow on line 39-1. Second, from Table 11.5, the sensitivities are highest for generators 6 and 9. As a result, the loading on these units has a greater influence on the tie-line flows, and tie-line oscillations, than other units.

Finally, the simulations are performed for a set of contingencies with fixed clearing time at $t_{cl}=0.05$ s. Again, the peak-to-peak sensitivities of tie-line powers with respect to generation are calculated. Table 11.6 gives the simulation results.

From Table 11.6, it can also be observed that the sensitivities are highest for generators 6 and 9. Again, the flow on tie-line 39-1 is more sensitive than other tie-lines in all cases. This provides further evidence of the important impact of generators 6 and 9 and tie-line 39-1 on the system security. Table 11.6 also indicates that sensitivity information can be used to rank the severity of contingencies. For instance, for contingencies involving lines 23-24, 4-14, and 6-7, the sensitivities are relatively small, so these contingencies are considered unimportant. The largest sensitivities correspond to outage of line 21-22 (generator 6) and line 25-26 (generator 9). Based on sensitivities, these contingencies would be ranked as most severe.

Table 11.6 Peak-to-peak sensitivities of tie-line powers with respect to generation for various line outages, $t_{cr}=0.5$ s for all cases

Generation number	Tie-line	Line outage					
		17-18	21-22	23-24	25-26	4-14	6-7
2	39-1	0.50	0.90	0.42	0.37	0.35	0.42
	4-3	0.11	0.13	0.06	0.06	0.18	0.21
	15-16	0.37	0.39	0.18	0.21	0.16	0.23
3	39-1	0.66	1.19	0.55	0.47	0.51	0.51
	4-3	0.15	0.16	0.09	0.09	0.20	0.24
	15-16	0.47	0.51	0.25	0.27	0.27	0.33
5	39-1	1.60	2.33	1.13	0.93	0.95	0.81
	4-3	0.31	0.31	0.14	0.12	0.16	0.10
	15-16	1.19	1.06	0.48	0.55	0.31	0.30
6	39-1	1.72	7.53	1.64	1.04	0.84	0.78
	4-3	0.34	0.73	0.23	0.12	0.17	0.09
	15-16	1.26	3.13	0.66	0.59	0.29	0.29
8	39-1	0.58	1.10	0.51	0.44	0.42	0.44
	4-3	0.14	0.13	0.06	0.30	0.08	0.06
	15-16	0.42	0.45	0.21	0.20	0.14	0.16
9	39-1	3.80	4.35	2.10	6.69	1.79	1.70
	4-3	1.00	0.47	0.26	1.24	0.37	0.22
	15-16	2.78	1.72	0.87	3.92	0.60	0.63

The assessment has been confirmed by simulation. The critical clearing times are 0.13 s for contingency on line 21-22 and 0.08 s for contingency on line 25-26. Further, delayed clearing of the fault on line 21-22 would result in losing synchronism of generator 6, whereas delayed clearing of the fault on line 25-26 would result in generator 9 losing synchronism. Note that different generators are critical for different contingencies.

11.6.2 Impact of Distributed Generation on System Stability

11.6.2.1 Distributed Generation Configuration

We assume that as load demand increases, it is met by the addition of Distributed Generation (DG) units at those buses. A new distributed load bus is introduced and connected to the original bus through a transformer, and the additional load is modeled at this new bus, as shown in Donnelly et al. (1996). This additional load is served by a DG that is connected to the load through another transformer as shown in Fig. 11.17.

The penetration factor that relates the additional load being met by the DG unit to the original load is defined as

$$\text{Penetration level (\%)} = \frac{P_{di}}{P_{di} + P_{Li}} \times 100$$

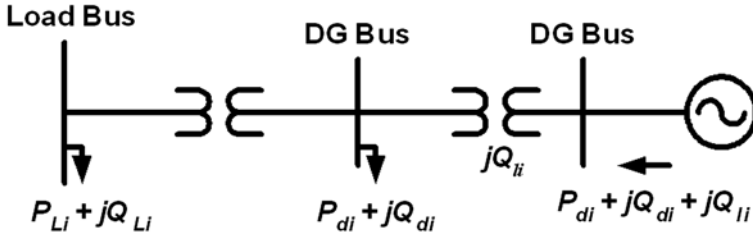


Fig. 11.17 Proposed configuration for DG

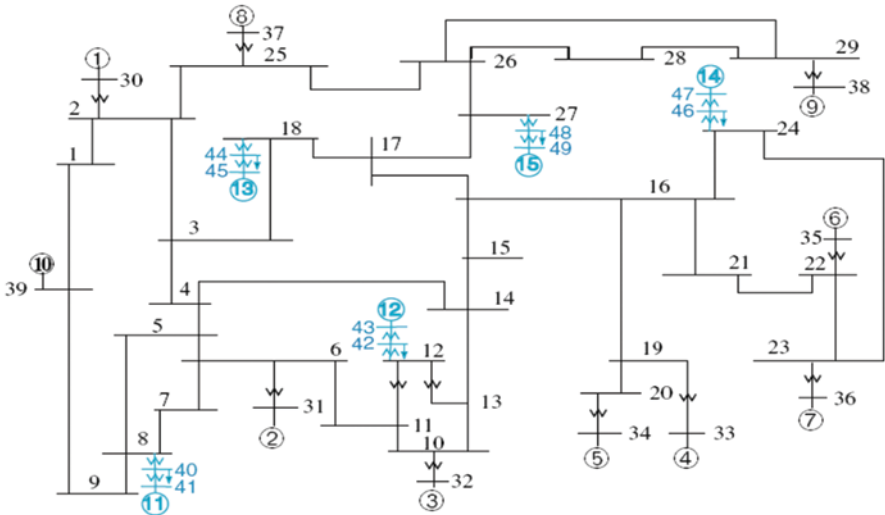


Fig. 11.18 The augmented system

In the above equation, P_{di} refers to the additional real load and P_{Li} is the original real load at the bus i where the DG is added. This relationship is also defined for reactive loads for the DGs. Also, the real power generation of the DG will match the new load added at the adjacent bus, and the reactive power generation will match the new load and loss in the transformer.

The 10-machine, 39-bus system from Fig. 11.3 is used as the original system for simulations. We assume that new loads $P_{di} + jQ_{di}$ ($i=1, \dots, 5$) have to be served at different system locations. These loads will be met by the configuration proposed in Fig. 11.17. With a penetration factor of 40% at each bus and adding DG at locations of the new loads, as shown in Fig. 11.18, we simulate for a fault at bus 15 followed by tripping line 15-16.

With a classical model for all generators and a clearing time of 0.22 s, the original system is stable (Fig. 11.19), but the augmented system is unstable (Fig. 11.20). The DG 11 is the unstable machine.

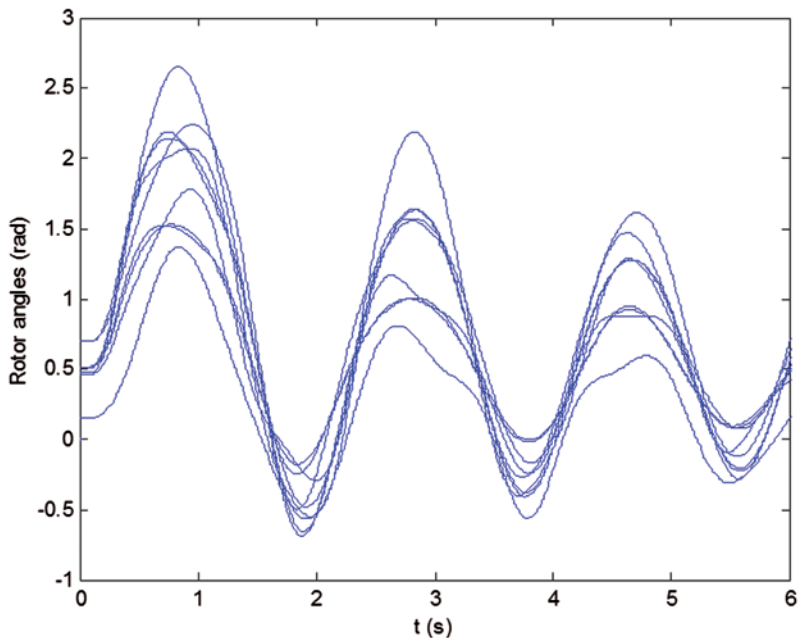


Fig. 11.19 Relative rotor angles for the original system with $t_{cl}=0.22$ s

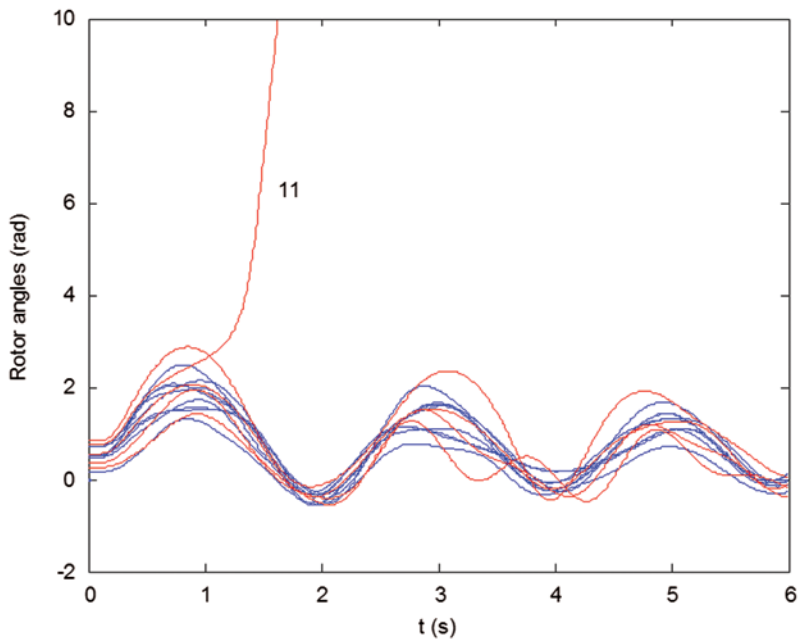


Fig. 11.20 Relative rotor angles for augmented system with $t_{cl}=0.22$ s

Table 11.7 Critical clearing time for different penetration levels

Penetration (%)	t_{cr} (s)	Unstable generators
Original	0.25	2, 3, 11
10	0.28	2, 3, 11
20	0.28	2, 3, 11
30	0.27	2, 3, 11
40	0.2	11
45	0.13	11
50	0.06	11

11.6.2.2 Effect of Penetration Levels on System Stability

With the augmented system shown in Fig. 11.18, we vary the penetration level to see how the system stability changes for the same fault. At 10% penetration, the system maintains stability up to a clearing time of 0.28 s. This is an improvement on the original system, which goes unstable at 0.26 s. When increasing the clearing time to 0.29 s, the system is unstable, and generators that go unstable are 2, 3, and 11.

At 20% penetration, the critical clearing time is 0.28 s, and the generators that go unstable are again 2, 3, and 11 when increasing clearing time slightly greater than the critical clearing time. At 30% penetration, the system still shows an improvement over the original, with a 0.27-s critical clear time, which is 0.02 s better than the original. Again, generators 2, 3, and 11 are advanced machines when clearing time is increased to 0.28 s.

At 40% penetration, the DG begins to adversely affect the system. Generator 11, i.e., one of the DGs, now goes unstable with a 0.21-s clearing time, which is worse than the original system. At 45% penetration, the critical clearing time drops to 0.13 s.

Generator 11 goes unstable when the clearing time is increased to 0.14 s. At 50% penetration, the critical clearing time is 0.06 s, and generator 11 goes unstable again when the clearing time is increased slightly above the critical clearing time. And at 55% penetration, the system is unstable for even a small amount of clearing time. The result is shown in Table 11.7.

The trend for this system is that penetration levels below 30% have little effect on system stability and can help the system slightly. However, once penetration begins to increase over 30%, clearing times allowed for stability diminish rapidly. The conclusion from this study is that DG is not a concern to system stability as long as it remains a small fraction of the overall system load.

11.6.2.3 Application of Trajectory Sensitivities

The augmented system (Fig. 11.18) is simulated with the fault at bus 15 and cleared by tripping line 15-16. The penetration level is varied from 10 to 40%. The clearing

Table 11.8 Normalized maximum variation for different penetration levels

Generator	Penetration levels (%)			
	10	20	30	40
1	0.0126	0.0125	0.0129	0.0214
2	0.0267	0.0264	0.0261	0.0719
3	0.0254	0.0251	0.0248	0.0678
4	0.0982	0.1003	0.1080	0.1606
5	0.1379	0.1433	0.1604	0.2473
6	0.0879	0.0915	0.1034	0.1697
7	0.0875	0.0910	0.1032	0.9
8	0.0272	0.0269	0.0270	0.0447
9	0.0632	0.0637	0.0687	0.1164
11	0.0775	0.0777	0.0884	1.0000
12	0.0963	0.0934	0.0909	0.0875
13	0.0888	0.0852	0.0836	0.0942
14	0.1095	0.1059	0.1485	0.7613
15	0.0811	0.0799	0.0807	0.1250

time is reduced to 0.18 s to make the system stable for all cases. With generator 10 chosen as reference, the sensitivities of relative rotor angles to the mechanical input power P_M at the various generators are computed. The maximum sensitivity variation for each relative rotor angle is normalized to unity for the generator having the highest variation. The results are shown in Table 11.8.

For the penetration level of 40%, it is found that generator 11 has the highest sensitivity variation. This suggests that the generator that goes unstable is 11 if the clearing time is set at a value larger than the critical one. This is consistent with the simulation results obtained in Sect. 11.6.2.2.

As can be seen from Table 11.8, for the penetration levels of 10, 20, and 30%, the sensitivities do not vary much. This suggests that the system stability is not affected much by those penetration levels. This also agrees with the simulation results in Sect. 11.6.2.2. When the penetration increases to 40%, the sensitivity variation changes significantly, especially for the potentially unstable generator 11. This result suggests that the system stability has been affected by this penetration level. Again, this agrees with the conclusion of the simulation in Sect. 11.6.2.2. Results from Table 11.8 have shown that there is a strong correlation between the system stability and the corresponding trajectory sensitivity of the dynamical system. The connection between system stability and trajectory sensitivity has been discussed for nonlinear dynamic systems in Tomovic (1963).

11.6.3 Relay Margin as Stability Indicator

Power system protection at the transmission system level is based on distance relaying. Distance relaying serves the dual purpose of apparatus protection and system protection. Significant power flow oscillations can occur on a transmission line or

a network as a result of major disturbances like faults and subsequent clearing, load rejection, etc. They are related to the swings in the rotor angles of synchronous generators. If the rotor angles settle down to a new stable equilibrium point, the disturbance is classified as stable. Otherwise, it is unstable. Hence, for stable disturbances, power swings die down with time.

Work based upon Lyapunov stability criterion has been reported by Singh and Hiskens (2001) to rank relays according to the severity of swings. Relay margin is used by Dobraca et al. (1990) as a measure of how close a relay is from issuing a trip command. Basically, it is the ratio of the time of the longest consecutive stay of a swing in zone to its Time Dial Setting (TDS).

For relays that see swing characteristics outside of their zone settings, the relay space margin is used. It is defined as the smallest distance between the relay characteristic and the swing trajectory in the R - X plane. To identify the most vulnerable relay, magnitude of the ratio of swing impedance to line impedance is used as a performance parameter. The most vulnerable relay corresponds to one with minimum ratio, where the search space extends over all the relays and time instants of simulation. The relay margin is computed by extensive simulations, and modifications of zone 2 or 3 settings are made to curtail relay operation on a stable swing (Vaidyanathan and Soman 2002).

The challenges to relaying in the restructured power system operation scenario have been discussed by Thorp and Phadke (1999). In such a scenario, there will be varying power flow patterns dictated by the market conditions. During the congestion period, relay margins and relay space margins will be reduced. This may pose challenges to system protection design. The vulnerability of a relay to power swings is directly dependent on the severity of oscillations in power flow observed in the primary transmission line and adjacent transmission lines that are covered by the backup zones. Hence, the problem of assessment of transmission protection system vulnerability to power swings translates into assessment of oscillations in power flow on a transmission system caused by disturbance.

Application of TSA to detect vulnerable relays in the system has been discussed by Soman et al. (2004). For each contingency, a quantity called branch impedance trajectory sensitivity (BITS; that is, trajectory sensitivity of rotor angles to branch impedance) is computed. This quantity is then used to locate the electrical center (weakest links; Kimbark 1950) in the transmission system and rank transmission system distance relays according to their vulnerability to tripping on swings. Its main advantage is that it can handle systems of any degree of complexity in terms of modeling and can be used as an online DSA tool. Detailed computation of BITS and its application in DSA can be found in Soman et al. (2004).

11.7 Conclusions

The trajectory sensitivity-based approach has been used to study various aspects of the DSA problem in power systems. The major advantage of this approach is the ability to handle complex models of power systems such as DAE, discrete event

coupled with DAE, and hybrid systems. A drawback of this approach is that an additional set of system sensitivity equations will have to be integrated along with the original dynamic system. The computational burden can be reduced by utilizing the common structure of the Jacobian of the two systems. Also, the advances in computer technology and capability in parallel computing, grid computing, and others have reduced the computational burden significantly.

References

- Abur A, Exposito AG (2004) Power system state estimation: theory and implementation. CRC , Boca Raton
- Ahmad M (2012) Power system state estimation. Artech House, London
- Alsac O, Stott B (1974) Optimal load flow with steady state security. *IEEE Trans Power App Syst* 93:745–754 (PAS)
- Athay T, Podmore R, Virmani S (1979) A practical method for direct analysis of transient stability. *IEEE Trans Power App Syst* 98(2):573–584 (PAS)
- Chaniotis D, Pai MA, Hiskens IA (2001) Sensitivity analysis of differential-algebraic systems using the GMRES method-application to power systems. In: *Proceeding of the IEEE International Symposium on Circuit System*, Sydney, 6–9 May 2001
- Dobraca F, Pai MA, Sauer PW (1990) Relay margins as a tool for dynamical security analysis. *Intl Electr Power Energy Syst* 12(4):226–234
- Donnelly MK, Dagle JE, Trudnowski DJ, Rogers GJ (1996) Impacts of the distributed utility on transmission system stability. *IEEE Trans Power Syst* 11(2):741–746
- Eslami M (1994) *Theory of sensitivity in dynamic systems*. Springer, New York
- Fouad AA (1988) Dynamic security assessment practices in North America. *IEEE Trans Power Syst* 3(3):1310–1321
- Fouad AA, Vittal V (1991) *Power system transient stability analysis using the transient energy function method*. Prentice Hall, Englewood Cliffs
- Frank PM (1978) *Introduction to system sensitivity theory*. Academic, New York
- Gan D, Thomas RJ, Zimmerman RD (2000) Stability-constrained optimal power flow. *IEEE Trans Power Syst* 15(2):535–540
- Hingorani NG, Gyu Gyi L (2000) *Understanding facts concepts and technology of flexible ac transmission systems*. IEEE Press, New York
- Hiskens IA, Pai MA (2000) Trajectory sensitivity analysis of hybrid systems. *IEEE Trans Circuits Syst I Fundam Theory Appl* 47(2):204–220
- Hiskens IA, Pai MA, Nguyen TB (1999) Dynamic contingency analysis studies for inter-area transfers. In: *Proceedings of the 13th power systems computation conference*, Trondheim, Norway
- Kimbark EW (1950) *Power System Stability. Power circuit breakers and protective relays*, vol II. Wiley, New York, p 160
- Kokotovic PV, Rutman RS (1973) Sensitivity of automatic control systems (survey). In: Cruz JB Jr (ed) *System sensitivity analysis*. Dowden, Hutchinson and Ross, Stroudsburg, pp 359–381
- Kumar ABR, Amelink H, Pang CK, Pai MA, Sauer PW (1987) Dynamic security assessment for power systems: research plan. EPRI report EL-4958, Aug 1987
- La Scala M, Trovato M, Antonelli C (1998) Online dynamic preventive control: an algorithm for transient security dispatch. *IEEE Trans Power Syst* 13(2):601–610
- Laufenberg MJ, Pai MA (1998) A new approach to dynamic security assessment using trajectory sensitivities. *IEEE Trans Power Syst* 13(3):953–958
- Laughton MA (1964) Sensitivity in dynamical system analysis. *J Electron Control* 17(5):577–791
- Monticelli A (2000) Electric power system state estimation. *Proceeding of the IEEE* 88(2):262–282

- Monticelli A (2007) *State estimation in electric power systems: a generalized approach*. Springer, New York
- Nguyen TB, Pai MA (2003) Dynamic security-constrained rescheduling of power systems using trajectory sensitivities. *IEEE Trans Power Syst* 18(2):848–854
- Nguyen TB, Pai MA, Hiskens IA (2002) Sensitivity approaches for direct computation of critical parameters in a power system. *Intl J Electr Power Energy Syst* 24(5):337–343
- Padiyar KR, Krishna S (2001) On-line detection of loss of synchronism using locally measurable quantities. In: *Proceedings of IEEE Transmission and Distribution Conference, Atlanta*
- Pai MA (1981) *Power systems stability*. North Holland Publishing Co., New York
- Pai MA (1989) *Energy Function Analysis for Power Systems*. Kluwer Academic, Boston
- Pavella M, Murthy PG (1994) *Transient stability of power systems: theory and practice*. Wiley, New York
- Pavella M, Ernst D, Ruiz-Vega D (2000) *Transient stability of power systems: a unified approach to assessment and control*. Kluwer Academic, Norwell
- Ruiz-Vega D, Pavella M (2003) A comprehensive approach to transient stability control: part I - Near optimal preventive control. *IEEE Trans Power Syst* 18(4):1446–1453
- Sauer PW, Pai MA (1998) *Power system dynamics and stability*. Prentice-Hall, Upper Saddle River
- Shubhanga KN, Kulkarni AM (2004) Stability-constrained generation rescheduling using energy margin sensitivities. *IEEE Trans Power Syst* 19(3):1402–1413
- Singh C, Hiskens IA (2001) Direct assessment of protection operation and non-viable transients. *IEEE Trans Power Syst* 16(3):427–434
- Soman SA, Nguyen TB, Pai MA, Vaidyanathan R (2004) Analysis of angle stability problems: a transmission protection systems perspective. *IEEE Trans Power Del* 19(3):1024–1033
- Thorp JS, Phadke AG (1999) Protecting power systems in the post-restructuring era. *IEEE Comput Appl Power* 12(1):33–37
- Tomovic R (1963) *Sensitivity analysis of dynamic systems*. McGraw-Hill, New York
- Tomovic R, Vukobratovic M (1972) *General sensitivity theory*. Elsevier, New York
- Vaidyanathan R, Soman SA (2002) Distance relay coordination considering power swings. In: *Proceedings of the international conference on power systems and communication systems infrastructure for the future*, Beijing, China
- Vittal V, Sauer PW, Meliopoulos S, Stofopoulos GK (2005) *Online transient stability assessment scoping study-final project report*. Power Systems Engineering Research Center, PSERC Publication 05-04
- Yuan Y, Kubokawa J, Sasaki H (2003) A solution of optimal power flow with multicontingency transient stability constraints. *IEEE Trans Power Syst* 18(3):1094–1102
- Zima M, Andersson G (2003) Stability assessment and emergency control method using trajectory sensitivities. In: *Proceedings of the IEEE PowerTech Conference, Bologna, Italy*
- Zimmerman R, Gan D (2005) *MATPOWER: a MATLAB power system simulation software package*. <http://www.pserc.cornell.edu/matpower>. Accessed 25 May 2005

Chapter 12

Model Predictive Real-Time Control of Electric Power Systems Under Emergency Conditions

Marek Zima and Göran Andersson

Abstract Model Predictive Control (MPC) is a widely used method in process industry for the control of multi-input and multi-output systems. It possesses features that make it attractive for power system applications. Power systems exhibit complex characteristics such as hybrid nature (mixed continuous and discrete dynamics), nonlinear dynamics, and very large size. The optimization computations involved in MPC further increase the challenge of handling such features in a reasonable time. Therefore, the reduction of the computational burden associated with MPC is a crucial factor for real-time applications. In this chapter, we describe a formulation of MPC for power systems based on trajectory sensitivities. Trajectory sensitivities are time-varying sensitivities derived along the predicted nominal trajectory of the system, which allow an accurate reproduction of the nonlinear system behavior using a considerable reduced computational burden as compared with the full nonlinear integration of the system trajectories. Therefore, their deployment opens application possibilities for MPC in new, previously restricted, areas.

12.1 Introduction

The model predictive control (MPC) approach entails the identification of an optimal control strategy by solving an optimization problem. An attractive feature of this problem's formulation is the explicit incorporation of control quality criteria and constraints imposed on system inputs, outputs, and states. The effect of controlled inputs on the system behavior (i.e., states and outputs) is predicted by using a model of the system.

However, the MPC has two drawbacks as well: open control loop nature and computational burden associated with the solution of the optimization problem. The first obstacle can be overcome by introducing an implicit feedback in the form of repetitive computation of control laws in a receding horizon manner. The second obstacle has

G. Andersson (✉)
Swiss Federal Institute of Technology, ETH Zurich, ETL G26, Physikstrasse 3, 8092 Zürich,
Switzerland
e-mail: andersson@eeh.ee.ethz.ch

M. Zima
Swissgrid, Laufenburg, Switzerland

restricted the application of MPC mostly to control of slower processes, with the dynamics in order of minutes, e.g., chemical industry, or linear systems, for which many efficient algorithms for optimization and describing system dynamics are available.

Power systems are large systems comprising many components (thus, the number of variables and states is very high), which interact with each other in various ways and in different time scales, i.e., dynamics speed ranging from milliseconds to years. Dynamics present in power systems may be very nonlinear and have a hybrid nature, i.e., both continuous and discrete state variables are involved. All these aspects complicate the employment of MPC in a power system, particularly in real-time applications.

Several authors have addressed the difficulties to apply MPC in power systems. Larsson (Larsson et al. 2002) analyzes Euler nonlinear and linear approximations with numerical computation of sensitivities to controlled inputs for prediction of the power system behavior. Geyer (Geyer et al. 2003) has proposed a Mixed Logic Dynamics (MLD) framework for dealing with the hybrid dynamics in MPC of power systems. A significant acceleration of MPC computations has been reported by Beccuti et al. (2004).

Coordinated secondary voltage control applied in the western part of France by Electricité de France (EdF) and reported in several publications, e.g., Vu et al. (1996), may probably be considered as the first industrial implementation of MPC in a real power system. Although it is not referred to in the literature as MPC, it possesses its features, i.e., continuous repetitive use of optimization for computing voltage set points of generators in the supervised region.

Our goal is to describe how an employment of trajectory sensitivities for the prediction of the system behavior and an effect of controlled inputs can help to significantly reduce the computational burden, while keeping a good reproduction of the system nonlinearities. By this, a further use of MPC for control applications in power systems would be possible.

The chapter starts with a short overview of MPC and associated computation burden reduction techniques. Then, we introduce a formulation of MPC based on trajectory sensitivities, which is described further in the Appendix. After that, we outline some possible applications in power systems and provide simulation results for the voltage control of a test power system. Finally, we discuss some implementation issues and future research challenges.

12.2 Model Predictive Control

12.2.1 General (Nonlinear) MPC

In a general system (no restrictions concerning the type of dynamics, etc.), MPC computes a sequence of control inputs, which yield an optimum (in most cases a minimum) of the objective function, while satisfying constraints imposed on the system inputs, outputs, and states. The objective function usually comprises several parts and represents a tradeoff between the quality of the control process and the effort needed to enforce it. The quality of the control process is usually expressed as a

difference between the desired and actual value of the output (when a tracking problem is considered). The control effort is the deviation of control inputs from their original values and/or their optimal values. This can mathematically be expressed as

$$\min_{u(t)} \Phi(x(t), y(t), u(t)) \quad (12.1)$$

subject to equality constraints:

$$\begin{aligned} \dot{x}(t) &= f(x(t), y(t), u(t)) \\ 0 &= g(x(t), y(t), u(t)) \end{aligned} \quad (12.2)$$

and inequality constraints:

$$0 \leq h(x(t), y(t), u(t)), \quad (12.3)$$

where $x(t)$ are the dynamic state variables, $y(t)$ are the algebraic state variables, and $u(t)$ are the control (manipulated) inputs, calculated at time t_0 , within the time horizon (interval) of the length T_h ; thus $t \in [t_0 + T_h]$. In addition, all types of variables can be nonlinearly bounded within corresponding spaces, i.e.,

$$\begin{aligned} x(t) &\in X \\ y(t) &\in Y \\ u(t) &\in U. \end{aligned} \quad (12.4)$$

The solution of the above-stated problem at the time t_0 is an optimal control inputs sequence $u^*(t)$. Since the above formulation fully relies on the system model and the system state at the time t_0 , an actual response of the system to the computed control sequence can differ due to the model imperfections and disturbances present in the system. Therefore, applying the initial part of control inputs and then solving MPC formulation again introduces a feedback. This procedure will be repeated at regular time intervals.

12.2.2 Approaches to Reduction of Complexity of General MPC Formulation

A complexity of solving (12.1–12.4) plays a crucial role in the feasibility of a control scheme based on MPC. There are several factors influencing it:

- Complexity of the cost function (12.1)
- Complexity of the boundaries (12.3) and (12.4)
- Size of the controlled system (i.e., number of variables in the system model)
- Complexity of the model behavior, e.g., internal structure, type of interactions within the model, etc., expressed by constraints (12.2)
- Length of the prediction horizon T_h

The length of the prediction horizon T_h should ideally be infinite, but this is practically impossible, hence it is one of the design parameters of the MPC to be considered in the tradeoff between the accuracy and computation time of the controller. Usually, T_h is chosen to be sufficiently long to capture the slowest dynamics of the controlled system.

The cost function itself has usually a simple form of either a linear or a quadratic function; boundaries are usually constant. However, both cost function and boundaries are linked/coupled to the system behavior description, i.e., (12.2).

Thus, the most decisive factor is the system dynamics. Many efficient, powerful, and robust computation techniques have been developed for linear systems, so in such a case, even a larger system size does not represent a major problem. But, often nonlinear and/or hybrid systems have to be controlled. In that case, solving (12.1–12.4) may represent a challenge. Therefore, significant effort has been invested into the research of techniques allowing reproduction of nonlinear system behavior with a minimal computational effort.

The first option is to use a full nonlinear model and computations, which is not only the most accurate but also the most time-consuming approach. Therefore, this is normally applicable only either for small-sized systems or for slow processes, where the slow dynamics implies that long computation times can be tolerated.

The second frequently used method is to linearize the system equations around the present operating point (equilibrium) and apply the linear MPC. Discrepancy between the linearized model and the actual system behavior is then compensated in the next controller step. However, this involves a risk that the system may undergo large excursions from the optimal trajectory and even violate imposed constraints.

The third approach is based on the approximation of the expected trajectory (Euler prediction) of the system if control inputs would remain unchanged and the numerical¹ computation of sensitivities of control inputs impact on this trajectory. A linear Euler prediction has similar properties as the ones described in the previous paragraph and is based on the strong assumption of monotonous time evolution of the system trajectory. Nonlinear Euler prediction is much more accurate. However, a numerical computation of sensitivities then means repetition of the system trajectory prediction as many times as the number of control inputs.

12.3 Proposed Control Theory

Our approach is closest to the last one described in the previous section. Let us assume discrete time control. The controller would then be employed (i.e., MPC optimization problem would be solved) in the regular time intervals of T_{cs} with the outlook of the prediction horizon (i.e., length of the sliding window) of T_h .

¹ A numerical computation of sensitivity to a change of a parameter is obtained by dividing the difference of trajectories with and without considering an incremental change of the parameter by the incremental change of the parameter.

Assume that the control should be executed at the time t_0 . Then the control method consists of three stages:

- A nominal trajectory of the system is predicted for the time interval $[t_0, t_0 + T_h]$ by employing discrete time form of (12.1–12.4) with the integration step of T_{ps} . This may be perceived as a time domain simulation. As a byproduct, trajectory sensitivities are computed with a little additional effort according to Hiskens and Pai (2000) and as explained in the Appendix.
- Controls are computed according to equations (12.5–12.10) and the description in the next paragraphs.
- The first set of computed controls is applied at the time t_0 (neglecting the time delay).

Note, that although we use a discrete time framework, we do not explicitly mention a particular number of samples but rather time instants. This is due to possible discrete events. To capture the discrete events properly, two samples in the same time instant are necessary. Moreover, it may happen between two regular samples; thus, the time of the discrete event occurrence has to be computed as well and the integration step T_{ps} is divided accordingly.

In most cases, the integration step has a relatively small size to capture dynamics properly. Therefore, $T_{ps} \leq T_{cs} \leq T_h$.

Using a quadratic cost function, the control objective can be expressed by (12.5). The first term represents the cost of the deviation from the reference value, so the corresponding algebraic variable is defined in the model description in the equality constraints (12.6). The third term penalizes the control employment, whereas the second term penalizes the deviation of the control from its initial value at the time t_0 . Note that all control deviations Δu refer to the initial point and not to the previous sample. However, a penalty on the deviation of the control from its previous sample value can easily be included by an appropriate choice of the nondiagonal elements of the matrix R_{du} .

$$\min_{\Delta U} \frac{1}{2} \sum_{k=0}^{N_{ps}-1} \{ y_k^T Q y_k + \Delta u_k^T R_{du} \Delta u_k + u_k^T R u_k \} \quad (12.5)$$

$$y_k = y_k^{nom} + \frac{\partial y_k}{\partial u_k} \Delta u_k \quad (12.6)$$

$$u_k = u_k^{nom} + \Delta u_k \quad (12.7)$$

$$y_k^{\min} \leq y_k \leq y_k^{\max} \quad (12.8)$$

$$u_k^{\min} \leq u_k \leq u_k^{\max}$$

$$\Delta u_k^{\min} \leq \Delta u_k \leq \Delta u_k^{\max}$$

$$\Delta U = \{ \Delta u_k \}_{k=0}^{N_{ps}-1} \quad (12.9)$$

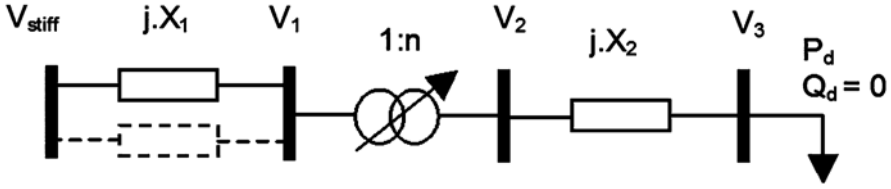


Fig. 12.1 Single line diagram of the simple system

$$\begin{aligned}
 u_k \in \mathfrak{R}^{N_u}, \Delta u_k \in \mathfrak{R}^{N_u}, \frac{\partial y_k}{\partial u_k} \in \mathfrak{R}^{N_y \times N_u}, y_k \in \mathfrak{R}^{N_y} \\
 \forall k \in KK = \{0, \dots, N_{ps} - 1\}
 \end{aligned} \tag{12.10}$$

N_u is the number of available controls (manipulated inputs), N_y the number of controlled variables (i.e., tracked outputs), and N_{ps} the number of samples in the prediction horizon. As discussed earlier, it is not necessarily constant. Unless the employed controls change significantly, trajectory sensitivities reproduce the system behavior quite accurately, even considering nonlinear dynamics. However, it is very difficult to bind a region, in which the changes can be considered “reasonably small.” Another possible source of errors may be certain types of discrete events. A discrepancy between the model and the actual system response can be corrected in the receding horizon manner.

The above-defined controller uses a quadratic cost function and hard constraints. But, this is not a limitation of the method. Soft constraints may be introduced, and slack variables and the whole problem can be restated in a form of linear programming.

12.4 Simulation Examples

We will now present two examples. The first one explains the principle of MPC based on trajectory sensitivities in a simple illustrative system. The second example shows a particular application for which the proposed control would suit well.

12.4.1 Illustrative Example

Consider the system described in Hiskens and Pai (2000) and Hiskens and Sokolowski (2001) and shown in Fig. 12.1. A simple radial system connected to a stiff network feeds load with a dynamic recovery. The system comprises three lines and a transformer equipped with a tap changer. The tap changer has its own traditional controller with a time constant of 20 s.

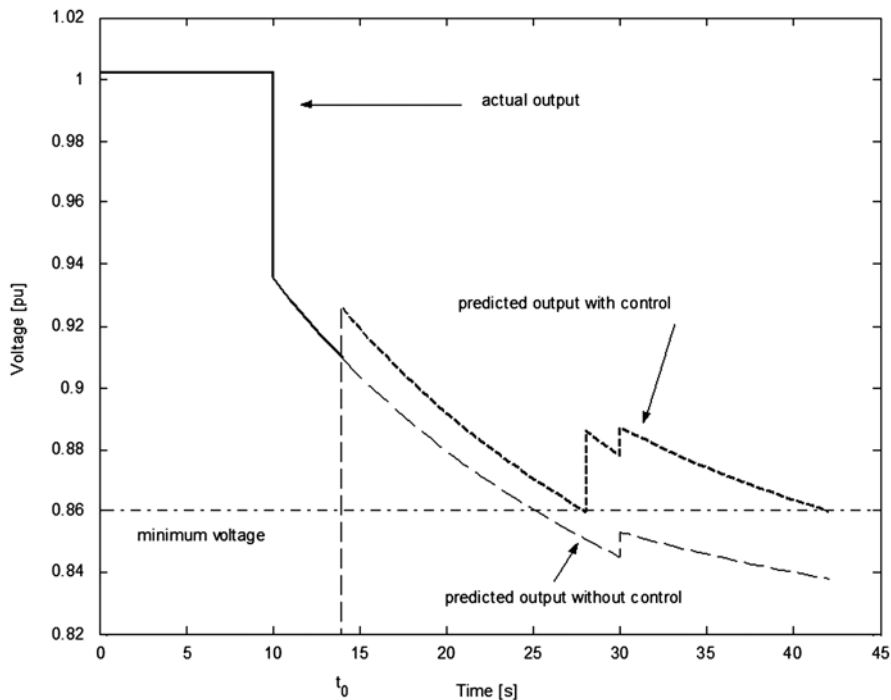


Fig. 12.2 Controller prediction at the time t_0

At the time equal to 10 s (from the beginning of the simulation), one of the parallel lines is tripped. As a consequence, the voltage in node 3 drops. The role of the controller is to keep the voltage in node 3 in the operation range (i.e., above 0.85 pu) by applying the smallest possible load shedding (in node 3). Load shedding is expressed by the factor k , which expresses which percentage (0 means no load shedding at all, 1 represents disconnection of entire load) of the initial value of the load is disconnected.

Let us assume that the controller is activated at the time t_0 as shown in Fig. 12.2.

First, the voltage magnitude in node 3 is predicted if no control change from its present value (i.e., in this case load shedding, present value of the load shedding is zero) is applied.

Simultaneously, trajectory sensitivities are computed using parts of the Jacobian evaluated during the prediction of the voltage evolution. Since the voltage drops under the minimal allowed value, MPC following formulation (12.5–12.10) computes the necessary load shedding to avoid it, see Fig. 12.4. The new trajectory predicted by the MPC controller would be as shown in Fig. 12.3.

The controller predicts the nominal trajectory (i.e., the one without any control input changes) and computes corresponding trajectory sensitivities for the time horizon of T_h equal to 28 s, which is divided into two intervals T_{cs} (equal to 14 s).

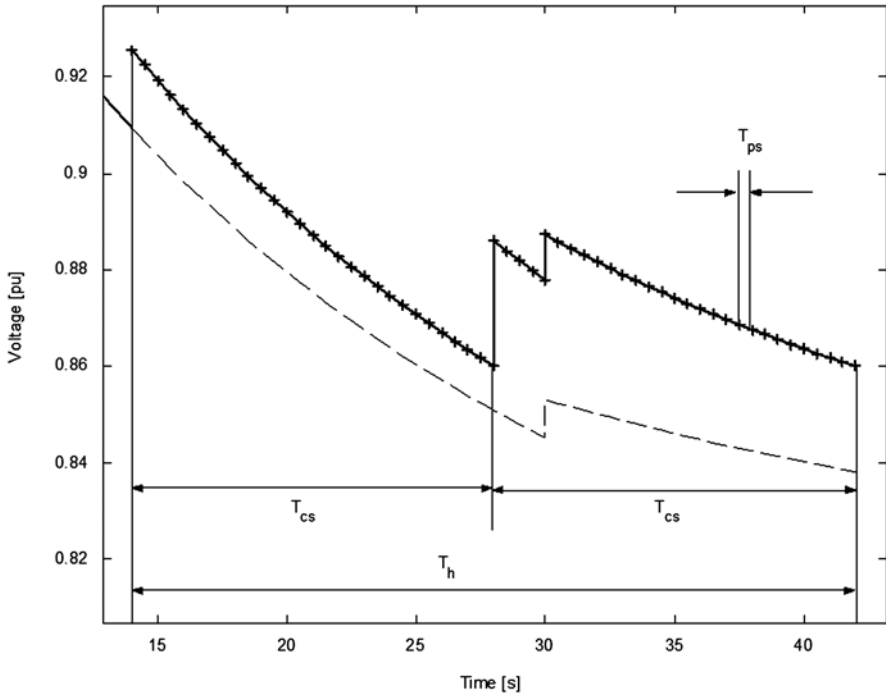


Fig. 12.3 Overview of time constants of the controller

Within each of them, control inputs remain constant. The integration step T_{ps} (prediction sampling), which is used for computations, is 0.5 s.

Figure 12.3 shows the relationship between all described time constants. Use of time constants instead of the number of samples (as it is a well-established practice in discrete time control) can be also explained with the help of Fig. 12.4.

The transformer tap changes its position (according to the prediction) in the beginning of the second control interval T_{cs} . It is a discrete event and it requires two samples at one time instant to capture this behavior appropriately. Therefore, the second control interval has one more sample than the first one.

Although two control intervals have been used, only the control inputs values of the first one are applied at the time t_0 (neglecting the time delay).

At the time $t_0 + T_{cs}$, the entire described procedure with the prediction and computation of necessary control inputs changes is repeated as shown in Fig. 12.5 and Fig. 12.6. As Fig. 12.7 shows, even when no external disturbance takes place, the system response slightly differs from the predicted one. Therefore, the value of the optimal control inputs to be applied at the time $t_0 + T_{cs}$ also may differ from the one envisioned for this time instant at the time t_0 , see Fig. 12.6.

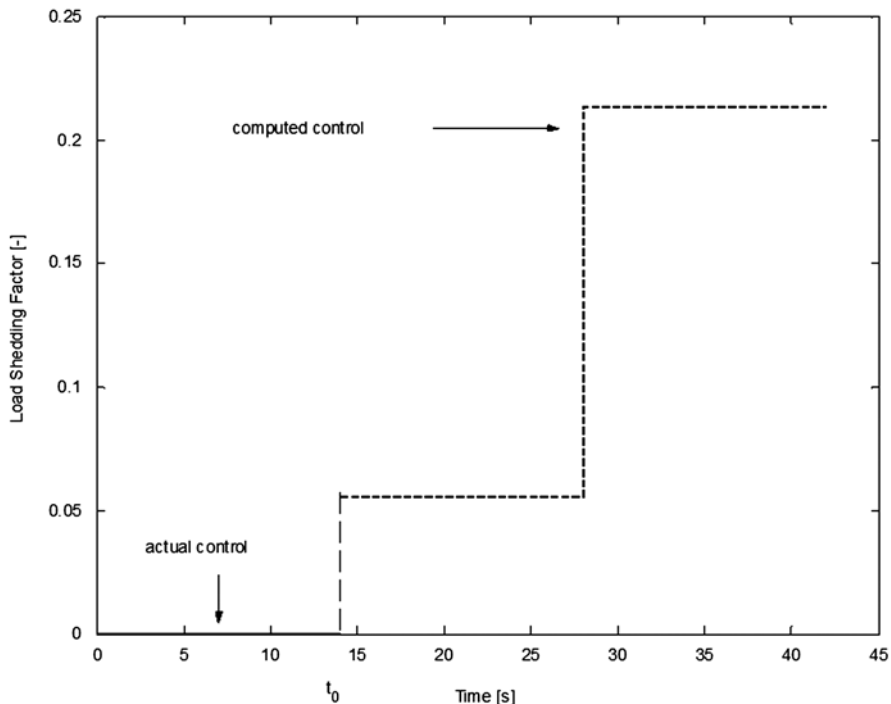


Fig. 12.4 Necessary load shedding as computed by the controller at the time t_0

The same procedure is then repeated at time instants corresponding to multiples of the control intervals T_{cs} . Thus, an implicit feedback control is introduced. The final voltage magnitude trajectory as well as load shedding factor after the decay of the transient voltage drop is plotted in Fig. 12.8.

12.4.2 Realistic Example

Voltage control (sometimes also referred to as reactive power management) in power systems has several goals. The approaches can be divided into two categories: economy and security oriented. From the long-term economic operation point of view, it is most desirable to avoid frequent under- or over-voltages, which increase aging and wear of the equipment, and to keep the losses generated in the system low.

This can be achieved by decrease of currents (recall that most of the losses are resistive: $R \cdot I^2$) by keeping the voltage profile high. From the security point of view, the main concern is the danger of encountering voltage instability and a possible voltage collapse. Here, the defense strategy is usually dependent on the system conditions.

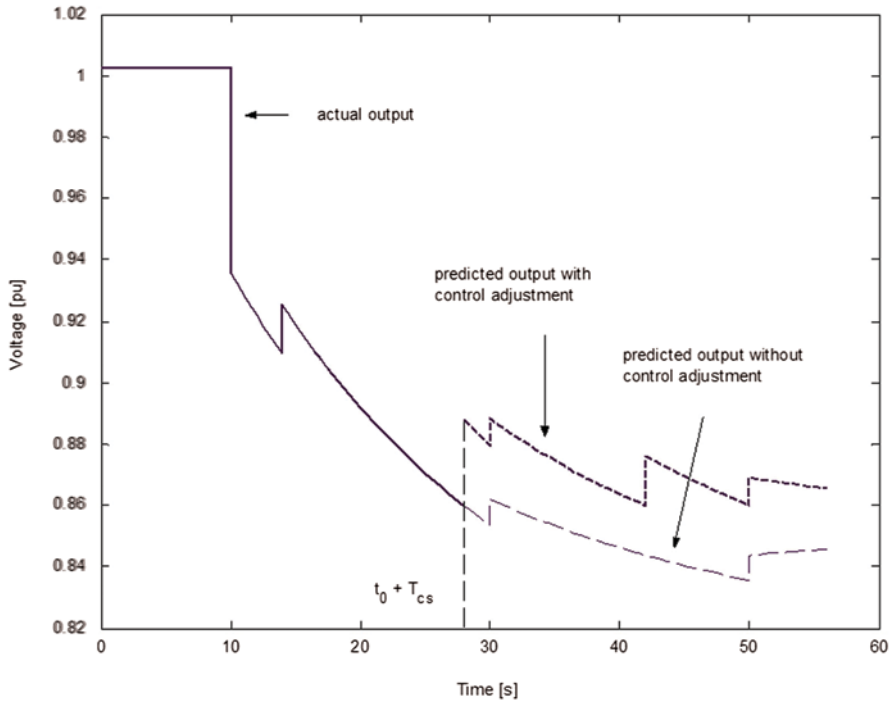


Fig. 12.5 Predicted trajectories at the time $t_0 + T_{cs}$

When the system is in an emergency state and voltages significantly drop, under-voltage load shedding relays trigger a disconnection of some loads. In normal operation conditions, the focus is on keeping the system robust and to strengthen its ability to withstand a disturbance (e.g., a line or a generator trip), which could possibly cause a voltage collapse. It is thus desirable to control the system in a way keeping large reactive power reserves of generators (in other words, keeping a low reactive power production of generators). Consequently, there should be a sufficient amount of reactive power available to avoid voltage problems in the case of a disturbance, as shown in Van Cutsem and Vournas (1998) and Kundur (1994) for explanation of coupling between the reactive power and voltage.

Consider the system described in Hiskens and Akke (1999) and shown in Fig. 12.9. The authors have used it for a study of power oscillations excited in Nordel (interconnected power system of Sweden, Norway, Finland, and eastern part of Denmark). We have introduced small modifications (e.g., changing the load character to constant power load instead of impedance load) allowing us to focus on the voltage-related issues.

An overview of basic system parameters is provided in the Table 12.1. Basic control circuits of generators are modeled too, e.g., *governors* controlling the turbine supplying torque and thus the active power, *automatic voltage regulators (AVR)*

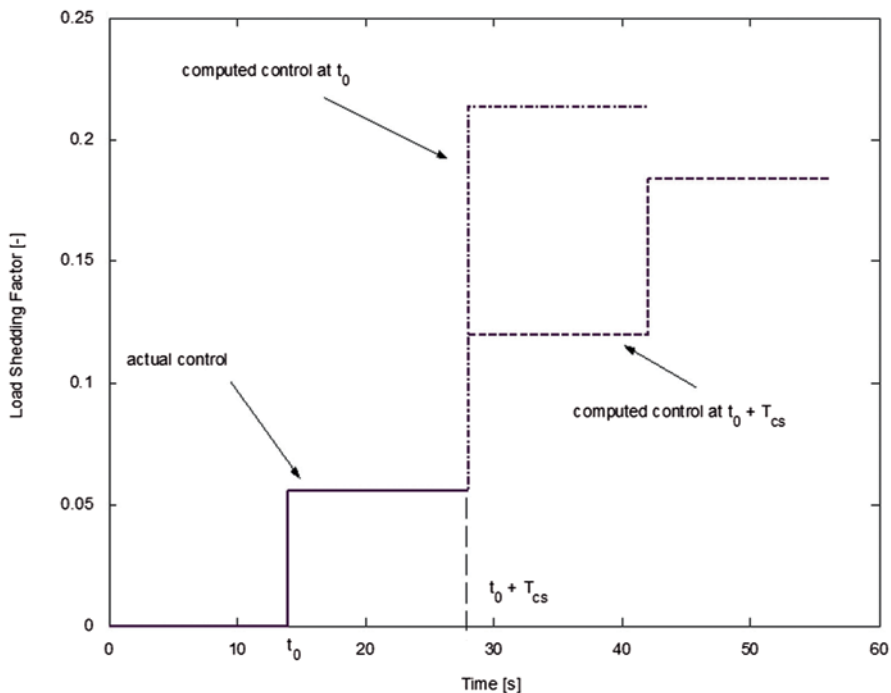


Fig. 12.6 Update of the value of optimal load shedding at the time $t_0 + T_{cs}$

controlling excitation circuits of the generator and thus the generator’s terminal voltage, and reactive power output and *Power System Stabilizers (PSS)* modulating the reference signal for the AVR to damp oscillations measured in the system frequency.

Altogether, the system model has 822 variables of all types (i.e., dynamic, algebraic, and discrete state variables, including controls). Tracked variables/outputs are voltages in all buses and reactive power production of all generators. Possible controls are reference voltages of all AVRs and load shedding of all loads.

Load shedding factor of each load can have a value between 0 (no load shedding at all) and 1 (complete load is shed) and determines to which extent the load is disconnected. The voltage boundaries are 0.95 pu (referred to the nominal voltage equal to 1 pu) and 1.15 pu, respectively (Fig. 12.10). Limits imposed on the reference voltages (i.e., controls, manipulated inputs) are 0.9 pu and 1.1 pu. Note that voltage boundaries, both of the outputs and inputs, are usually narrower in reality.

The goal of the controller is to continuously supervise the power system and minimize the absolute value of reactive power production of all generators. Under normal conditions, this should be achieved by selecting most suitable reference voltages for AVRs. Only when the system is seriously endangered, load shedding can be employed to recover the system into the acceptable operation region. The

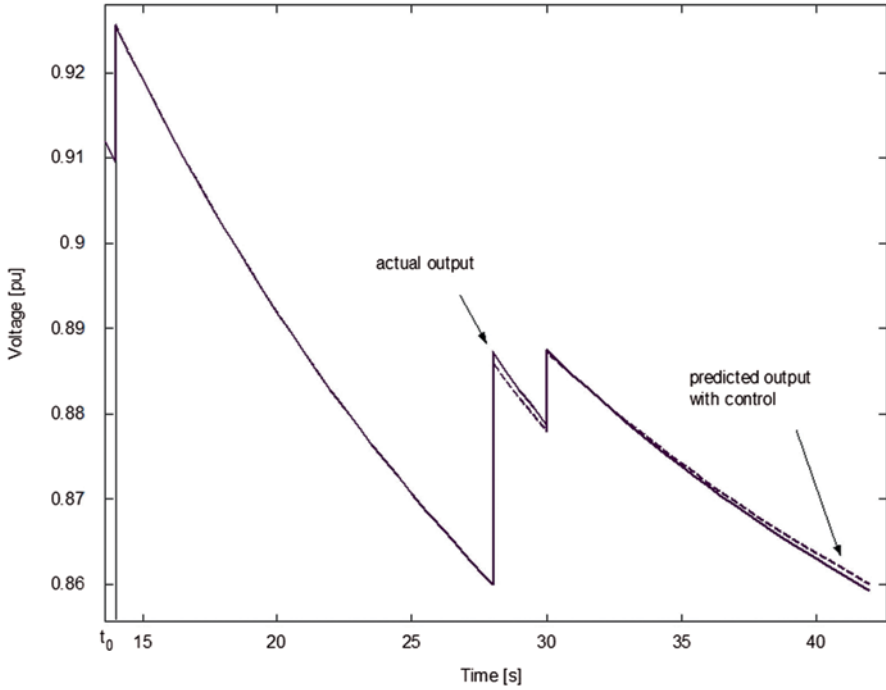


Fig. 12.7 Deviation of the actual trajectory from its predicted value even under the condition of no disturbance and using an ideal model

controller parameters have been chosen accordingly to serve this purpose. The nominal prediction sampling (i.e., integration step) T_{ps} is 0.5 s, prediction horizon T_h is 10 s, and controls sampling T_{cs} is 5 s. The controller follows the form defined by (12.5–12.10).

The upper plot in Fig. 12.11 represents the sum of absolute values of reactive powers produced by all generators. The lower plot shows buses' voltage magnitudes. To depict the controller's behavior, we have chosen two different scenarios. First, the system is subjected to a severe disturbance, which is disconnection of the faulty line between the buses 3 and 16.

As shown in Fig. 12.11, the line outage triggers an oscillation driving voltages outside of the secure operation region. Therefore, the controller orders load shedding at buses 1 and 3 in addition to the adjustment of generator voltage reference set points. The latter control action would be insufficient and too slow to save the system from more severe consequences, see Fig. 12.10.

In the second case, the system starts from the same initial conditions, but there is no disturbance. Therefore, the employed controls shown in Fig. 12.12 aim at decreasing the reactive power produced by generators as shown in Fig. 12.13.

Note that this type of control can be classified as secondary voltage control. That means that the system can be divided into areas, each of them supervised by one

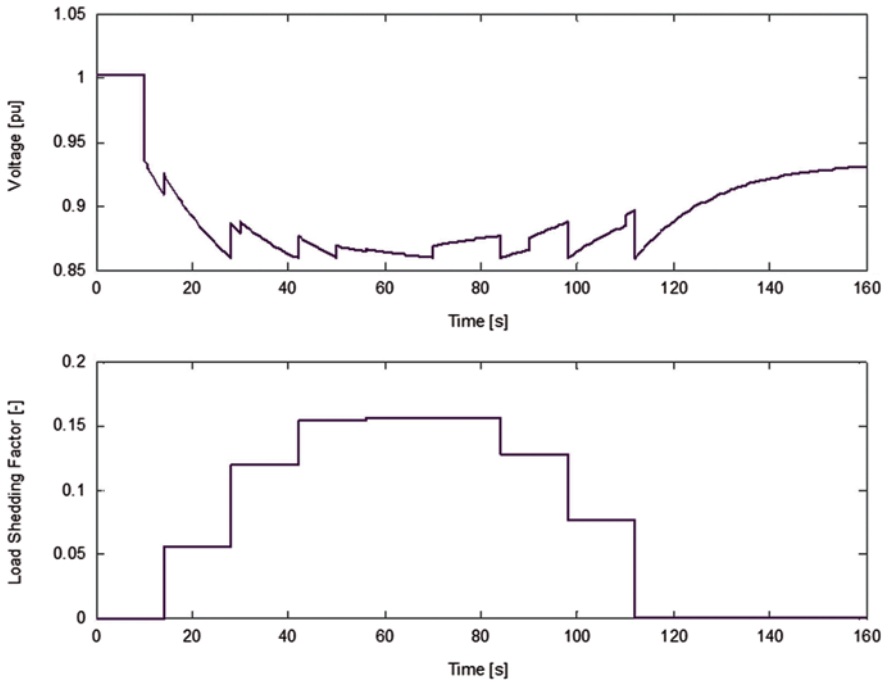


Fig. 12.8 Final voltage trajectory and applied control (i.e., load shedding)

controller. In addition to the presented example, the control objective can be extended for example by the term penalizing import and export of reactive power from and to other areas. Some aspects of possible interactions of controllers between each other are discussed on a conceptual level by Zima and Ernst (2005).

12.5 Implementation Issues

When implementing the control methodology described in the previous sections, several design aspects have to be considered in the overall control scheme design:

- Availability of accurate system models components
- Availability of control inputs
- Preprocessing of data, i.e., platform delivering the system topology, voltages, etc.
- Computational power
- Communication infrastructure

It is out of the scope of this chapter to discuss these issues further, but they need to be addressed carefully during the real implementation of the described control strategy. Reader interested in this topic may consult Zima et al. (2005).

Fig. 12.9 Single line diagram of the test system. Loads are connected in the *black* buses. The *dashed* line between nodes 3 and 16 is the line tripped in the disturbance scenario

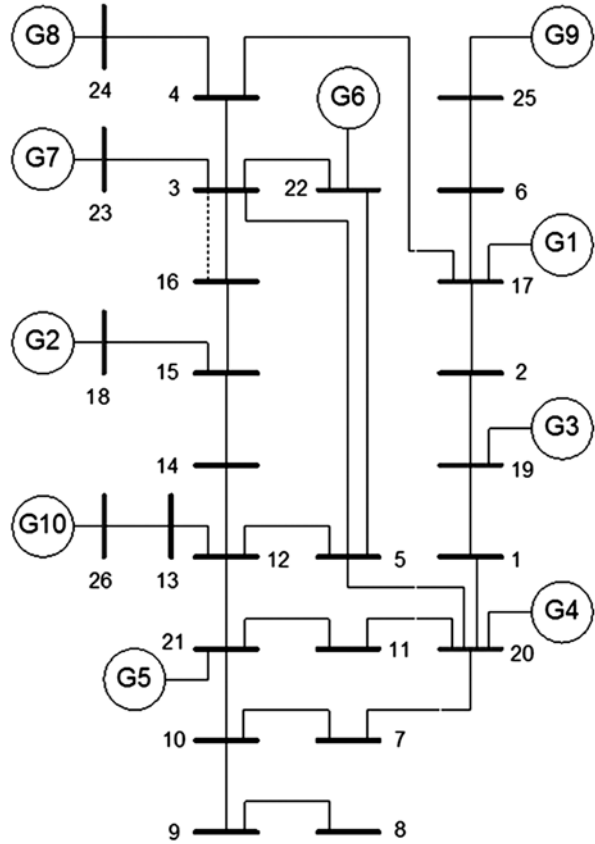


Table 12.1 The test system characteristic data

Component	Number/amount
Buses	26
Lines	31
Loads	17
Generators	10
Governors	10
AVRs	10
PSSs	3

12.6 Challenges and Possible Future Research Directions

The chapter describes an algorithm allowing relatively fast optimization computations, while keeping accurate track and description of the nonlinear behavior. We show the principle and theoretical description of the proposed algorithm and demonstrate its application on the reactive power and voltage control example.

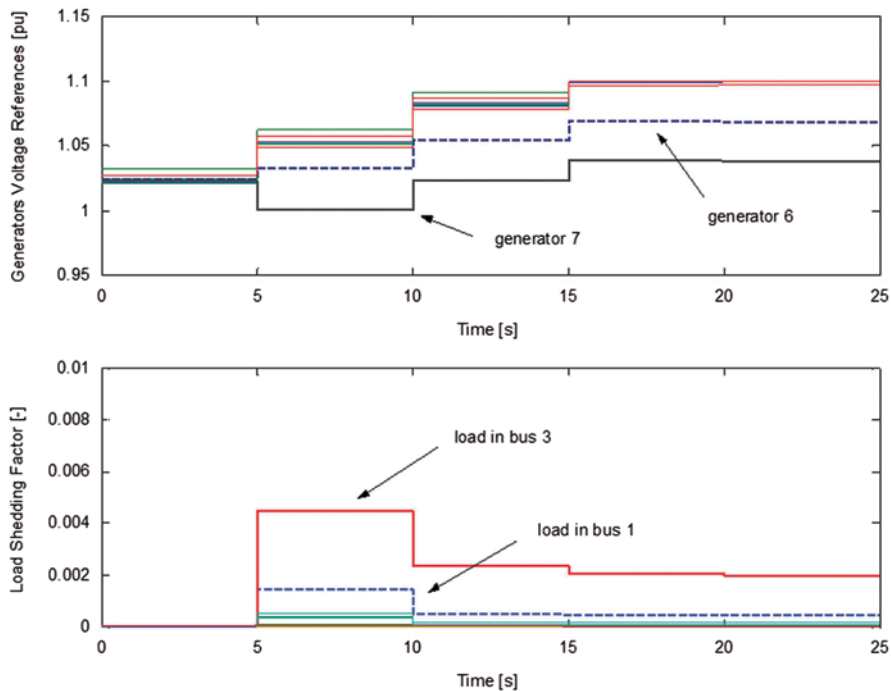


Fig. 12.10 Controls computed and executed by the controller. The test system is subjected to a severe disturbance. The *upper* plot shows reference voltages for generators’ AVRs. The *lower* plot shows load-shedding factors of all loads, closer explained in the text

Possible applications on other power systems’ control problems can be investigated. Research towards finding the most suitable implementation optimization algorithm, e.g., answering the question if linear programming with slack variables would be faster and numerically more robust, as well as introduction of explicit models of system-wide objectives, e.g., one model of the entire system reactive power generation, may further significantly improve the performance of the algorithm.

We believe that continuing advances in implementation platforms suited for MPC and computational power (i.e., hardware), as well as research activities towards more efficient algorithms, will make MPC more and more attractive for real-time applications in power systems.

Appendix: Trajectory Sensitivities Analysis

An efficient framework for modeling of nonlinear systems featuring discrete states has been presented in Hiskens and Pai (2000). Its application on power systems modeling has been further shown in Hiskens and Sokolowski (2001) and Hiskens

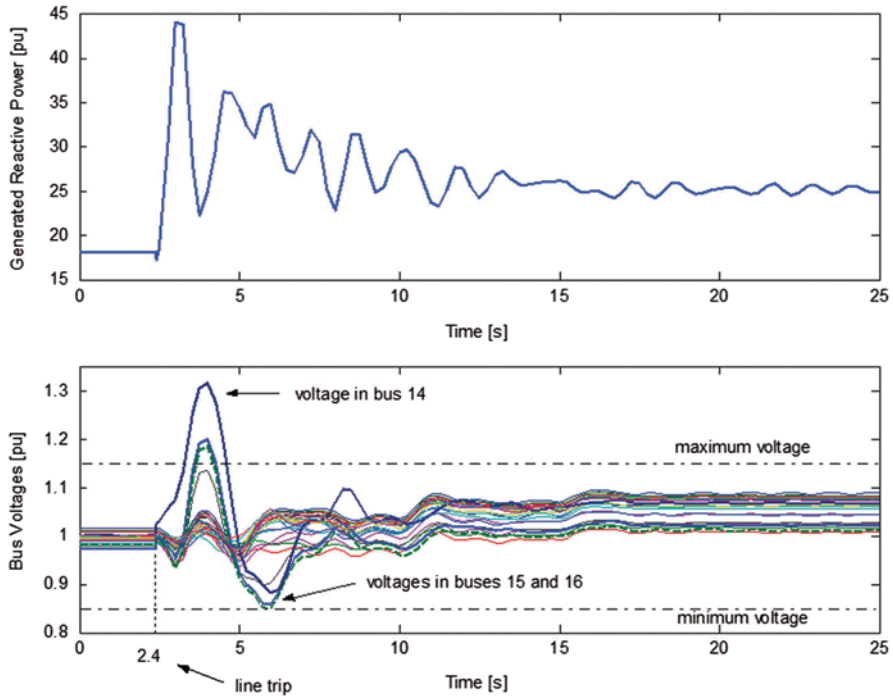


Fig. 12.11 Controlled system outputs. The test system is subjected to a severe disturbance

and Gong (2004), where a natural flexible modular structure following power systems components classification has been adopted.

Omitting parameter λ from the original formulation (Hiskens and Pai 2000) and introducing control input u , we can write the system equations in compact form:

$$\dot{x} = f(x, y, z, u), \tag{12.11}$$

$$0 = g^0(x, y, z, u), \tag{12.12}$$

$$0 = \begin{cases} g^{i-}(x, y, z, u) & y_{d,i} < 0 \\ g^{i+}(x, y, z, u) & y_{d,i} > 0 \end{cases} \quad i = 1, \dots, d, \tag{12.13}$$

$$\begin{aligned} z^+ &= h_j(x^-, y^-, z^-, u^-) & y_{e,j} &= 0 \\ \dot{z} &= 0 & y_{e,j} &\neq 0 \end{aligned} \quad j \in \{1, \dots, e\}, \tag{12.14}$$

$$\begin{aligned} y_d &= D.y \\ y_e &= E.y \end{aligned}, \text{and} \tag{12.15}$$

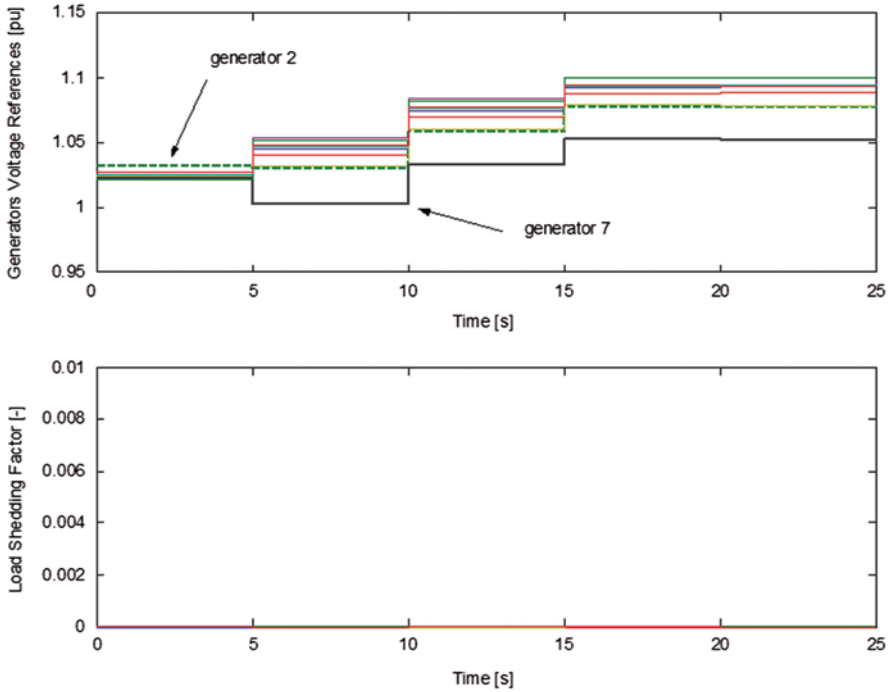


Fig. 12.12 Controls computed and executed by the controller. The test system is under normal conditions. The *upper* plot shows reference voltages for generators’ AVRs. The *lower* plot shows load-shedding factors of all loads, closer explained in the text

$$\begin{aligned}
 x \in X \subseteq \mathfrak{R}^n \quad z \in Z \subseteq \mathfrak{R}^k \\
 y \in Y \subseteq \mathfrak{R}^m \quad u \in U \subseteq \mathfrak{R}^l
 \end{aligned}
 \tag{12.16}$$

Dynamic state variables are denoted as x , algebraic state variables y , and discrete state variables z . Switching of the status of discrete variables is governed by the equation (12.14) when the corresponding auxiliary variables of y_e are equal to zero. Auxiliary variables y_d determine the region of validity of the equation (12.13). In the power systems context, this may be explained with an example of a line, which changes its status.

When the line is in service, equations linking the current through the line and voltages at both ends of the line as well as line parameters (line impedance and shunt admittance) are valid. When the line is out of service (i.e., disconnected), current flowing through it is zero. The auxiliary variable is in that case the difference between the time and the instant when the line was tripped.

Matrices D and E have normally a very sparse structure and their nonzero elements are equal to one in the positions aiming at the auxiliary variables.

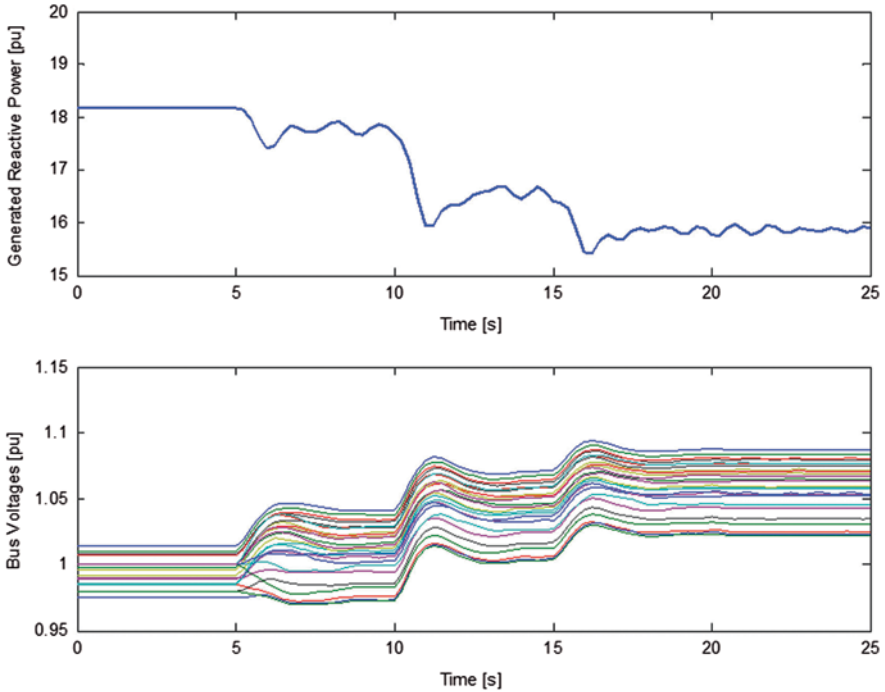


Fig. 12.13 Controlled system outputs. The test system is under normal conditions. The *upper* plot represents the sum of absolute values of reactive powers produced by all generators. The *lower* plot shows buses' voltage magnitudes

Flow (i.e., time evolution) of the system from its initial point can be characterized by the time evolution of its variables, e.g., for the algebraic state variables we can write

$$\varphi_y(y_0, t) = y(t). \quad (12.17)$$

Note that the initial state y_0 is obtained by solving equations (12.12–12.13) by substituting initial values of $x(t)$, $z(t)$, and $u(t)$ by x_0 , z_0 , and u_0 respectively.

An impact of small changes of the initial conditions on the system flow can be investigated by trajectory sensitivities. The impact of manipulated inputs (i.e., controls) on algebraic states time evolution can be obtained by a Taylor expansion of equation (12.17). When neglecting higher order terms:

$$\Delta y(t) = \frac{\partial y(t)}{\partial u_0} \cdot \Delta u_0. \quad (12.18)$$

Note that trajectory sensitivities are generally time-varying quantities. Note that a numerical approximation of trajectory sensitivities can be computed by

solving (12.11–12.16) for an incremental change of each control input. However, that would represent a large computation effort if many control inputs were considered. The methodology for computation of trajectory sensitivities, described in Hiskens and Pai (2000), involves only minimal additional computations, since it uses parts of Jacobian evaluated when solving (12.11–12.16).

References

- Beccuti AG, Geyer T, Morari M (2004) Temporal Lagrangian decomposition of model predictive control for hybrid systems, In: IEEE conference on decision and control, Atlantis, Bahamas, Dec 2004
- Geyer T, Larsson M, Morari M (2003) Hybrid emergency voltage control in power systems. In: Proceedings of the European control conference, Cambridge, UK, Sept
- Hiskens IA (2004) Power system modeling for inverse problems. *IEEE Trans Circuits Syst-I: Regul Papers* 51(3):539–551
- Hiskens IA, Akke M (1999) Analysis of the Nordel power grid disturbance of January 1, 1997 using trajectory sensitivities. *IEEE Trans Power Syst* 14(3):987–994
- Hiskens IA, Gong B (2004) Voltage stability enhancement via model predictive control of load. In: Bulk power systems dynamics and control VI, Cortina d’Ampezzo, Italy, 22–27 Aug 2004
- Hiskens IA, Pai MA (2000) Trajectory sensitivity analysis of hybrid systems. *IEEE Trans Circuits Syst-I: Fundam Theory Appl* 47(2):204–220
- Hiskens IA, Sokolowski PK (2001) Systematic modeling and symbolically assisted simulation of power systems. *IEEE Trans Power Syst* 16:2:229–234
- Kundur P (1994) Power system stability and control. Mc Graw-Hill Professional, New York
- Larsson M, Hill DJ, Olsson G (2002) Emergency voltage control using search and predictive control. *Int J Power Energy Syst* 24(2):121–130
- Van Cutsem T, Vournas C (1998) Voltage stability of electric power systems. Kluwer Academic, Norwell
- Vu H, Pruvot P, Launay C, Harmand Y (1996) An improved voltage control on large-scale power system, *IEEE transactions on power systems*, vol 11, no 3, pp 1295–1303, Aug 1996
- Zima M, Ernst D (2005) On multi-area control in electric power systems, PSCC, Paper 2 in Session 9, Liege, Belgium, Aug 2005, www.pscce.eu
- Zima M, Larsson M, Korba P, Rehtanz P, Andersson G (2005) Design aspects for wide area monitoring and control systems. *Proceedings of IEEE*, vol 93, no 5, May 2005, pp 980–996

Chapter 13

The Role of Power System Visualization in Enhancing Power System Security

Thomas J. Overbye

Abstract While the operation of much of the electric power grid is automated, the human operators and engineers are still very much “in the loop.” During times of emergency operation, when the system may be close to instability and collapse, having access to timely, pertinent information about a potentially rapidly changing system state could prove crucial in preventing major blackouts. This chapter examines the role power system visualization can play in providing this information to access the margin to system instability. The focus of the chapter is on techniques for the rapid analysis and display of information, based primarily on Supervisory Control and Data Acquisition (SCADA) data, which will allow operators and engineers to quickly assess the state of a large power grid, and then take effective control actions. It also examines how visualization can be used to provide an early warning as a secure power system state gradually approaches the system stability boundary.

13.1 Introduction

Around the world, the recent large-scale blackouts have dramatically demonstrated that even with modern Energy Management Systems (EMSs) cascading blackouts are still not a relic from the past. Based upon the investigations of these blackouts, it is clear that a number of changes can be made to decrease the risk of future blackouts, with some of these changes presented in the previous chapters. The goal of this chapter is to explore one additional area—the role improved power system visualization in the control centers can play in reducing blackout risk.

While the term “power system visualization” is somewhat generic, a good working definition is “a method for presenting large amounts of information in an interactive, graphical form in which the information is related by an underlying power system.” Hence, power system visualization is contained within the general “information visualization” field but is a unique subfield due to the impact of the

T. J. Overbye (✉)
University of Illinois at Urbana-Champaign, Champaign, IL, USA
e-mail: overbye@illinois.edu

underlying power system. Most of the research focus in this subfield has been directed towards the display of information associated with many electric substations, a topic known as wide-area visualization. Usually, this information has a geospatial component due to its location on a one-line diagram. While the one-lines themselves could be drawn in a geographically accurate form, usually they are only drawn in a pseudo-geographic form since the areas of most interest (i.e., those with a high concentration of electric facilities) may be geographically quite small.

The goal of power system visualization is to allow operators¹ to gain additional insight concerning the power system and ultimately make better decisions. For example, the visualizations may allow them to see patterns or rapidly locate interesting pieces of information (e.g., an overloaded transmission line). With power system models often containing tens of thousands of buses, and single studies producing hundreds of thousands of numeric values, it is no longer feasible to examine all or even a significant percentage of the numeric values.

From the point of view of reducing the risk of blackouts, power system visualizations play two distinct roles. First, they can be useful in preventing the power system from reaching an emergency operating state (i.e., one in which a blackout is imminent, and can only be prevented through emergency control). For example, a judicious display of Supervisory Control and Data Acquisition (SCADA) information and/or indices derived using the techniques discussed in the previous chapters could provide the operator with an early warning that the system may be moving towards an emergency state, allowing them to take preemptive action.

Second, during an emergency the visualizations can be useful in helping the operators maintain a good understanding of a potentially rapidly changing power system state (i.e., “situational awareness”), allowing them to take the necessary emergency control actions to prevent a bad situation from getting worse. Many blackout events have time frames of several minutes to a few dozen minutes—time frames that permit operator intervention. When seconds count and operator actions can prove crucial, the seconds and minutes spent figuring out what to do is time that is no longer available to actually get it done. This chapter discusses visualizations of both situations.

With respect to the question of what constitutes an optimal or even a good power system visualization, the answer is far from clear. While there is certainly much to learn from the general information visualization field and from the human factors field, to some extent a good visualization, like beauty, is in the eye of the beholder. Of course, the goal remains the same—help the operators make better decisions. But the devil is in the details.

What works great for some is despised by others, what works well during emergency operations does not during normal times, and what looks good initially does not after a month of operational experience. Those who desire the preciseness of mathematical equations should venture with trepidation into the visualization field.

¹ Here, the term “operator” is used generically to refer to any individual making operation decisions about the power system, either in real time or through day ahead or other types of planning studies.

This chapter presents several visualization techniques that are likely to be helpful. These include the use of graphic symbols, animation of power flow values, contouring, and three-dimensional (3D) visualization.

13.2 2D Power System Visualization

Traditionally, in an EMS system operational quantities, such as power flows and voltages, are usually represented as either analog fields on a set of substation one-line diagrams, or numeric fields on tabular displays. Dashed lines might be used to represent device status, while fonts may change color to indicate limit violations.

An overview of the system had only been available on a static map board with the only dynamic data shown using different colored lights. While such a representation might be desired for normal operation, or even during slowly developing system emergencies, the assertion here is it is inadequate for allowing operators to quickly comprehend a rapidly, and perhaps unexpectedly changing system state.

An alternative is to provide wide-scale visualizations that take advantage of the animation capabilities of modern computers to graphically show important system quantities. These quantities can include geospatially measured values, such as transmission line/transformer (line) flow values and bus voltages, geospatially derived values such as inter-area oscillation mode and participation values, and more abstract values such as distance to a loadability boundary. This section presents several of these techniques using the traditional 2D format.

13.2.1 Line Flow Pie Charts

One visualization technique that has proven useful for quickly indicating the location of overloads/outages in a transmission network has been the use of pie charts in which the percent fill of each pie chart is equal to the percentage loading on the line (Overbye et al. 1995). Optionally, a numeric text could also be superimposed on the pie chart to indicate the exact percentage. For displays with relatively few lines, where each individual line's pie chart can be viewed with sufficient detail, such pie charts can quickly provide an overview of the system loading. If desired, different color shadings could also be used with the pie charts to highlight those devices loaded above some threshold percentage.

However, for larger network overview displays there is insufficient space to show each individual pie chart. Instead, a supplementary technique is to dynamically size the pie charts based upon the line's percentage loading. In this approach, the percentage fill in each pie chart is still equal to the percentage loading on the line, but the size and color of the pie chart can be dynamically sized when the loading rises above a specified threshold. By increasing the size and/or changing the color of the pie charts only for the small number of elements loaded above a critical

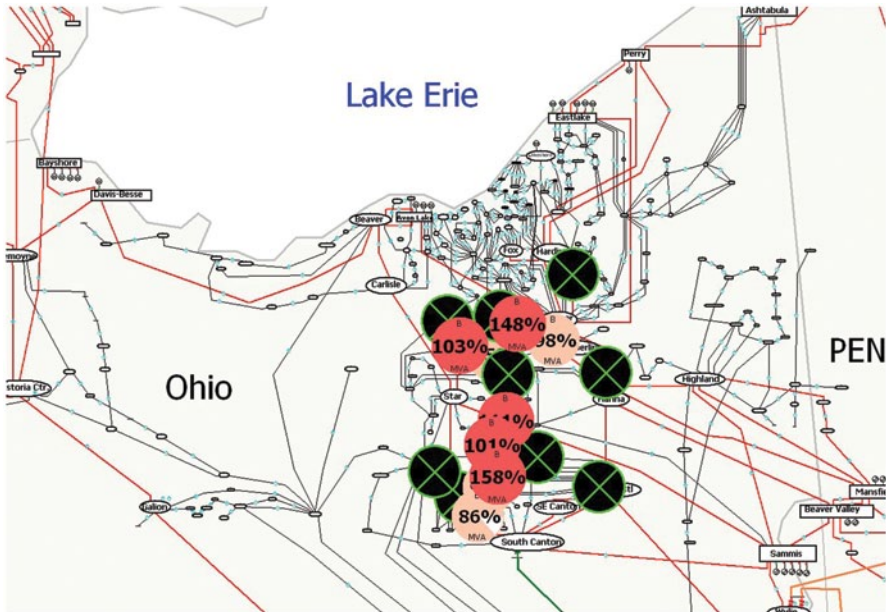


Fig. 13.2 Transmission system at 15:51 EDT

regularly loaded at a high percentage level. Common examples of this are generator step-up transformers. Such transformers are designed to be regularly loaded at a high percentage of their ratings, but because of their radial connection, they are in no danger of overloading. A straightforward solution to this problem is to either not show pie charts on such devices or to specify that the pie charts should not be dynamically resized.

Second, the use of dynamically sized pie charts involves a trade off between making the pie charts large enough to draw attention, yet not too large so as to obscure other important one-line elements. This is illustrated in Fig. 13.2, which shows the August 14th system at 15:51 EDT after three 345-kV lines and a number of 138-kV lines have opened. Note, the open transmission lines' pie charts can also be dynamically sized and can have their color/symbol changed to draw attention. In Fig. 13.2, the open lines are indicated by the large pie charts drawn with an "X" symbol.

The large number of overloads/line outages would make it much more difficult for an operator to rapidly locate the most crucially overloaded devices. Of course, this is a characteristic of any approach that uses dynamically sized one-line elements, including the approach from Mahadev and Christie (1996) of dynamically increasing the line widths to indicate overloads.

One solution for this problem is to filter the display to highlight certain lines, and attenuate the display of other lines. For example, Fig. 13.3 repeats the Fig. 13.2 display except now the lower voltage lines are blended into the background, helping to focus attention just on the more critical 345-kV lines. Now it becomes clear that

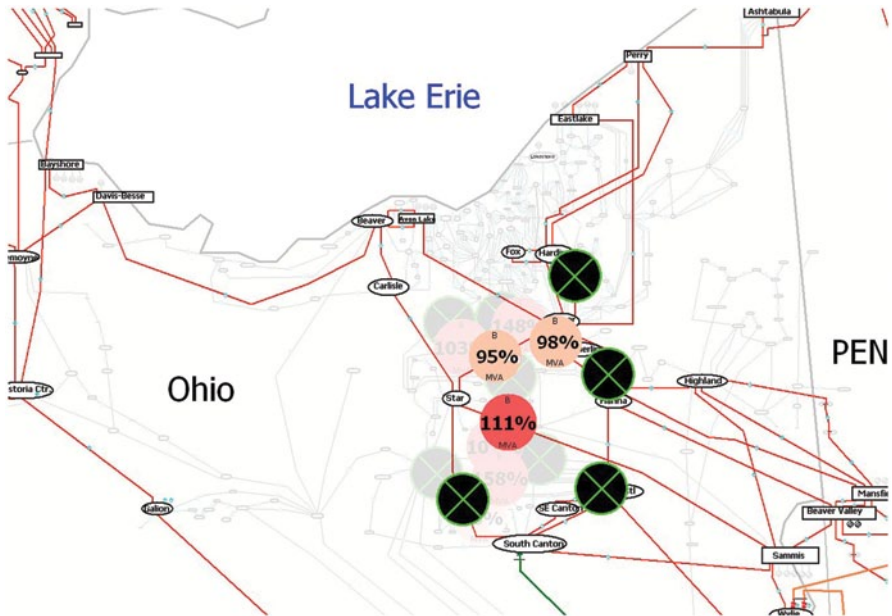


Fig. 13.3 Filtered Fig. 13.2 display with highlighting of just the 345 kV values

the Sammis-Star 345-kV line is overloaded, and that four 345-kV devices are open. Yet the lower voltage lines are still partially visible, helping both to provide context for the higher voltage lines and to allow continued monitoring of these lines.

A second potential solution would be to proportionally reduce the amount of resizing as the display is zoomed. For example, a maximum zoom value for full resizing could be specified. Once the display is zoomed past this value, the amount of pie chart resizing could be dynamically reduced until reaching some threshold value, such as the size of a normal pie chart. The visual effect during zooming is the resized pie chart that remains of the same size on the screen causing the overlap to eventually vanish. Figure 13.4 shows a zoomed view of the central portion of Fig. 13.2 using this technique. This technique could also be used with filtering.

13.2.2 *Animated Flows*

Useful as the pie charts may be, they still do not provide any indication of the direction of flow. During emergency operation, in which historical flows may have reversed, quickly conveying this information could prove crucial. One technique for displaying line flows is to superimpose small arrows on the lines, with the arrow pointing in the direction of the MW flow, and the size of the arrow proportional to either the MW or MVA flow on the line (Overbye et al. 1997). The size and color of these arrows can also be used to provide a visual reinforcement with respect

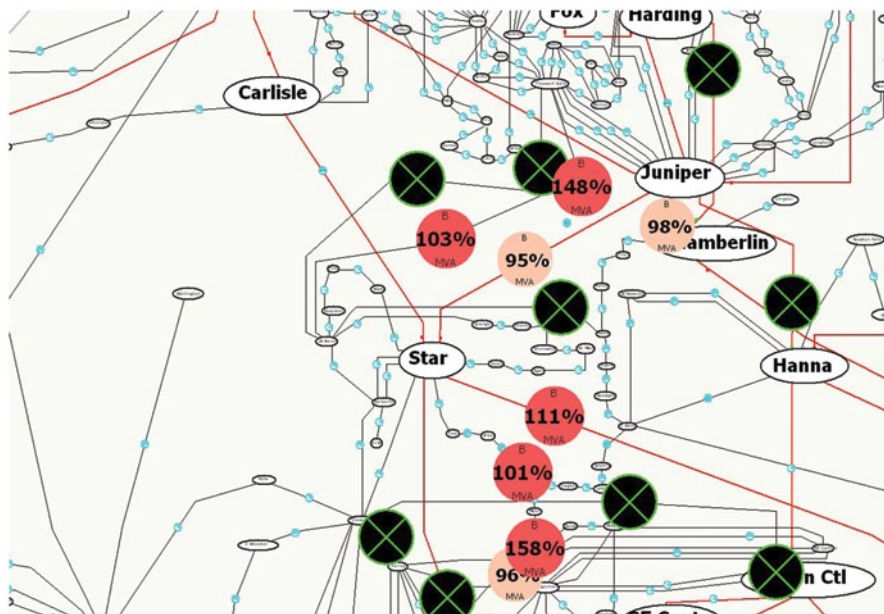


Fig. 13.4 Zoomed view of Fig. 13.3 using dynamic pie chart zoom control and no highlighting

to severity of the problem. Figure 13.5 demonstrates this enhancement using the Fig. 13.3 case with the arrows on the overloaded Sammis-Star line colored darker (red), while the net direction of the power flow into the Cleveland-Akron area could indicate a problem in that area.

To further emphasize the flow direction, the flows themselves could also be animated. With modern computer equipment, fairly smooth animations are possible even with rather large displays. For example, the Fig. 13.5 case can be animated at a rate of about ten times per second on a 1280 × 1024 pixel display. The effect of the animation is to make the system appear to “come to life.” Experience has shown that almost at a glance one can gain deep insight into the actual flows occurring on the system. The use of panning and zooming with conditional display of objects gives the user the ability to quickly study the flows even in a large system.

However, the application of such animated flows to larger systems has to be done with some care. It is certainly possible to create visualizations in which the presence of the animated flow arrows results in more clutter than insight. An example would be the Fig. 13.2 display. But if the view is filtered to just a particular voltage level, or zooming is utilized to focus on a particular portion of the grid, then the animated flow arrows can again be quite helpful.

The use of animation could also be restricted to just those lines of particular interest, allowing one to take advantage of the fact that motion is also preattentively processed, provided the number of elements moving on the screen is small. Selective use of animation can also convey a sense of urgency to the operator. The lack

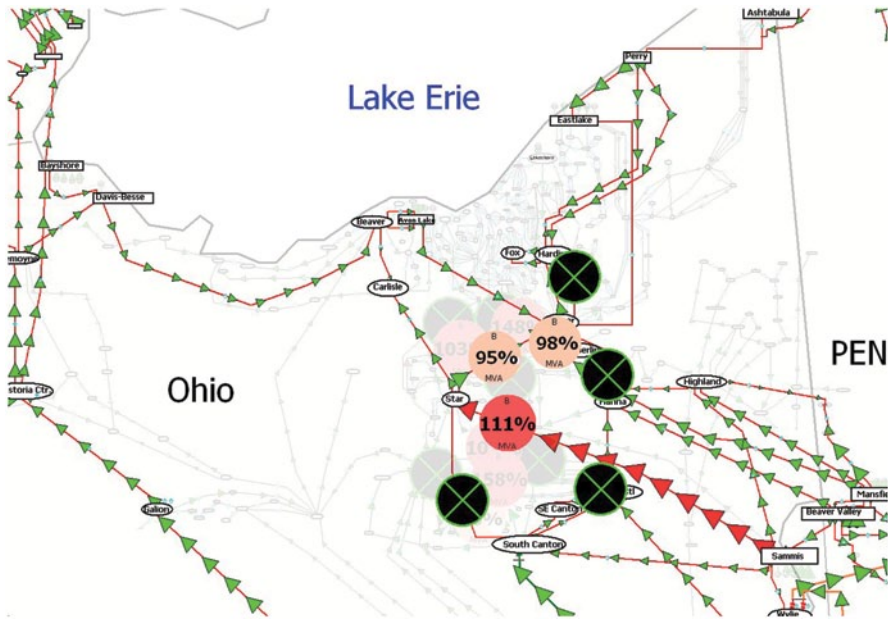


Fig. 13.5 Transmission system at 15:51 EDT with flow arrows

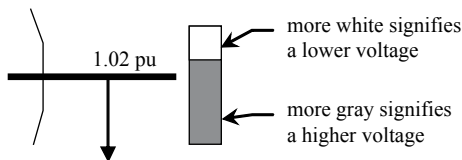
of a sense of urgency to remove a line overload was one of the main reasons for the 2003 Italian blackout (pp. 6 of UCTE 2004). Experimental results examining the impact of motion of flow visualization are presented in Wiegmann et al. (2014).

13.2.3 Symbolic Display of Values

The generic power system visualization question is how best to show a fairly large number of geospatially distributed real and/or complex values. Power system one-line examples of such values are numerous. These may be measured quantities such as bus voltage magnitudes and angles, generator values, LTC tap position, and switch shunt reactive power output. Or they may be derived quantities such as bus Locational Marginal Prices (LMPs), or a host of sensitivity values useful for stability analysis.

If the number of values is small, then numeric fields by themselves could be used. But for wide-area visualization, in which hundreds or thousands of values need to be shown, symbol displays of numeric values can have a significant advantage particularly if adjacent values are somehow related, something that is quite common in power visualizations in which the values are related through the underlying power system.

Fig. 13.6 Thermometer symbol used to show bus voltage magnitudes



For the symbolic display of real values, there are several common techniques. For example, if the numeric value is a normalized quantity, such as a percentage loading, one could use a pie-chart approach, perhaps dynamically sized, in which the amount of fill is used to indicate a percentage. Another technique is the “thermometer” type symbol (see Fig. 13.6; Mahadev and Christie 1994) in which a rectangular bar is filled to graphically indicate a value’s position within a range. This approach can be quite useful for showing numbers that share a common range. For example, Fig. 13.7 demonstrates the use of thermometers for showing the voltage magnitudes for a 37 bus case; here, the range is between 0.96 and 1.04 per unit.

Another common power system situation is the need to specify a normalized value, such as a percentage of a limit, while simultaneously indicating the magnitude of the limit. Examples might include transmission line flow values, or generator real/reactive power outputs. Certainly, the pie-chart approach could be used with either the diameter or area of the pie chart circle itself scaled based upon the value of the actual limit.

An alternative approach is to use the “circle method” in which a filled circle is contained within a hollow outer circle. Like the pie chart approach, the size of the outer circle can be scaled based upon the limit, whereas the size of the inner circle indicates the normalized (percentage) value. But a potential ambiguity arises—should the inner circle’s radius or area be used to show the value? The symbols on the left side of Fig. 13.8 show the radius approach, while those on the right use the area approach. Not knowing the value, what value would you guess for these circles?

While the circle approach is probably not superior to pie charts for displaying real numbers, it does have advantages for the display of complex numbers. Complex numbers are quite common in the analysis of power system stability, and, of course, a complex number requires the visualization of both its magnitude and its angle. While a pie chart could certainly be used for the display of angles, scaling its diameter by the magnitude would make for unreadable pie charts (and hence angles) for small values. A good alternative is shown in Fig. 13.9 in which the magnitude is indicated by the circle method while the angle is indicated by the angular position of an arrow superimposed on top of the circle.

As an example, consider the assessment and visualization of a power system’s oscillatory stability, a quantity that is quantified through the use of the eigen properties of the system state matrix (Rogers 2000; Kundur 1994). In order to provide an early detection of an impending blackout, understanding these values could be crucial. In particular, from a visualization perspective what is important is to quickly convey various geospatial values associated with a critical mode such as the normalized mode shapes for the generators (the right eigenvector of an oscillation

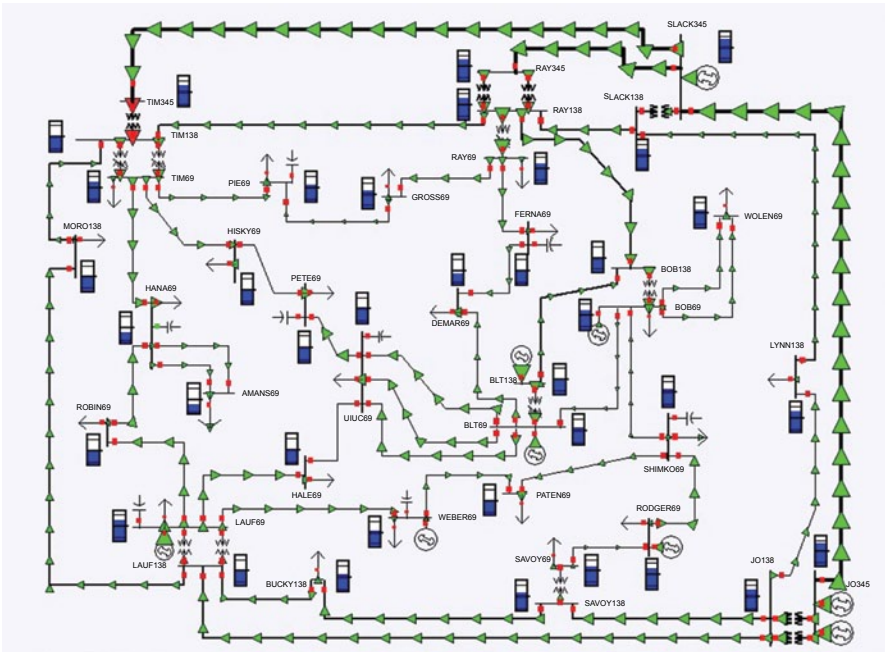


Fig. 13.7 Use of thermometers to display bus voltage magnitude

mode is called the mode). Figure 13.10 demonstrates the visualization of a mode shape for a 280 generator case. Note that almost at a glance the values for a large number of generators can be quickly interpreted.

13.2.4 Contouring

The use of discrete symbols for visualization can be quite helpful provided the number of individual symbols is relatively low (less than several hundred). However, as the number of values grows eventually the displays become too cluttered, making it difficult to detect any underlying patterns. Hence, for wide-area displays with many hundreds or thousands of values the use of contouring is preferred (Weber and Overbye 2000).

Contours have been used extensively for the display of spatially distributed continuous data in many other fields. However, there are three main issues with applying contouring to the display of bus-based power system information such as voltage magnitudes and angles and generator data. First, the buses themselves are not spatially continuous—bus data values only exist at the distinct, individual buses with no values in between.

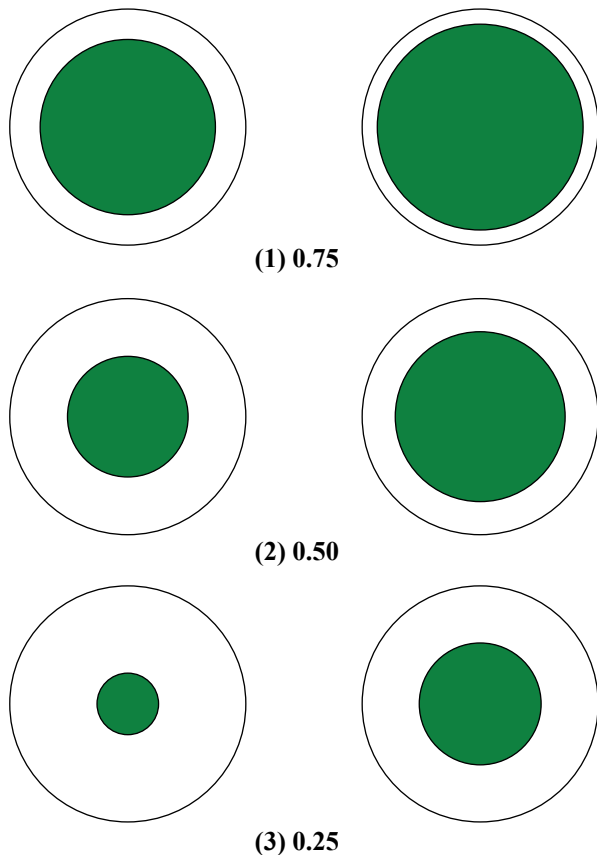
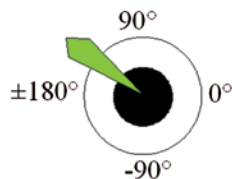


Fig. 13.8 Circle approach for showing values

Fig. 13.9 Visualization of complex numbers using circle approach



To address this issue, virtual values must be created to span the entire 2D contour region. The virtual value is a weighted average of nearby data points, with different averaging functions providing different results. Second, tap-changing transformers may introduce discrete changes in bus voltage magnitude values. Contour plots normally imply a continuous variation in value. However, this issue can be addressed by setting up a contour in which only bus values within a particular nominal voltage range (say only 138 kV) are contoured. Third, voltages that are near one another on

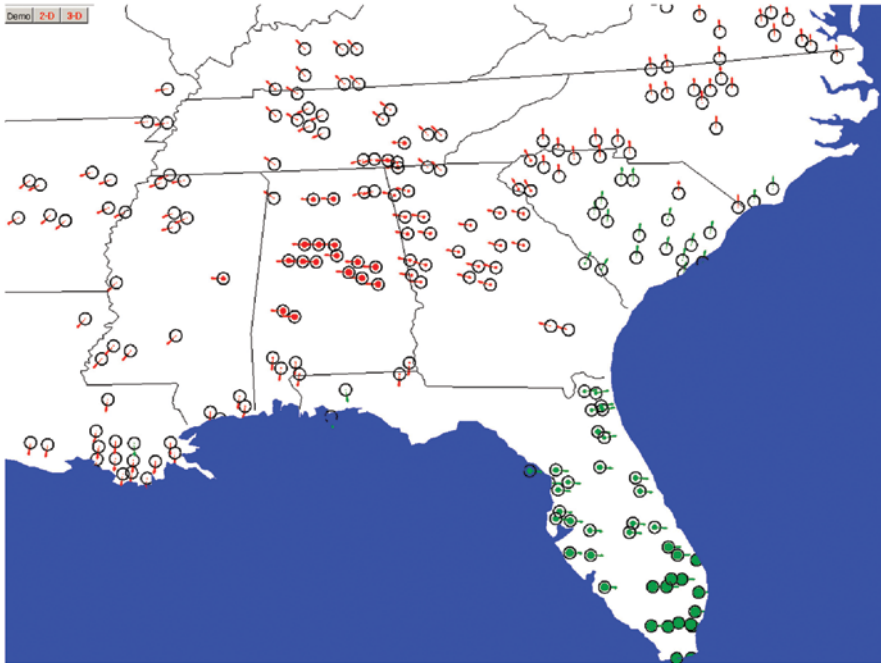


Fig. 13.10 Visualization of mode shape for 280 generators in southeast USA

a one-line diagram may not be “near” one another electrically. This issue can also be addressed by only contouring a particular voltage range, and perhaps by judicious construction of the contouring diagram. If a strictly geographical layout is used, normally buses of the same nominal voltage that are near each other geographically are also near electrically.

Once these virtual values are calculated, a color map is used to relate the numeric virtual value to a color for display on the screen. A wide variety of different color maps are possible, utilizing either a continuous or a discrete scaling (for a useful discussion of color mappings, see Brewer 1994). One common mapping is to use red for lower voltage values and blue for higher values, while another common mapping is the exact opposite. Standardization of contour color mappings, both within a control center and between control centers, could be beneficial.

Perceptually, contouring works well because the human visual system is well designed for detecting patterns. For example, Fig. 13.11 shows a voltage contour of about 5600 bus voltages in the Mid-Atlantic portion of North America at about 15:00 EDT on August 14 using a discrete gray color mapping. Notice that at a glance, the relatively low initial voltages in Ohio and Indiana are visible, with the extremely low voltages in southern Indiana due to line outages that occurred at about noon on August 14th.

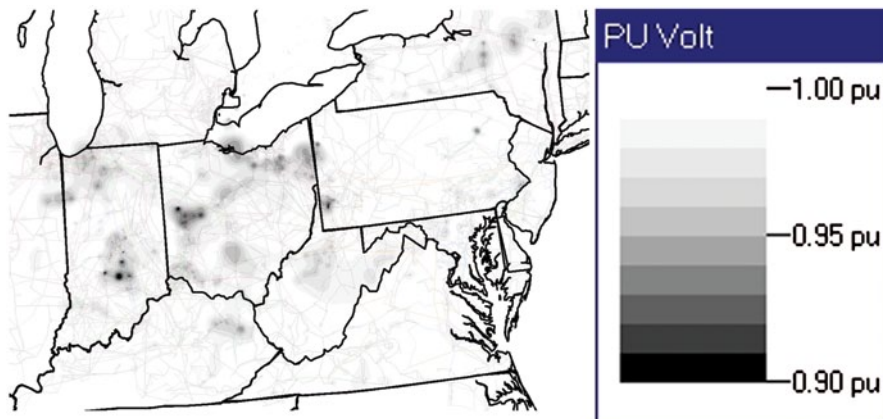


Fig. 13.11 Pre-blackout Ohio region 115–230-kV voltage contour

Human factors' testing of power system voltage contours indicates that it is useful both for increased speed and accuracy in problem diagnosis, particularly for situations with many voltage violations. This occurs because color serves as an effective highlighting feature that attracts attention to an area of a display and reduces the size of the search space, thus allowing for the rapid localization of problem areas. In addition, the use of color contouring has the ability to create global or holistic properties in the display, which are in contrast to the local or component parts that exist.

Global properties of objects depend on the interrelations between the component parts and generally refer to the Gestalt concept that the "whole is greater than the sum of its parts." Hence, color contouring may allow operators to assess the overall state of the system more readily (gain better situation awareness or develop a more accurate mental model) and therefore facilitate the choice of a more appropriate and timely corrective action.

Another advantage of contouring, which is impossible to show here, is the images can be readily animated to quickly show the progression of the system over time (similar to what is done with animated weather maps). During an emergency, this information could be used to rapidly convey the direction of the system state, and could also be used to rapidly bring late arriving people to the control room (such as engineers and management) up to speed on what is going on.

However, one does need to be careful about trying to convey too much information in a single display. For example, Fig. 13.12 combines transmission system information (pie charts and flow arrows) with the contour. While this may be tolerable if there are just a few problems, as more problems develop it would become increasingly cluttered.

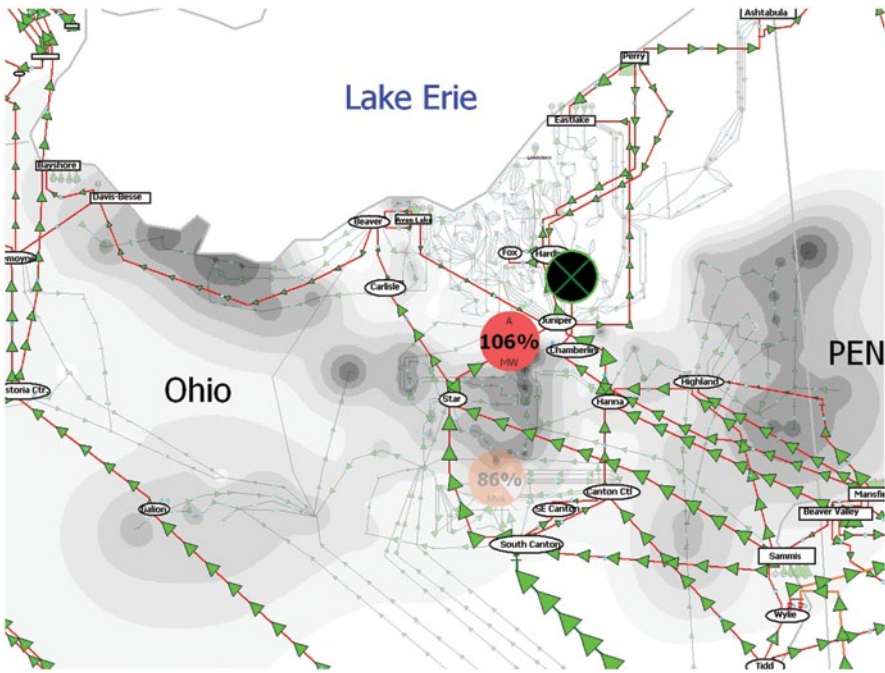


Fig. 13.12 Northeast Ohio voltage contour at 15:05 EDT

13.3 3D Power System Visualization

The previous data visualization techniques can be quite useful when one is primarily concerned with the visualization of one or perhaps two types of spatially oriented data such as bus voltages or transmission line flows. However, in power system stability analysis one is usually confronted with a large amount of multivariate data. Data of interest could include a potentially large list of independent and dependent variables, such as bus voltage magnitudes, transmission line loadings, generator real and reactive reserves, transformer tap and phase positions, scheduled and actual flows between areas, interface loadings, and oscillation mode shape. In more advanced applications, OPF, contingency analysis, and Available Transmission Capacity (ATC) calculations, this list of variables is even longer. This section discusses the use of an interactive 3D visualization to assist in analyzing this vast amount of information (Overbye et al. 2003a, b).

In developing such an environment, several key issues must be addressed. First, in visualizing power system data there is usually no corresponding “physical” representation for the variables. For example, there is no physical representation for the reactive power output of a generator, or for the percentage loading of a transmission line. Rather, these values are typically shown as a numerical value either on a one-line diagram or in a tabular display. This contrasts with the use of interactive 3D for

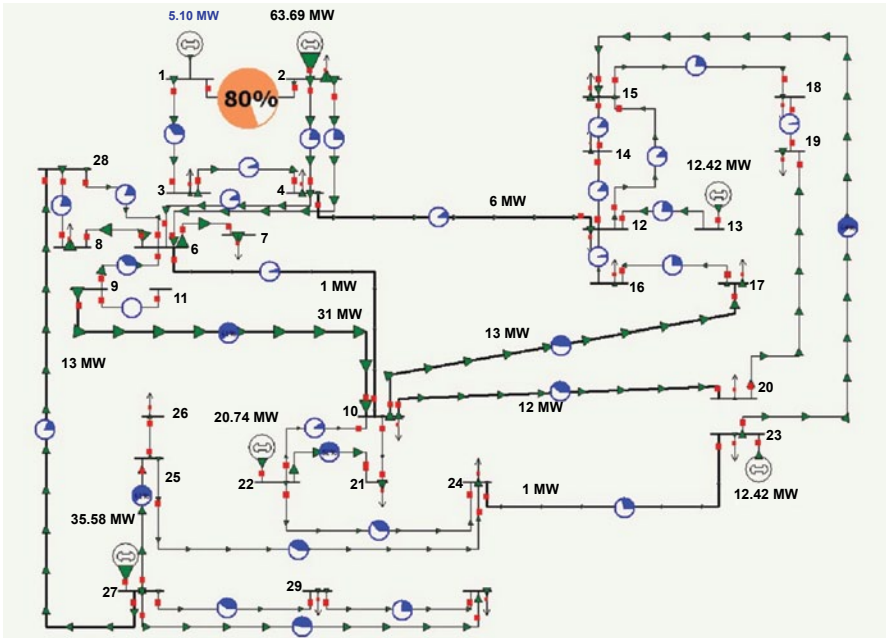


Fig. 13.13 2D one-line view of 30-bus system

power system operator training, in which the 3D environment seeks to mimic, as closely as possible, an existing physical environment. It also differs from the use of interactive 3D for some types of scientific visualization, in which the purpose of the environment is to visualize physical phenomena, such as flows in a wind tunnel or molecular interactions. To address this issue, an environment based upon the common one-line representation serves as a good starting point. The new environment differs from the one line in that a one line is a 2D representation, whereas the new one is 3D. How this third dimension can be exploited is discussed in the remainder of this section.

The second issue is the 3D environment must be highly interactive. In power systems, there are simply too much data to simultaneously display all the data that may be of interest. Rather, the operator should be able to quickly and intuitively access the data of interest.

To introduce such an environment, Fig. 13.13 shows a traditional 2D one line for a small 30-bus system, augmented using animation to show the system flows. Figure 13.14 shows the same one line in the 3D environment, with the exception that now the generators are represented using 3D cylinders of potentially varying heights. The one line has been mapped into 3D using a perspective projection. The one line is now oriented in the xy -plane (horizontal plane), while the generators extend in the z (vertical) direction. In Fig. 13.14, the height of each generator cylinder is proportional to its maximum real power capacity. The height of the lighter bottom

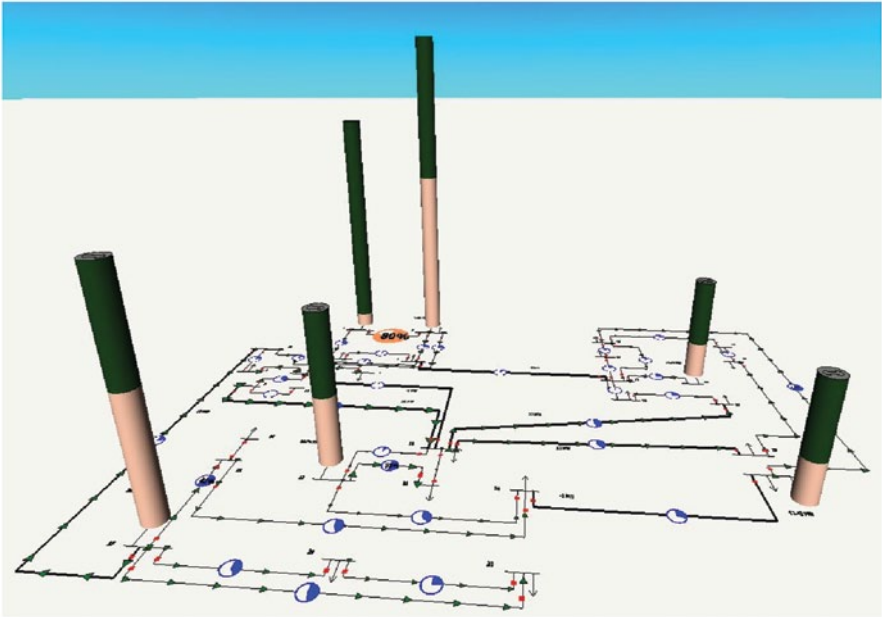


Fig. 13.14 3D view of 30-bus system

portion of the cylinder is proportional to current output of the generation, while the upper portion indicates the available reserve capacity.

One of the advantages of 3D is its ability to show the relationships between variables. For example, in studying the voltage stability of a system one is often interested in knowing both the location and magnitude of any low system voltages, and also the current reactive power output and the reactive reserves of the generators and capacitors. Such a situation is illustrated in Fig. 13.15 where the height of each generator cylinder is now proportional to the maximum reactive capacity of the generator; the darker region on the lower portion of the cylinder is proportional to the current reactive power output, while the lighter top portion represents the reactive power reserves. The bus voltage values are indicated using a contour, with only voltage values below 0.98 shaded.

Figure 13.16 shows a similar representation for the IEEE 118-bus system. Rapid navigation in such a visualization would be important to allow one to rapidly see the more distant parts of the display.

Note that in both figures it is apparent, almost at a glance, the location of the sources of reactive power generation and the reactive power reserves. The figures also do a good job of conveying qualitative information about the magnitude of these values. What they do not do is convey quantitative information. Thus, while one learns from Fig. 13.15 that the reactive power generation at bus 20 is about 50% of its maximum, one does not learn what the actual var output is nor the maximum var limit. In some situations, this could be a significant limitation. Thus,

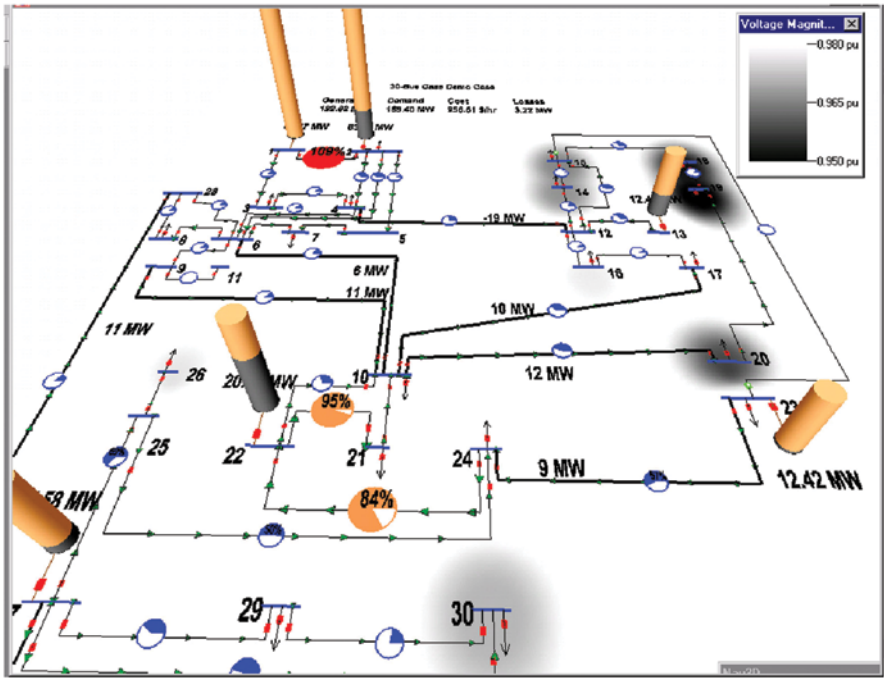


Fig. 13.15 Thirty-bus system generator reactive reserves

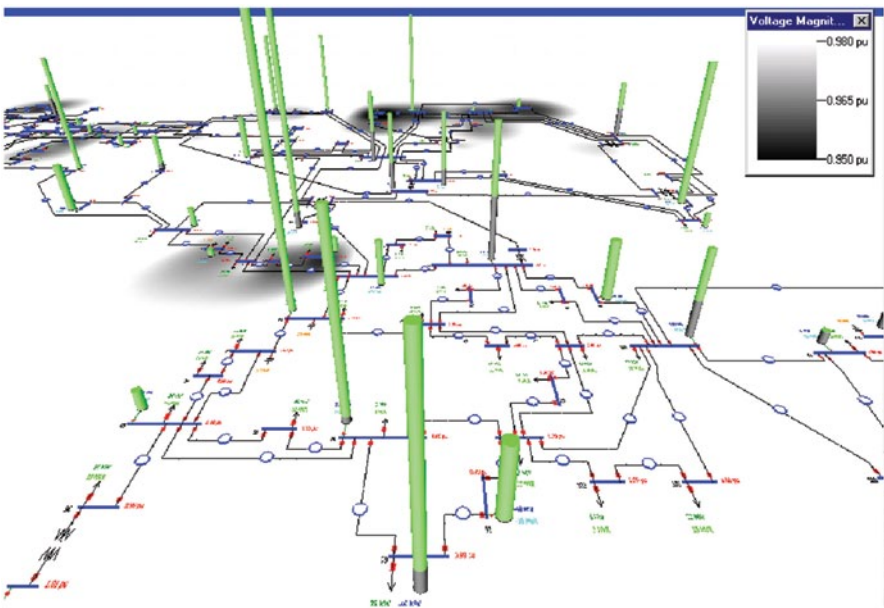


Fig. 13.16 118-bus system generator reactive reserves

the best use of interactive 3D would be to supplement, rather than to completely replace, existing one-line and tabular display formats.

However, in support of the 3D approach several observations are warranted. First, in many situations these qualitative relationships are sufficient. This is particularly true when one is studying a familiar system. For example, operators already know the reactive limits of their generators; what they need to know is how close those generators are to their limits in a qualitative sense. And one needs to know the value for only a few generators in order to get acceptable estimates for the remaining generators by comparing their relative sizes in the 3D environment. Second, there is nothing that prevents displaying numerical values of system quantities in the 3D environment, just as bus numbers and some line flows are shown in Fig. 13.15. However, a valid objection to this approach is if the viewpoint is changed (i.e., rotated) these fonts could be shown at unappealing angles. But this problem could be easily solved by having the 3D environment automatically rotate the fonts so they are always facing the viewer (provided the one line is designed with sufficient room for the fonts to rotate). Alternatively, the fonts could be shown in the vertical plane, such as on the surface of the generator cylinders.

A third approach would be to allow the operator to get additional information about system objects by selecting the object with the mouse. This allows the display to be relatively uncluttered, yet still allows rapid access to a large amount of quantitative information. Hint functionality, in which additional text-based information appears after a slight delay when the cursor is placed on an object, could also be used.

The use of 3D could certainly also be used for the display of stability related quantities such as mode shape and participation factor information. Figure 13.17 repeats the display of the Fig. 13.10 information, except now the height of the 3D cylinder is proportion to the magnitude of the mode shape value for each generator. The use of a perspective view allows for an emphasis on nearby generators (Florida in the Fig. 13.17 example), while the values for more distant generators are relatively smaller. Whether this is an advantage or disadvantage depends upon the application. If the operator is most interested in the nearby information, but would still like to get a feel for how that information fits in a global context, then a 3D perspective display is advantageous. Conversely, if the operator would like equal emphasis placed on each value then a 2D display would be preferred.

A final issue associated with 3D visualization that needs to be addressed is performance. In order to give the operator the feeling of interacting with the 3D environment it is crucial that the display refresh quickly and that there be little latency between the operator issuing a command, such as desiring to change position, and the display being updated.

How fast the display can be refreshed depends upon a number of factors, including the speed of the computer's processor, the speed of the display card, whether the display card has hardware support for the underlying 3D environment (e.g., OpenGL), and software considerations such as the level of detail of the display and the lighting model employed. Given the trend towards supporting 3D environments directly in the display card hardware, newer microprocessors with new commands

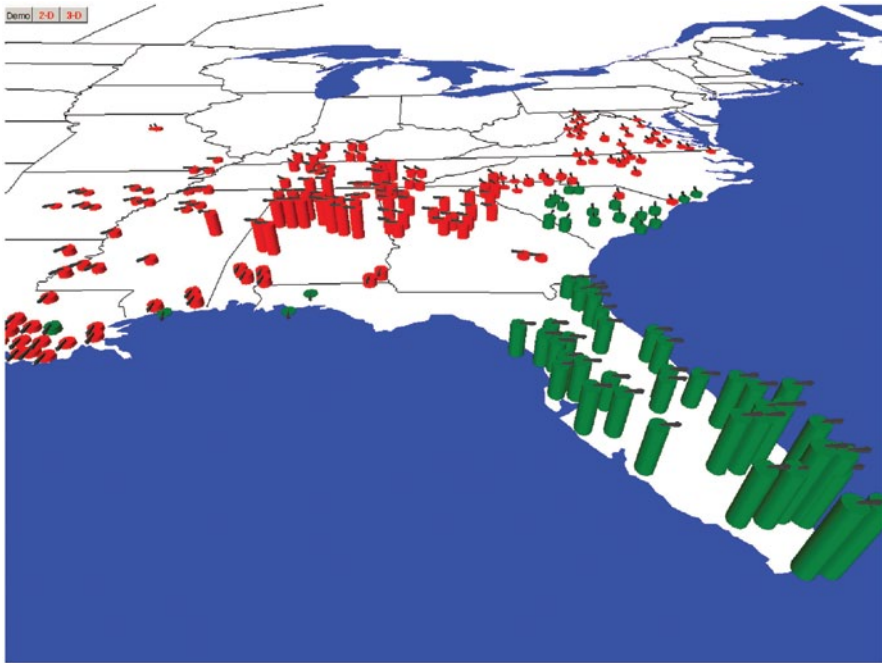


Fig. 13.17 3D visualization of Fig. 13.10 information

to directly support 3D graphics and faster processors in general, very good 3D performance is becoming widely available even for the display of relatively large systems.

For benchmarks, relatively small displays like Figs. 11.14 and 11.15 can be animated at about 60 frames/s on a 2.8-GHz PC. To demonstrate performance on a slightly more realistic system, Fig. 13.18 shows a one line of the Midwest electric grid, again using cylinders to visualize the generator outputs and reserves. The refresh rate for this reasonably detailed display, which contains about 1100 buses, 375 generators, and 1000 transmission lines, is around 4.5 frames/s.

13.4 Putting It All Together and Conclusion

Visualization can play a crucial role in reducing the risk of future blackouts by helping operators to quickly assess a potentially rapidly changing system state, and by helping them to formulate corrective control actions. This chapter has presented several methods that could be quite useful for the representation of this data both within the control room environment and for offline studies. Nevertheless, significant challenges remain. Key challenges are the problem of visualizing not just the

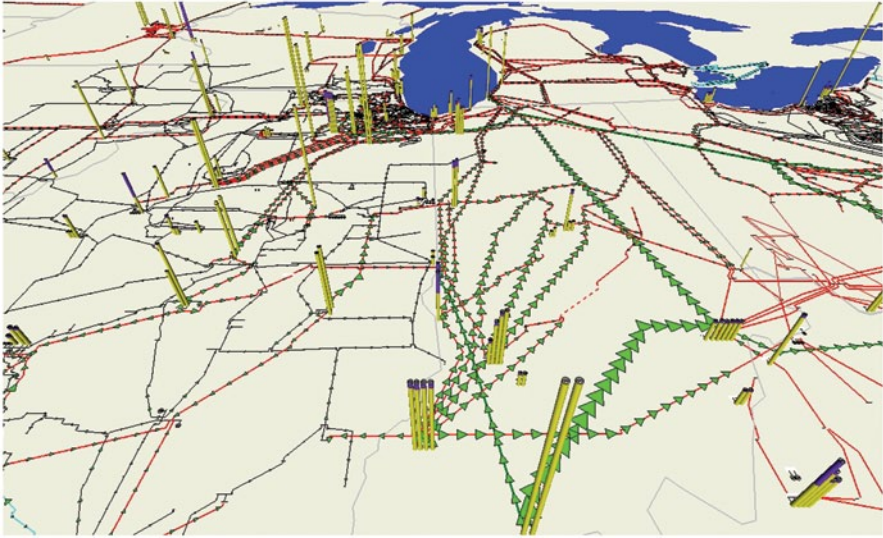


Fig. 13.18 3D view of Midwest power grid

current system state but also the potentially large number of contingency states, and the problem of visualizing not just a single time snapshot but rather the variation in the system operating conditions over time. More research is needed to develop better methods for visualizing this data, performing human factors assessments on these new techniques, and rapidly transferring the results to industry.

References

- Brewer CA (1994) Guidelines for use of the perceptual dimensions of color for mapping and visualization. Proceedings of the international society for optical engineering (SPIE), San Jose, February 1994, vol 2171, pp 54–63
- Kundur P (1994) Power system stability and control. McGraw-Hill, New York
- Mahadev PM, Christie RD (1994) Case study: Visualization of an electric power transmission system. Proceeding of visualization 1994, Washington D.C. October 17–21:1994
- Mahadev PM, Christie RD (1996) Minimizing user interaction in energy management systems: task adaptive visualization. IEEE Trans Power Syst 11(3):1607–1612 (PWRS)
- Overbye TJ, Sauer PW, Marzinzik CM, Gross G (1995) A user-friendly simulation program for teaching power system operations. IEEE Trans Power Syst 10:1725–1733 (PWRS)
- Overbye TJ, Gross G, Laufenberg MJ, Sauer PW (1997) Visualizing power system operations in the restructured environment. IEEE Comput Appl Power 10:53–58
- Overbye TJ, Wiegmann DA, Rich AM, Sun Y (2003a) Human factors aspects of power system voltage contour visualizations. IEEE Trans Power Syst 18:76–82 (PWRS)
- Overbye TJ, Sun Y, Klump RP, Weber JD (2003b) Interactive 3D visualization of power system information. Electr Power Compon Syst 31:1205–1215
- Rogers G (2000) Power system oscillations. Kluwer, Boston

- UCTE (2004) Final report of the investigation committee on the 28 September 2003 blackout in Italy, UCTE, April 2004
- US DOE (2004) Final report on the August 14, 2003 blackout in the United States and Canada: causes and recommendations, U.S. Department of Energy, April 2004
- Ware C (2004) Information visualization. ISBN:1-55860-819-2
- Weber D, Overbye TJ (2000) Voltage contours for power system visualization. IEEE Trans Power Syst 15:404–409 (PWRS)
- Wiegmann DA, Essenberg GR, Overbye TJ, Sun Y (2014) Human factors aspects of power system flow animation. IEEE Trans Power Syst 20:1233–1240

Index

2004 Summer Olympic Games 288

A

ABM integration method 168, 169
Aliveri 286, 288, 289, 326
ASTRE 322, 323
ATC 28, 151, 240, 306, 311
Athens 286, 288–290, 320, 322, 323, 325, 328
Available Transfer Capability *See* ATC 28
Avila-Rosales, R. 28, 46, 82, 237, 240, 260, 263

B

Barbier, C. 30, 31, 36, 38, 46, 51
Barret, J.P. 30, 31, 36
BDF integration method 168, 169
Binary search 299, 315–317
Blackout 118, 236, 279, 286–288, 330, 387, 388, 394, 405

C

CND 66, 70, 71, 76
Computations 31, 77, 237, 238, 261, 262, 337, 365, 367, 368
Contingency analysis 5, 18, 19, 24, 45, 139, 181, 228, 240, 260, 280, 297, 306–308, 315, 317–319, 322, 330, 342
Continuation parameter 165–167, 313
Continuation power flow 164, 165, 189
Control 123–125, 135–137, 139, 143–148, 150–156, 236, 240, 246, 254, 256, 263, 273, 276, 281, 291, 293, 306, 307, 312, 318, 319, 337, 340, 358, 367–370, 372, 373, 378, 381
Control centers 28, 59, 95, 98, 121, 242, 248, 398

Crary, S. 31

Critical 46, 54, 67–69, 71, 73–76, 79, 80, 83, 84, 125–129, 131–133, 135–138, 143, 144, 147, 148, 150, 151, 264, 318–320, 336, 337, 344, 345, 348, 353–355

D

Differential-Algebraic Equations (DAE) 337
Dimo, P. 28, 29, 31–33, 35, 38, 39, 43–48, 50, 51, 53, 58, 65, 66, 82, 83
Distance to instability 29, 32–35, 50, 51, 54–56, 58, 59, 66–77, 80–85, 125, 127, 128, 131, 135, 148, 151, 260, 264, 267, 275, 306, 312, 314–318, 322, 324, 325, 328, 335–337
Distributed generation 359, 362, 363
Dobson, I. 46, 283, 318, 320
Dynamic security assessment 98, 114, 138, 167, 181, 191, 196, 201, 205, 255, 321, 336
Dynamic Stability Assessment (DSA) 110, 139, 153, 155, 241, 305, 336, 364
Dynamics 131, 257, 283–285, 309, 310, 370

E

Electricity of Vietnam 77
Emergency SIME *See* E-SIME 143
Empresa de Transmisión Eléctrica S.A. *See* ETESA 66
Energy Management System (EMS) 118, 236, 289, 322, 387
Equilibrium 2, 17, 19, 23, 25, 308, 318
E-SIME 143, 145
ETESA 66, 70, 71, 76
Eurostag 139
EVN 66, 77, 78

F

FACTS 356
 FILTERA 139
 Flexible AC Transmission Systems *See*
 FACTS 356
 FVSS 70–77, 79, 80, 84

G

Generators 31, 32, 38, 43, 45, 46, 50, 56,
 58, 66, 67, 70, 71, 73–77, 81, 126,
 127, 129, 133, 134, 143, 146, 147,
 154, 264, 282–286, 289, 290, 292,
 308–310, 313, 314, 319, 326, 358,
 359, 376, 377
 Georgios 286, 323
 Giri, J. 28, 46, 237, 260
 Gonzalez, L. 70

H

Hellenic 139, 286–289, 320, 321, 325, 330
 Hiskens, I.A. 337, 339, 357, 364, 371, 372,
 376, 381, 382, 385
 Hurwitz 44
 Hydro-Quebec (H-Q) 295–299, 311, 317

I

Integrated security control 124, 152, 156
 Intelligent system 276
 Ionescu, S. 30, 31, 47, 51, 53

J

Jacobian 44, 50, 66, 152, 318–320

K

Kundur P. 261
 Kundur, P. 28, 30, 31, 64, 260, 279, 376

L

Limits 28, 29, 31–35, 47, 51, 54, 64, 68, 69,
 72, 74–77, 81, 84, 137, 236, 239,
 260, 280, 319, 325, 340
 Load 30, 50, 51
 Loadability 30, 47, 51, 66, 264, 282, 283,
 295, 311, 313, 314, 316–320, 322,
 326
 Load-flow 66, 68, 79, 80, 308, 313, 317
 Loads 124, 238, 265, 281, 288, 291–293, 295,
 297–301, 306, 310, 316, 317, 373,
 375–378
 Local Truncation Error (LTE) 170, 171
 Lyapunov 364

M

Magnien, M. 31, 65, 68
 MAIS 297, 299, 301
 Markets 28, 77, 238, 239, 261
 Maximum loadability 1, 16, 165, 166, 181
 Measurements 146, 147, 237, 239, 240,
 242–247, 254, 258, 259, 267, 272,
 276
 Megalopolis 286
 Methods 131, 238, 260, 301, 308–310, 313,
 317, 319, 322, 326, 328
 Models 31, 76, 77, 81, 283
 Modified SIME method 176, 181, 192
 Monitoring 11, 16, 18, 95, 98, 99, 236, 238,
 256
 Moraite, A. 32, 65, 68
 Morison, K. 31, 319

N

Nam, N.T. 66, 77, 81
 National Load Dispatch Center 66, 77
 NERC 28, 34
 Newton-Raphson method 163–165, 318
 Nguyen, T.B. 64, 340, 341, 348
 NLDC 66, 77, 79
 Nordel 376
 NTUA 290
 Numerical instability 161, 168, 190
 Nyquist 44

O

OMASES 138, 139, 320–323
 One Machine Infinite Bus (OMIB) 125–127,
 129–135, 143, 144, 150, 151
 Operations planning 66, 77
 Optimal Power Flow (OPF) 136–138, 148,
 153, 313, 318, 320, 340, 341, 343,
 344
 Overbye, T. 308

P

Pai, M.A. 30, 337, 339–341, 343
 Parallel 27, 160, 239, 262
 Pavella, M. 125, 128, 129, 135, 136, 143,
 147, 148, 152, 259
 PCLL 311, 315, 316, 318, 328
 Peloponnese 286, 288, 289
 Phasor Measurement Units (PMU) 25, 66, 98,
 203, 240, 243, 244, 246, 253, 254,
 258, 266
 Phasor measurements 66, 95, 118, 145, 238,
 243, 244

- Power flow 30, 70, 99, 111, 119, 161, 164, 192, 203, 271, 318
- Power system 27, 31, 51, 58, 67–71, 74, 76–81, 83–85, 124, 139, 140, 235–237, 239–241, 243, 245, 248, 254, 256–260, 264, 265, 275, 276, 285, 288, 290–293, 295, 306, 308, 309, 311, 314, 316, 324, 325, 337, 365, 375, 376
- Power-flow Jacobian 2, 5, 10, 11
- Predicting instability 143
- Preventive rescheduling 336, 345
- Prony 130–134, 179
- Protection Security Analysis (PSA) 121
- PSS/E 67, 70, 71, 73–76, 264
- P-V and Q-V relationships 30, 51, 281–283, 313, 322, 326, 328, 330
- Q**
- QuickStab 57, 65–67, 69, 71, 77, 121
- R**
- Real-time 28, 105, 119, 238, 336
- Regional Transmission Organization *See* RTO 242
- REI 35, 37–40, 43, 44, 48, 50, 51, 53–56
- Relay margin 260, 363, 364
- Reliability coordinators 28
- Risk 27, 31, 51, 54, 58, 70, 77, 280, 299
- RPTC 297
- RTO 242, 243
- S**
- Sauer, P.W. 30, 43, 66, 343
- Savulescu, S.C. 28, 68, 83, 257, 264
- SCADA/EMS 29, 35, 43, 56–58, 64, 67, 70, 77, 82, 84, 85, 139, 155, 236–243, 245, 247, 253, 254, 257–259, 261–264, 267, 272, 276, 289, 290, 321, 322, 330
- Security assessment 64, 138, 152, 281, 321, 335–337
- Security regions 153, 161, 182, 186
- Security-constrained optimization 337
- Sensitivity analysis 138, 139, 336, 337, 339, 340, 348, 350, 353–355, 357, 358, 364, 368, 371–373, 384, 385
- Short-circuit admittances 37–39, 41, 44, 48
- Shortcircuit currents 43
- Short-circuit currents 35, 42
- SIGUARD 120
- SIME 124–126, 129–133, 135–137, 139, 143, 146–148, 151, 153, 155, 337
- Single Machine Equivalent *See* SIME 125
- Small-signal stability 65, 206, 220
- Smart grids 86, 97, 266
- SSA 305, 307
- Stability 2, 8, 16, 28–35, 44–46, 48, 50, 51, 57, 58, 66, 67, 69, 71, 76, 77, 124–133, 135–137, 139, 142–144, 147, 148, 150–153, 156, 240, 252, 257, 260, 261, 268, 273, 279–282, 284–286, 291–293, 295, 297, 306, 308, 311, 318–320, 325, 326, 336, 337, 375, 376
- Stability assessment 45, 56, 57, 71, 74, 75, 82, 138, 145, 237, 240, 263, 306
- Stability constrained optimal power flow 340, 341
- Stability indicators 30, 32, 35, 48, 55, 81, 82, 85, 237, 242, 260, 264, 325
- Static and Dynamic Security Assessment System (SDSA) 161
- Steady-State Stability Limit (SSSL) 108
- Supervisory control and data acquisition (SCADA) 29, 56, 58, 70, 82, 105, 109, 118, 221, 241, 388
- Synchrophasors 98, 156, 246, 267, 268
- System dispatching 66, 77
- System stressing 46, 50, 54, 74, 152, 311, 312, 316, 317
- T**
- Tangent vector continuation method 165, 166
- Tap Changing Under Load (TCUL) 163
- Taylor, C. 44, 143, 280, 295, 384
- TDST 297, 299
- Testing and validation 66, 69, 71, 144, 262
- Time domain simulation 110, 160, 161, 167, 168, 170, 171, 178, 186, 187, 190, 192, 196, 371
- Time to insecurity (tti) 114
- Total Transfer Capability (TTC) 28, 34, 151, 311, 312
- Trajectory sensitivity analysis 338
- Transfer capability 77, 80
- Transient energy function 160, 171
- Transmission 25, 27, 38, 39, 51, 64, 66, 69, 83, 97, 109, 120, 219, 238, 256, 297, 306
- Transmission Reliability Margin (TRM) 28
- Transmission System Operator *See* TSO 280
- Trend 105, 112, 216, 362
- TSO 280
- Tweedy, J. 28, 46

U

Ungureanu, B. 31, 47, 51, 53

V

Van Cutsem, T. 46, 153, 280, 283, 284, 296,
300, 306, 307, 310, 312–314,
318–320, 322, 376

Variable-Step-Variable-Order (VSVO) 168

Venikov, V.A. 30, 43–46, 48, 49, 66

Vergara, J.S. 28, 33, 46, 51, 64, 70

Vietnam 78

Visualization 35, 38, 39, 54–57, 85, 95, 100,
107, 109, 114, 116, 207, 227, 237,
241, 243, 404, 405

Voltage stability 279, 287, 302

Vournas, C. 30, 66, 280, 283, 284, 286, 291,
306, 307, 312, 319, 320, 322

VSA 139, 153, 155, 289, 290, 305, 306, 318,
320–323, 330

W

WAMS 245, 250, 276, 335

Web Internet/Intranet 262

Wehenkel, L. 124, 154, 156

Wide area monitoring system *See* WAMS 276

WPSTAB 290, 322, 323

Z

Zima, M. 155, 379